许志琴地学成果系列（一）

青藏高原大陆动力学

（1984～2006）

地质出版社

The Geological Series Achievements (1) of Xu Zhiqin

The Continental Dynamics of the Qinghai-Tibet Plateau (1984 ~ 2006)

Geological Publishing House
Beijing

ISBN 7-116-05061-2

9 787116 050617 >

P·2755 定价:60.00元

许志琴地学成果系列

（一）

青藏高原大陆动力学
（1984～2006）

地质出版社

·北　京·

内 容 提 要

本书为作者研究青藏高原大陆动力学已发表的部分成果，涉及按地体和活动观对青藏高原结构的新划分、青藏高原北部早古生代地体构架及超高压变质带形成与折返机理、不同时期地体拼合/地壳缩短与碰撞造山类型、喜马拉雅大规模地壳变形、周缘造山带的崛起，以及大型走滑运动对青藏高原形成与演化的影响等。

本书对从事相关专业的科研、生产和教学人员具有重要参考价值。

图书在版编目(CIP)数据

青藏高原大陆动力学：1984～2006/许志琴等著. —北京：地质出版社，2006.12

(许志琴地学成果系列：1)

ISBN 7-116-05061-2

Ⅰ.青… Ⅱ.许… Ⅲ.①青藏高原—地球动力学—文集 Ⅳ.P548.27－53

中国版本图书馆 CIP 数据核字(2006)第 148529 号

QINGZANG GAOYUAN DALU DONGLIXUE (1984～2006)

组稿编辑：王大军 白 铁
责任编辑：白 铁
责任校对：王素荣
出版发行：地质出版社
社址邮编：北京海淀区学院路 31 号，100083
电 话：(010)82324508(邮购部)；(010)82324579(编辑部)
网 址：http://www.gph.com.cn
电子邮箱：zbs@gph.com.cn
传 真：(010)82310759
印 刷：北京地大彩印厂
开 本：787mm×1092mm 1/16
印 张：26.75
字 数：750 千字
印 数：1—1000 册
版 次：2006 年 12 月第一版·第一次印刷
定 价：60.00 元
ISBN 7-116-05061-2/P·2755

许志琴院士
（1941～　）

许志琴，女，构造地质学家。籍贯重庆，1941 年 8 月出生上海，1964 年北京大学地质地理系构造专业毕业，1986 年获法国博士学位。1995 年当选为中国科学院院士，曾获李四光科学奖和何梁何利科学奖。许志琴以大陆动力学为指导，运用微观构造与宏观构造相结合的手段，长期从事青藏高原、中国造山带及超高压变质带研究。1985 年以来一直担任中国造山带和青藏高原中法地学合作的中方负责人，又是中国大陆科学钻探工程（CCSD）及有关 CCSD 研究的国家 973 基础项目和国家基金重大项目的首席科学家。发表论文 200 余篇，专著 8 部。

自　序

青藏高原是一个正在快速隆起的大陆地块，印度板块与亚洲板块碰撞导致的青藏高原隆升是地球上新生代最壮观的事件，青藏高原的魅力使其成为全球地学家们研究的永恒课堂，成为当今“大陆动力学”研究的最佳实验室。

本人1964年踏进青藏川西高原，20世纪80年代初参加肖序常、李廷栋先生负责的中法喜马拉雅考察队，并在法国进修、获得博士学位，开始了“微构造与大地构造”相结合的连续20多年的青藏高原构造研究生涯。自1987年起担任中法青藏高原四个研究项目的中方负责人。本人涉足的地区有祁连山、阿尔金山、东-西昆仑山、巴颜喀拉山、松潘-甘孜、龙门山、可可西里和喜马拉雅。

本书选辑了作者等围绕青藏高原大陆动力学问题进行研究的部分成果，作为对具有强大吸引力的世界地学领地——青藏高原研究的微薄奉献。

2006年10月

目　录

青藏高原与大陆动力学——地体拼合、碰撞造山及高原隆升的深部驱动力[1]

许志琴　杨经绥　李海兵　张建新　曾令森　姜　枚
（中国地质科学院地质研究所　国土资源部大陆动力学重点实验室　北京　100037）

摘　要　运用地体和地体活动论观点，提出青藏高原结构划分的新方案；强调青藏高原的形成经历了新元古代以来长期活动的过程，青藏高原是一个“非原地”诸多地体会聚、拼合以及经历复合碰撞造山的“造山的高原”；大型走滑断裂在青藏高原形成中起着地体相对位移、侧向挤出、移置及使高原几何形态扭曲的作用。提出青藏高原隆升的“南缘超深俯冲（>600km）、北缘陆内俯冲、腹地深部热结构及岩石圈范围内的向NE右旋隆升”的多元驱动力机制。

关键词　青藏高原　非原地地体拼合　复合碰撞造山　走滑构造　多元驱动力
中图分类号：P541　　**文献标识码**：A　　**文章编号**：1000－3657(2006)02－0221－18

青藏高原是具有特殊几何形态和地貌景观的、正在快速隆起的大陆地块，高原内部是广阔又平坦的地域，其周缘为高峻陡峭、剧烈起伏的山链，构成了一堵与外界隔绝的屏障。

青藏高原是世界上最高、最厚、最新和体积最大的高原，具有十分复杂地质结构、物质组成、流变学特征和独特的深部物理状态。青藏高原隆升是地球上新生代最壮观的事件，它影响了资源的再分配及生存环境的变化，并在其内部及边缘诱发了至今异常活跃的地震灾害；青藏高原又是亚洲大陆的最后拼合体，它所显示出的地壳破损镶嵌结构，示踪了地质历史上诸地体多次离散、聚敛和碰撞造山动力学过程的证据，直至60～50Ma印度/亚洲的最终碰撞。印度/亚洲的重大碰撞事件形成了广泛的大陆变形域，作为世界地学瑰宝之一的青藏高原已成为公认的大陆动力学研究的最佳实验室和窗口。

1　青藏高原研究聚焦与大陆动力学

大陆岩石圈是一个不均一、不连续、具多层结构和复杂流变学特征的综合体。大陆地壳

---

[1] 中国地质，2006年第33卷第2期。

收稿日期：2006－03－14；改回日期：2006－03－20。
基金项目：本研究先后得到原地矿部中法“松潘-甘孜造山带造山过程”项目、中法“东昆仑及邻区岩石圈缩短机制研究”项目、国土资源部“祁连山-阿尔金山地质演化及岩石圈剪切作用”、国家自然科学基金重点项目“祁连造山带的组成及造山过程”及国土资源部科技专项“青藏高原的碰撞造山及其效应”课题“青藏高原地体边界及岩石圈剪切断裂”的资助。

作者简介：许志琴，女，1941年生，留法博士，中国科学院院士，从事大地构造学及构造地质学研究；E-mail：xzq@cesd.org.cn。

没有共同的成因和起源,它是由不同块体的不同物质组成的集合体,具有大范围变化的构造和热历史,流体和熔融体的相互作用又改变了流变学的结构。因此,比大洋岩石圈老得多、厚得多和具有复杂流变学结构和演化过程的大陆岩石圈使板块"登陆"受到很大阻力,大陆岩石圈并非刚性块体,变形作用也绝非只发生在板块边界的狭窄地带。人们愈来愈发现运用经典的板块理论很难解释大陆地质,譬如:长期活动的造山带的形成、大陆碰撞造山热的成因、印度/亚洲碰撞造成的巨大陆内变形域、青藏高原的隆升、大陆深俯冲和超高压变质作用以及超高温变质作用等难题。一个以解决大陆结构、行为、动态演化和驱动力,以及发展板块构造理论为目的的大陆动力学研究计划在20世纪90年代已经开始,在世界上大多数地学家中产生强烈反响。大陆动力学理论的完善是一场新的地学变革,是继"板块构造"之后固体地球科学发展的新的里程碑。

自19世纪末20世纪初开始[1~10],青藏高原研究已100多年,众多的中国和外国地学家前赴后继的研究和合作以及广泛的区域地质和地球物理调查,不仅揭示了青藏高原所显示的复杂镶嵌结构,示踪了地质历史上诸地体多次离散、聚敛、碰撞、移置、增生及联合[11~18],揭示了65~45Ma以来印度板块与欧亚大陆南部碰撞[19~28]及其产生的巨大效应[29~30];还初步揭示了青藏高原地壳、岩石圈及深地幔结构的基本构架[31~38]。

青藏高原具有"多陆块、多岛弧"组成的基本格架及显示"多洋(海)盆、多俯冲、多碰撞和多造山"的动力学作用过程。在不同历史阶段的洋盆开启和闭合致使块体汇聚和碰撞,多块体拼贴构筑成复合陆体;块体的碰撞产生碰撞造山带,碰撞造山带的拼贴及叠置又形成复合碰撞造山拼贴体。由复合地体和复合造山拼贴体组成的青藏高原是在新元古代以来长期活动、多期造山及新生代最后隆升的基础上形成的高原,又称为"造山的高原"(Orogenic Plateaux)[39]。

研究表明,组成青藏高原的诸多陆块和复合陆块并非原位,它们均来自靠近冈瓦纳大陆的一侧。陆块之间的会聚及俯冲使陆块消减,在地体碰撞过程中形成的大型剪切带及大型断裂的作用使陆块或复合陆块叠覆、错位、挤出和远离原地,后期大型盆地的形成又使块体和复合块体的原型遭到覆盖。因此,青藏高原的重大关键问题已不仅是65~45Ma以来印度和亚洲碰撞形成高原以及引起大陆岩石圈数千千米变形,再造巨大的地体拼合体和碰撞造山拼贴体相互作用及大陆增生的地质历史过程,成为青藏高原研究的重要内容。其包括了组成各陆块单元的古地理位置、原型、归属和特征,古洋盆的开启及消减,陆块之间相互运动的轨迹、拼合与叠置的方式,碰撞造山类型、造山过程、造山叠置以及造山机制,大型走滑构造的形成和对青藏高原结构的改造,以及深部结构、壳幔相互作用和驱动力等。青藏高原所具有的十分复杂的地壳-岩石圈流变学特征给青藏高原形成历史及动力学机制研究带来了很大困难。

因此,从大陆动力学和活动论的角度出发,结构、块体边界以及块体运动学是青藏高原大陆动力学研究的根本;印度/亚洲碰撞前和后的块体拼合及碰撞动力学的历史重塑为青藏高原大陆动力学研究的焦点,深部地壳、地幔结构的揭示和驱动力的探究是青藏高原大陆动力学研究的关键。

结合大陆动力学的研究,青藏高原的固体地球科学研究聚焦可以归结为如下关键问题:

(1)青藏高原的诸块体在地质历史中古地理位置、性质和归属。显生宙以来特提斯洋盆的开启、扩张、消减、转换和最终闭合的过程,以及如何促使诸块体的不断会聚、俯冲、增生和

拼合，形成巨型块体拼合体及“多洋(海)盆、多陆块、多岛弧、多俯冲、多碰撞”动力学过程？如何科学重建和确定青藏高原中诸块体会聚的前锋、会聚轨迹和洋壳/陆壳俯冲极性？

(2)显生宙以来青藏高原的诸块体会聚和碰撞的主要时期。是否存在晚古生代(华力西期)的碰撞造山？在块体会聚和碰撞过程中如何形成不同类型的俯冲-碰撞山链和叠置山链？山链及叠置山链的不同构造样式、造山极性及碰撞动力学？碰撞山链又如何不断生根、消融以及拆沉？大陆岩石圈如何在地体拼合中不断增生、保存和去除？俯冲-碰撞山链如何聚成长期活动的巨大碰撞造山拼贴体？造山热(花岗岩浆、高温变质作用及韧性变形)的产生主要与前造山的构造热背景还是与造山过程有关[40]？

(3)大印度板块变成小印度板块过程中，亚洲大陆一侧近2000km的南北向缩短量是以什么方式被吸收的[20,24]？印度/亚洲碰撞如何造成2500km宽的大陆变形域[29,30]？为什么新生代变形主要集中表现在高原的周缘及内部的地体边界或古构造带上，而广大地区为弥散变形？在挤压的大背景下，构造应力如何分解为缩短、伸展与走滑分量？目前一个重要的争论问题是：青藏高原的新生代变形是以连续均匀方式为主，还是以岩石圈刚性块体之间的变形(即不连续均匀变形)为主[30]？如果前者，则断裂作用对大陆生长过程不起重要作用，如果后者则相反。

(4)青藏高原的北缘(祁连山、阿尔金山)发现早古生代超高压变质带，揭示了洋壳/陆壳深俯冲的重大事件，洋壳/陆壳深俯冲的背景及其转换机制产生的条件？南缘(喜马拉雅山)保存了新生代超高压变质带，反映了印度陆壳的深俯冲作用，具浮力、较轻和低密度的陆壳如何俯冲至地幔深度形成含柯石英榴辉岩，然后又折返上来使超高压变质岩石出露在西北喜马拉雅的构造结部位[42,43]？

(5)印度/亚洲碰撞导致青藏高原内部高原地貌的形成和周缘造山带崛起。青藏高原内部高原地貌形成的表生地质过程与深部地质过程？青藏高原内部古高程的确定及对青藏高原隆起的制约？周缘造山带崛起受两种挤出机制的影响：一种是青藏高原南、北缘(喜马拉雅山和祁连山)高挤压速率(分别为18mm/a和16mm/a)下的物质垂(斜)向挤出；另一种是青藏高原物质的向东及南东方向的侧向挤出(逃逸)，使高原的东南缘几何形貌发生严重扭曲。在研究垂向和侧向两种“挤出”机制及其在青藏高原隆升中究竟起着何种作用时，应考虑如下问题：①周缘克拉通的制约？②下地壳熔体对下地壳流变学性质的影响及对物质挤出样式、方式的驱动？③大型走滑断裂及块体旋转对侧向挤出的规模、层次、运移方式、速率和时限的影响？④青藏高原复杂岩石圈流变学结构如何导致非板块行为？⑤周缘造山带、内部高原地貌及外侧盆地的三者互馈关系？

(6)青藏高原岩石圈/地幔结构的研究是揭开青藏高原隆升的深部驱动力内幕的关键，主要的问题是：青藏高原地壳/岩石圈流变学结构剖面和地幔各向异性的揭示和解释？碰撞造山及花岗岩浆作用的叠置性、长期性及多期性，以及它们与地壳的流变学特征、热结构与热历史以及壳幔相互作用的关系？地体边界上是否保留古岩石圈俯冲的“化石”残片和拆沉记录？大型走滑构造往下延伸深度？青藏腹地出现的大面积新生代碱性火山喷发与深地幔的低速异常结构的关系？印度岩石圈板块的俯冲几何学、运动学、俯冲深度、速率、时限及俯冲的最远距离？是否存在除南部印度板块向北俯冲以外的其他陆内俯冲的驱动力？

从上面思考和研究的问题来看，青藏高原固体地球科学的研究已经步入以大陆结构、行为和驱动力为主导的大陆动力学的研究轨道，远远超出青藏高原传统大地构造研究范畴。

青藏高原大陆动力学研究已经向地体拼合、碰撞动力学及高原隆升的深部驱动力研究方面聚焦,这是一个长期的任务。

2 青藏高原巨型地体拼合体的结构单元及活动体系

前人对青藏高原的基本构造单元的划分曾采用不同的名称:"板块"、"块体"、"陆块"和"地体"等。最近潘桂棠等[18]推出大地构造单元划分的"构造区"新版本:以青藏高原中多岛弧盆系的形成及洋/陆岩石圈体制转换为出发点,将碰撞结合带、夹持陆块与岩浆弧作为单元划分的基础,将青藏高原大地构造单元划分为"泛华夏大陆早古生代秦祁昆构造区"、"泛华夏大陆晚古生代羌塘-三江构造区"和"冈瓦纳北缘晚古生代-中生代冈底斯-喜马拉雅构造区"。该版本有许多新的思路,给笔者诸多启示。

2.1 地体单元

笔者主张以"地体"作为青藏高原结构划分的基本单元,其主要原因是:地体构造理论是板块构造理论的发展,地体概念最早由 Monger(1975, 1977)提出,David G. Howell 等[45]予以完善。地体实际上指的是"构造地层地体"或"变质地体"。是以断裂(或缝合带,或结合带)为边界的具有区域性延伸的地质实体,每个地体内的沉积、构造、火成作用和变质作用是统一连贯的,每个地体均有与相邻地体不同的地质历史。按地体运动学的观念,又分为"增生地体"及"移置地体"或"外来地体"。"增生地体"是指地体拼合到大陆前缘,成为大陆地壳的增生体(或增生楔),使大陆地壳在空间上扩大化,在性质上复杂化[46]。笔者认为运用地体和地体活动论的观点划分青藏高原基本构造单元有利于恢复和再造陆块的原型,有利于用运动学的眼光审视地体的增生、移置和挤出,有利于认识复杂化的生长的大陆地壳。

2.2 地体边界

地体边界的确定是准确划分地体单元的首要条件。地体边界记录了洋(海)盆开启、俯冲、会聚、闭合、碰撞造山及陆内俯冲的全过程,也包含了地体之间正向和斜向运动形成的各类大型断裂对地体制约的信息,因此地体边界对于大陆动力学的研究极其重要。印度/亚洲碰撞前的历史是诸多地体拼合和碰撞的过程,拼合和碰撞的动力学过程主要在地体的边界进行,并形成俯冲-碰撞的板块动力学体制和造山域。研究表明,俯冲-碰撞体制并不是一条狭窄的缝合带,而是一条宽数千米至数十千米的构造带。其组成包括两部分:

(1)俯冲杂岩带(Subduction Complex, SC)。由蛇绿岩、蛇绿混杂岩、弧前增生楔、俯冲剥蚀带及高压-超高压变质带组成。

1)蛇绿岩:分为洋脊型蛇绿岩(MORB)和洋壳俯冲上盘蛇绿岩(Super Subduction Zone, SSZ)两类,分别代表了洋盆打开和洋盆俯冲的背景和时代。蛇绿混杂岩代表了俯冲阶段洋壳物质与蛇绿岩、沉积岩块体的混杂体,在折返中和蛇绿岩残片伴生,就位于缝合带,或呈推覆体叠置在被动陆缘之上,如雅鲁藏布缝合带南部特提斯-喜马拉雅带上的蛇绿岩和蛇绿混杂岩的推覆体。

2)弧前增生楔与俯冲剥蚀带:大洋岩石圈俯冲时形成两类活动陆缘:加积板块边缘(accretionary plate margins),即弧前加积楔,在洋壳俯冲上盘形成;剥蚀板块边缘(erosive plate margins),即大洋岩石圈板片俯冲作用将上部板片中大量陆壳物质拖拽下去,在海沟地带形成板块边缘的剥蚀楔。已经证明在全球具有板块剥蚀边缘特征的地带有太平洋东岸中南段

的墨西哥-北智利、太平洋西岸的日本岛弧东侧的 Kurile-IsuMariana 及澳大利亚东岸的 Tonga-Kermadec，弧前增生楔经常变成剥蚀板块边缘的组分。

3）高压-超高压变质带：高压-超高压变质带（HP-UHP）的发现揭开了洋壳和大陆壳物质可以俯冲、深俯冲（100km）乃至超深俯冲（>200～300km）深度的重大事件中[47]。在青藏北部发育北祁连高压变质带是 480～460Ma 洋（海）盆俯冲的结果，由于都兰石榴石白云母片麻岩中柯石英的发现而确定的柴北缘超高压变质带[48]是 495～440Ma 的洋（海）盆深俯冲到陆壳深俯冲的复合产物[48～55]。在青藏南缘的喜马拉雅西构造结的南迦帕尔巴特地区先后找到榴辉岩[42～43]，并发现柯石英包裹体，超高压变质峰期的温压条件为 650℃ 和 2.6GPa，推测西构造结地区经历了大约 49Ma 印度陆壳的深俯冲作用。

（2）活动陆缘增生带。活动陆缘增生带（Active continental margin accretional zone，ACC）由火山岛弧岩浆带及弧后盆地组成。活动陆缘增生带是火山岩浆岛弧带在俯冲上盘活动陆缘一侧形成的增生体。洋壳俯冲形成的岛弧火山岩经常与“I”型花岗岩伴生，弧后盆地是洋壳俯冲在活动陆缘弧后拉张的产物。

这里需要指出的是洋盆岩石圈俯冲的物质有时没有被折返上来，因此在地体边界往往不保存俯冲杂岩带，如金沙江缝合带玉树及以西地带就没有发现古特提斯蛇绿岩；经历长期剥蚀的火山岩浆岛弧带还可能只剩下根部的岛弧花岗岩，如东昆仑北部布尔汗布达山的大片三叠纪岛弧花岗岩为活动陆缘根部的产物。洋盆岩石圈的深俯冲模拟实验[56]表明火山岛弧岩石还可以被拽到海沟中而消失。在上述情况下，会聚边界活动陆缘的前锋的确定是认识俯冲极性的重要标志，因此边界的研究需要综合的分析才能得出科学的结论。

2.3 青藏高原的地体单元和地体边界的划分及活动体系

组成青藏高原是诸多地体（或小陆块）在青藏高原形成的地质历史中，都曾身处异地，地体拼合的过程也是“非原地”的地体移置、拼贴和增生的过程，地球上最壮观的事件：60～50Ma 印度陆块与亚洲大陆的碰撞完成了最后的拼合及增生，使印度板块成为亚洲大陆最后的成员。

印度/亚洲前碰撞历史是从新元古代开始的长期活动历史，经历了早古生代、晚古生代-三叠纪和晚中生代的地体会聚-碰撞三个阶段，以及泥盆纪、三叠纪和晚侏罗世-早白垩世的多期碰撞造山事件。由于印度/亚洲前碰撞历史是以诸多地体的会聚为特征，因此可以通过地体结构及地体边界的研究以及各时期地体边界两侧陆壳的变形特征和动力学过程的揭示，来探究青藏高原形成前诸地体与亚洲北部逐渐拼合和大陆增生的过程。60～50Ma 印度/亚洲的最后碰撞，不仅使亚洲大陆增生了喜马拉雅地体，而且使亚洲大陆发生向东与南东的挤出，同时形成内部高原地貌和周缘新生代造山带的两个新的大地构造单元。

笔者提出“以地体的性质及地体边界作为地体划分依据，以显生宙以来地体拼合与碰撞的主要时期——早古生代、三叠纪、晚中生代以及新生代碰撞事件形成的复合地体、增生复合地体和增生、挤出及移置地体作为基本构造单元”，形成青藏高原基本单元新的划分方案。基于地体的裂解、运动、会聚、就位及改造是不停顿运动的结果，该方案以活动论为指导思路。

青藏高原大地构造单元组成可分为两大部分：

（1）60～50Ma 印度/亚洲碰撞前形成的两个复合（增生）地体。

1）“阿尔金-祁连-昆仑”早古生代复合地体。由祁连地体、柴达木地体、东昆北地体、东昆南地体、阿尔金地体、西昆北地体和西昆南地体等组成青藏高原北部的地体拼合体，地体

之间的边界有早古生代形成的北祁连俯冲杂岩带和活动陆缘增生带,柴北缘俯冲杂岩带和活动陆缘增生带,祁漫塔格俯冲杂岩带和活动陆缘增生带,昆中俯冲杂岩带和活动陆缘增生带,北阿尔金俯冲杂岩带和活动陆缘增生带,南阿尔金俯冲杂岩带和活动陆缘增生带以及库地俯冲杂岩带和活动陆缘增生带等。该复合地体向东与北秦岭早古生代地体及丹凤俯冲杂岩带和陆缘活动增生带相连。通过对阿尔金断裂两侧地体(祁连和阿尔金地体)和地体边界(北祁连和北阿尔金早古生代俯冲杂岩带,柴北缘南阿尔金早古生代俯冲杂岩带)的对比,确定了阿尔金山是祁连山的西延。

2)"松潘甘孜-羌塘-拉萨"三叠纪—早白垩世复合地体。松潘-甘孜地体、羌塘地体和拉萨地体拼合组成青藏高原中部的地体拼合体。地体之间的边界为昆南-阿尼玛卿俯冲杂岩带和活动陆缘增生带、金沙江俯冲杂岩带和活动陆缘增生带、班公湖-怒江俯冲杂岩带和活动陆缘增生带,以及由于新特提斯洋盆俯冲在拉萨地体南缘形成的雅鲁藏布江俯冲杂岩带及冈底斯活动陆缘增生带。

最新研究表明,在羌塘地体内部存在一条分割南、北羌塘的由二叠纪蛇绿岩和三叠纪高压变质带组成的双湖-龙木错俯冲杂岩带[57],使"松潘-羌塘-拉萨"复合地体的结构更复杂化。

(2)60～50Ma 印度/亚洲碰撞形成的增生-挤出-移置地体:印度/亚洲碰撞形成长2500km、宽300～500km、向南突出的 EW 向弧形"喜马拉雅"增生地体。在此过程中,印度/亚洲碰撞造成物质向东和南东运动,在走滑断裂——鲜水河左行走滑断裂、金沙江左行走滑断裂、嘉里-红河右行走滑断裂和三盖-民衮右行走滑断裂的制约下,使"松潘-羌塘-拉萨"复合地体向南东挤出,形成云南挤出地体和缅甸挤出地体,导致青藏高原几何形态的扭曲。

青藏高原北缘阿尔金主断裂和北阿尔金断裂的左行走滑作用,使其西侧的阿尔金地体和西昆仑地体向 SWW 方向移动,形成阿尔金移置地体和西昆仑移置地体。

此外,按现代的地貌-构造特征又可将青藏高原分为中央高原和周缘造山带(南缘喜马拉雅造山带、北缘西昆仑-阿尔金-祁连造山带及东缘龙门-锦屏造山带)两大基本单元(图1,表1)。

3 青藏高原地体拼合及"多(海)盆、多陆块、多岛弧、多俯冲、多碰撞"动力学过程

最新的古地磁研究进一步表明[58],组成青藏高原的诸地体的古地理位置、性质和归属,以及在各个重大历史阶段中的拼合和增生是与特提斯洋盆包括始特提斯洋(新元古代—早-中泥盆世)、古特提斯洋(中石炭世—早三叠世)和新特提斯洋(晚三叠世—晚白垩世)的不断开启与闭合以及印度洋的最后打开(早中新世—现在)有着密切的关系。

3.1 始特提斯洋盆与"多洋(海)盆/多地体/多岛弧"体系

初步研究表明,青藏高原北部带的"阿尔金-祁连-昆仑"早古生代造山带是由诸多的地体/岛弧组成,根据北祁连-北阿尔金带中代表初始洋壳的蛇绿岩年龄早于550Ma[59--61],柴北缘和库地蛇绿岩年龄早于510Ma[62--63],表明地体边界蛇绿岩中保留始特提斯洋盆(新元古代—早古生代)的记录。青藏高原北部早古生代板块体制重塑的研究表明,位于青藏北部的阿尔金-祁连地体、柴达木地体、东昆仑地体、阿尔金地体和西昆仑地体以及北秦岭地体中

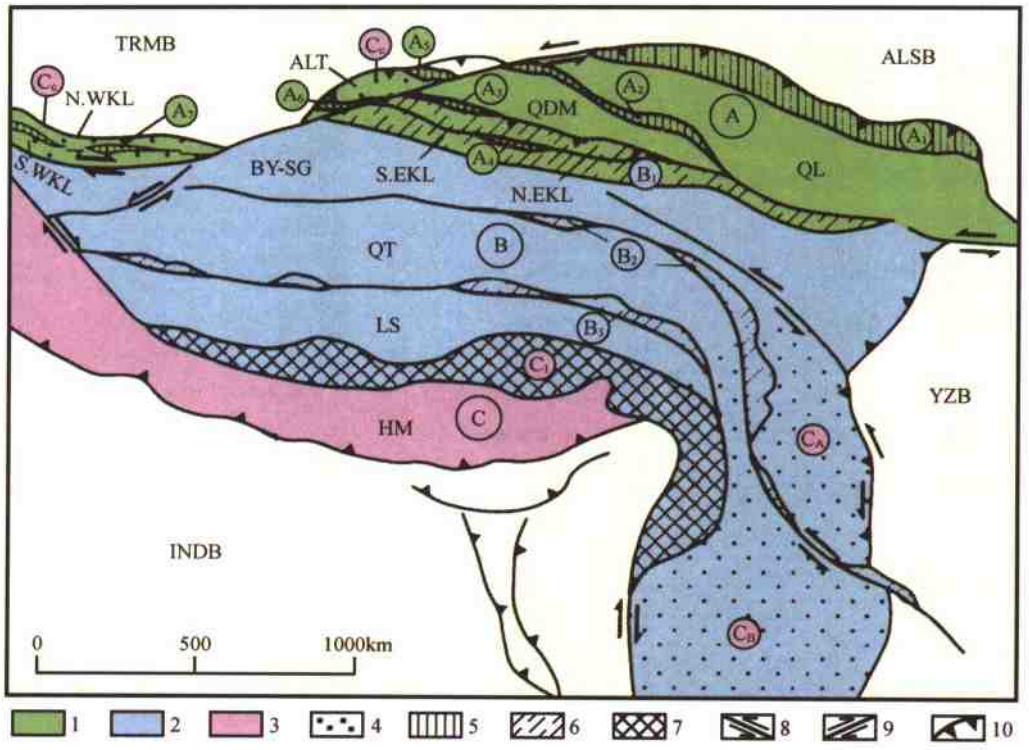

图 1　青藏高原结构图

Fig. 1　Map showing the structural architecture of the Qinghai-Tibet Plateau

1—早古生代复合地体;2—中生代增生复合地体;3—新生代增生地体;4—挤出-移置地体;5—早古生代俯冲杂岩带和活动陆缘带;6—早中生代俯冲杂岩带和活动陆缘带;7—晚中生代-早新近纪俯冲杂岩带和活动陆缘带;8—左行走滑断裂;9—右行走滑断裂;10—逆冲断裂

A—阿尔金-祁连-昆仑早古生代复合地体;QL—祁连地体;QDM—柴达木地体;N. EKL—东昆仑北地体;S. EKL—东昆仑南地体;ALT—阿尔金地体;N. WKL—西昆仑北地体;S. WKL—西昆仑南地体;B—松潘甘孜-羌塘-拉萨增生复合地体;BY-SG—巴颜喀拉-松潘甘孜地体,QT—羌塘地体,LS—拉萨地体;C—青藏高原周缘增生、挤出、移置地体;C—喜马拉雅增生地体;C_A—云南挤出地体;C_B—掸邦挤出地体;C_C—阿尔金-西昆仑移置地体

地体边界:A_1—北祁连早古生代俯冲杂岩带和活动陆缘带;A_2—柴达木北缘早古生代俯冲杂岩带和活动陆缘带;A_3—祁漫塔格早古生代俯冲杂岩带和活动陆缘带;A_4—昆中早古生代俯冲杂岩带和活动陆缘带;A_5—北阿尔金早古生代俯冲杂岩带和活动陆缘带;A_6—南阿尔金早古生代俯冲杂岩带和活动陆缘带;A_7—库地早古生代俯冲杂岩带和活动陆缘带;B_1—东昆仑-阿尼玛卿三叠纪俯冲杂岩带和活动陆缘带;B_2—金沙江三叠纪俯冲杂岩带和活动陆缘带;B_3—班公湖-怒江中生代俯冲杂岩带和活动陆缘带;C_1—雅鲁藏布江俯冲杂岩带和冈底斯活动陆缘带;INDB—印度陆块;YZB—扬子陆块;ALSB—阿拉善陆块;TRMB—塔里木陆块

1—Early Paleozoic composite terrane; 2—Mesozoic accretionary composite terrane; 3—Cenozoic accretionary terrane; 4—Extruded-displaced terrane;5—Early Paleozoic subduction complex zone and active continental-margin zone;6—Early Mesozoic subduction complex zone and active continental margin zone;7—Late Mesozoic-early Neogene subduction complex zone and active continental-margin zone;8—Sinistral strike-slip fault;9—Dextral strike-slip fault;10—Thrust fault

A—Early Paleozoic Altyn Qilian-Kunlun composite terrane; QL—Qilian terrane; QDM—Qaidam terrane; N. EKL—Northern East Kunlun terrane; S. EKL—Southern East Kunlun terrane; ALT—Altyn terrane; N-WKL—Northern West Kunlun terrane; S-WKL—Southern West Kunlun terrane; B-Songpan-Garzê—Qiangtang-Lhasa accretionary composite terrane; BY-SG—Bayan Har Songpan-Garzê terrane; QT—Qiangtang terrane; LS—Lhasa terrane; C—Accretionary; extruded and displaced terranes at peripheries of the Qinghai-Tibet Plateau; C—Himalaya accretionary terrane; C_A—Yunnan extruded terrane; C_B—Shan Ban extruded terrane; C_C—Altyn-W. Kunlum displaced terrane

Terrane boundaries: A_1—Early Paleozoic North Qilian subduction complex and active continental-marginzone; A_2—Early Paleozoic Northern Qaidam marginal subduction complex and active continental-margin zone; A_3—Early Paleozoic Qimantag subduction complex and active continental-margin zone; A_4—Early Paleozoic Central Kunlun subduction complex and active continental-margin zone; A_5—Early Paleozoic North Altyn subduction complex and active continental-margin zone; A_6—Early Paleozoic South Altyn subduction complex and active continental-margin zone; A_7—Early Paleozoic Küda subduction complex and active continental-margin zone; B_1—Triassic East Kunlun-A'nyêmaqên subduction complex and active continental-margin zone; B_2—Triassic Jinsha River subduction complex and active continental-margin zone; B_3—Mesozoic Bangong Co-Nujiang subduction complex and active continental-margin zone; C_1—Yarlung Zangbo subduction complex and Gangdise active continental-margin zone; INDB—Indian block; YZB—Yangtze block; ALSB—Alxa block; TRMB—Tarim block

表 1 青藏高原地体结构与地体边界

Table 1 Terrane structure and boundaries of the Qinghai-Tibet Plateau

编号	单元名称	地体组成	地体边界 俯冲杂岩带(SC) 活动陆缘增生带(ACA)
1	阿尔金-祁连-昆仑 (ALT-QL-KL) 早古生代复合地体	祁连(QL)地体 柴达木(QDM)地体 东昆仑北(N.EKL)地体 东昆仑南(S.EKL)地体 阿尔金(ALT)地体 西昆仑北(N.WKL)地体 西昆仑南(S.WKL)地体	北祁连逆冲断裂(NQLT) 北祁连 SC+ACA 柴北缘 SC+ACA 祁漫塔格 SC+ACA 昆中 SC+ACA 南阿尔金 SC+ACA 库地 SC+ACA 康西瓦 SC+ACA
Ⅱ	松潘-羌塘-拉萨增生地体 (SG-QT-LS) 晚侏罗世—早白垩世增生地体	松潘-甘孜(SP-GZ)地体 羌塘(QT)地体 拉萨(LS)地体	昆南-阿尼玛卿 SC+ACA 金沙江 SC+ACA
Ⅲ	喜马拉雅(HM)新生代增生地体	特提斯-喜马拉雅(THM)亚地体 高喜马拉雅(GHM)亚地体 低喜马拉雅(LHM)亚地体 次喜马拉雅(SHM)亚地体	雅鲁藏布江 SC+ACA
Ⅳ	侧向挤出-移置地体(新生代)	云南(YN)挤出地体 掸邦(SB)挤出地体 阿尔金-西昆仑(ALT-WKL)移置地体	鲜水河韧性左行走滑剪切带(XSHF) 班公湖-红河韧性走滑剪切带(BG-RRF) 雅鲁藏布江右行走滑断裂(YLZBF) 阿尔金断裂系(ALTF)

发育诸多早古生代火山岛弧——北祁连-北阿尔金火山岛弧、柴北缘-南阿尔金火山岛弧、祁漫塔克火山岛弧、中昆仑火山岛弧、库地火山岛弧及北秦岭二郎坪火山岛弧等,说明青藏高原北缘在早古生代曾处在始特提斯洋一侧的多地体/多岛弧环境。古地磁和全球大陆复原资料表明[58],在 550Ma 前冈瓦纳大陆与西伯利亚陆块、北美陆块和波罗的陆块之间存在始特提斯洋,北中国陆块和其他一系列小陆块一起,构成位于冈瓦纳大陆澳大利亚的西缘、始特提斯洋东侧的多陆块群(图 2)。推测它们之间分布的蛇绿岩和俯冲杂岩带代表具有扩张性质的边缘海盆的洋壳组分,而这些边缘海盆与外侧的始特提斯洋盆有密切的成因联系。因此尽管青藏高原北部陆块/岛弧群的确切位置尚未锁定,但是可以推测现地体/岛弧群曾经位于始特提斯洋盆和冈瓦纳大陆之间,是环始特提斯洋地体/岛弧群(活动带)的成员[54]。

3.2 始特提斯洋盆俯冲及活动陆缘带形成时限

代表洋(海)盆俯冲的北祁连高级蓝片岩形成的时代为 480～460Ma[64],与蓝片岩伴随的高压榴辉岩的锆石 SHRIMP U-Pb 定年的(463±6)Ma 和(468±13)Ma,代表了大洋板块俯冲至上地幔深度形成榴辉岩相的时限。北祁连火山岛弧时代 486～438Ma[64]、柴北缘火山岛弧时代 U-Pb 年龄是 514～486Ma[60,62,66]及中昆仑火山岛弧时代(530～518Ma)[54],表明冈瓦纳大陆澳大利亚西侧边缘海盆俯冲(即火山岛弧带形成的时代)自外向里有渐新的趋势,这是早古生代多地体/岛弧的加积作用的反映。

上述表明,组成现在青藏高原北部的诸地体在 510～460Ma 期间曾位于靠近冈瓦纳大陆的一侧,由于始特提斯洋盆的俯冲作用,成为"始特提斯洋南缘地体/火山岛弧群"的一部分。在 420～390Ma 期间这些地体又通过"弧-陆"和"陆-陆"先后拼合及碰撞造山[55],并与

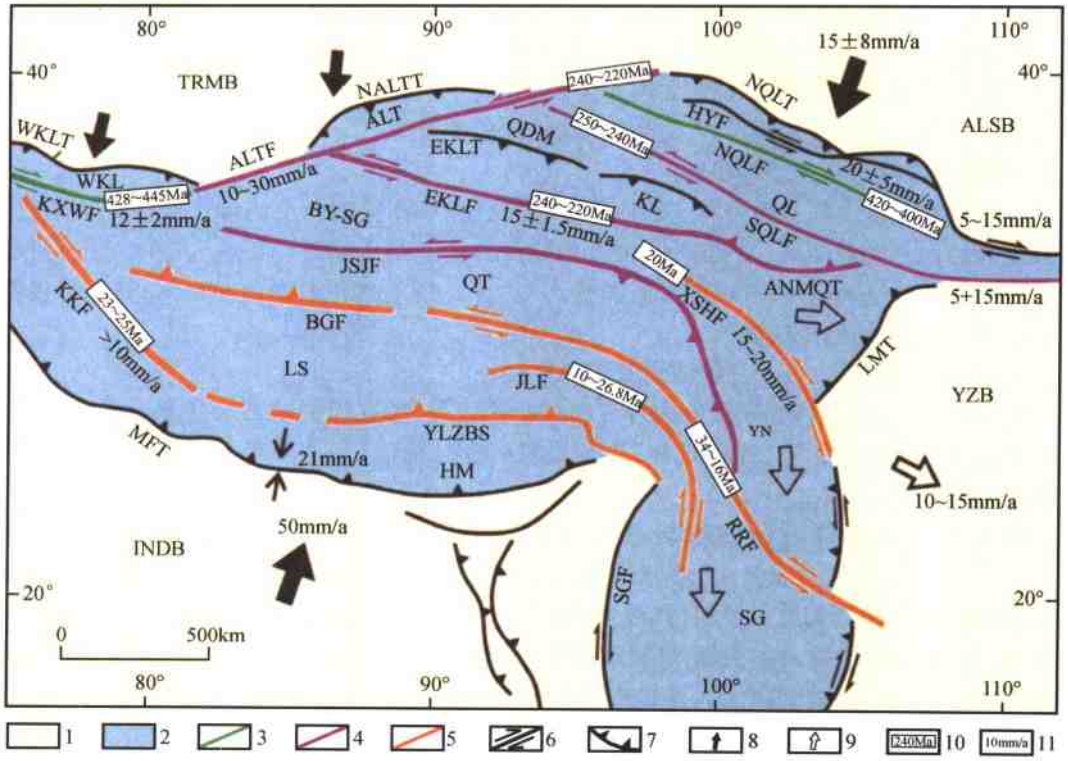

1 2 3 4 5 6 7 8 9 240Ma 10 10mm/a 11

图 2　青藏高原大型走滑构造图

Fig. 2　Map showing large strike-slip structures of the Qinghai-Tibet Plateau

1—青藏高原周边克拉通;2—青藏高原;3—早古生代形成的韧性走滑剪切带;4—三叠纪形成的韧性走滑剪切带;5—新生代形成的韧性走滑剪切带;6—走滑断裂;7—逆冲断裂;8—板块挤压运动方向;9—板块挤出运动方向;10—走滑构造形成时代;11—运动速率

走滑断裂:HYF—海源走滑断裂;NQLF—北祁连走滑断裂;SQLF—南祁连南缘走滑断裂;ALTF—阿尔金走滑断裂;EKLF—东昆仑走滑断裂;XSHF—鲜水河走滑断裂;JSJF—金沙江走滑断裂;BGF—班公湖走滑断裂;JLF—嘉黎走滑断裂;KXWF—康西瓦走滑断裂;RRF—红河走滑断裂;KKF—喀喇昆仑走滑断裂;QMF—恰曼走滑断裂;SGF—三盖明衮走滑断裂;逆冲断裂:NQLT—北祁连逆冲断裂;ANMQT—阿尼玛卿逆冲断裂;MFT—喜马拉雅主前锋逆冲断裂;NALTT—北阿尔金逆冲断裂;WKLT—西昆仑逆冲断裂;LMT—龙门山逆冲断裂;EKLT—东昆仑逆冲断裂;ALT—阿尔金亚地体;BY-SG—巴颜喀拉-松潘甘孜地体;HM—喜马拉雅增生地体;INDB—印度陆块;KL—昆仑断裂;LS—拉萨亚地体;QDM—柴达木地体;QL—祁连地体;QT—羌塘地体;SG—松潘甘孜地体;WKL—西昆仑亚地体;YLZBS—雅鲁藏布江缝合带;YN—云南地体;YZB—扬子陆块;ALSB—阿拉善陆块;TRMB—塔里木陆块

1—Cratons at peripheries of the Qinghai-Tibet Plateau;2—Qinghai-Tibet Plateau;3—Ductile strike-slip shear zone formed in the Early Paleozoic;4—Ductile strike-slip shear zone formed in the Triassic;5—Ductile strike-slip shear zone formed in the Cenozoic;6—Strike-slip fault;7—Thrust fault;8—Direction of plate compression; 9—Direction of plate extrusion; 10—Age of strike-slip structure; 11—Movement rate

Strike-slip faults: HYF—Haiyuan strike-slip fault; NQLF—North Qilian strike-slip fault; SQLF—South Qilian strike-slip fault; ALTF—Altyn Tagh strike-slip fault; EKLF—East Kunlun strike-slip fault; XSHF—Xianshuihe strike-slip fault; JSJF—Jinshajiang strike-slip fault; BGF—Bangong Co strike-slip fault; JLF—Lhari strike-slip fault; KXWF—Kangxiwar strike-slip fault; RRF—Red River strike-slip fault; KKF—Karakorum strike-slip fault; QMF—Qimantag strike-slip fault; SGMGF—Sangai-Minggun strike-slip fault

Thrust faults: NQLT—North Qilian thrust; ANMQT—A'nyêmaqên thrust; MFT—Main Front Thrust; NALTT—North Altyn Tagh thrust; WKLT—West Kunlun thrust; LMT—Longmenshan thrust; EKLT—East Kunlun thrust ALT-Altyn Tagh subterrane; BY-SG—Bayan Har-Songpan-Garzê subterrane; HM—Himalaya accretionary terrane; INDB—Indian block; KL—Kunlun fault; LS—Lhasa subterrane; QDM—Qaidam subterrane; QL—Qilian subterrane; QT—Qiangtang subterrane; SG—Songpan-Garzê terrane; WKL—West Kunlun terrane; YLZBS—Yarlung Zangbo suture; YN—Yunnan terrane; YZB—Yangtzeblock; ALSB—Alxa block; TRMB—Tarim block

中朝、塔里木陆块(克拉通)等一起组成位于冈瓦纳西缘的"始北中国早古生代复合地体"。

必须提及的问题是在"始北中国早古生代复合地体"中发现了重要的早古生代柴北缘-南阿尔金超高压变质带和北祁连-北阿尔金变质带[67],它们的形成可能与早古生代始特提斯洋盆有关的边缘海盆的深俯冲及继后的陆壳深俯冲有关[55]。

3.3 特提斯洋盆演化与俯冲极性

古地磁和全球大陆复原资料还表明[58],继始特提斯洋盆闭合及地体拼合(D_3)之后,中石炭世开始西伯利亚陆块、北美陆块、波罗的陆块和冈瓦纳大陆开始汇聚,在中二叠世拼合成"联合大陆"(Pangaea)。同时特提斯洋盆产生,并经历了古特提斯(C_2-T_{1-2})和新特提斯(T_3-E_1)洋盆发育的两个阶段。

3.3.1 古特提斯(C_2-T_{1-2})洋盆演化及俯冲极性

中石炭世开始,古特提斯洋盆的打开和不断扩张使"始北中国早古生代复合地体"、"始华南早古生代复合地体"、"Siam 地体"和基墨里(羌塘)地体[68～69]等先后朝北运移,并接受了海相沉积。

根据古特提斯洋盆的蛇绿岩残片研究,已确定昆南-阿尼玛卿蛇绿岩带形成于C-P[70～72]和早三叠世向北俯冲形成东昆仑活动陆缘带;金沙江-理塘蛇绿岩带形成于 C-P,早三叠世向南和南西俯冲于羌塘(昌都)地体之下,形成包括义敦-玉树火山岛弧带和理塘弧后盆地(具洋壳性质)在内的羌塘-昌都活动陆缘带[73]。上述两条蛇绿岩带代表的古特提斯洋盆可分别称之为古特提斯北大洋和古特提斯南大洋。洋盆的消减是通过反向俯冲(北大洋向北和南大洋向南的俯冲极性)实现的。

洋盆的闭合使 3 个地体会聚及碰撞。由于包含中朝陆块、阿拉善陆块和塔里木陆块的"北中国板块"北面联合大陆中的西伯利亚陆块已经连接。南面与"扬子地体"首先在东端(大别-苏鲁)碰撞,并在 240～220Ma 产生陆壳的深俯冲[74]。与此同时,基墨里-羌塘地体与"扬子地体"的 SW 部分(保山-中甸)拼合、碰撞。由于古特提斯洋盆"反向俯冲"的运动学极性,致使在"北中国板块"、"扬子地体"和基墨里-羌塘地体之间形成宽阔的倒三角形的松潘甘孜被动陆缘海盆,堆积了巨厚复理石建造。三叠纪末的 3 个地体在西部的碰撞实现了南北块体之间的完全碰撞,形成"松潘-羌塘三叠纪复合增生地体",并形成由早古生代和三叠纪两个时代复合碰撞造山构成的 4000km 长的中国中央造山带及超高压变质带[50]。

3.3.2 新特提斯(T_{1-2}-K_1)洋盆演化及俯冲极性

中二叠世—早三叠世开始,联合大陆冈瓦纳陆块北缘的新特提斯洋盆开启和扩张,成为古特提斯洋盆消减的驱动力。班公湖-怒江蛇绿岩带与雅鲁藏布江蛇绿岩研究表明它们分别标志新特提斯北洋盆和新特提斯南洋盆的存在。位于"松潘-羌塘复合增生地体"与"拉萨地体"之间的新特提斯北洋盆开启于早-中三叠世,在晚三叠世洋壳发生俯冲,由于在羌塘地体南缘活动陆缘增生带发育不明显,关于俯冲极性问题由于北侧的活动陆缘带不清楚,而最近又发现拉萨地体中印支火山岛弧带的存在[75],推测印支火山岛弧带是新特提斯北洋盆(班公湖-怒江洋盆)向南俯冲的结果[76]。新特提斯北大洋闭合及地体碰撞时间在侏罗纪。

由于雅鲁藏布江蛇绿岩时代提早到晚三叠世(215～195Ma),潘桂棠等[18]提出新特提斯南大洋形成时代为晚二叠世—早白垩世。冈底斯火山岛弧带形成初始时期为 J_3-K_1,主期为 K-E_1,表明新特提斯南大洋(雅鲁藏布蛇绿岩)的初始裂解为 T_3,向北俯冲的时间为 J_3-E_1。因此,新特提斯北大洋的形成、扩张及消减的演化历史比新特提斯南大洋的老。

69Ma 开始，印度陆块从冈瓦纳大陆裂解，印度洋打开并使印度陆块向亚洲大陆方向推进，新特提斯南洋盆的消减和俯冲在主动陆缘的拉萨地体一侧形成白垩-新近纪冈底斯火山岛弧及花岗岩浆带，被称为“转换喜马拉雅带”(Transhimalaya zone)[77]。约 55Ma 开始印度大陆与亚洲大陆碰撞形成印度-雅鲁藏布缝合带和“喜马拉雅新生代增生地体”。此时“阿-祁-昆-秦”早古生代复合地体与“松潘-羌塘三叠纪复合增生地体”和“拉萨侏罗纪增生地体”已完全连在一起，拼贴在南亚大陆之上。

3.3.3 洋盆演化、地体增生及大陆生长

综上所述，早古生代始特提斯洋盆形成在冈瓦纳大陆的西侧，中石炭世以来的特提斯洋盆形成在联合大陆的东部，始特提斯洋盆和特提斯洋盆有成因联系，但产生的大背景决然不同[58]。“始北中国早古生代复合地体”中的诸地体作为冈瓦纳大陆和始特提斯洋盆之间的多地体/多岛弧群产出，它们之间为一系列具初始洋壳的边缘海盆(类似日本海)相隔，这些边缘海盆与始特提斯洋盆有成因联系，为始特提斯大洋岩石圈板片俯冲造成的上盘活动陆缘增生带上扩张的弧后盆地。

始特提斯→特提斯(古和新)洋盆的转化使羌塘地体和拉萨地体先后从冈瓦纳大陆附近向北运动，由于洋盆的发育一般经历了开启、扩张和消减的过程，一个洋盆的收缩与另一个洋盆的打开在时限上往往具有穿时性，因此新特提斯南大洋的开启与新特提斯北大洋扩张或收缩时期同时，在新特提斯南大洋关闭时保留在缝合带中的早期(T_3)初始洋壳残片是很正常的。

4 造山的高原——青藏高原巨型碰撞造山拼贴体与造山的叠置性

青藏高原形成的基础背景比世界上其他的许多高原都来得复杂，譬如，北美的科罗拉多高原构筑在稳定的古生代地台之上，法国中央高原的基础是欧洲华力西造山带。而青藏高原的前身是早古生代以来形成的巨型复合碰撞造山拼贴体，因此有人又把青藏高原称为“造山作用的高原”(Orogenic Plateaux)。

青藏高原的地体拼合与碰撞造山作用同时进行，显生宙以来主要的碰撞造山时限为早古生代、三叠纪、晚侏罗-早白垩世和新生代以来。因此青藏高原巨型碰撞造山拼贴体形成主要是 600Ma 以来长期活动及多期造山的过程，巨型碰撞造山拼贴体的形成是亚洲大陆的自北往南的增生和造山迁移过程的标志。

研究表明全球性造山作用涉及大范围的陆壳变形、变质及花岗岩浆活动，造山作用可以发生在板块碰撞前的俯冲期(俯冲型山链)、主碰撞期(碰撞型山链)及后碰撞期(陆内型山链)。

4.1 早古生代弧-陆碰撞及多地体/岛弧的造山动力学

早古生代时期的地壳变形与碰撞造山事件主要记录在“阿尔金-祁连-昆仑”早古生代复合地体中，但是位于中部和南部的羌塘地体和喜马拉雅地体也曾经历了早古生代或泛非-早古生代造山事件形成原始喜马拉雅山，并成为现今的喜马拉雅造山带的早古生代变质褶皱基底[78]。因此早古生代造山运动(或泛非-早古生代造山运动)的范围几乎遍及整个青藏高原各地体之中，但是它们的原位在南半球的冈瓦纳大陆周缘的不同部位[58]。

上述表明青藏北部的早古生代碰撞造山带的形成是由于与始特提斯洋盆有关的边缘海

盆(地体/岛弧相间)的闭合而引起,其导致地体/岛弧群的拼合与碰撞,经历了弧/陆和陆/陆碰撞的过程,从俯冲型山链向碰撞型山链转化[65]。可以看出,柴北缘超高压变质带的形成也起始于边缘海盆初始洋壳的深俯冲作用,而早古生代复合造山带的"三多"的构造格局显示了早古生代造山带形成前的弧后活动带的背景。最近研究提出美洲科迪勒拉造山带是位于弧后及现代弧后域的长期活动带上的造山带,具有长期弱化、低强度、薄和热的岩石圈,由造山带中造山花岗岩基、高级变质作用和韧性变形所指示的造山热能来自原先的弧后热岩石圈,而不是来自于造山变形过程本身[40]。因此推测青藏高原北部早古生代造山带形成前的广大的活动带是弧后活动带,提供了造山类型转化及陆-陆碰撞强烈造山作用必备的热的条件。

4.2 晚古生代(华力西期)的碰撞造山?

前人曾提出东-西昆仑山为华力西期造山带[70,78]。"十五"青藏高原空白区填图成果中也报道了在布青山以北的南昆仑、北羌塘和西昆仑地区等存在晚古生代地层之间的"角度不整合",因而晚古生代(华力西期)碰撞造山存在与否成为研究青藏高原碰撞造山作用的值得注视的问题。

碰撞造山事件是以大规模褶皱、伴随的变质作用、区域性角度不整合、大规模的花岗岩浆活动及代表造山结束的磨拉石盆地沉积为标志的。经与有关区调人员最近在成都(会议由潘桂棠主持)讨论初步表明:西昆仑地区的华力西碰撞造山:木孜塔格北 J_1 陆相沉积不整合在 P_2 之上、阿其克库都克 P_1 不整合在 S_{1-2} 之上,克里雅河地区时代没有确定的 T_{1-2} 的磨拉石不整合在 C_3-P_2 弧后盆地沉积之上,以及朝阳湖 P_3-T_2 与 C_3-P_1 之间砾岩层(性质未定)和上下地层整合的特点,表明西昆仑华力西碰撞造山运动证据不足;在东昆仑布青山蛇绿岩以北地区,局部发现宽缓褶皱的 P_3 灰岩不整合在同劈理褶皱的 C-P_2 板岩夹中基性火山岩之上,可以解释为洋壳俯冲带上盘 C-P_2 弧前加积楔中存在的局部披盖不整合效应。北羌塘地区发现的局部 P_3 与 C-P_2 之间微角度的不整合可以认为是被动陆缘的伸展不整合的效应。

另外,前人曾认为东昆仑地区华力西期花岗岩浆活动强烈,是华力西期洋盆向北俯冲的结果[70]。经重新测试,原定为东昆仑布尔汗布达山的"晚古生代"花岗岩,通过 $^{206}Pb/^{238}U$ 和 ^{39}Ar-^{40}Ar 年龄的测定(陈文),获得的绝大部分年龄为三叠纪弧型花岗岩(226～239Ma),表明为三叠纪古特提斯洋盆向北俯冲于东昆仑地体之下的结果,而小范围存在的晚古生代花岗岩可能与后加里东碰撞造成的陆内岩浆活动有关(许志琴等,未刊资料)。

据古地磁资料表明,晚泥盆世之后,始特提斯洋闭合及石炭-二叠纪古特提斯洋打开,位于冈瓦纳大陆周缘已拼合的"始中国早古生代复合地体"开始往北和北西方向移动,向联合大陆(Pangeae)靠拢,直至晚三叠-早侏罗世古特提斯洋盆自东往西逐渐闭合,南北陆块会聚形成中央碰撞造山带。因此古地磁资料不支持在此之前南北陆块之间碰撞形成华力西造山带的观点(没有碰撞的机会)。

所以,根据青藏高原现有地质资料分析,晚古生代不存在以大规模褶皱、伴随的变质作用、区域性广泛角度不整合、大规模的花岗岩浆活动及代表造山结束的磨拉石盆地沉积为标志的碰撞造山运动。

4.3 三叠纪碰撞造山及叠置造山

三叠纪是青藏高原中地体碰撞造山的重要时期。三叠纪的地壳变形主要分布在东-西

昆仑地体的南部、巴颜喀拉-松潘甘孜地体、羌塘地体及青藏高原东南部横断山的广大地域，构成巨型三叠纪碰撞造山带，由于后期的改造，三叠纪碰撞造山带几何学呈现“T”形，由纬向印支带和经向印支带组成。纬向印支带自西往东从西昆仑南部甜水海地体、越过阿尔金断裂连接巴颜喀拉-松潘甘孜、羌塘地体，向东与南秦岭、大别-苏鲁相连，全长 3000km；经向印支带自北往南从松潘-甘孜-川滇-印度尼西亚，全长 2000km。

昆南-阿尼玛卿和金沙江蛇绿岩所代表的石炭-二叠纪古特提斯洋盆的闭合造成昆仑、松潘和羌塘 3 个地体与“阿-祁-昆”早古生代复合地体在晚三叠-早侏罗世拼合，同时形成近东西向的昆仑-松潘-羌塘晚三叠-早侏罗世碰撞造山系。研究表明，在昆南-阿尼玛卿缝合带北缘的东昆仑主动陆缘一侧发育逆冲-推覆叠置岩片结构，而在扬子被动陆缘一侧发育新元古代变质基底和盖层之间的韧性挤压型滑脱体系[73]，两侧都具有向南的造山极性，并伴随三叠纪以来的花岗岩浆活动。昆南-阿尼玛卿缝合带两侧的“逆冲-滑脱结构”与东秦岭十分类似。

晚侏罗-早白垩世的碰撞造山造成的地壳变形主要分布在青藏联合地体南部的羌塘地体和拉萨地体范围内。

尽管青藏高原中各时期的地体拼合、增生过程与碰撞造山同时进行，但是碰撞造山作用（包括地壳变形、基底活化及花岗岩浆活动）所涉及范围远远越出地体边界的狭窄地域，造成叠置造山作用。譬如，由于古特提斯洋盆闭合形成的强烈印支碰撞造山还影响到东昆仑南缘早古生代复合地体，形成叠覆造山带。在阿尔金-祁连-昆仑早古生代复合地体的北部，在早古生代变形之上叠置了印支陆内变形。在东昆仑南地体的万宝沟地区，早中三叠世地层的同心褶皱叠置在早古生代绿片岩系紧闭褶皱及加里东期花岗岩之上，羌塘地体玉树以南格拉山的泥盆-石炭纪陆相地层的同心褶皱叠置在早古生代褶皱之上。

4.4 印度/亚洲碰撞及巨大的陆内变形域

青藏高原的形成是地质历史过程中板块或地体连续碰撞和拼合的结果，最后一次是 60～50Ma以来的印度/亚洲碰撞。目前，绝大多数人接受了青藏高原的隆升是印度板块与亚洲大陆碰撞的结果的观点[30,80]。研究表明，印度/亚洲大陆碰撞之后，板块之间的作用并未终止，印度板块仍以 44～50mm/a 的速率往北推进，至少 1500km 的南北向缩短量被吸收，使青藏高原成为 2 倍于正常地壳厚度的巨厚陆壳体，并形成印度与西伯利亚板块之间南北 2000km、东西 3000km 巨大范围的新生代陆内变形域[29,81～82]。现今青藏高原南部喜马拉雅的南北向缩短率为 18mm/a，北部祁连山的缩短率为 15mm/a，腹地的东西向伸展速率为 10mm/a[83]，由此形成了“中央高原”和“周缘造山带”两个新生代青藏高原特级大地构造单元。

4.4.1 大印度板块变成小印度板块

印度/亚洲大陆碰撞之前比现在的范围大得多的印度板块（即大印度板块）往北相对南亚大陆运动了 2500km[84～85]，由于沿着走滑断裂往北运移的速度的差异，大印度板块东西两端与南亚大陆的碰撞产生了时间上的先后：西端的碰撞在 52Ma（可能更早），东端的碰撞大约 45Ma，比西端晚了 10Ma。印度板块的东西界分别为两条大型的走滑断裂：西界是恰曼（Chaman）左行走滑断裂，东界是沙盖-明衮（Sagaing-Minggun）右行走滑断裂，这两条断裂都伴随强烈褶皱，水平位移至少 1000km，这些构造形成了著名的两个喜马拉雅东西构造结：南迦帕巴（Nanga Parbat）西构造结和布玛（Burma）东构造结[86]。

4.4.2 巨大的弧后变形域

新特提斯洋盆往北俯冲形成的冈底斯岩浆岛弧带作为活动增生陆缘带拼贴在拉萨地体之上,冈底斯岩浆岛弧带以北的广大地域都可以看作弧后域。由于印度/亚洲碰撞产生的大规模的变形及主要构造事件表现为:弧后地域(青藏腹地)的裂谷伸展作用和大规模碱性火山活动,周缘造山带的挤压逆冲变形及垂向挤出,地体边界(或古构造带的再活化)以及斜向碰撞形成的大型走滑断裂以及大量物质向东和南东方向的侧向挤出,而北部广大地区除地体边界外则表现为弥散的弱变形。周边克拉通上的陆相盆地的形成与高原隆升及周缘造山带崛起呈互馈关系。

4.4.3 周缘现代造山带的崛起和喜马拉雅造山机制

印度/亚洲碰撞造山的巨大影响使喜马拉雅增生地体最后崛起,喜马拉雅山的最后形成是30Ma以来印度板块往北陆内俯冲在亚洲大陆之下的结果[87],与此同时的北缘、东缘和西缘周边造山带以不同的挤出样式:东缘龙门山和西北缘阿尔金山的"挤压转换-逆冲式"及东北缘祁连山"双向逆冲式"崛起[88]。最新的研究[89]表明,高喜马拉雅(GHM)亚地体北缘的藏南拆离断裂(STD)向北延伸在特提斯-喜马拉雅(THM)亚地体之下,与自南而北剪切滑移的康马-拉轨岗日拆离带(KLDT)相连。由于拆离构造作用同时及稍后形成的淡色花岗岩的侵位使康马-拉轨岗日拆离带隆起,形成康马-拉轨岗日穹隆带。在高喜马拉雅(GHM)亚地体南部发育的逆冲断层具有挤压转换性质,在北部发现EW向近水平的韧性拆离构造,以发育EW向拉伸线理及缓倾的糜棱面理和自西向东水平滑移的剪切指向为特征。提出高喜马拉雅(GHM)亚地体的EW向水平滑移是垂向挤出和侧向挤出的变形综合反映。喜马拉雅地体中的东西和南北向拆离构造的存在为喜马拉雅现代造山机制提供了再讨论的基础[89]。

5 大型走滑构造对青藏高原地体结构的改造

青藏高原的几何学形态十分奇特,这与大型走滑构造对青藏高原中先后形成的拼合地体和碰撞造山系的重要制约、改造以及碰撞造成的青藏高原东南缘大量物质向SE及S方向逃逸(侧向挤出)[90~94]有关。

青藏高原中不同历史时期形成的大型走滑构造主要有两类,一类是产于地壳深部的韧性走滑剪切带,由于后期的抬升而出露地表,包括400Ma左右前形成的北祁连南缘韧性右行走滑剪切带和西昆仑康西瓦韧性右行走滑剪切带[73,95~96],240~220Ma前形成的南祁连南缘韧性左行走滑剪切带[73]、东昆仑韧性左行走滑剪切带[95]、金沙江韧性左行走滑剪切带及阿尔金韧性左行走滑剪切带[96];20Ma前后形成的鲜水河韧性左行走滑剪切带[73]、喀喇昆仑韧性右行走滑剪切带和红河韧性右行走滑剪切带[97]等。其中阿尔金韧性左行走滑剪切带是中亚最大的走滑构造带,南祁连南缘韧性左行走滑剪切带向东沿至东秦岭可能和丹凤韧性左行走滑剪切带相连,全长2500km。这些地壳深部的韧性走滑剪切带在后期抬升过程中,由韧性→韧脆性→脆性应变转化。另一类是产于地壳浅部的脆性走滑断裂,如海源左行走滑断裂[98]等。在印度/亚洲碰撞以来大型韧性走滑构造主要发育在高原南部,而且在喜马拉雅的东、西两侧,如喀喇昆仑韧性右行走滑断裂、嘉黎-高黎贡山韧性右行走滑断裂、红河韧性右行走滑断裂和鲜水河韧性左行走滑断裂;其他地区特别是北部以脆性断裂为主,

表现为古韧性剪切带的再活动及新生断裂，如阿尔金左行走滑断裂、东昆仑左行走滑断裂、雅鲁藏布江右行走滑断裂和海源左行走滑断裂。

大型走滑构造在青藏高原地体拼合及碰撞造山中的作用主要表现如下：

5.1 地体的相对位移及斜向碰撞

位于地体边界的走滑构造使地体相对位移，是地体斜向碰撞的产物。如 400Ma 左右形成的北祁连南缘韧性右行走滑剪切带，是阿拉善地体与祁连地体拼合碰撞后期的斜向碰撞导致两地体相对位移的结果；昆南韧性左行走滑剪切带使东昆仑地体和松潘地体相对位移数十千米，反映了晚三叠世-早侏罗世阶段地体斜向碰撞的影响。

5.2 地体错位及移置

与青藏高原北部"阿-祁-昆"早古生代复合地体及"松潘-羌塘"三叠纪复合增生地体斜交的阿尔金主断裂(NEE-SWW 走向)是中亚最大的走滑断裂，研究表明阿尔金地体与祁连地体具可对比性，阿尔金地体为祁连加里东造山带的西延部分。它与祁连加里东造山带的分开是由于印支期(240～220Ma)开始的阿尔金主断裂的左行走滑运动及之后多期再活动的结果。根据断裂两侧构造单元及地体边界特征的详细对比，已提出沿阿尔金主断裂两侧的北阿尔金俯冲杂岩带与北祁连俯冲杂岩带的累计错距 350km，南阿尔金俯冲杂岩带与柴北缘俯冲杂岩带的累计错距 400km，沿阿尔金断裂北缘的若羌断裂可能平移 200km 的认识[99]。阿尔金断裂现今的走滑速率：北东段 5mm/a，中段 20mm/a 和西段 30mm/a，使阿尔金地体和西昆仑地体成为现在的移置地体。

位于青藏高原西南缘的喀喇昆仑右行走滑断裂的活动时间开始于 23～27Ma 以前，比前人的看法(8～11Ma)提前。目前对于断裂的累积位移量的估算存在着较大的分歧(～300～66km)[100]。根据笔者以断裂两侧的地体边界为标志的研究，认为班公缝合带相对阿克拜塔尔缝合带右行位移 400km，狮泉河缝合带相对什约克缝合带右行位移 280km，累计走滑位移量至少在 250～300km 以上。最新的研究还表明，喀喇昆仑断裂形成以来的长期的平均滑移速率为 10±3mm/a，说明从印度板块与欧亚大陆碰撞后，青藏高原西南缘约 27Ma 以来产生大规模右旋走滑，使得高原物质沿这一滑移线以约 10mm/a 滑移速率向东挤出[101]。

5.3 地体的侧向挤出

在印度陆块楔与南欧亚大陆碰撞同时，大规模的走滑作用使南欧亚大陆南部的松潘、羌塘和冈底斯地体向东南方向强烈侧向挤出，构成"云南挤出地体"和"禅邦挤出地体"(图 1)，而制约块体挤出的主要走滑断裂(或韧性走滑剪切带)为鲜水河韧性左行走滑剪切带、嘉黎-红河韧性走滑剪切带、雅鲁藏布江右行走滑断裂等(图 2)。

6 青藏高原隆升的多元深部驱动力

自 20 世纪 90 年代初以来，由许志琴、杨经绥、姜枚和 P.Tapponnier 组织的中法青藏高原地学合作开展了地质和地球物理多学科的研究和探测。其中姜枚和 Hirn 及 Wittlinger 负责的中法地球物理合作小组在青藏高原实施了 8000km 长的天然地震探测剖面，包括横穿青藏高原中部及南部的格尔木-唐古拉-嘎拉剖面(3000km)，位于青藏高原腹地东部的共和-玉树剖面(3000km)，横穿青藏高原西北部柴达木盆地和阿尔金山的乌图美仁-若羌剖面(1000km)，以及横穿青藏高原西部昆仑山的叶城-狮泉河剖面(1000km)。这些剖面几乎穿

过了青藏高原所有地体，并通过了主要地体边界，获得地壳和地幔速度图像及地震波各向异性，揭示了青藏高原400km深度范围内的地幔结构特征：①青藏高原地体的地壳结构及复杂流变学特征；②青藏高原腹地可可西里下面的深地幔羽存在；③大型走滑断裂为超岩石圈或地幔剪切带；④古大洋岩石圈"化石"残片与拆沉的地球物理证据；⑤印度大陆岩石圈板片俯冲的样式和距离等，为人们提供了讨论有关青藏高原深部地壳、岩石圈以及深地幔结构的背景资料[36,102－106]。

青藏高原各地体的厚度及地壳平均地震波速度特征反映了拼合的各地体的物质组成、结构差异及低速层的存在；400km深度范围内的地幔速度图像揭示了青藏高原腹地深地幔中存在以大型低速异常体为特征的地幔羽，并通过热通道与可可西里地表大面积分布的新生代高钾碱性火山作用有成因联系；伸入＞200km以下的5条伴有局部熔融及高热物质的垂向低速异常带代表了大型超岩石圈或地幔剪切带；数条不连续的高速异常带被解释为地体拼合历史过程中可能保留的大洋或大陆岩石圈化石残片，是"拆沉"的地球物理依据；由巨大的断续高速异常带(厚100～300km)组成的印度岩石圈板片往北缓缓地插入雅鲁藏布江缝合带以北400km远的唐古拉山之下，并被若干条深达400km以上的垂向低速异常带切割[106]。

最近以S.P.Grandt[107]，R.Van Der Voo *et al*[41]，S.Widiyantoro[108]和H. Bigwaard[38]等为首的科学家通过对最新的全球地震层析资料所揭示的地幔中地震波速变化的研究，发现有的板块可以俯冲到过去不可想象的核幔边界(2891km深)。在大陆板块会聚边界，地幔地震层析图像不仅显示了岩石圈板片的超深俯冲，还保存了拆沉的岩石圈化石残片的重要信息。通过印度、西藏及邻近印度洋的西喜马拉雅地幔层析剖面[38,41]揭示了若干高速异常体的存在。在北东阿富汗的兴都库什的上地幔600km范围内，高速板片向北倾斜并与印度板块岩石圈连接；在北巴基斯坦，同样的高速板片显示了印度板片以"翻转"几何形态俯冲至800～1000km的地幔深度，并发现印度次大陆之下1000～2300km深度范围内出现与浅部异常体分离的高速异常体，甚至掉到核幔边界的深度。R.V.der Voo等[41]把这些下地幔中的高速异常体解释为拆沉的新特提斯大洋岩石圈残片。这一新的信息为青藏高原形成的深部驱动力探究提供了新的思考。

结合有关的青藏高原深部探测资料，讨论青藏高原隆升的多元深部驱动力的几个问题：

(1)印度岩石圈板片俯冲样式和俯冲深度。印度和欧亚板块碰撞及青藏高原形成的研究一直是地学界关注的热点。自Argand E.提出印度板块往北俯冲在欧亚大陆之下的观点以来，地球物理的探测不断提供了岩石圈范围内的俯冲证据[109－112]。印度岩石圈板块究竟往北俯冲多远，以何种样式俯冲，是印度/亚洲碰撞及青藏高原隆升的重要制约因素。长期以来各种推测和讨论都是以岩石圈尺度所获得的地球物理资料为依据的。横越西-中喜马拉雅的地震层析剖面[38,41]揭示了印度岩石圈板块往北以特殊的样式超深俯冲于青藏高原之下，即印度岩石圈俯冲板片的上部往北缓倾、中部直立向下以及下部往南翻转的几何学形式[87]；喜马拉雅的地幔地震层析图像中还揭示了中下地幔范围内保存了若干高速异常体，说明岩石圈板片可以俯冲到地幔深部，一部分成为拆沉的化石残片，一部分在碰撞的过程中折返上来，折返上来的板片保存了大量地幔动力学的信息，包括超高压变质岩石的发现[113]。

横穿青藏高原的地震层析资料研究进一步表明，在翻卷板片的上部(400km以上)，代

表印度岩石圈板块的高喜马拉雅高速异常带以缓倾角度俯冲至雅鲁藏布江缝合带以北400km远的唐古拉山下面，切割印度岩石圈板片的垂向低速异常带解释为印度岩石圈翻卷板片造成的地幔上升熔融柱，这些上升的熔融柱在印度岩石圈板片上部组成以低速异常层为特征的地壳熔融层。

(2)青藏高原周缘古老变质体的挤出及北缘克拉通的陆内俯冲。青藏高原周缘高耸的山峰构成了高原的屏障，南缘为喜马拉雅山，东缘为龙门山-锦屏山，北缘和西缘为祁连山-阿尔金山-西昆仑山，山脉的外围是稳定地块之上的前陆沉积盆地。青藏高原的周缘造山带是如何在新生代崛起？原来埋在深部的岩石为什么快速折返到地表形成高山？深部的驱动力是什么？

在大约55Ma，印度板块与亚洲大陆碰撞之前比现在的范围大得多的印度板块(即大印度板块)往北相对南亚大陆运动了2500km[25,84~85]。由于沿着走滑断裂往北运移的速度的差异，大印度板块东西两端与南亚大陆的碰撞产生了时间上的先后：西端的碰撞在52Ma(可能更早)，东端的碰撞大约45Ma[28]，晚了10Ma。印度板块的向北推挤导致喜马拉雅增生地体的形成与喜马拉雅山脉的崛起，缩短率为18%，之间会聚与碰撞方式是以挤压为主，构造造型是从雅鲁藏布缝合带逐步往南扩展的逆冲叠覆作用为特征，因此印度板块北部被动陆缘的变质基底及古生代-中生代沉积盖层均卷入地壳增生楔中。在60～50Ma形成雅鲁藏布江上幔逆冲断层，40Ma形成特提斯喜马拉雅的北喜马拉雅逆冲断层，20Ma同时形成高喜马拉雅和低喜马拉雅之间的主中央冲断层(MCT)和高喜马拉雅与特提斯喜马拉雅之间的藏南拆离断裂(STD)。在MCT和STD的制约下，高喜马拉雅古老变质体从下地壳呈挤出样式折返。

青藏高原北部周缘克拉通向南的陆内浅俯冲作用使高原北缘的祁连山-阿尔金山-西昆仑山在地壳的强烈挤压下以“双向式逆冲挤出”样式和“逆冲转换挤出”样式缩短并崛起。河西走廊-北祁连地震反射剖面[33]和乌图美仁-若羌天然地震层析剖面[102,105]提供了陆内俯冲的证据，叶城-狮泉河剖面也显示了塔里木地块向南俯冲于西昆仑之下。

(3)岩石圈-地幔剪切带与“右旋隆升”的新机制。根据青藏高原大型走滑断裂研究已提出青藏高原向NE方向的“右旋隆升”新机制[94]，新的地震层析资料表明青藏高原新生代活动的走滑断裂大部分为岩石圈-地幔剪切带，因此可以认为高原“右旋隆升”的机制受到岩石圈-地幔断裂的制约。笔者认为在青藏高原腹地的上地幔剪切波各向异性方向自西往东从EW→NE→SE→NNE→SSW的转化与“右旋隆升”的观点相吻合。

(4)青藏高原腹地深部的热结构及地幔羽。位于青藏高原腹地100km深度以下的巨型地幔羽与可可西里火山作用有成因联系，表明青藏高原腹地深部具有热结构，青藏高原南缘的陆内超深俯冲与北缘的陆内浅俯冲对高原产生南北向挤压及东西向拉伸，深部挤压环境导致物质熔融和地幔羽的形成，以及物质在地幔中的向东运动，浅部东西向拉伸环境造成南北向裂谷及腹地的火山喷发。格尔木-唐古拉天然地震探测剖面及根据其与周围资料从新处理获得的阿克塞-花石峡天然地震探测剖面还揭示了可可西里为中心的由大型低速异常体组成深部地幔羽结构(深度150～400km以下)的存在[38~39]，并且在柴达木盆地下部发现宽300km、厚80km的地震波低速异常层，该地震波低速异常层又与可可西里深部大型低速异常体组成地幔羽相连[114]。

许志琴[88]曾提出青藏高原隆升的“周缘陆内俯冲及内部地幔底辟”的碰撞动力学机制

模型。根据新的地震层析资料及地震反射资料,对上述模式应作进一步修改,新的模式可归结为"青藏高原南部印度岩石圈板片的陆内超深俯冲,北缘克拉通的陆内浅俯冲,腹地深地幔热结构以及超岩石圈范围的"右旋隆升"及物质向东挤出"(图3)。

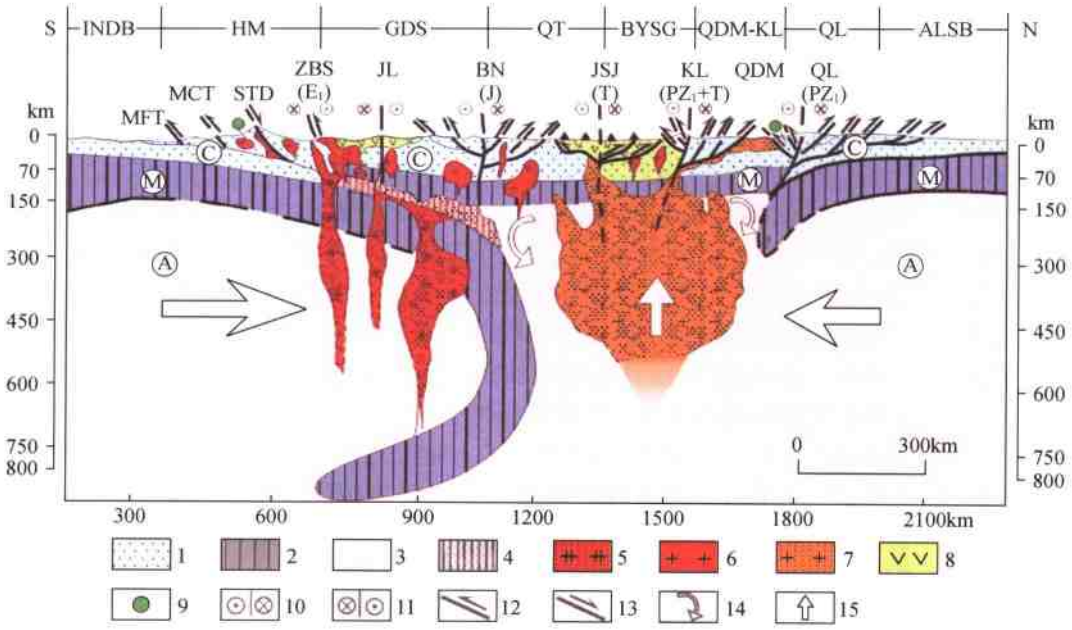

图3　青藏高原深地幔结构及动力学模式图

Fig. 3　Deep mantle structure and dynamic model of the Qinghai-Tibet Plateau

1—地壳;2—岩石圈地幔;3—软流圈;4—局部熔融体;5—深部熔融体;6—花岗岩;7—地幔底辟;8—火山岩;9—超高压变质岩石;10—左行走滑断裂;11—右行走滑断裂;12—逆冲断裂;13—正断层;14—挤压力;15—上升力。IND—印度陆块;HM—喜马拉雅增生地体;GDS—冈底斯地体;QT—羌塘地体;BYSG—巴颜喀拉-松潘甘孜地体;QDM-KL—柴达木-昆仑地体;QL—祁连地体;ALSB—阿拉善陆块;MFT—主前锋逆冲断裂;MCT—主中央冲断裂;STD—藏南拆离断裂;ZBS—藏布缝合带;JL—嘉黎断裂;BN—班公湖-怒江缝合带;JSJ—金沙江缝合带;KL—昆仑断裂;QDM—柴达木地体

1—Crust; 2—Lithospheric mantle; 3—Asthenosphere; 4—Partial melt; 5—Deep melt; 6—Granite; 7—Mantle diapir; 8—Volcanic rocks; 9—Ultra-high pressure metamorphic rocks; 10—Sinistral strike-slip fault; 11—Dextral strike-slip fault; 12—Thrust; 13—Normal fault; 14—Compression; 15—Uplifting force; IND—Indian block; HM—Himalaya accretionary terrane; GDS—Gangdise terrane; QT—Qiangtang terrane; BYSG—Bayan Har-Songpan-Garzê terrane; QDM-KL—Qaidam-Kunlun terrane; QL—Qilian terrane; ALSB—Alxa block; MFT—Main Front Thrust; MCT—Main Central Thrust; STD—South Tibet detachment; ZBS—Zangbo suture; JL—Lhari fault; BN—Bangong Co—Nujiang suture; JSJ—Jinshajiang suture; KL—Kunlun fault; QDM—Qaidam terrane

青藏高原大陆动力学的研究刚刚开始,笔者在本文中提出的浅见愿与同仁们讨论。

鸣谢:本文为笔者等近15年青藏高原研究的部分成果综述。在成文过程中向M. Mattauer教授、肖序常院士、莫宣学教授、潘桂棠研究员等请教,受益匪浅。图件由张晓卫绘制,唐哲民、蔡志慧协助整理参考文献,一并感谢。

参 考 文 献

[1] Suess E. Das Antlitz der Erde. 1888; 2. Wien:F. Tempsky.

[2] Suess E. Das Antlitz der Erde. 1901a, 3, pt. 1. Wien:F. Tempsky.

[3] Suess E. Abschieds-Vorlesung der Professors Eduard Suess: Beitrage zur Palaontologie und Geologie Osterreich-Ungarns and des Orients. 1901b, 14: 1～18.

[4] Suess E. Das Antlitz der Erde, v. Ⅲ 2 (Dritter band. Zweite Halfte. Schluss des Gesamtwerkes). 1909. Wien: F. Tempsky, and Leipzig: G. Freytag.

[5] Suess E. Uber die Donau. Vortrag gehalten in der a.o. Festversammlung der k. Akad. Wiss. am 9. Marz 1911. Wien: Alfred Holder.

[6] De Launay L. La Géologie et les Richesses Minerales de L'Asie Historique-Industrie-Production-Avenir-metallogenie-Sibérie-Oural-Caucase-Turkestan-Met Egee-Asie-Mineure-Perse-Inde-Insulinde-IndoChine-Japon, etc. Paris: Ch. Beranger. 1911.

[7] Leuchs, K. Beitrage zur Geologie des westlichen Kwenlun und Westtibets, nach Zugmayer's Beobachtungen. Zeitschrift der Deutschen Geologischen Gesellschaft[J]. Monatshefte. 1913. 65:173～185.

[8] Argand E. La tectonique de l'Asie. In: Congres Géologique International, Comptes Rendus de la XIIIe Session, premier fascicule[M]. Liege: Vaillant-Carmanne, 1924.

[9] Fromaget J. Etudes géologiques sur le nord de L'Indochine centrale. Theses presentées a la Faculté des Sciences de L'Université de Lyon pour obtenir le grade de Docteur de L'Université de Lyon [M]. Hanoi: imprimerie de L'Extreme Orient, 1927.

[10] Dainelli G. La Serie dei Terreni, parte prima. Spedizione Cinese(1913～1914). Serie Ⅱ Resultati Geologici et Geografici, vol.2. Publication sotto la direzione di Giotto Dainelli, Bologna: Nicola Zanichelli, 1933.

[11] Huang T K. An outline of the tectonic characteristics of China[J]. Eclogae Geol. Helv. 1978, 71:611～635.

[12] Huang T K, Chen B W. The Evolution of the Tethys in China and Adjacent Regions (English and Chinese bilingual text)[M]. Beijing: Geological Publishing House, 1987.

[13] 肖序常,李廷栋,李光岑,等.喜马拉雅岩石圈构造演化[M].北京:地质出版社,1988.
Xiao Xuchang, Li Tingdong, Li Guangqin, *et al*. Tectonic Evolution of the Crust-upper Mantle of the Qinghai-Xizang(Tibet)Plateau [M]. Beijing: Geological Publishing House, 1988(in Chinese with English abstract).

[14] 肖序常,李廷栋. 青藏高原的构造演化与隆升机制[M]. 广州:广东科技出版社, 2000.
Xiao Xuchang, Li Tingdong. Tectonic Evolution and Uplift of Qinghai-Xizang (Tibet) Plateau [M]. Guangzhou: Guangdong Science & Technology Press, 2000(in Chinese with English abstract).

[15] Chang C F, Pan, Y S, Sury Y Y. The tectonic evolution of the Qinghai-Tibet plateau: a review[A]. In: Sengor A M C (ed.). The Tectonic Evolution of the Tethyanions [C]. Dordrecht: Kluwer, 1989. 415～476.

[16] 潘裕生. 喀喇昆仑山-昆仑山地区地质演化[M]. 北京:科学出版社,2000. 525.
Pan Yusheng. Geological Evolution of the Karakrum-Kunlun Mountains [M]. Beijing: Science Press, 2000. 525(in Chinese).

[17] 钟大赉. 滇川西部古特提斯造山带[M]. 北京:科学出版社, 1998. 1～231.
Zhong Da lai. Paleotethyan Orogenic Belt in Yunnan-Western Sichuan[M]. Beijing: Science Press, 1998. 1～231(in Chinese).

[18] 潘桂棠,李兴振, 王立金. 青藏高原及邻区大地构造单元初步划分[J]. 地质通报,2002, 21(11):701～707.
Pan Guitang, Li Xingzhen, Wang Lijin, *et al*. Preliminary division of tectonic units of the Qinghai-Tibet plateau and its adjacent regions [J]. Geological Bulletin of China, 2002, 21(11):701～707(in Chinese with English abstract).

[19] Courtillot V, Besse J, Vandamme D, *et al*. Deccan flood basalts at the Cretaceous/Tertiary boundary? [J]. Earth Planet. Sci. Lett, 1986, 80: 361～374.

[20] Jaeger J J, Courtillot V, Tapponnier P. Paelontological view of the ages of the Deccan Traps, the Cretaceous/tertiary boundary, and the India/Asia collision[J]. Geology, 1989, 17:316～319.

[21] Searle M P. Tigraphy, structure and evolution of the Tibetan-Tthys zone in Zanskar and the Indus suture zone in the Ladakh Himalaya [J]. Trans. R. Soc. Edinburgh Earth Sci., 1983, 73:205～219.

[22] Searle M P, Windley B F, Coward M P, *et al*. The closing of Tethys and the tectonics of the Himalaya [J]. Geol. Soc. Am. Bull., 1987, 98:678～701.

[23] Treloar P J, Coward M P. Indian plate motion and shape: Constraints on the geometry of the Himalaya orogen [J]. Tectonophysics, 1991, 191: 189～198.

[24] Dewey J F, Cande S, Pitman W C. Tectonic evolution of the India-Eurasia collision zone[J]. Eclogae. Geol. Helv., 1989, 82:717～734.

[25] Besse J V, Courtillot J P, Pozzi M, *et al*. Paleomagnetic estimates of crustal shortening in the Himalayan thrusts and Zangbo suture [J]. Nature, 1984, 311:621～626.

[26] Critelli S, Garzanti E. Provenance of the Lower Tertiary Murree redbeds (Hazara-Kashmir syntaxis, Pakistan) and initial rising of the Himalayas [J]. Sediment. Geology, 1994, 89:265～284.

[27] Le Pichon X, Fournier M, Jolivet L. Kinematics, topography and extrusion in the India-Eurasia collision [J]. Tectonics, 1992, 1:1085～1098.

[28] Rowley D B. Age of initiation of collision between India and Asia: a review of stratigraphic data [J]. Earth Planet. Sci. Lett., 1996, 145:1～13.

[29] Molnar P, Tapponnier P. Cenozoic tectonics of Asia: Effects of a continental collision [J]. Science, 1975, 189:419～426.

[30] Tapponnier P, Peltzer G, Armijo A. On the mechanics of the collision between India and Asia, in Collision Tectonics [A]. In: Coward M P and Riess A C (ed.). Geol. Soc. Spec. Publ. (C). London, 1986, 19: 115～157.

[31] Barazangi M, Ni J. Propagation characteristics of Pn beneath the Himalayan arc and Tibetan plateau: possible evidence for underthrusting of Indian continental lithosphere beneath Tibet[J]. Geology, 1982, 10: 179～185.

[32] 沈显杰,李文仁,杨淑贞．青藏高原南北地体壳幔热结构差异的大地热流证据[J]．中国地质科学院院报，1990，21:203～214.

Shen Xianjie, Zhang Wenren, Yang Shuzhen, *et al*. Heat flow evidence for the differentiated crust-mantle thermal structures of the northern and southern terranes of the Qinghai-Xizang plateau[J]. Bulletin of the Chinese Academy of Geological Sciences, 1990, 21:203～214(in Chinese with English abstract).

[33] 吴宣志,吴春玲,卢杰．利用深地震反射研究北祁连-河西走廊地壳细结构[J]．地球物理学报，38(增刊 Ⅱ)，1995，29～35.

Wu Xuanzhi, Wu Chunling, Lu Jie. Research on the fine crustal structure of the northern Qilian-Hexi corridor by deep seismic reflection [J]. Acta Geophysica Sinica, 38, 1995, 29～35 (in Chinese with English abstract).

[34] 高锐,黄东定,卢德源,等．横过西昆仑造山带与塔里木盆地结合带的深地震反射剖面[J]．科学通报，2000，45(17)：1874～1879.

Gao Rui, Huang Dongding, Lu Deyuan, *et al*. Deep seismic reflection profile across Juncture zone between Tarim basin and west Kunlun Mountain[J]. Chinese Science Bulletin, 2000, 45(17):1874～1879(in Chinese with English abstract).

[35] 滕吉文,王绍舟,姚振兴．青藏高原及其邻近地区的地球物理场特征与大陆板块构造[J]．地球物理学报，1980，23(3):254～268.

Teng Jiwen, Wang Shaozhou, Yao Zhenxing. Characteristics of the geophysical fields and plate tectonics of the Qinghai-Xizang plateau and its neighbouring regions [J]. Acta Geophysica Sinica, 1980, 23(3):254～268(in Chinese with English abstract).

[36] 姜枚,吕庆田,史大年,等．用天然地震探测青藏高原中部地壳,上地幔结构[J]．地球物理学报，1996，39(4)：470～481.

Jiang Mei, Lu Qingtian, Shi Danian, *et al*. The study on the structure of crust and upper mantle with natural earthquakes in central Tibetan plateau[J]. Acta Geophysica Sinica, 1996, 39(4):470～481(in Chinese with English abstract).

[37] Bigwaard H, Sjakman, Win. Closing the gap between regional and global travel tomography [J]. Journ. Geoph. Res, 1998, 103: 30055～30078.

[38] Xu Z QJiang M, Yang J S. *et al*. Mantle diapir inward intracontinental subduction: A discussion on the mechanism of uplift of the Qinghai-Tibet plateau [J]. Geological Society of America, Special Paper, 1999, 328: 19～31.

[39] Dewey J F. Orogeny can be very short [J]. Proceeding of the National Academy of Sciences, 2005, 102: 15286～15293.

[40] Hyndman R D, Currie C A, Mazzotti S P. Subduction zone backarcs, mobile belts, and orogenic heat[J]. GSA Today, 2005, 15(15): 4～10.

[41] Van der Voo R, Spakman W, Bijwaad H. Mesozoic subducted slabs under Siberia [J]. Nature, 1999, 397: 246～249.

[42] Pognante U, Spencer D A. First record of eclogites from the High Himalayan belt, Kaghan valley(northern Pakistan) [J]. Eur. J. Mineral., 1991, 3(3): 613～618.

[43] Guillot S, de Sigoyer J, Lardeaux J M, *et al*. Eclogitic metasediments from the Tso Morari area (Ladakh, Himalaya): Evidence for continental subduction during India-Asia convergence[J]. Contrib. Mineral. Petrol., 1997, 128: 197～212.

[44] David G Howell. Terrane Tectonics-Mountain Building Continental Growth? [M]. 1983.

[45] 郭令智，施央申，马瑞士．论地体构造-板块构造理论研究的最新问题[J]．中国地质科学院院报，1984，(10)：27～34.

Guo Lingzhi, Shi Yangshen, Ma Ruishi. On terrane-A latest concept in the study of plate tectonics[J]. Bulletin of the Chinese Academy of Geological Sciences, 1984, (10): 27～34(in Chinese with English abstract).

[46] Cong B L. Ultrahigh-Pressure Metamorphic Rocks in the Dabieshan-Sulu Region of China[M]. Beijing: Science Press, 1996. 1～224.

[47] Liou J G, Zhang R Y, Ernst W G, *et al*. High-pressure minerals from deeply subducted metamorphic rocks. In: Ultrahigh-pressure mineralogy: physics and chemistry of the Earth's deep interior[A]. In: Hemley R J (ed.). Reviews in Mineralogy[C]. Washington D. C.: Mineralogical Society of America, 1998. 37: 33～96.

[48] 杨经绥，宋述光，许志琴，等．柴北缘早古生代高压-超高压变质带发现典型超高压矿物——柯石英[J]．地质学报，2001，75(2)：175～179.

Yang Jingsui, Song Shuguang, Xu Zhiqin, *et al*. Discovery of Coesite in the North Qaidam Early Paleozoic ultrahigh-high pressure(UHP-UHP) metamorphic belt, NW China [J]. Acta Geoscientica Sinica, 2001, 75(2): 175～179(in Chinese with English abstract).

[49] 杨经绥，许志琴，李海兵，等．柴北缘地区榴辉岩的发现及潜在的地质意义[J]．科学通报，1998，43(14)：1544～1549.

Yang Jingsui, Xu Zhiqin, Li Haibing, *et al*. Discovery of Eclogite in the North Qaidam and its geological significance [J]. Chinese Science Bulletin, 1998, 43(14): 1544～1549 (in Chinese with English abstract).

[50] 杨经绥，许志琴，宋述光，等．青海都兰地区榴辉岩的发现及对中国中央造山带高压-超高压变质带研究的意义[J]．地质学报，2000，74(2)：156～168.

Yang Jingsui, Xu Zhiqin, Song Shuguang, *et al*. Discovery of Eclogite in Dulan, Qinghai Province and its significance for studing the HPUHP metamorphic belt along the central orogenic belt of China[J]. Acta Geoscientica Sinica, 2000, 74(2): 156～168(in Chinese with English abstract).

[51] 张建新，张泽明，许志琴，等．阿尔金构造带两段榴辉岩的 Sm-Nd 及 U-Pb 年龄——阿尔金中加里东期山根存在的证据[J]．科学通报，1999，44(10)：1109～1112.

Zhang Jianxin, Zhang Zeming, Xu Zhiqin, *et al*. The ages of Sm-Nd and U-Pb of eclogite from the west Altyn tectonic belt [J]. Chinese Science Bulletin, 1999, 44 (10): 1109～1112 (in Chinese with English abstract).

[52] 张建新，杨经绥，许志琴，等．柴北缘榴辉岩的峰期和退变质年龄：来自 U-Pb 及 Ar-Ar 同位素测定的证据[J]．地球化学，2000，29(3)：217～222.

Zhang Jianxin, Yang Jingsui, Xu Zhiqin, *et al*. Peak and retrograde age of eclogites at the northern margin of Qaidam basin, northwestern China: Evidences from U-Pb and Ar-Ar dates [J]. Geochimica, 2000, 29(3): 217～222(in Chinese with English ab stract).

[53] 张建新，杨经绥，许志琴，等．阿尔金榴辉岩中超高压变质作用证据[J]．科学通报，2002，47(3)：231～234.

Zhang Jianxin, Yang Jingsui, Xu Zhiqin, *et al*. Evidence of UHP metamorphism in eclogite of Altyn mountain [J]. Chinese Science Bulletin, 2002, 47 (3): 231～234.

[54] Xu Zhiqin, *et al*. Abstract for AGU Fall Meeting. 2005.

[55] Xu Zhiqin, Yang Jingsui, Wu Cailai, *et al*. Timing and mechanism of formation and exhumation of the Northern Qaidam ultrahighpressure metamorphic belt [J]. JAES, 2006(in press).

[56] Chemenda A I, Burg P, Mattauer M. Evolutionary model of the Himalaya-Tibet system: geopoem based on new modeling, geological and geophysical data[J]. Earth Planet. Sci. Lett. 2000, 174: 397～409.

[57] 李才,翟庆国,程立人,等. 青藏高原羌塘地区几个关键地质问题的思考 [J]. 地质通报, 2005, 24(4): 295～301.
Li Cai, Zhai Qingguo, Cheng Liren, *et al*. Thought on some key geological problems in the Qiangtang area, Qinghai-Tibet plateau [J]. Geological Bulletin of China, 2005, 24(4): 295～301 (in Chinese with English abstract).

[58] Gradstein F M, Ogg J G, Smith A G, *et al*. A Geologic Time Scale[M]. New York: Columbia University Press, 2004.

[59] 夏林圻,夏祖春,徐学义. 北祁连山海相火山岩岩石成因[M]. 北京: 地质出版社, 1996.
Xia Linqi, Xia Zuchun, Xu Xueyi. Genetic Environments of Early Paleozoic Marine Volcanics of North Qilian [M]. Beijing: Geological Publishing House, 1996(in Chinese with English abstract).

[60] 史仁灯,杨经绥,吴才来,等. 北祁连玉石沟蛇绿岩形成于晚震旦世的 SHRIMP 年龄证据[J]. 地质学报, 2004b, 78(5): 649～657.
Shi Rendeng, Yang Jingsui, Wu Cailai, *et al*. First SHRIMP dating for the formation of the Late Sinian Yushigou ophiolite, North Qilian mountains [J]. Acta Geoscientica Sinica, 2004b, 78(5): 649～657(in Chinese with English abstract).

[61] 刘良,车自成,王焰,等. 阿尔金高压变质带的特征及其构造意义[J]. 岩石学报, 1999, 15(1): 57～64.
Liu liang, Che Zicheng, Wang Yan, *et al*. Characters and tectonic significance of Altun high pressure metamorphic belt [J]. Acta Petrologica Sinica, 1999, 15(1): 57～64(in Chinese with English abstract).

[62] 史仁登,杨经绥,吴才来,等. 柴北缘超高压变质带中的岛弧火山岩[J]. 地质学报, 2004, 78(1): 53～64.
Shi Rendeng, Yang Jingsui, Wu Cailai, *et al*. Island arc volcanic rocks in the north Qaidam UHP metamorphic belt[J]. Acta Geoscientica Sinica, 2004, 78(1): 53～64(in Chinese with English abstract).

[63] 肖序常,王军,苏犁,等. 再论西昆仑库地蛇绿岩及其构造意义[J]. 地质通报, 2003, 22(10): 745～750.
Xiao Xuchang, Wang Jun, Su Li, *et al*. A further discussion of the Kuda ophiolite, West Kunlun, and its tectonic significance [J]. GeoLogical Bulletin of China, 2003, 22(10): 745～750 (in Chinese with English abstract).

[64] 许志琴,徐惠芬,张建新,等. 北祁连走廊南山加里东俯冲杂岩石地体及动力学[J]. 地质学报, 1994, 69(1): 1～14.
Xu Zhiqin, Xu Huifen, Zhang Jianxin, *et al*. The Zhoulangnanshan Caledonian subductive complex in the northern Qilian Mountains and its dynamics [J]. Acta Geologica Sinica, 1994, 69(1): 1～14(in Chinese with English abstract).

[65] Xu Z Q, Zhang J X, Li H B. Architecture and orogeny of the Northern Qilian Orogenic Belt, Northwestern China[J]. Journal of the Geological Society of China, 2000, 43: 125～141.

[66] 李怀坤,陆松年,赵凤清,等. 柴达木北缘新元古代重大地质事件年代格架[J]. 现代地质, 1999, 13(2): 224～225.
Li Huaikun, Lu Songnian, Zhao Fengqing, *et al*. Geochronological framework of the Neoproterozoic major geological events in the northern margin of the Qaidam basin [J]. Geoscience, 1999, 13(2): 224～225(in Chinese with English abstract).

[67] Yang J S, Xu Z Q, Li H B, *et al*, A Caledonian convergent border along the Qilian terraine, NW China: Evidence From eclogite, garnet-peridotite, ophiolite, and S-type granite[J]. J. of the Geological Society of China, 2000, 43(1): 142～160.

[68] Sengor A M Celai. Tethyan evolution of Turkey: A plate tectonic approach[J]. Tectonophysics, 1981, 75(3－4): 181～190.

[69] Sengor A M Celai, Plate tectonics and orogenic research after 25 years: A Tethyan Perspwetive [J]. Earth-Sacience Reviews, 1990, 27(1·2): 1～34.

[70] 姜春发,杨经绥,冯秉贵,等. 昆仑开合构造[M]. 北京: 地质出版社, 1992.
Jiang Chunfa, Yang Jingsui, Feng Binggui, *et al*. Opening-Closing Tectonics of Kunlun Mountains [M]. Beijing: Geo-

logical Publishing House, 1992(in Chinese with English abstract).

[71] Yang J S, Robison P T, Jiang C F, *et al*, Ophiolites of the kunlun Mountains, China and their tectonic implications[J]. Tectonophysics, 1996, 258:215~231.

[72] 杨经绥,王希斌,史仁灯,等. 青藏高原北部东昆仑南缘德尔尼蛇绿岩:一个被支解了的古特提斯洋壳[J]. 中国地质,2004,31(3):226~229.
Yang Jingsui, Wang Xibin, Shi Rendeng, *et al*. The Dur'ngoi ophiolite in East Kunlun, northern Qinghai-Tibet Plateau: a fragment of paleo-Tethyan oceanic crust [J]. Geology in China, 2004, 31(3):226~229(in Chinese with English abstract).

[73] 许志琴,侯立玮,王宗秀,等. 中国松潘-甘孜造山带的造山过程[M]. 北京:地质出版社, 1992. 1~190.
Xu Zhiqin, Hou Liwei, Wang Zongxiu, *et al*. Orogenic Processes of the Songpan-Garze Orogenic Belt of China [M]. Beijing: Geological Publishing House, 1992. 1~190(in Chinese with English abstract).

[74] 刘福来,许志琴,宋彪. 苏鲁地体超高压和退变质时代的厘定:来自片麻岩锆石微区 SHRIMP U-Pb 定年的证据[J]. 地质学报,2003,77 (2): 229~237.
Liu Fulai, Xu Zhiqin, Song Biao. Determination of UHP and retrograde metamorphic ages of the Sulu Terrane: Evidence from SHRIMP U-PB dating on zircons of gneissic rocks [J]. Acta Geo logical Sinica, 2003,77(2):229~237(in Chinese with English abstract).

[75] 郑来林,廖光宇,耿全如,等. 墨脱县幅地质调查新成果及主要进展[J]. 地质通报,2004,23(5~6):458~462.
Zheng Lailin, Liao Guangyu, Geng Quanru, *et al*. New results and major progress in regional geological survey of the Medog County sheet[J]. Geological Bulletin of China, 2004,23(5~6): 458~462 (in Chinese with English abstract).

[76] 潘桂棠,王立全,朱弟成. 青藏高原区域地质调查中几个重大科学问题的思考[J]. 地质通报,2004, 23(1): 12~19.
Pan Guitang, Wang Liquan, Zhu Dicheng. Thoughts on some important scientific problems in regional geological survey of the Qinghai-Tibet Plateau [J]. Geological Bulletin of China, 2004, 23 (1): 12~19(in Chinese with English abstract).

[77] Hodges K V, Geissman J W E, Glazner A F E. Tectonics of the Himanaya and southern Tibet from two perspectives. Special focus on the Himalaya[J]. Geol. Soc. Am. Bull., 2000, 112:324~350.

[78] 许志琴,杨经绥,梁凤华,等. 喜马拉雅地体的泛非-早古生代造山时间年龄记录[J]. 岩石学报,2005,21 (1): 1~12.
Xu Zhiqin, Yang Jingsui, Liang Fenghua, Pan-African and Early Palewozoic orogenic events in the Himalaya terrane: Inference from SHRIMP U-Pb zircon ages [J]. Acta Petrologica Sinica, 2005, 21(1):1~12(in Chinese with English abstract).

[79] 任纪舜,肖黎薇. 1:25 万地质填图进一步揭开了青藏高原大地构造的神秘面纱[J]. 地质通报,2004,23(1): 1~11.
Ren Jishun, Xiao Liwei. Lifting the mysterious veil of the tectonics of the Qinghai-Tibet plateau by 1:250000 geological mapping[J]. Geological Bulletin of China, 2004, 23(1):1~11 (in Chinese with English abstract).

[80] Molnar P. A review of geophysical constraints on the deep structure of the Tibetan Plateau, the Himalaya and the Karakoram, and their tectonic implications[J]. Phil Trans R Soc Lond, 1988, A326:33~88.

[81] Gansser A. Geology of the Himalayas[M]. London: Wiley Interscience, 1964. 289.

[82] Powell C Mc A, Conaghan PJ. Plate tectonics and the Himalayas [J]. Earth and Planetary Science Letters, 1973, 20: 1~12.

[83] Avouac J-P, Tapponnier P. Kinematic model of active deformation in central Asia[J]. Geophys, Res. Lett., 1993, 20: 895~898.

[84] Patriat P, Achache J. India-Eurasia collision chronology has implications for crustal shortening and driving mechanisms of plates [J]. Nature, 1984, 311: 615~621.

[85] Tapponnier P, Meyer B, Avouac J P. Active thrusting and folding in the Qilian Shan, and decoupling between upper crust and mantle in northeastern Tibet[J]. Earth Planet Sci. Lett., 1990, 97:382~403.

[86] Mattauer M. La tectonique sous les plaques [J]. Science (Edition Francaise de Scientific American), 2002, 295:70~75.

[87] Van der Voo R, Spakman W, Bijwaard H. Tethyan subducted slabs under India [J]. Earth Planet. Sci. Lett., 1999, 171:7~20.

[88] 许志琴,杨经绥,姜枚,等. 大陆俯冲作用及青藏高原周缘造山带的崛起[J]. 地学前缘, 1999,6(3): 139~151.
Xu Zhiqin, Yang Jingsui, Jiang Mei, *et al*. Continental subduction and uplifting of the orogenic belts at the margin of the Qinghai Tibet plateau [J]. Earth Science Frontiers, 1999,6 (3): 139~151 (in Chinese with English abstract).

[89] 许志琴,杨经绥,戚学祥. 印度/亚洲碰撞——SN 向和 EW 向拆离构造与喜马拉雅造山机制的再讨论[J]. 地质通报,2006,25(1~2):1~14.
Xu Zhiqin, Yang Jingsui, Qi Xuexiang. India/Asia collision——A fruther discussion of N-S-and E-W-directed detachements and Himalaya orogenic mechanism [J]. Geological Bulletin of China, 2006,25(1~2): 1~14 (in Chinese with English abstract).

[90] Tapponnier P, Peltzer G, Le Dain Y, *et al*. Propagating extrusion tectonics in Asia: New insights from simple experiments with plasticine[J]. Geology, 1982,10:611~616.

[91] Peltzer G, Tapponnier P. Formation and evolution of strike slip faults, rifts, and basins during the India-Asia collision: An experimental approach[J]. Journal of Geophysical Research; 1988,93(12):1508~1517.

[92] Peltzer G, Tapponnier P, Gaudemer Y. Offsets of late Quaternary morphology, rate of slip and recurrence of large earthquakes on the Changma Fault[J]. J. Geophys. Res., 1988b, 93:7793~7812.

[93] Avouac J-P, Tapponnier P. Kinematic model of active deformation in central Asia[J]. Geophys, Res. Lett., 1993,20: 895~898.

[94] Tapponnier P, Xu Zhiqin, Roger F, *et al*. Oblique stepwise rise and growth of the Tibet plateau[J]. Sciences, 2001, 294: 1671~1677.

[95] 许志琴,李海兵,杨经绥,等. 东昆仑山南缘大型转换挤压构造带和斜向俯冲作用[J]. 地质学报,2001, 75(2): 156~164.
Xu Zhiqin, Li Haibing, Yang Jingsui, *et al*. A Large transpression zone at the south margin of the east Kunlun mountains and oblique subduction [J]. Acta Geoscientica Sinica, 2001, 75(2): 156~164 (in Chinese with English abstract).

[96] 李海兵,杨经绥,许志琴,等. 阿尔金断裂带印支期走滑活动的地质纪年代学证据[J]. 科学通报,2001,46(16): 1333~1338.
Li Haibing, Yang Jingsui, Xu Zhiqin. Geological and chronological evidence of Indo-Chinese strike-slip movement in the Altyn Tagn fault zone[J]. Chinese Science Bulletin, 2001, 46(16): 1333~1338(in Chinese with English abstract).

[97] Tapponnier P, Molnar P. Active faulting and tectonics in China [J]. J. Geophys, Res., 1977,82:2905~2930.

[98] 邓起东,张维歧,张培震,等. 海源走滑断裂带及其尾端挤压构造[J]. 地震地质, 1989,11(1): 1~14.
Deng Qidong, Zhang Weiqi, Zhang Peizhen, *et al*. Haiyuan strikeslip fault zone and its compressional structures of the End [J]. Seismology and Geology, 1989,11(1)1~14 (in Chinese with English abstract).

[99] 许志琴,杨经绥,张建新,等. 阿尔金断裂两侧构造单元的对比及岩石圈剪切机制[J]. 地质学报, 1999, 73(3): 193~205.
Xu Zhiqin, Yang Jingsui, Zhang Jianxin, *et al*. A comparison between the tectonic units on the two sides of the Altun sinistral strike-slip fault and the mechanism of lithospheric shearing[J]. Acta Geoscientica Sinica, 1999b, 73(3):193~205(in Chinese with English abstract).

[100] Matte Ph, Tapponnier P, Arnaud N, *et al*. Tectonics of Western Tibet between the Tarim and Indus[J]. Earth and Planet. Sci. Lett. 1996,142: 311~330.

[101] 李海兵,Valli F,许志琴,等. 喀喇昆仑断裂的变形特征及构造演化[J]. 中国地质,2006,33(2): 239~255.
Li Haibing, Valli F, Xu Zhiqin, *et al*. Deformation and tectonic evolution of the Karakorum Fault, Western Tibet [J]. Geology in China, 2006,33(2):239~255.(in Chinese with English abstract).

[102] 姜枚,许志琴,薛光琦,等. 青海茫崖-新疆若羌地震探测剖面及其深部构造研究[J]. 地质学报, 1999,73(2): 153~161.
Jiang Mei, Xu Zhiqin, Xue Guangqi, *et al*. Seismic profiling between Mangnai, Qinghai and Ruoqiang, Xinjiang and infrastructure study[J]. Acta Geoscientica Sinica, 1999,73(2):153~161 (in Chinese with English abstract).

[103] Jiang Mei, Qian Hui, *et al*. Telesesismic anisotropy and its features in the upper mantle beneath the Tibet plateau and neighboring areas[J]. Metallogenic Implications Global Tectonics and Metallogeny, 2003, 8(1－4): 1～2.

[104] Wittinger G, Masson F, Poupinet G, *et al*. Seismic tomography of northern Tibet and Kunlun: Evidence for crustal blocks and mantle velocity contests [J]. Earth Planet Sci, Lett, 1996, 139: 263～279.

[105] Wittinger G F, Tapponier P, Poupinet G, *et al*. Tomographic evidence for localized lithospheric shear along the Altyn Tagh fault[J]. Science, 1998. 74～76.

[106] 许志琴，姜枚，杨经绥，等．青藏高原的地幔结构：地幔羽，地幔剪切带及岩石圈俯冲板片的拆沉[J]．地学前缘，2004, 11(4): 329～343.

Xu Zhiqin, Jiang Mei, Yang Jingsui, *et al*. Mantle structure of Qinghai-Tibet Plateau: Mantle plume, mantle shear zone and delamination of lithospheric slab [J]. Earth Science Frontiers, 2004, 11 (4): 329～343(in Chinese with English abstract).

[107] Grandt S P, *et al*. Global seismic tomography: a snapshot of convection in the Earth[J]. Nature, 1997, 386: 578～584.

[108] Widiyantoro S, Van der Hils R D T. The slab of subducted lithosphere beneath the Sunda arc, Indonesia [J]. Science, 1996, 271: 1566～1570.

[109] Molnar P. A review of geophysical constraints on the deep structure of the Tibetan Plateau, the Himalaya and the Karakoram, and their tectonic implications [J]. Phil Trans R Soc Lond, 1988, A326: 33～88.

[110] Beghoul N, Barazangi M, Isacks B L. Lithospheric structure of Tibet and western north America: mechanisms of uplift and a comparative study [J]. Journal of Geophysical Research, 1993, 98: 1997～2016.

[111] Hirn A, Jiang M, Sapin M, *et al*. Seismic anisotropy as an indicator of mantle flow beneath the Himalayas and Tibet [J]. Nature 1995, 375: 571～574.

[112] Zhao W J, Nelson K D and Project INDEPTH Team. Deep seismic reflection evidence for continental underthrusting beneath southern Tibet[J]. Nature, 1993, 366: 557～559.

[113] O'Brien PJ, Zotv N, Law R, *et al*. Coesite in Himalayan eclogite and implications for models of India-Asia collision [J]. Geology, 2001, 29: 435～438.

[114] 许志琴，曾令森，杨经绥，等，走滑断裂、"挤压性盆山构造"与油气资源关系的探讨[J]．地球科学，2004, 29(6): 631～643.

Xu Zhiqin, Zeng Lingsen, Yang Jingsui, *et al*. Role of large-scale strike-slip faults in the formation of petroleum-bearing compressional basin-mountain range systems[J]. Earth Science-Journal of China University of Geosciences, 2004, 29 (6): 631～643(in Chinese with English abstract).

The Qinghai-Tibet plateau and continental dynamics: A review on terrain tectonics, collisional orogenesis, and processes and mechanisms for the rise of the plateau

XU Zhi-qin YANG Jing-sui, LI Hai-bing,
ZHANG Jian-xin, ZENG Ling-sen, JIANG Mei
(Key Laboratory for Continental Dynamics, MLR, Institute of Geology,
Chinese Academy of Geological Sciences, Beijing 100037, China)

Abstract Recent studies on the compositions and structures of multiple terrains within the Qinghai-Tibet plateau have offered us an opportunity to examine how this plateau was assem-

bled in the context of terrain tectonics. The formation of this plateau resulted from long-term tectonic activities since the late Paleozoic which is represented by (1) convergence and welding of a number of exotic terrains, and (2) collision induced "orogenic plateaux" and has reached its climax in the Cenozoic. Large-scale strike-slip faults (commonly act as terrain boundary faults) has played a central role in controlling the relative offset, magnitude of lateral extrusion, and the geometry of these terrains. The final assembly and rise of the Qinghai-Tibet plateau may result from a combination of contemporaneous processes, e.g. super-deep subduction (>600km) at its southern margin, intra-continental subduction at its northern margin, inland deep thermal processes, and NE-trending right lateral uplift of mantle lithosphere.

Key words Qinghai-Tibet Plateau "non-in-situ" terrane assembly compounding-collisional orogeny strike-slip structure multi-component driving force

About the first author: XU Zhi-qin, female, born in 1941, received a doctor degree in France, academician of the Chinese Academy of Sciences, her research interests include tectonics and structural geology; E-mail: xzq@ccsd.org.cn.

造山的高原——青藏高原巨型造山拼贴体和造山类型❶

许志琴　李海兵　杨经绥

（中国地质科学院　地质研究所　国土资源部大陆动力学重点实验室　北京　100037）

摘　要　青藏高原是一个巨型碰撞造山拼贴体，它的形成与始特提斯、古特提斯和新特提斯洋盆的先后开启、消减、闭合以及古大陆的裂解、诸地体的移动、会聚和拼合有关。造山类型形成于不同时期海（洋）盆俯冲、地体碰撞和陆内会聚的不同阶段。多地体/多岛弧/多弧前海的构架表明，诸多的俯冲型山链可以产生在地体边界的活动陆缘一侧，古特提斯南、北两洋盆的双向俯冲构筑了双向俯冲型山链；碰撞型山链由于地体边界与块体驱动方向的几何学关系形成"正向碰撞型"和"斜向碰撞型"造山类型。"斜向碰撞型山链"与走滑断裂的形成、规模及其运动学直接相关。50～60Ma 印度/亚洲碰撞不仅形成青藏高原造山拼贴体的最后成员——喜马拉雅山链，而且在拼贴体的北缘由于陆内俯冲作用使早期形成的山链在整修后又一次崛起。青藏高原的周缘山链铸成屏障与外侧的克拉通相隔。青藏高原巨型碰撞造山拼贴体的形成是亚洲大陆自北往南的增生和造山迁移的生长结果，其所反映的活动长期性、非原地性、俯冲/碰撞/陆内造山类型的多样性、碰撞造山的多期性以及造山的复合叠置性比世界上任何一个复合山链（或造山拼贴体）来得复杂、多彩。

关键词　造山的高原　青藏高原　巨型造山拼贴体　造山类型

中图分类号：P54　　**文献标识码**：A　　**文章编号**：1005－2321(2006)04－0001－17

0　前言

造山作用是形成山脉的过程[1]，100 多年来研究山链的专家一直认为造山作用是构造的起源，而不是指山脉地形的起伏[2]。造成山链的构造作用过程，包括地壳上部的褶皱、逆掩和断裂以及下部的塑性变形、变质和深成岩浆活动，并认为造山运动发生于较短时间，在一条线性地带内发生了强烈变形。20 世纪 60 年代以来板块构造理论赋予"造山作用"新的内涵，把大陆山链的造山过程看作岩石圈板块相互运动和作用的表征。板块之间的运动通过三种类型（离散型、会聚型和转换型）的边界进行，造山"形变"只发生在会聚板块边缘的窄

❶　地学前缘，2006 年第 13 卷第 4 期。

收稿日期：2006－05－22。

基金项目：国土资源部科技专项（2001010101）；中国地质调查局重点项目（200313000058）

作者简介：许志琴（1941　　），女，研究员，中国科学院院士，构造地质学专业，主要从事显微构造、大地构造和大陆动力学研究，长期从事青藏高原构造研究工作。

部。威尔逊把板块构造引入造山作用中,强调了造山运动的三维观念:洋脊的拉张、原始山链的挤压及两侧的旋转,并根据北美科迪勒拉山的造山特征,认为造山带可借助走滑断层将大量较小的"碎块"聚集起来重新分布而形成[3]。

20 世纪 70 年代以来,致力于大陆山链研究的地质学家通过山链实体解剖,发现造山形变不限于会聚板块边缘的窄带,而可以扩展到板内达数百乃至上千千米的宽域。地质学家发现,造山作用涉及大范围的陆壳变形、变质及花岗岩浆活动,可以发生在板块碰撞前的俯冲期(俯冲型山链)、主碰撞期(碰撞型山链)及后碰撞期(陆内型山链)。Mattauer(1980)[4]按板块运动阶段曾把山链划分为"俯冲型"(即安第斯型)、"仰冲型"(阿曼型)、"碰撞型"(喜马拉雅-阿尔卑斯型)及"陆内型";许志琴(1994)[5]曾根据构造造型划分"滑脱型"、"挤压型"、"叠覆型"、"平移型"和"热隆伸展型"山链。

Sergor(1987)[6],曾认为,大量会聚板块边界在时空活动中形成的众多的造山带组成造山区,这种造山区可以用"造山拼贴体"(orogenic collage)[7]术语来描述。许志琴(1987,1994)[5,8]在研究中国造山带时曾认为中国的某些山链经历了长期的地质历史演化过程,形成"复合"山链。"复合"的含义包括"增生"和"叠置"两个方面;又将复合山链划分为"增生型复合山链"、"双向型复合山链"及"叠覆型复合山链"。

研究表明,世界上许多造山带是长期活动(>300Ma)的复合造山带,活动域的宽度可超过 1000km,是大陆生长的最好见证。近 10 年来,对全球造山带的研究已由单一造山带向复合造山带研究深入,复合造山带是大范围、多期和多造山类型相互作用的结果。

复合造山带长期活动的原因、大陆增生机制、造山带的流变学结构和造山热对造山作用的控制等已成为当前大陆动力学研究的关键科学问题。

近 10 年来,对"俯冲型"山链的研究又有了新的进展。在许多山链中,地质学家发现由剪断的大陆碎片和肢解的俯冲蛇绿岩、混杂堆积、高压-超高压变质带组成的俯冲杂岩带的上部(活动陆缘),发育由弧前增生楔、钙碱性火山岛弧系及弧后盆地组成的活动陆缘增生带。不同成因块体的活动陆缘可以形成不同的陆缘增生带,其形成均早于大陆块体之间的碰撞界限——缝合带,并且在很多的情况下,俯冲上盘的陆缘增生带未固结物质对于上部板块的变形及造山带的形成起重要的作用[9]。譬如南美的安第斯山链、北美科迪勒拉山以及亚洲东南部菲律宾马尼亚拉地带均有弧前增生带。其中南美的安第斯山不存在多岛弧的增生,以巨型火山岛弧岩浆带为主体,是南太平洋向东俯冲于南美板块之下形成的俯冲型山链。而东南亚洲在第三纪时期以来经历了小的块体与亚洲大陆长时间会聚和对接的增生历史,对接过程包括边缘盆地的不断打开、多岛弧的增生和上部俯冲板片的缩短[9]。Sengor(1996)[10]在研究中亚阿尔泰(Altaids)碰撞造山系时提出"中亚型"或"土耳其型"山链类型,认为在此山链中,一个或两个大陆的前碰撞历史包含了大规模的俯冲加积杂岩的形成,在俯冲加积杂岩中岩浆弧轴迁移,并致使大陆不断增生扩大。因此俯冲带上部遭受了包括俯冲增生历史在内的前碰撞的演化,并形成俯冲型山链,是研究俯冲过程、俯冲极性和活动陆缘增生历史以及前碰撞山链的最佳场所。

地球上的许多山链构筑在俯冲板块(被动陆缘)一侧,被动陆缘伸展盆地中的沉积盖层和变质基底在板块碰撞过程中遭受强烈的变形,形成碰撞型山链。典型的例子是位于非洲-意大利板块下部的欧洲俯冲板块一侧的阿尔卑斯山链和位于亚洲板块下部的印度俯冲板块一侧的喜马拉雅山链,这是由叠覆逆冲岩片组成的具陆壳增生楔结构特征的"阿尔卑斯-喜

马拉雅”型碰撞造山带。研究表明，俯冲型山链在板块碰撞后与碰撞型山链拼贴在一起，往往通过弧/陆碰撞→陆/陆碰撞的方式，形成“俯冲-碰撞型”山链。有些弧/陆碰撞引起的造山变形过程本身可能是短暂的，如欧洲英国-爱尔兰加里东造山带的弧/陆碰撞造山作用从大陆边缘俯冲开始到前碰撞缩短的结束只持续了 18Ma，碰撞造山缩短和变质演化延续了 8Ma，地壳拉伸和下地壳折返延续 1.5Ma，俯冲极性反转后的造山缩短为 4.5Ma[11]。

研究还发现在板块碰撞之后可以继续造山（后造山）或者在远离缝合带的地区造山。这种陆内造山活动突出表现为山脉的剧烈隆升，产生新的逆冲、走滑构造并伴随着强烈的岩浆和变质作用，出现地壳尺度的伸展-剥离以及山体抬升和塌陷。

青藏高原是地球上最大、最高和最年轻的高原，青藏高原形成的基础背景比世界上其他的许多高原都来得复杂，比如，北美的科罗拉多高原构筑在稳定的古生代地台之上，法国中央高原的基础是欧洲华力西造山带。而青藏高原是在新元古代以来长期活动、多期造山及新生代最后隆升的基础上形成的高原，经历了显生宙以来洋盆不断消减和闭合，是诸地体（或陆块）不断会聚、碰撞和增生的产物，具有“多陆块、多岛弧”组成的基本格架及显示“多洋（海）盆、多俯冲、多碰撞和多造山”的动力学作用过程。不同历史阶段洋盆的开启和闭合致使地体会聚和碰撞，多地体拼合构筑成复合地体，地体间的碰撞产生碰撞造山带，碰撞造山带的拼合及叠置又形成复合碰撞造山拼贴体。因此青藏高原形成的基础是经过长期拼合的复合地体和复合的造山拼贴体，而在其周缘又被再崛起的造山带所包围，因此有人称青藏高原为“造山作用的高原”（orogenic plateau）[11]。

青藏高原在长期地质历史演化中，形成不同时期从俯冲、碰撞到陆内各种造山类型组成的山链和复合山链，青藏高原的造山类型之多样及丰富称得上是世界造山类型之大全。识别这些丰富的造山类型并与世界上典型的造山类型对比，是研究碰撞动力学的重要内容。本文将通过青藏高原形成过程中不同时期、不同阶段造山类型和造山作用、造山机制的解析，来说明青藏高原为什么是个造山的高原。

1 高原基本地体构架

研究表明，组成青藏高原的诸多陆块和复合陆块并非原位，它们均来自靠近冈瓦纳大陆的一侧[12~13]。陆块之间的会聚及俯冲使陆块消减，在地体碰撞过程中形成的大型剪切带及大型断裂的作用使陆块或复合陆块叠覆、错位、挤出和远离原地，后期大型盆地的形成又使块体和复合块体的原型遭到覆盖。因此，青藏高原的关键问题已不仅是 50～60Ma 以来印度和亚洲碰撞形成高原以及引起波及大陆岩石圈数千千米变形，再造巨大的地体拼合体和碰撞造山拼贴体的形成、地体之间的相互作用及大陆增生的地质历史过程，成为青藏高原研究的重要内容。其包括了组成各陆块单元的古地理位置、原型、归属和特征，古洋盆的开启及消减，陆块之间相互运动的轨迹、拼合与叠置的方式，碰撞造山类型、过程、造山叠置以及造山的机制；大型走滑构造的形成和对青藏高原结构的改造，以及深部结构、壳幔相互作用和驱动力等。青藏高原所具有的十分复杂的地壳-岩石圈流变学特征给青藏高原形成历史及动力学机制研究带来了极大的困难。

印度/亚洲前碰撞历史是从新元古代开始的长期活动历史，经历了早古生代、晚古生代—三叠纪和晚中生代的地体会聚的三个阶段，和泥盆纪、晚三叠世和晚侏罗—早白垩世的多期

撞造山事件。由于印度/亚洲前碰撞历史是以诸多地体的会聚为特征,因此通过地体结构及地体边界的研究以及各时期地体边界两侧陆壳的变形特征和动力学过程的揭示,研究青藏高原形成前诸地体与亚洲北部逐渐拼合和大陆增生的过程。50～60Ma 印度/亚洲的最后碰撞,不仅增生了喜马拉雅地体,而且使亚洲大陆发生向东与南东的挤出以及形成内部高原地貌和周缘新生代造山带的两个新的大地构造单元。

青藏高原大地构造单元组成可分为三大部分:①青藏高原北部"阿尔金-祁连-昆仑"早古生代复合地体;②青藏高原腹地"松潘甘孜-羌塘-拉萨"中生代复合增生地体;③青藏高原南部喜马拉雅新生代增生地体。①和②组成印度/亚洲前碰撞的"青藏联合陆块"构架,③为 60～50Ma 印度/亚洲碰撞的最后拼接体[14](图 1)。

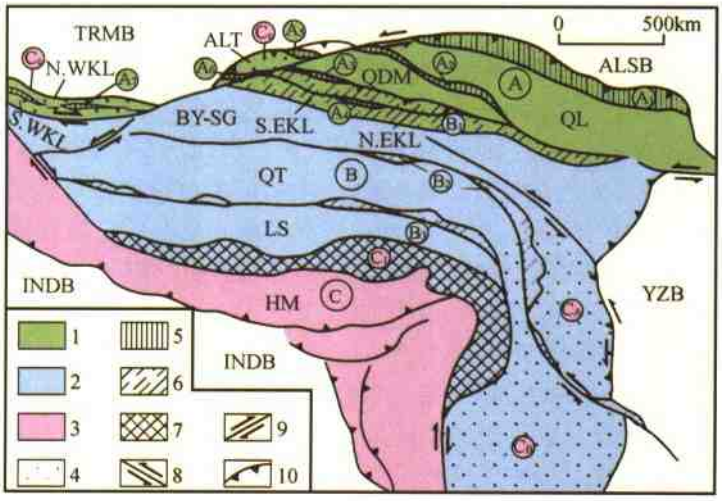

图 1　青藏高原结构图

(据许志琴等,2006)

Fig. 1　Structural architecture of the Qinghai-Tibet plateau

1—早古生代复合地体;2—中生代增生复合地体;3—新生代增生地体;4—挤出-移置地体;5—早古生代俯冲杂岩带和活动陆缘带;6—中生代俯冲杂岩带和活动陆缘带;7—晚中生代—早新近纪俯冲杂岩带和活动陆缘带;8—左行走滑断裂;9—右行走滑断裂;10—逆冲断裂

地体组成:A—阿尔金-祁连-昆仑早古生代复合地体;QL—祁连地体,QDM—柴达木地体,N. EKL—东昆仑北地体,S. EKL—东昆仑南地体,ALT—阿尔金地体,N. WKI—西昆仑北地体,S. WKL—西昆仑南地体;B—松潘甘孜-羌塘-拉萨增生复合地体;BY-SG—巴颜喀拉-松潘甘孜地体,QT—羌塘地体,LS—拉萨地体;C—青藏高原周缘增生、挤出、移置地体;HM—喜马拉雅增生地体;C_A—云南挤出地体;C_B—掸邦挤出地体,C_C—阿尔金-西昆仑移置地体

地体边界:A_1—北祁连早古生代俯冲杂岩带和活动陆缘带,A_2—柴达木北缘早古生代俯冲杂岩带和活动陆缘带,A_3—祁漫塔格早古生代俯冲杂岩带和活动陆缘带,A_4—昆中早古生代俯冲杂岩带和活动陆缘带,A_5—北阿尔金早古生代俯冲杂岩带和活动陆缘带,A_6—南阿尔金早古生代俯冲杂岩带和活动陆缘带,A_7—库地早古生代俯冲杂岩带和活动陆缘带;B_1—东昆仑-阿尼玛卿三叠纪俯冲杂岩带和活动陆缘带,B_2—金沙江三叠纪俯冲杂岩带和活动陆缘带;B_3—班公湖-怒江中生代俯冲杂岩带和活动陆缘带;C_1—雅鲁藏布江俯冲杂岩带和冈底斯活动陆缘带

INDB—印度陆块,YZB—扬子陆块;ALSB—阿拉善陆块;TRMB—塔里木陆块

青藏高原北部"阿尔金-祁连-昆仑"早古生代复合地体的组成包括阿拉善-敦煌地体、祁连-阿尔金地体、柴达木地体、东昆仑北地体、东昆仑南地体、西昆仑北地体和西昆仑南地体,

地体边界包括早古生代俯冲杂岩带(蛇绿岩、混杂堆积和高压-超高压变质)和活动陆缘增生带(弧前增生楔、火山岛弧岩浆带和弧后盆地)两部分,有北祁连俯冲杂岩带和活动陆缘增生带、柴北缘俯冲杂岩带和活动陆缘增生带、祁漫塔格俯冲杂岩带和活动陆缘增生带、昆中俯冲杂岩带和活动陆缘增生带、北阿尔金俯冲杂岩带和活动陆缘增生带、南阿尔金俯冲杂岩带和活动陆缘增生带以及库地俯冲杂岩带和活动陆缘增生带等。该复合地体向东与北秦岭早古生代地体相连。通过对阿尔金断裂三叠纪形成[12]及其两侧地体(祁连和阿尔金地体)和地体边界(北祁连和北阿尔金早古生代俯冲杂岩带,柴北缘南阿尔金早古生代俯冲杂岩带)的对比,确定了阿尔金山是祁连山的西延[15]。

在"松潘甘孜-羌塘-拉萨"中生代复合地体中,地体之间的边界昆南-阿尼玛卿俯冲杂岩带和活动陆缘增生带、金沙江俯冲杂岩带和活动陆缘增生带、班公湖-怒江俯冲杂岩带和活动陆缘增生带,以及由于新特提斯洋盆俯冲在拉萨地体南缘形成的雅鲁藏布江俯冲杂岩带及冈底斯活动陆缘增生带。在青藏高原东南部三江地区由于印度/亚洲碰撞造成物质的侧向挤出和逃逸[16~17],构造格架由 EW 向转为 NS 向,自东向西为与金沙江俯冲杂岩带相连接的甘孜-理塘俯冲杂岩带和巴塘-元江俯冲杂岩带及伴随的义敦和江达火山岛弧带[18~19](图 2)。最新研究表明,在羌塘地体内部存在一条分割南、北羌塘的由二叠纪蛇绿岩(辉长岩,U-Pb,299~314Ma;玄武岩,Rb-Sr,318Ma)和三叠纪高压蓝片岩和榴辉岩(蓝闪石,^{39}Ar-^{40}Ar,220~221Ma)变质带组成的双湖-龙木错俯冲杂岩带[20~21],该带可能与青藏高原东南部三江地区分割"昌康-思茅地体"和"保山地体"的澜沧江蛇绿岩带(C-P)相连,与澜沧江蛇绿岩带伴随还有"杂多-昌都火山岛弧带"及"澜沧火山岛弧带"(C_3-P)[19]相连(图 2)。

通过最新的古地磁研究[13],组成青藏高原的诸地体的古地理位置、性质和归属的"非原地性"得以进一步证明,青藏高原在各个重大历史阶段中的地体拼合和增生是与特提斯洋盆包括始特提斯洋(新元古代-早、中泥盆世)、古特提斯洋(中石炭世-早三叠世)和新特提斯洋(晚三叠世-晚白垩世)的不断开启与闭合以及印度洋的最后打开(早中新世-现在)有着密切的关系。而且新的研究进一步证实青藏高原在印度/亚洲碰撞前的地体构架具有典型的"多洋(海)盆、多地体、多岛弧"的特征和"多俯冲、多碰撞、多造山"的动力学过程。在60~50Ma 印度/亚洲碰撞前的地体构架为"阿尔金-祁连-昆仑"早古生代复合地体和"松潘甘孜-羌塘-拉萨"中生代复合增生地体组成的"青藏联合陆块",北以西昆仑北缘冲断裂、阿尔金北缘冲断裂和北祁连北缘冲断裂为界,南缘界限为雅鲁藏布江缝合带。

60~50Ma 印度/亚洲碰撞造成"青藏联合陆块"的右旋隆升及物质向东挤出[22]以及联合陆块之西北缘发生地体移置,分别形成叠置的云南挤出地体、缅甸挤出地体和阿尔金-西昆仑移置地体[14](图 1)。

2 青藏高原的俯冲/碰撞/陆内造山类型

纵观青藏高原的造山类型可以分为三大类型:俯冲型山链、碰撞型山链及陆内型山链。俯冲型山链包括正向俯冲型(冈底斯白垩纪-早古新世俯冲型山链、东昆仑-阿尼玛卿三叠纪俯冲型山链和玉树-义敦三叠纪俯冲型山链)、正向俯冲增生型(阿尔金-祁连-昆仑早古生代俯冲增生型山链);碰撞型山链包括正向碰撞型(喜马拉雅新生代逆冲叠覆-挤出型山链、松潘甘孜晚三叠世滑脱-逆冲型山链)和斜向碰撞型(巴颜喀拉晚三叠世挤压转换型山链、西缅

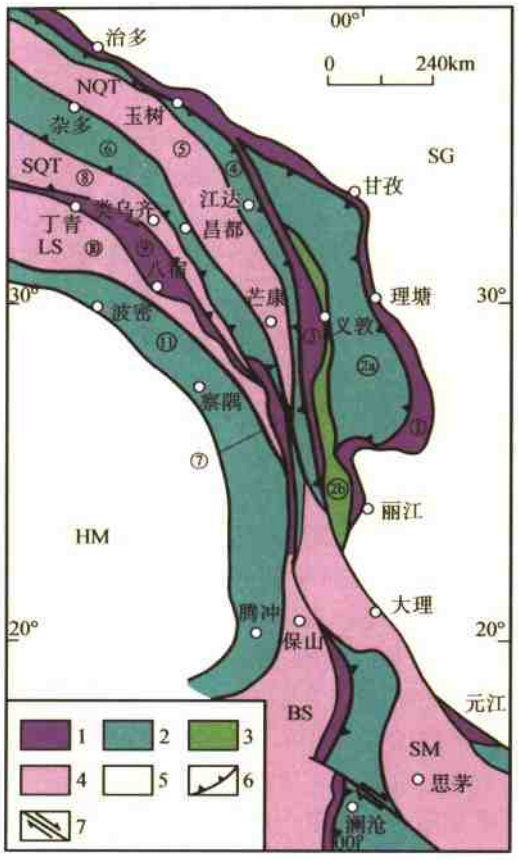

图 2　青藏高原三江地区构造图

(据刘增乾等,1993 修改)

Fig. 2　Tectonic map of the Sanjiang area of the Qinghai-Tibet plateau

1—俯冲杂岩带;2—火山岛弧带;3—弧后盆地;4—地体;5—周缘地体;6—俯冲极性;7—走滑断裂;①甘孜-理塘俯冲杂岩带;②义敦火山岛弧(㉔)和弧后盆地(㉕);③巴塘-元江俯冲杂岩带;④江达火山岛弧带;⑤北羌塘(芒康-思茅)地体;⑥杂多-昌都火山岛弧带;⑦澜沧江-孟良俯冲杂岩带;⑧南羌塘(类乌齐-保山)地体;⑨丁青-八宿俯冲杂岩带;⑩拉萨地体;⑪波密-腾冲火山岛弧带

甸新生代挤压转换山链,西巴基斯坦新生代挤压转换山链);陆内型山链包括挤压-转换型山链(青藏高原北缘新生代挤压转换型山链)和转换-挤出型山链(阿尔金-西昆仑新生代陆内挤出转换型山链)(表 1)。图 3 示意了青藏高原的主要造山类型的三维样式。

2.1　俯冲型山链

俯冲型山链是指地体碰撞及复合地体拼合之前的形成的山链类型。根据碰撞前地体会聚的几何学特征分析,在青藏高原有两种俯冲型山链:①正向俯冲型山链;②俯冲加积型增生山链。

2.1.1　正向俯冲型山链——冈底斯山链

典型例子为由冈底斯火山岛弧带及弧前加积楔组成的"俯冲型山链"。在印度和亚洲碰撞之前,由于新特提斯洋壳向北俯冲在亚洲大陆南缘形成增生的大陆弧,被称为转换喜马拉

表 1　青藏高原俯冲/碰撞型山链类型

Table 1　Types of subduction/collision mountain chains of Qinghai-Tibet plateau

类型	分类	典例
俯冲型山链	正向俯冲型	冈底斯白垩纪-早古新世俯冲型山链 东昆仑-阿尼玛卿三叠纪俯冲型山链 玉树-义敦三叠纪俯冲型山链
	正向俯冲增生型	阿尔金-祁连-昆仑早古生代俯冲增生型山链
碰撞型山链	正向碰撞型	喜马拉雅新生代逆冲叠覆-挤出型山链
	斜向碰撞型	松潘甘孜晚三叠世滑脱-逆冲型山链 巴颜喀拉晚三叠世挤压转换型山链 西缅甸新生代挤压转换山链 西巴基斯坦新生代挤压转换山链
陆内型山链	挤压-转换型	青藏高原北缘新生代挤压转换型山链
	挤出-转换型	阿尔金-西昆仑新生代陆内挤出转换型山链

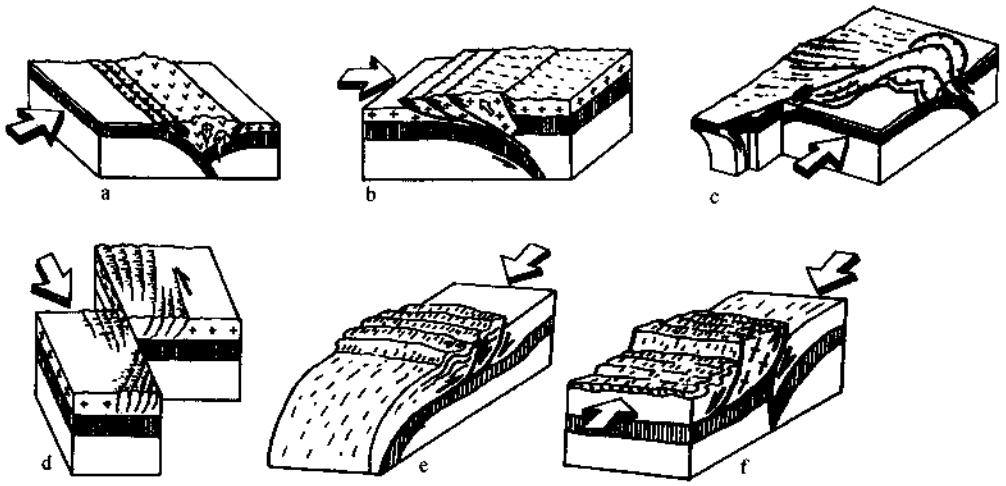

图 3　青藏高原俯冲/碰撞/陆内造山类型立体示意图

Fig.3　Stereoscopic simplified diagrams showing subduction/collision/intracontinental orogenic types of the Qinghai-Tibet plateau

a—俯冲型山链；b—碰撞型陆壳叠置增生山链；c—碰撞型"平行挤压转换"山链；d—碰撞型"斜向挤压转换"山链；e—碰撞型滑脱-逆冲山链；f—碰撞/陆内型挤出山链

雅带[23~24]。转换喜马拉雅带(即冈底斯带)由火山岩浆岛弧组成，它们的围岩为前寒武纪到中生代的变质岩系，白垩纪-第三纪的前陆盆地沉积一般保存不好。火山岩浆岛弧带主要发育在两个地段：西面巴基斯坦-印度 Koshistan-Ladakh 段[25~26]和东面的拉萨-日喀则段[27]。

在西部，沿晚白垩纪 Shyok 缝合带分布的 Koshistan-Ladakh 岛弧杂岩的碰撞是喜马拉雅增生事件的前兆。其上部为早白垩世钙碱性岛弧火山岩与沉积岩单元，被辉长岩和花岗岩岩基所侵入；下部为早白垩世席状杂岩的基性-超基性层状深成岩体，以及高度变形基性变火山岩和变质深成岩，其中可能包含火山弧底部的新特提斯洋底残片[28]。最老的 Koshistan-Ladakh 岛弧杂岩岩基的年龄是 100Ma，最年轻的是晚古新世[26,29~30]。

在中部,沿雅鲁藏布缝合带的拉萨-日喀则段(即冈底斯带)是发育在晚侏罗世与亚洲拼合的拉萨地体的大陆边缘岛弧带。拉萨地体的稳定地壳包括了为泥盆纪-晚白垩世浅水陆-海相夹火山岩地层所不整合的前寒武纪—寒武纪变质地层[27]。沿拉萨地体南缘的冈底斯火山岛弧带主要由林芝杂钙碱性火山岩及冈底斯花岗岩基组成,岩浆活动年龄为94～42Ma,大部分年龄是古新世-始新世[29,31-33]。与西部比较,具有西部老(晚早白垩世)中部新(古近纪)的特征。上述表明冈底斯带和"安第斯山链"一样是典型的前碰撞俯冲型山链。

类似冈底斯俯冲型山链的还有由东昆仑-阿尼玛卿活动陆缘增生带和玉树-义敦活动陆缘增生带组成的两条俯冲型山链。前者是以东昆仑-阿尼玛卿蛇绿岩带为标志的古特提斯北洋盆向北俯冲于东昆仑地体下的产物;后者为以西兰乌金-金沙江-甘孜-理塘蛇绿岩带为标志的古特提斯南洋盆向南和南西俯冲于羌塘地体之下而形成。由于昆南-阿尼玛卿古特提斯洋壳向北俯冲,在东昆仑地体中形成宽度50～80km、长度800km、具有弧火山性质的布尔汗不达钙碱性系列花岗岩带,侵位时限为220～240Ma,其和东昆仑南缘三叠纪弧前增生楔和共和弧后盆地组成的活动陆缘带构成碰撞前的初始山链。大规模的岛弧花岗岩基的出露表明其曾经位于火山岛弧带的根部,由于后期强烈的抬升剥蚀而裸露地表。因此东昆仑印支期岛弧型花岗岩基代表了阿尼玛卿洋盆往北俯冲在主动陆缘一侧形成的火山岛弧带的深部物质,反映了受深度剥蚀的安第斯俯冲型山链的根部。

2.1.2 俯冲增生型山链

大部分大陆地壳是构筑在俯冲带上部,俯冲作用导致之后的大陆碰撞[34-38]。在青藏高原北部"阿尔金-祁连-昆仑"早古生代复合地体的前碰撞历史中,可以重塑两种类型"俯冲加积型"山链:一种为与海沟倒退有成因联系的北祁连活动陆缘增生山链,位于北祁连走廊南山早古生代主火山岛弧带南缘伴随弧前火山链和加积楔的三条高压变质带是早古生代洋盆倒退俯冲的表征[5,39]。与海沟倒退有关的北祁连"俯冲加积型"增生山链与三次倒退俯冲形成的西太平洋菲律宾东部马尼亚拉"俯冲加积型"山链相似(图4)。另一种是在"阿尔金-祁连-昆仑"早古生代复合地体中,诸地体的前碰撞历史包含了俯冲加积杂岩增生过程而形成的"俯冲型"山链,类似于"中亚型俯冲山链"。这种类型是Sengor[10]在1996年提出的,指陆块碰撞前的一个或两个陆块包含有俯冲加积杂岩增生的前碰撞历史,是中亚Altaids碰撞造山带中普遍发育的造山类型(图3),在俯冲过程中,由于火山岩浆弧向海沟方向迁移,俯冲加积杂岩随时间而变宽,在卷入碰撞后俯冲杂岩产生强烈变形、缩短以及加厚。"阿尔金-祁连-昆仑"早古生代地体的俯冲加积增生型山链包含了"马尼亚拉"和"中亚型"两种叠置的"俯冲加积型"增生山链类型(图4)。

2.2 碰撞型山链

2.2.1 正向碰撞型山链

板块(或地体)之间正向(或近于正向)的碰撞过程中,在被动陆缘一侧的陆壳变形由碰撞边界向外扩展,形成由前缘一系列逆冲叠覆岩片、后缘伸展断裂组成的陆壳增生山链。

(1)典型实例1:喜马拉雅新生代陆壳叠置增生-挤出山链。60～50Ma期间印度/亚洲正向碰撞使印度被动陆缘一侧形成喜马拉雅增生地体或喜马拉雅山链。喜马拉雅增生地体的组成自北往南为:特提斯-喜马拉雅亚地体、高喜马拉雅亚地体、低喜马拉雅亚地体和次喜马拉雅亚地体,亚地体之间的界限分别为藏南拆离断层(STD)(20Ma形成)、主中冲断裂(MCT)(20Ma形成)、主边冲断裂(MBT)(10Ma形成)、主前锋冲断裂(MFT)(5Ma形成)[14,40-47]。

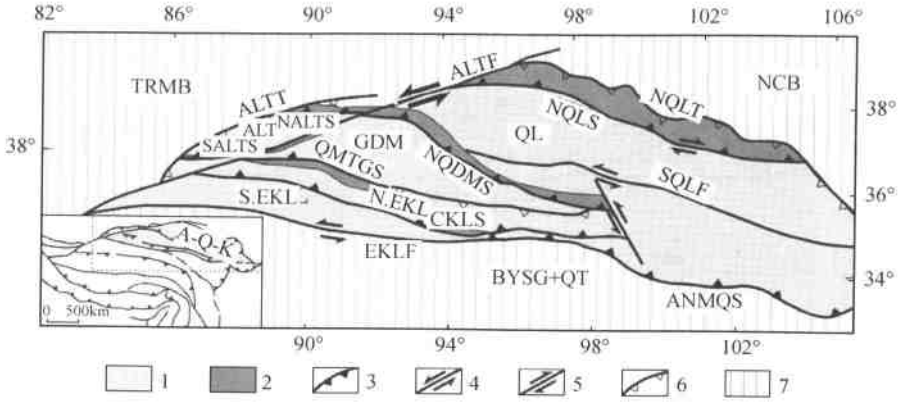

图 4 “阿尔金-祁连-昆仑”俯冲增生山链平面图

Fig. 4 The“Altyn-Qilian-Kunlun”mountain chains of subduction accretional type

1—阿尔金-祁连-昆仑(A-Q-K)早古生代复合地体;2—早古生代俯冲杂岩带和活动陆缘带;3—缝合带;4—左行走滑断裂;5—右行走滑断裂;6—逆冲断裂;7—周缘地体。TRMB—塔里木地块;NCB—北中国陆块;BYSG+QT—巴颜喀拉-松潘甘孜地体+羌塘地体;NQLT—北祁连逆冲断裂;NQLS—北祁连俯冲杂岩带;QL—祁连地体;SQLF—南祁连走滑断裂;NQDMS—柴北缘俯冲杂岩带;GDM—柴达木地体;QMTGS—祁漫塔格俯冲杂岩带;N.EKL—东昆仑北地体;CKLS—昆中俯冲杂岩带;S.EKL—东昆仑南地体;EKLF—东昆仑走滑断裂;ANMQS—阿尼玛卿俯冲杂岩带;ALTF—阿尔金走滑断裂;NALTS—北阿尔金俯冲杂岩带;SALTS—南阿尔金俯冲杂岩带;ALT—阿尔金地体;ALTT—阿尔金逆冲断裂

研究表明,喜马拉雅山链的前缘结构为由 MCT、MBT 和 MFT 组成的具有向南造山极性的逆冲叠覆岩片[41],地震反射剖面揭示,喜马拉雅逆冲断裂系与喜马拉雅深部逆冲断裂(MHT)相连[48]。新的研究表明,高喜马拉雅亚地体北缘的藏南拆离断裂(STD)向北延伸在特提斯-喜马拉雅亚地体之下,与具有自南向北剪切滑移性质的康马-拉轨岗日拆离带(KLD)相连,由于深部地壳局部熔融物质上涌造成花岗岩侵位,使康马-拉轨岗日拆离带隆起,形成康马-拉轨岗日穹窿带[14]。因此,喜马拉雅山链与一般碰撞型陆壳逆冲叠置增生山链(如阿尔卑斯山链)不同之处在于,喜马拉雅逆冲叠置增生陆壳的后部产生巨大的拆离伸展构造(STD+KLD),使 STD+KLD 与 MCT 之间的由结晶变质岩片组成的高喜马拉雅亚地体成为与挤出机制有关的新生代碰撞型陆壳叠置增生-挤出山链(图 5)。

(2)典型实例 2:松潘甘孜三叠纪碰撞型滑脱-逆冲型山链。在东昆仑-阿尼玛卿古特提斯缝合带东段南侧,扬子板块被动陆缘之上大面积出露的巨厚三叠纪复理石岩系组成了松潘造山带的主体,三叠纪西康群的变形发育“西康式”无劈理的弯滑型及含劈理的尖棱型直立褶皱[18]。在震旦-三叠纪盖层与其下的新元古代变质基底之间,发育一条大规模(延展达 300km)的缓倾(倾角 10°～20°)的呈向南凸出的弧形韧性滑脱剪切带,厚度达到 5～6km。滑脱剪切带之上的盖层板片中的劈理与褶皱轴面自上而下由直立-倾斜-近水平的变化,滑脱剪切带内糜棱岩及下部盖层岩片中发育近 SN 向拉伸线理,普遍发育“A”型褶皱及“A”型流动褶皱,大量花岗质脉体贯入,滑脱面上下的剪切应变指示滑脱带具从北往南的剪切指向特征[18]。研究表明,自滑脱带向上的热变质相带由混合岩化带→矽线石带→蓝晶石-十字石带→铁铝榴石带→黑云母带递退演变,矽线石带的形成温度 $T=600℃$,蓝晶石-十字石带的 $T=550～570℃$,铁铝榴石带 $T=500～540℃$,黑云母带 $T=400～500℃$。在滑脱带后缘发

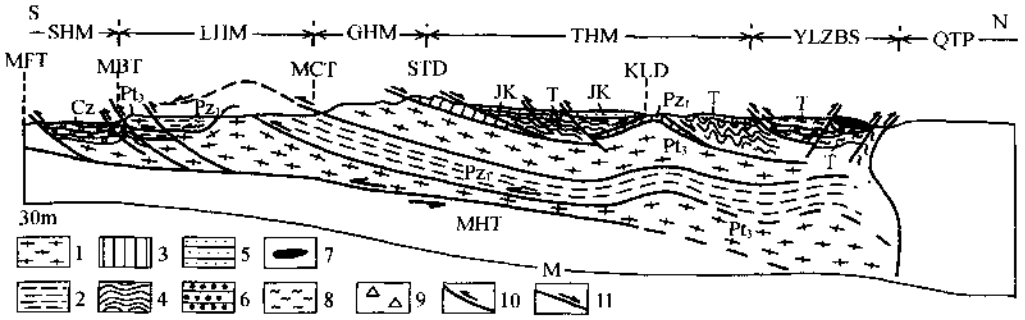

图 5 喜马拉雅碰撞型山链构造剖面

(地表构造剖面据 Brunel, 1986; 许志琴等, 2006 修改。深部地球物理资料据 Zhao *et al*., 1993)

Fig. 5 Tectonic profile of the Himalaya collision mountain chains

1—前寒武纪变质岩系; 2—早古生代浅变质岩系; 3—早古生代拆离层; 4—三叠纪地层; 5—侏罗-白垩纪地层; 6—新生代西瓦里克磨拉石; 7—蛇绿岩; 8—三叠纪复理石沉积; 9—混杂堆积; 10—逆冲断裂; 11—拆离断裂。QTP—青藏高原; YLZBS—雅鲁藏布缝合带; THM—特提斯-喜马拉雅带; GHM—高喜马拉雅带; LHM—低喜马拉雅带; SHM—次喜马拉雅带; KLD—康马-拉轨岗日拆离带; STD—藏南拆离带; MCT—主中逆冲断裂; MBT—主边逆冲断裂; MFT—主前锋逆冲断裂; MHT—主喜马拉雅逆冲断裂; M—莫霍面

育了印支期同构造花岗岩。上述研究表明,该滑脱剪切带为高温韧性滑脱剪切带。在滑脱带上部的盖层岩片中伴随一系列的向南剪切的韧性和韧-脆性逆冲断裂,在滑脱带的前缘发育朝南指向的逆冲断裂,使元古宙变质基底岩石抬升逆冲在志留纪片岩之上,志留纪片岩又逆冲在二叠纪灰岩、砂板岩和变玄武岩之上(图 6)[18]。这一典型的滑脱-逆冲型的构造样式同样出现在扬子被动陆缘的南秦岭一侧[49],归于三叠纪碰撞型滑脱-逆冲型山链类型。

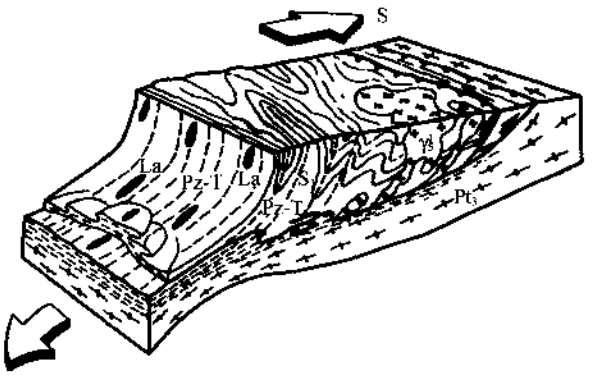

图 6 松潘甘孜晚三叠世滑脱-逆冲型山链立体图

Fig. 6 Stereoscopic diagram showing the Late Triassic Songpan-Ganzi Mountain chains of "detachment-thrust type"

Pt_3—新元古代变质岩系, Pz-T—古生代-三叠纪地层; γ_5^3—三叠纪花岗岩; La—拉伸线理; S_1—劈理

2.2.2 斜向碰撞型山链

青藏高原结构的一个重要特征是大型走滑断裂的发育,在地体之间斜向会聚和碰撞过程中,沿地体边界产生走滑断裂,并形成与走滑构造伴生的褶皱与逆冲断裂,筑建了挤压转

换型山链。

(1)典型实例1:巴颜喀拉-东昆仑三叠纪斜向挤压-转换型山链。巴颜喀拉-松潘甘孜地体和东昆仑地体的边界为东昆仑-阿尼玛卿俯冲杂岩带,NW-SE走向的东段(布青山-阿尼玛卿段)以发育典型的蛇绿岩和蛇绿混杂堆积为特征[50~51],而近EW走向的西段(木孜塔格-东昆仑南缘)仅少量蛇绿岩露头[52],为长达1000km的大型东昆仑左行走滑断裂所占位。研究表明,三叠纪时期(220~240Ma)东昆仑左行走滑断裂形成[12],由于后期抬升,深部韧性左行走滑剪切带出露地表,并叠置了韧脆性和脆性应变。断裂北侧是以早古生代碰撞造山带为基底的东昆仑三叠纪弧前增生楔的斜坡相沉积;断裂南侧为长条形狭窄巴颜喀拉带,带内广布三叠系巨厚的巴颜喀拉群复理石沉积岩系,与东面倒三角形松潘甘孜地体中的三叠系巨厚的西康群复理石沉积岩系相连;两侧的变形以与EW向东昆仑走滑断裂斜交(NW-SE向)的直立或扇形褶皱轴面伴随密集流劈理和折射劈理为特征,发育高角度逆冲断裂,构成NW-SE向斜列状褶皱山系。为东昆仑地体与羌塘地体之间斜向俯冲-碰撞导致EW向走滑及NE-SW向挤压的产物(图7,图8)。

(2)典型实例2:西缅甸-西巴基斯坦斜交挤压-转换型山链。印度和亚洲会聚过程中,印度板块的几何形态决定了其像楔子一样插向亚洲大陆,印度和亚洲的正向会聚一侧形成冈底斯俯冲型山链及继后形成的喜马拉雅碰撞型陆壳叠覆式增生山链。根据古地磁资料,印度洋盆初始开启在白垩纪,50~60Ma期间由于新特提斯洋盆闭合及印度/亚洲碰撞在印度陆块的东、西两侧分别形成孟加拉湾和阿拉伯湾[13],并在印度/亚洲侧向(斜向)会聚之东侧(即喜马拉雅东构造结之南)形成以近NS走向的密支那右行走滑断裂(又称90°东海岭断裂)及相伴生的与之平行的新生代逆冲断裂和褶皱山系(勃固山-若开山)组成的宽达500km的西缅甸山链;在西侧形成以NNE-SSW走向的恰曼左行走滑断裂及相伴生的一系列与之平行的新生代逆冲断裂和褶皱山系(莱曼山)组成的宽达400km的西巴基斯坦山链。山链的构造变形以平行的走滑与挤压构成的挤压转换样式为特征,归为"斜向碰撞型"平行挤压-转换山链(图9)。

2.3 陆内山链

印度/亚洲(55±10)Ma碰撞之后,板块之间的作用并未终止,印度板块仍以44~50mm/a的速率往北推进,致使亚洲大陆一侧1500km的南北向缩短量被吸收,形成2倍于正常地壳厚度的巨厚陆壳体(平均厚度70km),营造了世界上最高、最大的青藏高原。印度一侧的陆壳增生形成亚洲大陆的最后拼贴体——喜马拉雅增生地体[53],构筑了最高的喜马拉雅山链[42,46,53~58]。值得注意的是,青藏高原北缘的"阿尔金-祁连-昆仑"早古生代造山带及变质基底再次崛起,形成长达数千千米的青藏高原北缘"西昆仑-阿尔金-祁连"巨型山链和高原屏障。这一巨型山链究竟何时开始隆起?又以什么构造样式铸造什么类型的山链?是归于陆内山链研究的范畴。

(1)典型实例1:阿尔金-北祁连斜交挤压-转换型山链。位于青藏高原北缘的中亚最大走滑断裂——NEE-SWW走向的阿尔金左行走滑断裂的南侧,分布着很多大大小小的NWW-SEE走向的山脉,由北往南分别为:祁连山、大雪山、野马山、党和南山、柴达木-宗务隆山、柴达木盆地褶皱带和祁漫塔格山等,并出现一系列盆地与山脉相间的地貌格局(图1),类似于美国西部圣安德列斯走滑断裂及其西地部美国南加州挤压盆-山构造体系,在走滑断裂一旁的盆地内均富含油气[59]。

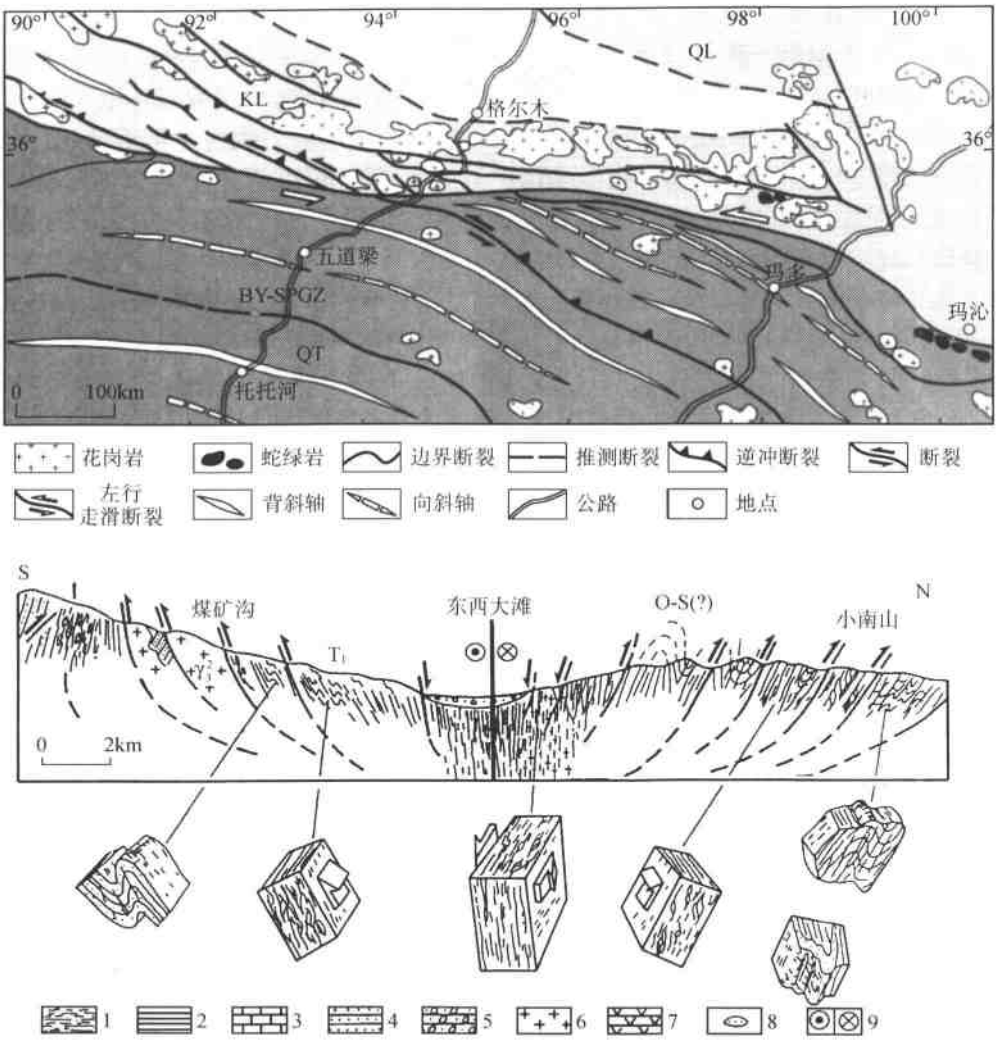

图 7 巴颜喀拉-东昆仑晚三叠世斜向"挤压-转换型"山链构造平面图(上)、剖面图(下)
(据 Li *et al*., 1996)

Fig. 7 Tectonic map and structural cross-section showing the Late Triassic Bayanhar-E. Kunlun mountain chains of "oblique transpression" type

1—糜棱岩;2—板岩;3—灰岩;4—砂岩;5—砂砾岩;6—花岗岩;7—变火山岩;8—砂岩透镜体;9—走滑断裂

这些山脉或褶皱带的走向与阿尔金断裂带呈一定的角度过渡关系。研究表明,阿尔金左行走滑断裂形成于三叠纪,在其继后的左行走滑过程中,至少在 120Ma(白垩纪)左右开始伴随相对的快速隆升作用,并在逆冲断裂前接受沉积,形成早期的山前盆地。约 110～100Ma 左右,在阿尔金断裂带东端出现局部拉张环境,发生火山作用,并在逆冲体西段开始发生顺时针旋转,形成山间盆地;到了 80Ma 左右,走滑伴随的逆冲作用使得前白垩纪地质体(祁连山早古生代造山带)上隆再成山,山前、山间盆地已成规模[60]。

这些山脉和褶皱,尤其是山前逆冲断裂的形成,是在阿尔金断裂带的统一左行走滑剪切

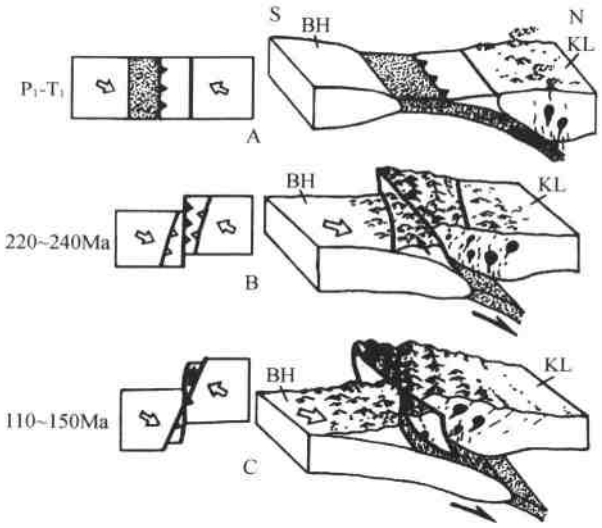

图 8　巴颜喀拉-东昆仑晚三叠世斜向"挤压-转换型"山链形成演化立体图示

Fig.8　Stereoscopic diagram showing formation and evolution for the Late Triassic Bayanhar-E. Kunlun mountain chains of oblique"transpression"type

A—P_1-T_1 古特提斯北洋盆斜向俯冲于东昆仑地体下，形成东昆仑活动陆缘增生带；B—220～240Ma 东昆仑挤压-转换型走滑断裂形成，两侧地体形成与断裂斜交的褶皱系；C—110～150Ma 东昆仑挤压转换型走滑断裂继续活动，"挤压-转换型"碰撞山链定型；BH—巴颜喀拉地体；KL—昆仑地体

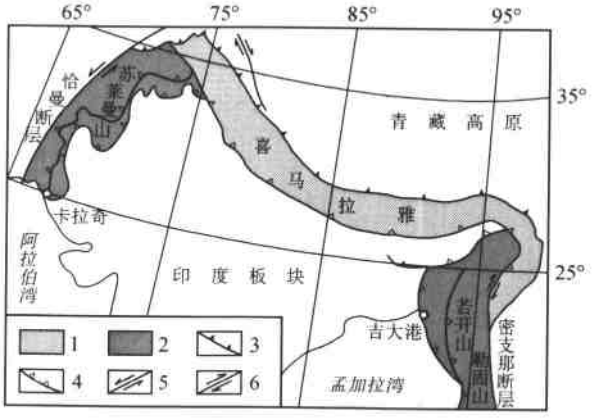

图 9　西缅甸-西巴基斯坦"平行挤压-转换型"山链平面图

Fig.9　Tectonic simplified map showing the West Burma-West Pakistan mountain chains of"parallel transpression"type

1—喜马拉雅地体；2—"平行挤压-转换型"山链；3—缝合带；4—逆冲断裂；5—左行走滑断裂；6—右行走滑断裂

应力场作用下形成的。沿阿尔金断裂带各山体或古老(前新生代)块体的边界大多数都由新生代断裂控制，或者说这些山体或古老块体的抬升成山是在新生代完成的。并构成现今的高原北部山链面貌[61～62]。

由于新生代的再活动,在断裂南侧的祁连山中,形成与之相伴随的斜交的(NW-SE 向)新生代挤压型盆-山构造体系,盆-山之间分布了平面上向 NE 方向突出的逆冲断裂体系,逆冲断裂的活动使山脉不断抬升,此类与陆内走滑断裂活动有关的挤压型山链为陆内"斜向挤压转换"山链(图 10)。

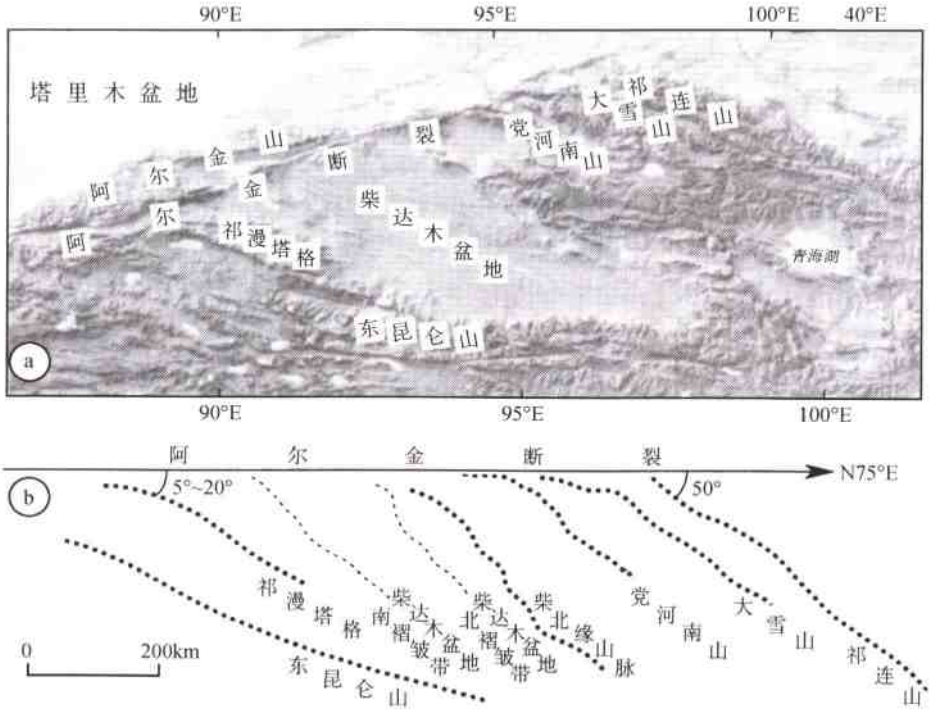

图 10　阿尔金走滑断裂与南侧挤压型山系 DEM 图像(a)及断裂南侧山系展布图(b)

Fig.10　DEM image(a)and mountain system distributions(b)of the Altyn-Tagh strike-slip fault and its southern side

(2)典例实例 2:西昆仑、阿尔金平行挤压-转换型山链。青藏高原西北缘以早古生代造山为特征的阿尔金地体和西昆仑地体,在新生代时期再度崛起,形成现今的地貌-构造景观。阿尔金地体的南缘为新近纪强烈活动的 NEE-SWW 向的阿尔金左行走滑主断裂[22],北缘为与之平行的挤压型的阿尔金逆冲断裂,往北叠覆在塔里木盆地之上。西昆仑地体的北缘为 EW 向西昆仑北缘逆冲断裂系,根据山/盆结合带中塔西南凹陷的上白垩统、古新统、始新统、渐新统和中新统砂岩的磷灰石裂变径迹年龄为 80～90Ma[63]、50～70Ma[64]、10～30Ma和 2～5Ma[65]。塔西南凹陷的沉积物来自其南侧的西昆仑造山带,表明白垩纪-新近纪时期,西昆仑造山带存在强烈的热构造活动;而在西昆仑南缘的康西瓦左行走滑断裂自白垩纪(100～120Ma)至今也有强烈的活动表现[66]。因此,阿尔金地体和西昆仑地体的最后隆升受到相互平行的前缘逆冲断裂和后缘走滑断裂,即前缘挤压后缘旋转的应变制约,西昆仑、阿尔金"平行挤压-转换"山链与高喜马拉雅山链的挤出机制不同,为"半挤出-转换"机制的产物。

3 青藏高原巨型造山拼贴体

两个或两个以上时期形成的造山带构成复合或叠置的造山拼贴体，为复合叠置山链。例如，发育在太平洋东岸、美洲大陆西海岸宽近 1000km、长度超过 10000km 的科迪勒拉造山带，主要是晚古生代和早白垩-早古新世的两条平行造山带构成的复合造山拼贴体；阿尔卑斯造山带叠置在欧洲华力西造山带上，阿尔卑斯外带(Helvc 带)中出露 6 个华力西结晶基底(Mt. Balanc, Aiguilles, Rouges, Belledonne, Des Grandes Rousses, Pelvoux 和 L'Argentera)，它们被断裂所撕裂，在基底岩石中保留 NE60°方向的华力西期的拉伸线理及褶皱构造，被阿尔卑斯期的近 EW 向拉伸线理及剪切应变所叠置[67]。青藏高原显示了一个巨型复合/叠置造山拼贴体的形成过程。

青藏高原的地体拼合与碰撞造山作用同时进行，显生宙以来主要的碰撞造山时限为早古生代、晚三叠世、晚侏罗世-早白垩世和新生代以来，青藏高原巨型碰撞造山拼贴体形成主要是 500～600Ma 以来长期活动、多期造山及造山叠置的过程，因此青藏高原的诸多地体中保存了多期复合/叠置的地壳变形和造山的记录。

3.1 青藏高原不同时期的碰撞造山

3.1.1 早古生代的"弧-陆、陆-陆"俯冲/碰撞造山

早古生代时期的地壳变形与碰撞造山事件主要记录在"阿尔金-祁连-昆仑"早古生代复合地体中，此外在青藏腹地——羌塘地体及其东南延展部分的思茅地体和保山地体中广泛显示[68]。青藏南部喜马拉雅地体也曾经历了早古生代或泛非-早古生代造山事件形成原始喜马拉雅山，并成为现今的喜马拉雅山链的早古生代变质褶皱基底[53,59]。因此早古生代造山运动(或泛非-早古生代造山运动)的范围几乎遍及整个青藏高原各地体之中(图 3)。

青藏北部的"阿尔金-祁连-昆仑"早古生代复合地体是以早古生代多地体/多岛弧群及地体/岛弧相间的与始特提斯洋盆有关的具有洋壳的多弧前海为基本特征的地体结构，始特提斯洋盆及相关的含洋壳的多弧前海的消减和闭合导致地体/岛弧群的拼合与碰撞，形成"阿尔金-祁连-昆仑"早古生代碰撞造山带，即经历弧/陆→陆/陆碰撞的过程，从俯冲型山链向碰撞型山链转化[39]。而早古生代复合造山带的"三多"构造格局显示了早古生代造山带形成前的弧后活动带的背景。在"阿尔金-祁连-昆仑"早古生代复合地体中广泛发育的垂直山链的拉伸线理反映了地体/岛弧的运动矢量。

3.1.2 三叠纪双向俯冲/碰撞造山

亚洲中南部的三叠纪碰撞造山带呈"T"字几何形态展布，东西延绵 8000km，从中东-帕米尔-西昆仑南部甜水海地体越过阿尔金断裂连接巴颜喀拉-松潘甘孜、羌塘地体，向东与南秦岭、大别-苏鲁相连；南北延绵 2000km，从阿尼玛卿-松潘-木里-藏东到印度尼西亚地块两侧。在青藏高原范围内，主要分布在巴颜喀拉-松潘甘孜地体、羌塘地体以及思茅地体和保山地体中。晚古生代时期形成古特提斯洋盆(C-P)可分为两支，即分别位于基墨里地体北、南边的北洋盆和南洋盆。碰撞造山带是古特提斯北洋盆(以东昆仑-阿尼玛卿蛇绿岩为标志)和南洋盆(以金沙江-元江蛇绿岩为标志)的三叠纪末期闭合及劳亚板块、扬子板块和从冈瓦那大陆分裂的基墨里地体(东段为羌塘地体)之间碰撞造山的产物。

阿尼玛卿三叠纪俯冲杂岩带为古特提斯洋壳北支俯冲的产物，由阿尼玛卿蛇绿岩、混杂

堆积、弧前增生楔及高应变滑脱带组成,超镁铁质岩、辉长岩及拉斑玄武岩组成的蛇绿岩残片呈不规则长条状及块状混杂体产于中下三叠系砂板岩中,并混杂了大量含化石的石炭-二叠纪灰岩及三叠纪浊积岩等外来岩块[50]。在北洋盆往北及方向俯冲同时,在北大陆南缘形成三叠纪活动陆缘带(东昆仑活动陆缘带)自南往北发育俯冲杂岩带、弧前增生楔、岛弧岩浆带与弧后盆地的沟-弧-盆体系。位于布青山-玛沁火山岛弧南侧的T_{1-2}含浊积岩的复理石岩系中,发育北倾的不协调褶皱,底界为高应变俯冲滑脱面,由安山质糜棱岩组成,发育NNE-SSW向拉伸线理、"A"型剪切褶皱及向南逆冲指向的剪切应变。

标志古特提斯南洋盆的金沙江蛇绿岩带(C_1-T_1)在玉树以东转为SN走向的甘孜-理塘蛇绿岩带和巴塘-元江蛇绿岩两带,甘孜-理塘蛇绿岩/俯冲杂岩带西侧的义敦火山岛弧带和弧后盆地以及巴塘-元江蛇绿岩/俯冲杂岩带以西的昌都火山岛弧带均代表古特提斯南洋盆具有向羌塘地体方向的俯冲(P_2-T_3)极性。

由于古特提斯北洋盆和北洋盆的"双向"俯冲,即北洋盆向北俯冲于东昆仑地体之下,南洋盆向南和南西俯冲于羌塘地体之下,因此俯冲和碰撞造成的地壳变形分别叠置在东昆仑(北侧)和羌塘(南侧)活动陆缘一侧,形成Pz_1+T的叠置山链。特别是昆南-阿尼玛卿缝合带两侧构成完整的主动和被动陆缘的俯冲/碰撞山链:北缘的东昆仑主动陆缘一侧发育逆冲-推覆叠置岩片结构,而在南缘的扬子被动陆缘一侧发育新元古代变质基底和盖层之间的韧性挤压型滑脱-逆冲体系[18],两侧都具有垂直山链的横向拉伸线理及标志向南造山极性的剪切指向,并伴随三叠纪的同构造花岗岩浆活动。

根据晚三叠世山链是由两条古特提斯洋盆的双向俯冲/闭合和东昆南地体/羌塘地体/扬子地体碰撞而造成的,因此它是一个特殊的双向俯冲-碰撞型复合山链,晚三叠-早侏罗世和北部早古生代山链实现了拼贴和叠置,构成此时的劳亚大陆的一部分。

新生代以来印度/亚洲碰撞而造成的物质向SE侧向挤出,使三叠纪山链几何形貌发生扭曲,成为今日的"T"型几何状态。

3.1.3 晚侏罗-早白垩世的碰撞造山

班公湖-怒江蛇绿岩带(向东及南东与三江地区的丁青-八宿蛇绿岩带相连)所代表的新特提斯北洋盆开启和扩张(T-J_2)发生在从冈瓦纳大陆裂解的拉萨地体与基墨里地体之间,地体之间的会聚及碰撞与新特提斯北洋盆的消减、闭合有关。晚侏罗-早白垩世碰撞造山造成的地壳变形主要分布在班公湖-怒江缝合带两侧的羌塘地体南部和拉萨地体范围内,还叠置在三江地区的保山地体西部。

3.1.4 晚白垩世以来的俯冲/碰撞/陆内造山

以雅鲁藏布江蛇绿岩为代表的新特提斯南洋盆主要扩张期在侏罗纪,白垩纪-始新世新特提斯南洋盆往北俯冲形成的以冈底斯岩浆岛弧带为主体的冈底斯俯冲型山链作为活动增生陆缘带拼贴在拉萨地体之上。50Ma左右新特提斯南洋盆闭合使印度/劳亚大陆碰撞,大印度陆块的继续推进使其俯冲在劳亚大陆之下[60～70],20Ma开始印度陆块北缘形成具有向南极性的典型的喜马拉雅逆冲叠覆岩片构造[42,45～46,58,71～72]。喜马拉雅地体在逆冲叠覆-挤出机制下形成世界最高的喜马拉雅山链[73～74]。最新的研究确定了高喜马拉雅北缘的藏南拆离断裂(STD)规模巨大,向北延伸并与特提斯-喜马拉雅的康马-拉轨岗日拆离带(KLD)相连[14]。上述情况不仅表明高喜马拉雅岩片的快速挤出,而且在高喜马拉雅结晶岩片中东西拆离构造的发现,说明现代高喜马拉雅隆升是垂向挤出和侧向挤出两种机制的综

合效应[14]。

与此同时，青藏高原北缘的"阿尔金-祁连-昆仑"早古生代山链在经过长期的演化调整之后，东北缘的祁连地区在阿尔金走滑断裂活动影响下以陆内"转换-挤压型"造山样式再度隆升，阿尔金-西昆仑地区以及青藏东缘的龙门山以陆内"转换-挤出型"造山样式再度崛起[75]。

3.2 青藏高原的复合叠置造山与巨型造山拼贴体的形成

尽管青藏高原中各时期的地体拼合、增生过程与碰撞造山同时进行，但是碰撞造山作用(包括地壳变形、基底活化及花岗岩浆活动)所涉及范围远远越出地体边界的狭窄地域，造成叠置造山作用。比如，青藏高原北部的"阿尔金-祁连-昆仑"早古生代复合地体的主体是早古生代碰撞造山带，在其南部的东昆仑地体中叠置了古特提斯北洋盆俯冲和消减(C-T)形成的三叠纪活动陆缘岛弧岩浆带及强烈变形的三叠纪弧前增生楔和弧后盆地；在复合地体北部，早古生代碰撞造山变形体系之上叠置了变形较弱的以同心宽缓褶皱为特征的陆内造山变形。新生代由于阿尔金走滑运动及北缘的陆内俯冲作用使青藏北部古老造山带再次崛起，因此，青藏高原北部的"阿尔金-祁连-昆仑"早古生代复合地体自显生宙以来经历了三次叠置造山。

图 11 表示了新生代前东昆仑山是早古生代与三叠纪叠置的复合山链。在东昆仑地体南部的早古生代地层中保留了完好的早古生代变形记录，震旦-志留纪地层中强烈同轴挤压应变形成含流劈理的紧闭直立不协调褶皱，伴随绿片岩相变质作用。晚泥盆世磨拉石沉积不整合盖在早古生代褶皱岩系上表明造山运动的结束，早中三叠世地层的同心褶皱叠置在早古生代绿片岩系紧闭褶皱及早古生代花岗岩之上。在东昆仑南缘的东昆仑-阿尼玛卿俯冲杂岩带北缘的古特提斯活动陆缘增生带叠置在早古生代褶皱山链之上，明显见到三叠纪布尔汗不达岛弧岩浆带穿过早古生代褶皱地层，小南川-阿尼玛卿三叠纪弧前增生楔自北而南含少劈理→折射劈理→流劈理的直立→同斜褶皱系叠置在早古生代褶皱系之上。形成典型的 $Pz_1 + T$ 复合叠置山链。

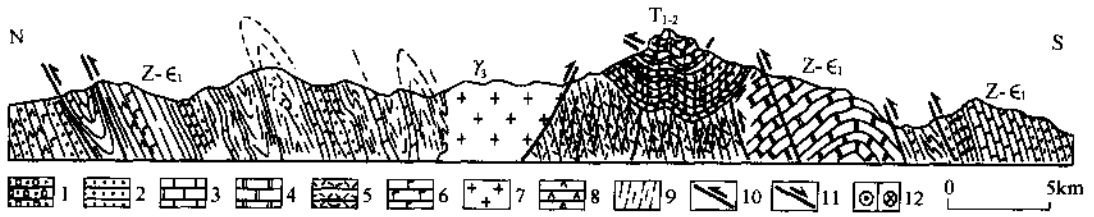

图 11 东昆仑早古生代山链上的三叠纪叠置变形剖面

Fig. 11 Structural cross-section showing the Triassic superimposed deformation on the East Kunlun Early Paleozoic mountain chains

1—含砾砂岩；2—砂岩；3—灰岩；4—大理岩；5—凝灰岩；6—变玄武岩；7—花岗岩；8—变中性火山岩；9—板岩；10—逆冲断裂；11—正断裂；12—走滑断裂

位于"巴颜喀拉-松潘甘孜"晚三叠世碰撞山链南部(羌塘)的基底为早古生代山链，后期又受到新生代喜马拉雅运动的影响，因此其为 $Pz_1 + T + Cz$ 的复合叠置山链；阿尔金和西昆仑早古生代山链之上叠置了新生代变形，成为 $Pz_1 + Cz$ 复合叠置山链；喜马拉雅山链为泛

非-早古生代与新生代叠置山链已被证实[53,76～77]。

4　结论和讨论

(1)地球上的许多复合造山带或碰撞造山拼贴体都是构筑在长期活动带之上。例如,宽达1000km的科迪勒拉造山带变形的地质历史纪录表明,该带从600Ma一直活动到现在,主要的造山期是晚古生代和早白垩-早古新世[42]。青藏高原是在巨型碰撞造山拼贴体基础上构筑的,青藏高原巨型碰撞造山拼贴体的形成是亚洲大陆的自北往南的增生和造山迁移的生长结果。但是巨型碰撞造山拼贴体所反映的活动长期性、非原地性、俯冲/碰撞/陆内造山类型的多样性、碰撞造山的多期性以及造山的复合叠置性比世界上任何一个复合山链(或造山拼贴体)来得复杂、多彩(图12)。

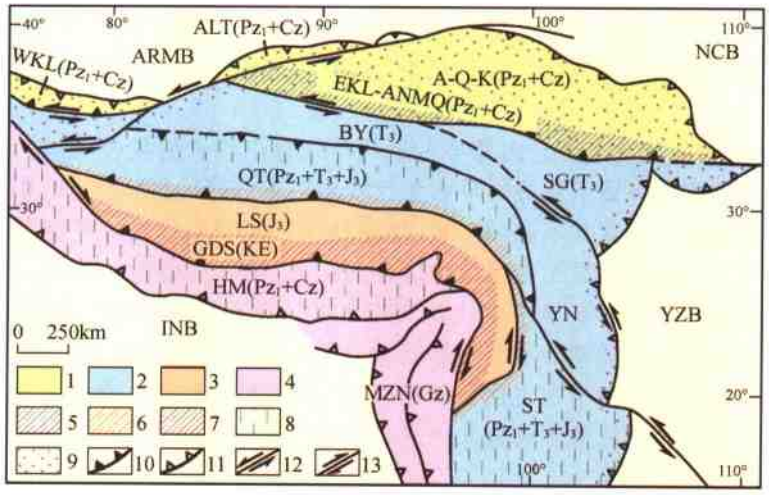

图12　青藏高原巨型碰撞造山拼贴体组成图示

Fig. 12　The huge collision orogenic collage of the Qinghai-Tibet plateau

1—早古生代(Pz_1)碰撞山链;2—晚三叠世(T_3)碰撞山链;3—晚侏罗世(J_3)碰撞山链;4—新生代(Cz)碰撞山链;5—叠置的晚三叠世(T_3)俯冲型山链;6—叠置的晚侏罗世(J_3)俯冲型山链;7—叠置的白垩-第三纪(K-E)俯冲型山链;8—基底为早古生代(Pz_1)山链;9—叠置的新生代(Cz)陆内山链;10—缝合带;11—逆冲断裂;12—左行走滑断裂;13—右行走滑断裂

(2)青藏高原造山拼贴体的形成与始特提斯、古特提斯和新特提斯洋盆的先后开启、消减、闭合以及古大陆的裂解、诸地体的移动、会聚和拼合有关。造山类型形成在不同时期洋盆俯冲、地体碰撞和陆内会聚的不同阶段,多地体/多岛弧的构架表明诸多的俯冲型山链可以产生在地体边界的活动陆缘一侧,古特提斯两洋盆的反向俯冲构筑了反向俯冲型山链;地体碰撞形成的碰撞型山链以及后碰撞形成的陆内山链由于地体边界与块体驱动方向的几何学关系形成"正向碰撞/陆内型"和"斜向碰撞/陆内型"造山类型。"斜向碰撞/陆内型山链"与走滑断裂的形成、规模及其运动学直接相关。

50～60Ma印度/亚洲碰撞不仅形成青藏高原造山拼贴体的最后成员——喜马拉雅山链,而且在拼贴体的北缘和东缘由于陆内俯冲作用使早期形成的山链在整修后又一次崛起。

青藏高原的周缘山链铸成屏障与外侧的克拉通相隔。

本文是笔者等10余年来研究青藏高原的部分成果。成文中与曾令森博士进行了有益的讨论，图件由张晓卫、柴耀楚和张淼绘制，唐哲民协助整理参考文献，在此一并感谢。

References

[1] GILBERT G K. Report on the geology of the Henry Mountains[R]// U S Geol Survey. Rocky Mtn Region, Report, 1890:160.

[2] STILLE H. Bemerkungen zu James Gillulys "Distribution of Mountain Building in Geologic Time" [J]. Geol Rundsch, 1950, 38:91～102.

[3] WILLSON J T. Convection and continental drift in the southwest Pacific [J]. Tectonophysics, 1966(3):69.

[4] MATTAUER M. La formation des chaines de montagnes[J]. Science edition francaise de scientific American, 1981, 46: 40～56.

[5] XU Zhiqin, XU Huifen, ZHANG Jianxin, *et al*. The Zhoulangnanshan Caledonian subductive complex in the northern Qilian mountains and its dynamics[J]. Acta Geologic Sinica, 1994, 69(1):1～14(in Chinese).

[6] SENGOR A M C. Tectonics of the Tethysides: orogenic collage development in a collisional setting[J]. Ann Rev Earth Planet Sci, 1987, 15: 213～244.

[7] HELWIG J E. Eugeosynclinal basement and a college concept of orogenic belts[J]. Soc Econ Paleontol Mineral, 1974, 19: 359～376.

[8] XU Zhiqin. Large deep-level decollement structure on the northern margin of the Yangtze Plate and its dynamic analysis [J]. Regional Geology of China, 1987 (4) : 289～300 (in Chinese).

[9] MANUEL P, JASON A, CHRISTOPHE M. Cenozoic plate interaction of the Australia and Philippine sea plates: "hitand-run"tectonics[J]. Tectonophysics, 2003, 363 (3/4): 181～199.

[10] SENGOR A M C, NATALIN B A. Turkic-type orogeny and its role in the making of the continental crust[J]. Annu Rev Earth Planet Sci, 1996, 24:263～337.

[11] DEWEY J F. Orogeny can be very short[J]. Proceeding of the National Academy of Sciences, 2005(102):15286～15293.

[12] LI Haibing, YANG Jingsui, XU Zhiqin. Geological and chronological evidence of Indo-Chinese strike-slip movement in the Altyn Tagh fault zone[J]. Chinese Science Bulletin, 2001, 46 (16):1333～1338(in Chinese).

[13] GRADSTEIN F M, OGG J G, SMITH A G, *et al*. A geologic time scale [M]. New York:Columbia University Press, 2004.

[14] XU Zhiqin, YANG Jingsui, LI Haibing, *et al*. The Qinghai-Tibet plateau and continental dynamics: a review on terrain tectonics, collisional orogenesis, and processes and mechanisms for the rise of the plateau[J]. Geology in China, 2006, 33 (2): 221～238(in Chinese).

[15] XU Zhiqin, LI Haibing, YANG Jingsui, *et al*. A large transpression zone at the south margin of the East Kunlun Mountains and oblique subduction[J]. Acta Geoscientia Sinica, 2001, 75(2) : 156～164(in Chinese).

[16] TAPPONNIER P, PELTZER G, DAIN L, *et al*. Propagating extrusion tectonics in Asia: new insights from simple experiments with plasticine[J]. Geology, 1982, 10: 611～616.

[17] TAPPONNIER P, PELTZER G, ARMIJO R. On the mechanics of the collision between India and Asia, in collision tectonics[C] // COWARD M P, RIESS A C. Geol Soc Spec Publ, London, 1986, 19:115～157.

[18] XU Zhiqin, HOU Liwei, WANG Zongxiu, *et al*. Orogenic processes of the Songpan-Garze orogenic belt of China[M]. Beijing: Geological Publishing House, 1992:1～190 (in Chinese).

[19] LIU Zengqian, LI Xingzhen, YE Qingtong, *et al*. Division of tectono-magmatic zones and the distribution of deposits in the Sanjiang Area [M]. Beijing: Geological Publishing House, 1993: 245 (in Chinese).

[20] ZHAI Qingguo, LI Cai, CHENG Liren, *et al*. Geological features of Permian ophiolite in the Jiaomuri area, Qiangtang, Tibet, and its tectonic significance [J]. Geological Bulletin of China, 2004, 23 (12): 22～24(in Chinese).

[21] LI Cai, ZHAI Qingguo, DONG Yongsheng, *et al*. Discovery of eclogite of the Central Qiangtang of the Qinghai-Tibet Plateau[J]. Chinese Science Bulletin, 2006, 51(1): 70～74 (in Chinese).

[22] TAPPONNIER P, XU Zhiqin, ROGER F, *et al*. Oblique stepwise rise and growth of the Tibet Plateau[J]. Science, 2001, 294:1671～1677.

[23] DEWEY J F, BIRD J M. Mountain belts and the new global tectonics [J]. Journal of Geophysical Research, 1970, 75: 2625～2647.

[24] TAPPONNIER P, MATTAUER M, PROUST F, *et al*. Mesozoic ophiolites, sutures, and large-scale tectonic movements in Afghanistan[J]. Earth and Planetary Science, 1981, 52(2): 355～371.

[25] SEARLE M P, CHICHESTER U K, JOHN W, *et al*. Geology and tectonics of the Karakoram Mountains[M]. Chichestep: John Wiley and Sons, 1991:358.

[26] HONEGGER K, DIETRICH V, FRANK W, *et al*. Magmatism and metamorphism in the Ladakh Himalayas (the Indus-Tsangpo suture zone)[J]. Earth Planet Sci Lett, 1982, 60: 253～292.

[27] BURG P, HARRISJEAN L B, SAUNJAC S. Strain distribution within the Pardailhan Nappe (Montagne Noire, France) and structure of its basal thrust zone:implications for events associated with nappe emplacement[J]. Journal of Structural Geology, 1983, 5 (3/4): 431～440.

[28] TRELOAR P J, PETTERSON M G, JAN M Q, *et al*. A re-evaluation of the stratigraphy and evolution of the Kohistan arcsequence, Pakistan Himalaya: implications for magmatic and tectonic arc-building processes [J]. Geological Society Journal, 1996, 153: 681～693.

[29] SCHARER U, HAMET J, ALLEGRE C J. The Trans-Himalayan(Gangdese) plutonism in the Ladakh region: U-Pb and Rb-Sr study [J]. Earth and Planetary Science Letters, 1984, 67: 327～339.

[30] PETTERSON M G, WINDLEY B F. Rb-Sr dating of the Kohistan arc-batholith in the Trans-Himalaya of north Pakistan, and tectonic implications [J]. Earth and Planetary Science Letters, 1985, 74:45～57.

[31] XU R H, SHARER U, ALLEGRE C J. Magmatism and metamorphism in the Lhasa Block (Tibet): an U-Pb geochronological study[J]. J Geol, 1985, 93: 42～57.

[32] COULON C, MALUSKI H, BOLLINGER C, *et al*. Mesozoic and Cenozoic volcanic rocks from central and southern Tibet: ^{39}Ar-^{40}Ar dating, petrological characteristics, and geodynamical significance[J]. Earth Planet Sci Lett, 1986, 79: 281～302.

[33] COPELAND P H, YUN T M, KIDD P, *et al*. Thermal evolution of the Gangdese batholith, southern Tibet: a history of episodic unroofing[J]. Tectonics, 1995, 14: 223～236.

[34] TAYLOR J C. The origin and growth of continents[J]. Tectonophysics, 1967, 4(1): 17～34.

[35] JACOBS M, LOWRIE R W. Magnetic properties and mineralogy of four deep-sea cores[J]. Earth and Planetary Science Letters, 1972, 15(2): 157～168.

[36] DEWEY M. A test of terminal mesozoic catastrophe [J]. Earth and Planetary Science Letters, 1981, 53 (1): 103～108.

[37] ALLEGRE C J, JAUPART C. Continental tectonics and continental kinetics [J]. Earth and Planetary Science Letters, 1985, 74(2/3): 171～186.

[38] SENGOR A M, CELAL. Plate tectonics and orogenic research after 25 years: a Tethyan perspective[J]. Earth-Science Reviews, 1990, 27(1/2): 1～34.

[39] XU Z Q, ZHANG J X, LI H B. Architecture and orogeny of the Northern Qinling orogenic belt, Northwestern China [J]. Journal of the Geological Society of China, 2000, 43 (1): 125～141.

[40] BURG J P, CHEN G M. Tectonics and structural formation of southern Tibet, China[J]. Nature, 1984, 311:219～223.

[41] BRUNEL M. Ductile thrusting in the Himalayas: shear sense criteria and stretching lineations[J]. Tectonics, 1986, 5 (2): 247～265.

[42] BURCHFIEL B C, CHEN Z, HODGES K V, *et al*. The South Tibetan detachement system, Himalayan orogen: extension contemporancous with and parallel to shortening in a collisional mountain belt[J]. Geol Soc Am Spec Pap, 1992, 269: 1~41.

[43] CUI Junwei, ZHU Hong, WU Changde, *et al*. Deformation and dynamics of the lithosphere in Qinghai-Xizang Plateau [M]. Beijing. Geological Publishing House, 1992:1~164 (in Chinese).

[44] CUI Junwei, TANG Zhemin, DENG Jinfu, *et al*. Altun fault system[M]. Beijing: Geological Publishing House, 1996: 249(in Chinese).

[45] BROOKFIELD M E. The Himalayan passive margin from Precambrian to Cretaceous[J]. Sedimentary Geol, 1993, 84: 1~35.

[46] Le FORT P. Evolution of the Himalaya[M]//YIN A, HARRISON T M. In the tectonics of Asia[M]. New York: Cambridge University Press, 1996:95~106.

[47] YIN A, HARRISON T M. Geologic evolution of the Himalayan-Tibetan orogen[J]. Rev Earth Planet Sci, 2000, 28: 211~228.

[48] ZHAO W J, NELSON K D, Project INDEPTH Team Deep seismic reflection evidence for continental underthrusting beneath southern Tibet[J]. Nature, 1993, 366: 557~559.

[49] XU Zhiqin, LU Yilun, TANG Yaoqing, *et al*. *Formation of the composite eastern Qinling chains*[M]. *Beijing*: China Environmental Science Press, 1986:1~158(in Chinese).

[50] JIANG Chunfa, YANG Jingsui, FENG Binggui, *et al*. Opening-closing tectonics of Kunlun mountains[M]. Beijing: Geological Publishing House, 1992(in Chinese).

[51] YANG J S, ROBISON P T, JIANG, C F, *et al*. Ophiolites of the Kunlun Mountains, China and their tectonic implications [J]. Tectonophysics, 1996, 258:215~231.

[52] MOLNAR P, BURCHFIEL B C, LIANG K U, *et al*. Geomorphic evidence for active faulting in the Altyn Tagh and northern Tibet and qualitative estimates of its contribution to the convergence of India and Eurasia[J]. Geology, 1987, 15: 249~253.

[53] HODGES K V, GEISSMAN J W E, GLAZNER A F E. Tectonics of the Himalaya and southern Tibet from two perspectives, special focus on the Himalaya[J]. Geol Soc Am Bull, 2000, 112:324~350.

[54] GANSSER A. Geology of the Himalayas[M]. London: Wiley Interscience, 1964:289.

[55] Le FORT P, DEBON F, SONET J. The Lower Paleozoic(Lesser Himalayan) granitic belt: emphasis on the Simchar pluton of central Nepal [M] // SHAMS F A. *Granites of the Himalaya Karakoram and Hindu Kush*. Lahore: Institute of Geology, Punjab University, 1983:235~256.

[56] BURG J P, CHEN G M. Tectonics and structural formation of southern Tibet, China[J]. Nature, 1984, 311:219~223.

[57] HARRISON T M, RYERSON F J, Le FORT P, *et al*. A late Miocene-Pliocene progin for the central Himalayan inverted metamorphism [J]. Earth and Planetary Science Letters, 1997, 146:E1~E7.

[58] YIN A, HARRISON T M. Geologic evolution of the Himalayan-Tibetan orogen[J]. Rev Earth Planet Sci, 2000, 28: 211~280.

[59] XU Zhiqin, YANG Jingsui, LIANG Fenghua, *et al*. Pan-African and Early Palaeozoic orogenic events in the Himalaya terrane: inference from SHRIMP U-Pb zircon ages[J]. Acta Petrologica Sinica, 2005, 21 (1): 1~12 (in Chinese).

[60] LI Haibing, YANG Jingsui. Evidence for Cretaceous uplift of the northern Qinghai-Tibetan plateau[J]. Earth Science Frontiers, 2004, 11(4): 345~359(in Chinese).

[61] LI Jijun, FANG Xiaomin, MA Haizhou, *et al*. Geomorphological and environmental evolution in the upper reaches of Yellow River during the Late Cenozoic[J]. Science in China: Series D, 1996, 26(4):316~322(in Chinese).

[62] FANG X M, GARZIONE C, van der VOO, *et al*. Flexural subsidence by 29 Ma on the NE edge of Tibet from the magnetostratigraphy of Linxia basin, China[J]. Earth Planet Sci Lett, 2003, 210(3/4): 545~560.

[63] CUI Junwen, ZHANG Xiaowei, TANG Zhemin. Tectonic divisions of the Qinghai-Tibet Plateau and structural characteristics of deformation on their boundaries[J]. Geology in China, 2006, 33 (2): 256~267 (in Chinese).

[64] DING Daogui, WANG Daoxuan, LIU Weixin, *et al*. The western Kunlun orogenic belt and basin[M]. Beijing: Geological Publishing House, 1996:1～249(in Chinese).

[65] SOBEL E R, DUMITRU T A. Thrusting and exhumation around the margins of the western Tarim basin during the India-Asia collision[J]. Joul Geo Res, 1997, 102(B3): 5043～5063.

[66] MATTE P, TAPPONNIER P, AMAUD N, *et al*. Tectonics of western Tibet, between the Tarim and the Indus [J]. Earth Planet Sci Lett, 1996, 142:311～330.

[67] XU Zhiqin Crustal deformation and microstructures[M]. Beijing: Geological Publishing House, 1984: 131 (in Chinese).

[68] LIU Zengqian, LI Xingzhen, YE Qingtong, *et al*. Division of tectono-magmatic zones and the distribution of deposits in the Sanjiang area [M]. Beijing: Geological Publishing House, 1993: 245 (in Chinese).

[69] BESSE J V, COURTILLOT J P, POZZI M, *et al*. Paleomagnetic estimates of crustal shortening in the Himalayan thrusts and Zangbo suture[J]. Nature, 1984, 311: 621～626.

[70] PATZELT A, LI H, WANG J, *et al*. Paleomagnetism of Cretaceous to Tertiary sediments from Southern Tibet: evidence for the extent of the northern margin of India prior to the collision with Eurasia[J]. Tectonophysics, 1996, 259: 259～284.

[71] MOLNAR P, TAPPONNIER P. Cenozoic tectonics of Asia: effects of a continental collision[J]. Science, 1975, 189: 419～426.

[72] BROOKFIELD M E. The Himalayan passive margin from Precambrian to Cretaceous[J]. Sedimentary Geol, 1993, 84: 1～35.

[73] CHEMENDA A I, MATTAUER M, MALAVIELLE J, *et al*. A mechanism for syn-collisional rock exhumation and associated normal faulting: results from physical modeling[J]. Earth and Planetary Science Letters, 1995, 132:225～232.

[74] CHEMENDA A I, BURG P, MATTAUER M. Evolutionary model of the Himalaya-Tibet system: geopoem based on new modeling, geological and geophysical data[J]. Earth Planet Sci Lett, 2000, 174:397～409.

[75] XU Zhiqin, YANG Jingsui, ZHANG Jianxin, *et al*. A comparison between the tectonic units on the two sides of the Altun sinistral strike slip fault and the mechanism of lithospheric shearing[J]. Acta Geoscientica Sinica, 1999, 73(3): 193～205(in Chinese).

[76] LIU Wencan, LIANG Dingyi, WANG Keyou, *et al*. The Ordovician discovery in the Kangma region of the south Tibet and its geological significance[J]. Earth Science Frontiers, 2002, 9(4):247～248 (in Chinese).

[77] XU Zhiqin, ZENG Lingsen, YANG Jingsui, *et al*. Role of large-scale strike-slip faults in the formation of petroleum-bearing compressional basin-mountain range systems [J]. Earth Science, 2004, 29(6): 631～643 (in Chinese).

参 考 文 献

[5] 许志琴,徐惠芬,张建新,等. 北祁连走廊南山加里东俯冲杂岩石地体及动力学[J]. 地质学报,1994,69(1):1～14.

[8] 许志琴. 扬子板块北缘的大型深层滑脱构造及动力学分析[J]. 中国区域地质,1987,4:289～300.

[12] 李海兵,杨经绥,许志琴,等. 阿尔金断裂带印支期走滑活动的地质纪年代学证据[J]. 科学通报,2001,46(16):1333～1338.

[14] 许志琴,杨经绥,李海兵,等. 青藏高原研究聚焦——地体拼合、碰撞造山及高原隆升的深部驱动力[J]. 中国地质,2006,33(2):221～238.

[15] 许志琴,李海兵,杨经绥,等. 东昆仑山南缘大型转换挤压构造带和斜向俯冲作用[J]. 地质学报,2001,75(2):156～164.

[18] 许志琴,侯立玮,王宗秀,等. 中国松潘-甘孜造山带的造山过程[M]. 北京:地质出版社,1992:1～190.

[19] 刘增乾,李兴振,叶庆同,等. 三江地区构造岩浆带的划分与矿产分布规律[M]. 北京:地质出版社,1993:245.

[20] 翟庆国,李才,程立人,等. 西藏羌塘角木日地区二叠纪蛇绿岩地质特征及构造意义[J]. 地质通报,2004,23(12):

22～24.
[21] 李才，翟庆国，董永胜，等．青藏高原羌塘中部榴辉岩的发现及其意义[J]．科学通报，2006，51(1)：70～74.
[43] 崔军文，朱红，武长得，等．青藏高原岩石圈变形及其动力学[M]．北京：地质出版社，1992：1～164.
[44] 崔军文，唐哲民，邓晋福，等．阿尔金断裂系[M]．北京：地质出版社，1996：249.
[49] 许志琴，卢一伦，汤耀庆，等．东秦岭复合山链的形成——变形、演化及板块动力学[M]．北京：中国环境科学出版社，1986：1～158.
[50] 姜春发，杨经绥，冯秉贵，等．昆仑开合构造[M]．北京：地质出版社，1992.
[59] 许志琴，杨经绥，梁凤华，等．喜马拉雅地体的泛非-早古生代造山事件年龄记录[J]．岩石学报，2005，21(1)：1～12.
[60] 李海兵，杨经绥．青藏高原北部白垩纪隆升的证据[J]．地学前缘，2004，11(4)：345～359.
[61] 李吉均，方小敏，马海州，等．晚新生代黄河上游地貌演化与青藏高原隆起[J]．中国科学：D辑，1996，26(4)：316～322.
[63] 崔军文，张晓卫，唐哲民．青藏高原的构造分区及其边界的变形构造特征[J]．中国地质，2006，33(2)：256～267.
[64] 丁道桂，王道轩，刘伟新，等．西昆仑造山带与盆地[M]．北京：地质出版社，1996：1～249.
[67] 许志琴．地壳变形和显微构造[M]．北京：地质出版社，1984：131.
[68] 刘增乾，李兴振，叶庆同，等．三江地区构造岩浆带的划分与矿产分布规律[M]．北京：地质出版社，1993：245.
[75] 许志琴，杨经绥，张建新，等．阿尔金断裂两侧构造单元的对比及岩石圈剪切机制[J]．地质学报，1999，73(3)：193～205.
[76] 刘文灿，梁定益，王克友，等．藏南康马地区奥陶系的发现及其地质意义[J]．地学前缘，2002，9(4)：247～248.
[77] 许志琴，曾令森，杨经绥，等．走滑断裂、"挤压性盆-山构造"与油气资源关系的探讨[J]．地球科学，2004，29(6)：631～643.

An orogenic plateau-the orogenic collage and orogenic types of the Qinghai-Tibet plateau. Earth Science Frontiers

XU Zhi-qin　LI Hai-bing　YANG Jing-sui
(Key Laboratory for Continental Dynamics of MLR, Institute of Geology, Chinese Academy of Geological Sciences, Beijing 100037, China)

Abstract　The *Qinghai-Tibet plateau, a major collisional orogenic collage up to 1500km wide*, was formed by tectonic processes related to the opening, consumption and closure of the Proto-Tethyan, Paleo-Tethyan and Neo-Tethyan oceans. The breakup of Gondwanan supercontinents produced numerous continental blocks and microcontinents that eventually converged and collided against Asia. Thus, the plateau contains a long record of oceanic (or small oceanic basin) subduction, terrane collision and intra-continental convergence. The present-day collage is composed of numerous distinct terranes separated by ophiolites, arc volcanic rocks and forearc sedimentary rocks. The observable tectonic framework suggests that volcanic arcs and related mountain chains are common on active continental margins, such as those that occurred on both sides of Paleo-Tethys. Subduction and collision was both normal and oblique, depending on the direction of block movements and on the configurations of individual blocks. Oblique collision led to the formation of strike-slip faults, many of which played a major role in mountain build-

ing. The initial of India and Asia in 50～60Ma not only formed the High Himalaya along the southern margin of the plateau but caused uplift of pre-existing Palaeozoic mountain belts farther to the north. These rejuvenated belts now form significant intra-continental mountain chains accompanied by intra-continental subduction. The Qinghai-Tibet orogenic collage formed by progressive accretion of blocks and terranes to the Asian continent as orogenesis migrated from north to south over a protracted period of time. The tectonic evolution of the region was episodic, with multiple periods of basin formation, subduction and intracontinental block collisions. The plateau has had a longer and more complex geologic history than many of the other orogenic belts in the world.

Key words orogenic plateau Qinghai-Tibet plateau huge orogenic collage orogenic types

印度/亚洲碰撞——南北向和东西向拆离构造与现代喜马拉雅造山机制再讨论❶

许志琴　杨经绥　戚学祥　崔军文　李海兵　陈方远
（中国地质科学院地质研究所　国土资源部大陆动力学重点实验室　北京　100037）

摘　要　印度/亚洲碰撞形成的喜马拉雅增生地体由特提斯-喜马拉雅（THM）、高喜马拉雅（GHM）、低喜马拉雅（LHM）和次喜马拉雅（SHM）亚地体组成。通过喜马拉雅增生地体中变质基底和盖层的组成、变质演化、变形机制与形成时代的对比，确定高喜马拉雅（GHM）亚地体北缘的藏南拆离断裂（STD）向北延伸于特提斯-喜马拉雅（THM）亚地体之下，与形成在大于650℃温度、具有自南向北剪切滑移性质的康马-拉轨岗日拆离带（KLD）相连，深部地壳局部熔融、物质上涌造成的花岗岩侵位，使康马-拉轨岗日拆离带隆起，形成康马-拉轨岗日穹隆带。在高喜马拉雅（GHM）亚地体北部（普兰—吉隆—聂拉木—亚东一带）的变质基底与盖层之间发现EW向近水平的高喜马拉雅韧性拆离构造（GHD），以发育EW向拉伸线理、缓倾的糜棱面理及具有自西向东水平滑移为特征；而在GHM南部靠近主中央冲断裂（MCT）北侧发育具有挤压转换性质的韧性走滑-逆冲断层。高喜马拉雅亚地体从南到北具有由逆冲→斜向逆冲→EW向伸展→斜向伸展→SN向伸展的连续变形和转换的特征，是在现代喜马拉雅垂向挤出和侧向挤出的耦合造山机制下综合变形的响应。喜马拉雅地体中的东西向和南北向拆离构造的存在为喜马拉雅现代造山机制再讨论提供了基础。

关键词　喜马拉雅　NS向和EW向拆离构造　垂向和侧向挤出　造山机制
中图分类号：P542⁺.4；P542⁺.2　**文献标识码**：A　**文章编号**：1671－2552(2006)01～02－0001－14

1　前言

印度/亚洲于(55±10)Ma碰撞之后，板块之间的作用并未终止，印度板块仍以44～50mm/a的速率往北推进，致使亚洲大陆一侧1800km（西部）和2750km（东部）的南北向缩短量被吸收[1]，形成2倍于正常地壳厚度的巨厚陆壳体（平均厚度70km），在青藏高原南缘形成喜马拉雅增生地体。印度/亚洲碰撞导致喜马拉雅造山带崛起（包括变质、变形、隆升与剥蚀作用）和青藏高原隆升事件已为许多学者所描述[1～9]，碰撞造成的青藏高原南缘大量物质向SE方向逃逸（侧向挤出）的观点[10～13]为越来越多的地学家接受，经研究确定的喜马

❶　地质通报，2006年第25卷第1～2期。
收稿日期：2006－02－08；修订日期：2006－02－14。
科技项目：国土资源部科技专项《青藏高原的碰撞造山及其效应》的课题《青藏高原地体边界及岩石圈剪切断裂》资助。
作者简介：许志琴（1941－），女，研究员，中国科学院院士，从事大地构造学及构造地质学研究。

拉雅增生地体的结构及边界断裂已经成为造山带的经典。

长期以来现代喜马拉雅造山带的形成引起地学家们的极大兴趣,特别是制约高喜马拉雅结晶变质岩片的自 20Ma 以来形成的主中央冲断裂(MCT)和藏南拆离断裂(STD)备受关注。Chemenda 等[14]曾通过陆-陆碰撞岩石圈模拟实验提出了岩石圈板片的"挤牙膏"式折返模式,即岩石圈板片俯冲过程中造成底侵构造并形成冲断裂,在折返过程中岩石圈板片像牙膏一样挤出,并伴随正断裂产生。该模式可用以解释喜马拉雅的造山机制,即主中央冲断裂(MCT)和藏南拆离断裂(STD)夹持的高喜马拉雅结晶变质岩片是在南北向 18mm/a 的挤压缩短率下垂向挤出机制下折返的。

提出的问题是:在印度/亚洲陆-陆碰撞中,喜马拉雅的垂向挤出与青藏东南缘的侧向挤出之间的关系是如何在高喜马拉雅增生地体的新生代变形记录中体现的?本文将通过喜马拉雅增生地体中现代喜马拉雅变形几何学、运动学及变形机制转换的微观—宏观构造的研究,重新厘定藏南拆离断裂(STD)的规模及其形成条件,揭示在高喜马拉雅增生地体中垂向挤出和侧向挤出的变形反映,进一步解析高喜马拉雅崛起的造山机制。

2 构造背景

喜马拉雅增生地体呈向南突出的 EW 向弧形展布,长 2500km,宽 300~500km,北侧以印度斯-雅鲁藏布江缝合带与拉萨地体南部的冈底斯活动陆缘带为邻,南侧以喜马拉雅前锋冲断裂(MFT)与印度地台上的西瓦里克前陆磨拉石盆地为界。喜马拉雅增生地体的东侧为由呈 NS 向的三盖-民衣右行走滑断裂及伴随的褶皱-逆冲带组成的挤压转换带,延长 2000km 以上,并与印度尼西亚岛弧带相连;西侧为由呈近 NS 向的恰曼左行走滑断裂及伴随的褶皱-逆冲带组成的挤压转换带,延长 1000km。2 条挤压转换带往北分别系在喜马拉雅的东构造结(Namche Barwa)和西构造结(Nanga Parbat)上,与喜马拉雅带相连(图 1)。

喜马拉雅增生地体自北往南分为 4 部分:特提斯-喜马拉雅亚地体(THM)、高喜马拉雅(GHM)亚地体、低喜马拉雅(LHM)亚地体和次喜马拉雅(SHM)亚地体(图 2)。特提斯-喜马拉雅(THM)亚地体与高喜马拉雅(GHM)亚地体的界线为藏南拆离断裂(STD),高喜马拉雅(GHM)亚地体与低喜马拉雅(LHM)亚地体的界线为主中央冲断裂(MCT),低喜马拉雅(LHM)亚地体与次喜马拉雅(SHM)亚地体的界线为主边冲断裂(MBT),次喜马拉雅(SHM)亚地体与印度克拉通的界线为主前锋冲断裂(MFT)[4~7,9,15~17]。主中央冲断裂(MCT)和藏南拆离断裂(STD)均为强变形的韧性剪切带,在尼泊尔 MCT 厚达 6km,STD 的厚度约 1km。

2.1 特提斯-喜马拉雅亚地体

特提斯-喜马拉雅(THM)亚地体呈 EW 向弧形带状延展,宽达 100~120km。出露印度陆块的变质基底和古生代—中生代被动陆缘盖层,南部的古生代地层由于拆离作用明显减薄或缺失。

特提斯-喜马拉雅(THM)亚地体的北界——雅鲁藏布江缝合带由白垩纪日喀则群弧前盆地、蛇绿岩带和混杂堆积带组成。白垩纪日喀则群弧前盆地宽达 10~30km,沿冈底斯火山岛弧带南缘分布,变形以东西轴向宽缓褶皱为特征,其底部为著名的雅鲁藏布江蛇绿岩带。位于蛇绿岩带以南的混杂堆积带宽 20~40km,以三叠纪—白垩纪复理石为基质,含有

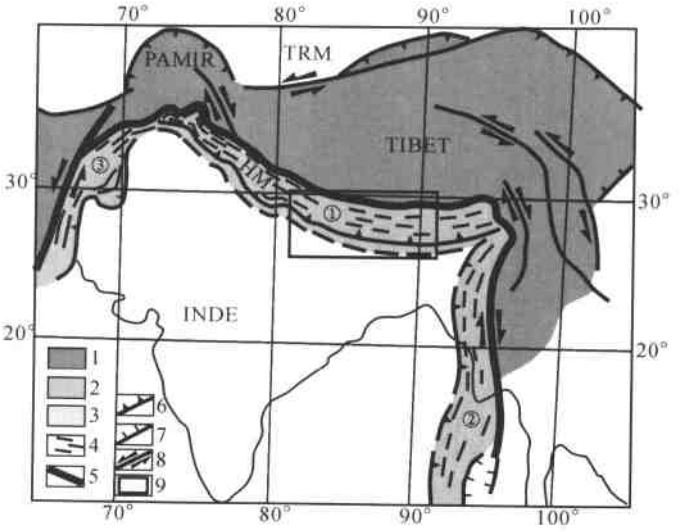

图 1　青藏高原-喜马拉雅构造简图

（本图底图由 Mattauer 提供）

Fig. 1　Tectonic sketch map of the Qinghai-Tibet Plateau and Himalayas

1—高原；2—喜马拉雅增生地体；3—喜马拉雅东、西侧挤压转换带；4—构造线；5—缝合带；6—逆冲断层；7—正断层；8—走滑断层；9—图 2 范围；INDE—印度板块；TIBET—青藏高原；TRM—塔里木地块；PAMIR—帕米尔高原；HM—喜马拉雅；①喜马拉雅主带；②③喜马拉雅东侧带和西侧带

大量灰岩、硅质岩和蛇绿岩的块体，基质的变形表现为紧密的同劈理褶皱，轴面向南陡倾，往南渐缓。

特提斯-喜马拉雅（THM）亚地体以发育大片显生宙沉积盖层为特征。在亚地体中部的拉轨岗日-康马 250km 范围内出露 8 个大小不等的变质穹隆，变质穹隆核部由拉轨岗日群组成，为一套高角闪岩相的副变质岩系和混合岩化片麻状花岗岩组合，与高喜马拉雅的聂拉木群相似。最新的锆石 SHRIMP U-Pb 测年表明，拉轨岗日-康马变质穹隆带的基底岩石——花岗质片麻岩的原岩形成时代为 835～869Ma，并经历了泛非造山事件（504～528Ma）的影响。古生代基本上为一套连续沉积的稳定的台型碳酸盐岩-碎屑岩沉积，属印度地台沉积盖层，总厚逾 3300m。沉积盖层与前震旦纪变质基底之间的强烈拆离，使震旦纪—寒武纪岩石变质成石榴黑云片岩及绿泥石英片岩，其与古生代盖层一并减薄[16,18]。康马穹隆边部发现下奥陶统的底砾岩[19,20]，并提出底砾岩可作为泛非事件的地质标志[20]，这一认识与上述泛非事件的年代学测定结果吻合。变质穹隆带的南北两侧发育中生代—始新世的海相沉积盆地，侏罗纪—白垩纪地层的变形以轴向东西、宽缓的同心弯滑褶皱为特征；三叠纪—白垩纪复理石地层变形以含破劈理的圆滑褶皱和含流劈理的尖棱褶皱组合为特征，轴向东西，轴面近直立。中生代地层的变形样式反映了上部收缩与下部压扁的机制。

2.2　高喜马拉雅（GHM）亚地体

高喜马拉雅（GHM）亚地体呈 EW 向宽 150km 的弧形展布，出露大范围的前震旦纪变质岩。高喜马拉雅的前震旦纪变质岩屑印度地台北缘结晶基底的组分，在主带上称聂拉木群，为一套高角闪岩相的富铝变质岩系，局部混合岩化，原岩是砂岩及砂质粘土岩，总厚

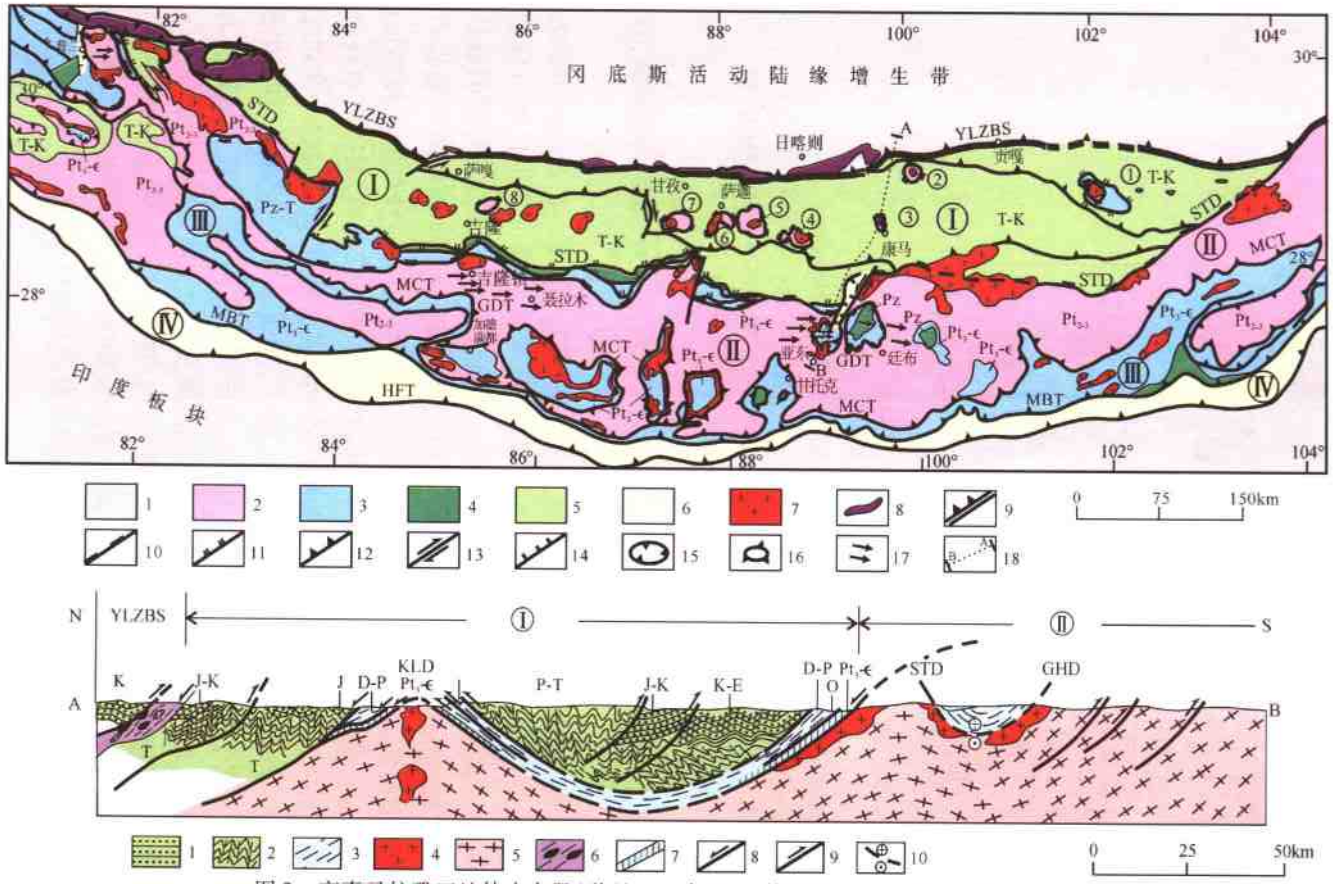

图2　高喜马拉雅亚地体中东段(普兰—亚东地区)构造图(上)及构造剖面图(下)

Fig. 2　Tectonic map and section of the east-central segment (Burang-Yadong area) of the Grearer Himalaya subterrane

构造图:1—喜马拉雅地体周缘地区;2—古-中元古代变质基底岩石;3—新元古代-早古生代地层;4—晚古生代地层;5—中生代地层;6—新生代地层;7—花岗岩;8—蛇绿岩;9—缝合带;10—主拆离断层带;11—拆离断层;12—逆冲断层;13—走滑断层;14—正断层;15—飞来峰;16—构造窗;17—滑移方向;18—构造剖面位置构造图以中国地质调查局和成都地质矿产研究所编制的青藏高原1:500万地质图(2005)为基础,结合本研究成果编制。

构造剖面图:1—中、新生代沉积;2—三叠纪同劈理褶皱;3—古生代盖层;4—浅色花岗岩;5—元古宙片麻岩;6—俯冲杂岩带;7—新元古代-寒武纪变质片岩;8—剪切运动方向;9—逆冲断裂;10—拆离断裂面上盘向里(E)下盘向外(W)运动。Ⅰ—特提斯-喜马拉雅亚地体;Ⅱ—高喜马拉雅亚地体;Ⅲ—低喜马拉雅亚地体;Ⅳ—次喜马拉雅亚地体;YLZBS—雅鲁藏布江缝合带;KLD—康马-拉轨岗日拆离带;STD—藏南拆离带;GHD—高喜马拉雅拆离带;MCT—主中央冲断层;MBT—主边冲断层;MFT—主前锋冲断层;①～⑧变质穹隆

6000～9000m。前人曾认为喜马拉雅地体变质基底岩石的形成年龄为中新元古代[21-25]。最近运用锆石 SHRIMP U-Pb 测年获得普兰片麻岩的最老年龄值为 1863.8Ma，表明聂拉木群的时代应为中新元古代。并记载了高喜马拉雅亚地体的变质基底岩石卷入泛非-早古生代事件(529～457Ma)的历史。

值得注意的是，在西构造结南迦帕尔巴特的喀格罕山谷、斯达克及东拉达克地区先后找到榴辉岩[26-29]，O'Brien 等(1998)又在喀格罕山谷榴辉岩中发现了柯石英包裹体，计算了含柯石英的 UHP 榴辉岩的温压条件为 650℃ 和 2.6GPa，超高压变质年龄为 49Ma ± 7Ma[30]，推测西构造结地区的印度/亚洲碰撞时间应早于 49Ma，并且经历了大约 49Ma 以来的陆壳深俯冲和折返作用。

在东构造结南迦巴瓦群中高压麻粒岩的发现及研究表明，前震旦纪的变质基底曾到达下地壳的深度(T=750～850℃，p=1.4～1.8GPa)，其峰变质年龄为 45～69Ma。高喜马拉雅结晶岩系中分布有平行喜马拉雅构造线走向的浅色花岗岩带，主要岩石类型有电气石花岗岩、白云母花岗岩和二云母花岗岩，属 S 型花岗岩，岩体常伴随有强烈的混合岩化、流劈理化和糜棱岩化作用。岩体的同位素年龄值有 4 组：1800～650Ma、500～400Ma、43.3Ma 和 18.6～10.5Ma[1]。

高喜马拉雅(GHM)亚地体中沉积盖层发育齐全，包括古生代、中生代、古—始新统的海相沉积及渐新世以来的陆相沉积。在高喜马拉雅亚地体的加里满都—甘托克一带，高喜马拉雅结晶岩片之下出露若干个为 MCT 制约的由低喜马拉雅新元古代—寒武纪绿片岩相组成的构造窗和半构造窗。由于特提斯-喜马拉雅(THM)亚地体的沉积盖层与高喜马拉雅(GHM)亚地体结晶变质岩系之间的强烈拆离(STD)，拆离层上部的震旦纪—寒武纪岩石强烈变质并且减薄，位于喜马拉雅东段的古生代地层几乎全部缺失，三叠系直接覆盖在高喜马拉雅结晶岩系之上。

2.3 低喜马拉雅(LHM)亚地体

低喜马拉雅(LHM)亚地体位于喜马拉雅结晶岩带的南侧，震旦系—下古生界绿片岩相浅变质岩系以主中央冲断裂(MCT)与高喜马拉雅结晶岩系相隔，大致可与特提斯喜马拉雅(THM)亚地体的震旦系—下古生界相对比，同属于印度地台的盖层沉积。上古生界分布在震旦系—下古生界以南，为冈瓦纳系沉积，因缺乏化石依据，暂定为石炭系—二叠系。主要岩性为黑色页岩、含复杂岩屑的泥岩和长石石英砂岩。低喜马拉雅(LHM)亚地体沿主边冲断裂(MBT)叠置在次喜马拉雅(SHM)亚地体之上。

2.4 次喜马拉雅(SHM)亚地体

由中中新世—第四纪西瓦里克沉积盆地组成，盆地西起巴基斯坦的白沙瓦，东延经西里克山、印度阿萨姆，至缅甸的掸邦高原，长达数千千米，为总厚达 6000m 的前陆盆地山麓相沉积。次喜马拉雅(SHM)亚地体沿喜马拉雅前锋冲断裂(MFT)往南推覆在印度克拉通之上。

3 喜马拉雅地体中的 SN 向和 EW 向大型韧性拆离构造

笔者的研究工作是在中国境内的雅鲁藏布江缝合带及以南的特提斯-喜马拉雅和高喜马拉雅亚地体中进行的。穿越的 4 条剖面(自东而西)为：仁布-江孜-康马-嘎拉-亚东剖面、

门布-赖西-聂拉木-樟木剖面、萨噶-马拉-吉隆-吉隆镇剖面和门士-普兰剖面,经过的地层有:属于雅鲁藏布江俯冲杂岩带的白垩纪日喀则群弧前盆地、蛇绿岩带、三叠纪—白垩纪复理石为基质的混杂堆积和厚逾1000m的属于印度次大陆被动陆缘的晚白垩世海相沉积、三叠纪—早侏罗世厚1000m左右的陆棚-斜坡相浅水-半深水相碳酸盐岩-碎屑岩类复理石沉积、泥盆纪—二叠纪浅海相碎屑岩-碳酸盐岩沉积、早古生代浅变质碎屑岩-碳酸盐岩以及由聂拉木群前震旦纪角闪岩相—绿片岩相的孔兹岩系(形成年龄为800～1800Ma)为代表的变质基底。通过构造变形几何学、运动学和动力学的研究,进一步确定了喜马拉雅增生地体中的SN向拆离构造——位于特提斯-喜马拉雅和高喜马拉雅亚地体之间的藏南拆离断裂带(STD)与位于特提斯-喜马拉雅亚地体中的康马-拉轨岗日拆离带(KLD)的关系,高喜马拉雅亚地体中新发现EW向拆离构造的存在,讨论了变形机制的内在联系(图2)。

3.1 特提斯-喜马拉雅(THM)亚地体中的SN向拆离构造

在特提斯-喜马拉雅(THM)亚地体中部的吉隆-拉轨岗日-康马300km的长度范围内,出露8个以元古宙变质基底岩石为核部和被古生代—中生代地层围绕的穹隆构造,自东向西依次为曲松穹隆、仁布穹隆、康马穹隆、哈金桑惹穹隆、萨迦穹隆、拉轨岗日穹隆(普弄抗日、总布荣和阿马穹隆)和吉隆穹隆。平面上呈圆形、椭圆形及长条形等几何形态,又称康马-拉轨岗日穹隆带。

Burg等[4]最早提出康马穹隆核部由变形的眼球状片麻岩组成,形成年龄为562Ma±4Ma(U-Pb)[31]。康马变质基底与古生代—中生代盖层之间的拆离断层(STD)为NS向伸展变形的产物,形成时代由正片麻岩的黑云母坪年龄20.4Ma±0.6Ma和白云母坪年龄15.5Ma而确定[18]。

笔者通过对康马穹隆的详细微构造观测和研究获得以下进一步的认识(图3、图2)。

(1)康马穹隆核部为聂拉木群的富铝深变质岩系,呈NS向椭圆状产出,叶理面向四周缓倾,倾角10°～25°。康马变质穹隆的基底岩石——花岗质片麻岩的原岩形成时代为835～869Ma,并经历了泛非造山事件(504～528Ma)的影响[32]。聂拉木群之上出露盖层震旦纪—奥陶纪、泥盆纪—二叠纪及三叠纪地层,逐次围绕在聂拉木群的四周,盖层强烈变形及减薄。

(2)康马穹隆变质基底的聂拉木群片麻岩与盖层之间发育由基底的花岗质糜棱岩和盖层的千糜岩组成的厚约250m的韧性拆离剪切带,穹形产出。糜棱面理上发育由长英质脉的布丁构造和石榴子石压力影构成的拉伸线理,在穹隆北部为SN向,南部为NWN-SES向。剪切带中发育平行拉伸线理方向的紧闭"A"型褶皱。XZ面上的S/C构造、σ型长石碎斑体系及长英质脉的不对称褶皱等剪切应变均显示了自南而北(或自南南东至北北西)的运动方向(图3、图4)。糜棱面理(S1)的重褶形成S2面理,S2上同样发育NS向拉伸线理及形成以S2为轴面的"B"型褶皱。震旦纪—奥陶纪、泥盆纪—二叠纪地层及三叠纪地层之间自下而上发育由韧性→脆性转化、厚度由几十米减薄到几米、拆离方向自南而北的次级拆离断层带,均显示了自南而北的剪切应变特征。后期的改造使拆离断层带呈现穹形构造样式,核部聂拉木群变质岩系出露地表。

(3)石英组构的EBSD测定。运用先进有效的电子背散射(electron backscatter diffraction, EBSD)技术,通过观测反向散射电子的衍射图像来提供微米级的晶体空间取向信息,使用日本电子公司(JEOL)制造的jsm-56101v型扫描电镜和丹麦HKL公司制造的CHANNEL5型号的EBSD仪器,将样品的XZ面定向薄片(X轴为拉伸线理方向,XY面为面理,Z

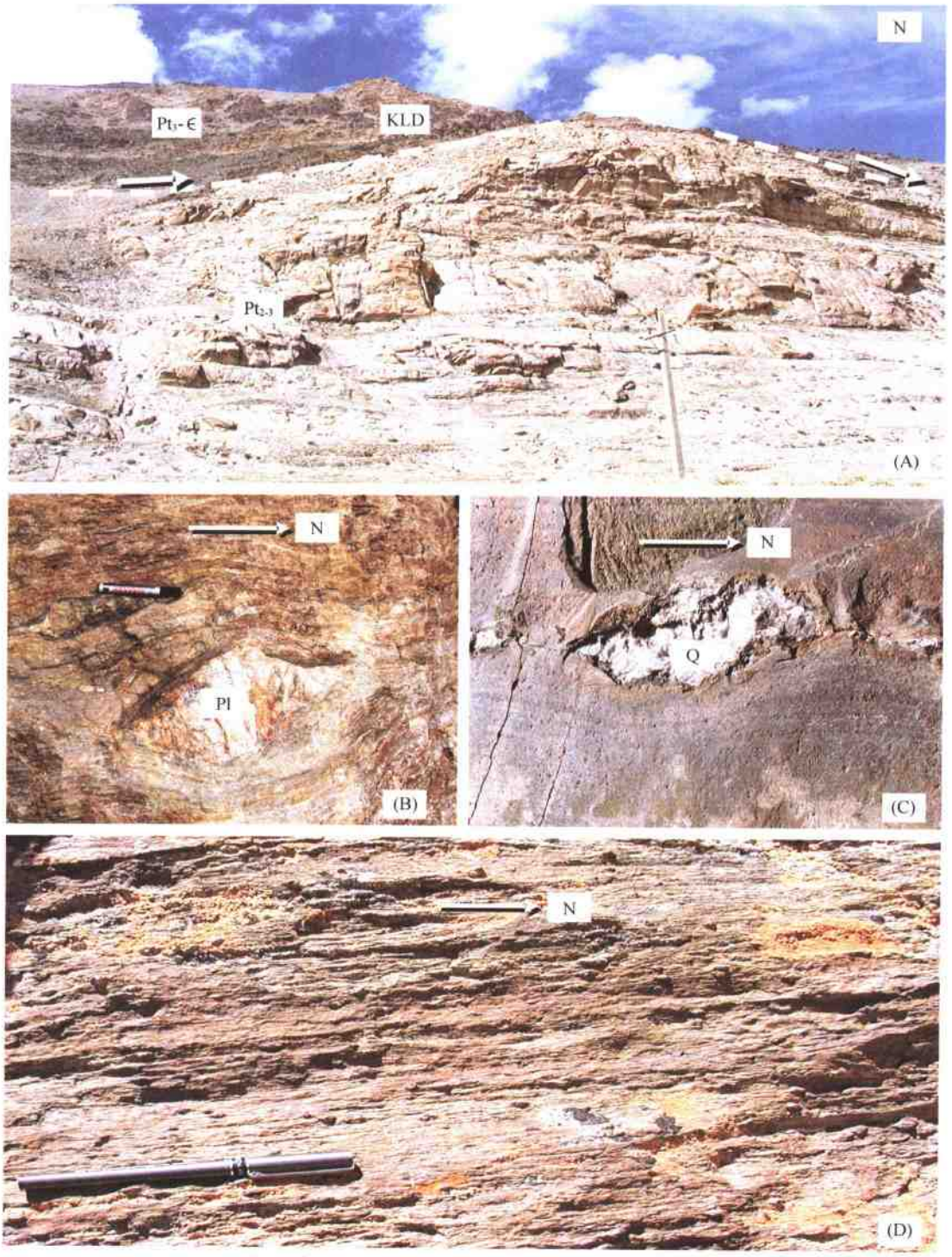

图 3　康马 SN 向韧性拆离构造带变形构造野外照片

Fig. 3　Field photo showing deformation structure in the N-S-trending Kangmar ductile detachment

(A):KLD—康马-拉轨岗日拆离带;Pt_{2-3}—中-晚元古代花岗片麻岩;Pt_3—∈—新元古代-寒武纪变质岩系;(B)、(C)、(D):Pl—斜长石斑晶,Q—石英脉

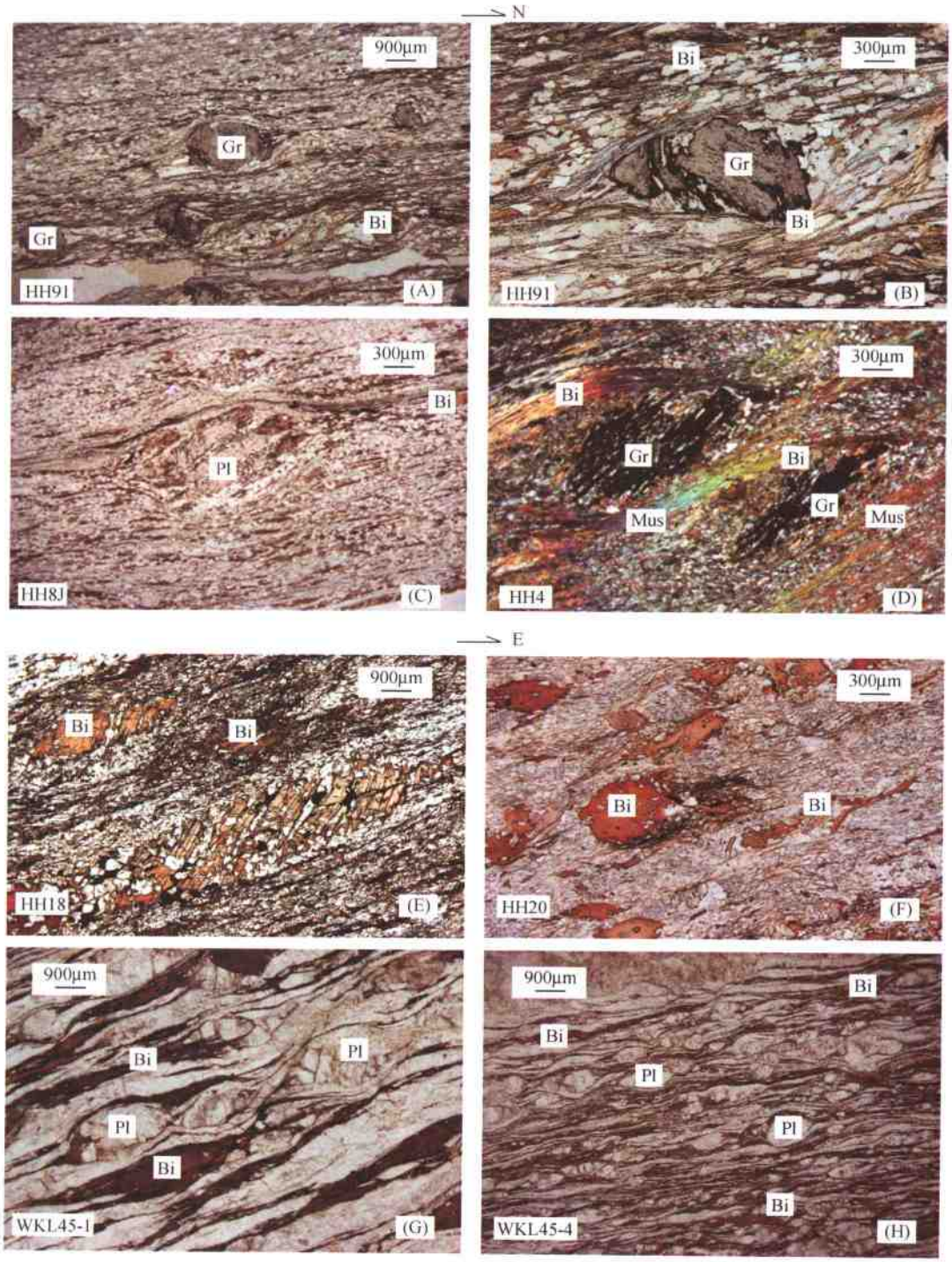

图 4　喜马拉雅增生地体中 NS 向和 EW 向拆离构造带的显微照片

Fig. 4　Photomicrograph showing N-S-and E-W-trending detachments in the Himalaya accretionary terrane

(A)、(B)、(C)、(D)—康马 SN 向拆离构造带的显微照片,显示自 S 而 N 的剪切应变;(E)、(F)、(G)、(H)—亚东 EW 向拆离构造带的显微照片,显示自 W 往 E 的剪切应变;Gr—石榴子石;Bi—黑云母;Mus—白云母;Pl—斜长石

轴垂直面理方向)精细抛光后置于20kV的扫描电镜电子束电压下,首先利用EBSD系统确定矿物的电子背散射通道衍射花样(electron backscatter pattern EBSP),标明衍射点的指数,然后在薄片范围内进行石英颗粒的优选方位测定,每类矿物大约测试3000～15000点。采集康马穹隆变质基底与盖层之间主拆离韧性剪切带中5个样品的石英颗粒进行测定,3个样品为变质基底的糜棱岩化花岗片麻岩(HH5、HH6、HH8),2个样品为盖层底部震旦纪—寒武纪的千糜岩化石榴子石石英片岩(HH18)和石英片岩(HH95),所测数据点的范围为2538～6887。通过下半球投影获得的石英EBSD图(图5-A)显示了基底糜棱岩化花岗片麻岩的石英组构类型为中高温(450～550℃)棱面$(10\bar{1}\,\bar{1})$<a>组构、柱面$(10\bar{1}0)$<a>组构和高温(>650℃)柱面$(10\bar{1}0)$<c>组构,剪切指向为自南向北;盖层底部千糜岩化石榴子石石英片岩(HH18)和石英片岩的石英组构表现为早期中高温(450～550℃)菱面$(10\bar{1}\,\bar{1})$<a>组构和叠置后期的低温(<350℃)底面(0001)<a>组构,剪切指向同样为自南向北(图6)[33]。表明康马拆离带形成于高温(>650℃)条件下,并经历了中温(450～550℃)→中低温(350～450℃)→低温(<350℃)的递退过程[34]。

上述研究表明,康马穹隆的形成主要经历了20Ma以来的伸展作用,形成基底与盖层之间自南而北的韧性拆离断层,继后东西向挤压使韧性拆离断层弯曲,形成穹隆构造。

李德威等[35]在研究藏南萨迦的拉轨岗日穹隆带时同样提出NS向拆离构造带的存在。拉轨岗日穹隆带由3个小穹隆——普弄抗日、总布容和阿马穹隆组成,穹隆核部的花岗片麻岩、混合花岗岩夹角闪斜长岩和榴闪岩的深变质岩系之上为由云母石英片岩、石榴子石云母片岩、十字石蓝晶石片岩、石英岩和大理岩组成的薄层中等变质(角闪岩—绿片岩相)岩系,其周围分别与下二叠统、三叠系和下侏罗统未变质岩系直接接触,缺失整个早古生代—泥盆纪地层[35]。笔者认为,穹隆核部深变质岩系之上的中等变质岩系可与康马穹隆拆离带之上的新元古代—寒武纪变质岩系对比,并且在穹隆的核部均有淡色花岗岩底辟侵位。因此,康马-拉轨岗日穹隆带中包含了同一条SN向拆离断层带的证据,可称为"康马-拉轨岗日拆离断层带"(KLD)。

3.2 藏南拆离断层(STD)与康马-拉轨岗日拆离断层(KLD)的连接

藏南拆离带(STD)是特提斯-喜马拉雅亚地体(THM)与高喜马拉雅亚地体(GHM)之间的边界,是一条发生在中-新元古代变质基底(下板片)和盖层(上板片)之间的一条规模巨大的向北缓倾并具有自南向北滑移的拆离构造带[5,16]。笔者观测了亚东帕里—聂拉木—吉隆镇以北地区,STD之下为高喜马拉雅角闪岩相—绿片岩相的富铝质片麻岩系,其顶部约2km厚的岩层强烈剪切应变和糜棱岩化,卷入拆离构造带中;拆离构造带之上的盖层显示出自下而上由角闪岩相→绿片岩相→低绿片岩相→未变质的递退变质和由强剪切变形→弱剪切变形的递退应变的演化规律,以及由于拆离作用盖层厚度明显减薄甚至尖灭。研究表明,STD中段450km的范围内,拆离带上部盖层岩片的底部均出露厚度仅几十米的新元古代—早寒武世强烈糜棱岩化的石榴子石云母片岩和二云石英片岩,其上寒武系—奥陶系为低绿片岩相(含有绿泥石、绿帘石和绢云母等矿物)的千枚岩、石英变质砂岩、钙质片岩、石英岩和大理岩,在平面上呈透镜状,厚度0～300m。

上板片的上部为厚度不等(几十到几百米)的未变质的泥盆纪石英砂岩-砂页岩-灰岩、石炭纪—二叠纪陆缘碎屑岩夹含砾板岩、三叠纪石英砂岩夹细砾岩和侏罗纪砂岩-粉砂岩。在上板片的新元古界—下寒武统、上寒武统—奥陶系、泥盆系—石炭二叠系和三叠系盖层之间均有

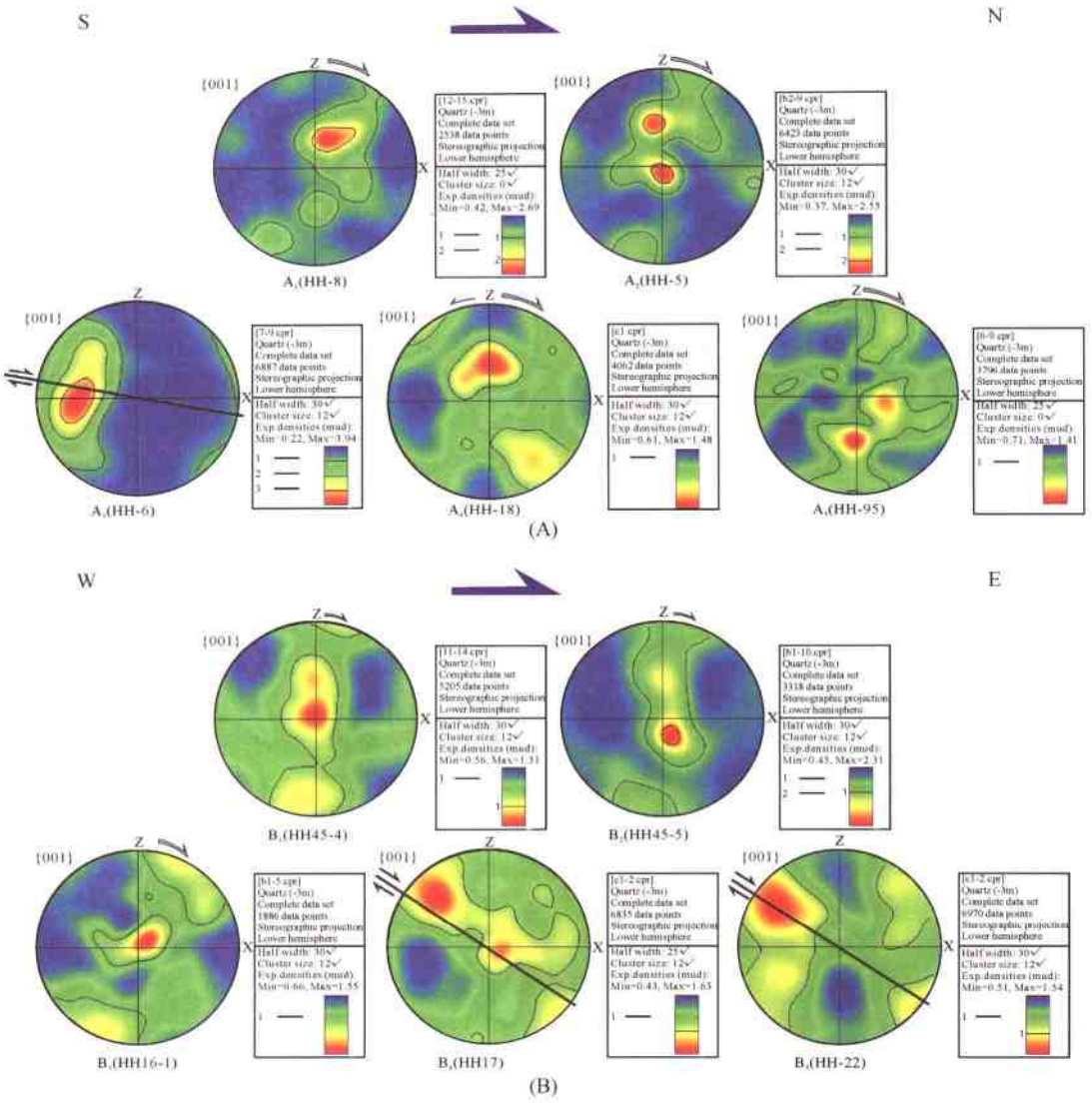

图 5　喜马拉雅增生地体中 SN 向和 EW 向拆离构造带的石英组构图

(EBSD 方法测试)

Fig. 5　Quartz fabrics in N-S-and E-W-trending detachments in the Himalaya accretionary terrane

(analyzed by EBSD)

(A)康马 NS 向拆离构造带中石英组构的 EBSD 测量结果,剪切指向自 S 向 N;

(B)高喜马拉雅亚地体 EW 向拆离构造带中石英组构的 EBSD 测量结果,剪切指向自 W 向 E

自下而上从韧性—韧脆性—脆性递变的次级平行拆离断裂系间隔。STD 东段和西段还显示高喜马拉雅结晶岩系与中生代不同地层直接接触,新元古代—古生代地层全部缺失或部分缺失。

前人已经开始注意到藏南拆离断层(STD)与康马-拉轨岗日拆离断层(KLD)之间的关系[17,35,36]。笔者的研究进一步提出藏南拆离断层(STD)与康马-拉轨岗日拆离断层(KLD)相连接的如下证据。

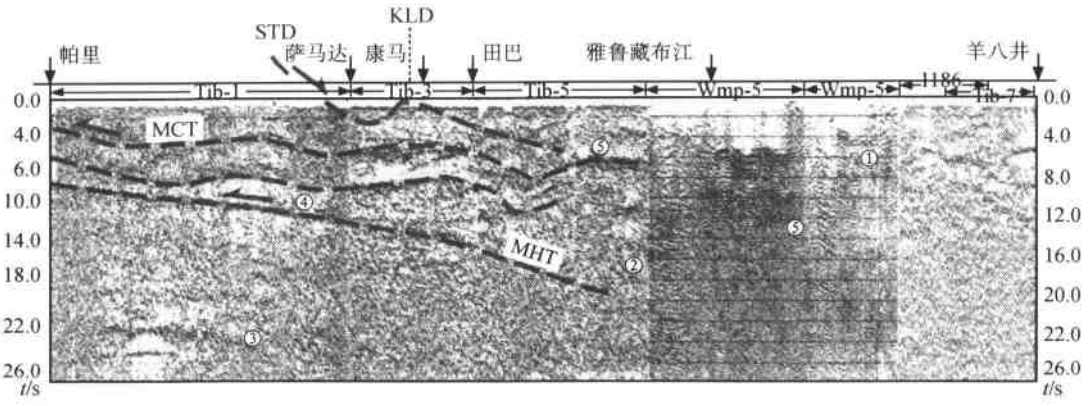

图 6　穿越喜马拉雅的地震反射剖面解释图

(原始资料据赵文津等,2001)[36]

Fig.6　Interpretation of the seismic reflection profile across the Himalayas

MCT—主中央逆断层;MHT—主喜马拉雅冲断层(深部);STD—藏南拆离断层;KLD—康马-拉轨岗日拆离断层

(1)位于藏南拆离带(STD)和康马-拉轨岗日(KLD)拆离带以下的变质基底原岩均为富铝质沉积岩系组合,原岩年龄大约 800～1800Ma,以中新元古代为主,并共同经历了泛非—早古生代(599～429Ma)造山事件[32],具有共同的变形和变质演化历史,表明它们为喜马拉雅地体的统一基底。

(2)藏南和康马-拉轨岗日拆离断层带均由韧性-韧脆性-脆性拆离断裂系组成,主拆离带岩石强烈糜棱岩化,糜棱面理上发育相同的近 SN 向拉伸线理,剪切应变显示自南往北的指向。

(3)拆离断层之上均为角闪岩相—绿片岩相—低绿片岩相的震旦纪—早古生代盖层岩片,强烈的剪切应变及自上而下的铲式构造样式同样显示了自南往北的剪切指向。由于拆离作用影响,上板片中的地层明显减薄和缺失,如康马拆离断层以上震旦统—下古生界的厚度减薄到只有 1km,藏南拆离断层带之上的震旦纪—早古生代盖层仅有 2.5～3km 厚。康马-拉轨岗日拆离断层带中变质基底与拆离断裂带之上不同时代的盖层(新元古界—寒武系、下古生界、石炭—二叠系、二叠—三叠系、三叠系和三叠—侏罗系等接触,拆离断裂带中盖层不同程度地减薄和尖灭可能与拆离强度在纵向上的不均一性有关,这与藏南拆离带的情况相同。

(4)前人资料表明藏南拆离断裂(STD)开始活动的时间早于 22Ma[37],中中新世和第四纪再活动[38](Hurtado *et al*,未发表)。康马拆离断裂(KLD)开始活动的时间为 20Ma,二云母花岗岩和淡色花岗岩侵入体的独居石 U-Th-Pb 年龄为 9.5～17.6Ma[8,31]。上述表明藏南拆离断层带(STD)与康马拆离断层带(KLD)形成时代基本相当。由此,康马拆离断层带(KLD)与藏南拆离断层带(STD)实为同一条拆离断层带。

(5)藏南/康马-拉轨岗日拆离带连接的深部证据。康马拆离断层带(KLD)与藏南拆离断层带(STD)为同一条拆离断层带,那么康马-拉轨岗日穹隆带是如何形成的?中美合作进行的 INDEPTH 计划所获得的横穿拉萨地体和喜马拉雅地体的羊八井-帕里(INDEPTH-Ⅱ)地震反射剖面揭示 MCT 和 STD 界面向北缓倾,延伸于特提斯-喜马拉雅亚地体之下,2

个界面均在康马穹隆的下部拱起,并继续往北延至雅鲁藏布江缝合带附近,表明康马拆离断层带(KLD)与藏南拆离断层带(STD)在深部连接(图 6)[33]。由于康马-拉轨岗日拆离带的穹隆核部均有淡色花岗岩体的侵位(9.5~17.6Ma)[8,31],表明康马-拉轨岗日穹隆带的形成与深部 STD 和 MCT 界面的拱起及花岗岩的侵入有关。地震反射剖面还揭示喜马拉雅地体之下的深部逆冲断裂(MHT)向北以缓倾角插入冈底斯地体之下,它的活动可能是壳下局部熔融物质的上涌形成花岗岩体的原因。

3.3 高喜马拉雅亚地体北部的 EW 向韧性拉伸变形构造

在高喜马拉雅(GHM)亚地体中主要发育以聂拉木群片麻岩系为主的印度次大陆变质基底,在东段亚东一带变质基底之上出露寒武纪—奥陶纪浅变质岩系组成的盖层,构成向形构造。新的变形构造研究厘定了高喜马拉雅单元(中国境内)中反映现代喜马拉雅变形特征的 3 种韧性变形样式:①自北而南的韧性逆冲剪切变形构造;②自南而北的韧性正滑变形构造;③EW 向韧性拉伸变形构造。特别是 EW 向韧性拉伸变形构造的发现为讨论喜马拉雅造山机制提供了新的思考。

沿高喜马拉雅亚地体北部普兰—吉隆—聂拉木—亚东长约 800km 一带,在变质基底与盖层中普遍发育以 EW 向拉伸线理为特征的面形韧性拆离构造,笔者称其为高喜马拉雅(普兰—亚东)东西向拆离带(GHD),证据如下。

(1)高喜马拉雅(普兰—亚东)东西向拆离带(GHD)的微构造特征

西部普兰地区:普兰纳木那尼峰下的聂拉木群为由含石榴子石斜长角闪片麻岩、硅线石榴黑云斜长片麻岩、长英质片麻岩和大理岩等组成的变质岩系,普遍糜棱岩化,糜棱面理近水平,发育近 EW 向拉伸线理,显示了角闪石定向排列及长英质脉布丁的微构造特征。XZ 面定向薄片上的 S/C 构造、"σ"和"δ"型长石碎斑体系、不对称云母鱼、拖曳褶皱和多米诺骨牌构造等均显示自西往东的剪切指向(图 7)。

中部吉隆和聂拉木地区:珠穆朗玛峰以西的吉隆和聂拉木地区以硅线石榴黑云斜长片麻岩为主的变质岩系中,均发现 EW 向韧性伸展变形,在向北缓倾的面理上发育 EW 向水平拉伸线理,剪切应变指示自西向东的滑移(图 7)。

东部亚东地区:在亚东地区的震旦纪—寒武纪盖层与前震旦纪变质基底之间存在一条具有 EW 向拉伸线理的面形韧性剪切带,厚度约 1km,韧性剪切带呈向形构造样式产出,表明韧性剪切带又经历了后期南北向挤压作用(图 7)。面形韧性剪切带下部前震旦纪变质岩系中,根据斜长角闪岩的透镜体的雁行状排列、不对称长英质脉体的布丁及不对称褶皱等剪切应变特征,判断剪切指向为自西往东;而形韧性剪切带上部角闪岩相—绿片岩相的震旦纪—寒武纪沉积盖层强烈变形,与变质基底的变形具有连续性、递进性,普遍发育 EW 向拉伸线理,出现近平卧不对称协调褶皱系列,根据褶皱轴面的倾伏、石榴子石旋转、S/C 构造和不对称布丁化石英脉的微构造特征,确定剪切指向自 W 往 E(图 8、图 4-B)。

(2)高喜马拉雅(普兰—亚东)东西向拆离带石英组构的 EBSD 测量

选择普兰地区变质基底糜棱岩化花岗片麻岩(HH45-4、HH45-5)和亚东地区盖层的石英榴闪岩(HH16-1、HH17)、黑云母变质砂岩(HH22)共 5 个样品,获得花岗片麻岩中石英颗粒的中高温(450~650℃)$(10\bar{1}0)<a>$、$(10\bar{1}\,\bar{1})<a>$滑移系和低温(<350℃)的(0001)<a>滑移系的 EBSD 组构图,无论是卷入剪切带的基底还是盖层的强剪切变形岩石均显示了自西往东的运动指向(图 5-B)。

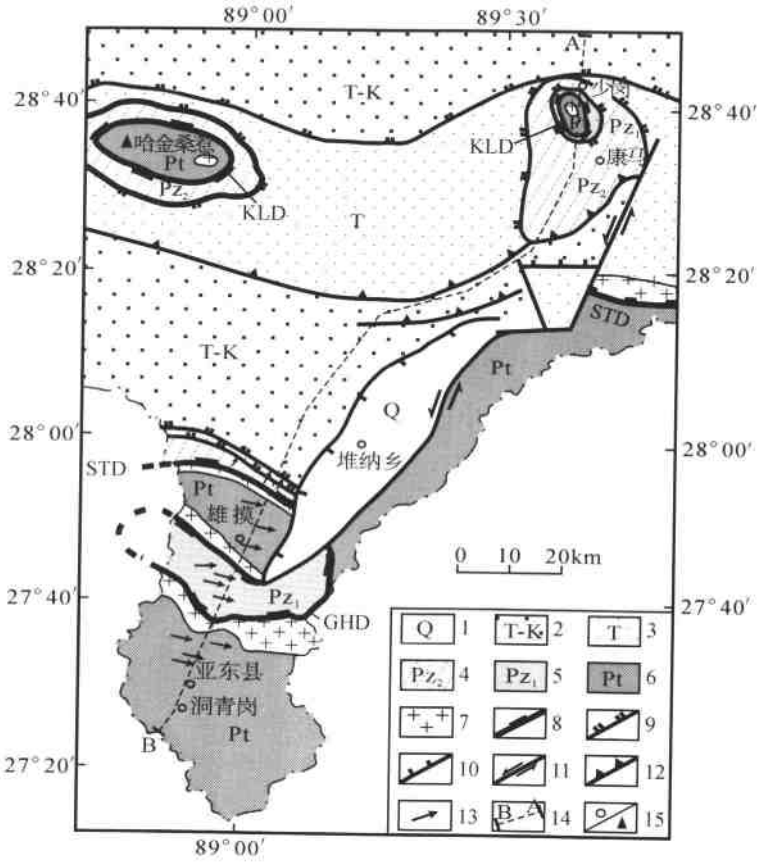

图 7　亚东-康马地区构造图

（由丁孝忠提供的新编亚东 1:25 万地质图作为基础背景而编制）

Fig.7　Tectonic map of the Yadong-Kangmar area

1—第四纪裂谷盆地；2—三叠纪—白垩纪地层；3—三叠纪地层；4—晚古生代地层；5—早古生代浅变质岩系；6—中新元古代变质基底；7—花岗岩；8—拆离断层主界面；9—拆离断层；10—正断层；11—走滑断层；12—逆冲断层；13—拉伸线理及剪切指向；14—剖面线；15—地名及山峰

3.4　高喜马拉雅中 EW 向伸展构造与 NS 向逆冲构造的转换关系

在聂拉木南樟木海关一带的基底变质岩系中发育近 EW 走向 N 倾的渗透性面理，倾角 25°～40°，面理上发育近水平的 EW 向拉伸线理，剪切应变显示自西向东。自北而南可见 EW 向拉伸线理在面理上逐渐由水平变为向西斜倾，并且由缓倾渐变为陡倾（W＜35°→W＜63°），剪切应变由自西向东的运动指向逐渐变为自北而南的逆冲运动指向，由近水平的向东滑移的构造样式逐渐转为右行逆冲和逆冲的应变样式。

在亚东和吉隆镇南部变质基底中也发现与聂拉木南樟木海关一带相同的 2 组拉伸线理方向（NS 和 EW 向）转换的情况，过渡区域的剪切应变指示了右行逆冲的运动指向。

3.5　喜马拉雅事件年龄

主中冲断裂（MCT）中淡色花岗岩的角闪石 ^{39}Ar-^{40}Ar 测试和 U-Pb 定年表明 MCT 形成早于 23～20Ma[37,39]，但它在晚中—上新世还继续活动[8]，并显示了全新世活动的证据

图 8　亚东地区 EW 向韧性拆离构造带变形构造野外照片

Fig. 8　Field photo showing deformation structure in the E-W-trending Yadong ductile detachment

(A)GHD—高喜马拉雅拆离带;Pt_{2-3}—中-新元古代变质基底;Pt_3—∈—新元古代-寒武纪变质岩系;(B)长英质脉的旋转布丁构造显示自 W 向 E 的剪切应变;(C)A 型剪切平卧褶皱;(D)EW 向拉伸线理

(Hodges *et al*,未发表)。藏南拆离断裂(STD)开始活动的时间也早于 22Ma[37],中中新世和第四纪再活动[38](Hurtado *et al*,未发表)。上述表明制约高喜马拉雅亚地体的主中央冲断裂(MCT)和藏南拆离断裂(STD)几乎是同时产生和活动的,高喜马拉雅崛起的机制是"向上的挤出机制"[14,40]。伴随挤出机制产生的大量淡色花岗岩的 U-Th-Pb 年龄为 22～23Ma[37,41]到 12～13Ma[42],在东西构造结获得最年轻的淡色花岗岩的年龄(<4Ma)[43,44]。

本研究通过亚东硅线石榴黑云斜长片麻岩样品(HH32)中 3 个变质锆石及变质增生锆石(Th/U =0.01～0.03)所测得的年龄(27Ma ±1Ma、19Ma ±14Ma、12Ma ±5Ma)为一致年龄,加权平均值 19.3Ma ±6.7Ma;聂拉木地区 3 颗变质锆石(Th/U <0.1)所测的年龄(20Ma ±0.6Ma、19Ma ±0.5Ma、19Ma ±0.5Ma)为一致年龄,平均值为 19.29Ma ±0.63Ma[32](表 1)。新的 SHRIMP 测年数据结果代表了喜马拉雅事件的记录,与前人大量研究结果一致。

表 1 亚东(HH32)和聂拉木(HH72)片麻岩中锆石 SHRIMP U-Pb 定年数据

Table 1 SHRIMP U-Pb dating data for zircons from the Yadong(sample HH32)and Nyalam(sample HH72)gneisses

样品号	$U/10^{-6}$	$Th/10^{-6}$	$^{206}Pb/10^{-6}$	Th/U	$^{235}U/^{207}Pb^*$	$^{238}U/^{206}Pb^*$	$^{206}Pb^*/^{238}U$ 年龄/Ma
HH32-18.1	375	9	1.35	0.03	15.8479±1.3154	237.90±9.2780	27±1
HH32-3.2	40	1	0.30	0.03		342.00±249.66	19±14
HH32-6.1	109	1	0.38	0.01		546.00±212.94	12±5
HH72-22.1	4031	7	10.8	0.00	78.7402±16.5354	328.10±9.5149	20±0.6
HH72-13.1	9171	30	23.8	0.00	60.9756±5.2439	335.00±9.3800	19±0.5
HH72-19.1	5795	12	14.9	0.00	56.1798±4.6067	337.60±9.4528	19±0.5
HH72-23.1	18403	52	43.2	0.00	49.4315±1.8290	366.50±9.8955	18±0.5

4 现代喜马拉雅造山机制的再讨论

研究表明,特提斯洋的影响使印度陆块上的原始喜马拉雅泛非—早古生代造山带之上覆盖了晚古生代至白垩纪的特提斯型海相沉积,69Ma 开始印度陆块向北移动,大约 55Ma 印度与亚洲碰撞,使印度陆块俯冲消减和大印度陆块变成小印度陆块。新生代开始,喜马拉雅再次崛起,现代喜马拉雅造山带成为亚洲/印度陆-陆碰撞的最好例子。印度与亚洲的拼贴不仅产生了喜马拉雅山链,还形成了 5km 高的青藏高原、巨大范围的变形域和地壳缩短加厚。地壳的缩短主要通过喜马拉雅地体中及雅鲁藏布江缝合带以北地区的变形——逆冲断裂、褶皱和早期构造的再活化表现出来。对喜马拉雅地体变形构造的研究提出了对喜马拉雅造山机制的新思考。

4.1 主中冲断层(MCT)实质上为一条陆内转换挤压带

主中央冲断层(MCT)的主界面位于本研究区域以外的国外部分,因此缺乏对它的直观认识。但在高喜马拉雅亚地体的亚东—聂拉木—吉隆南部靠近边境一带,出现具有与横向拉伸线理斜交的右行逆冲剪切应变体系,如果这样的剪切应变体系是主中冲断层(MCT)在本研究区的反映,那么可以推测,主中冲断层带是一条具有斜向碰撞性质的相当规模的陆内转换挤压带,即具平移性质的逆冲带。古地磁记录已表明,自碰撞早期以来印度以反时针的旋转方式继续向北推进[45,46],因此主中冲断层系的运动学是印度/亚洲板块斜向碰撞的见证。

4.2 喜马拉雅 SN 向拆离带——藏南拆离带(STD)+康马-拉轨岗日拆离带(KLD)

已揭示了喜马拉雅地体中高喜马拉雅亚地体的北界为向北缓倾的藏南拆离断裂(STD),以 SN 向拉伸线理、自南往北的正向滑移及强烈韧性剪切应变为特征;南界为向北缓倾的主中央冲断裂(MCT),以 SN 向拉伸线理、自北往南的逆冲指向及强烈韧性剪切应变为特征,并在南缘形成一系列的逆冲叠覆岩片构造,由古老变质基底岩石组成的高喜马拉雅构造单元总体显示了南缘逆冲、北缘拆离的"挤出构造岩片"的特征[40]。特提斯-喜马拉雅亚地体中的康马-拉轨岗日穹隆带核部由串珠状分布的古老变质岩石组成,其与高喜马拉雅亚地体的基底物质组成和形成演化时代大体一致。穹隆核部与周边震旦纪—寒武纪石榴子石黑云母片岩、绿泥石英片岩及上部盖层之间为自南往北剪切并呈穹形的韧性拆离带。研

究表明,藏南拆离断裂(STD)和主中央冲断裂(MCT)的形成年龄大致从20Ma开始,是喜马拉雅造山事件的产物[4-7,9],本文中获得的喜马拉雅事件记录(亚东27～12Ma,聂拉木20～19Ma)也证明了这一点。研究提出,康马-拉轨岗日拆离带(KLD)和藏南拆离带(STD)为位于高喜马拉雅亚地体后缘(北缘)的同一条伸展式断层,向北延伸于特提斯-喜马拉雅亚地体之下,推测南北延伸达200km,是一条巨型拆离带。它的规模已远远超出前人的认识范围。

4.3 高喜马拉雅EW向拉伸拆离构造

高喜马拉雅EW向拉伸拆离构造首先在西段被发现。西喜马拉雅尼泊尔北西部Gurla Mandhada-Humla剪切带为一条缓倾角(20°)的拆离带,厚度2m,拉伸线理近EW向,剪切指向自E往W。石榴子石中独居石的Th-Pb测年结果显示石榴子石生长在16～10Ma期间。本研究揭示高喜马拉雅中东段(普兰—吉隆—聂拉木—亚东长约800km一线)发育大面积自W往E的拉伸拆离构造,与西段遥相呼应,高喜马拉雅EW向拉伸拆离构造成为现代喜马拉雅构造变形的新标记。

4.4 "垂向挤出"和"侧向水平挤出"机制的耦合

在高喜马拉雅亚地体中东段自南而北呈现相互转换的韧性构造样式:斜向逆冲→EW向伸展→斜向伸展→SN向伸展。前缘斜向逆冲与MCT有关,后缘斜向伸展与SDT有关,说明20Ma以来高喜马拉雅变质体的隆升受到斜向向上挤出机制的制约。根据EW向拉伸构造与NS向斜向逆冲、斜向伸展的渐变和转换关系,以及整个高喜马拉雅亚地体西段自东往西和中东段自西往东近水平滑移的运动学特征,推测其反映高喜马拉雅中东段物质向东、西段物质向西逃逸的特征。因此,EW向拉伸构造是印度/亚洲岩石圈碰撞的近NS向挤压背景下古老基底岩石从深部斜向挤出并导致近水平滑移的造山机制的综合效应(图9)。

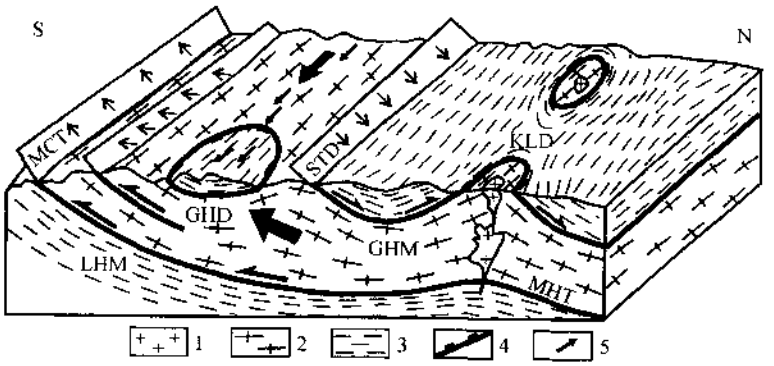

图9 高喜马拉雅造山机制模式图

Fig.9 Model showing the orogenic mechanism of the Greater Himalaya

1—浅色花岗岩;2—中新元古代变质岩系;3—早古生代浅变质岩系;4—拆离断层主界面;5—拉伸线理;STD—藏南拆离断层;MCT—主中央冲断层;GHD—高喜马拉雅拆离断层;KLD—康马-拉轨岗日拆离断层;GHM—高喜马拉雅亚地体;LHM—低喜马拉雅亚地体

4.5 喜马拉雅缩短量的再重塑

对喜马拉雅地壳缩短量已做了许多工作,曾推测MCT与MFT之间的缩短量为414～

550km[47]，西尼泊尔低喜马拉雅 MBT 和 MCT 之间的缩短量为 228km[48,49]，东尼泊尔低喜马拉雅和次喜马拉雅之间缩短 70km，MCT 及藏南地区缩短 150～170km 等。因而，进一步又提出喜马拉雅地体两翼的缩短为 465～808km[1]，MFT 和 MMT 的总缩短量 620km[50,51]。笔者认为，高喜马拉雅的实际变形包括了"原始喜马拉雅"变形和"现代喜马拉雅"变形两部分，新生代变形又包含了挤压、走滑和伸展机制造成的变形，因此实际的"现代"缩短量应该比上述估算的小。

致谢 SHRIMP 年龄测试在中国地质科学院地质研究所同位素实验室进行，EBSD 组构测量在中国地质科学院地质研究所大陆动力学实验室进行，在成文中与肖序常院士和赵文津院士进行了有益的讨论，文中图件由张晓卫绘制，参考文献由蔡志慧、唐哲民协助整理，在此一并感谢。

参 考 文 献

[1] Dewey J F, Cande S, Pitman W C. Tectonic evolution of the India/Eurasia Collision zone [J]. Eclogae Geologicae Helvetiae, 1989, 82: 717～734.

[2] Gansser A. Geology of the Himalayas[M]. London, Wiley Interscience, 1964.289.

[3] Le Fort P, Debon F, Sonet J. The Lower Paleozoic "Lesser Himalayan" granitic belt: Emphasis on the Simchar pluton of central Nepala. in: Shams F A ed. Granites of the Himalaya arakoram and Hindu Kush[C]. Lahore, Institute of Geology, Punjab University, 1983, 235～256.

[4] Burg J P, Chen G M. Tectonics and structural formation of southern Tibet, China[J]. Nature, 1984, 311: 219～223.

[5] Burchfiel B C, Chen Z, Hodges K V, *et al*. The South Tibetan Detachement System, Himalayan orogen: extension contemporaneous with and parallel to shortening in a collisional mountain belt[J]. Geol. Soc. Am. Spec.Pap., 1992, 269: 1～41.

[6] Brookfield M E. The Himalayan passive margin from Precambrian ti Cretaceous[J]. Sedimentary Geol., 1993, 84: 1～35.

[7] Le Fort P. Evolution of the Himalaya[A]. In: A Yin, T M Harrison, The Tectonics of Asia[C]. New York: Cambridge Univ. Press, 1996, 95～106.

[8] Harrison T M, Ryerson F J, LeFort P, *et al*. A late Miocene—Pliocene progin for the central Himalayan inverted metamorphism[J]. Earth and Planetary Science Letters, 1997, 146: E1～E7.

[9] Yin A, Harrison T M. Geologic evolution of the Himalayan—Tibetan orogen[J]. Rev.Earth Planet. Sci, 2000, 28: 211～280.

[10] Tapponnier P, Peltzer G, Le Dain Y, *et al*. Propagating extrusion tectonics in Asia: New insights from simple experiments with plasticine[J]. Geology, 1982, 10: 611～616.

[11] Peltzer G, Tapponnier P. Formation and evolution of strike-slip faults, rifts, and basins during the India-Asia collision: An experimental approach[J]. Journal of Geophysical Research, 1988, 93(12): 1508～1517.

[12] Avouac J-P, Tapponnier P. Kinematic model of active deformation in central Asia[J]. Geophys. Res. Lett., 1993, 20: 895～898.

[13] Tapponnier P, Xu Zhiqin, Roger F, *et al*. Oblique stepwise rise and growth of the Tibet Plateau[J]. Scieces, 2001, 294: 1671～1677.

[14] Chemenda A I, Mattauer M, Bokun A N. Continental subduction and a mechanism for exhumation of high-pressure metamorphic rocks: New modeling and field data from Oman [J]. Earth and Planetary Science Letters, 1996, 143: 173～182.

[15] Burchfiel B C, Royden, L H. North-south extension within the convergent Himalaya region[J]. Geology, 1985, 13:

679～682.

[16] 崔军文,朱红,武长得,等．亚东-格尔木 GGT,青藏高原岩石圈变形及其动力学[M]．北京:地质出版社,1992,1～164.

[17] 崔军文．喜马拉雅碰撞带的构造演化[J]．地质学报,1997,71(2):105～112.

[18] Chen Z, Liu Y, Hodges K V, *et al*. The Kangmar dome: A metamorphic core complex in southern Xizang (Tibet) [J]. Science, 1990, 250: 1552～1556.

[19] 刘文灿,梁定益,王克友,等．藏南康马地区奥陶系的发现及其地质意义[J]．地学前缘,2002,9(4):247～248.

[20] 周志广,刘文灿,梁定益．藏南康马奥陶系及其底砾岩的发现并初论喜马拉雅沉积盖层与统一变质基底的关系[J]．地质通报,2004,23(7):655～663.

[21] Krummenacher D. Determination d'age isotopique faite sur quelques roches de L'Himalaya du Nepal par la methode K/Ar[J]. Bull. Suisse, Min. Petr., 1961, 41/2:273.

[22] Xu R H, Sharer U, Allegre C J. Magmatism and metamorphism in the Lhasa Block (Tibet): An U-Pb geochronological study[J]. J. Geol., 1985, 93:42～57.

[23] Acharyya. Stratigraphy and tectonic features of the Eastern Himalayas[A]. In: Saklani P S ed. Tectonic geology of the Himalaya[C]. Today and Tomorrow's Pub., 1997. 243～268.

[24] Thakur V C. Tectonics of the Central crystallines of western Himalaya[J]. Tectonophysics, 1980, 62:141～154.

[25] Gehrels G E, Decelles P G, Martin A, *et al*. Initiation of the *Himalayan orogen as an Early Paleozoic* Thin-skinned Thrust belt[J]. GSA Today, 2003, 13:4～9.

[26] Pognante U, Spencer D A. First record of eclogites from the High Himalayan belt, Kaghan valley(northern Pakistan) [J]. Eur. J. Mineral., 1991, 3/3:613～618.

[27] Guillot S, Mascle G, Lardeaux J M, *et al*. A new discovery of eclogites from the Himalaya, Tso Morari dome unit (northwestern India) [J]. Mitteilungen des Geologischen Institut ETH Zürich and Universitat Zürich, Neue Folge, 1995, 298: 84～87.

[28] Guillot S, de Sigoyer J, Lardeaux J M. *et al*. Eclogitic metasediments from the Tso Morari area (Ladakh, Himalaya): Evidence for continental subduction during India-Asia convergence [J]. Contrib. Mineral. Petrol., 1997, 128: 197～212.

[29] Le Fort P, Guillot S, Pecher A. HP metamorphic belt along the Indus suture zone of NW Himalaya: New discoveries and significance[J]. C. R. Acad. Sci. Paris, 1997, 325: 773～778.

[30] Tonarini S, Villa I, Oberli M, *et al*. Eocene age of eclogite metamorphism in Pakistan Himalaya: Implications for IndiaEurasia collision[J]. Terra Nova, 1993, 5:13～20.

[31] Scharer U, Xu R, Allegre C. U-(Th)-Pb systematics and ages of Himalayan leucogranites, south Tibet [J]. Earth and Planetary Science Letters, 1986, 77:35～48.

[32] 许志琴,杨经绥,梁凤华,等．喜马拉雅地体的泛非-早古生代造山事件年龄记录[J]．岩石学报,2005,21(1):1～12.

[33] Zhao W J, Nelson K D, Project INDEPTH Team. Deep seismic reflection evidence for continental underthrusting beneath southern Tibet[J]. Nature, 1993, 366:557～559.

[34] Mainprice D, Boucher T-L, Blumenfeld P, *et al*. Dominant c slip in naturally deformed quartz: implications for dramatic plastic softening at high temperature[J]. Geology, 1986, 14:819～822.

[35] 李德威,刘德民,廖群安,等．藏南萨迦拉轨岗日变质核杂岩的厘定及其成因[J]．地质通报,2003,22(5)303～307.

[36] 赵文津及 INDEPTH 项目组著．喜马拉雅山及雅鲁藏布江缝合带深部结构与构造研究[M]．北京:地质出版社．2001.369.

[37] Hodges K V, Parrish R R, Searle M P. Tectonic evolution of the central Annapurna Range, Nepalese Himalayas[J]. Tectonics. 1996.15: 1264～1291.

[38] Hodges K V. The thermodynamics of Himalayan orogenesisA. In: Treloar P. J, O'Brien P eds. What drives metamorphism and metamorphic reactions[C]. Geological Society, 1998.270.

[39] Hubbard M S. Thermobarometric constraints on the thermal history of the Main Central thrust zone and Tibetan slab,

eastern Nepal Himalaya[J]. Journal of Metamorphic Geology, 1989, 7: 19～30.

[40] Chemenda A I, Burg P, Mattauer M. 2000, Evolutionary model of the Himalaya-Tibet system: geopoem based on new modeling, geological and geophysical data [J]. Earth Planet. Sci. Lett., 2000, 174: 397～409.

[41] Harrison T M, Mahon K I, Guillot S, *et al*. New constraints on the age of the Manaslu leucogranite: Evidence for episodic tectonic denudation in the central Himalaya: Discussion and reply[J]. Geology, 1995, 23: 478～480.

[42] Wu C L, Nelson K D, Wortman G, *et al*. Yadong cross structure and South Tibetan detachment in the east central Himalaya (89°-90°E)[J]. Tectonics, 1998, 92: 28～45.

[43] Zeitler P K, Chamberlain C P, Smith H A. Synchronous anatexis, metamorphism, and rapid denudation at Nanga Parbat(Pakistan Himalaya) [J]. Geology, 1993, 21: 347～350.

[44] Burg J P, Nievergelt P, Seward D, *et al*. The Namche Barwa syntaxis: Evidence for exhumation related to compressional crustal folding[J]. Journal of Asian Earth Sciences, 1998, 16: 239～252.

[45] Patriat P, Achache J. India-Eurasia collision chronology has implications for crustal shortening and driving mechanisms of plates[J]. Nature, 1984, 311: 615～621.

[46] Klootwijk C T, Gee J S, Peirce J W, *et al*. An early India-Asia contact: Paleomagnetic constraints from Ninetyeast Ridge, ODP Leg 121[J]. Geology, 1992, 20: 395～398.

[47] Srivastava P, Mitra G. Thrust geometries and deep structure of the outer and lesser Himalaya, Kumaun and Garhwal (India): Implications for evolution of the Himalayan fold and thrust belt[J]. Tectonics, 1994, 13: 89～109.

[48] DeCelles P G, Gehrels G E, Quade J, *et al*. Eocene-early Miocene foreland basin development and the history of Himalayan thrusting, Weston and central Nepal [J]. Tectonics, 1998, 17: 741～765.

[49] DeCelles P G, Gehrels G E, Quade J, *et al*. Eocene-early Miocene foreland deposits, erosional unroofing, and the kinematic history of the Himalayan fold-thrust belt, western Nepal[J]. Geology Society of America Bulletin, 1998, 110: 2～21.

[50] Lyon-caen H, Molnar P. Constraints on the structure of the Himalaya from an analysis of gravity, anomalies and a flexural model of the lithosphere [J]. Journal of Geophysical Research, 1983, 88: 8171～8191.

[51] Molnar P. Structure and tectonics of the Himalaya: Constraints and implications of geophysical data[J]. Annual Review of Earth and Planetary Sciences, 1984, 12: 489～518.

India-Asia collision: A further discussion of N-S- and E-W-trending detachments and the orogenic mechanism of the modern Himalayas

XU Zhi-qin　YANG Jing-sui　QI Xue-xiang　CUI Jun-wen
LI Hai-bing　CHEN Fang-yuan
(Key Laboratory of Continental Dynamics of the Ministry of Land and Resources, Institute of Geology, Chinese Academy of Geological Sciences, Beijing 100037, China)

Abstract　India-Asia collision formed the Himalaya accretionary terrane, which is composed from north to south of the Tethys-Himalaya (THM), Greater Himalaya (GHM), Lesser Himalaya (LHM) and Subhimalaya (SHM) subterranes. Comparison of the compositions, metamorphisms and evolutions, deformation mechanisms and formation ages of metamorphic basements and covers in the Himalaya accretionary terrane indicates that the southern Tibet detachment (STD) on the northern margin of the GHM subterrane extends northward beneath the

THM subterrane and is connected with the Kangmar-Lhagoi Kangri detachment (KLD) that formed at >650℃ and has the nature of north-directed shear slip motion, and that partial melting of the crust and material upwelling resulted in granite emplacement and uplift of the KLD, forming the Kangmar-Lhagoi Kangri gneiss domes. An E-W-trending subhorizontal ductile detachment (GHD) is found between the metamorphic basement and cover in the northern part (Burang-Gyirong-Nyalam-Yadong area) of the GHM subterrane, which is characterized by E-W stretching lineation and gently dipping mylonitic foliation and shows the east-directed horizontal slip shear sense; whereas near the north side of the Main Central Thrust (MCT) in the southern part of the GHM subterrane there occur ductile strike slip-thrust faults of transpressional nature. From south to north the GHM subterrane has the features of continuous deformation and transition from Thrust→oblique thrust→E-W trending extention→oblique extention→S-N trending extention, which are the response to the composite deformation under the orogenic mechanism of coupling of vertical and lateral extrusions. The existence of the E-W-and N-S-trending detachments in the Himalaya terrane provide a basis for a further discussion of the modern orogenic mechanism of the Himalayas.

Key words Himalaya N-S- and E-W-trending detachments vertical and lateral extrusions orogenic mechanism

Timing and mechanism of formation and exhumation of the Northern Qaidam ultrahigh-pressure metamorphic belt●

Xu Zhiqin● Yang Jingsui Wu Cailai Li Haibing
Zhang Jianxin Qi Xuexiang Song Shuguang Qiu Haijun
(Laboratory of Continental Geodynamics, Institute of Geology, Chinese Academy of Geological Sciences, Baiwanzhuang Road 26, Beijing 100037, China)

Abstract The Qilian Caledonian orogenic belt on the north margin of the Qinghai-Tibet Plateau were formed by convergence and collision of the Alxa terrain, Qilian terrain and Qaidam terrain. The 350-km-long, WNW-ESE-trending North Qaidam ultrahigh-pressure (UHP) metamorphic belt, lying between the Qilian and Qaidam terrains, was formed between 495 and 440Ma by deep subduction of the South Qilian Sea and the Qaidam continental crust beneath the Qilian terrain. The UHP belt was exhumed by a process of 'oblique extrusion' during transformation from 'normal' to 'oblique' intracontinental subduction between the Qilian and Qaidam terrains. Exhumation began at 470～460Ma and was completed by 406～400Ma. Exhumation structures are well-preserved in the UHP rocks and record extensive retrograde metamorphism.

Key words Northern Quaidam UHP metamorphic belt Exhumation Mechanism

1 Introduction

The northern Qinghai-Tibet plateau (NQTP) is a mosaic of multiple terrains and island/continental arcs. The NQTP composite terrain is composed of the Qilian terrain, Qaidam terrain, northern part of the eastern Kunlun terrain, southern part of the eastern Kunlun terrain and Altyn terrain. Lying in the northern margin of the Qinghai-Tibet Plateau, the Qilian Caledonian orogenic belt form a WNW-ESE trending belt about 800km long and 400km wide (Fig.1). This belt is bounded on the north by the Hexi Corridor, on the south by the Qaidam basin, on the east by the West Qinling Mountains and on the west by the Altyn Tagh fault. It is considered to be the product of convergence and collision of the Alxa terrain (west segment of the North China plate), the Qilian and the Qaidam terrain during the Caledonian. Subduction complexes along both sides of the Qilian terrain separate the three terrains (Xu *et al*., 2000). Late Devonian molasse deposits rest unconformably on the Lower Palaeozoic folded metamor-

● Journal of Asian Earth Sciences 28(2006)160～173.
● Corresponding author. E-mail address: xzq@ccsd.cn (X. Zhiqin).

phic rocks and Caledonian granites, indicating the end of the Caledonian orogeny.

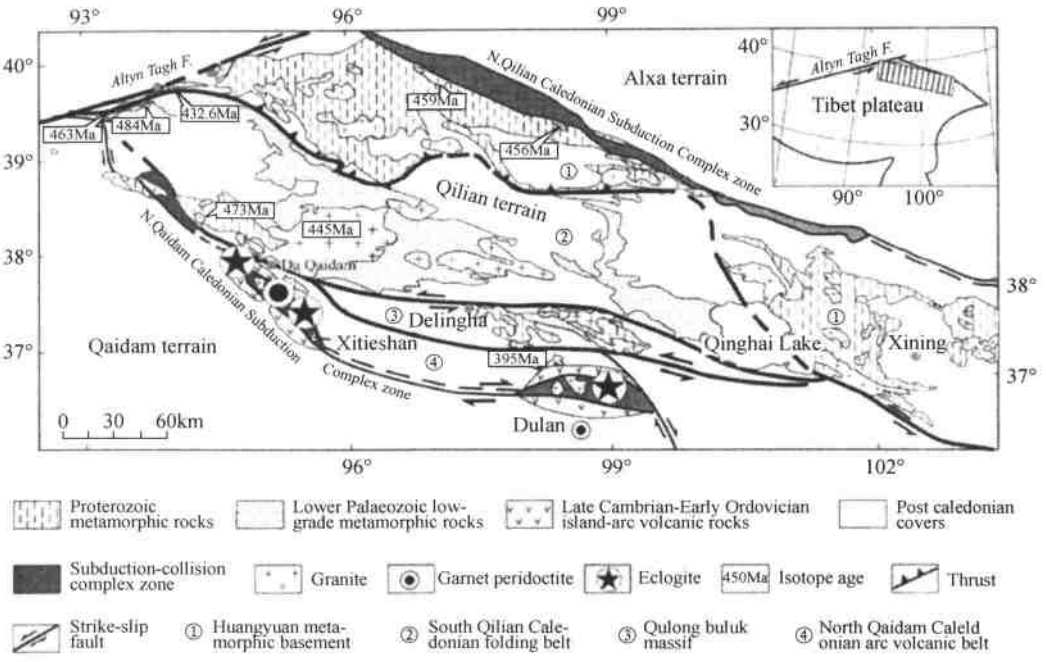

Fig.1 Tectonic map of the Qilian terrain and the northern Qaidam area.

The subduction complex between the Alxa and Qilian terrains consists of ophiolites, mélange and high-pressure (HP) metamorphic rocks (Xiao *et al*., 1978; Wu *et al*., 1993). The North Qilian continental arc complex to the north, combined with an accretionary wedge, records an active continental-margin accretionary system on the southern margin of the Alxa terrain (Xu *et al*., 1994; Xia and Xia, 1991; Xia *et al*., 1998; Zhang and Xu, 1995). Geochronological studies on the timing of either formation or peak metamorphism for the HP or magmatic rocks from these terrains by using various radiometric methods yielded the following results: ①gabbros from the ophiolite of the northern Qilian indicating the North Qilian sea have a SHRIMP U/Pb zircon age of 500 ± 17Ma (Shi *et al*., 2004), and the HP eclogites have SHRIMP U/Pb zircon age of 463～468Ma representing the North Qilian sea was subducted to a depth of at least 60km (Song *et al*., 2004). These ages are earlier than the formation age (440～460Ma) of the blue schist (Wu *et al*., 1993; Xu *et al*., 1994; Zhang and Xu, 1995). ②The northern Qilian volcanic arc formed at 486～438Ma and the marine volcanic rocks at a back-arc spreading ridge formed at 469～454Ma (Xu *et al*., 2000).

The Caledonian arc-trench-basin system distribution and ductile thrust structures with south-to southwest-directed polarity in the North Qilian active continental margin between the Alxa terrain and the Qilian terrain suggest that the North Qilian Sea was subducted northward or northeastward beneath the Alxa terrain (Cui *et al*., 1996; Xu *et al*., 2000).

Recently, an ultrahigh-pressure (UHP) belt, 350km long and 10km wide, named the north Qaidam UHP metamorphic belt, was found in the Da Qaidam-Xitieshan-Dulan area between the Qilian and Qaidam terrains (Yang *et al*., 1998, 2000, 2001; Zhang *et al*., 1999, 2000a, b). Coesite inclusions in zircon from garnet-bearing muscovite gneiss that hosts the Dulan eclogite (Yang *et al*., 2001) demonstrate that the belt formed by deep subduction of continental crust. Estimated conditions of the peak UHP metamorphism are $P \geqslant 2.8$GPa and $T \geqslant 700 \sim 800$℃.

The study shows that volcanic rocks of the Tanjianshan Group on the northern margin of the Qaidam terrain are islandarc in character and inferred the existence of a major tectonic boundary between the two terrains. LA-ICP-MS U/Pb analyses on zircons from a tholeiite of the northern Qaidum volcanic arc yielded an age of 514.2 ± 8.5Ma (Shi *et al*., 2004). U/Pb zircon and SHRIMP U/Pb zircon ages on the cal-alkaline volcanic rocks have ages from 496 to 440Ma (Li *et al*., 1999; Wu *et al*., 2001). In summary, these analyses show that the ophiolite representing the south Qilian oceanic basin has an age of about more than 514Ma, and the subduction of this oceanic basin and formation of the volcanic arc complex occurred at about 500～440Ma.

Previous studies have shown that the Qilian terrain and the Altyn terrain which are on either side of the Altyn Tagh strike-slip fault have similar structures, age of formation, and compositions. In particular, the northern Qilian HP belt and northern Qaidam UHP belt can be correlated with the northern Altyn HP belt and the southern Altyn UHP belt (Liu *et al*., 1996; Zhang *et al*., 2001), respectively. Correlation of these two belts suggests a left-lateral offset of at least 400km on the Altyn Tagh Fault (Xu *et al*., 1999).

In this paper, mainly through an intensive study of the Caledonian tectonic system of the Qilian terrain, we further confirm the existence and nature of the terrain boundary and reveals the formation mechanism of the northern Qaidam UHP metamorphic belt, and through a study of the tectonic styles and geometric and kinetic characteristics formed in the process of exhumation of the UHP metamorphic belt and its geochronology, we analyze the mechanism of exhumation and timing of the belt and present a model for its formation and exhumation.

2 Caledonian tectonic system of the Qilian terrain and the northern Qaidam UHP metamorphic belt

2.1 Caledonian tectonic units of the Qilian terrain

The Qilian terrain, about 600km long and 240km wide, is located between the Alxa and Qaidam terrains. Its northern and southern boundaries, respectively, are the northern Qilian subduction complex and the northern Qaidam subduction complex. From north to south, the Caledonian tectonic units of the terrain may fall into four parts: (1) the Huangyuan metamorphic basement, (2) the South Qilian Caledonian fold belt, (3) the Oulongbuluk block, and (4) the northern Qaidam Caledonian volcanic island-arc zone (Fig.1).

2.1.1 Huangyuan metamorphic basement

The Huangyuan metamorphic basement is mainly distributed in the northern part of the Qilian terrain. It is composed of 900～1000Ma high-grade metamorphic series (high amphibolite facies) and its overlying greenschist-facies metamorphic series. Study suggests that the Huangyuan metamorphic basement is similar to those of the northern Qaidam, Qaidam terrain and Yangtze block, being the basement that developed during the formation of the supercontinent Rodinia in the Jinningian period at 900～1000Ma (Wan *et al*., 2000). The metamorphic basement is superimposed by the Caledonian metamorphic event (Nd-Sm age 396～567Ma) (Juang and Sun, 2002) and intruded by Caledonian granite, suggesting that the Huangyuan metamorphic basement was reactivated in the Caledonian period and involved in the Caledonian orogeny. In addition, several ophiolite zones and ultramafic zones occur at Lajishan in the eastern part and Danghe Nanshan in the western part of the Huangyuan metamorphic basement.

2.1.2 South Qilian Caledonian fold belt

The South Qilian Caledonian fold belt is located in the southern part of the Huangyuan metamorphic basement, where Cambrian-Ordovician strata are widespread. Cambrian-Ordovician strata, which consist of lava flows, pyroclastic rocks and abyssal and bathyal deposits, contain both 'Southeast China-type' and 'transition-type' faunas. Silurian sedimentary rocks and Early Silurian graptolite faunas belong to the 'Southeast China' type (Bureau of Geology and Mineral Resources of Qinghai Province, 1991). This flysch series was strongly folded in the Caledonian orogeny, resulting in the formation of tight upright folds accompanied by flow cleavages in argillaceous rocks and gentle upright folds accompanied by fracture cleavages or spaced cleavages in arenaceous rocks, and are intruded by late Caledonian granites.

2.1.3 Oulongbuluk block

The Oulongbuluk block in the southern part of the Qilian terrain is composed of the granulite facies and amphibolite facies rocks of the Daken Daban Group (Zhang *et al*., 2001). It mainly formed at 900～1000Ma (Wan *et al*., 2000). Overlying the metamorphic basement are Sinian to Ordovician covers, and platform-type sediments containing typical 'North China-type' faunas occur in Cambrian-Ordovician strata composed of limestone and phyllite (Bureau of Geology and Mineral Resources of Qinghai Province, 1991), implying that the Oulongbuluk block may possibly be a block divorced from the Alxa terrain. Sinian to Ordovician strata suffered Caledonian folding and thrusting. The tectonic styles in the Cambrian-Ordovician strata are manifested by the gradual transformation from syncleavage folds with a north-dipping axial plane to recumbent folds from north to south. These folds are accompanied by ductile thrusts with southward shearing and intruded by late Caledonian granite. The features of Caledonian tectonic deformation in this block show the south-ward orogenic polarity and its boundaries are constrained by two ductile sinistral strike-slip shear zones formed at 240～250Ma (Xu *et al*., 2002).

2.1.4 Northern Qaidam Caledonian volcanic island-arc zone

On the southern margin of the Qilian terrain, the greenschist-facies volcanic and volcani-

clastic rocks of Tanjianshan and Shaliuhe Groups (Bureau of Geology and Mineral Resources of Qinghai Province, 1991) extend intermittently for nearly 400km along the belt and are accompanied by a subduction complex. It is very narrow, being only more than 10km wide. The volcanic rocks are unconformably overlain by Late Devonian molasse deposits.

Recently, through a study of the volcanic rocks of the Tanjianshan Group in the northern Qaidam marginal area it has been indicated that the volcanic rocks belong to the calc-alkaline series. They are characterized by enrichment of LREE and their trace element distribution patterns are similar to those of Pearce's island-arc volcanic rocks. This indicates that these Early Paleozoic volcanic rocks are island-arc tholeiite and that the tectonic environment of the volcanic rocks should belong to the volcanic island-arc one (Shi *et al*., 2004). Moreover, the gabbro intruded into the Tanjianshan Group has a zircon U-Pb age of 496.3 ± 6.3Ma (Yuan *et al*., 2002) and the island-arc tholeiite and intermediate-acid volcanic rocks of the same group have zircon U-Pb ages of 514.2 ± 8.5Ma by LA-ICPMS analysis (Shi *et al*., 2004) and 486 ± 13Ma, respectively (Li *et al*., 1999), implying a Late Cambrian-Early Ordovician age for the volcanic island arc produced by subduction of the south Qilian sea.

A suite of I-type monzodiorite-quartz monzodiorite-granodiorite-monzogranite of calc-alkaline affinity also occurs along the Aulaoshan-Luliangshan area, west segment of the northern Qaidam zone, exhibiting marked negative Th and Nb anomalies as well as positive P, Ti and Ba anomalies, features typically of I-type island-arc granitic rocks (Wu *et al*., 2000, 2001).

Both the I-type granites and volcanic rocks were formed at an active continental margin during subduction of the South Qilian Sea. The subducted sea crust was metamorphosed from greenschist facies through amphibolite facies to eclogite facies. Dehydration of the crust during metamorphism expelled fluids into the overlying mantle wedge, causing partial melting to form the island arc lavas and I-type granites.

2.2 Northern Qaidam UHP metamorphic belt

The northern Qaidam UHP belt is intimately associated with Cambrian-Ordovician island-arc volcanic rocks and intruded by Caledonian granites. It extends discontinuously for 350km and is the most important component part of the northern Qaidam Caledonian subduction complex zone. This UHP metamorphic belt is comprised of eclogite, coesitebearing gneiss and garnet peridotite. Metamorphic conditions varied between the eastern and western segments of the belt. In the west, the Da Qaidam eclogite formed at temperatures of 620～730℃ and pressures of 2.3～2.8GPa and the Xitieshan eclogite at 810～850℃ and > 1.4GPa. In the eastern segment, the eclogite was formed at temperatures of 610～680℃ and pressures of 2.6GPa. The presence of coesite in the garnet-muscovite gneiss in Dulan, which hosts the eclogites, indicates that it reached temperatures of 700℃ and pressures of 2.8GPa (Yang *et al*., 1998, 2000; Zhang *et al*., 2001). The presence of coesite in these rocks provides strong evidence that the supercrustal rocks were subducted to a depth of at least 100km (Liou *et al*., 1994; Coleman and Wang, 1995).

The Dulan UHP metamorphic rocks have zircon SHRIMP age ranging between 495 and 465Ma and Sm-Nd ages of 496～444Ma. The Da Qaidam garnet peridotite has zircon SHRIMP ages of 497～436Ma and the Da Qaidam eclogite formed at 495Ma (Yang *et al*, 1998, 2000, 2002; Zhang *et al*., 2000a, b). These dates indicate that the northern Qaidam UHP belt formed approximately at 495～440Ma.

2.3 Caledonian tectonic regime of the Qilian terrain and formation of the northern Qaidam UHP metamorphic belt

Based on the above analysis, we make the following preliminary observations of the Caledonian plate regime for the Qilian terrain.

(1) According to the composition of the Qilian terrain, it may be found that the Qilian terrain is composed of several small blocks. To the north lies the Huangyuan metamorphic block, to the south is the Oulongbuluk block composed of the metamorphic basement and Lower Paleozoic 'North China-type' platform deposits, and in the center is the abyssal-bathyal sea basin composed of Lower Paleozoic (Cambrian-Silurian) flysch deposits, containing 'South China-type' faunas.

(2) In the southern part of the terrain there is an island-arc volcanic-magmatic zone, which formed in Late Cambrian-Early Ordovician. It is inferred that its formation was related to the northward subduction of the South Qilian Sea. It is an accretional island-arc terrain resulting from subduction. A thick (>3000m) sequence of mid-late Ordovician-Silurian (460～410Ma) flysch crops out extensively in the northern part of UHP belt. It consists of sandy slate, phyllite and intermediate-basic volcanic rocks, representing deposits formed in a back-arc basin.

(3) On the convergent boundary between the Qilian and Qaidam terrains, there occurs the northern Qaidam Caledonian subduction complex zone, which is composed of ophiolites and UHP metamorphic rocks. The northern Qaidam ophiolite consists of peridotite, gabbro, cumulates and diabase-gabbro dike swarms (Xia *et al*., 1998; Yang *et al*., 2000). Xia *et al*. (1998) thought that the northern Qaidam ophiolite represents the tectonic environment of the South Qilian Sea and formed in the Early-Middle Cambrian. Therefore it is inferred that the North and South Qilian seas may have been linked and that the terrain occurred in the same Sea.

(4) Coesite was found in eclogite-bearing country rocks-garnet-muscovite gneiss-in Dulan (Yang *et al*., 2001), suggesting that the UHP metamorphic rocks are the product of deep subduction of continental crust. The UHP rocks formed at 495～440Ma BP, after the formation of the island-arc volcanic-magmatic zone accompanying the subduction of oceanic crust. As now no exact evidence indicates that the protoliths of the UHP rock were a (relic) component of the Early Paleozoic south Qilian Sea. Therefore, there is a possibility that the UHP metamorphic slices formed by the deep subduction of Sea crust beneath the South Qilian may have been 'delaminated' down and not have been exhumed or may have been exhumed but not have been found. Later, the continental crust of the Qaidam terrain continued to be subducted to

very great depths to form the North Qaidam UHP metamorphic zone.

(5) The Caledonian tectonic deformation of the Lower Paleozoic strata in the south-central part of the Qilian terrain is manifested by the features of south directed polarity: the deformation changes from upright folds→south-overturned congruous folds→recumbent folds from north to south, accompanied by southward ductile thrusts. This provides tectonic evidence for the northward subduction of the Qaidam terrain beneath the Qilian terrain.

3 Exhumation structures of the northern Qaidam UHP Terrain

The principal structures preserved in the northern Qaidam UHP metamorphic belt were formed during exhumation. Structures formed during the subduction stage are only rarely preserved because of the extensive retrograde metamorphism. In this section, we discuss the structural styles, mechanisms, and timing of exhumation in the northern Qaidam terrain.

The northern Qaidam UHP metamorphic belt may be divided into an eastern segment (north Dulan UHP metamorphic zone) with striking NW-SE and 10km of width, and a western segment (Da Qaidan-Luliangshan-Xitieshan UHP metamorphic zone) with striking E-W and exceeding 3～5km of width.

3.1 Structural features of the Dulan segment

The Dulan UHP metamorphic zone is located at the Yematan-Shaliuhe area of Dulan, eastern segment of the North Qaidam UHP belt. It is accompanied with the late Cambrian-early Ordovician island arc volcanic rocks and intruded by Late Caledonian granites. Late Devonian molasse deposits rest unconformably on the island arc volcanic rocks at the south. The east extending of the Dulan UHP zone is cutting off by a NNW-SSE striking fault (Fig.2a).

The Dulan UHP rocks consist chiefly of K-feldspar-plagioclase gneiss, biotite-K-feldspar-plagioclase gneiss, plagioclase gneiss, granitic gneiss, coesite-bearing garnet-muscovite-plagioclase gneiss, amphibolite, K-feldspar-plagioclase schist, felsic biotite schist, jadeite quartzite, taurolite-bearing garnet-biotite-plagioclase gneiss, kyanite-bearing biotite-plagioclase gneiss, kyanite-bearing two-mica-quartz schist, two-mica-quartz schist and marble. There are many nodules and lenses of gabbro, diabase, serpentinized harzburgite, dunite, eclogite and garnet amphibolite in the gneiss and schist. During exhumation, the rocks underwent retrograde metamorphism, which is expressed as: ①Omp→Cpx + Pl (Ab＞75%), ②Omp + H_2O→Amp + Ab, ③Omp + Grt + H_2O→Amp + Pl, ④Phe + Qtz + Ca^{2+} + Na^{+}→Bi + Pl, and ⑤ Rt + Al^{3+} + Ca^{2+}→Spn (The abbreviation of mineral names after Kretz, 1983). These reactions suggest that the rocks were first retrograded under amphibolite facies conditions (500～650℃ and 1.5GPa) at mid-crustal levels, but that as exhumation continued, the rocks moved into the greenschist facies, as indicated by the presence of hydrated minerals, such as muscovite, chlorite and actinolite. This later stage is estimated to have occurred at T＜500℃ and P＜0.5GPa in the upper crust (Song, 2001).

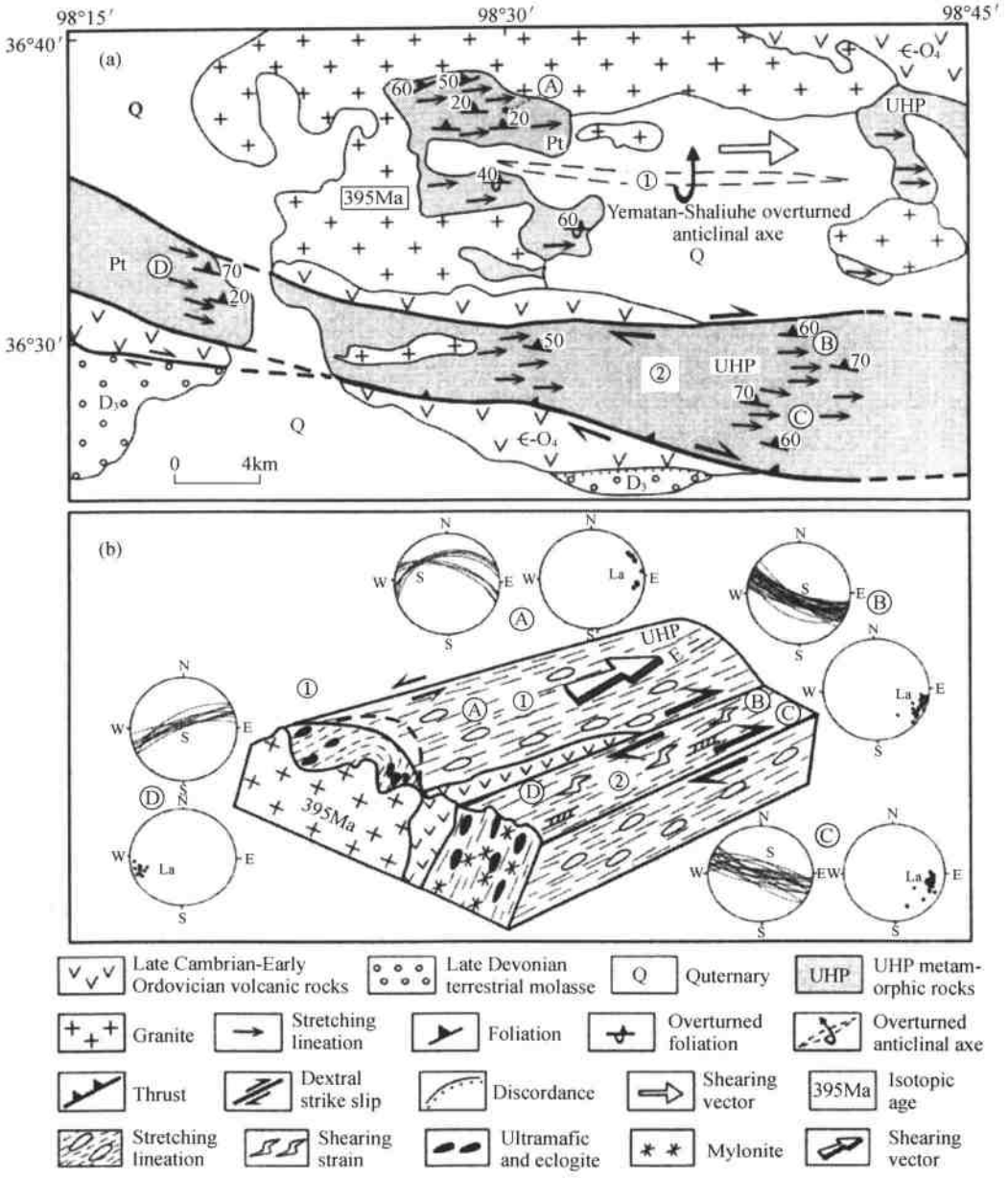

Fig.2 Geological sketch map (a) and stereoscopic structural model (b) of Dulan UHP metamorphic zone (modified from the 1∶200000 Geological Map of the Dulan region, Qinghai Bureau of Geology and Mineral Resources). Diagrams at Fig.2(b) border show projection of foliation (S) and stretching lineation (La) of the Dulan UHP metamorphic rocks: (Schimith circle, lower hemisphere projection): ①Yematan overturned anticline; ②Shaliuhe ductile dextral shear zone. Ⓐ: lower hemisphere projection of gently dipping foliation (S) and stretching lineation (La) in the middle part of the overturned anticlinal structure. Ⓑ, Ⓒ, Ⓓ: lower hemisphere projection of steep dipping foliation (S) and stretching lineation (La) in the southern limb of the overturned anticlinal structure.

The exhumation structures of the Dulan UHPM terrain are composed of the Yematan overturned anticline at the north and the Shaliuhe dextral ductile transpression shear zone at the south.

3.1.1 Yematan overturned anticline

The foliation in the Dulan UHP zone generally strikes E-W and is folded into an overturned anticline. In the north limb of the anticline, the steeply northward-dipping foliation gradually flattens to the south, whereas along the southern limb the foliation is overturned and becomes the steeply north dipping (Fig. 2a, b).

The most striking structural feature of the Dulan UHP zone is the development of longitudinal, subhorizontal stretching lineations in the foliation, i.e. the stretching lineation is parallel to the strike of the zone and the orientation of the mountain belt. The lineation is manifested as stretching and breaking of eclogite bands, stretching and preferred orientation of kyanite grains, stretching of felsic minerals and development of boudins in granitic rocks and chert bands.

On the basis of measurements of foliation and stretching lineation in the overturned anticline, it shows that the stretching lineation has a constant attitude whether foliation varied. Where the foliation is steeply dipping, we found that the vertical stretching lineation is cut by a horizontal stretching lineation, which may represent the vector of movement at great depth during the early stages of exhumation.

Shear strain in the Dulan UHP zone is marked by σ-and δ-type porphyroclasts systems, S-C structures, asymmetric drag folds, domino structures and rotation of inclusions in garnet. In the gentle foliation of the top of the overturned anticline, the shear strain caused by the eastward slip of the hanging wall can be observed on the XZ plane perpendicular to the foliation (Fig.3(a)). Steeply northward-dipping foliation zones are developed on both the north and south limbs of the overturned anticline and the shear strain is manifested by sinistral strike-slip movement on the north limb and dextral strike-slip movement on the south limb (Fig.3c).

The sense of the shear strain was also determined by measuring the preferred orientation of 3 types of quartz in the subhorizontal foliation zone (Fig.3b); stretched quartz, rectangular quartz in quartz bands and mylonitic quartz (<0.1mm). Stretched quartz is observed on the *XZ* plane where the grains show marked wavy extinction and a subgrain structure. $X:Z$ ratios may reach 10 : 1 or even 20 : 1 in these grains. The preferred orientation of these grains is formed by a basal-face fabric with the system (0001)$<$a$>$, a rhombic-face fabric with the slip system $\{10\bar{1}0\}$ $<$a$>$ and a prismatic-face fabric with the slip system $\{10\bar{1}0\}$ $<$a$>$, reflecting the fabric patterns of quartz grains medium to medium-low temperature (600－350℃). The rectangular quartz grains have length to width ratios on the *XZ* plane of 1.5:1－2:1. The patterns of preferred orientation are similar to those of stretched quartz showing medium-to medium-low-temperature fabrics of the slip systems (0001) $<$a$>$, $\{10\bar{1}\,\bar{1}\}$ $<$a$>$ and $\{10\bar{1}0\}$ $<$a$>$ (Mainprice *et al.*, 1986). The mylonitic quartz is characterized by very small grain size (<0.1mm) but its preferred orientation is the same as that of stretched quartz and rectangular quartz.

Therefore, preferred orientation of quartz from the subhorizontal foliation shows also east-

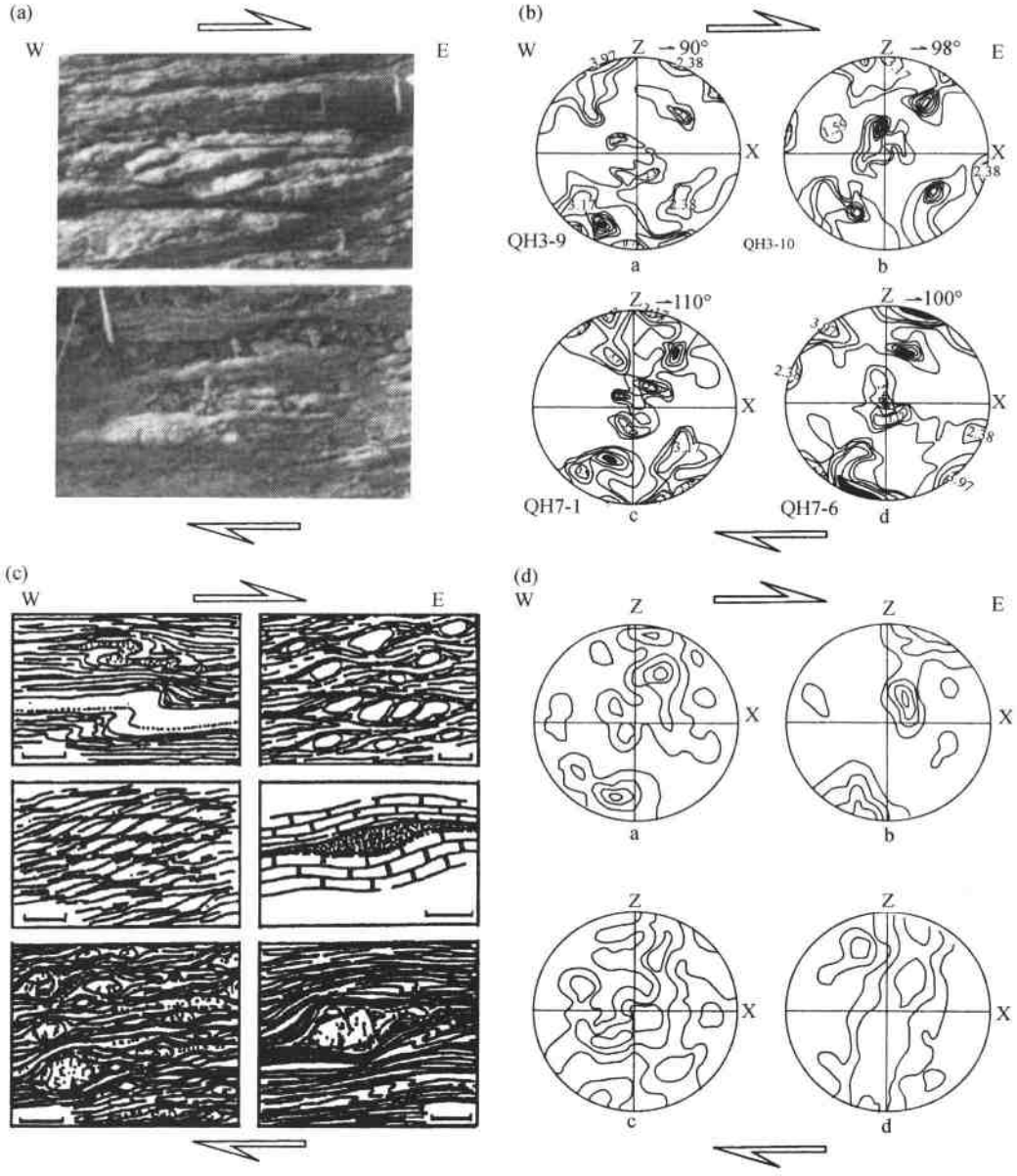

Fig. 3 Shearing strain and Letters Preferred Orientation of quartz of the Dulan UHP metamorphic rocks: (a) Photomicrograph on the gently dipping foliation of granitic gneiss at the middle part of the Yematan overturned anticline showing shearing sense eastward. (b) Lattice Preferred Orientations of quartz from granitic gneiss at the middle part of the Yematan overturned anticline showing shearing sense eastward. (Equal-area projection, lower hemisphere; 150 grains, Contours: 1-3-5-7-9-11%). (c) Shear strain of granitic mylonite in the Shaliuhe ductile dextral strike-slip shear zone. (d) Lattice Preferred Orientations of quartz from granitic mylonite of the Shaliuhe ductile dextral strike-slip shear zone (Equal-area projection, lower hemisphere; 150 grains, Contours: 1-3-5-7-9-11%).

ward slip of the hanging wall.

3.1.2 Shaliuhe dextral ductile transpression shear zone

The Shaliuhe ductile shear zone composed of granitic mylonite, mylonizated gneiss and intense shearing stain schiste is characterized by subvertical foliation and subhorizontal stretching lineation. A-type folds are well developed and the dextral strike-slip feature is shown on the *XZ* plan. In addition, southward thrusting is observed on the *YZ* plane, which indicating formation in a ductile transpression zone.

The preferred orientation of quartz in this ductile transpression shear zone is shown in Fig. 3b. The quartz grains show three types of preferred orientation, (0001) <a>, $\{10\bar{1}\,\bar{1}\}$ <a> and $\{10\bar{1}0\}$ <a>. These formed at medium-high to medium-low temperatures (400～650℃) and reflect the dextral strike-slip motion of the hanging wall (Fig. 3d). The mineral assemblages in this foliation zone are Ab + Q + Bi + Mus, Mus + Bi + Mic + Pl + Q and Bi + An + Chl + Q, suggesting that amphibolite-facies to greenschist-facies metamorphism occurred during strike-slip shearing.

3.2 Structural features of the Da Qaidam segment

The NW-SE-trending Da Qaidam terrain is made up of the Xitieshan, Luliangshan and Iqe sub-terrains, each with a width of ～3～4km. The country rocks are composed of granitic gneiss and paragneiss of the Daken Dawan Group, and these contain nodules and lenses of eclogite, garnet peridotite and ophiolite lithologies. Although no coesite has been found in the Da Qaidam terrain, the *P-T* conditions of the eclogite and presence of coesite pseudomorphs provide evidence of UHP metamorphism (Zhang *et al*., 2000a, b).

The exhumed structures of the Xitieshan terrain are characterized by overtured anticline form caused by refolded foliation. The regional foliation generally strikes NNW. A NW-SE, subhorizontal stretching lineation marked by elongate sillimanite and feldspar grains, as well as felsic veins in the foliation, is similar to that in the Dulan terrain (Fig. 4).

Gneiss of the Xitieshan UHP terrain and Cambrian-Ordovician volcanic rocks have both been mylonitized and they exhibit southeast-oriented shear strain in the subhorizontal to gently dipping foliation at the top of the Xitieshan overturned anticline. The preferred orientations of mylonitic quartz and recrystallized rectangular quartz in the mylonitized gneiss are manifested by transformation from medium-to high-temperature (>600～450℃) fabrics $\{10\bar{1}0\}$ <c> and $\{10\bar{1}0\}$ <a> to medium-to low-temperature (450～350℃) fabrics $\{10\bar{1}\,\bar{1}\}$ <a> and (0001) <a> (Fig. 5a, b).

Gneiss of the Xitieshan UHP zone and Cambrian-Ordovi-cian volcanic rocks have both been mylonitized in the southwest part of the Xitieshan anticline. The foliation of mylonite zone dips steeply to the north and the stretching lineations dip gently to the southeast with rake angles of 20°～30°. The preferred orientations of mylonite quartz and recrys-tallizing rectangular quartz also show a transformation from medium-high to medium-low temperatures, and the shear strain indicates dextral strike-slip movement (Fig.5c). The dextral strike-slip on the *XZ* plan and compression deformation on the *YZ* plan, which indicating dextral transpression features is

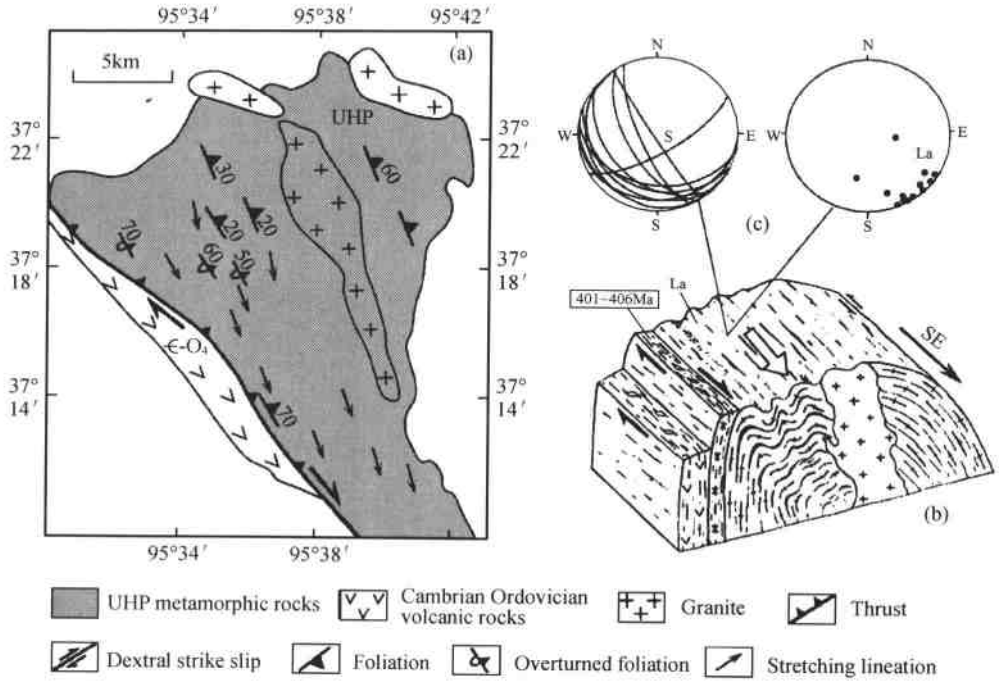

Fig.4 Geological sketch map and stereoscopic structural model of the Xitieshan UHP metamorphic zone: (a) Geological sketch map of the Xitieshan UHP metamorphic zone. (b) Projection of gently dipping foliation (S) and stretching lineation (La) of the middle part of the Xitieshan overturned anticlinal structure. (c) Stereoscopic diagram of foliation (S) and stretching lineation (La) in the Xitieshan UHP metamorphic zone.

similar to those of the Dulan UHP zone.

4 Timing of exhumation of the northern Qaidam UHP zone

In order to determine the exhumation age in the northern Qaidam UHP zone, we dated muscovite from the subhorizontal foliation in the Dulan overturned anticline and the subvertical mylonite foliation in the Xitieshan dextral transpression shear zone. We also dated granitic plutons intruded into the Dulan terrain.

In order to date the horizontal mylonite foliation we separated muscovite from coesite-bearing granitic gneiss. The rock dips 20°N and is mylonitized. The muscovite formed during mylonitization and shear deformation displays east-directed slip features. The sample 99-Y-117 was dated by the ^{39}Ar-^{40}Ar method at the Institute of Geology, Chinese Academy of Geological Sciences, Beijing. The sample yielded a very good plateau age of 401.5 ± 0.5Ma (Fig. 6a). On the isochron diagram the ^{40}Ar-^{36}Ar intercept age is 209.2 ± 52.5Ma and the isochron age is 406 ± 4.5Ma, in good agreement with the plateau age (Table 1) (Fig. 6a, b). The muscovite closure temperature of 350 ± 50℃ for the K-Ar system reflects the time at which the UHP metamorphic terrain reached shallow depths of ~10km.

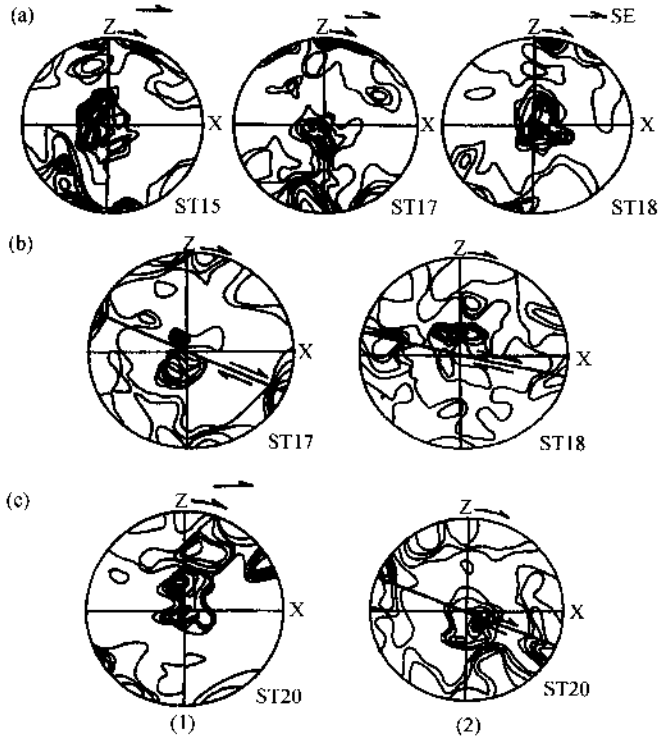

Fig. 5 Diagram showing the lattice preferred orientations of mylonite quartz in the Xitieshan UHP metamorphic zone. (a) Preferred orientation of rectangular recrystallized quartz in gentle-dipping mylonite foliation at the top of the Xitieshan overturned anticline (Equal-area projection; lower hemisphere; 150 grains. Contours: 1-3-5-7-9-11%). (b) Preferred orientation of mylonite quartz in gentle-dipping mylonite foliation at the top of the Xitieshan overturned anticline (Equal-area projection; lower hemisphere; 150 grains. Contours: 1-3-5-7-9-11%). (c) Preferred orientations of mylonite quartz (left) and recrystallized quartz (right) in the Xitieshan ductile dextral strike-slip shear zone (Equal-area projection; lower hemisphere; 150 grains. Contours: 1-3-5-7-9-11%).

Table 1 ^{39}Ar-^{40}Ar data for muscovite from granitic gneiss on the horizontal mylonitic foliation

T(℃)	$(^{40}Ar/^{39}Ar)m$	$(^{36}Ar/^{39}Ar)m$	$(^{37}Ar/^{39}Ar)m$	$^{39}Ar(\times10^{-14}$, mol)	^{39}Ar(%)	Age (Ma, 2σ)
400	22.9034	0.0276	0.0595	99.19	1.07	302.9±5.90
500	18.6586	0.0073	0.0745	236.08	3.61	336.0±4.70
600	19.9941	0.0063	0.0316	305.57	6.9	366.1±3.70
700	20.4162	0.0032	0.0185	839.40	15.96	390.1±3.90
800	20.8262	0.0028	0.0132	860.45	25.22	399.5±4.00
900	20.8751	0.0020	0.0102	1659.08	43.09	404.9±4.20
980	20.7693	0.0026	0.0081	835.61	52.09	399.9±4.00
1080	20.8971	0.0028	0.0146	679.56	59.42	400.8±4.40
1180	21.2045	0.0038	0.0242	1057.32	70.81	401.0±3.90
1280	20.8729	0.0025	0.0058	1492.20	86.88	402.3±4.10
1400	20.8007	0.0022	0.0411	1217.60	100	402.7±4.60

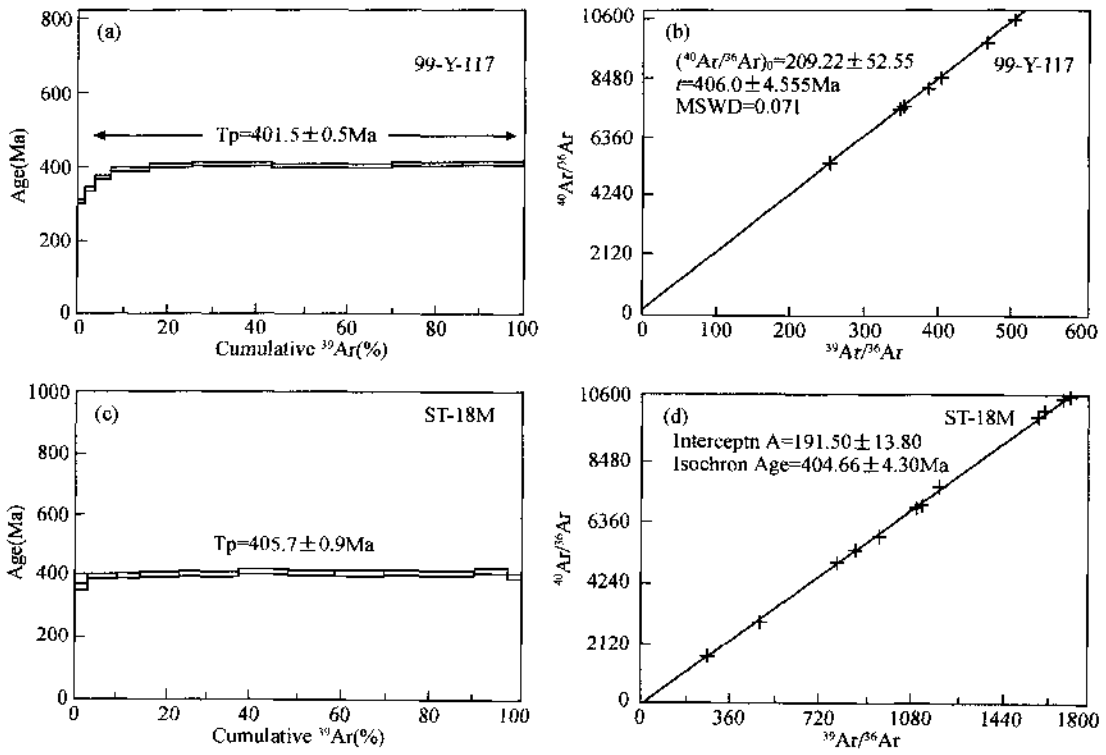

Fig.6 Muscovite ^{39}Ar-^{40}Ar age diagram of the northern Qaidam.

UHP metamorphic rocks: (a) Muscovite ^{39}Ar-^{40}Ar plateau age diagram of garnet-muscovite gneiss in the northern Dulan UHP zone. (b) Muscovite ^{39}Ar-^{40}Ar isochron age diagram of garnet-muscovite gneiss in the northern Dulan UHP zone. (c) Muscovite ^{39}Ar-^{40}Ar plateau age diagram of mylonitized granitic gneiss in Xitieshan. (d) Muscovite ^{39}Ar-^{40}Ar isochron age diagram of mylonitized granitic gneiss in Xitieshan.

Muscovite from the mylonitized granitic gneiss sample ST18M of the south side of the Xitieshan zone was used to date the steeply dipping foliation. The mylonite foliation in this sample dips SE at 80° and the stretching lineation dips 145° at 30°. The plateau age obtained through 12 heating steps is 405.7 ± 0.9Ma, and the ^{40}Ar-^{36}Ar intercept age on the isochron is 191.50 ± 13.80Ma. The isochron age is 404.66 ± 4.3Ma, similar to the plateau age (Table 2) (Fig. 6c, d).

The Yematan granite, intruded into the Dulan terrain, was dated at 397 ± 4Ma using the zircon SHRIMP method sample (Wu *et al.*, 2000). The Ar-Ar ages of mica cited above suggest that the gently-dipping and steeply-dipping or subvertical foliations in the zone formed at approximately the same time (400～406Ma). This corresponds to the last stage of exhumation of the zone to shallow depths. The intrusion of the 397Ma granite marks the end of exhumation of the UHP belt.

Table 2 ^{39}Ar-^{40}Ar data for muscovite from granitic gneiss on the subvertical mylonitic foliation. Data step heating for ST-18M (Weight = 91.00 mg, J = 0.012948)

T(℃)	($^{40}Ar/^{39}Ar$)m	($^{36}Ar/^{39}Ar$)m	($^{37}Ar/^{39}Ar$)m	F	$^{39}Ar(\times10^{-14}$, mol)	^{39}Ar(%)	Age(Ma)
500	36.66670	0.08890	0.52190	10.43660	9.00	0.09	228.70±27.80
600	18.66670	0.00370	0.03130	17.58110	300.00	2.96	370.00±4.70
700	79.48950	0.00110	0.03600	19.17720	666.00	9.34	400.10±4.40
800	19.65430	0.00060	0.01530	19.48060	1562.00	24.31	405.80±4.50
900	19.64010	0.00060	0.01830	19.45590	1306.00	36.82	405.30±4.50
1000	19.95830	0.00080	0.02000	19.70900	1200.00	48.31	410.00±4.50
1100	19.79770	0.00060	0.02310	19.60990	1038.00	58.26	408.20±4.50
1200	19.64290	0.00090	0.02140	19.37610	1120.00	68.99	403.80±4.50
1250	19.80580	0.00120	0.02790	19.45920	515.00	73.92	405.40±4.50
1300	19.64910	0.00060	0.02800	19.47400	1710.00	90.30	405.60±4.50
1350	19.94900	0.00130	0.06110	19.57260	784.00	97.82	407.50±4.50
1400	19.21050	0.00220	0.42020	18.59380	228.00	100.00	389.20±4.30

5 Mechanism of exhumation and model of evolution of the northern Qaidam UHP belt

5.1 Mechanism of exhumation of the northern Qaidam UHP belt

Exhumation of UHP metamorphic rocks from the deep mantle to the shallow crustal levels is a difficult problem that has not yet to be completely solved. A number of different models have been proposed, which fall into four categories: (1) erosion and buoyancy (Platt, 1993), (2) extension (Harrison, 1992), (3) vertical extrusion (Chemenda *et al*., 1995, 1996), and (4) extension of the upper crust and shortening of the lower crust (Anderson and Jamerit, 1990; Ballevere *et al*., 1990; Blake and Jayko, 1990).

The most striking exhumation structures in the north Qaidam UHP belt are the antiform formed by arching of the foliation, the longitudinal, subhorizontal ductile stretching lineation, and the shear strain displaying evidence of eastward slip and dextral transpression. Based on the isotopic age data (400~406Ma), which show that the eastward slip and the dextral transpression structures are coeval, we suggest that exhumation involved a combination of vertical extrusion and transpression.

The vertical extrusion model suggests that during plate collision and deep subduction of continental crust, the UHP metamorphic slab ruptures and plate convergence causes the subducting slice to be exhumed by buoyancy forces. As a result of upward extrusion of soft material within rigid walls, the foliation in the upper part of the subducting slice is arched and a horizontal stretching lineation forms. This process is distinguished from simple horizontal compression in that the latter usually produces a vertical foliation and vertical stretching lineation.

The overturned anticline in the north Qaidam belt dips to the southeast and east and sinistral and dextral transpression structures occur on both limbs of the overturned anticline. The occurrence of the transpression structures at the south margin of the overturned anticline indicates that the driving force during exhumation was oblique convergence. Thus, the combination of oblique collision and subduction results in both 'vertical extrusion' and 'transpression'. We call this combined mechanism 'oblique extrusion'.

The Black Mountain axial zone of the Hercynian orogen in France is a metamorphosed dome composed of Precambrian gneiss, where the antiform due to foliation folding and longitudinal (nearly E-W-trending) stretching lineation are quite similar to the basic features of the northern Qaidam UHPM terrain (Fig. 7a). However, there are differences between the two belts. For example, the sense of shear strain on the east and west sides of the Black Mountain axial zone are just opposite to each other, i.e. the shear strain on the east side has an easterly sense, while that on the west side has a westerly sense, showing bidirectional shear. In contrast, the northern Qaidam UHP zone is not a domal anticline but an elongate body and the shear strain has an easterly sense, showing unidirectional shear. Matte *et al*. (1998) proposed that the Hercynian Black Mountain axial zone is not a metamorphic core complex but an anticlinal nappe resulting from N-S coaxial compression and longitudinal extension.

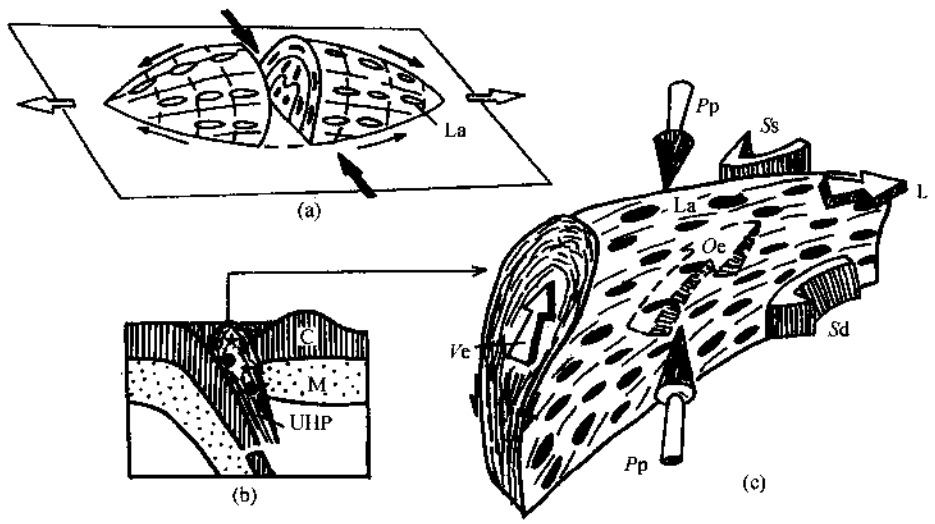

Fig. 7 Three-dimensional model for exhumation mechanism of the north Qaidam UHP metamorphic zone: (a) Three-dimensional model for the formation of the Black Mountain metamorphosed dome in France. (b) Exhumation model of a UHP metamorphic slice. (c) Three-dimensional model for the exhumation model of the north Qaidam UHP metamorphic terrane. Abbreviations: *P*p, direction of the principal stress of oblique collision and subduction; *O*e, oblique extrusion; L, eastward slip component; *V*e, vertical extrusion component; *S*s, sinistral transpression component; *S*d, dextral transpression component.

The mechanism of oblique extrusion for the northern Qaidam UHP belt is much more complex than that for the Black Mountain axial zone. Fig. 7b, c show a hypothetical three-dimensional model of 'oblique extrusion', showing that under the principal stress (Pp) produced by oblique plate convergence the UHP metamorphic slice is subjected to 'oblique extrusion' (Oe), which may be resolved into an eastward slip component (L), a vertical extrusion component (Ve), a sinistral transpression component (Ss) and a dextral transpression component (Sd) (Fig. 7).

'Oblique extrusion' implicates the Qilian terrain was moved easterly opposite to the Qaidam terrain at about 400Ma. It is not unique, but has its counterpart, the Alxe terrain was moved easterly opposite to the Qilian terrain at the same time (Xu *et al*., 1996). It is inferred that relative convergence between the Alxe and Qilian terrains was transformed from 'normal' to 'oblique' intracontinental subduction in late Caledonian.

5.2 Model for the formation and exhumation of the northern Qaidam UHP metamorphic belt

Paleomagnetism and global tectonic reconstruction studies (Hallam, 1992; Gradstein *et al*., 2004) suggested that the proto-Tethys Oceanic basin was present at the southern hemisphere between the Gondwanaland, Siberian plate, North America plate, and Baltic plate at ~ 550Ma, while the North China plate, South China plate and a series of other small terrains that constitute the northern Qinghai-Tibet composite terrain such as the Qilian-Altin terrain, the Qaidam terrain, the northern part of the eastern Kunlun terrain and the southern part of the eastern Kunlun terrain, were located probably between the proto-Tethys Oceanic basin and the Gondwanaland. These small terrains were separated by some seas such as the North Qilian Sea and the South Qilian Sea linked with the proto-Tethys Oceanic basin and formed a Caledonian chain of archipelago at late Devonian. During 500～440Ma, the North Qilian Sea was subducted beneath the North China plate to 30～60km deep and resulted in the northern Qilian HP metamorphic belt, while the South Qilian Sea and Qaidam continental crust were subducted beneath the Qilian terrain to 100km deep and led to the formation of the northern Qaidam UHP metamorphic belt. Later arc-arc, arc-continent and continent-continent collisions at 410～400Ma led to the juxta-position and amalgamation of these terrains. Such collisional events were responsible for the intensive deformation of the accretional wedge above a subducted slab, formation of the Devonian molasses basins and large amounts of granitic intrusions in this region. Eventually, these terrains were welded with the North China plate to form the 'Early Paleozoic China collage'.

Above-mentioned studies provide the following geological records for the formation and exhumation of the northern Qaidam UHP metamorphic belt: ① the proto-Tethys ocean basin formed at 515Ma before; ②the volcanic island arc by the subduction of the ocean basin and seas occurred at about 515～485Ma; ③ the north Qaidam UHP belt formed between 495 and 440Ma; ④ the exhumation of the UHP terrain began at 470～460Ma and completed at 400～406Ma. The evolution history of the north Qaidam UHP terrain should be divided into the four stages (Fig.8).

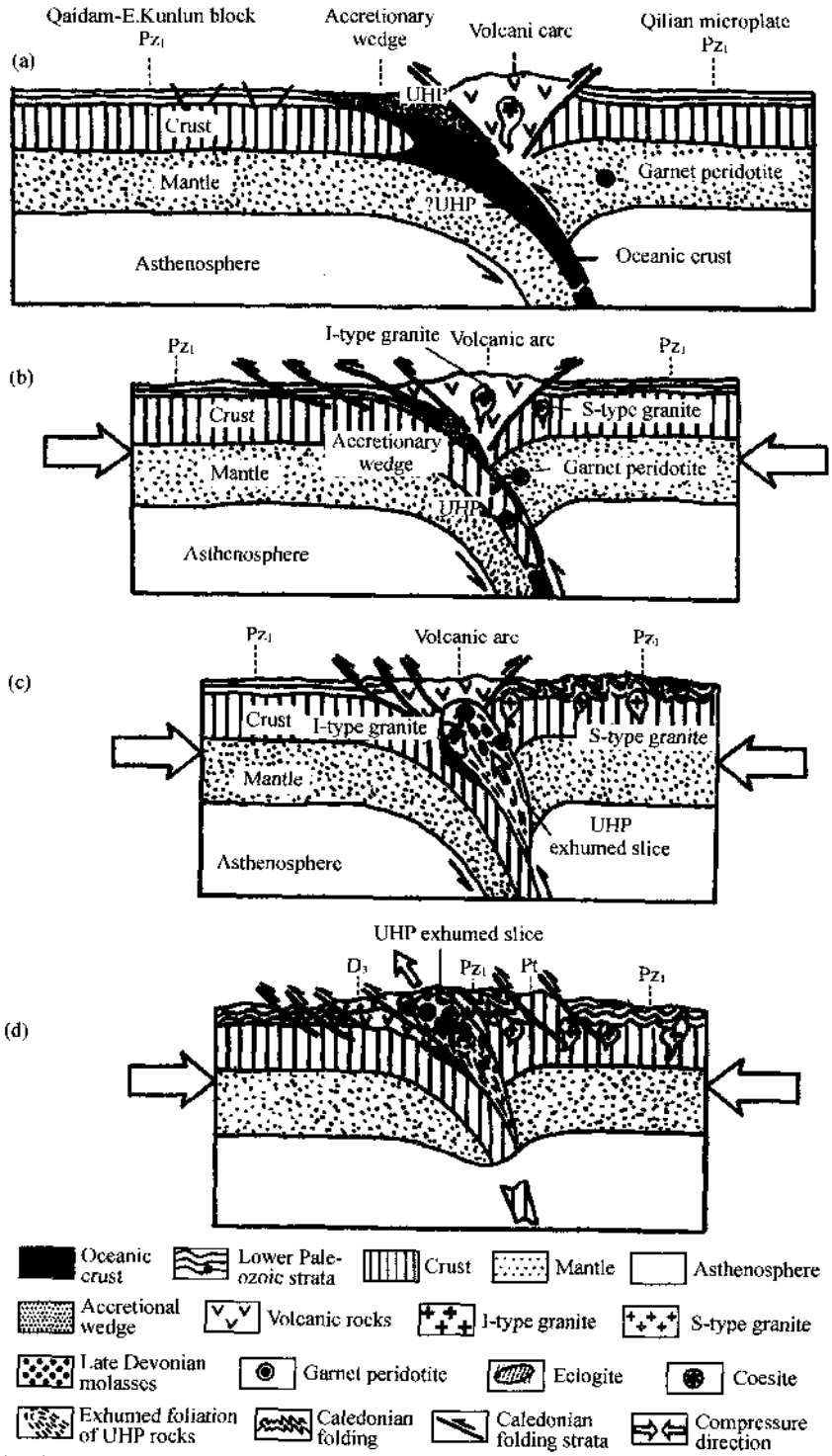

Fig.8 Model of the formation and exhumation of the northern Qaidam UHP metamorphic zone: (a) Subduction of the South Qilian ocean basin (Late Cambrian-Early Ordovician). (b) Continentao deep subduction of the Qaidam-East Kunlun plate (495～440Ma). (c) Exhumation of the Northern Qaidam UHP metamorphic slice (470～400Ma). (d) Caledonides (after 400Ma).

5.2.1 Subduction stage of the South Qilian Sea

The South Qilian Sea lying between the Qilian terrain and the Qaidam terrain was formed during Early-Middle Cambrian (about 515Ma before). The South Qilian Sea was subducted northward beneath the Qilian terrain, the interaction of the subducted lithosphere and asthenosphere in the mantle wedge between the two terrains made the side of the obducted Qilian terrain to be weaked and spreaded, and the volcanic island arc was happened at 515～485Ma.

5.2.2 Continental deep subduction stage of the Qaidam terrain

After the South Qilian Sea subduction, the continental crust including metamorphic basement of the Qaidam was carried deeply to be a great depth of more than 100km and underwent UHP metamorphism between 495 and 440Ma. Meanwhile the continued deep subduction, the exhumation of the subducted slice began at 470～460Ma.

5.2.3 Exhumation stage of the north Qaidam UHP zone

The UHP zone was exhumed by a process of 'oblique extrusion' during transformation from 'normal' to 'oblique' intracontinental subduction between the Qilian and Qaidam terrains. Overall exhumation was occurred at 460～440Ma and was completed by 406～400Ma. Meanwhile, extensive retrograde metamorphism, reactivation of the metamorphic basement intensive folding of the Lower Paleozoic strata occurred and intruded of a large number of S-type collision granites.

5.2.4 End of Caledinian orogeny

The Qilian Mountains were built by Caledinian orogeny. Late Devonian molasses deposits indicating the end of Caledonian orogeny were cumulated in the foreland of the Caledonian folding belt by uplift and erosion at 372～354Ma.

6 Summary and conclusions

The South Qilian Sea basin was subducted northward beneath the Qilian terrain beginning at 515～490Ma, while a volcanic island arc, I-type granites and a fore-arc accretionary wedge (pyroclastic rocks + marble) formed along the southern margin of the Qilian terrain. Later (495～440Ma), deep subduction (>100km) of continental crustal rocks (including 900～1100Ma metamorphosed basement) of the Qaidam terrain produced the north Qaidam UHPM zone. The initial stage of exhumation for the UHPM slice began at 470～440Ma. The overall exhumation occurred at 440～410Ma. The final exhumation happened at 400～406Ma accompanied by retrograde metamorphism and intrusion of voluminous S-type collision granites. Deep subduction of continental crust slice and exhumation of the UHPM slice were happened alternately during 470～440Ma.

The entire UHPM slice was exhumed by 'oblique extrusion' was transformed from 'normal' to 'oblique' intracontinental subduction in late Caledonian and underwent retrograde metamorphism. Driven by buoyancy forces, the UHP block was indented into the volcanic island-arc and fore-arc belt and was juxtaposed against the island arc.

Acknowledgements

This research was supported by the key project 'Material Composition and Orogenic Process of the Qilian Orogenic Belt' of the National Natural Science Foundation of China (grant G 1998040800), the key fundamental research project of the Ministry of Land and Resources and Sino-French cooperative project 'Tectonic Evolution and Lithosphere Shearing of the Qilian-Altun Mountains' (1966～2000) and the China Geological Survey project 'Tectonic Framework and Mineralization in the Qilian Mountains'. The authors are grateful to Prof. P. Lobinson of Canada and Prof. M. Mattauer of France for their helpful suggestions on the exhumation mechanism outlined in this paper and Zhang Xiaowei, Tang Zhemin, Liang Fenghua and Wu Guixiang for their assistance in the completion of the manuscript.

References

Anderson, T.B., Jamerit, B., 1990. Uplift of deep crust during orogenic extensional collapse: A model based on field studies in the Sogn-Sunnfjord region of Western Norway. Tectonics 9, 1097～1111.

Ballevere, M., Lagabrille, Y., Merlr, O., 1990. Tertiary ductile normal faulting as a consequence of lithospheric stacking in the Western Alpes. Memoirs of the Geological Society of France 156, 227～236.

Blake, M.C.J., Jayko, A.S., 1990. Uplift of very high pressure rocks in the western Alps: evidence for structural attenuation along low-angle fault. Memoirs of the Geological Society of France 156, 237～246.

Bureau of Geology and Mineral Resources of the Qinghai Province, 1991, 1991, 1991. Anon., 1991. Regional Geology of Qinghai Province. Geological Publishing House, Beijing pp. 1～662.

Chemenda, A.I., Mattauer, M., Malavielle, J., Bokun, A.N., 1995. A mechanism for syn-collisional rock exhumation and associated normal faulting: Results from physical modelling. Earth and Planetary Science Letters 132, 225～232.

Chemenda, A.I., Mattauer, M., Bokun, A.N., 1996. Continental subduction and a mechanism for exhumation of high-pressure metamorphic rocks: New modeling and field data from Oman. Earth and Planetary Science Letters 143, 173～182.

Coleman, R.G., Wang, X., 1995. Ultrahigh-Pressure Metamorphism. Cambridge University Press.

Cui, J.W., Tang, Z.M., Deng, J.F., Yue, Y.J., Meng, L.S., Yu, Q.F., 1996. Altun Fault System. Geological Publishing House, Beijing p. 249.

Gradstein, F.M., Ogg, J.G., Smith, A.G., Agterberg, F.P., Bleeker, W., Cooper, R.A., Davydov, V., Gibbard, P., Hinnov, L., House, M.R., Lourens, L., Luterbacher, H.-P., McArthur, J., Melchin, M.J., Robb, L.J., Shergold, J., Villeneuve, M., Wardlaw, B.R., Ali, J., Brinkhuis, H., Hilgen, F.J., Hooker, J., Howarth, R.J., Knoll, A.H., Laskar, J., Monechi, S., Plumb, K.A., Powell, J., Raffi, I., Rohl, U., Sanfilippo, A., Schmitz, B., Shackleton, N.J., Shields, G.A., Strauss, H., Van Dam, J., Van Kolfschoten, T., Veizer, J., Wilson, D., 2004. A geologic time scale 2004. Columbia University Press, New York.

Hallam, A., 1992. Phenerozoic Sea-level Changes. Columbia University Press, New York p. 266.

Harrison, C.G.A., 1992. Rates of continental erosion and mountain buiding, Proceedings of the 21th IGC. Kyoto, Japan p. 2.

Juang, W.S., Sun, M.Z., 2002. Isotopic and geochemistry evidence of granitoids of reactivation of basement of the Qilian Fold Belt, The Third (2002) Cross-Strait Conference on Geology of Qilian Mountains and Adjacent Area-Evolution of the Central Orogenic Belt, pp. 120～122 Liou, J.G., Zhang, R.Y., Ernst, W.G., 1994. An introduction to ultrahigh-pressure metamorphism. The Island Arc 3, 1～24.

Kretz, R., 1983. Symbols for rock-forming minerals. American Mineralogist 68, 277～279.

Li, H.K., Lu, S.N., Zhao, F.Q., 1999. Chorology of upper-proterozoic main strata events in North Qaidam. Geochemica 13, 224～225.

Liou, J.G., Zhang, R.Y., Ernst, W.G., 1994. An introduction to ultrahigh-pressure metamorphism. The Island Arc 3, 1～24.

Liu, L., Che, Z.C., Luo, J.H., Wang, Y., Gao, Z., 1996. Determination of ecologite in the west segment of Altun mountains and its geological significance. Chinese Science Bulletin 41, 1458～1488.

Mainprice, D., Boucher, T.L., Blumenfeld, P., Tubia, J.M., 1986. Dominant <c> slip in naturally deformed quartz: implications for dramatic plastic softening at high temperature. Geology 14, 819～822.

Matte, Ph., Lancelot, J., Mattauer, M., 1998. La Zone axiale hercynienne de la Montagne Noiren'est par un 'metamorphic core complex' extensive mais un anticlinal post nappe a coeur anatectique. Geodinamica Acta, Paris 11, 13～22.

Platt, J.P., 1993. Exhumation of high pressure rocks: A review of concepts and processes. Terra Nova 5, 119～133.

Shi, R.D., Yang, J.S., Wu, C.L., Tsuyoshi, I., Takakumi, H., 2004. Island Arc volcanic Rocks in the North Qaidam UHP metamorphic Belt. Acta Geologica Sinica 78, 52～64.

Song, S.G., 2001. Petrology, mineralogy and metamorphic evolution of the Dulan UHP terrane in the northern Qaidam, NW China, and its tectonic implications. PHD dissertation, Cags: 1～96.

Song, S.G., Zhang, L.F., Niu, Y., Song, B., Liu, D.Y., 2004. Early Paleozoic plate-tectonic evolution and deep continental subduction on the northern margin of the Qinghai-Tibet Plateau. Geological Bulletin of China 23, 918～925.

Wan, Y.S., Yang, J.S., Xu, Z.Q., Wu, C.L., 2000. Geochemical characteristics of the Maxianshan complex and Xinglongshan group in the eastern segment of the Qilian orogenic belt. Journal of the Geological Society of China (Taiwan) 43, 52～68.

Wu, C.L., Yang, J.S., Li, H.B., Shi, R.D., 2000. Petrogenesis of the granitoides from Lenghu, northern margin of Qaidam basin, NW China. Journal of the Geological Society of China (Taiwan) 43, 107～124.

Wu, C.L., Yang, J.S., Ireland, T., Wooden, J., Li, H.B., Wan, Y.S., 2001. The SHRIMP age of zircon for Aulaoshan granite in the south Qilian, and its significance. Acta petrological sinica 17, 215～221.

Wu, H.Q., Feng, Y.M., Huo, Y.G., Song, S.G., 1993. Metamorphism and deformation of blueschist belts and their tectonic implications, North Qilian Mountain, China. Journal of Metamorphic Geology 11, 523～536.

Xia, L.Q., Xia, Z.C., 1991. Marine volcanic rocks in Qilian-Qinling Mountains. Geological publishing house of China university of Geosciences, Wuhan pp. 59～105.

Xia, L.Q., Xia, Z.C., Ren, Y.X., Zuo, G.C., Qiu, J.X., 1998. Volcanism and Mineralization in Qilian Mountains and Its Adjacent Area. Geological publishing house, Beijing p. 215.

Xiao, X.C., Cheng, G.M., Zhu, Z.Z., 1978. The geologic-tectonic significance of ophiolite in Qilian Mountains. Acta Geologica sinica 52, 195～287.

Xu, Z.Q., Xu, H.F., Zhang, J.X., 1994. Zoulangnanshan Caledonian subduction complex in north Qilian Mountains and its dynamics. Acta Geologica Sinica 68, 1～5.

Xu, Z.Q., Cui, J.W., Zhang, J.X., 1996. Deformation Dynamics of Continental Mountain Chains. Metallurgical industrial publishing house, Beijing pp. 1～246.

Xu, Z.Q., Yang, J.S., Zhang, J.X., Jian, M., Li, H.B., Cui, J.W., 1999. A comparison between the tectonic units on the two sides of the Altyn Tagh sinistral strike-slip fault and the mechanism of lithospheric shearing. Acta Geologica Sinica 73, 193～205.

Xu, Z.Q., Zhang, J.X., Li, H.B., 2000. Architecture and orogeny of the northern Qilian orogenic belt, NW China. Journal of the Geological Society of China (Taiwan) 43 (1), 125～141.

Xu, Z.Q., Li, H.B., Chen, W., Wu, C.L., Yang, J.S., Jin, X.C., Chen, F.Y., 2002. Acta Geologica Sinica 76 (2), 183～193.

Yang, J.S., Xu, Z.Q., Li, H.B., Wu, C.L., Cui, J.W., Zhang, J.X., Chen, W., 1998. Discovery of eclogite in the north Qaidam. Chinese Science Bulletin 43, 1544～1549.

Yang, J.S., Xu, Z.Q., Li, H.B., Wu, C.L., 2000. A Caledonian convergent border along the Qilian terrain, NW China: evidence from eclogite, garnetperidotite, ophiolite, and S-type granite. Journal of the Geological Society of China 43, 142~160.

Yang, J.S., Song, S.G., Xu, Z.Q., Wu, C.L., Shi, R.D., Zhang, J.X., Li, H.B., Wan, Y.S., Liu, Y., Qiu, H.J., Liu, F.L., 2001. Discovery of coesite in the north Qaidam early Paleozoic ultrahigh-high pressure (UHP-HP) metamorphic belt, NW China. Acta Geologica Sinica 75, 175~179.

Yang, J.S., Xu, Z.Q., Zhang, J.X., Song, S.G., Wu, C.L., Shi, R.D., Li, H.B., Maurice, B., 2002. Early Paleozoic North Qaidam UHP metamorphic belt on the northeastern Tibetan plateau and a paired subduction model. Terra Nova 14, 397~404.

Yuan, B.G., Wang, M.G., Li, H.M., Hao, G.J., Xin, H.T., Zhang, B.H., Wang, Q.H., Tian, Q., 2002. The U-Pb age of Zircon from gabbro of the Luiliangshan area at the northern margin of Qaidam basin and its significance. Researching Progresses of Precambrian 25, 36~40.

Zhang, J.X., Xu, Z.Q., 1995. Caledonian subduction accretionary complex/volcanic arc belt in middle sector of the north Qilian mountains and its deformational features. Acta Geoscientia Sinica, 154~163.

Zhang, X.T., Lu, H.Q., Cheng, Z.X., 1999. Discovery and preliminary study of high pressure metamorphic rock-eclogite facies in Shaliuhe area, north Qaidam. Qinghai geology 2, 1~12.

Zhang, J.X., Zhang, Z.M., Xu, Z.Q., Yang, J.S., Cui, J.W., 2001. Petrology and geochrology of eclogite from the western segment of the Altyn Tagh, northwestern China. Lithos 56, 187~206.

Zhang, J.X., Yang, J.S., Xu, Z.Q., Zhang, Z.M., Chen, W., Li, H.B., 2000a. Peak and retrograde age of eclogites at the northern margin of Qaidam basin, northwestern China: evidences from U-Pb and Ar-Ar dates. Geochemica 29, 217~222.

Zhang, J.X., Yang, J.S., Xu, Z.Q., Zhang, Z.M., Li, H.B., Chen, W., 2000b. U-Pb and Ar-Ar ages of ecologites from the northern margin of the Qaidam basin, northwestern China. Journal of the Geological Society of China (Taiwan) 43, 161~169.

A New Caledonian Khondalite Series in West Kunlun, China: Age Constraints and Tectonic Significance[1]

Xu Zhiqin[2] Qi Xuexiang Liu Fulai
Yang Jingsui Zeng Lingsen and Wu Cailai
(Key Laboratory for Continental Dynamics, MLR, Institute of Geology,
Chinese Academy of Geological Sciences, Beijing 100037, China)

Abstract The Kangxiwar ductile strike-slip shear zone marks the southern boundary of the West Kunlun terrane, a large, nearly E-W trending metamorphic terrane in the western Qinghai Tibet Plateau region. This ductile shear zone is ~7km wide, and consists of mylonitized khondalites. Protoliths of the khondalites were alumina-rich pelitic sedimentary and subordinate volcanic rocks. The pelitic khondalites have pronounced positive Th anomalies and subdued positive Ce and Zr anomalies, whereas the metavolcanic rocks have positive Nb and Zr anomalies. Both types of khondalite are LREE enriched, and show weak HREE depletions and moderate negative Eu anomalies. P-T conditions for the formation of the khondalites are estimated to be 6.8 kbar and 700℃. The khondalites formed in the Caledonian orogeny (428~445Ma) and underwent strong shear deformation during the Indosinian (250~210Ma). SHRIMP dating of detrital zircons in the khondalites suggests that they were derived from an older metamorphic basement, probably older than 644Ma. The Kangxiwar khondalites are similar in their protoliths, trace-element and rare-earth element geochemistry, P-T conditions, and age of formation to those of the South Altyn Tagh khondalite series. This lateral correlation suggests that the West Kunlun and Altyn Tagh terranes were once contiguous, and provides evidence for the existence of a Caledonian orogenic belt in this region.

Introduction

THE NEARLY E-W-trending West Kunlun terrane is located in the northern part of the western Qinghai Tibet Plateau. It is a narrow terrane about 100km wide, bounded on the north by the Tarim Basin, on the south by the Karakorum Mountains, and on the east by the Altyn Tagh fault. Geologic observations suggest that it can be divided into two subterranes South Kunlun and North Kunlun separated by the Küdi-Oytog suture. The Kangxiwar suture that separates the South Kunlun from the Tianshuihai terrane (the western extension of the Bayan Har terrane) defines the southern boundary of the West Kunlun terrane (Matte *et al.*, 1996; Pan, 2000) (Fig.1).

[1] International Geology Review, Vol.47.2005, p.986~998.
[2] Corresponding author; email: xzq@cgsd.org.cn.

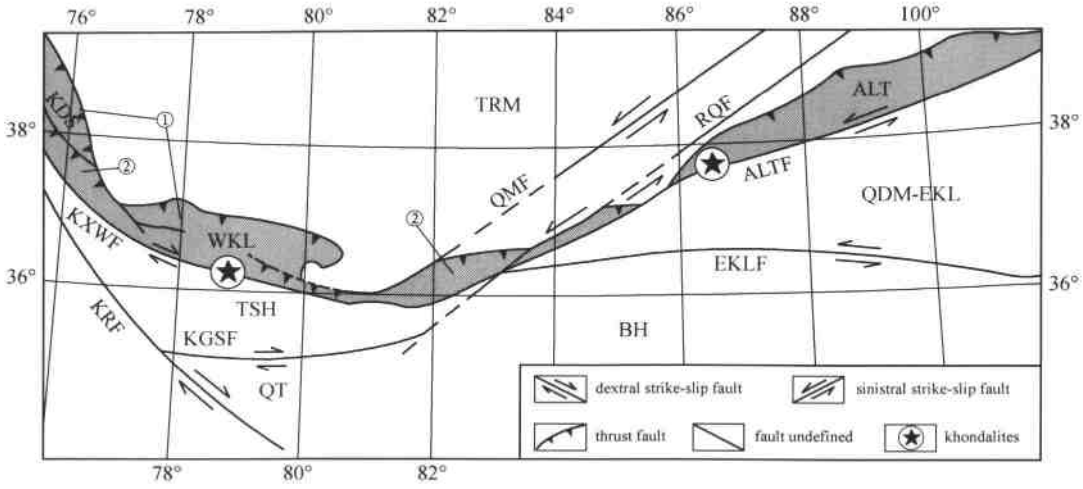

Fig. 1 Tectonic sketch map of the West Kunlun.

Legend: 1 = thrust; 2 = sinistral strike-slip fault; 3 = dextral strike-slip fault; 4 = fault; 5 = khondalites. Abbreviations: WKL = West Kunlun terrane; ALT = Altyn terrane; TSH = Tianshuihai terrane; QDM + EKL = Qaidam-East Kunlun terrane; BH = Bayan Har terrane; QT = Qiantang terrane; ALT F = Altyn Tagh fault; EKL F = East Kunlun fault; KXW F = Kangxiwar fault; KR F = Karakunlun fault; KGS F = Konggushan fault; KD S = Küdi-Oytog suture; RQ F = Ruoqiang fault; QM F = Qiemo fault. Legend: circled number 1 = North Kunlun tectonic zone; circled number 2 = South Kunlun tectonic zone.

The oldest North Kunlun basement rocks have a zircon U-Pb age of ～2261Ma and a Sm-Nd isochron age of ～2800Ma. They are overlain by Precambrian schists, gneisses, and marbles with subordinate quartzites and mafic to intermediate volcanic rocks. Ordovician to Lower Silurian sedimentary sequences consist of deep-water sedimentary rocks and fan deposits that formed in continental shelf and continental slope settings. The Lower and Middle Devonian strata consist of terrestrial clastic and carbonate rocks, whereas Upper Devonian strata are marked by marine variegated clastic rocks intercalated with continental equivalents which contain plant fossils (XBGMR, 1985).

A granodiorite intrusion has ^{40}Ar-^{39}Ar ages of 449 and 474Ma, and a zircon U-Pb age of 458Ma (Matte *et al*., 1996), suggesting that the North Kunlun terrane experienced a Caledonian magmatic event. Such an inference is also supported by biotite Ar/Ar and whole-rock Rb-Sr ages from 384 to 480Ma for calc-alkaline plutons in the North Kunlun (Xu *et al*., 2000). The Küdi-Oytog ophiolitic mélange, which lies in the Küdi-Oytog suture zone, consists of disrupted ophiolite rocks, siliceous pelites, and derivatives from arc volcanism. The ophiolite sequence consists of ultramafic rocks, mafic cumulates, mafic dike swarms, and tholeiitic basalts, which we regard as fragments of oceanic crust and uppermost mantle. The sequence as a whole represents rocks formed in either an island-arc or a continental arc environment (Jiang *et al*., 1992; Ding *et al*., 1996). The juxtaposition of ophiolitic malerial and an arc assemblage suggests that the West Kunlun terrane experienced Sinian to Early Paleozoic seafloor spreading, subduction, and finally collision (Ding *et al*., 1996).

The South Kunlun subterrane is a broad dome 15km wide that contains Paleoproterozoic intermediate-to high-grade granitic gneiss in its core, overlain by low-amphibolite to greenschist facies schists, marbles, and metavolcanic rocks. These high-grade basement rocks were intruded by granitic plutons that fall into two age groups: a Variscan group with ages of 377Ma (U/Pb zircon), 392 ± 35Ma (whole-rock Rb-Sr), and 381 ± 4Ma (biotite Ar/At) (Arnaud *et al.*, 1991); and an Indosinian group with ages of 211 ± 8Ma (whole-rock), 180 ± 10Ma(K-feldspar and plagioclase Ar/Ar), and 180 ± 10Ma (whole-rock Rb-Sr isochron) (Matte *et al.*, 1996). These results suggest that: ①the granitic gneisses underwent metamorphism sometime between 420 and 380Ma; and ② the metamorphic basement of the South Kunlun was involved in both Caledonian and Indosinian orogeneses.

The Kangxiwar fault is located along the southern margin of the South Kunlun subterrane, and extends eastward from Uzbel Pass, Kazakhstan through Bandinorth of Taxkorgan, Mazar. Sanshiliyingfang, Kangxiwar, and Muztag to Qong Muztag, where it is cut by the Allyn Tagh fault. The rocks of the South Kunlun sublerrane are similar to those in the North Kunlun. Precambrian metamorphic basement is exposed in the northwestern part of the Tianshuihai terrane and is overlain by Lower Paleozoic (O-S) continental-margin slope flysch and siliceous rocks of abyssal basin facies, which are strongly foliated and folded. Middle Devonian strata were formed in a stable marine depositional environment, whereas Upper Devonian strata consist of continental variegated coarse clastic rocks (Ding *et al.*, 1996). A very thick Permian-Triassic (P-T) flysch sequence consists of Paleo-Tethyan sedimentary rocks, which have been strongly foliated and folded and intruded by Indosinian granites (Xu *et al.*, 2000; Matte *et al.*, 1996). Most of the regional deformation and metamorphism in the Tianshuihai terrane is believed to be related to the Indosinian orogeny. The Taishuihai terrane and the Bayan Har-Songpan Garzê terrane together constitute a large-scale NW-trending Indosinian orogenic belt.

The Kangxiwar Khondalite Series

Khondalite-series rocks have recently been identified within the Kangxiwar shear zone. The Kangxiwar ductile shear zone is up to 7km wide and consists of mylonites and mylonitized metamorphic rocks. Although the rocks in the shear zone have been subjected to strong brittle and ductile deformation, their compositions and textural characteristics are sufficiently preserved to allow identification of their protoliths. Such data are critical for reconstructing their environment of formation, and for tracing the deformational history of the shear zone. We have analyzed a suite of rocks from the shear zone in order to characterize major, trace-, and rare earth element compositions. Zircons were extracted from one of the samples for SHRIMP U/Pb dating. The radiometric age data, combined with the geochemical data, are used to constrain the tectonic history of the Kangxiwar khondalites. Field, petrologic, and geochemical studies (presented here) indicate that the protoliths of rocks in the Kangxiwar ductile shear zone were khondalites.

Khondalite series

Khondalites have long been considered to be alumina-rich, high-grade metamorphic rocks that formed during the early stages of continental crustal development. They consist dominantly of highly metamorphosed supracrustal rocks, potassic granites, and granulites that contain aluminous minerals such as sillimanite and garnet. Khondalites have been found on all continents and share a number of common features in the nature of their protoliths, metamorphism, magmatism, and ore potential (Narayanaswami, 1975; Banerji, 1982; Chacko *et al*., 1987; Lu *et al*., 1996). In China, most of the khondalites occur in Precambrian terranes in the northern and central parts of the country (Jiang, 1991; Lu and Jiang, 1992; Lu *et al*., 1992), although one occurrence of Phanerozoic (450Ma) khondalite has been described from Qiemo, in the South Altyn Tagh Mountains (Zhang *et al*., 1999).

Field and petrographic observations show that the khondalites found along the Kangxiwar ductile shear zone have complicated lithologies dominated by aluminous gneisses (e.g., garnet-sillimanite rich gneisses and pyroxene-amphibole gneisses) with subordinate marbles (Fig.2). Two types of gneiss as well as serpentinized marbles are present in the South Altyn Tagh mountains.

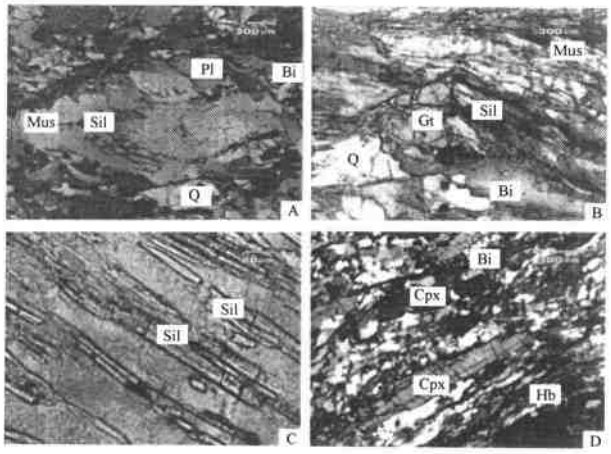

Fig.2 Photomicrographs of the Kangxiwar khondalites.

A-C—Sillimanite-garnet-rich gneiss. D—Pyroxene-amphibole-garnet-biotite monzonitic gneiss. Abbreviations: Sil = sillimanite; Gt = garnet; Bi = biotite; Mus = muscovite; Cpx = clinopyroxene; Q = quartz; Hb = hornblende; pl = plagioclase.

1. *Garnet-sillimanite-rich gneisses* (*khondalite series sensu stricto*). The garnet-sillimanite rich gneisses possess medium-to coarse-grained, nematoblastic to granoblastic textures and a gneissic structure. They consist of sillimanite, biotite, almandine, graphite, quartz, K-feldspar, and plagioclase. Based on mineral compositions, this suite of rocks includes garnet-sillimanite-biotite-plagioclase gneisses, sillimanite-biotite-plagioclase gneisses, garnet-sillimanite-two-mica-plagioclase gneisses, and garnet-graphite-biotite-(two-mica) plagioclase gneisses.

2. *Pyroxene-amphibole-bearing garnetbiotite-plagioclase-K-feldspar gneisses*. These vari-

eties occur along a ~50 m wide belt in the central part of the ductile shear zone. They have medium-to fine-grained, nematoblastic-granoblastic textures and a gneissic structure, or augen-mylonitic textures and a banded structure. The dominant minerals are diopside, zoisite, hornblende, with or without garnet, titanite, scapolite, biotite, quartz, microcline, plagioclase, and calcite.

3. *Serpentinized phlogopite-olivine marbles*. The marbles occur as lenses 1 to 2 m wide in the khondalite series in the northern part of the ductile shear zone. The marbles in the middle of the lenses have weakly deformed, weakly foliated, granular textures with a grain size of < 1mm to 1cm, whereas those at the edges of the lenses have strongly deformed, pervasive-foliated mylonitic textures. The dominant minerals are forsterite, diopside, phlogopite, and hornblende, with minor euhedral-granular apatite. Some of the rocks are extensively serpentinized.

Geochemical characteristics of the khondalite series

Major, trace element, and REE analyses were carried out on 12 samples of the Kangxiwar khondalites at the Chinese National Research Center for Geoanalysis, Beijing. Major oxides and some trace elements were determined by standard XRF techniques, whereas the remainder of the trace elements and rare earth elements (REE) were determined by ICP-MS. The analyzed samples include garnet-sillimanite rich (GSR) gneisses (WKL30-18a, WKL30-18b, WKL30-22, WKL30-33, WKL30-3, WKL30-19, and WKL30-20a) and pyroxene-amphibole-garnet-plagioclase (PAGP) gneisses (WKL30-35, WKL30-36, WKL30-31, WKL30-32, and WKL30-28). As shown in the following discussion, the protolith of the garnet-sillimanite-rich gneisses was a peraluminous sedimentary rock, whereas that of the pyroxene-amphibole-garnet-plagioclase gneiss was a volcanic rock (Fig. 3). Analytic results are listed in Table 1 and are discussed in the following sections.

1. *Major element geochemistry*. The major element geochemistry of the khondalites provides a good guide to their protoliths. The GSR gneisses have the following characteristics: ① their SiO_2 contents are mostly between 59.09 and 66.85 wt%, with the exception of sample 30~20a that has 71.44 wt% SiO_2; ② their K_2O, MnO, and TiO_2 contents are negatively correlated with SiO_2; ③ they have Al_2O_3 contents ranging from 10.66 to 19.58 wt%, with three samples (30-18a, 30-18b, and 30-33) having more than 17 wt% Al_2O_3. Such high Al_2O_3 is typical for peraluminous sedimentary rocks of the type formed in a stable continental margin environment. Samples of PAGP gneisses have: ① Al_2O_3 contents ranging from 9.70 to 11.73 wt%, far lower than those of the GSR gneisses; ② SiO_2 contents that vary between 65 and 72 wt%, similar to those in the GSR gneisses; and ③ high CaO of 5.04~7.39 wt%. Major element compositions suggest that they are calc-silicate rocks. When major element compositions of both types of rocks are converted into Niggli values and plotted in an Si (Al + fm) (c + alk) diagram, the GSR gneisses concentrate close to the pelitic end-member in the pelitic-psammitic sedimentary rock field, whereas all of the PAGP gneisses fall in the volcanic rock field (Fig.3). Thus, protoliths of the analyzed samples are believed to be either pelitic sedimentary rocks or intermediate-silicic volcanic rocks. The association of pelitic sedimentary

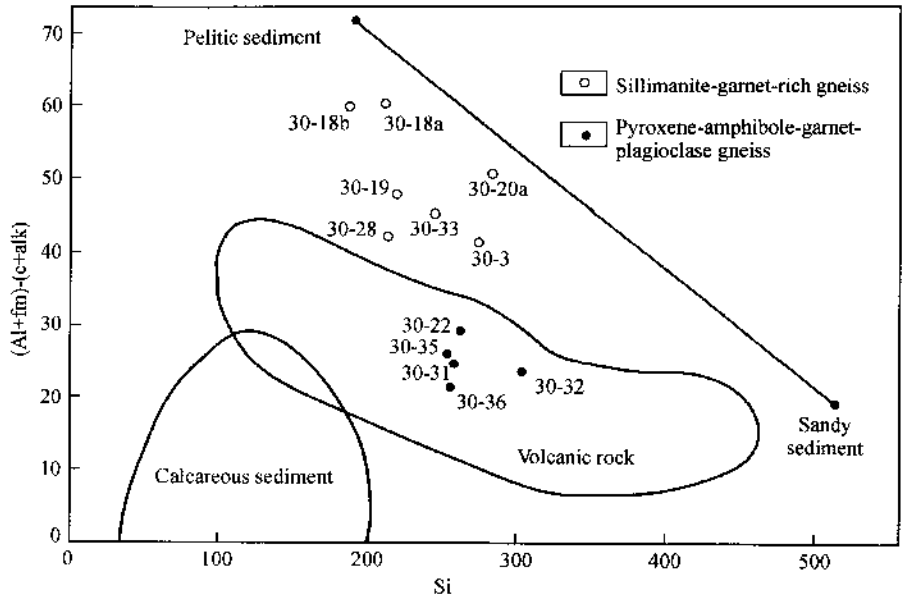

Fig. 3 Si-(Al + fm)-(c + alk) diagram of the Kangxiwar khondalites (after Simonen, 1953).
Legend: 1 = sillimanite-garnet-rich gneisses; 2 = pyroxene-amphibole-garnet-plagioclase gneisses. Sample numbers are the same as in Table 1.

rocks with intermediate-silicic volcanic rocks is typical for rocks formed in an arc environment (Saleeby and Busby, 1993), and we suggest that protoliths of the Kangxiwar khondalites formed in the margin of an extinct continental arc.

2. *Trace element and REE geochemistry*. Concentrations of the large-ion lithophile elements (LILEs) such as K, Rb, and Ba, as well as Th, Nb, and Ce in the Kangxiwar khondalites are far higher than the MORB values given by Pearce et al. (1984). In contrast, the P_2O_5 contents and Sr, Zr, and Sm concentrations are highly variable, all lower than MORB values (Table 1). In primitive mantle normalized spider diagrams (Fig. 4), the GSR gneisses show pronounced positive Th, Ce, and Zr anomalies, reflecting a crustal source of the protoliths. The PAGP gneisses have no Th anomaly, but do have positive Nb and Zr anomalies, which distinguish them from the GSR gneisses. Both the trace element and major oxide compositions of these khondalites suggest that they originated from igneous rocks.

The total REE contents of the khondalites range from 115.43 to 187.28 ppm (Table 1). The LREE/ HREE ratios vary from 2.34 to 3.63, indicating relative enrichment in LREE over HREE. Such enrichment in LREE is also consistent with the chondrite-normalized trace element distribution patterns (Fig. 4). Eu shows moderate depletion and Eu/Eu^* is generally scattered around 0.6, with values up to 0.83. All of the samples have high $(La/Sm)_N$ ratios ranging from 2.59 to 3.65, and $(Gd/Yb)_N$ values exceeding 1.0. High $(La/Sm)_N$ ratios indicate enrichment of LREE over HREE, whereas near unity ratios of $(Gd/Yb)_N$ signify weak or no HREE fractionation. In summary, the rare earth element geochemistry shows that the khondalite series is characterized by relative enrichment in LREE, high degrees of REE frac-

Table 1 Chemical Composition of the Kangxiwar Khondalites①

Sample	30-18a	30-22	30-33	k30-3	30-18b	30-19	30-20a	30-28	30-31	30-32	30-35	30-36
SiO_2	60.93	66.85	59.09	65.49	62.63	65.62	71.44	65.67	69.96	72.07	69.91	69.2
TiO_2	0.84	0.43	0.7	0.74	0.87	0.88	0.58	0.67	0.46	0.44	0.45	0.38
Al_2O_3	19.58	10.66	18.07	15.71	17.43	15.97	13.35	15.78	11.73	10.32	9.7	12.06
Fe_2O_3	2.09	1.02	2.55	1.12	0.59	0.61	0.33	1.14	0.74	0.53	0.64	1.27
FeO	4.67	2.57	3.75	4.02	5.91	5.26	4.22	4.01	2.53	2.39	3.2	2.35
MnO	0.07	0.08	0.07	0.12	0.07	0.09	0.1	0.07	0.06	0.18	0.11	0.14
MgO	3.3	2.64	3.02	2.3	3.24	2.46	1.91	2.3	2.24	1.89	3.85	1.97
CaO	1.23	10.56	0.76	1.92	1.4	1.53	1.4	2.52	5.04	6.66	6.91	7.39
Na_2O	2.08	1.38	2.81	3.17	1.84	2.73	2.16	3.37	2.19	1.1	1.65	1.59
K_2O	3.61	1.39	6.73	2.86	3.5	3.12	2.73	2.95	2.76	1.36	1.01	1.51
P_2O_5	0.19	0.09	0.14	0.21	0.34	0.17	0.27	0.16	0.08	0.08	0.07	0.08
H_2O^+	1.39	0.72	1.74	1.22	1.5	1.28	1.35	0.6	0.84	1.08	0.68	0.62
CO_2	0.22	2.06	0.22	0.48	0.09	0.05	0.07	0.4	1.1	1.8	1.32	0.93
Total	100.2	100.45	99.65	99.36	99.41	99.77	99.91	99.64	99.73	99.9	99.5	99.49
Sr	156	175	55.2	207	153	197	181	113	185	153	204	267
Rb	130	36.1	176	93.3	134	113	90.8	93.5	77.7	58.6	33.7	52.8
Ba	549	441	777	459	508	480	460	314	420	249	204	267
Th	14.1	8.73	16.9	10.9	13.7	12.8	9.72	8.61	8.27	6.91	7.71	8.4
Nb	13.3	8.59	13.4	11.8	12.6	12.6	9.24	176	49.7	51.6	138	37.4
Zr	206	100	168	208	197	206	162	192	163	169	278	128
Sm	7.04	4.46	6.86	5.72	7.62	6.27	5.38	5.31	3.78	3.59	7.66	4.1
Y	24.7	22	30	28.8	32.6	23.2	26.1	23.1	18.2	17.5	33.5	19.4
Sc	15.4	9.33	14.6	12.5	13.8	12.3	10.3	9.98	6.47	6.23	8.2	7.74
La	38.4	39.8	30.4	31.4	29.3	22.2	22.9	28.6	22.3	21.5	43.8	22.6
Ce	78.8	82.2	62	73.3	68.8	54.8	45.8	57.7	43.5	40	85.8	45.6
Pr	9.14	9.24	7.32	9.26	8.36	6.69	5.44	6.73	5.02	4.77	10	5.32
Nd	34.8	34.7	27.9	34.8	31.3	24.7	21	26.5	19	17.9	37.8	19.9
Sm	7.04	6.86	5.72	7.62	6.27	5.38	4.46	5.31	3.78	3.59	7.66	4.1
Eu	1.3	1.27	1.39	1.44	1.51	1.42	0.89	1.12	0.81	0.81	1.61	0.8
Gd	5.38	5.45	4.76	6.97	5.38	4.95	3.71	4.96	3.61	3.4	7.51	3.78
Tb	0.9	0.94	0.83	1.16	0.86	0.87	0.67	0.82	0.55	0.55	1.2	0.6
Dy	5.11	5.64	5.29	6.71	4.78	5.28	4.09	4.64	3.4	3.3	7.23	3.75
Ho	0.94	1.13	1.11	1.27	0.93	1.06	0.85	0.91	0.72	0.69	1.49	0.74
Er	2.56	3.32	3.34	3.37	2.59	2.91	2.55	2.5	2.12	2.13	4.31	2.28
Tm	0.34	0.48	0.5	0.44	0.37	0.43	0.36	0.38	0.32	0.32	0.62	0.34
Yb	2.22	3.15	3.34	2.69	2.4	2.67	2.35	2.43	2.14	1.97	3.97	2.22
Lu	0.35	0.48	0.53	0.4	0.38	0.41	0.36	0.36	0.33	0.32	0.63	0.34
ΣREE	187.28	194.66	154.4	180.43	163.23	133.77	115.43	143	107.6	101.3	213.6	112.4
LREE/HREE	9.52	8.45	6.84	6.86	8.23	6.2	6.73	7.41	7.16	6.99	6.92	7
δEu	0.62	0.61	0.79	0.59	0.78	0.83	0.65	0.66	0.66	0.7	0.64	0.61
$(La/Sm)_N$	7.41	7.41	7.41	7.41	7.41	7.41	7.41	3.39	3.71	3.77	3.6	3.47
$(Gd/Yb)_N$	2.62	2.62	2.62	2.62	2.62	2.62	2.62	1.65	1.36	1.39	1.53	1.37

① Units for major elements are in wt %; trace elements and REE are in ppm.

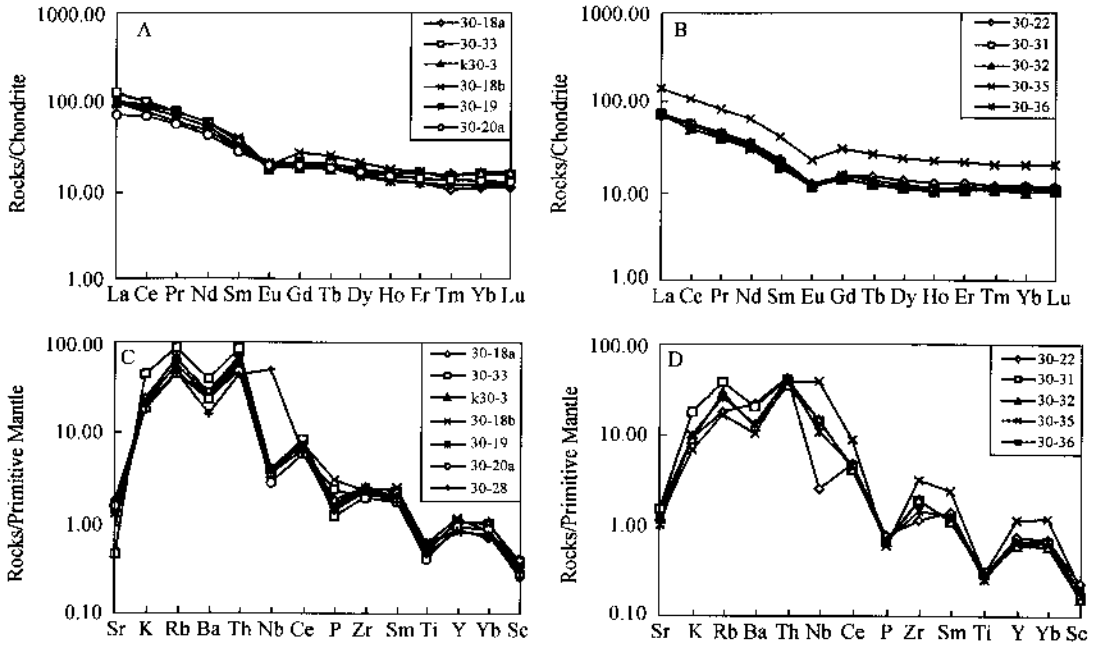

Fig.4 Trace element spidergram and REE distribution patterns of the Kangxiwar khondalite series.

A—Sillimanite-garnet-rich gneiss, B—Pyroxene-amphibole-garnet-plagio-clase gneiss. C—Sillimanite-garnet-rich gneiss. D—Pyroxene-amphibole-garnet-plagioclase gneiss. Sample numbers are the same as in Table 1.

tionation, relatively low degrees of HREE fractionation, and moderate Eu depletion.

Estimates of P-T conditions for the formation of the khondalites

Six samples of fresh khondalite were selected for microprobe study at the Electron Microprobe Laboratory of the Institute of Mineral Resources, Chinese Academy of Geological Sciences (CAGS), Beijing. Operating conditions were an accelerating voltage of 20kV and a beam current of 20nA. The analyzed samples contain fresh biotite, muscovite, plagioclase, and garnet that are thought to represent equilibrium assemblages. The *P-T* conditions of metamorphism were calculated from the mineral data using Thermo Calc software developed by Powell and Holland (1994) and Holland and Powell (2001). The results show that peak metamorphism occurred at $T=668\sim729$℃ with a mean of 701℃ and $P=6.6\sim7.1$ kbar with a mean of 6.8 kbar.

Zircon SHRIMP U/Pb Ages of the Kangxiwar Khondalite Series

Sample 30～36, a PAGP gneiss, was collected from the khondalite series in the Kangxiwar ductile shear zone, West Kunlun. The rock is greyish white and has a mylonitic structure with well-developed foliation and stretching lineation. The dominant minerals are garnet, sillimanite, diopside, biotite, microcline, K-feldspar, and quartz. Zircon grains were separated at the Langfang Institute of the Geological Survey, Hebei Province, and euhedral crystals were

handpicked under the microscope. The grains were then mounted and polished for laser Raman and SHRIMP analyses. The crystal shapes and internal structure of the zircons were observed with a laser Raman spectrometer and microscope at the Laboratory for Continental Dynamics of the Instituie of Geology, CAGS. Cathodoluminescence images were obtained at the Laboratory of Electron Microprobe of the Institute of Mineral Resources, CAGS.

Most zircons are prismatic with a length of 0.1～0.2 mm. The length/width ratio averages about 2.5∶1 but may reach 3.5∶1 in some grains. A few zircons have relatively complete crystal edges or faces, whereas others are rounded or granular in shape, with small sizes ranging from 0.05 to 0.1mm. Some grains contain cracks parallel to the prismatic face, suggesting that these zircons were modified by late-stage geological processes after formation. Cathodoluminescence (CL) images show two different types of structures in the zircons—those with a distinct overgrowth around a primary relict core, and those showing obvious growth lamellae characteristic of magmatic crystallization (Fig.5). The different shapes and geometries of the zircons in this sample indicate that they are the products of multi-stage geological processes.

Fig.5 Cathodoluminescence images of zircons from sample 30～36 of the Kangxiwar khondalite series. SHRIMP analytical spot numbers and the corresponding $^{206}Pb/^{238}U$ ages are shown in the images.

The zircon U-Pb dating was carried out with the SHRIMP II ion microprobe at the Isotope Laboratory of the Institute of Geology, CAGS. Detailed analytical procedures have been described by Stern (1997). Ion microprobe analyses were made on 26 spots of different types of zircon (relict core, overgrowth rim, and growth lamellae). The analytical results are listed in Table 2, and plotted on a U-Pb concordia diagram (Fig. 6). Most of the data fall on the $^{207}pb/^{235}U$-$^{206}pb/^{238}U$ concordia, and the others points plot close to the concordia. Four age groups: 197～214Ma, 245～256Ma, 428～445Ma, and 618～718Ma can be recognized in the diagram (Fig. 6).

Table 2 SHRIMP U-Pb Data for Zircons from the Khondalite Series (sample 30～36)

Sample	Zircon domain	Content							Age, Ma	
		U	Th	$^{206}Pb^*$	Th/U	$^{238}Pb/^{206}U$		$^{207}Pb^*/^{206}Pb^*$	$^{206}Pb/^{238}U$	
30-36-63	Rim	679	51	18.4	0.08	32.2	±3.5	0.0488	±5.0	197.1	±6.7
30-36-58	Rim	628	22	17	0.04	32	±3.5	0.0536	±4.5	198.5	±6.8
30-36-30.2	Rim	462	8	13.8	0.02	29.5	±3.5	0.0582	±9.5	214.8	±7.5
30-36-41	Rim	158	85	5.43	0.55	25.75	±3.7	0.0528	±12.0	245.6	±8.8
30-36-34	Rim	351	182	12.4	0.54	25.64	±3.7	0.042	±24.0	246.6	±9.0
30-36-50	Rim	669	2882	23.2	4.45	25.44	±3.5	0.053	±6.0	248.6	±8.5
30-36-42	Core	530	5	18.5	0.01	24.91	±3.5	0.0541	±3.7	253.7	±8.6
30-36-48	Rim	1224	478	43.2	0.4	24.65	±3.4	0.0499	±3.3	256.4	±8.6
30-36-54	Rim	470	131	17.6	0.29	23.37	±3.5	0.0532	±6.3	270.1	±9.2
30-36-33	Mantle	460	194	18.6	0.43	21.57	±3.5	0.0562	±4.1	292.2	±9.9
30-36-37	Mantle	667	218	32.1	0.34	18.09	±3.5	0.0652	±2.9	347	±12.0
30-36-38	Mantle	1031	364	43.7	0.36	20.55	±3.5	0.0509	±5.9	306	±10.0
30-36-47.1	Core	248	155	15.4	0.65	13.98	±3.5	0.054	±4.7	445	±15.0
30-36-46	Core	227	68	13.7	0.31	14.58	±3.5	0.0636	±6.8	428	±15.0
30-36-32	Core	416	251	25.1	0.62	14.39	±3.5	0.0578	±3.2	433	±15.0
30-36-56	Core	318	97	19.3	0.32	14.38	±3.5	0.0546	±5.5	433	±15.0
30-36-67	Core	306	11	21.1	0.04	12.62	±3.6	0.0668	±5.2	492	±17.0
30-36-44	Core	433	73	39.2	0.17	9.52	±3.5	0.05962	±1.6	644	±21.0
30-36-49	Core	176	57	16.4	0.33	9.44	±3.5	0.0647	±5.3	649	±22.0
30-36-59	Core	48	21	4.39	0.46	9.95	±3.9	0.07	±15.0	618	±23.0
30-36-45	Core	562	25	56.4	0.05	8.65	±3.4	0.1438	±1.3	705	±23.0
30-36-35	Core	235	21	24.7	0.09	8.49	±3.5	0.0631	±6.6	718	±24.0
30-36-31	Core	232	246	29.2	1.09	6.89	±3.5	0.0726	±2.3	873	±28.0
30-36-60	Core	70	50	15.1	0.74	4.06	±3.6	0.1091	±3.4	1419	±46.0
30-36-42.2	Core	387	52	116	0.14	2.878	±3.5	0.16671	±0.50	1923	±57.0

Pb^* = corrected for common Pb using ^{204}Pb. All errors are 1 sigma of standard deviation.

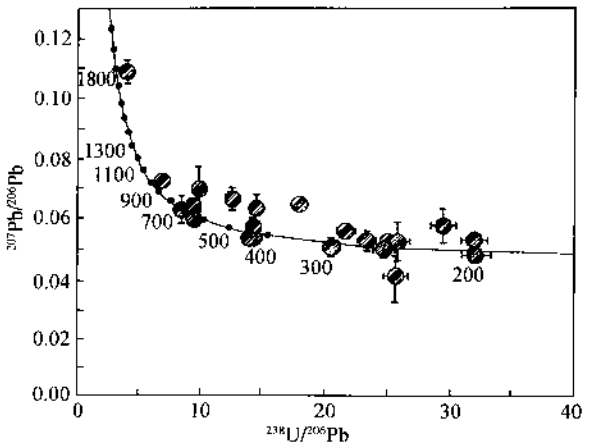

Fig.6 Concordia diagram of SHRIMP U-Pb zircon ages for sample 30~36 of the Kangxiwar khondalites.

The first group includes three data points from the zircon overgrowths, which have ages of 197.1Ma, 198.5Ma, and 214.8Ma, with a mean of 203Ma. U and Th contents are relatively constant, varying from 462 to 679 ppm and from 8 to 51 ppm. respectively, giving Th/U ratios of less than 0.1. These features are similar to those of metamorphic zircons (Claesson *et al.*, 2000; Rubatto, 2002)(Fig. 5).

The second group includes five spots from concentrically zoned zircon, which have ages of 245.6Ma, 246.6Ma, 248.6Ma, 252.7Ma, and 256.4Ma, with a mean of 250.2Ma. These zircons have widely varying U and Th concentrations. Except for spot 30-36-42, which has a Th/U ratio of <0.1, all the grains have Th/U ratios >0.4. Because of growth zoning, these zircons are interpreted as having a magmatic or anatectic origin (Hanchar and Miller, 1993; Sue *et al.*, 1999).

Zircons in the third group yielded four ages of 445Ma, 428Ma, 433Ma, and 492Ma, with an average of 435Ma. A few individual data points fall below the concordia, suggesting a possible loss of Pb. The U/Th ratios of these grains are relatively constant, ranging from 0.31 to 0.65 (Fig.7). In the cathodoluminescence images, these zircons have distinct growth zoning, implying that they may represent a growth stage related to an important regional tectonothermal event. The ages obtained from these zircons provide a key constraint on the timing of the Caledonian orogenic event.

Ages of 644, 649, 618, 705, 718, and 873Ma, all of which fall on or close to the concordia, comprise the fourth group (Fig.6). Their mean value is 667Ma. Zircons from this group have highly variable U concentrations but relatively constant Th concentrations, with Th/U ratios varying between 0.05 and 0.46 (Fig. 7). As shown in the CL images, all of these analyses were carried out on relict cores, and the ages probably represent the ages of the old metamorphic basement in the surrounding regions.

In addition to these four main groups of ages, two other clusters were obtained, one with

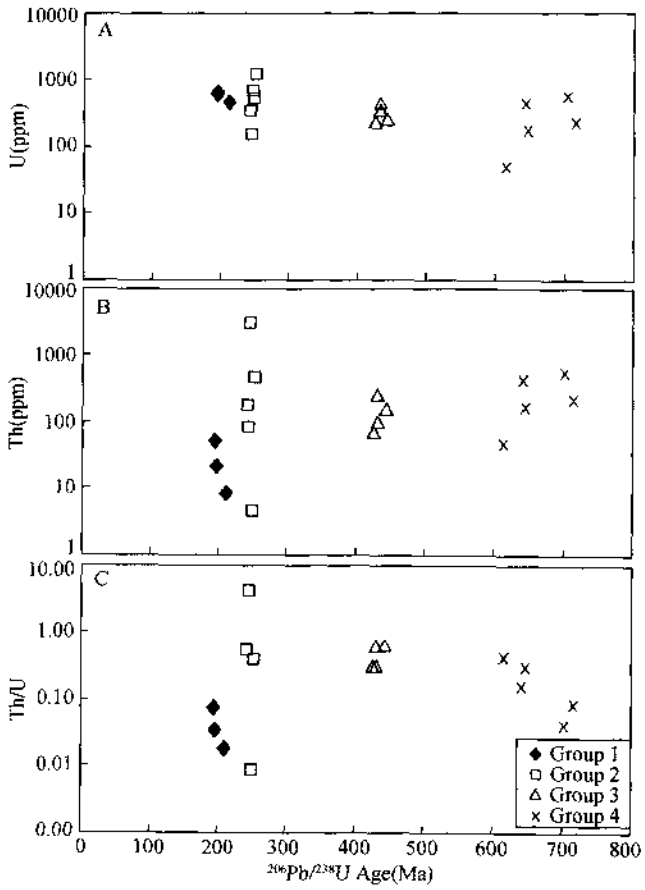

Fig.7 Plots of U versus $^{206}Pb/^{238}U$ ages (A), Th versus $^{206}Pb/^{238}U$ ages (B), and Th/U versus $^{206}Pb/^{238}U$ ages (C) for zircons from sample 30～36, showing that these zircons can be divided into four age groups.

ages of 873～1923Ma and the other with ages of 292～347Ma. Analytical spots of the first group are all from the relict cores of zircons, and these ages may reflect the presence of event older metamorphic basement components in the Kangxiwar khondalites. The second age group represents spots located in the transitional area between the relict cores and overgrowths. These are mixed ages and have no geological significance.

Discussion and Conclusions

A 7km wide ductile shear zone at Kangxiwar in the southern part of the West Kunlun terrane contains a mylonitized khondalite series. The rocks are chiefly garnet-sillimanite-rich gneisses, pyroxene-amphibole-bearing garnet-biotite-plagioclase-K-feldspar gneisses, and serpentinized phlogopite-olivine marbles. The khondalite protoliths were aluminum-rich pelitic or pelitic-psammitic sedimentary rocks and interlayered intermediate to silicic volcanic rocks.

Khondalites derived from pelitic sedimentary rocks have pronounced positive The anomalies and relatively subdued positive Ce and Zr anomalies. In contrast, those derived from metavolcanic rocks have positive Nb and Zr anomalies. Both types are relatively enriched in LREE, relatively depleted in HREE, and moderately depleted in Eu. This khondalite series may have been derived from rocks that formed at an ancient rifted continental margin. Khondalites in the vicinity of Tura in the western segment of the Altyn Tagh terrane are composed of peraluminous gneisses with garnet-hornblende-two-pyroxene gneisses, whose protoliths were alumina-rich pelitic and peliticpsammitic sedimentary rocks and basalts. This khondalite series is also thought to have formed in a continental-margin environment (Zhang *et al.*, 1999). The Kangxiwar khondalite series is similar to that of the Altyn Tagh khondalite series.

The Kangxiwar khondalites have experienced granulite-facies metamorphism, as suggested by peak metamorphic temperatures and pressures of 800 ± 50℃ and 6～9 kbar, respectively. However, relatively low metamorphic temperatures in the range of 650℃ to 750℃ determined for a few samples, suggest that metamorphism may have been transitional between high-amphibolite facies and granulite facies conditions (Lu *et al.*, 1996). Because no granulites have been found in the Kangxiwar khondalite series, the peak metamorphic P and T of 6.8 kbar and 700℃ for the peraluminous gneisses imply that they have also undergone transitional metamorphism. Granulites in the Altyn Tagh khondalite series have peak temperatures and pressures 700～850℃ and 8～12 kbar, respectively (Zhang *et al.*, 1999), similar to those of the Kangxiwar khondalites. Therefore, we conclude that the P-T conditions for the formation of the West Kunlun khondalites were comparable to those of the Altyn Tagh khondalites.

Zircon SHRIMP U/Pb dating of the Kangxiwar khondalites indicates that: ① detrital zircons with ages from 644 to 873Ma or older in the khondalites represent materials derived from pre-existing metamorphic terranes older that 644Ma; ② the khondalites were formed by high-grade metamorphism of pelitic sedimentary rocks and subordinate volcanic rocks at 428～445Ma; and ③ the khondalites underwent strong shear strain in the Indosinian (250～210Ma). Zhang *et al.* (1999) reported U-Pb and Pb-Pb ages of 447～462Ma for metamorphic zircons, and upper intercept ages of 1027 and 2571Ma for relict zircons from the Altyn Tagh khondalites. The older ages probably represent ancient source components in the protoliths for the Altyn Tagh khondalites. The sparse U-Pb zircon age data reported by Zhang *et al.* (1999) do not put a tight constraint on the potential old source components in the Altyn Tagh khondalites, as it is the case of the Kangxiwar khondalite. The available data indicate that the metamorphic ages of the two khondalite series are similar, and that the relict grains represent detrital zircons derived from an older metamorphic basement.

Khondalites in Kangxiwar and the Altyn Tagh are similar in age, chemical composition, protolith chemistry, and P-T conditions of formation (Zhang *et al.*, 1999), and we suggest they may be originally part of the same terrane. SHRIMP dating on zircons collected from the ductile shear zones of the Altyn Tagh fault suggests that the main trace of the Altyn Tagh fault to the south of the Altyn Tagh terrane might have been initiated in Indosinian time (Li *et al.*,

2001). Recent field, petrologic, and geochemical observations demonstrate excellent correlations between the Caledonian subduction complexes (e.g., the Northern Qilian subduction complex with the Northern Altyn Tagh, and the Northern Qaidam Mountain ultrahigh pressure metamorphic complex with the Southern Altyn Tagh) (Yang *et al*., 1998, 2000; Zhang *et al*., 2000a, 2000b). Such correlations on both sides of the main trace of the Altyn Tagh fault suggest an approximately 400km left-lateral strike-slip motion along it (Xu *et al*., 1999). The ENE-WSW-trending Ruoqiang fault that is subparallel to main trace of the Altyn Tagh fault may be one of the abandoned branches of the paleo-Altyn Tagh fault and defines the northern boundary of the Altyn Tagh terrane (Fig. 1). It joins the Altyn Tagh fault at its southwestern end. Field observations and satellite images around this junction indicate that it is probably where the South Kunlun terrane meets the Altyn Tagh terrane. If the Altyn Tagh and South Kunlun terranes were once a coherent block and later offset by the Ruoqiang strike-slip fault, then about 150 to 200km left-lateral strike-slip movement can be added to the total amount of slip on the Altyn Tagh fault system. Therefore, we suggest a total dextral slip of up to 600km along the Altyn Tagh fault since the Indosinian.

The khondalite series has long been considered a peraluminous, high-grade metamorphic complex that developed in the early stages of crustal formation (Narayanaswami, 1975; Banerji, 1982; Chacko *et al*., 1987; Lu *et al*., 1996). Khondalites occur mainly in Early Precambrian terranes in the northern and central parts of China (Lu *et al*., 1992; Jiang, 1991). The khondalite series discovered at Kangxiwar of the West Kunlun and Qiemo of the South Altyn Tagh Mountains (Zhang *et al*., 1999) consist of high-grade metamorphic rocks located in the mountain root zones formed during the Caledonian, and thus have great significance for understanding the Caledonian orogeny and tectonic evolution of this region.

Acknowledgments

This study was supported by the "Terrane Boundaries and Lithospheric Shear Faults in the Qinghai-Tibet Plateau" section of the special project of the Ministry of Land and Resources "Collisional Orogeny of the Qinghai-Tibet Plateau and Its Effects." Thanks to Paul Robinson and J. G. Liou for their support and suggestions that greatly helped to improve the quality of this manuscript, and Fenghua Liang and Xiaowei Zhang for assistance in preparation of the figures.

References

Arnaud, N., Xu, R., and Zhang, Y., 1991, Nouvelles donnees thermochronologique sur le batholite du kunlun et L'histoire thermique du Nord du Plateau Tibetain: Compte Rendus de l'Academie Sciences Paris, t. 312, Serie II, p. 905～911.

Banerji, P. K., 1982, The khondalites of Orissa, India—a case history of confusing terminology: Journal of the Geological So-

ciety of India, v. 23, p.155～159.

Chacko, T., Ravindra, K. G. R., and Newton, R. C., 1987, Metamorphic P-T conditions of Kerala (South India) khondalite belt: A granulite facies supracrustal terrain: Journal of Geology, v. 95, p. 343～358.

Claesson, V. S., Vetrin, T., and Bayanova, H. D., 2000, U-Pb zircon ages from a Devonian carbonatite dyke, Kola peninsula, Russia: A record of geological evolution from the Archean to the Palaeozoic: Lithos, v. 51, p. 95～108.

Ding, D. G., Wang, D. X., Liu, W. X., and Liu, W. X., 1996, The western Kunlun orogenic belt and basin: Beijing, China, Geological Publishing House (in Chinese). Hanchar, J. M., and Miller, C. E, 1993, Zircon zonation patterns as revealed by cathodoluminescence and backscattered electron images: Chemical Geology, v. 110, p. 1～13.

Holland, T. J. B., and Powell, R., 2001, Calculation of phase relations involving haplogranitic melts using an internally consistent thermodynamic data set: Journal of Petrology, v. 42, p. 673～683.

Jiang, C. F., Yang, J. S., Feng, B. G., Zhu, Z. Z., Zhao, M., Chai, Y. C., Shi, X. D., Wang, H. D., and Hu, J. Q., 1992, Opening-closing tectonics of Kunlun mountains: Beijing, China, Geological Publishing House, p. 224 (in Chinese).

Jiang, 1. S., 1991, Main-period areal metamorphism and evolution of khondalite series from the Mashan group: Acta Petrologica et Mineralogica, v. 11, no. 2, p. 97～110.

Li, H. B., Yang, J. S., Xu, Z. Q., Wu, C. L., Wang, Y. S., and Shi, R. D., 2001, Geological and geochronogy evidence of Indosinian strike-slip movement for the Altyn Tagh fault: Chinese Science Bulletin. v. 46, no. 16, p. 1333～1338 (in Chinese with English abstract).

Lu, L. Z., and Jiang, J. S., 1992, Metamorphic evolution of the khondalic series from the early Proterozoic Kongling group, western Hubei Province, in Augustithis, S. S., ed., High-grade metamorphism: Athens, Greece, Theophrastus Publications, S.A., p. 265～296.

Lu, L. Z., Jin, S. Q., Xu, X. C., and Liu, F. L., 1992, Origin of an early Precambrian Khondalite series in southeastern inner Mongolia and its mineralization: Changchun, China, Jiling Science and Technology Press, 152 p. (in Chinese with English abstract).

Lu, L. Z., Xu, X. C., and Liu, F.L., 1996, Early Cambrian khondalite series in northern China: Changchun, China, Changchun Publishing House, 276 p. (in Chinese).

Matte, P. H., Tapponnier, P., Arnaud, N., Bourjot, L., Avouac, J. P., Vidal, P. H., Liu, Q., Pan, Y. S., and Wang, Y., 1996, Tectonics of western Tibet, between the Tarim and the Indus: Earth and Planetary Science Letters, v. 142, p. 311～330.

Narayanaswami, S., 1975, Proposal for charnockite-khondalite and Sargur-Nellore-Khamman-Bengpal-Deogarh-Pallahare-mahagiri rock groups—older than Dharwar type greenstone belts in the Peninsular Archaean: India Mineralogist, v. 16, p. 16～25.

Pan, Y. S., 2000, Geological evolution of the Karakorum-Kunlun Mountains: Beijing, China, Science Press, 525 p. (in Chinese with English abstract).

Pearce, J. A., Harris, N. B. W., and Tindle , A. G., 1984, Trace element discrimination diagrams for the tectonic interpretation of granitic rocks: Journal of Petrology, v. 25, p. 956～983.

Powell, R., and Holland, T. J. B., 1994, Optimal geothermometry and geobarometry: American Mineralogist, v. 79, p. 120～133.

Rubatto, D., 2002, Zircon trace element geochemistry: Partitioning with garnet and the link between U-Pb ages and metamorphism: Chemical Geology, v. 184, p. 123～138.

Saleeby, J. B., and Busby, C., 1993, Paleogeographic and tectonic setting of axial and western metamorphic framework rocks of the southern Sierra Nevada, California, *in* Dunn, G., and MacDougall, K., eds., Mesozoic paleogeography of western United States-II: Pacific Section SEPM, Book 71, p. 197～226.

Simonen, A., 1953, Stratigraphy and sedimentation of the Svecofennidic, early Archean supracrustal rocks in southwestern Finland: Bulletin de la Commission Géologique de Finlande, v. 160, p. 64.

Stern, R. A., 1997, The GSC Sensitive High Resolution Ion Microprobe (SHRIMP): Analytical techniques of zircon U-Th-

Pb age determinations and performance evaluation, *in* Radiogenic age and isotopic studies: Geological Survey of Canada, Current Research, Report 10. p. 1～31.

Sue, K., David, S., and William, C., 1999, Identifying granite sources by SHRIMP U-Pb zircon geochronology: An application to the Lachlan fold belt: Contributions to Mineralogy and Petrology, v: 137, p. 323～341.

XBGMR (Xinjiang Bureau of Geology and Mineral Resources). 1985, 1∶1 M Regional Geological Survey report on the Bulungkol-Qarlun area, West Kunlun Mountains: Beijing, China: Geological Publishing House, p. 14～89 (in Chinese).

Xu, R. H., Zhang Y. Q., Xie, Y. W., Vidal, P. H., Arnaud, N., Zhang. Q. D., and Zhao, D. M., 2000, Isotopic geochemistry of plutonic rocks, *in* Yusheng, P., ed., Geological evolution of the Karakoram and Kunlun mountains: Beijing, China, Scientific Publishing House, p. 324～392 (in Chinese).

Xu, Z. Q., Yang, S., Zhang, J. X, Jiang, M., Li, H. B, and Cui, J. W., 1999, A comparison between the tectonic units on the two sides of the Altun sinistral strike-slip fault and the mechanism of lithospheric shearing: Acta Geologica Sinica, v. 73, no. 3, p. 193～205 (in Chinese with English abstract).

Yang, J. S., Xu, Z. Q., Li, H. B., Wu, C. L., Cui, J. W., Zhang, J. X., and Chen, W., 1998, Discovery of eclogite at northern margin of Qaidam basin, NW China: Chinese Science Bulletin, v. 43, p. 1755～1760.

Yang, J. S., Xu, Z. Q., Li, H. B., Zhang, J. X., Wu, C. L., Zhang, J. X., and Shi, R. D., 2000, A Caledonian convergent border along the Qilian terraine, NW China: Evidence from eclogite, garnet-peridotite, ophiolite, and S-type granite: Journal of the Geological Society of China, v. 43, no. 1, p. 142～160.

Zhang, J. X., Xu, Z. Q., Yang, J. S., Li, H. B., and Wu, C. L., 2000a, The Altun-North Qaidam eclogite belt in western China—another HP-UHP metamorphic belt truncated by large-scale strike-slip fault in China: Earth Science Frontiers. v. 7 (suppl.), p. 254～255.

Zhang, J. X., Zhang, Z. M., Xu, Z. Q., Cui, J. W., and Yang, J. S., 1999, Discovery of khondalite series from the western segment of Altyn and their petrological and geochronological studies: Science in China (Series D), v. 29, no. 4. p. 298～305.

Zhang, J. X., Zhang, Z. M., Xu, Z.Q., Yang, J. S., and Cui, J. W., 2000b, Discovery of khondalite series from the western segment of Altyn and their petrological and geochronological studies: Science in China (Series D), v. 43, p. 308～316.

喜马拉雅地体的泛非-早古生代造山事件年龄记录❶

许志琴[1] 杨经绥[1] 梁凤华[1] 戚学祥[1] 刘福来[1] 曾令森[1]
刘敦一[2] 李海兵[1] 吴才来[1] 史仁灯[1] 陈松永[1]
(1. 中国地质科学院地质研究所大陆动力学重点实验室 北京 100037;
2. 中国地质科学院地质研究所北京离子探针中心 北京 100037)

摘 要 喜马拉雅地体是55±10Ma以来印度陆块与欧亚大陆碰撞而形成的增生地体,位于其中的高喜马拉雅与特提斯-喜马拉雅构造单元的变质基底主要由角闪岩相的富铝变质沉积岩和花岗质片麻岩组成。对两类岩石中锆石的SHRIMP U-Pb测年结果表明,除了记录了20Ma以来的构造事件年龄外,主要保存了529~457Ma的变形和变质事件记录,另外还保存了更早期(>835Ma)的年龄信息。根据20Ma以来崛起的喜马拉雅挤出岩片中包含早期强烈褶皱和向南的斜向逆冲构造以及伴随的角闪岩相变质作用记录,结合岩石测年所获得的大量泛非-早古生代年龄和奥陶纪底砾岩的发现,说明曾位于南半球印度陆块北部的变质基底岩石经历过泛非-早古生代造山事件,同位素年代学数据表明:①原始喜马拉雅山是泛非-早古生代造山事件的产物;②印度陆块早-中元古代变质基底的再活化在原始喜马拉雅山形成中起重要的作用;③现在的喜马拉雅山是在泛非-早古生代造山事件基础上再造山的结果。

关键词 喜马拉雅 泛非-早古生代造山事件 SHRIMP测年
中图法分类号:P534.4;P542.2;P597.3

1 引言

位于青藏高原南缘的喜马拉雅地体具地球上最高的地貌地形,被称为世界"屋脊"。地体的主带呈EW向延展2500km,宽300~500km,其北界为雅鲁藏布江缝合带,南界为喜马拉雅前陆冲断裂(HFT)。地体在印度板块的西北端及东北端分别形成高地貌的Nanga Parbat构造结和Namche Barwa构造结,在东、西构造结处地体往南转成南北走向,分别成为90°东海岭右行走滑断裂及恰曼左行走滑断裂(图1)。

喜马拉雅地体是55±10Ma以来印度板块与欧亚大陆碰撞而形成的增生地体(Argand, 1922),由于印度板块与欧亚大陆碰撞导致喜马拉雅造山带的崛起的事件(包括变质、变形、

---

❶ 岩石学报,2005年第21卷第1期。

本研究得到国土资源部科技专项《青藏高原的碰撞造山及其效应》课题"青藏高原地体边界及岩石圈剪切断裂"的资助。

第一作者简介:许志琴,女,1941年生,中国科学院院士,主要从事显微构造、大地构造和大陆动力学研究,长期从事青藏高原构造研究。

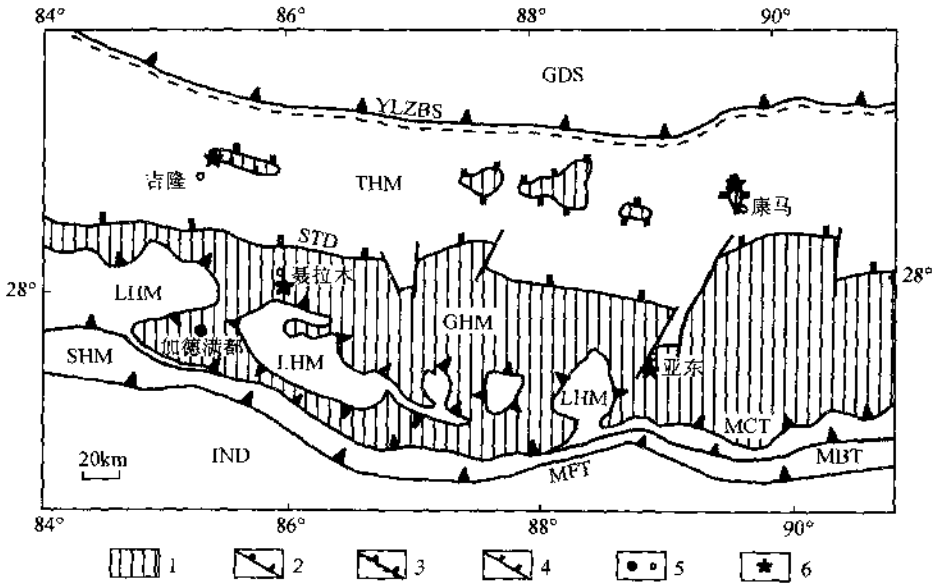

图 1 喜马拉雅地体构造图

Fig. 1 Tectonic Sketch map of the Himalaya terrane

1—变质基底;2—逆冲断层;3—缝合带;4—拆离断层;5—地名;6—采样位置。THM—特提斯喜马拉雅构造单元;GHM—高喜马拉雅构造单元;LHM—低喜马拉雅构造单元;SHM—次喜马拉雅构造单元。GDS—冈底斯地体;IDN—印度陆块;YLZBS—雅鲁藏布缝合带;STD—藏南拆离断层;MCT—主中冲断层;MBT—主边冲断层;MFT—主前锋冲断层

1—metamorphic basement; 2—thrust; 3—*suture zone*; 4—*detachment*; 5—*locations*; 6—collected location. THM—Tethys-Himalaya tectonic unit; GHM—Greater Himalaya tectonic unit; LHM—Lesser Himalaya tectonic unit; SHM—Subhimalaya tectonic unit; GDS—Gangdise terrane; IND—India plate; YLZBS—Yaluzangbu suture; STD—South Tibetan Detachment; MCT—Main Central Thrust; MBT—Main Boundary Thrust; MFT—Main Frontier Thrust

隆升与剥蚀作用)已为许多学者所描述(Argand, 1922; Gansser, 1964; Tapponnier *et al*., 1982; Le Fort *et al*., 1983; Le Fort, 1996; Harrison *et al*., 1997; Hodges, 2000; DeCelles *et al*., 2000, 2001)。

喜马拉雅构造带的物质组成包括了印度板块北缘的前震旦纪变质基底和特提斯类型的古生代、中生代、古始新世的海相沉积,以及渐新世以来的陆相沉积。喜马拉雅增生地体自北往南分为 4 个构造单元:特提斯-喜马拉雅构造单元、高喜马拉雅构造单元、低喜马拉雅构造单元及次喜马拉雅构造单元。特提斯-喜马拉雅构造单元位于雅鲁藏布缝合带(YLZBS.)与藏南拆离断裂(STD)之间,高喜马拉雅构造单元的南界为主中冲断裂(MCT),低喜马拉雅构造单元的南界为主边冲断裂(MBT),次喜马拉雅构造单元的南界以主前锋冲断裂(MFT)与印度板块相接(Burg and Chen, 1984; Burchifiel *et al*., 1992; Brookfield, 1993; Le Fort, 1996; Yin and Harrison, 2000)。

喜马拉雅地体的前震旦纪变质基底岩石主要分布在高喜马拉雅构造单元及特提斯-喜马拉雅构造单元的拉轨岗日-康马一带的 4 个变质穹隆中。高喜马拉雅的前震旦纪变质岩

属印度地台北缘结晶基底的组分，在主带上称聂拉木群，为一套高角闪岩相-绿片岩相的副变质岩系，以含蓝晶石、十字石、矽线石的石榴石片岩和片麻岩为主，夹变粒岩、大理岩和石英岩，原岩为含铝的沉积岩砂岩及砂质粘土岩（可能为孔兹岩系），局部为混合岩化花岗质片麻岩，总厚 6000～9000m。前人资料表明，尼泊尔纳瓦科特云母石英岩的白云母年龄为 728±2Ma（Krummenacher, 1961），锡金查尔群中角闪石年龄为 819±80Ma（Krummenacher, 1961），聂拉木群黑云斜长片麻岩中锆石 U-Pb 年龄为 1250Ma（Xu Ronghua *et al*., 1985），侵入聂拉木群的东喜马拉雅林格斯花岗岩 Rb-Sr 等时线年龄为 1050Ma（Acharyya, 1977）以及库蒙地区穆尼亚片麻岩的全岩等时线年龄 1800±100Ma（Thakur, 1980）。在尼泊尔高喜马拉雅的前奥陶纪变质岩中碎屑锆石的年龄主要为 1000～1300Ma，此外还有 1500Ma 和 2500Ma（Gehrels *et al*., 2003）的年龄。

特提斯-喜马拉雅构造单元的变质穹隆核部拉轨岗日群也是一套高角闪岩相-绿片岩相的副变质岩系，以含蓝晶石、十字石、矽线石的石榴石片岩、片麻岩及花岗质片麻岩为主，原岩由含铝的沉积岩砂岩、砂质粘土岩及混合岩化片麻状花岗岩组成，与高喜马拉雅的聂拉木群相似。

喜马拉雅地体中沉积盖层发育齐全，包括古生代、中生代及古始新统的海相沉积以及渐新世以来的陆相沉积。古生代基本上为一套连续沉积的、稳定的台型碳酸盐-碎屑岩沉积，属印度地台沉积盖层，总厚 3300 余米。由于在北喜马拉雅构造单元的沉积盖层与高喜马拉雅构造单元结晶岩系之间的强烈拆离（STD），拆离层上部的震旦-寒武纪岩石变质成石榴石黑云母片岩及绿泥石英片岩，并且减薄，位于喜马拉雅东段的古生代地层几乎全部缺失，三叠系直接覆盖在高喜马拉雅结晶岩系之上。

由于高喜马拉雅地体的中奥陶纪底砾岩的发现及同位素年代学的测试结果，使原始喜马拉雅的形成成为讨论的焦点（Gehrels *et al*., 2003）。自 1964 年 Gansser 提出关于喜马拉雅造山带形成于早古生代的观点以来，Stocklin and Bhattarai（1977）、Stocklin（1980）、Le Fort *et al*.（1983）、Garzanti *et al*.（1986）、Thakur（1992）、Brookfield（1993）、Valdiya（1995）和 Gehrels *et al*.（2003）通过尼泊尔及北印度地区的工作同意此观点，主要证据如下：（1）中尼泊尔新元古代-早古生代地层被同造山的花岗岩侵位（Stocklin and Bhattarai, 1977；Stocklin, 1980），北印度高喜马拉雅的变质作用的时代为 534Ma（Sm-Nd, Argles *et al*., 1999），矽线石蓝晶石片岩被 488Ma 的花岗岩侵位和北西喜马拉雅的变质年龄为 467Ma（Foster, 2000），中尼泊尔变质年龄为 484Ma（U-Pb，独居石和锆石；Godin *et al*., 2001），变形花岗岩的年龄为 484Ma，未变形的花岗岩脉的年龄为 472Ma 和 476Ma（Gehrels *et al*., 2003），东尼泊尔变质年龄为 436～548Ma（Th-Pb，独居石；Catlos *et al*., 2002）；（2）早古生代隆升与剥蚀的证据：在北印度的喜马拉雅，中奥陶统砾岩角度不整合盖在组成山体的变质沉积岩之上（Garzanti *et al*., 1986）；在中尼泊尔，奥陶纪砾岩和长石砂岩层记录了同造山沉积作用（Stocklin and Bhattarai, 1977；Kumar *et al*., 1978；Stocklin, 1980）；在西尼泊尔，发现一层 30m 厚的含 40cm 直径砾石的奥陶统砾岩层（Gehrels *et al*., 2003）；另外在砾岩层之上的奥陶纪-泥盆纪地层中含有大量 480～530Ma 年龄的锆石颗粒（Gehrels *et al*., 2003）。

最近，中国境内高喜马拉雅的聂拉木和特提斯-喜马拉雅的康马穹隆边部发现早奥陶统的底砾岩（刘文灿等，2002；周志广等，2004），并提出底砾岩可作为泛非事件的地质标志（周志广等，2004）。

本项研究是从喜马拉雅地体变质基底的地质演化历史复原的角度出发,通过对中国境内高喜马拉雅构造单元东段(亚东)、中段(聂拉木)及特提斯-喜马拉雅构造单元(康马、吉隆镇北)变质基底的角闪岩相富铝变质沉积岩和花岗质片麻岩样品的锆石进行 SHRIMP U-Pb 同位素测年,探求如下问题:(1)喜马拉雅地体变质基底所经历的重要地质演化历史记录;(2)原始喜马拉雅造山事件的时限及其成因。

2 喜马拉雅地体变质基底岩石的 SHRIMP 锆石测年

2.1 测试样品位置及地质背景

测试样品取自于特提斯-喜马拉雅构造单元的康马和吉隆北以及高喜马拉雅构造单元的亚东和聂拉木(图 2)。

其中,HH-5 位于特提斯-喜马拉雅构造单元中拉轨岗日穹隆带东部的康马变质穹隆北缘西侧,康马变质穹隆主要由黑云二长片麻岩、二云二长片麻岩、矽线石榴黑云斜长片麻岩和矽线二云二长片麻岩等组成,HH-5 为含褐帘石黑云二长片麻岩,片状-柱粒状变晶结构,片麻状构造,主要矿物组成:斜长石 + 钾长石 + 石英 + 黑云母 + 褐帘石 + 石榴石等,暗色矿物定向排列;HH-42 位于特提斯-喜马拉雅构造单元的拉轨岗日穹隆带西部吉隆镇北佩枯错西,1∶150 万青藏高原及邻区地质图(中国地质科学院成都地质矿产研究所,1988)上原定为喜马拉雅期花岗岩,呈长条状东西向展布,位于侏罗纪与白垩纪浅海相地层之间,研究表明其为含电气石二云二长片麻岩,片状-柱状变晶结构,片麻状构造,主要矿物组成为:斜长石 + 钾长石 + 石英 + 黑云母 + 白云母 + 电气石等,具弱糜棱岩化,花岗片麻岩与侏罗纪与白垩纪浅海相地层为断层接触,南缘为逆冲断层,北缘为正断层,佩枯错花岗片麻岩体为变质基底的组分,呈挤出构造岩片产出;HH-32 位于高喜马拉雅构造单元东部亚东镇南西离锡金边境 18km 处,亚东地区的岩石主要为石榴矽线黑云斜长片麻岩、矽线黑云斜长片麻岩、二云二长片麻岩、黑云二长片麻岩等,HH-32 为矽线石榴黑云斜长片麻岩,片状-柱状变晶结构,片麻状构造,主要矿物组成为:斜长石 + 石英 + 黑云母 + 石榴石 + 矽线石等,暗色矿物定向排列明显;HH-72 位于高喜马拉雅构造单元西部聂拉木镇南樟木北 13km 友谊隧道,聂拉木地区的岩石主要由矽线石榴二云二长片麻岩、蓝晶石矽线石二云二长片麻岩、白云母斜长片麻岩、黑云斜长片麻岩、含十字石石榴蓝晶黑云片岩和透辉石大理岩等组成,HH-72 为矽线石榴二云二长片麻岩,片状-柱粒状变晶结构,片麻状构造,主要矿物组成为:斜长石 + 钾长石 + 石英 + 黑云母 + 白云母 + 石榴石 + 矽线石等(图 2)。

2.2 测试方法

选用单颗粒锆石 SHRIMP U-Pb 原位定年的方法对上述样品进行时代的确定。首先用常规方法粉碎样品并分选出锆石,在双目镜下挑选出晶形和透明度较好的锆石颗粒,将其和标准锆石参考样 TEM 在玻璃板上用环氧树脂固定、抛光,然后进行透射光及反射光照相;阴极发光照相在中国地质科学院矿产资源研究所电子探针室完成。U-Pb 同位素年龄的测定是在中国地质科学院地质研究所北京离子探针中心 SHRIMP II 上完成的,SHRIMP U-Pb 分析方法参考 Williams 等(1987)和 Compston 等(1992)。

2.3 分析结果

2.3.1 康马(HH-5)

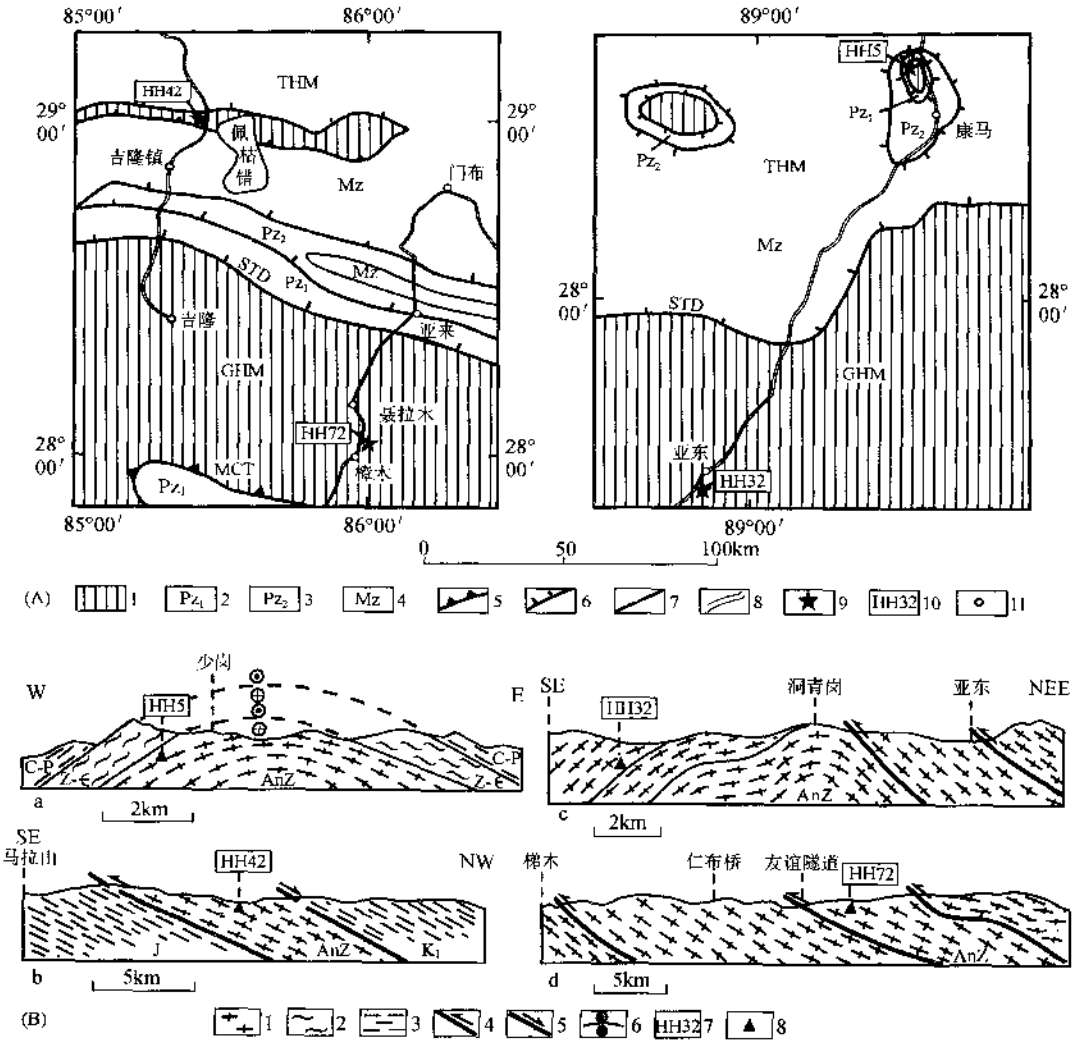

图 2 SHRIMP U-Pb 测年采样位置的地质平面图及地质剖面图

(据 1/150 万青藏高原地质图修改,1988)

Fig.2 The geologic map and profiles of the collected location of the SHRIMP U/Pb dating

(by the 1/1.5 million geological map of the Qinghai-Tibet plateau, 1988, revised)

(A)采样位置地质平面图:1—喜马拉雅前寒武纪变质基底;2—早古生代地层;3—晚古生代地层;4—中生代地层;5—逆冲断层;6—拆离断层;7—国界线;8—主要公路;9—采样位置;10—样品编号;11—地名

(B)采样位置地质剖面图:a—康马-少岗地质剖面;b—吉隆镇北佩枯错西-马拉山地质剖面;c—亚东镇南-乃堆拉山口地质剖面;d—聂拉木樟木-友谊隧道地质剖面。1—片麻岩;2—片岩;3—沉积岩;4—逆冲断层;5—正断层;6—上盘向里,下盘向外的剪切指向;7—样品号;8—采样位置

(A) The geologic map: 1—Precambria metamorphic basement of the Himalaya; 2—Early Paleozoic strata; 3—Late Paleozoic strata; 4—Mesozoic strata; 5—thrust; 6—detachment; 7—national boundary; 8—the main road; 9—collected locations; 10—sample's number; 11—locations

(B) The geologic profiles: a—the profile from Kangma to Shaogang; b—the profile from western Peikucuo located in the north of Jilong to the Malashan; c—the profile from southern Yadong to the Naiduilashan pass; d—the profile from Nielamu-Zhangmu to the friendship tunnel; 1—gneiss; 2—schist; 3—sediment; 4—thrust; 5—fault; 6—shear sense: the upper wall northward and the lower wall southward; 7—sample's number; 8—collected locations

含褐帘石黑云二长片麻岩(HH-5)中挑选了 15 颗锆石,均为短柱状,核幔结构比较发育,共测得两组年龄值:

(Ⅰ)504～528Ma, 9 颗锆石的$^{206}Pb/^{238}U$ 年龄数据(528 ± 14Ma, 528 ± 14Ma, 522 ± 14Ma, 518 ± 15Ma, 511 ± 15Ma, 511 ± 14Ma, 510 ± 14Ma, 507 ± 14Ma, 504 ± 13Ma)都投在谐和线上(表 1)(图 3),平均值为 515.4 ± 9.3Ma。锆石的特点有三类,一类位于继承性晶核的幔部(图 4(A)中 HH5-5.1),第二类为变质重结晶锆石(图 4(A)中 HH5-15.1),第三类为新生长的变质锆石(图 4(A)中 HH5-2.1)。锆石的 Th/U 比值都>0.1。这组年龄记录了泛非事件的年龄。

表 1 康马片麻岩中锆石 SHRIMP U-Pb 定年数据

Tabel 1 SHRIMP U-Pb data for zircons from the kangma gneiss

Sample	Content(ppm)			Th/U	$^{235}U/^{207}Pb^*$	$^{238}U/^{206}Pb^*$	Age: $^{206}Pb^*/^{238}U$(Ma)
	U	Th	^{206}Pb				
HH5-9.1	670	555	83.2	0.85	0.7519 ± 0.0233	6.93 ± 0.1871	869 ± 22
HH5-3.1	236	122	28.3	0.53	0.7849 ± 0.0290	7.18 ± 0.2010	840 ± 22
HH5-12.1	116	115	13.9	1.03	0.79050.0372	7.230.2386	835 ± 26
HH5-8.1	632	487	50.5	0.80	1.42250.0469	10.790.2913	571 ± 15
HH5-13.1	272	276	21.2	1.05	1.40250.0589	11.080.3102	557 ± 15
HH5-14.1	346	275	26.3	0.82	1.39860.0517	11.320.3170	546 ± 15
HH5-7. 1	438	600	32.2	1.42	1.46410.0542	11.720.3282	528 ± 14
HH5-15.1	462	354	34.0	0.79	1.55760.0592	11.710.3279	528 ± 14
HH5-4.1	760	556	55.3	0.76	1.54320.0525	11.850.3200	522 ± 14
HH5-1.1	144	154	10.3	1.11	1.43680.0790	11.950.3705	518 ± 15
HH5-6.1	157	163	11.3	1.07	1.76990.1770	12.130.3639	511 ± 15
HH5-2.1	395	143	28.0	0.37	1.46200.0512	12.110.3391	511 ± 14
HH5-10.1	367	305	26.0	0.86	1.54800.0619	12.140.3399	510 ± 14
HH5-16.1	250	201	17.7	0.83	1.65840.0912	12.220.3544	507 ± 14
HH5-5.1	459	347	32.2	0.78	1.60260.0657	12.290.3441	504 ± 13

Note: Pb^* corrected for common Pb using ^{204}Pb. All errors are 1 sigma of standard deviation.

(Ⅱ)869～835Ma, 3 颗锆石的$^{206}Pb/^{238}U$ 年龄数据(869 ± 22Ma, 840 ± 22Ma, 835 ± 26Ma)投在谐和线上(表 1)(图 3),平均值为 849 ± 27Ma,代表泛非事件(500～600Ma)前的年龄记录。锆石都为继承性晶核(图 4(A)中 HH5-3.1),均保留原生的生长环带,测点位于晶核的幔部,Th/U 比值均>0.1,为继承性岩浆锆石。

2.3.2 吉隆(HH-42)

含电气石二云二长片麻岩(HH-42)中共挑选了 15 颗锆石,形状有长柱状、短柱状、浑圆状,主要获得一组年龄值:529～483Ma,其中 10 颗锆石的$^{206}Pb/^{238}U$ 年龄(529 ± 14Ma, 523 ± 14Ma, 522 ± 15Ma, 521 ± 14Ma, 519 ± 13Ma, 516 ± 14Ma, 511 ± 13Ma, 511 ± 13Ma, 510 ± 13Ma, 483 ± 13Ma)中的数据点投在谐和线上(表 2)(图 3 中 HH-42-2),平均值为 514.0 ±

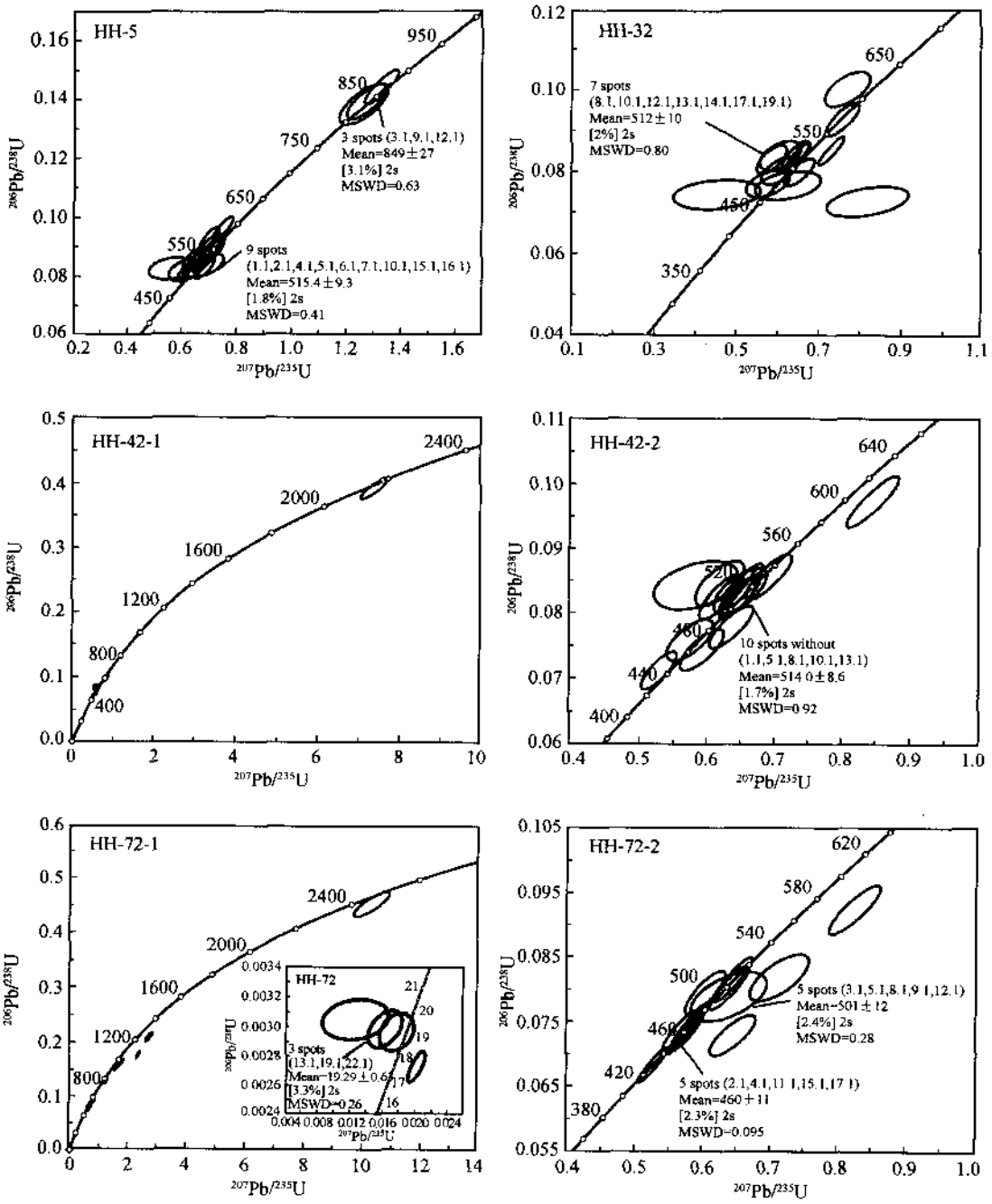

图 3　喜马拉雅地体变质基底岩石的 SHRIMP U-Pb 年龄谐和曲线图

Fig.3　Concordant diagram of the SHRIMP U-Pb age for the metamorphic basement rocks in the Himalaya terrane

HH-5：康马；HH-42：吉隆；HH-32：亚东；HH-72：聂拉木

HH-5: Kangma sample; HH-42: Jilong sample; HH-32: Yadong sample; HH-72: Nielamu sample

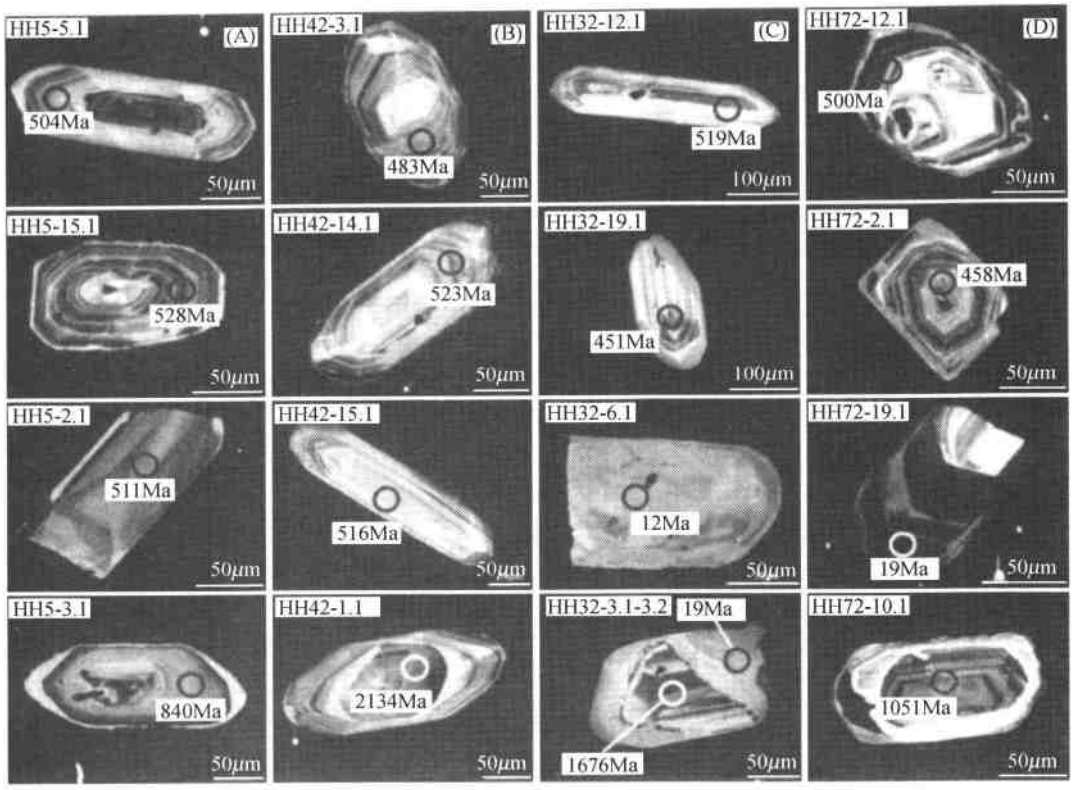

图 4　喜马拉雅地体变质基底岩石的锆石阴极发光照片

Fig.4　Cathodoluminescence image for the zircons of the metamorphic basement rocks in the Himalaya terrane

(A)康马 HH-5;(B)吉隆 HH-42;(C)亚东 HH-32;(D)聂拉木 HH-72

(A) Kangma: HH-5; (B) Jilong: HH-42; (C) Yadong: HH-32; (D) Nielamu: HH-72

8.6Ma。这组锆石多是长柱状-短柱状的结晶锆石(图 4(B)中 HH42-3.1、14.1),锆石原有的结晶环带有的已明显被改造,具有变质重结晶的特点(图 4(B)中 HH42-15.1),绝大多数锆石的 Th/U 比值<0.1。这组年龄主要代表了泛非事件的年龄。

另外还有 1 颗锆石的继承性核部所测得的$^{207}Pb/^{206}Pb$年龄为 2183±24Ma,落于谐和线上(图 3 中 HH-42-1)(图 4(B)中 HH42-1.1),该年龄为古老的残余锆石年龄,由于数据太少,只供参考。

2.3.3　亚东(HH-32)

在样品矽线石榴黑云斜长片麻岩(HH-32)中挑选了 18 颗锆石,锆石晶形为长柱状、短柱状和浑圆状等,共测 19 个点,主要获得的年龄值为 525～494Ma,其中 7 颗锆石的$^{206}Pb/^{238}U$测年数据(525±14Ma, 520±14Ma, 519±14Ma, 518±13Ma, 513±14Ma, 496±13Ma, 494±13Ma)投在谐和线上(表 3)(图 3),平均值为 512±10Ma。锆石主要是变质重结晶锆石(图 4(C)HH32-12.1、19.1),具有比较均匀的生长环带,Th/U 比值>0.1。该组年龄代表了泛非-早古生代的变质年龄。

表 2 吉隆片麻岩中锆石 SHRIMP U-Pb 定年数据

Table 2 SHRIMP U-Pb data for zircons from the Jilong gneiss

Sample	Content(ppm)			Th/U	$^{235}U/^{207}Pb^*$	$^{238}U/^{206}Pb^*$	Age: $^{206}Pb^*/^{238}U$(Ma)
	U	Th	^{206}Pb				
HH42-1.1	496	35	167.0	0.07	0.1353±0.0041	2.55±0.0688	2134±49
HH42-10.1	1328	190	111.0	0.15	1.1820±0.0355	10.89±0.2776	599±15
HH42-7.1	775	16	57.1	0.02	1.4430+0.0462	11.69±0.3156	529±14
HH42-14.1	833	73	60.8	0.09	1.6129±0.0629	11.82±0.3191	523±14
HH42-6.1	319	36	23.3	0.12	1.7094±0.1214	11.87±0.3442	522±15
HH42-9.1	932	44	67.4	0.05	1.5291±0.0489	11.89±0.321	521±14
HH42-11.1	3984	50	287.0	0.01	1.5480±0.0433	11.93±0.3221	519±13
HH42-15.1	439	31	31.5	0.07	1.5361±0.0614	11.99±0.3357	516±14
HH42-2.1	805	146	57.2	0.19	1.5361±0.0476	12.11±0.327	511±13
HH42-12.1	739	36	52.5	0.05	1.6129±0.0532	12.13±0.3275	511±13
HH42-4.1	959	60	67.9	0.06	1.5361±0.0476	12.13±0.3275	510±13
HH42-3.1	595	44	39.8	0.08	1.5699±0.0534	12.85±0.3598	483±13
HH42-5.1	527	65	34.4	0.13	1.7361±0.0694	13.18±0.369	471±13
HH42-8.1	391	116	25.0	0.31	1.6835+0.0606	13.45±0.3766	462±12
HH42-13.1	1717	733	105.0	0.44	1.8868±0.0623	14.05±0.3794	443+11

Note: Pb^* corrected for common Pb using ^{204}Pb. All errors are 1 sigma of standard deviation.

表 3 亚东片麻岩中锆石 SHRIMP U-Pb 定年数据

Table 3 SHRIMP U-Pb data for zircons from the Yadong gneiss

Sample	Content(ppm)			Th/U	$^{235}U/^{207}Pb^*$	$^{238}U/^{206}Pb^*$	Age: $^{206}Pb^*/^{238}U$(Ma)
	U	Th	^{206}Pb				
HH32-3.1	514	28	131.00	0.06	0.1395±0.0039	3.37+0.0909	1676±40
HH32-7.1	1165	353	155.00	0.31	0.3660+0.0102	6.49±0.1752	924±23
HH32-15.1	935	656	105.00	0.72	0.8361±0.0242	7.64±0.2063	793±20
HH32-4.1	216	66	18.70	0.32	1.2987+0.0623	10.00±0.2800	614±17
HH32-11.1	680	179	54.20	0.27	1.3193±0.0475	10.80±0.3024	571±15
HH32-8.1	1803	155	132.00	0.09	1.3699±0.0397	11.77±0.3178	525±14
HH32-17.1	714	107	51.60	0.16	1.5552±0.0529	11.91±0.3216	520±14
HH32-12.1	358	258	26.00	0.74	1.6529±0.0909	11.94±0.3343	519+14
HH32-10.1	1627	23	117.00	0.01	1.5432±0.0478	11.96±0.3229	518±13
HH32-13.1	485	76	34.70	0.16	1.7094±0.0701	12.07±0.3380	513±14
HH32-19.1	427	195	29.50	0.47	1.6584±0.0779	12.49+0.3497	496±13
HH32-14.1	291	115	19.90	0.41	1.5337±0.0014	12.54±0.3511	494±13
HH32-1.1	257	97	17.10	0.39	1.7361+0.1059	12.99±0.3767	478+13
HH32-5.1	120	48	7.94	0.41	1.6026±0.1362	13.08±0.4055	475±14
HH32-20.1	131	61	8.51	0.48	2.2124±0.3540	13.46±0.4307	462±14
HH32-16.1	93	7	5.84	0.08	1.2225±0.0978	13.79±0.4551	451±15
HH32-18.1	375	9	1.35	0.03	15.8479±1.3154	237.90±9.2780	27±1
HH32-3.2	40	1	0.30	0.03		342.00±249.66	19+14
HH32-6.1	109	1	0.38	0.01		546.00±212.94	12±5

Note: Pb^* corrected for common Pb using ^{204}Pb. All errors are 1 sigma of standard deviation.

另外还测到3个年轻的$^{206}Pb/^{238}U$年龄(27±1Ma, 19±14Ma, 12±5Ma)(表3),这组锆石部分为新生长的变质锆石(图4(C)中HH32-6.1),或是在古老晶核(图4(C)中HH32-3.1)四周发育的变质增生边(图4(C)中HH32-3.2)。它们的Th/U值均<0.1(0.01～0.03),其年龄值可能代表喜马拉雅事件年龄。

2.3.4 聂拉木(HH-72)

矽线石榴二云二长片麻岩(HH-72)中共挑选了22颗锆石,短柱状为多,少数不规则,主要测得两组年龄值:

(Ⅰ)509～457Ma,其中10颗锆石的$^{206}Pb/^{238}U$测年数据(509±14Ma, 507±13Ma, 500±13Ma, 495±13Ma, 492±15Ma; 466±12Ma, 461±12Ma, 460±12Ma, 458±12Ma, 457±12Ma)呈两组投在谐和线上(表4)(图3中HH-72-2),平均值分别为501±12Ma和460±11Ma。这些锆石多为结晶锆石,具明显环带(图4(D)中HH72-12.1、2.1),Th/U比值不一致,有的>0.1,有的<0.1。该组年龄代表泛非-早古生代事件年龄。值得注意的是,该锆石样品的寄主岩石矽线石榴二云二长片麻岩(HH72)经历了较强烈的深熔作用,部分锆石可能为熔体结晶过程中形成的,因此,该组年龄可能也代表了孔兹岩系的深熔年龄。

表4 聂拉木片麻岩中锆石SHRIMP U-Pb定年数据

Tabel 4 SHRIMP U-Pb data for zircons from the Nienamu gneiss

Sample	Content(ppm)			Th/U	$^{235}U/^{207}Pb^*$	$^{238}U/^{206}Pb^*$	Age: $^{206}Pb^*/^{238}U$(Ma)
	U	Th	^{206}Pb				
HH72-6.1	31	29	12.2	0.94	0.0970±0.0038	2.21±0.0730	2404±66
HH72-7.1	368	149	66.6	0.42	0.3663±0.0114	4.76+0.1285	1228±31
HH72-10.1	2986	336	454.0	0.12	0.4237±0.0114	5.65±0.1526	1051±26
HH72-1.1	966	212	136.0	0.23	0.5643±0.0158	6.13±0.1655	975±24
HH72-18.1	580	156	77.2	0.28	0.6238±0.0187	6.45±0.1742	929±24
HH72-20.1	167	139	18.5	0.86	0.8197±0.0361	7.79±0.2259	778±21
HH72-16.1	1733	209	138.0	0.12	1.2092+0.0375	10.82±0.2921	570±15
HH72-8.1	251	100	17.8	0.41	1.4006±0.0560	12.18±0.3410	509±14
HH72-5.1	1683	123	118.0	0.08	1.5480±0.0449	12.22±0.3299	507+13
HH72-12.1	1701	138	118.0	0.08	1.5625±0.0469	12.41±0.3351	500±13
HH72-3.1	1422	1132	97.8	0.82	1.6556±0.0546	12.52±0.3380	495±13
HH72-9.1	141	112	9.7	0.82	1.5649±0.0908	12.61±0.3909	492+15
HH72-15.1	4084	210	263.0	0.05	1.7271±0.0484	13.33±0.3599	466±12
HH72-17.1	1434	116	91.5	0.08	1.7637±0.0529	13.49±0.3642	461+12
HH72-4.1	1948	206	124.0	0.11	1.7331±0.0503	13.52±0.3650	460±12
HH72-2.1	3605	147	228.0	0.04	1.7483±0.0490	13.59±0.3669	458±12
HH72-11.1	523	479	33.1	0.95	1.5504+0.0543	13.62±0.3814	457±12
HH72-14.1	3897	79	231.0	0.02	1.9011±0.0532	14.52±0.3920	429±11
HH72-22.1	4031	7	10.8	0.00	78.7402±16.5354	328.10±9.5149	20±0.6
HH72-13.1	9171	30	23.8	0.00	60.9756±5.2439	335.00±9.3800	19±0.5
HH72-19.1	5795	12	14.9	0.00	56.1798±4.6067	337.60±9.4528	19±0.5
HH72-23.1	18403	52	43.2	0.00	49.4315±1.8290	366.50±9.8953	18±0.5

Note: Pb^* corrected for common Pb using ^{204}Pb. All errors are 1 sigma of standard deviation.

(Ⅱ)20～19Ma,3 颗锆石的$^{206}Pb/^{238}U$ 年龄(20±0.6Ma,19±0.5Ma,19±0.5Ma)投在谐和线附近(表 4)(图 3 中 HH72-1 小图),平均值为 19.29±0.63Ma。这组锆石为结晶核(未测)的变质环带(图 4(D)中 HH72-19.1),测点位于边部。Th/U 值明显偏低,表明本区孔兹岩系明显经历了喜马拉雅热事件的改造。

另外,还测得 1 个锆石古老残核(图 4(D)中 HH72-10.1)的$^{207}Pb/^{206}Pb$ 年龄 2513±36Ma,落在谐和线上(图 3 中 HH72-1)。但因数据少,只作参考。

3 喜马拉雅的古地理复原及变质基底再活化

重塑喜马拉雅的雏形,首先需要复原喜马拉雅在地质历史中的古地理位置和构造背景,认识喜马拉雅变质基底再活化的阶段和过程。

3.1 喜马拉雅的地质历史复原

目前,国际地学界关注的罗迪尼亚超大陆的形成和裂解使新元古时期重大地质事件的研究再次成为热点(陆松年,2002)。喜马拉雅地体位于印度陆块的北缘,根据古地磁的最新成果,在 1000～750Ma 期间,以劳伦大陆为中心,聚合澳大利亚、南极、印度、西伯利亚、波罗的、亚马逊、西非、刚果和北非等陆块,形成罗迪尼亚超大陆(Hoffman, 1991; Condie, 2001),华北与华南小陆块分别位于西伯利亚陆块的两侧(Li, *et al*., 1995, 1996a)。比现今范围大得多的印度陆块为罗迪尼亚超大陆的成员,位于赤道以南的澳大利亚陆块、南极陆块和非洲陆块之间。750～600Ma 期间罗迪尼亚超大陆发生裂解形成两个重要的构造带:一个是位于东、西冈瓦纳之间的莫桑比克带,以中压麻粒岩带为重要标志,另一条位于东、西非之间并延至南美东部(Acharyya, 2000)。根据在圣保罗西南发现的具有典型洋壳组合蛇绿岩套中变辉长岩的 U-Pb 年龄为 628±9Ma,以及巴西东南部岩浆弧的存在,证明南美与非洲西部之间存在刚果-巴西泛非洋盆(Tassinari *et al*., 2001)。

500～600Ma 期间,泛非洋盆闭合,出现泛非造山幕,形成莫桑比克和刚果-巴西泛非造山带(Acharyya, 2000)(图 5)。泛非造山带的形成促使东冈瓦纳与西冈瓦纳大陆块体联合,即冈瓦纳大陆诞生。石炭-二叠纪末,冈瓦纳大陆与劳亚大陆汇合形成联合超大陆(Pangea)。早侏罗世时期特提斯大洋扩张,69Ma 开始位于赤道以南的大印度陆块向北运移(Gradstein *et al*, 2004),50Ma 左右与劳亚大陆碰撞,大印度陆块的继续推进使其俯冲在劳亚大陆之下(Besse *et al*., 1984; Patzelt *et al*., 1996),20Ma 开始印度陆块北缘形成具有向南极性的典型的喜马拉雅逆冲叠复岩片构造(Molnar and Tapponnier, 1975; Burg and Chen, 1984; Burchifiel *et al*., 1992; Brookfield, 1993; Le Fort, 1996; Yin and Harrison, 2000),喜马拉雅地体在挤出机制下崛起(Chemenda *et al*., 1995; Chemenda *et al*., 2000)。

3.2 喜马拉雅地体古老变质基底的再活化事件

本研究为喜马拉雅地体的中国部分提供了大量有用的测年数据,有利于对事件的解析。在这里我们将喜马拉雅的历史分为原岩形成时代、泛非-早古生代原始喜马拉雅造山事件及现代喜马拉雅造山事件。

(1)喜马拉雅地体变质基底岩石的形成年龄

在特提斯-喜马拉雅和高喜马拉雅构造单元中,代表古老变质基底的有中元古代(康马 835～869Ma)的年龄记录,说明喜马拉雅地体曾为罗迪尼亚大陆的一部分;变质基底还包含

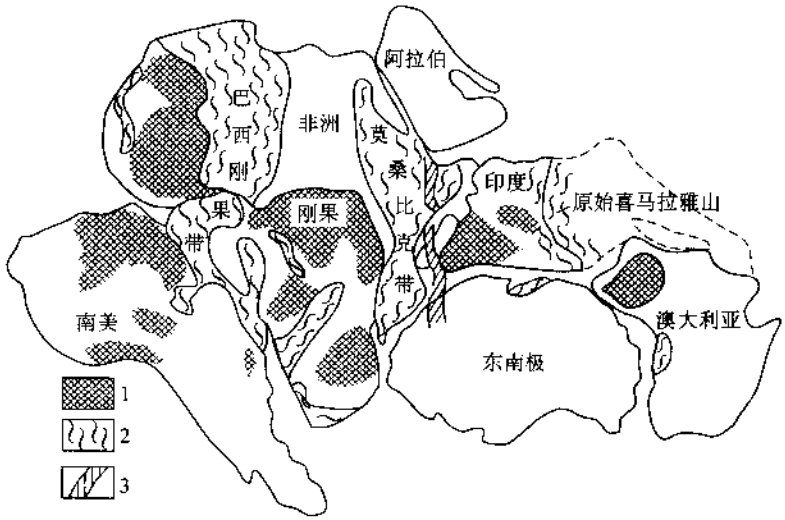

图 5 罗迪尼亚超大陆复原图
(据 Acharyya, 2000 修改)
Fig.5 Reconstruction of the hypothetical Rodinia Supercontinent
(by Acharyya, 2000, revised)
1—克拉通;2—泛非造山带;3—麻粒岩带
1—Craton; 2—Pan-Africa orogen; 3—granulitic zone

有早元古代年龄(聂拉木的 2404±66Ma 和吉隆的 2134±49Ma),结合前人资料:尼泊尔纳瓦科特云母石英岩的白云母年龄为 728±2Ma(Krummenacher, 1961),锡金查尔群中角闪石年龄为 819±80Ma(Krummenacher, 1961),聂拉木群黑云斜长片麻岩中锆石 U-Pb 年龄为 1250Ma(Xu Ronghua *et al*., 1985),侵入聂拉木群的东喜马拉雅林格斯花岗岩 Rb-Sr 等时线年龄为 1050Ma(Acharyya, 1977)以及库蒙地区穆尼亚日片麻岩的全岩等时线年龄 1800±100Ma(Thakur, 1980)。在尼泊尔高喜马拉雅的前奥陶纪变质岩中碎屑锆石的年龄主要为 1000～1300Ma,此外还有 1500Ma 和 2500Ma(Gehrels *et al*., 2003)的年龄等,进一步证明喜马拉雅地体变质基底岩石的形成年龄为早中元古代。

(2)喜马拉雅地体泛非-早古生代事件的记录

泛非事件是指大约 550±100Ma 前发生的一次重要的深成事件,其影响的非洲大部分及相邻的冈瓦纳地区被称为泛非造山带(Kennedy, 1964),泛非造山带包括变质和变形的表壳岩及局部再活化基底,特别在莫桑比克、喀麦隆和尼日利亚等地带(Windley B F, 1978)。本测年结果表明,在特提斯-喜马拉雅变质基底和高喜马拉雅变质岩石中,有 36 个锆石 SHRIMP 测试数据在 529～457Ma 范围,其中康马:528～504Ma,平均年龄值为 515.4±9.3Ma;吉隆:529～483Ma,平均年龄值为 514.0±8.6Ma;亚东:525～494Ma,平均年龄值为 512±10Ma;聂拉木:509～457Ma,平均年龄值为 501±12Ma 和 460±11Ma。记载了喜马拉雅地体的变质基底岩石既卷入泛非事件中,又在 500Ma 之后继续卷入早古生代事件的历史。

(3)喜马拉雅事件记录

虽然只有 6 个新的年龄数据:亚东:27～12Ma,聂拉木 20～19Ma,但是集中代表了喜马

拉雅事件记录，与前人大量研究结果一致。

上述结果表明，在喜马拉雅造山之前，喜马拉雅地体古老变质基底的再活化主要记录了泛非-早古生代造山事件的历史。

4 讨论与结论

4.1 喜马拉雅地体中泛非-早古生代事件年龄记录的存在

运用锆石 SHRIMP 测年获得喜马拉雅地体变质基底岩石的原岩年龄为早-中元古代，其后又经历了泛非-早古生代事件以及喜马拉雅事件的地质历史。

本研究的大量 SHRIMP 测试数据集中在中晚寒武世时期，康马、吉隆和亚东地区的 SHRIMP 平均年龄值分别为 515.4±9.3Ma、514.0±8.6Ma 和 512±10Ma，聂拉木地区除了中晚寒武世(平均年龄值 501±12Ma)外，还有中奥陶世(平均年龄值 460±11Ma)的变质年龄，表明了泛非事件在中国境内的特提斯-喜马拉雅和高喜马拉雅构造单元中普遍存在，高喜马拉雅的中西部还受到早古生代事件的影响。

4.2 喜马拉雅地体的泛非-早古生代事件为造山事件

(1)泛非-早古生代的变形构造记录

已揭示了喜马拉雅地体中高喜马拉雅构造单元的北界为向北缓倾的藏南拆离断裂(STD)，以 SN 向拉伸线理、自南往北的正向滑移及强烈韧性剪切应变为特征；南界为向北缓倾的主中逆冲断裂(MCT)，以 SN 向拉伸线理、自北往南的逆冲指向及强烈韧性剪切应变为特征，并在南缘形成一系列的逆冲叠覆岩片构造，由古老变质基底岩石组成的高喜马拉雅构造单元总体显示了南缘逆冲北缘拆离的"挤出构造岩片"的特征(Chemenda A I *et al*., 1995；Chemenda A I, *et al*., 2000)。特提斯-喜马拉雅构造单元中拉轨岗日穹隆带核部由串珠状分布的古老变质岩石组成，其与高喜马拉雅构造单元的物质组成和形成时代大体一致。穹隆核部与周边震旦-寒武纪石榴石黑云母片岩和绿泥石石英片岩之间为自南往北剪切的韧性穹形拆离带，其很可能与特提斯-喜马拉雅构造单元南缘的藏南拆离断裂(STD)相连。研究表明藏南拆离断裂(STD)和主中逆冲断裂(MCT)的形成年龄大致从 20Ma 开始，是喜马拉雅造山事件的产物(Burg and Chen, 1984；Burchifiel *et al*., 1992；Brookfield, 1993；Le Fort, 1996；Yin and Harrison, 2000)，本文中获得的喜马拉雅事件记录(亚东：27～12Ma，聂拉木 20～19Ma)与前人研究吻合。

组成喜马拉雅地体变质基底的实体是角闪岩相的富铝变质沉积岩和花岗质片麻岩，在这套岩系中的早期构造应变主要表现为大范围的强烈非同轴褶皱和 NWW-SEE 走向的韧性斜向逆冲构造，伴随角闪岩相变质作用，反映了深层次的变形构造特征，并为喜马拉雅期的浅层次的韧性-韧脆性-脆性变形构造所切割。根据采集样品均为角闪岩相的富铝变质沉积岩和花岗质片麻岩，HH32 和 HH72 样品又位于 NWW-SEE 方向的韧性斜向逆冲构造带中，因此测得的泛非-早古生代 SHRIMP U/Pb 年龄应反映大规模褶皱、韧性变形及角闪岩相变质作用的造山事件的时代。

(2)泛非-早古生代造山事件的不整合证据

康马、吉隆和亚东地区的 SHRIMP 平均年龄值分别为 515.4±9.3Ma、514.0±8.6Ma 和 512±10Ma，聂拉木地区除了中晚寒武世(平均年龄值 501±12Ma)外，还有中奥陶世(平

均年龄值460±11Ma)的变质年龄,表明了泛非事件在中国境内的特提斯-喜马拉雅和高喜马拉雅构造单元中普遍存在,高喜马拉雅的中西部还受到早古生代事件的影响。

周志广等(2004)曾认为康马地区发现的早奥陶统底砾岩为泛非造山的不整合证据。Gehrels等(2003)将尼泊尔喜马拉雅地区中奥陶纪底砾岩作为确定早古生代造山事件不整合的地质标志,并认为奥陶纪的碎屑岩层在造山过程中因逆冲作用的向南扩展而堆积在前陆盆地中,由于剥蚀深度大,寒武-奥陶纪深成岩体的岩屑在同造山的奥陶纪-泥盆纪地层中占很大的比例。

本文年龄测试所获康马、吉隆和亚东地区的中晚寒武纪(512～515Ma)的变质年龄的存在与周志广认识完全吻合,而聂拉木地区的中晚寒武世—中奥陶世年龄反映了泛非事件延续到早古生代时期,与Gehrels等(2003)在尼泊尔喜马拉雅地区奥陶纪底砾岩的发现和研究结果吻合。但由于高喜马拉雅单元北缘的拆离作用的影响,早古生代地层明显减薄,甚至缺失,地层之间为构造接触,特别是尼泊尔的底砾岩归属时代尚不确切,因此泛非-早古生代造山事件的地质依据尚需进一步验证。

综上所述,曾位于南半球印度陆块北部的变质基底岩石经历过泛非-早古生代造山事件,形成了原始喜马拉雅山,印度陆块早-中元古代变质基底的再活化在原始喜马拉雅山形成中起重要的作用,现在的喜马拉雅山则是在泛非-早古生代造山事件的基础上再造山的结果。

致谢 本研究得到国土资源部科技专项《青藏高原的碰撞造山及其效应》课题"青藏高原地体边界及岩石圈剪切断裂"的资助,SHRIMP年龄测试在中国地质科学院地质研究所北京离子探针中心进行。

References

Acharyya S K. 2000. Break up of Australia-India-Madagascar Blok, Openning of the Indian Ocean and Continental Accretion in Southeast Asia with special reference to the characteristics of the Peri-Indian Collision Zones. Gondwana Research, 3 (4): 425～443.

Acharyya. 1977. Stratigraphy and tectonic features of the Eastern Himalayas. In: Tectonic Geology of the Himalaya, P. S. Saklani Ed., Today and Tomorrow's Pub: 243～268.

Argand E. 1922. La tectonique de l'Asie. C R Cong Geol Int. Liege, XIII Sess., Fasc. 1, 171～372.

Argles T W, Prin C I, Foster G L, Vance D. 1999. New garnets for old? Cautionary tales from young mountain belts. Earth and Planetary Science Letters, 172: 301～309.

Besse J *et al*. 1984. Paleomagnetic estimates of crustal shortening in the Himalayan thrusts and Zangbo suture. Nature, 311: 621～626.

Brookfield M E. 1993. The Himalayan passive margin from Precambrian to Cretaceous. Sedimentary Geol., 84: 1～35.

Burchifiel B C, Chen Z, Hodges K V, Liu Y, Royden L H, *et al*. 1992. The South Tibetan Detachement System, Himalayan orogen: extension contemporaneous with and parallel to shortening in a collisional mountain belt. Geol. Soc. Am. Spec. Pap., 269:1～41.

Burg J P, Chen G M. 1984. Tectonics and structural formation of southern Tibet, China. Nature, 311:219～223.

Carlos E J, Harrison T N, Manning C E, Grove M, Rai S M, Hubbard M S, Upreti B N. 2002. Records of the evolution of the Himalayan orogen from in situ Th-Pb ion microprobe dating of monazite: Eastern Nepal and western Garhwal. Journal of Asian Earth Sciences, 20:459～479.

Chemenda A I, Burg J P, Mattauer M. 2000. Evolutionary model of the Himalaya-Tibet system: geopoem based on new midelling, geological and geophysical data. Earth and Planetary Science Letters, 174:397～409.

Chemenda A I, Mattauer M, Malavielle A N, Bokun A. 1995. A mechanism for syn-Collisional deep rock exhumation and associated normal faulting: results from physical modeling. Earth Plenet. Sci. Lett., 132: 225～232.

Compston W, Williams I S, and Kirschvink J L. 1992. Zircon U-Pb ages for the Early Cambrian time-scale. Journal of the Geological Society, 149 : 171～184.

Condie K C. 2001. Continental grough during formation of Rodinia at 1.35～0.9Ga. Gondwana Research, 4(1): 5～16.

DeCelles P G, Gehrels G E, Quade J, Lareau B, Spurlin M. 2000. Tectonic implications of U-Pb zircon ages of the Himalayan orogenic belt in Nepal. Science, 288:497～499.

DeCelles P G, Robison D M, Quade J, Ojha T P, Garzione C N, Copel P, Upreti B N. 2001. Stratigraphy, structure and tectonic evolution of the Himalayan fold-thrust belt in western Nepal. Tectonics, 20: 487～509.

Foster G L. 2000. The pre-Neogene thermal history of the Nanga Parbat Haramosh Massif and the NW Himalaya [Ph.D. dissertation]. The Open University, United Kingdom, 345.

Gansser A. 1964. The Geology of the Himalayas. London, Wiley Interscience: 289.

Garzanti E, Casnedi R, Jadoul F. 1986. Sedimentary evidence of a Cambro-Ordovicin orogenic event in the northwestern Himalaya. Sedimentary Geology, 48:237～265.

Gehrels G E, DeCelles P G, Martin A, Ojha T P, Pinhassi G, Upreti B N. 2003. Initiation of the Himalayan Orogen as an Early Paleozoic Thin-skinned Thrust Belt. GAS TODAY, 13(9): 4～9.

Godin L., Parrish R R, Brown R L, Hodges K V. 2001. Crustal thickening leading to exhumation of the Himalayan metamorphic core of central Nepal: Insight from U-Pb geochronology and $^{40}Ar/^{39}Ar$ themochronology. Tectonics, 20: 729～747.

Gradstein F M, Ogg J G, Smith A G *et al*. 2004. A Geologic Time Scale; Geological Survey of Canada, Miscellaneous Report: 86.

Harrison T M, Ryerson F J, Le F P, Yin A, Lovera O, Catlos E J. 1997. A late Miocene-Pliocene progin for the central Himalayan inverted metamorphism. Earth and Planetary. Science Letters, 146: E1～E7.

Hodges K V. 2000. Tectonics of the Himalaya and southern Tibet from two perspectives. Geological Society of America Bulletin, 112:324～350.

Hoffman P F. 1991. Did the breakup of Laurentia turn Gonwana inside out? Science, 252: 1409～1412.

Institute of Chengdu Geology and Mineral Resources, Chinese Academy of Geological Sciences. 1988. Geological Map of the Qinghai-Tibet Plateau and Adjacent Region. Beijing: Geological Publishing House

Kennedy W Q. 1964. The structural defferentiation of Africa in the PanAfrica (± 500m. y.) tectonic episode. Res. Inst. African Geol. Univ. Leeds 8th Ann. Rep., 48.

Krummenacher D. 1961. Determination d' age isotopique faite sur quelques roches de L'Himalaya du Nepal par la methode K/Ar Bull. Suisse, Min. Petr. 41(2): 273.

Kumar R, Shan A N, Bingham D K. 1978. Positive evidence of a Precambrian tectonic phase in central Nepal, Himalaya. Journal of the Geological Society of India, 19:519～522.

Le Fort P, Debon F, Sonet J. 1983. The Lower Paleozoic Lesser Himalayan granitic belt: Emphasis on the Simchar pluton of central Nepal, In: Shams F A (ed.), Granites of the Himalaya arakoram and Hindu Kush: Lahore, Institute of Geology, Punjab University:235～256.

Le Fort P. 1996. Evolution of the Himalaya. In: The Tectonics of Asia, ed. A Yin, TM Harrison, New York: Cambridge Univ. Press: 95～106.

Li Z X, Zhang L H, Powell C M. 1995. South China in Rodinian: part of the missing link between Australia-East Antarrctic and Laurentia? Geology, 23 (5):407～410.

Li Z X, Zhang L H, Powell C M. 1996. Positions of the East Asian cratons in the Neoproterozoic supercontinent Rodinia. In: Li Z X, Metcalfe I, Powell C M (eds.) Breakup of Rodinia and Gondwanal and assembly of Asia. Australia J. Earth Science, 43 (6): 593～604.

Liu W C, Liang D Y, Wang K Y. 2002. The Ordovician discovery in the Kangma region of the south Tibet and its geological significance. Earth Science Frontiers, 9 (4): 247～248 (in Chinese).

Lu S N. 2002. Preliminary in the North Qinghai-Tibet Plateau. Beijing: Geological Publishing House, 125 (in Chinese).

Molnar R, Tapponnier P. 1975. Cenozoic tectonics of Asia: Effects of a continental collision. Science, 189: 419～426.

Patzelt A, Li H, Wang J, Appel E. 1996. Paleomagnetism of Cretaceous to Tertiary sediments from Southern Tibet: evidence for the extent of the northern margin of India prior to the collision with Eurasia. Tectonophysics, 259: 259～284.

Stocklin J, Bhattarai K D. 1977. Geology of the Kathmandu area and central Mahabharat Range, Nepal: Department of Mines and Geology, Himalayan Report: 86.

Stocklin J. 1980. Geology of Nepal and regional frame. Geological Society [London] Journal, 137: 1～34.

Tapponnier P, Peltzer G, Le Dain A Y. 1982. Propagating extrusion tectonics in Asia: New insights from simple experiments with plasticine. Geology, 10:611～616.

Tassinari C C G, Munha J M U, Ribeiro A, Correia C T. 2001. Neoproterozoic oceans in the Ribeira belt (southern Brazi): the Pirapora do Bom Jesus ophiolitic complex. Episode, 24 (4): 245～251.

Thakur V C. 1980. Tectonics of the central crystallines of western Himalaya. Tectonophysics, 62: 141～154.

Thakur V C. 1992. Geology of the western Himalaya. Oxford, Pergammon Press, 363.

Valdiya K S. 1995. Proterozoic sedimentation and Pan-African geodynamic development of the Himalaya. Precambrian Research, 74:35～55.

Williams I S, Cleasson S. 1987. Isotope evidence for the Precambrian province and Caledonian metamorphism of high grade paragneiss from the Seve Nappes, Scandinavian Caledonides, II. Ion microprobe zircon U-Th-Pb. Contrib. Mineral. Petrol., 97:205～217.

Windley B F. 1978. The Evolving Continents, Library of Congress Cataloging in Publication Data: Typese in LinotronTimes and printed by Arrowsmith J W. Ltd., Brstol, John Wiley & Sons. 385.

Xu R H, Sharer U, Allegre C J. 1985. Magmatism and metamorphism in the Lhasa Block (Tibet): an U-Pb geochronological study. J. Geol., 93:42～57.

Yin A, Harrison T M. 2000. Geologic Evolution of the Himalayan-Tibetan Orogen. Rev. Earth Planet. Sci., 28: 211～280.

Zhou Z G, Liu W C, Liang D Y. 2004. Discovery of the Ordovician and its basal conglomente in the Kangmar area, southern Tibet with a discussion of the relation of the sedimentary cover and unifying basement in the Himalayas. Geological Bulletin of China, 23 (7): 655～663 (in Chinese).

中文参考文献

刘文灿,梁定益,王克友等.2002.藏南康马地区奥陶系的发现及其地质意义.地学前缘,9(4):247～248.

周志广,刘文灿,梁定益.2004.藏南康马奥陶系及其底砾岩的发现并初论喜马拉雅沉积盖层与统一变质基底的关系.地质通报,23(7):655～663.

陆松年.2002.青藏高原北部前寒武纪地质初探.北京:地质出版社,125.

中国地质科学院成都地质矿产研究所.1988.青藏高原及邻区地质图.北京:地质出版社.

Pan-African and Early Paleozoic orogenic events in the Himalaya terrane: Inference from SHRIMP U-Pb zircon ages

XU ZhiQin[1] YANG JingSui[1] LIANG FengHua[1] QI XueXiang[1]
LIU FuLai[1] ZENG LingSen[1] LIU DunYi[2] LI HaiBing[1]
WU CaiLai[1] SHI RenDeng[1] and CHEN SongYong[1]
(1. Key Laboratory for Continental Dynamics, Institute of Geology, Chinese Academy of Geological Sciences, Beijing 100037, China;
2. Beijing SHRIMP Center, Institute of Geology, Chinese Academy of Geological Sciences, Beijing 100037, China)

Abstract The Himalayan terrane is an accretional terrane formed during the collision between the India Plate and the Eurasian Plate since 55 ± 10Ma. SHRIMP U-Pb dating has been performed on zircons from the amphibolite facies aluminum-rich metasediments and granitic gneisses from the Greater Himalaya and the Tethyan-Himalayan units of the Himalayan terrane. The dating results indicatean widespread 529 ~ 457Ma deformation and metamorphism event, and greater than 835Ma metamorphic basement formation age, except for the latest tectonic event at 12 ~ 20Ma. Field observations on the Himalayan slice which has been exhumed since 20Ma have documented earlier than Cenozoic tectonic events represented by the early intense folding, oblique southward thrusting and concurrent amphibolite facies metamorphism and the Ordovician basal conglomerate. Recent studies also yielded a number of Pan-African and Early Paleozoic ages for the metasedimentary and metamorphic basement rocks by Ion Probe U-Pb zircon dating. These lines of evidence together with our new dating results lead us to propose that the Early middle Proterozoic metamorphic basement of the India block once located in the southern hemisphere has undergone the Pan-African-Early Paleozoic orogenic events. The geochronological data suggest that: (1) the Proto-Himalaya formed as a result of the Pan-African and the Early Paleozoic orogenic events; (2) reactivation of the Early-middle Proterozoic metamorphic basement of the India block has played a key role in the formation of the Proto-Himalayan Mountains; (3) the building of the present-day Himalaya Mountains may have been initiated as early as the Pan-African and the Early Paleozoic.

Key words Himalaya Pan-African and Early Paleozoic orogenic events SHRIMP dating

走滑断裂、“挤压性盆-山构造”与油气资源关系的探讨●

许志琴[1]　曾令森[1]　杨经绥[1]　李海兵[1]　姜　枚[1]
金之钧[2]　郑和荣[2]　郭齐军[2]
（1. 中国地质科学院地质研究所大陆动力学部重点实验室　北京　100037；
2. 中国石油化工股份有限公司　北京　100083）

摘　要　了解含油气盆地的形成及其演化的影响因素对于含油气盆地的勘探和开发是至关重要的。以美国西部的圣安德烈斯断裂带及伴生的南加州油气盆地作为参考，对中国青藏高原北部与阿尔金走滑断裂系相关的盆-山构造进行了剖析。探讨阿尔金走滑断裂系在其演化过程中，怎样控制区域应力场、变形构造及盆地的形成，进而制约油气的迁移和圈闭。分析结果表明与圣安德烈斯断裂带在美国南加州的盆-山构造体系所起的作用相比较，阿尔金走滑断裂系在青藏高原北部的盆-山构造体系的形成和演化中起相似的作用。青藏高原相对于塔里木盆地的斜向运动导致在阿尔金走滑断裂的东南形成走滑-挤压构造域。形成一系列的走滑和推覆构造，在地形上表现为包括柴达木盆地在内的有序的盆-山相间的构造体系。与南加州富含油气的盆地相似，阿尔金走滑断裂及相配套的走滑-逆冲推覆构造促使在这些盆地中形成富集油气的构造。

关键词　走滑断裂　挤压型盆-山构造　油气资源
中图分类号：P544　**文章编号**：1000－2383(2004)06－0631－13　**收稿日期**：2004－08－01

0　引言

大型走滑断裂以其规模大、地震活动性强以及沿断裂带有序的地貌（有序的起伏、伸长的隆起和盆地）吸引了众多地质及地球物理学家的注意力。自从 Sylvester 在 1988 年美国地质学会成立 100 周年之际全面详细评述走滑断裂在过去 100 年的研究历史和进展之后，又过去了 15 年。在这 15 年中，观测及实验技术（GPS、地震层析、深部地震反射和震中的定位）的进步，走滑断裂的研究在以下方面取得长足的进展：①走滑断裂的深部构造特征（Zhu, 2000）；②走滑断裂与深部流（气）体的关系（Kennedy *et al*., 1997）；③走滑断裂的应变承载及分解机制（Kranzh, 1995；Jones, 2003）；④走滑断裂的活动特征与地震活动的关系（Liu *et al*., 2003；Liu *et al*., 2004）；⑤走滑断裂与其两侧的地形地貌的关系（Spotila *et al*.,

● 地球科学—中国地质大学学报，2004 年第 29 卷第 6 期。
基金项目：国土资源部重点基础项目“东昆仑造山带的构造演化”，“祁连山—阿尔金山地质演化及岩石圈剪切作用”（No.9501106）；国土资源部科技专项“青藏高原演化与资源”的课题“地体边界和岩石圈断裂对青藏高原形成的贡献”（No.2001010201）；国家自然科学基金重点项目“祁连造山带的组成及造山过程”（No.49732070）。
作者简介：许志琴（1941—），女，留法博士，研究员，中国科学院院士，长期从事大地构造学和构造地质学研究。

1998; Yule and Sieh, 2003)。在这些进展的基础上,很有必要重新审视大型走滑断裂与其两侧盆-山构造的关系,探讨它们在油气勘探中的意义。

走滑断裂在不同的构造环境下有以下几种产出:①板块或地体边界的走滑断层:如美国的圣安德烈斯断裂带、新西兰的 Alpine 断裂带(King, 2000)、土耳其的 North Anatolian 断裂带及我国阿尔金断裂带等;②斜向俯冲或碰撞造成的板内走滑断裂:如印度尼西亚的 Sumatra 断层;③不均一的俯冲作用导致的走滑断层:如中美洲的加勒比海和南美洲南端的 Scotia 海的南北两侧的走滑断层;④板内伸展或挤压作用导致的走滑断层:如美国西部的盆岭省(basin and range Province)中一系列北西向的连接低角度正断层的走滑断裂带。

根据走滑断裂与周缘的断裂带的关系,可区分两种类型的走滑断裂:主动型走滑断裂和被动型走滑断裂。主动型走滑断裂是指走断裂两侧伸展或挤压构造受走滑断裂控制,这些断裂往往是板块或地体的边界断层,切穿岩石圈,可能为来自地幔或下地壳的深部流体提供有效的迁移通道;而被动型走滑断裂是指那些由于大规模的伸展或挤压作用,所形成的连接一系列正断层或逆冲断层的走滑断裂,其变形和运动特征受伸展或挤压作用控制。被动型走滑断裂实际上是伸展作用或挤压作用的应变承接带(accommodation zone),其作用是承载由伸展或挤压应变所造成的不同地块之间几何学上不相容的剪切应变。

最近的研究表明,由于复杂的板块边界及断裂带的相互作用,板块边界的变形往往表现为被滑移分解(slip partitioning)所控制,具体表现为一条或多条直立断裂为水平的走滑运动,而在这些断裂之间发育逆冲推覆断裂带(Jones, 2003)。同时,由于断裂带几何形态的不协调(如大拐弯)、板块的斜向运动促使大型板块边界走滑断裂带在区域上形成局部压扭性应力场。在这种压力场中,区域构造主要表现为以推覆构造所制约的盆-山构造体系,在区域上表现为盆地与高山相间的有序的盆-山体系。在逆冲推覆构造的上盘生成的一系列断层扩展褶皱,这些褶皱不但成为褶皱山,而且成为油气储存的有利构造。同时以频繁的地震活动为特征的活动断裂运动不但作为地幔或下地壳的流体和气体的通道(Kennedy *et al*., 1997; Fuis *et al*., 2001),而且为油气提供有利的迁移空间和动力。

本文首先简要地评述圣安德烈斯断裂带与南加州地区的含油气盆地的关系,进而详细的解剖我国西部阿尔金断裂南侧从昆仑山到祁连山之间的盆-山构造体系特征,强调走滑作用与挤压性盆-山构造的关系及油气的远景。

1 圣安德烈斯断裂带与挤压型盆-山构造

作为世界上研究程度最高的一条板块边界的走滑断裂带,圣安德烈斯断裂带在美国加利福尼亚州含油气盆地的形成及演化中起着举足轻重的作用。以位于圣安德烈斯断裂带西南的洛杉矶盆地为例,探讨走滑断层对含油气盆地的制约作用。

南加州的陆上及海岸地带分布着一系列构造相似的富含油气的新生代沉积盆地,其中规模较大的自南往北依次为:洛杉矶盆地、Santa Barbara-Ventura 盆地和 Santa Maria 盆地。洛杉矶盆地长约 300km,宽约 110km, Santa Maria 盆地长约 200km,宽约 20～80km, Santa Barbara-Ventura 盆地长约 240km,宽约 90km,后两个盆地的构造演化历史和洛杉矶盆地相似,并且这些盆地都具有丰富的陆上和近海油气藏。位于南加州的横向山脉(Transverse Range)和半岛山脉(Peninsular Range)之间洛杉矶盆地最大,储油量最丰,是世界上最富集

石油天然气的区域之一,美国的第二大城市洛杉矶市就坐落于这个盆地之上。这个盆地在新近世形成,和圣安德烈斯断裂带的形成紧密相关,盆地的中心沉积了高达 10km 的海相及河流冲积相沉积物。自盆地形成以来,盆地经历了复杂的多旋回构造变形,表现为:①在渐新世和中新世期间,主要为伸展及走滑构造变形;②在晚新世和第四纪,圣安德烈斯断层在南加州地区的南北 2 个大转弯和太平洋板块的北东向的运动导致在南加州地区形成挤压构造变形域(图 1),大地变形表现为推覆和走滑断裂作用相结合的斜向缩短。这种变形在南加州的横向山脉区域及洛杉矶盆地内形成大量的地震活动频繁的低角度盲逆冲断层,在断层的上盘形成与盲逆冲断层相配套的断层扩展皱褶(Shaw and Shearer,1999;Dolan *et al.*,2003;Oskin *et al.*,2000)。这些部位成为美国石油公司(如 Conoco、Chevron、Union 和 Exxon)竞相争取的油气勘探目标(图 2a)。

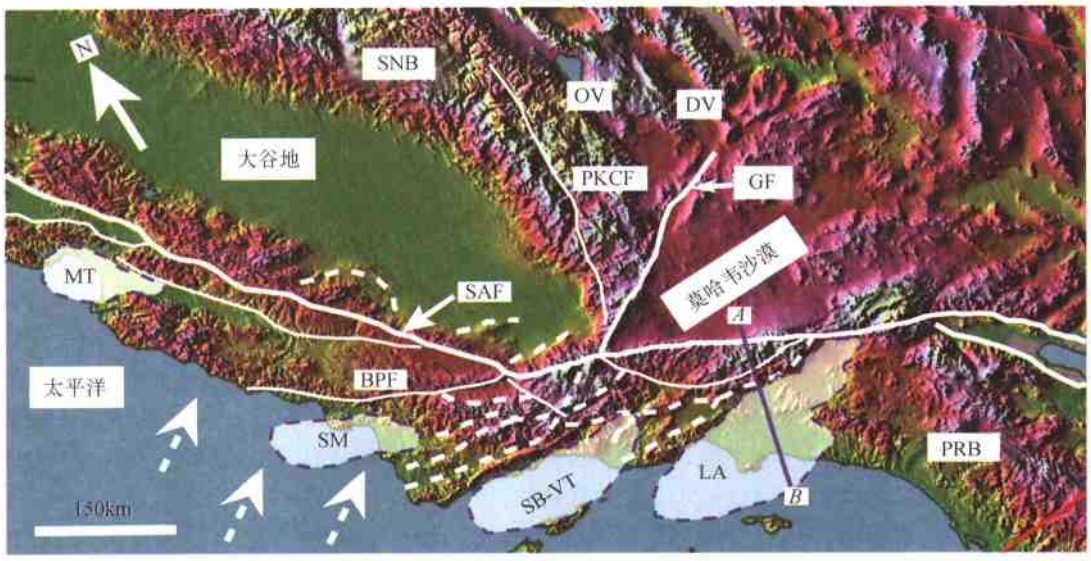

图 1　圣安德烈斯断裂带与南加州近海和陆上的含油气盆地及地貌简化示意图

Fig. 1　Simplified map showing the San Andreas fault and its adjacent costal and in land petroleum-bearing Cenozoic basins in southern California, USA

SNB—Sierra Nevada 花岗岩岩基;PRB—半岛山脉花岗岩岩基;SAF—圣安德烈斯断裂;GF—Garlock 断裂;PKCF—古 Kern Canyon 断裂;BPF—Big Pine 断裂;SM—Santa Maria 盆地;LA—洛杉矶盆地;SB VT—Santa Barbara Ventura 盆地;MT—Montery 湾盆地;*A-B*—为相应于图 2 中的横穿洛杉矶盆地和 San Gabriel 山脉的剖面线。实线为走滑断裂,虚线为逆冲推覆断层,带箭头的虚线为太平洋板块相对于北美板块的现今运动方向。图中的大谷地为中生代的弧前盆地,也是美国主要的油区之一

从数字化地形图看,圣安德烈斯断裂带以西的南加州地区主要表现为错落有致的盆地与山脉相间分布。山脉的前沿往往为出露的或盲逆冲断层。自 20 世纪 70 年代以来,南加州地区频繁、高强度地震活动引起地质学家及地震学家研究盆地中蕴震构造的兴趣。高精度地震定位、古地震、钻孔、详细的地质填图及深地震反射(南加州地震中心的 LARSE 研究项目)的研究(Fuis *et al.*,2001;Shaw and Shearer,1999)揭示出一系列盲逆冲推覆构造(图 2)。

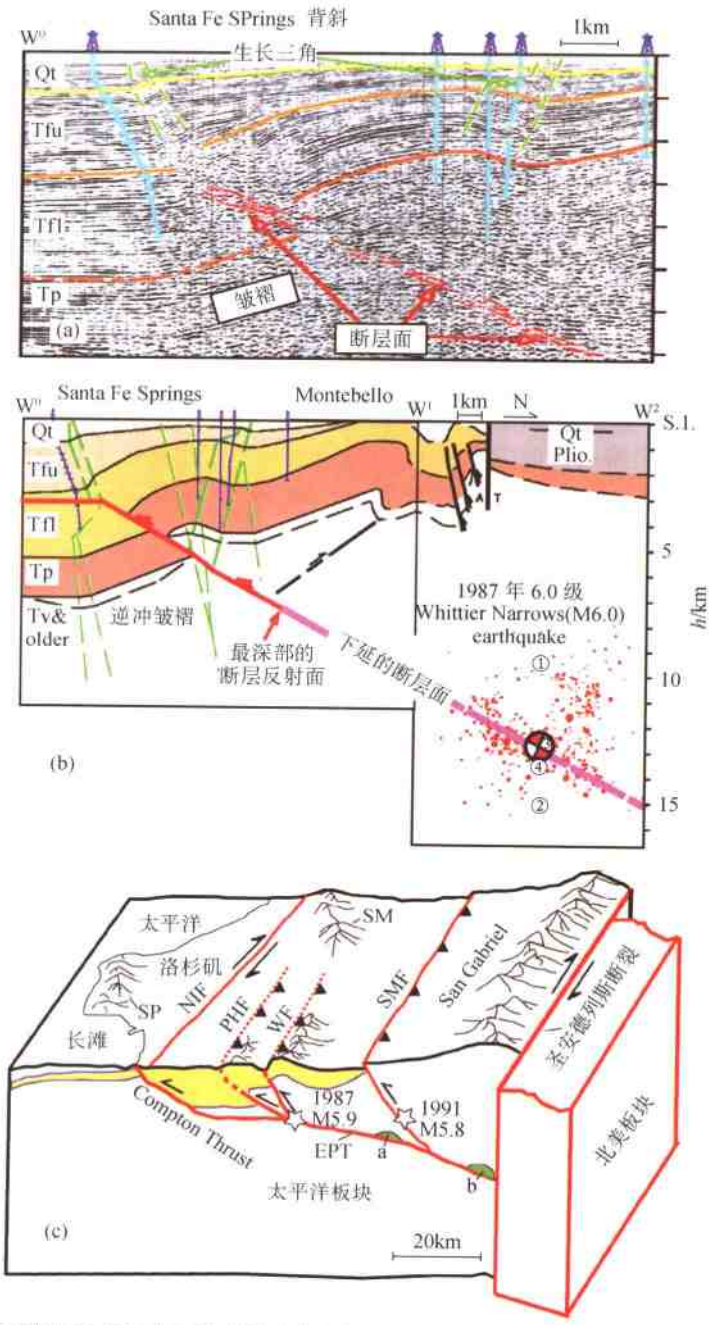

图 2　地震反射剖面、石油勘探及地震定位所揭示的洛杉矶盆地中一系列的盲逆冲推覆构造

Fig. 2　Blind and exposed thrust fault and fold structures revealed by seismic reffection profiling, oil-drilling and relocation of earthquake focus in the Los Angeles basin

(a)地震反射剖面及石油钻探揭示的盲逆冲推覆构造及断层生长褶皱(据 Shaw and Shreaer,2000);(b)图 2a 中所揭示的逆冲断层向深部延伸和 1987 年 Whittier Narrows 地震发生所在的断面相吻合(据 Dolan *et al.*,2003);(c)LARSE 综合研究项目所确定的从南加州海岸线到 Mojave 沙漠的简化构造剖面(据 Fuis *et al.*,2001 修改). NIF—Newport-Inglewood 走滑断层;EPT—Elysian Park 逆冲断层;WF—whittier 逆冲断层;PHF—Puente Hills 逆冲断层;SMF—Sierra Madre 逆冲断层;SP—San Pedra 山脉;SM—Santa Monica 山脉;(a)和(b)为地震反射所揭示的可能为液态物质的亮点 Qt—第四纪沉积;Tfu,Tfl,Tp 和 Tv 为第三纪含油气沉积地层;Plio—上新世;S. L—为海平面

为简单起见,我们在图中仅列出了规模较大的逆冲推覆构造。图 2c 为从南加州海岸线到 Mojave 沙漠的简化构造剖面图,图中显示了 4 条分支逆冲断层(Compton, Puente Hills, Whittier 和 Sierra Madre)在深部汇聚于 Elysian Park 主逆冲断层(EPT)上,其中 1991 年和 1987 年的地震分别发生在 Whitter 和 Sierra Madre 逆冲断层上。而 1994 年的 Northridge 6.7 级大地震也发生在位于洛杉矶北部的另一条盲逆冲断层上。这些频繁的地震活动有可能造成局部应力场和断裂的开闭,为流体的迁移提供动力和空间。a 和 b 为地震反射所揭示的亮点,它们可能代表着沿逆冲断层迁移的流(气)体。这些综合研究结果说明在走滑-挤压构造域中,油气田形成和演化、流(气)体的沿断裂带的分布和迁移、地震活动性与大型走滑断裂相关的挤压构造之间存在紧密关系。

概括地说,圣安德烈斯断裂带和太平洋板块的共同作用导致洛杉矶盆地的强烈缩短作用,发育一系列的盲逆冲断层,在这些断裂的上盘发育断层生长褶皱,在这些褶皱的核部形成褶皱山。这种有序的挤压型盆-山构造体系是南加州主要的地形地貌特征,成为油气开发的主要目标。

2 青藏高原北部的走滑断裂与新生代挤压型"盆-山"构造

位于阿尔金走滑断裂、东昆仑走滑断裂及阿拉善地体之间的青藏高原的北部地区,出现一系列新生代盆地与山脉相间的地貌格局(图 3),类似于美国西部的盆岭省(basin and range province),但它们的构造背景却不同,美国西部的盆岭省是拉伸构造作用的产物,而青藏高原的北部的盆-山构造体系是挤压和走滑共同作用的结果。在形成机制上青藏高原的北部的盆-山构造体系却与上述的美国南加州盆-山构造系相似,并且位于走滑断裂一旁的挤压盆地均为富含油气的盆地。

2.1 青藏高原北部的走滑断裂系

制约青藏高原的北部新生代盆-山体系发育的 3 条大型(上千千米延伸)走滑断裂是:NEE-SWW 向阿尔金走滑断裂、近 EW 向的东昆仑走滑断裂及近 EW 向的海源断裂。阿尔金走滑断裂与东昆仑走滑断裂和海源断裂斜交,它们均为左行走滑断裂。这些大型左行走滑断裂的浅部及深部结构显示了如下的特征:

2.1.1 阿尔金左行走滑断裂的特征

阿尔金断裂带位于青藏高原西北边界,祁连山、柴达木盆地和东昆仑山的西侧,在平面上由一系列 NEE-SWW 向平行断裂组成,主断裂位于阿尔金山的南侧,全长 1800km,自西藏北部的郭扎错、拉竹龙,经新疆硝尔库勒、阿羌、吐拉、索尔库里、老阿克赛县城延至甘肃玉门的宽滩山,地表宽度 6～15km。研究表明阿尔金主断裂为韧-脆性走滑剪切带,形成于印支期(李海兵等,2001),经历多期活动,是一条至今仍在活动的走滑断裂,沿阿尔金主断裂最大左行走滑位移达 400km(许志琴等,1999)。阿尔金断裂带的基本构造样式表现为:以走滑断裂为中心的两侧反向逆冲断裂系、北西侧的阿尔金逆冲断裂及其后部发育的同倾向正断层(李海兵等,2001)。

2.1.2 东昆仑左行走滑断裂的特征

近东西向的东昆仑断裂为东昆仑地体与巴颜喀拉-松甘地体之间的界线,往东与阿尼玛卿缝合带相连。东昆仑断裂为一条韧-脆性左行走滑剪切带,其基本构造样式表现为以

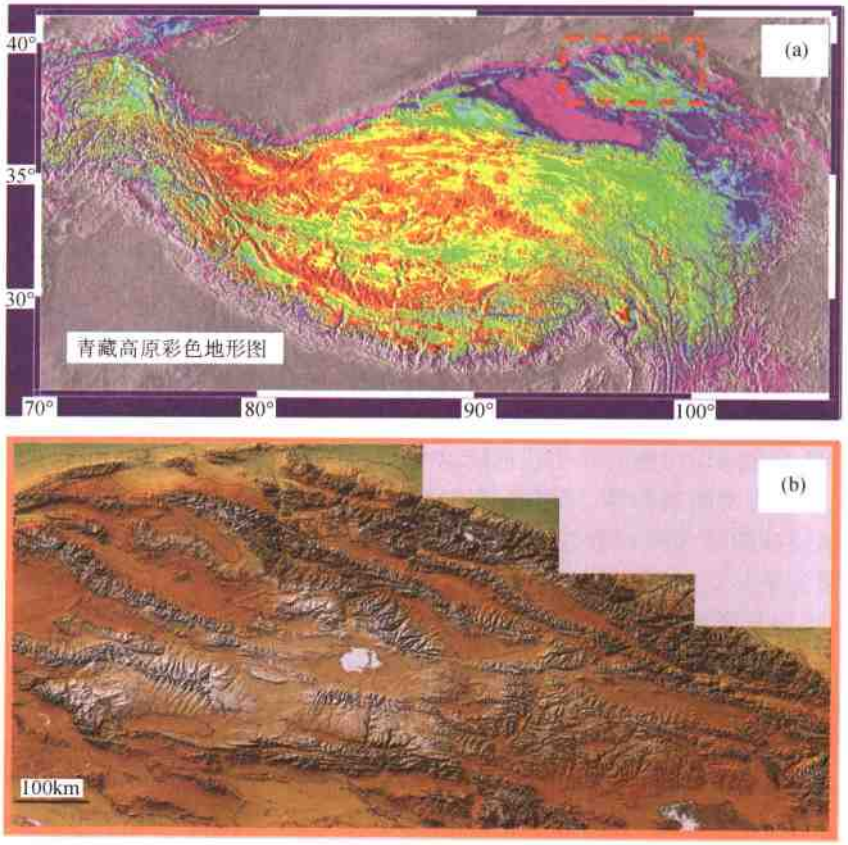

图 3　青藏高原(a)及柴达木盆地北缘到祁连山地区(b)的彩色数字地形图

Fig. 3　Color shade relief map of the Qinghai-Tibet plateau(a) and the areas from the northern margin of the Qaidam basin to the Oilian Mountain(b)

走滑断裂为中心的两侧反向逆冲断裂系,形成于印支期,150Ma 以来又有多次强烈活动,至今还具有左行走滑活动性质,并伴随地震活动(Li *et al.*,1996)。2001 年 11 月 14 日在东昆仑断裂西段可可西里地区发生了 $M=8.1$ 极大地震,并形成了约 430km 长的地表破裂带。格尔木-唐古拉山口剖面揭示东昆仑断裂为垂向低速异常带组成的延伸达 250km 深度的地幔剪切带(许志琴等,2001)。

2.1.3　海源左行走滑断裂的特征

海源断裂位于青藏高原北缘及东北缘,是一条巨型的弧形构造带,全长达 1000 多千米。自西向东从疏勒南山的哈拉湖北部向东经青海的门源北部,过甘肃天祝、古浪、景泰及宁夏海源,向东南至固原与六盘山相连及渭河地堑西端(Peltzer *et al.*,1985),至陇县、宝鸡与西秦岭北缘断裂相连(Zhang *et al.*,1995;刘锁旺等,1997)。它是我国西部的一条重要活动断裂,晚第四纪以来以左行活动为特征(刘锁旺等,1997;Lasserre,1999; Tapponnier and Molnar,1977;Zhang *et al.*,1988;国家地震局地质研究所和宁夏地震局,1990),最大左行走滑位移达 110km(刘锁旺等,1997),滑动速率达(12 ±4)mm/a(刘锁旺等,1997)。上世纪的 2 次极大地震(1920 年 $M=8.7$ 以及 1927 年 $M=8.3$)就发生在海源断裂带上,1920 年的极

大地震($M=8.7$)形成了长达 230km 长的地表破裂带(Burchfiel *et al*., 1991; Deng, 1986)。海源断裂西段以小角度斜切了祁连山,它是将祁连山与秦岭相连的主要断裂。

2.2 青藏高原北部的挤压型"盆-山"构造域

青藏高原的北部新生代大型左行走滑断裂系之间的盆-山构造系由 3 个构造域组成(图 4):位于阿尔金断裂东段与海源断裂之间的祁连盆-山构造域、位于阿尔金断裂中段、海源断裂与东昆仑断裂之间的柴达木盆-山构造域和位于东昆仑断裂与鲜水河断裂之间的巴颜喀拉-松甘盆-山构造域。

2.2.1 祁连盆-山构造域

自北而南祁连盆-山构造地貌域的展布依次为酒泉盆地、祁连山、昌马-黑河盆地、大雪山、野马河-哈拉湖盆地、野马山、党河盆地及党河南山。呈 NWW-SEE 走向的盆-山体系与上述两条走滑断裂均以 30°角度相交,盆-山之间的界线为逆冲断层(图 5)。

酒泉盆地为祁连山山前的新生代前陆盆地,长 1000km,宽 20～80km,是该域最大的盆地。西以阿尔金走滑断裂为界,南以北祁连北缘逆冲推覆带与祁连山连接,东为六盘山褶皱带,北以双塔逆冲断层与阿拉善沙漠相隔。自西往东分布了酒泉盆地、武威盆地及张掖盆地,其中酒泉盆地是已发现的含油气盆地。

酒泉盆地的基底为北祁连加里东褶皱带及后造山的泥盆纪—三叠纪陆相—海陆交互相山间盆沉积,其上被侏罗纪—上新统的近 6000m 的沉积地层不整合覆盖。侏罗—白垩纪陆相沉积地层厚度 4000m,沉积速率为 5.7～6.2mm/100a;新生代时期,酒泉盆地接受了渐新—全新统碎屑堆积,总厚度达 2 500m 以上,估计沉积速率的变化为:渐新世 7.5mm/100a,中新世 3.1mm/100a,上新世 20.8mm/100a,更新世 51mm/100a,全新世 0.1mm/100a(何登发等,1996)。

分隔酒泉盆地与祁连山的北祁连北缘逆冲推覆带为一系列南倾的铲式逆冲断裂及逆冲推覆岩片组成的薄皮构造,祁连山逐步向北逆冲推覆在酒泉盆地之上,逆冲断裂的活动始于中生代,白垩纪—第三纪地层不整合在逆冲断裂之上,在新生代继续活动,并使山体不断朝北推进,自中新世后期以来可能至少水平推移了 18km(Peltzer *et al*., 1985)。地震反射剖面资料揭示了阿拉善地块沿河西盆地以北的双塔逆冲断裂带以 30°角度插入河西盆地及祁连山下 30km 的深度(吴宣志等,1995)。据近年研究表明,晚第四纪期间北祁连的上升速率为 0.9～3.1mm/a(Tapponnier *et al*., 1990),如果以这样的速率在早期也保持不变的话,北祁连山脉应是在第四纪期间隆起的。

2.2.2 柴达木盆-山构造域

柴达木盆-山构造域位于阿尔金走滑断裂中段、海源走滑断裂及东昆仑走滑断裂之间,面积约 640000km^2。柴达木盆-岭构造域是以柴达木盆地为中心,柴达木盆地北侧为柴北缘盆-山构造系:以党河南山为北界,由苏海盆地、宗务隆山、柴北缘盆地(包括塞什腾-海马凹陷、欧北凹陷、埃北凹陷等)(姜洪川和高焕章,1989)及柴北缘山(包括塞什腾山、锡铁山、欧龙布鲁克山、埃姆尼克山)组成,柴北缘山东段以北发育菱形的青海湖盆地、共和盆地、西宁盆地和贵德盆地,明显受 NWW-SEE 向温泉右行走滑断裂及海晏右行走滑断裂的控制。柴达木盆地南侧为柴南缘盆-山构造系:由祁漫塔格山、阿牙库木克盆地、阿奇克库都克盆地、东昆仑山及阿奇克库洛湖盆地组成,沿东昆仑走滑断裂带的中段发育东西大滩拉分盆地。

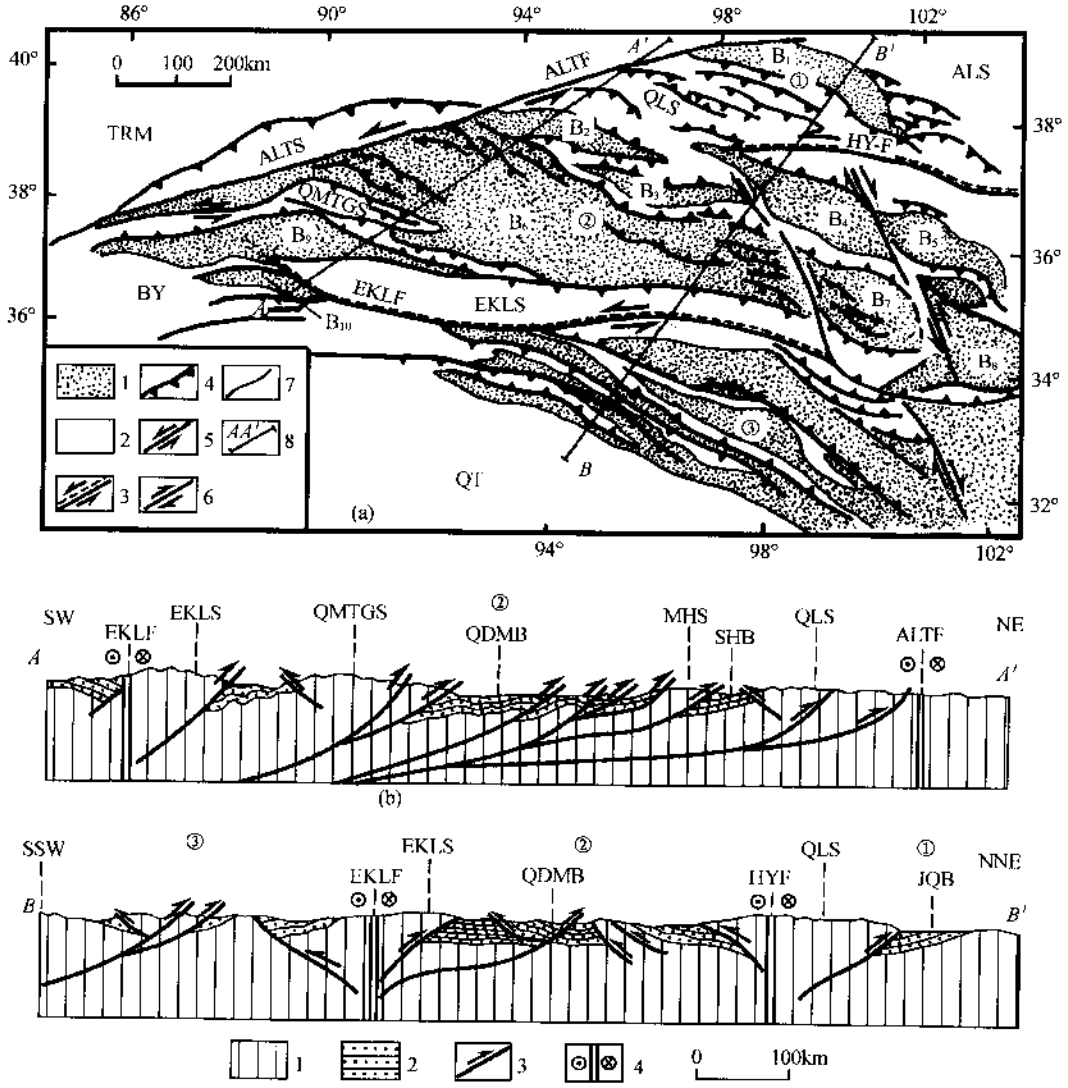

图 4 青藏高原北部的新生代构造平面及构造剖面

Fig. 4 Simplified geologic map showing the Cenozoic structures and cross-sections showing the characteristic structures in the northern Qinghai-Tibet plateau

(a)青藏高原北部的新生代构造平面图：1—盆地；2—山脉；3—大型左型走滑断裂；4—逆冲断裂；5—左行走滑断裂；6—右型走滑断裂；7—地质界线；8—剖面位置。(b)青藏高原北部构造剖面图：1—山体；2—盆地；3—逆冲断裂；4—左行走滑断裂。①祁连盆-山构造域；②柴达木盆-山构造域；③巴颜喀拉-松甘盆-山构造域。盆地：B_1—酒泉盆地；B_2—苏海盆地；B_3—柴北缘盆地；B_4—青海湖盆地；B_5—西宁盆地；B_6—柴达木盆地；B_7—共和盆地；B_8—贵德盆地；B_9—阿牙库木克盆地；B_{10}—阿奇克库都克盆地；QDMB—柴达木盆地；SHB—苏海盆地；JQB—酒泉盆地。山脉：QLS—祁连山；ALTS—阿尔金山；QMTGS—祁漫塔格山；EKLS—东昆仑山；ALS—阿拉善地体；TRM—塔里木地体；BY—巴颜喀拉地体；QT—羌塘地体；MHS—马海山。走滑断裂：ALTF—阿尔金左行走滑断裂；HYF—海源左行走滑断裂；EKLF—东昆仑左行走滑断裂

柴达木盆地是青藏高原中最大的一个中新生代陆相沉积盆地，盆地内的中新生界厚达5000～6000m 至 10000m，最厚达 16000m。柴达木盆地是在柴达木地块的基础上发育的，中新生界盆地的前新生代基底主要由前震旦纪变质岩系及部分震旦纪—古生代褶皱盖层和加

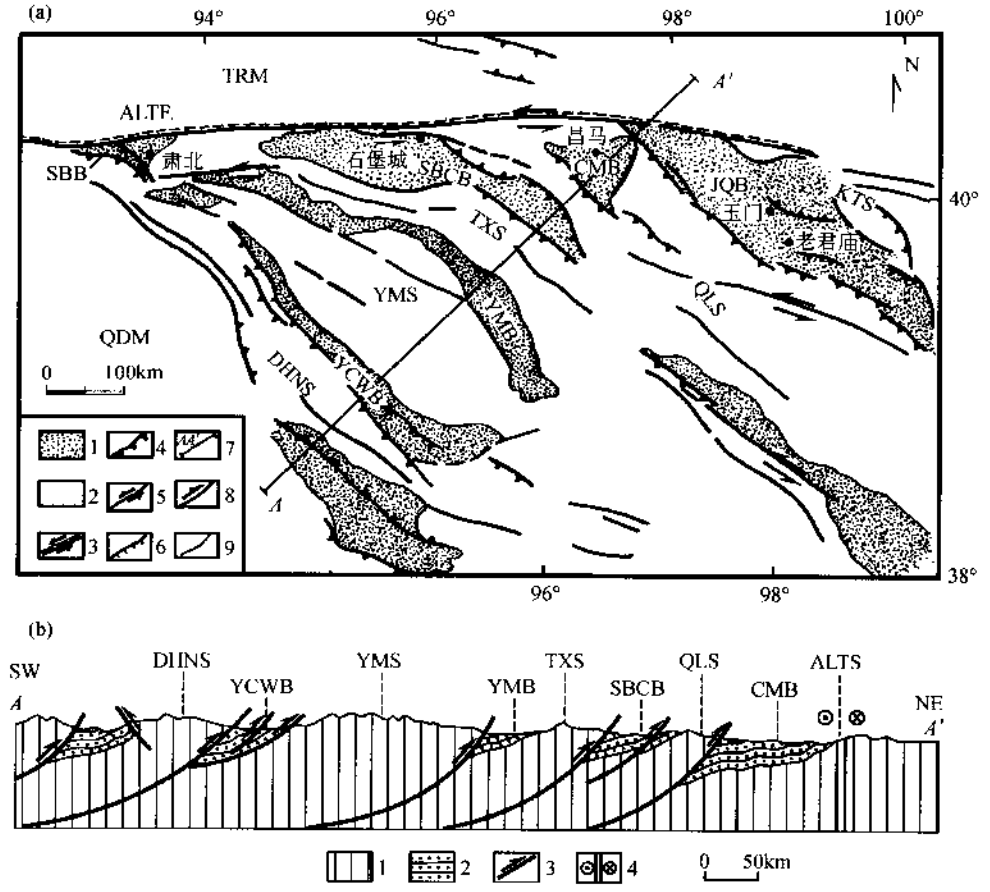

图 5　祁连山新生代构造平面及构造剖面

Fig. 5　Simplified geologic map showing the Cenozoic structures and cross-sections showing the characteristic structures in the Qilian Mountains

(a)祁连山新生代构造平面图;1—盆地;2—山脉;3—大型左型走滑断裂;4—逆冲断裂;5—左行走滑断裂;6—正断裂;7—剖面位置;8—逆冲断裂;9—地质界线。(b)祁连山新生代构造剖面图;1—山体;2—盆地;3—逆冲断裂;4—左行走滑断裂。KTS—宽堂山;QLS—祁连山;TXS—大雪山;YMS—野马山;DHNS—党河南山;ALTS—阿尔金山;ALTF—阿尔金断裂;TRM—塔里木地体;QDM—柴达木地体;JQB—酒泉盆地;CMB—昌马盆地;SBCB—石堡城盆地;SBB—肃北盆地;YMB—野马盆地;YCWB—盐池湾盆地

里东花岗岩组成,古生代—三叠纪可能一直处于相对隆起的地块状态。自印支运动以来,柴达木地块由于东昆仑地体与南面的巴颜喀拉-松潘-甘孜地体、羌塘地体、冈底斯地体不断会聚、碰撞与拼贴,形成印支和中生代造山带,而柴达木地块则相对沉降。新生代以来,接受了来自周边的大量剥蚀物质,形成巨厚陆相沉积。

在柴达木盆地的北缘及南缘分别发育了柴北缘及柴南缘大型逆冲推覆断裂带,它们均向山脉方向(祁连山和东昆仑山)倾斜,向盆地方向逆冲。柴达木盆地内沉积层发生轻微变形,形成宽缓的弯滑直立褶皱,无劈理,轴向 NW-SE,伴随逆冲断层,反映了挤压盆地的特征。盆地向东收缩,宽度缩小近一倍。

东昆仑山-阿牙库木克盆地-祁漫塔格山-柴达木盆地-马海山-苏海盆地-党河南山的构造

示意剖面(图 4)显示了柴达木盆地浅部逆冲叠覆的薄皮构造,推测柴达木盆地表层的褶皱-逆冲挤压体系与发育在盆地沉积层与前中生代基底之间及前中生代基底内部的深部滑脱断裂构造有关,滑脱断裂以 5°～10°向南倾伏,伸入祁漫塔格山和东昆仑山之下,向北滑脱断裂前缘的马海山一带隆起,出露基底变质岩石,把柴达木盆地与苏海盆地隔开。

在柴北缘盆-山构造系中,向 NWW 缓倾的宗务隆山南缘逆冲断层使宗务隆山压在中新生代的欧北盆地之上,中新生代沉积褶皱并伴随外缘逆冲断层系构成薄皮构造,在靠近断层一侧的背形构造部位利于油藏的富集(姜洪川和高焕章,1989)(图 6)。

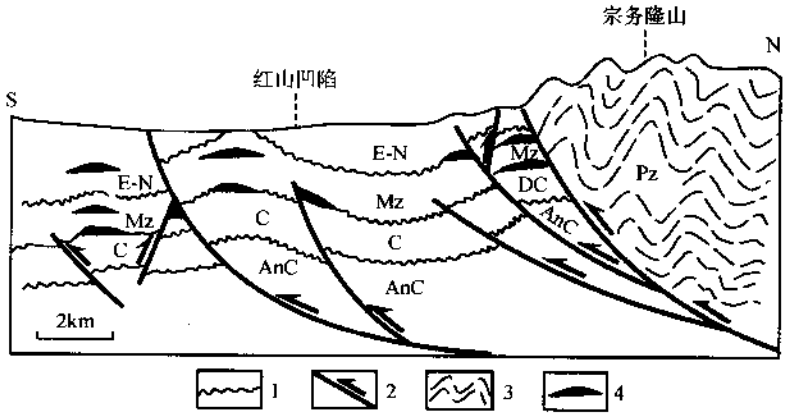

图 6　柴达木北缘欧北凹陷红山地区逆冲推覆构造
(据姜洪川等,1989)

Fig.6　Cross-section showing the thrust fault and associated structures in the Hongshan area of Oubei depression, North Qaidam

1—不整合;2—逆冲断裂;3—早古生代褶皱;4—有利的含油气构造部位 .AnC—前石炭纪;C—石炭纪;DC—泥盆纪-石炭纪;Mz—中生代;Pz—古生代;E-N—老第三纪—新第三纪

在柴达木南缘盆-岭构造系中,盆地主要发育在靠近阿尔金断裂一侧,平面呈透镜状,阿牙库木克盆地南北两侧发育反向逆冲断层,盆地内新生代地层变形形成轴向近 EW 的宽缓褶皱。

2.2.3　巴颜喀拉-松甘盆-山构造域

巴颜喀拉-松甘盆-山构造域位于巴颜喀拉-松甘地体东北部的近 EW 向的东昆仑断裂与 NW-SE 向的鲜水河断裂之间的三角形地区,盆-岭展布呈 NW-SE 方向,与东昆仑断裂相交约 30°。山体岩石为三叠纪复理石,盆地中主要堆积中-上新统的红色陆相沉积,厚度可达 3000m。盆-岭之间以逆冲断层为界,NE 部以向 NE 倾斜的逆冲断层为主,SW 部主要发育向 SW 倾斜的逆冲断层。

2.3　青藏高原北部的新生代盆-山省与走滑作用的关系

青藏高原北部的新生代盆-山域是在青藏高原隆升中形成的,并构成青藏高原特殊的构造-地貌景观,三大盆-山域的提出是对青藏高原北部新生代构造格架认识的深化。"盆-山"只是一种地貌的概念,关键在于成因。青藏高原北部的新生代盆-山挤压构造与走滑构造带究竟有没有成因联系?走滑构造带如何制约挤压型含油气盆地的发育?下面将要讨论两个

问题:①新生代盆-岭省与走滑构造的组构关系;②盆-岭省的地壳缩短及与高原地貌的形成。

青藏高原北部新生代盆-山构造域的地壳变形一方面表现了盆地内部的挤压变形(褶皱与逆冲断层)特征,同时构造线的方向显示了与走滑断裂斜交的组构特征,并且在靠近走滑断裂处出现构造的转折与绕曲,表现为盆地的不对称透镜形态、褶皱轴和逆冲断裂的转弯等。盆-山构造域与走滑断裂的组构关系均表明了3条走滑断裂的左行平移性质,盆-山构造域中的盆地,除沿断裂带的拉分盆地外,其他均为挤压型盆地,并且与走滑构造有成因联系。

以阿尔金断裂东段肃北地区的党河南山和肃海盆地为例,解析走滑作用与盆-山关系,选择在芦草湾和西水沟(河)地区研究阿尔金走滑作用与其南侧逆冲作用的成因联系(李海兵,2001;李海兵等,2001)。

①肃北地区西水沟的走滑速率约为22mm/a和17mm/a,而在东侧仅相距7～8km左右的芦草湾的走滑速率为17～13mm/a,这两地的走滑速率存在4～5mm/a之差。说明阿尔金断裂的走滑速率向东减少;②在阿尔金断裂东段南侧西水沟东南,由于逆冲构造使得T1、T2、T3均被抬升16～18m、35m±及50～55m,成为党河南山的前缘,逆冲断裂逆冲方向由SW到NE,估算T2阶地形成以来的抬升速率为(4.2±0.3)mm/a,党河南山北侧的缩短速率至少为4mm/a。

估算表明4～5mm/a的走滑速率差恰好与通过阶地抬升已估算的抬升速率4mm/a相近。这是因为走滑的一部分的能量转化到阿尔金断裂南侧,形成了南侧的逆冲断裂。上述表明走滑与逆冲可以相互调节和转化。走滑变形过程中伴随有逆冲作用形成山脉,同时逆冲作用使上隆的山体物质剥蚀,堆积在逆冲断裂之下盘,形成盆地。

2.4 新生代盆-山省与地壳缩短及高原地貌的形成

2.4.1 新生代盆-山省与地壳缩短

Tapponnier(2000)以美国国防制图局1992年提供的30弧秒分辨率(约900 m)的数字高程模型作为地形学基础,计算出位于阿拉善、塔里木和东昆仑之间的青藏高原北部的面积大约$5.4\times10^5km^2$,其中在盆地第三纪沉积体中保存下来的地下物质埋藏量大约等于$0.44\times10^6km^3$,表明第三纪盆地周围地壳加厚造成的区内岩石体积在1500m基准面之上增加了$1\times10^6km^3$。假定青藏高原东北部为均衡补偿区域,地壳与地幔的密度分别为$2750kg/m^3$和$3300kg/m^3$,并且将沉积物质考虑在内的话,位于西藏东北部的地壳岩石体积应为$6.8\times10^6km^3$。如果这个体积是由于地壳缩短造成的,那么未变形时原始地壳厚度应相当于未变形的阿拉善地台的地壳厚度(47.5±5)km,并获得$1.4\times10^5km^2$的地表面积减少量。晚新生代时缩短量大约相当于目前西藏东北部面积的26%,也相当于区内海拔2000m以上的山区面积的40%(约$3.5\times10^5km^2$),这可以解释为什么沿N30°E的地壳缩短。根据区域质量平衡法获得的沿N30°E方向大多数剖面缩短大于100km,在靠近阿尔金断裂处可达200km。考虑到区外沉积物的大量流失:黄河将大量携带到东部,疏勒河和党河在地史上的气候润湿期向西流向罗布泊,因此区外加厚的地壳物质可能损失百分之几,故地壳缩减量应比估计的还大。估算的缩短量的其中一部分被转换到柴达木地块往南俯冲到昆仑山之下。上述表明青藏高原北部的新生代盆-山省是在地壳缩短的挤压背景下形成的,是与美国西部盆岭省完全不同性质的"盆-山省",尽管它们在地貌上表现出相似特征。

2.4.2 新生代挤压型盆地的封闭及高原地貌的形成

一系列宽阔、平坦且高海拔的新第三纪盆地构成了青藏东北部的显著景观。由于受各种方向的晚新生代断层所限，许多盆地呈菱形或三角形，并且大部分盆地没有现在的河流出口，分别形成局部的基准面。典型的例子如共和盆地、青海湖盆地、哈拉湖盆地、苏海盆地、柴达木盆地、阿牙库木克盆地和阿奇克库都克盆地等。少数盆地虽然四周被山脉包围，但仍有大河通向外界(党河、疏勒河及黄河)，这些河流的切割能力与山体的增长速率相同。然而这些河流的输出速率却受气候变化的影响，流向周围低地的出水口很难保持稳定，例如黄河在共和及贵德盆地堆积了千米厚的第四纪沉积物，向上游方向横切青海南山和大石山，形成了数百米深的峡谷(Tapponnier, 2000)。

特别指出的是，逆断层上盘的构造快速抬升像水坝一样切割了汇水盆地的出口，随着山脉的增高和断裂的加大，使盆地处于隔离的状态，变成向内部排泄的封闭"水库"或"浴盆"。走滑断裂对此起至关重要的作用，因为走滑断裂与逆冲断层有一定的角度，水系与山脉平行，形成较高而且与附近低地不相连的局部基准面。随着来自周围山脉的碎屑物的流入，基准面继续升高，直到侵蚀残留高度，众多盆地的基准面共同形成高的、平滑的表面。

柴达木盆地的四周完全被新生代断层及 5000～6000m 的高山包围，它的基准面的平均海拔为 2800m，面积 103000km^2。盆地内的上新世—第四纪沉积物快速充填(等于或大于现在平原和冲积扇的充填速率)，说明构造作用切断了盆地流向黄河的出口，使大量的沉积物堆积在盆地内部。这种"坝式"沉积作用及"浴盆"式的填充方式使盆地高程抬升，表面平整。随着相对高差的减少，沿盆地周围山脉边缘的侵蚀速率降低，沉积物充填减慢，从而没有沉积物的溢出(Tapponnier, 2000)(图 7)。

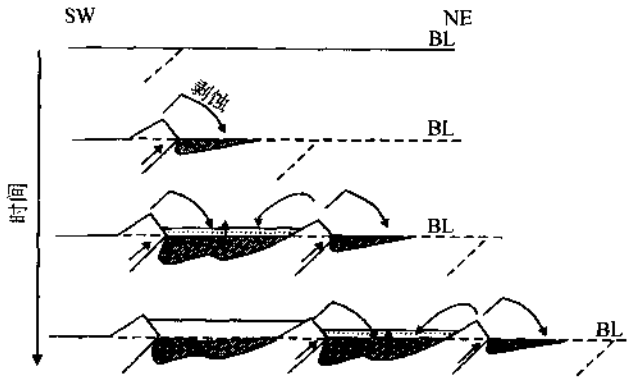

图 7 青藏高原北部盆-山构造域中盆地封闭及快速堆积

(Tapponnier, 2000)

Fig.7 Schematic diagram showing closure of the basins and rapid deposition within the basin-mountain system in the northern Qinghai-Tibet plateau

BL—基准面

2.5 青藏高原北部的深部构造与油气通道的探索

中法地球物理合作在青藏高原北部进行的乌图美仁-茫崖-若羌和格尔木-唐古拉天然地震探测剖面揭示了如下深部构造特征(Wittinger *et al*., 1996; Wittinger *et al*., 1998; 许志琴

等,2001);①乌图美仁-茫崖-若羌天然地震探测剖面揭示了阿尔金主断层的深部存在宽度为60～80km延伸超过400km的地震波低速异常带,是一条近直立的地幔(或超岩石圈)剪切带。低速异常带由低速度、低密度的高热物质组成,推测与大规模韧性剪切产生局部熔融有关。代表上地幔物质剪切流动矢量的SKS波各向异性强度大,各向异性方向与断裂带一致,也反映了该断裂带在上地幔深部发生了剪切位移(许志琴等,1996;Xu *et al.*,1999;许志琴等,2001)。②格尔木-唐古拉天然地震探测剖面及根据其与周围资料重新处理获得的阿克塞-花石峡天然地震探测剖面(图8)所显示的地幔图像,不仅揭示了东昆仑断裂为由低速异常带组成的深入250km的地幔剪切带(许志琴等,2001),以及昆仑山口-花石峡为中心的由大型低速异常体组成深部地幔羽结构(深度150～400km以下)的存在(许志琴等,1996;Xu *et al.*,1999),而且在柴达木盆地下部发现宽度300km、厚度达80km的地震波低速异常层,该地震波低速异常层又与昆仑山口-花石峡为中心的深部大型低速异常体组成地幔羽相连。

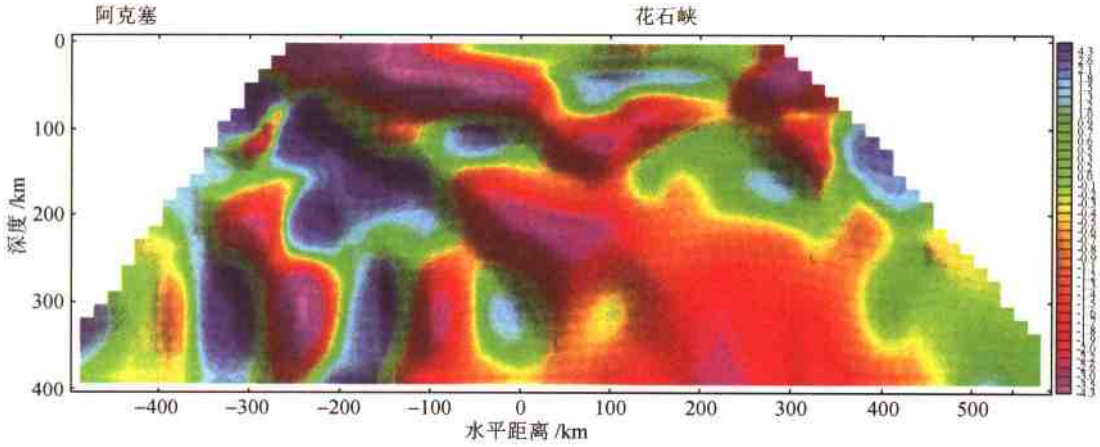

图8　阿克塞-花石峡天然地震探测剖面

Fig. 8　Natural seismic tomographic profile from Akesai to Huashixia

上述深部构造特征表明,柴达木盆地的周缘存在由高热低密度物质组成的地幔剪切带,盆地下部为高热低密度物质组成的底垫,为盆地的油气资源提供了有利的通道和背景。

3　讨论与结论

以上讨论表明青藏高原北部走滑断裂/盆-山体系与美国加州南部的圣安德烈斯走滑断裂/盆-山体系具有相似的特征。阿尔金断裂新生代以来的运动和印度板块与欧亚板块的碰撞紧密相关,是青藏高原地块与塔里木地块之间的边界断层。而圣安德烈斯断裂带是太平洋板块和北美板块之间的转换断层,其形成与三联点的上陆、向两侧的移动相关。虽然它们的现今大地构造背景不同,但两者之间在构造地质、地形地貌及含油气盆地等方面存在许多相似的特征:①青藏高原相对于塔里木地块与太平洋相对于北美板块的斜向运动相似,分别

在青藏高原的东北部和美国南加州横向山脉地区形成区域挤压缩短应变区。②与走滑运动相伴生的挤压缩短应变导致在青藏高原北部的昆仑山-祁连山地区形成有序的盆-山构造体系。相似地,太平洋板块和圣安德烈斯断裂相互作用也导致在南加州形成有序的盆-山构造体系。③与走滑运动有关的强烈的挤压缩短应变导致一系列出露地表或盲逆冲推覆构造的产生,并在逆冲断层的上盘形成断层生长皱褶和皱褶山,这些部位为油气圈闭、成藏的有利构造位置。④阿尔金断裂和圣安德烈斯断裂作为板块或地体边界走滑断裂,具有地慢剪切带的特征,与其相配套的高度地震活动性的逆冲推覆断裂带为深部流体或气体向上的迁移提供有利的通道,促使油气在与推覆构造相伴生的褶皱核部聚集和圈闭。⑤逆冲断层的褶皱核部为油气圈闭的有利部位和油气勘探的主要目标。

基于大型走滑断裂在挤压型盆-山构造体系中的重要作用(刘和甫等,2004;许志琴等,2004)和上述的特点,我们认为应该利用新技术和实验手段来详细研究与大型走滑断裂带相关的盆-山构造体系的地质地貌特征,重新审视和评价其油气资源的前景。

References

Burchfiel, C., Zhang, P., Wang, Y., *et al*., 1991. Geology of the Haiyuan fault zone, Ningxia-hui autonomous region, China, and its relation to the evolution of the northeastern margin of the Tibetan plateau. Tectonics, 10:1091~1110.

Deng, Q., 1986. Variations in the geometry and amount of slip on the Haiyuan (Nanxi-Haushan) fault zone, China, and the surface rupture of the 1920 Haiyuan earthquake. Geophys. Monogr. Ser., 37:169~182.

Dolan, J. F., Christofferson, S. A., Shaw, J. H., 2003. Recognition of paleoearthquakes on the Puente Hills blind thrust fault, California. Science, 300:115~118.

Fuis, G. S., Ryberg, T., Godfrey, N. J., *et al*., 2001. Crustal structure and tectonics from the Los Angeles basin to the Mojave desert, southern California. Geology, 29:15~18.

He, D. F., Lu, X. X., Lin, Y. H., *et al*., 1996. Foreland basin analysis. Petroleum Industry Press, Beijing, 212 (in Chinese).

Institute of Geology and Ningxia Institute of Seismology, SSB, 1990. Active tectonics of the Haiyuan fault. Seismology Press, Beijing (in Chinese).

Jiang, H. C., Gao, H. Z., 1989. A study on the thrust and nappe structure in the north margin of Chaidamu basin and its oil and gas prospect. Northwestern University Press, Xi'an, China, 79 (in Chinese).

Jones, C. H., 2003. How faults accommodate plate motion. Science, 300: 1105~1106.

Kennedy, B. M., Kharaka, Y. K., Evans, W. C., *et al*., 1997. Mantle fluids in the San Andreas fault system, California. Science, 278:1278~1281.

King, P. R., 2000. New Zealand's changing configuration in the last 100 million years: Plate tectonics, basin development, and depositional setting. 2000 New Zealand Petroleum Conference Proceedings, 15.

Kranzh, R. W., 1995. The transpressional strain model applied to strike-slip, oblique-convergent and oblique-divergent deformation. Journal of Structural Geology, 17(8):1125~1137.

Lasserre, C., 1999. Postglacial left slip-rate and past occurrence of $M \geqslant 8$ earthquakes on the western Haiyuan fault, Gansu, China. J. Geophys. Res., 104 (17): 633~17,651.

Li, H. B., 2001. Timing of the initation of the Altyn Tagh fault and its contribution to the uplift of the Northern Tibetan plateau. Ph. D. Thesis, Chinese Academy of Geological Sciences, Beijing (in Chinese).

Li, H. B., Xu, Z. Q., Chen, W., 1996. Deformational features and tectonic evolution of the south Kunlun strike-slip shear zone, East Kunlun Mountains. Acta Geoscientia Sinica, Special Issue: 16~21.

Li, H. B., Yang, J. S., Shi, R. D., *et al*., 2001. The relationship between faulted basin and mountain ranges along the Altyn Tagh Fault. Chinese Science Bulletin, 47 (1):63~67 (in Chinese).

Li, H. B., Yang, J. S., Xu, Z. Q., *et al*., 2001. Geological and geochronogy evidences of Indosinian strike-slipping for the Altyn Tagh fault. Chinese Science Bulletin, 46(16): 1333～1338 (in Chinese).

Liu, S. W., Gan, J. S., Yao, Y. S., *et al*., 1997. Strike-transform deformation of the northern margin fault of the West Qinling and the Haiyuan fault and their relation with the Longshan massif. Crustal Deformation and Earthquake, 17 (3): 73～83 (in Chinese with English abstract).

Liu, H. F., Li, X. Q., Liu, L. Q., *et al*., 2004. Petroleum play analysis and strike-slip system basin-mountain coupling. Geoscience, 18: 139～150 (in Chinese with English abstract).

Liu, J., Klinger, Y., Sieh, K., *et al*., 2004. Six similar, sequential ruptures of the San Andreas fault, Carrizo plain, California. Geology, 32 (8): 649～652.

Liu, J., Sieh, K., Hauksson, E., 2003. A structural interpretation of the aftershock "cloud" of the 1992 Mw7. 3 Landers earthquake. Bull. Seism. Soc. Am., 93(3): 1333～1344.

Oskin, M., Sieh, K., Rockwell, T., *et al*., 2000. Active parasitic folds on the Elysian Park anticline: Implications for seismic hazard in central Los Angeles, California. Geological Society of America Bulletin, 112: 693～707.

Peltzer, G., Tapponnier, P., Zhang, Z., *et al*., 1985. Neogene and Quaternary faulting in and along the Qinling Shan. Nature, 317: 500～505.

Shaw, J. H., Shearer, P. M., 1999. An elusive blind-thrust fault beneath metropolitan Los Angeles. Science, 283: 1516～1518.

Spotila, J., Farley, K., Sieh, K., 1998. Uplift and erosion of the San Bernardino Mountains associated with transpression along the San Andreas fault, California, as constrained by radiogenic helium thermochronometry. Tectonics, 17: 360～378.

Sylvester, A. G., 1988. Strike-slip faults. Geological Society America Bulletin, 100: 1666～1703.

Tapponnier, P., 2000. Neotectoincs. In: Xu, Z. Q., Yang, J. S., Tapponnier, P., *et al*., eds., Field trip guide, international symposium on geoscience of the northern Qinghai-Tibet plateau—Marking the 20th Anniversary of the Sino-French cooperative research on geoscience. Dunhuang, China.

Tapponnier, P., Meyer, B., Avouac, J. P., 1990. Active thrusting and folding in the Qilian Shan and decoupling between upper crust and crust and mantle in northeastern Tibet. Earth and Planetary Sciences Letters, 97: 382～403.

Tapponnier, P., Molnar, P., 1977. Active faulting and tectonics in China. J. Geophys. Res., 82: 2905～2930.

Wittinger, G. F., Tapponier, P., Poupinet, G., *et al*., 1998. Tomographic evidence for localized lithospheric shear along the Altyn Tagh fault. Science, 74～76.

Wittinger, G., Masson, F., Poupinet, G., 1996. Seismic tomography of northern Tibet and Kunlun: Evidence for crustal blocks and mantle velocity contrasts. EPSL, 139: 263～279.

Wu, X. Z., Wu, C. L., Lu, J., 1995. Research on the fine crustal structure of the northern Qilian-Hexi corridor by deep seismic reflection. Acta Geophysica Sinica, 38(suppl. II): 29～35 (in Chinese with English abstract).

Xu, Z. Q., Li, H. B., Yang, J. S., *et al*., 2001. A large transpression zone at the south margin of the east Kunlun Mountains and oblique subduction. Acta Geologica Sinica, 75(2): 156～164 (in Chinese with English abstract).

Xu, Z. Q., Jiang, M., Yang, J. S., 1996. Tectonophysical process at depth for the uplift of the northern part of the Qinghai-Tibet plateau: Illustrated by the geological and geophysical comprehensive profile from Golmud to the Tanggula mountains, Qinghai Province, China. Acta Geologica Sinica, 70: 195～206 (in Chinese with English abstract).

Xu, Z. Q., Jiang, M., Yang, J. S., *et al*., 1999. Mantle diapir inward intracontinental subduction: A discuss on the mechanism of uplift of the Qinghai-Tibet plateau. Geological Society of America, Special Paper, 328: 19～31.

Xu, Z. Q., Yang, J. S., Jiang, M., 2001. Deep structure and lithospheric shear faults in the East Kunlun-Qiangtang region, northern Tibetan plateau. Science in China (Series D), 31(Suppl.): 1～7 (in Chinese).

Xu, Z. Q., Yang, J. S., Li, H. B., *et al*., 2004. The assembly of the Qinghai-Tibet plateau by amalgamation of terranes and its collisional dynamics. Geological Publication House, Beijing (in Press, in Chinese).

Xu, Z. Q., Yang, J. S., Zhang, J. X., *et al*., 1999. A comparison between the tectonic units on the two sides of the Altun sinistral strike-slip fault and the mechanism of lithospheric shearing. Acta Geologica Sinica, 73 (3): 193～205 (in Chinese with English abstract).

Yule, D., Sieh, K., 2003. Complexities of the San Andreas fault near San Gorgonio pass: Implications for large earthquakes. Journal of Geophysical Research, 109, B11, 2548, ETG 9, doi: 10. 1029/2001JB000451.

Zhang, P., Molnar, P., Barchfiel, B. C., *et al*., 1988. Bounds on the Holocene slip rate of the Haiyuan fault, northcentral China. Quat. Res., 30: 151～164.

Zhang, W., Jiao, D., Zhang, P., *et al*., 1987. Displacement along the Haiyuan fault associated with the great 1920 Haiyuan, China, earthquake. Bull. Seismol. Soc. Am., 77:117~131.

Zhang, Y. Q., Vergely, P., Mercier, J., 1995. Active faulting in and along the Qinling Range (China) inferred from SPOT imagery analysis and extrusion tectonics of South China. Tectonophysics, 243: 69~95.

Zhu, L., 2000. Crustal structure across the San Andreas fault, southern California from teleseismic converted waves. Earth and Planetary Sci. Lett., 179:183~190.

中文参考文献

何登发,吕修祥,林永汉,等,1996.前陆盆地分析.北京:石油工业出版社,212.

国家地震局地质研究所,宁夏地震局,1990.海源活动断裂带.北京:地震出版社.

姜洪川,高焕章,1989.柴达木盆地北缘逆冲推覆构造及其含油气性研究.西安:西北大学出版社,79.

李海兵,2001.阿尔金断裂的形成时代及其走滑作用对青藏高原北部隆升的贡献.中国地质科学院研究生院博士论文.

李海兵,杨经绥,史仁灯,等,2001.阿尔金走滑断陷盆地的确定及其与山脉的关系.科学通报,47(1):63~67.

李海兵,杨经绥,许志琴,等,2001.阿尔金断裂带印支期走滑活动的地质及年代学证据.科学通报,46(16):1333~1338.

刘锁旺,甘家思,姚运生,等,1997.西秦岭北缘断裂与海源断裂的走滑转换变形及其与陇山地块的相互作用.地壳变形与地震,17(3):73~83.

刘和甫,李晓清,刘立群,等,2004.走滑构造体系盆山耦合与区带分析.现代地质,18(2):139~150.

吴宣志,吴春玲,卢杰,1995.利用深地震反射研究北祁连-河西走廊地壳细结构.地球物理学报,38(增刊Ⅱ):29~35.

许志琴,李海兵,杨经绥,等,2001.东昆仑山南缘大型转换挤压构造带和斜向俯冲作用.地质学报,75(2):156~164.

许志琴,姜枚,杨经绥,1996.青藏高原北部隆升的深部构造物理作用.地质学报,70(3):195~206.

许志琴,杨经绥,姜枚,等,2001.青藏高原北部东昆仑-羌塘地区的岩石圈结构及岩石圈剪切断层.中国科学(D辑),31(增刊):1~7.

许志琴,杨经绥,张建新,等,1999.阿尔金断裂两侧构造单元的对比及岩石圈剪切机制.地质学报,73(3):193~205.

许志琴,杨经绥,李海兵,等,2004.青藏高原的地体拼合及碰撞动力学.北京:地质出版社(待刊).

Role of Large-Scale Strike-Slip Faults in the Formation of Petroleum-Bearing Compressional Basin-Mountain Range Systems

XU Zhi-qin[1] ZENG Ling-sen[1] YANG Jing-sui[1] LI Hai-bing[1]
JIANG Mei[1] JIN Zhi-jun[2] ZHENG He-rong[2] GUO Qi-jun[2]
(1. Key Laboratory for Continental Dynamics, MLR, Institute of Geology, Chinese Academy of Geological Sciences, Beijing 100037, China;
2. China Petroleum and Chemical Corporation, Beijing 100083, China)

Abstract Understanding the factors that affect the formation and evolution of petroleum-bearing sedimentary basins plays a critical role in the prospecting and exploitation of oil fields. The formation and evolution of the highly-order coastal and inland petroleum-bearing Cenozoic basins and their bounding mountain ranges in southern California, USA were initiated and controlled by the San Andreas fault system, a large-scale plate boundary transform fault that

separates the Pacific plate from the North American plate. The northeast oblique movement of the Pacific plate relative to the North American plate in conjunction with the big bend of the San Andreas fault in southern California produces intense contractional strain across the Transverse Ranges and leads to the formation of a series of fault and fold structures that shape the salient landscape of southern California. For comparison, we have conducted detailed structural analyses on the basin-mountain range systems in the northern Qinghai-Tibet plateau to discuss the role of the Altyn Tagh fault in ①development of regional contractional stress field; ②formation of structures and sedimentary basins; ③generation of structures that facilitate the migration and capture of oil and gas. Results show that the Altyn Tagh fault has played a similar role in the formation of the spectacular basin-mountain systems to that of the San Andreas fault. The oblique convergence of the Qinghai-Tibet terrane relative to the Tarim basin resulted in the formation of transpressional tectonic regime to the southeastern of the Altyn Tagh fault. Such oblique convergence resulted in a series of strike-slip and thrust faults. As a consequence, the areas from the Kunlun Mountains to the Qilian Mountains form spectacular landforms characterized by alternations of basins and mountain ranges. For both cases of the southern California and the northern Qinghai-Tibet plateau, thrust faulting not only provides a viable mechanism for the migration of oil or gas, but also resulted in fault-propagation folds which serve as the favorable capture structure for oil and gas. One of the key factors that generate such a highly organized petroleum-bearing basin-mountain system is oblique convergence induced slip partitioning which results in the dextral horizontal slip along a major strike slip faultand vertical slip along numerous blind or exposed thrust faults.

Key words strike-slip fault compressional basin-mountain range system petroleum resources.

青藏高原的地幔结构：地幔羽、地幔剪切带及岩石圈俯冲板片的拆沉❶

许志琴[1]　姜　枚[1,2]　杨经绥[1]　薛光琦[1,2]　宿和平[1]
李海兵[1]　崔军文[1]　吴才来[1]　梁凤华[1]
（1. 中国地质科学院　地质研究所　大陆动力学部重点实验室　北京　100037；
2. 中国地质科学院　矿产资源研究所　北京　100037）

摘　要　通过横穿青藏高原近 8000km 长的 4 条天然地震层析剖面，获得 400km 深度以上的地壳和地幔速度图像及地震波各向异性，揭示了青藏高原 400km 深度范围内的地壳和地幔结构特征。地幔速度图像显示，青藏高原腹地的深地幔中存在以大型低速异常体为特征的地幔羽，其可能通过热通道与大面积分布的可可西里新生代高钾碱性火山作用有成因联系；阿尔金、康西瓦、金沙江、嘉黎及雅鲁藏布江等走滑断裂可下延至 300～400km 深度，显示了低速高热物质组成的垂向低速异常带特征及大型超岩石圈或地幔剪切带的产出；发现康西瓦、东昆仑-金沙江、班公湖-怒江和雅鲁藏布缝合带下部存在不连续的高速异常带，可以解释为青藏高原地体拼合及碰撞过程中可能保留的加里东、古特提斯和中特提斯大洋岩石圈“化石”残片，是“拆沉”的地球物理证据。印度大陆岩石圈的巨厚俯冲板片以 15°～20°倾角向北插入唐古拉山下 300km 深处，并被高热物质组成的地幔剪切带分开。结合新的横穿喜马拉雅及青藏高原的地幔层析资料，提出青藏高原碰撞动力学新模式：青藏高原南部印度岩石圈板片的翻卷式陆内超深俯冲，北缘克拉通向南的陆内俯冲，腹地深部的地幔羽上涌，以及地幔范围内的高原“右旋隆升”及物质向东及北东方向运动及挤出。

关键词　青藏高原　地震层析剖面　地幔羽　地幔剪切带　岩石圈板片拆沉
中图分类号：P542＋.4　**文献标识码**：A　**文章编号**：1005－2321(2004)04－0329－15

0　引言

青藏高原的结构是由祁连地体、东昆仑-柴达木地体、西昆仑地体、巴颜喀拉-松潘甘孜地体、羌塘地体、冈底斯地体和喜马拉雅地体组成的。在青藏高原的各地体之间存在着地质历史中形成并保留下来的地体边界，其中有加里东期形成的祁连-阿尔金[1～4]和西昆仑库地缝合带[5～8]，古特提斯期形成的东昆仑阿尼玛卿及金沙江缝合带[9～13]，中特提斯期形成的班公湖-怒江缝合带及新特提斯期形成的雅鲁藏布江缝合带[14,15]等，它们分别是早古生

❶ 地学前缘，2004 年第 11 卷第 4 期。
收稿日期：2004－07－16；修订日期：2004－07－29。

作者简介：许志琴(1941—)，女，研究员，中国科学院院士，构造地质学专业，主要从事显微构造、大地构造和大陆动力学研究，长期从事青藏高原构造研究工作。

代洋盆、古特提斯洋盆、中特提斯洋盆及新特提斯洋盆消减和地体碰撞的见证。研究表明，地体边界及内部由于地体之间的相对斜向会聚与碰撞而形成大型走滑构造[16～19]，其中有加里东期以来的北祁连南缘韧性走滑剪切带[20]和西昆仑康西瓦韧性走滑剪切带[21]，印支期以来的南祁连南缘韧性走滑剪切带[22]、阿尔金韧性走滑剪切带[23,24]、东昆仑南缘韧性走滑剪切带及金沙江韧性走滑剪切带[25,19]，新生代以来形成的喀喇昆仑韧性走滑剪切带[26,27]、鲜水河韧性走滑剪切带[11,28]、红河韧性走滑剪切带[29]、嘉黎韧性走滑剪切带和海源走滑断裂等大型走滑构造以及古韧性走滑剪切带的再活化[17,18,30]。青藏高原大型走滑构造的研究导致青藏高原地体向东及东南方向的侧向挤出[31,17]以及"右旋隆升"动力学机制的提出[32]。

喜马拉雅地体是大约65～50Ma以来印度板块与欧亚大陆碰撞形成的增生地体[33]，目前人们已普遍接受了"大印度"板块(即碰撞前印度次大陆的面积比现在要大得多)的观点，即"大印度"板块通过向北插入青藏高原以下上千千米而消减[34]。最新的全球地幔地震层析资料不仅揭示了东太平洋和西太平洋岩石圈板片可以俯冲到美洲及亚洲大陆之下的深地幔或核幔边界，而且通过西喜马拉雅的地幔层析剖面[35,36]揭示了西喜马拉雅构造结部位的印度岩石圈板片以高速异常体的形式从地表往北下插，向下变成直立，最后在深部又往南翻转(overroll)的几何形态，俯冲至800～1000km的地幔深度。

自20世纪90年代初以来，由许志琴和P. Tapponnier组织的中法青藏高原地学合作开展了地质和地球物理多学科的研究和探测。其中姜枚和Hirn及Wittlinger G.负责的中法地球物理合作小组在青藏高原实施了8000km长的天然地震探测剖面[37,38]，包括横穿青藏高原中部及南部的格尔木-唐古拉-嘎拉剖面(3000km)，位于青藏高原腹地东部的共和-玉树剖面(3000km)，横穿青藏高原西北部柴达木盆地和阿尔金山的乌图美仁-若羌剖面(1000km)，以及横穿青藏高原西部西昆仑山的叶城-狮泉河剖面(1000km)。这些剖面几乎穿过了青藏高原所有地体，并通过了主要地体边界。上述剖面的成果大部分已发表，并作了初步地质解释，提出了有关青藏高原北部大型岩石圈断裂和腹地地幔底辟存在以及塔里木地块俯冲于阿尔金地体之下[39～41]等观点。

本文对青藏高原地震层析资料作了进一步处理，并在此基础上进行综合地质解析，对青藏高原地壳和地幔的结构、物理性质和状态、高原隆升及碰撞动力学机制作新的探讨。需要说明的是本文在重新处理"格尔木-唐古拉-嘎拉"地震层析剖面时参考使用了国土资源部中美INDEPTH项目在该剖面南段西侧的有关地震层析数据(图1中示意)。

1 青藏高原400km深度范围内的天然地震层析图像

通过转换波计算的地壳中地震速度层、地震横波分裂处理的地震各向异性资料及三维走向获得的400km深度以上的地幔速度图像，为进行青藏高原400km深度范围内地壳与地幔的天然地震层析图像的分析提供了研究的基础。

1.1 地壳厚度及地震波速度层

根据天然地震转换波计算速度层编绘而成的各地体地层速度剖面图(图2)显示了青藏高原各地体地壳结构、地壳厚度和层速度变化的特征。获得了自北往南各地体地壳平均厚度如下：祁连地体62km，柴达木地体54km，东昆仑地体64km，巴颜喀拉地体66～68km，羌

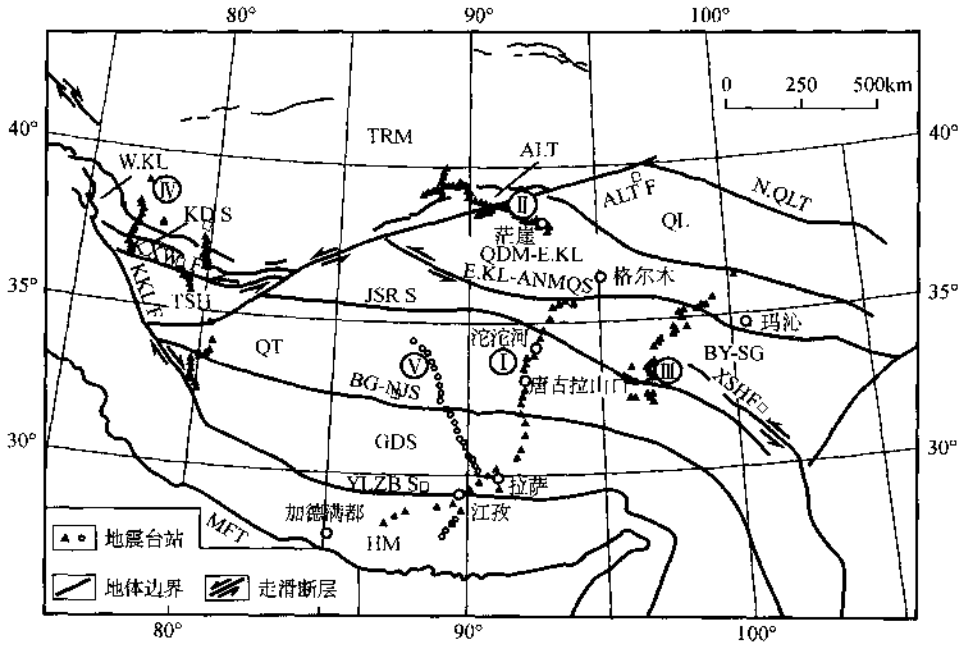

图 1 横穿青藏高原的天然地震层析剖面位置图

Fig. 1 Locations of the seismic tomographic profiles across the Qinghai-Tibet Plateau

Ⅰ—格尔木-唐古拉-嘎拉剖面;Ⅱ—乌图美仁-若羌剖面;Ⅲ—共和-玉树剖面;Ⅳ—叶城-狮泉河剖面;V—INDEPTH组的地震探测路线。QL—祁连地体;QDM-E.KL—柴达木-东昆仑地体;BY-SG—巴颜喀拉-松潘甘孜地体;QT—羌塘地体;GDS—冈底斯地体;HM—喜马拉雅地体;ALT—阿尔金地体;W.KL—西昆仑地体;TSH—甜水海地体;TRM—塔里木地体;E.KL-ANMQ S.—东昆仑-阿尼玛卿缝合带;JSR S—金沙江缝合带;BG-NJ S—班公湖-怒江缝合带;YLZB S—雅鲁藏布江缝合带;KD S—库地缝合带;KXWF—康西瓦缝合带;KKL F—喀喇昆仑断裂;ALTF—阿尔金断裂;N.QLT—北祁连北缘逆冲断裂;MFT—喜马拉雅主前缘逆冲断裂

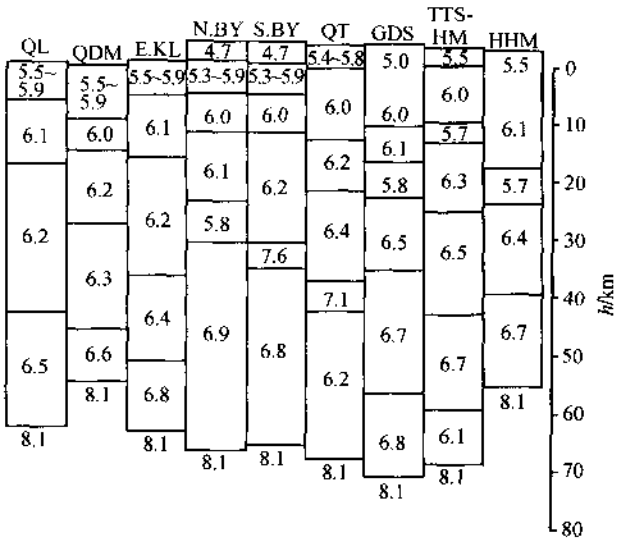

图 2 青藏高原地体的地震波平均速度剖面图

Fig. 2 Average seismic wave velocity sections of various terranes in Qinghai-Tibet Plateau

QL—祁连地体;QDM—柴达木盆地;E.KL—东昆仑地体;N.BY—北巴颜喀拉地体;S.BY—南巴颜喀拉地体;QT—羌塘地体;GDS—冈底斯地体;TTS-HM—特提斯-喜马拉雅地体;HHM—高喜马拉雅地体

塘地体 67km,冈底斯地体 71km,喜马拉雅地体中的特提斯喜马拉雅 68km,高喜马拉雅 55km。其中,冈底斯地体的地壳最厚,柴达木地体和高喜马拉雅地体的地壳最薄。

青藏高原各地体的地震波速度剖面揭示各地体的如下结构特征:

(1)存在上部地壳中的地震波低速层。在东昆仑地体以南的巴颜喀拉地体北部、冈底斯地体及喜马拉雅地体的上部地壳中存在地震波低速层,但低速层的深度及厚度有所不同:巴颜喀拉地体北部低速层位于深度 23～30km,厚度 7km,冈底斯地体低速层位于深度 16～22km,厚度 6km;喜马拉雅地体北部的特提斯喜马拉雅低速层位于深度为 10～13km,厚度 3km;高喜马拉雅低速层位于深度 17～22km,厚度 5km。

(2)下部地壳中的地震波低速层和高速层。在羌塘地体的 Moho 面(v_p=8.1km/s)之上,43～68km 深度处出现 25 m 厚的低速层,地震波层速度为 v_p=6.2km/s;在特提斯喜马拉雅的下地壳(v_p=6.7km/s)与上地幔(v_p=8.2km/s)之间 60～68km 深度处出现 v_p=6.1km/s 的低速层。在巴颜喀拉地体南部正常的下地壳(33～66km)波速(v_p=6.8km/s)之上和羌塘地体低速层之上均出现厚 3～5km 的高速层(v_p=7.6km/s 和 v_p=7.1km/s)。

(3)各地体地震波速度剖面反映了各地体的物质组成及结构的差异,表明青藏高原是地质历史时期地体拼合的产物。

1.2 青藏高原地幔速度图像

横穿青藏高原的格尔木-嘎拉天然地震层析剖面(图 3-A)、乌图美仁-若羌天然地震层析剖面(图 4-A_1)、共和-玉树天然地震层析剖面(图 4-A_2)和叶城-狮泉河天然地震层析剖面(图 4-A_3),显示了 400km 深度范围的青藏高原深部结构是由高波速和低波速相互交错、镶嵌组成的复杂图像,分别对这些图像进行解析,为我们探讨青藏高原地幔结构提供了基础。

1.2.1 地震波低速异常图像

天然地震层析剖面显示了 400km 深部范围内的两种类型地震波低速图像:大型深地幔地震波低速异常体和地震波垂向低速异常带。①大型深地幔地震波低速异常体:在格尔木-嘎拉天然地震层析剖面(图 3-A)中,可观察到青藏高原腹地(柴达木-东昆仑地体、巴颜喀拉地体和羌塘地体北部)100km 以下存在以昆仑山口为中心(北抵柴达木盆地,南到雁石坪)的深部地震波低速异常体。地幔低速异常体宽度约 600km,深度从 100km 延到 400km 以下,可与相邻的乌图美仁-若羌天然地震层析解析剖面(图 4-A_1)及共和-玉树天然地震层析解析剖面(图 4-A_2)中揭示的东昆仑-巴颜喀拉-羌塘地体及柴达木盆地下面的深地幔地震波低速异常体相连,表明高原腹地的深地幔中存在大型地震波低速异常体。同时在格尔木-嘎拉剖面中的深部地幔低速异常体通过低速异常通道直达可可西里地表的新生代高钾火山岩区。②垂向地震波低速异常带:垂向低速异常带出现在地体边界及大断裂的下部,雅鲁藏布江垂向低速异常带宽 50～100km,从地表一直延伸至 400km 以下;嘉黎低速异常带与班公湖-怒江低速异常带发育在 100～200km 深度以下,并在 350km 深处相连(图 3-A)。在乌图美仁-若羌天然地震层析剖面(图 4-A_1)中,垂向低速异常带清晰地显示在阿尔金断裂带之下,阿尔金低速异常带宽度超过 100km,延伸深度大于 300km。③近水平低速异常层:在图 3 中,从雅鲁藏布江缝合带往北至唐古拉之下 200km 深处,存在一条往北缓倾的不规则形态的厚度约 20～50km 的地震波低速异常层,其下部与雅鲁藏布江、嘉黎和班公湖-怒江垂向低速异常带相连(图 3-A)。

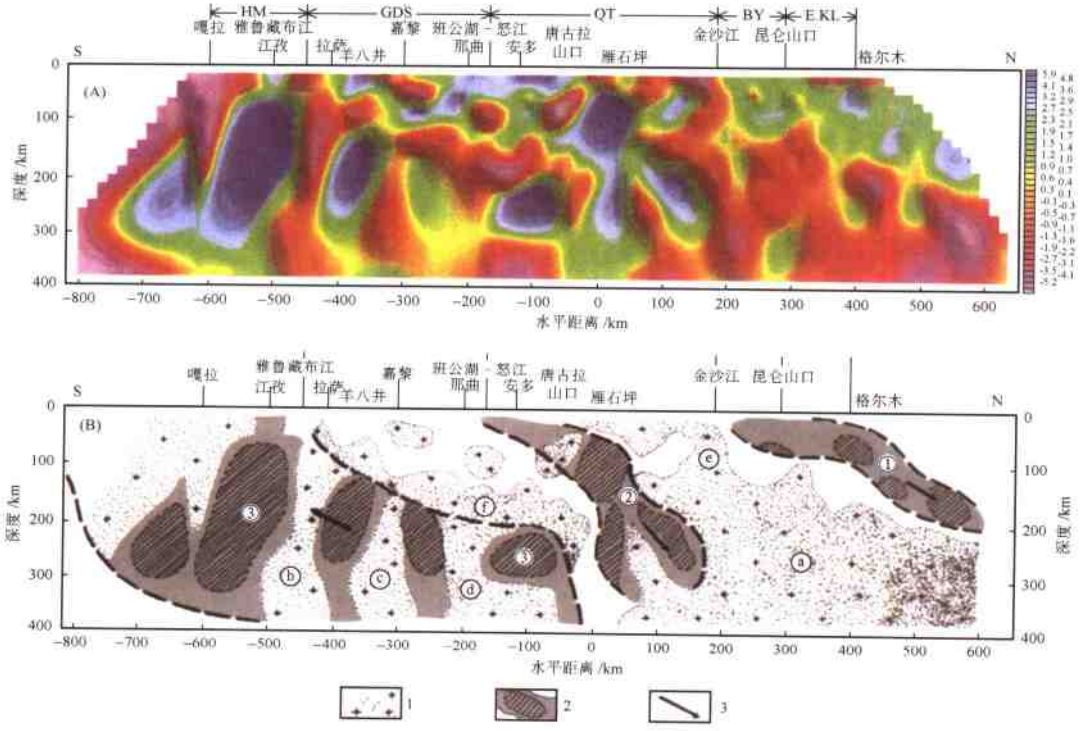

图 3　格尔木-嘎拉天然地震层析剖面及解释剖面

Fig. 3　Golmud-Gala seismic tomographic cross-section and geological interpretation

(A)格尔木-嘎拉天然地震层析剖面;E. KL—东昆仑地体;BY—巴颜喀拉地体;QT—羌塘地体;GDS—冈底斯地体;HM—喜马拉雅地体。(B)格尔木-嘎拉天然地震层析解释剖面:1—低速异常域;2—高速异常域;3—岩石圈板片俯冲方向。ⓐ青藏高原腹地深部大型低速异常体解释为地幔羽;ⓑ雅鲁藏布江地震波低速异常带解释为雅鲁藏布江地幔剪切带;ⓒ嘉黎地震波低速异常带解释为嘉黎地幔剪切带;ⓓ班公湖-怒江地震波低速异常带解释为班公湖-怒江地幔剪切带;ⓔ金沙江地震波低速异常带解释为金沙江地幔剪切带;ⓕ印度岩石圈板片上部的地壳低速熔融层;①东昆仑-金沙江高速异常带解释为古特提斯岩石圈俯冲残片;②班公湖-怒江高速异常带解释为中特提斯岩石圈俯冲残片;③印度高速异常带解释为印度岩石圈俯冲残片

1.2.2　地震波高速异常图像

地震层析剖面中的地震波高速异常图像主要是通过浅部的地震波高速异常体和抵达300～400km 地幔深度的地震波高速异常带的形式表现出来的。

最明显的浅部地震波高速异常体——阿尔金地震波高速异常体在乌图美仁-若羌天然地震层析剖面(图 4-A_1)的浅部低速图像背景中映出,该高速异常体被阿尔金走滑断裂和阿尔金逆冲断裂所夹持,呈楔形几何学产出[42],宽度约 150km,最大厚度 100km,表明了阿尔金地体的无根特征。

格尔木-嘎拉地震层析剖面(图3-A)显示了3 条明显的高速异常带:①位于东昆仑-金沙江缝合带下部的地震波高速异常带,由若干个小型高速异常体组成,整体向北倾斜,倾角约30°～40°,其底界达 200km。②班公湖-怒江缝合带下部的地震波高速异常带(图 3-A),包含3 个高速异常体,以中等角度向北伸入至 300km 深度。③位于青藏高原南部巨厚的喜马拉雅-印度地震波高速异常带(图 3-A),该地震波高速异常带厚达 300km,整体向北缓倾(15°～

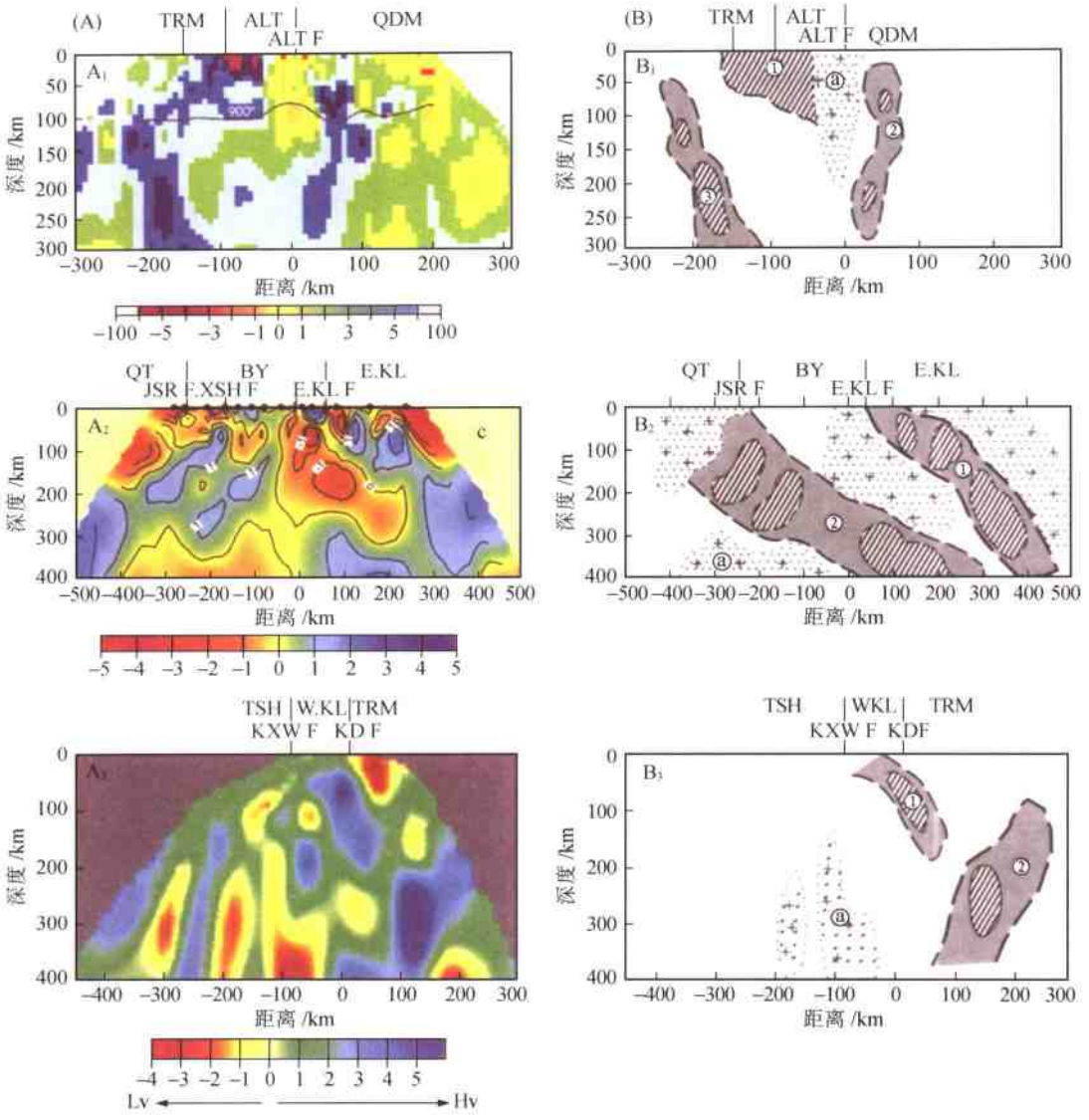

图4　青藏高原乌图美仁-若羌、共和-玉树及叶城-狮泉河天然地震层析剖面及解释剖面

Fig. 4　Urt Moron-Ruoqiang, Gonghe-Yushu and Yecheng-Shiquanhe seismic tomographic cross-sections and geological interpretation of the Qinghai-Tibet Plateau

(A)青藏高原乌图美仁-若羌、共和-玉树及叶城-狮泉河天然地震层析剖面。(B)青藏高原乌图美仁-若羌、共和-玉树及叶城-狮泉河天然地震层析解释剖面;TRM—塔里木地体;ALT—阿尔金地体;QDM—柴达木地体;QT—羌塘地体;BY—巴颜喀拉地体;E. KL—东昆仑地体;TSH—甜水海地体;W. KL—西昆仑地体;ALT F—阿尔金断裂;E. KL F—东昆仑断裂;XSH F—鲜水河断裂;JSR F—金沙江断裂;KD S—库地缝合带;KXW F—康西瓦断裂。A_1—乌图美仁-若羌天然地震层析剖面。B_1:乌图美仁-若羌天然地震层析解释剖面,ⓐ阿尔金地震波垂向低速异常带可解释为阿尔金地幔剪切带;①阿尔金高速异常楔形体表明阿尔金地体为无根地体;②南阿尔金高速异常带可能为加里东期大洋岩石圈俯冲残片;③东塔里木高速异常带可解释为塔里木岩石圈向南东俯冲于阿尔金山之下的俯冲板片。A_2—共和-玉树天然地震层析剖面。B_2—共和-玉树天然地震层析解释剖面,ⓐ青藏高原腹地深部大型低速异常体解释为地幔羽;①东昆仑高速异常带;②金沙江高速异常带,相当于图3中的东昆仑-金沙江高速异常带所代表的古特提斯岩石圈俯冲残片。A_3—叶城-狮泉河天然地震层析剖面。B_3—叶城-狮泉河天然地震层析解释剖面,ⓐ康西瓦深部低速异常带,可能代表深部地幔剪切带;①库地-康西瓦地震波高速异常带,可能代表加里东(印支?)大洋岩石圈俯冲残片;②南塔里木地震波高速异常带代表向南俯冲的塔里木岩石圈板片

20°)，插入雅鲁藏布江以北 400km 的唐古拉山下，顶面达 200km 的深处。该带被若干条垂向低速异常带分割成 4 个断续的近直立椭球形的高速异常体。

此外，在共和-玉树剖面(图 4-A_2)中位于东昆仑-金沙江缝合带下部的地震波高速异常带分为两条，特征十分明显。在叶城-狮泉河天然地震层析剖面中(图 4-A_3)，库地-康西瓦地震波断续高速异常带位于康西瓦缝合带的下部，包含 3 个小型高速异常体，该带在 150km 深度以上以 30°～40°往北倾斜，至 150km 以下变为近直立产出，并伴随强烈地震活动，震源深度达 150km；南塔里木地震波高速异常带(图 4-A_3)位于塔里木地体南缘，地震波高速异常带往南以 60°倾角伸入库地缝合带之下大于 400km 的深度，在 200km 深处似乎将往北倾的康西瓦高速异常带切割。在乌图美仁-若羌天然地震层析剖面(图 4-A_1)中，位于阿尔金低速异常带南侧 50～280km 的深度范围存在一条南阿尔金高速异常带。

1.3 上地幔剪切波各向异性特征

地震波在上地幔中的扩散经常是各向异性的，地震波各向异性可用以示踪地幔动力学。弹性各向异性出现在地震波速度与它的方向有关的地方，在地幔中各向异性构造主要是由于流变引起矿物的优选方位而产生的，这些构造可以用来推测地球内部的流变几何学。地震产生挤压波(P)和剪切波(S)在各向异性岩石中的耦合导致波的散射、双折射和复杂的偏振，这些不同的特征将帮助我们揭示地幔和地壳中岩石结构，及研究地球历史中岩石圈板块的形成和大陆的增生。

青藏高原上地幔剪切波各向异性分布[43～47](图 5)显示了以下特征：①雅鲁藏布江以南喜马拉雅地体的上地幔剪切波各向异性方向为 NNW-SSE 向。②雅鲁藏布江以北青藏高原腹地的上地幔剪切波各向异性方向表现为 NEE-SWW 及 NE-SW 向；羌塘地体中部的上地幔剪切波各向异性方向为近 EW 向，而中东部转为 NEE-SWW 向；在巴颜喀拉地体上地幔剪切波各向异性方向由中部的 SW-NE 向转为东部 NNE-SSW 向，沿金沙江缝合带的玉树一带上地幔剪切波各向异性方向变为平行缝合带的 NW-SE 向；在柴达木-东昆仑地体的上地幔剪切波各向异性方向以 NW-SE 向为主。③上地幔剪切波各向异性在青藏高原西北缘的阿尔金地体中为近 EW 方向，沿阿尔金断裂为平行断裂 NEE-SWW 向。

上述表明上地幔剪切波各向异性的方向在雅鲁藏布江缝合带南北有明显区别，在青藏腹地的北部(柴达木-东昆仑地体)及中南部(巴颜喀拉-羌塘-冈底斯)也有不同，青藏腹地中南部的上地幔剪切波各向异性的方向自西往东由近 EW→NE→NNE 方向转换；沿地体边界及断裂有时出现与之平行的上地幔剪切波各向异性的方向。

2 青藏高原的地幔结构

地震波低速异常体、垂向低速异常带及高速异常带是青藏高原下 400km 深度范围内的最重要的地幔层析图像，对这些图像进行综合地质解释是研究青藏高原地幔结构的初步尝试。

2.1 深部地震波低速异常体及地幔羽

位于青藏高原腹地(东昆仑地体、巴颜喀拉地体及羌塘地体)400km 深度范围内，存在宽度 600km、厚度大于 300km 的巨型地震波低速异常体(图 3-A)，许志琴等曾认为该大型低速异常体为一地幔底辟，与可可西里新生代高钾质火山喷发[48,49]有成因联系[32,41]。现根

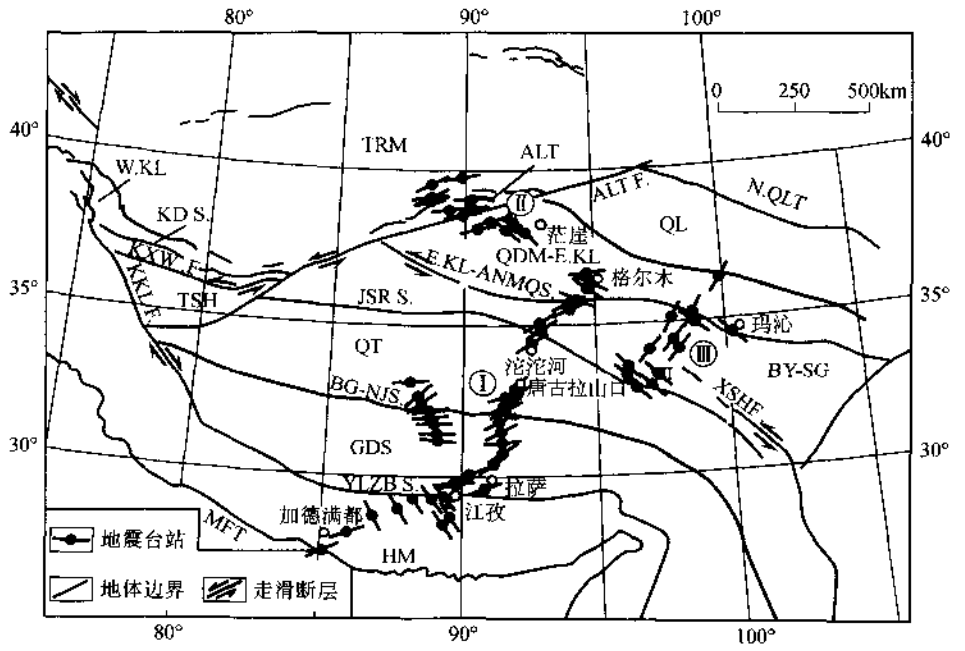

图 5 青藏高原剪切波各向异性图[43]

Fig.5 Shear-wave anisotropy of the Qinghai-Tibet Plateau

Ⅰ—格尔木-唐古拉-嘎拉剖面；Ⅱ—乌图美仁-若羌剖面；Ⅲ—共和-玉树剖面。QL—祁连地体；QDM-E.KL—柴达木-东昆仑地体；BY-SG—巴颜喀拉-松潘甘孜地体；QT—羌塘地体；TSH—甜水海地体；TRM—塔里木地体；GDS—冈底斯地体；HM—喜马拉雅地体；W.KL—西昆仑地体；E.KL-ANMQS.—东昆仑—阿尼玛卿缝合带；JSR S.—金沙江缝合带；BG-NJ S.—班公湖-怒江缝合带；YLZB S.—雅鲁藏布江缝合带；MFT—主前缘逆冲断裂；KXW F.—康西瓦断裂；KKL F.—喀喇昆仑断裂。表示地震波各向异性的黑短线方向代表剪切波快速波方向，黑短线中心的黑点为快速波与慢速波的时间延迟，表示各向异性强度

据地震层析新资料，又可以圈出一个相当规模的深部三维地幔低速异常体，大致相当P.Molnar(1988)[50]的Sn波的缺失区的位置，推测其是由低速高热物质组成，往南有一条低速高热的通道与可可西里火山岩区相连(图6)。

高分辨的全球地震层析结果已经揭示了由高热低速异常体组成的超地幔羽可以在核幔边界存在，并从核幔边界往上横跨上、下地幔之间的不连续面(660km深处)到达浅部地幔中的其它边界，形成小的地幔羽[51]，或者抵达地壳上部，形成一系列的热点[52]，如冰岛、东非、卡那利群岛和黄石公园等之下的热点。热点往往是一些孤立的火山中心，推测其下面有悬浮着的地幔羽状物，热点的膨胀区紧紧夹住悬浮流，热流量由地幔羽传导。世界上最典型的超地幔羽是东非超地幔羽，东非超地幔羽是由低的剪切波速异常体组成的，位于核幔边界。东非超地幔羽的热上涌往上部向东和北东方向偏移，并与东非大裂谷地表的碱性火山岩相连，这种偏移被解释为冈瓦纳大陆的分裂致使非洲板块向北东迁移的结果[53－55]。由此可见，超地幔羽-地幔羽状物-热点是高热低速异常从地球深部到浅部的反映。

青藏腹地的地震波低速异常体位于100～400km深度范围，因此我们可以把它看作为浅部的地幔羽状物，地幔羽的热上涌往上向南偏移，导致可可西里高钾火山岩的喷发，其原因尚待探讨。

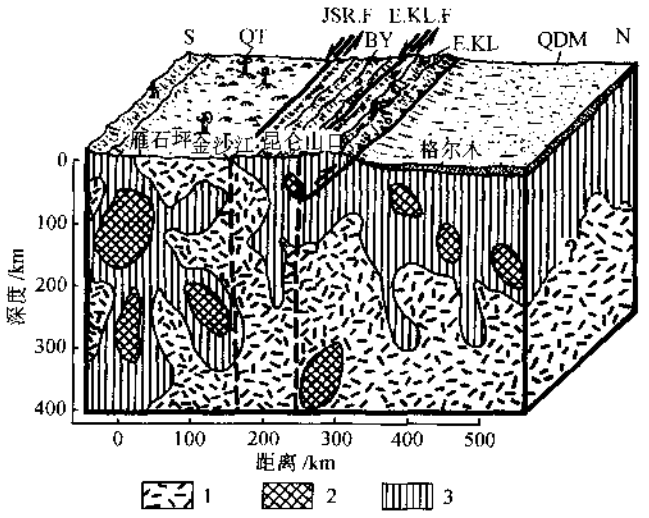

图 6　青藏高原腹地深部地幔羽的立体图示

Fig.6　Block diagram of the mantle plume in the deep interior of the Qinghai-Tibet Plateau

1—地震波低速异常；2—地震波高速异常；3—地震波中速域；QDM—柴达木盆地；E.KL—东昆仑地体；BY—巴颜喀拉地体；QT—羌塘地体；E.KL.F—东昆仑断裂；JSR.F—金沙江断裂

2.2　地幔剪切带

横穿青藏高原的 4 条地震层析剖面揭示了若干条延至地幔深部的垂向地震波低速异常带，它们大多位于地体边界，表明地幔剪切带（或超岩石圈）的特征（图 3，图 4）。

2.2.1　青藏高原北缘的地幔剪切带

阿尔金断裂带位于青藏高原北缘，其主体为 NEE-SWW 向，全长 1800km，自西藏北部的郭扎错、拉竹龙，经新疆硝尔库勒、阿羌、吐拉、索尔库里、老阿克塞县城至甘肃玉门的宽滩山，地表宽度 6～15km。研究表明阿尔金主断裂为韧-脆性走滑剪切带，形成于印支期[23]，经历多期活动，是一条至今仍在活动的走滑断裂，沿阿尔金主断裂走滑位移达 400km[56]。阿尔金断裂带的基本构造样式表现为：以走滑断裂为中心的两侧反向逆冲断裂系、北西侧的阿尔金逆冲断裂及其后部发育的同倾向正断层[23]。乌图美仁-茫崖-若羌天然地震探测剖面（图 4-A_1，图 4-B_1）揭示了阿尔金主断层的深部存在一宽度为 60～80km、延伸超过 400km 的低速异常带，是一条近直立的超岩石圈-地幔剪切带[56]。低速异常带由低速度、低密度的高热物质组成，推测与大规模韧性剪切产生局部熔融有关。代表上地幔物质剪切流动矢量的 SKS 波各向异性强度大，各向异性方向与断裂带一致，也反映了该断裂带在上地幔深部发生了剪切位移。

2.2.2　青藏高原腹地的地幔剪切带

近 EW 向的金沙江断裂西段位于青藏高原腹地巴颜喀拉-松潘甘孜地体与羌塘地体之间，共和-玉树地震层析剖面（图 4-A_2）和格尔木-嘎拉地震层析剖面（图 3-A）均通过该断裂。金沙江断裂在地表由糜棱岩带组成，具左行走滑特征，形成时代为印支期，后经多期活动，也是一条现代活动断裂[19]。格尔木-嘎拉地震层析剖面揭示了金沙江断裂由垂向的地震波低速异常带组成，与北面的巴颜喀拉高速体相间，垂向低速异常带抵达 100km 深度后，插入青藏高原腹地的巨型低速异常体之中，成为与地幔羽沟通的地幔剪切带（图 3）。

2.2.3 青藏高原南部的地幔剪切带

"格尔木-嘎拉"地震层析剖面(图 3-A)揭示了青藏高原南部有 3 条垂向的地震波低速异常带深入地幔之中。位于羌塘地体与冈底斯地体之间的班公湖-怒江走滑断裂叠置在晚侏罗世形成的班公湖-怒江缝合带之上,该断裂的 100km 以下为一条垂向的地震波低速异常带;位于冈底斯地体内部的嘉黎断裂是一条现代大型右行走滑断裂,在剖面中显示了地壳上部有一小型低速体,从深度 100km 到 380km 为垂向低速异常带,后转向北与班公湖-怒江垂向低速异常相连;印度板块与欧亚板块之间的雅鲁藏布江走滑断裂是雅鲁藏布江缝合带基础上发育的,层析图像显示的垂向低速异常带向下延伸超过 400km。上述 3 条地震波低速异常带都是沿剪切断裂向下延伸至地幔深处,并由高热低速的部分熔融物质组成,表明它们是超岩石圈或地幔剪切带(图 3-B)。

2.3 岩石圈俯冲及拆沉的地震层析证据

以 S.P.Grand(1997)[52], R.Van der Voo(1999)[36], R.D.Van der Hilst(1997)[57], H.Bigwaard 和 W.Sjakman(1998)[35]等为首的科学家通过对全球地震层析资料所揭示的地幔中地震波速变化的研究,发现地震资料显示了有的板块可以俯冲到过去不可想象的核幔边界(2891km 深), R.D.Van der Hilst 等(1997)[57]利用体波分辨下地幔中的高速板片构造,发现它们中的大部分可往上一直到达地球表面板块汇聚的俯冲带位置,往下可追踪到核幔边界,提供了从地表俯冲带经地幔一直到核幔边界的由高速体组成的超深俯冲的影像。

横穿北美洲南部的地幔层析剖面[52]揭示了由高速异常体组成的太平洋法拉隆大洋岩石圈板片从北美洲南部海沟表面插到下地幔;通过西喜马拉雅构造结的地幔层析剖面[34,35](图 7)揭示了印度岩石圈板片以高速异常体的形式从地表往北下插,向下变成直立,最后在深部又往南翻转(over-roll)的几何形态,一直俯冲至 800～1000km 的地幔深度;中喜马拉雅的地幔层析剖面揭示了印度岩石圈向北俯冲的板片延伸至 500km 深度,在其下侧存在两个

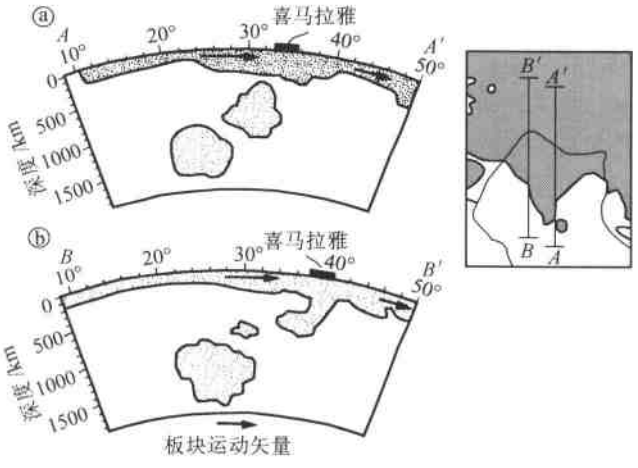

图 7 通过西喜马拉雅和中喜马拉雅地幔地震层析示意剖面[58]

Fig.7 Schematic seismic tomographic cross-sections across the West and Central Himalayas[58]

ⓐ据中喜马拉雅地幔地震层析示意剖面[35]表示的俯冲在中喜马拉雅下的岩石圈位置;ⓑ据西喜马拉雅地震层析示意剖面[35]表示的俯冲在西喜马拉雅下的岩石圈位置

孤立的高速异常体，分别代表25Ma和45Ma之前俯冲和拆沉的印度次大陆的岩石圈残片[58]；穿西伯利亚的地震层析剖面[35]揭示了蒙古-鄂霍茨克-科里亚克高速异常带(M)及其东部的西太平洋高速异常带(P)达到2300km深度，不仅提供了现代太平洋板块同样往西垂直俯冲到核幔边界的地球物理证据，而且揭示了西伯利亚板块与蒙古-北中国板块碰撞所保存的蒙古-鄂霍茨克侏罗纪古大洋岩石圈深俯冲和"拆沉"的历史记录。

上述研究不仅提供了现代大洋和大陆岩石圈超深俯冲的地球物理证据，而且通过大陆板块会聚带的地幔地震层析成果寻找古大洋岩石圈俯冲和"拆沉"的地球物理证据和重塑这一历史过程已成为可能[59]。

青藏高原格尔木-嘎拉剖面(图3-B)、乌图美仁-若羌剖面(图4-B_1)、共和-玉树剖面(图4-B_2)以及叶城-狮泉河剖面(图4-B_3)中位于加里东、古特提斯、中特提斯及新特提斯缝合带下部的高速异常带为我们提供了400km深度范围内大洋/大陆岩石圈俯冲和"拆沉"的新的地球物理证据；塔里木地块向南陆内俯冲于西昆仑之下的证据也在乌图美仁-若羌剖面(图4-A_1，图4-B_1)和叶城-狮泉河剖面(图4-A_3，图4-B_3)的层析图像中得到进一步的显示。

我们曾根据阿尔金断裂两侧加里东构造单元特别是柴北缘与南阿尔金超高压变质带的对比以及阿尔金糜棱岩的年代学测定，指出阿尔金左行走滑断裂形成于印支期(240～220Ma)。由于沿阿尔金断裂分布一系列加里东期蛇绿岩岩块，笔者曾怀疑这些岩块并不一定是印支期阿尔金断裂走滑造成的，可能早在加里东期就存在。乌图美仁-若羌剖面(图4-A_1)中的南阿尔金高速异常带可能代表加里东期沿阿尔金转换带分布的大洋岩石圈俯冲板片拆沉的"化石"残片。在叶城-狮泉河剖面中的库地-康西瓦高速异常带可能代表早期(加里东或印支?)大洋岩石圈俯冲板片拆沉的"化石"残片(图4-B_3)。

在中生代早期，羌塘和巴颜喀拉-松潘甘孜地体以及冈底斯地体已成为从冈瓦纳大陆分离的基墨里大陆的组成部分。伴随新特提斯洋在南面的打开，古-中特提斯大洋岩石圈先后消减，羌塘和巴颜喀拉-松潘甘孜地体成为亚洲大陆在晚三叠世末的增生地体，冈底斯地体成为晚侏罗世-早白垩世的增生地体。我们认为高速异常带出现在古、中特提斯缝合带之位置并向北倾斜产出，可能分别代表了古、中特提斯大洋岩石圈板片曾先后往北俯冲的历史记录，在这些断续的高速异常带中出现若干孤立的高速异常体可以解释为岩石圈板片"拆沉"的结果，为俯冲的"化石"残片。

新特提斯大洋的闭合和印度板块与欧亚大陆碰撞事件发生在50～60Ma前[33]，位于青藏高原南缘的喜马拉雅-印度高速异常带可以认为是印度岩石圈板片插入青藏高原之下的印证。高速异常带的巨厚(300km)特征是与作为地盾的印度岩石圈的厚度相吻合。印度岩石圈板片往北缓倾，直达雅鲁藏布江以远400km的唐古拉山之下。喜马拉雅-印度巨型高速异常带是被地幔剪切带切割成若干个直立椭圆形高速异常体，组成了一条断续高速异常带，这种几何学的特征类似于剪切布丁构造，直立椭圆形高速异常体可以相当于在印度岩石圈板片俯冲过程中分离的残片。笔者认为在400km深度范围的印度岩石圈俯冲板片中不存在新特提斯大洋岩石圈的残片。根据西中喜马拉雅的地幔层析剖面[34,35](图7)，古特提斯大洋岩石圈的残片可能位于800～1000km深度之下。

乌图美仁-若羌剖面(图4-B_1)和叶城-狮泉河剖面(图4-B_3)还揭示了塔里木地块向南俯冲的高速异常带图像：以60°～70°角度向南东俯冲在阿尔金地体下面大于300km的深度，向南俯冲在西昆仑地体下面大于400km的深度。

3 青藏高原碰撞动力学机制的再探讨

在青藏高原形成的碰撞动力学机制问题上一直存在不同的认识:一种认为高原的隆升是整个高原的连续加厚及壳幔之间的广泛性黏性流动的结果,或者是印度板块以低角度往北大规模俯冲于青藏高原之下,形成双层地壳,尔后由于重力均衡造成高原隆升[60,61],藤吉文等(1999)[62]根据地震面波三维速度结构,深部地震探测资料(宽角反射、折射与近垂直反射)和天然地震资料的研究进一步提出"双层楔板"的模式。另一种认为印度板块岩石圈以高角度往北深俯冲于青藏高原之下[63,65];Tapponnier 等人(1977)[16]用印度板块楔往北俯冲造成欧亚大陆向东挤出,来解释印度和欧亚板块碰撞所形成的陆内变形远程效应。某些学者还提出青藏高原的高度是由于地幔的"拆沉"作用[66]或软流圈中的对流作用[50]造成的。最近 Tapponnier 等又提出高原隆升与会聚拼合的岩石圈地体之间的剪切作用有关,提出印度和亚洲大陆碰撞以来斜向右旋隆升和增生的机制使青藏高原向东和北东方向不对称增生,它类似于具走滑分量的加厚地壳的板块构造[33]。

3.1 青藏高原碰撞动力学机制的新模型

在讨论青藏高原碰撞动力学机制时,有必要明确以下几个关键问题:

3.1.1 关于印度岩石圈板片俯冲样式和俯冲深度

印度岩石圈板块究竟往北俯冲多远?以何种样式俯冲?这些是印度-欧亚板块碰撞及青藏高原隆升的重要制约因素。长期以来各种推测和讨论都是依据岩石圈尺度所获得的地球物理资料,并且对俯冲的倾角仍有缓倾和陡倾两种观点。横越西喜马拉雅的地震层析剖面(图 7)揭示了印度岩石圈板块呈翻卷几何学的样式往北超深俯冲于青藏高原之下 800km 深度,但是印度岩石圈板片的前缘在何处,俯冲有多远并不清楚。本研究表明,印度岩石圈板块的喜马拉雅-印度断续高速异常带以极缓的倾角俯冲至雅鲁藏布江缝合带以北 400km 之远的唐古拉山下面 200km 深处,比曾融生等(1998)和 Kosarev 等(1999)认为印度板块前缘到达班公湖-怒江缝合带[67,68]还要远。

在格尔木-嘎拉剖面中,由高速异常体组成的印度岩石圈板片被若干垂向低速异常带所分割,构成以孤立的高速异常体为特征的不连续岩石圈板片,在印度岩石圈板片的上部还存在向北缓倾的不规则的顶面起伏的低速异常层,似乎把垂向低速异常带连接起来。我们对上述复杂的速度图像试作如下讨论:①不连续高速异常体可能反映了被分割的印度岩石圈板片,而不是拆沉的证据。根据西-中喜马拉雅的地震层析剖面的解释,新特提斯大洋岩石圈的"化石"残片已掉入 500km 以下直至 1800km 深的地幔中[34,35](图 7)。②垂向低速异常带位于雅鲁藏布江、嘉黎和班公湖-怒江断裂带的下部,可以解释为地幔剪切带。③印度岩石圈板片以上由低速异常层组成的近水平的地壳熔融层可能也与来自地幔剪切带深部的上升熔融柱有成因联系,高热低速物质通过地幔剪切带聚集在欧亚板块与印度岩石圈板片之间。④印度岩石圈板片的超深俯冲作用可以解释高喜马拉雅变质地体经历超高压变质作用、形成含柯石英的超高压变质带[69~71]的事实。

3.1.2 青藏高原北部周缘克拉通的陆内俯冲新证据

笔者曾认为,青藏高原北部周缘克拉通向南的陆内俯冲作用使祁连山-阿尔金山-西昆仑山崛起以及地壳的强烈缩短[41]。但是河西走廊-北祁连地震反射剖面[72]和格尔木-额济

纳旗地学断面[73,74]虽然揭示了阿拉善地块向南插入祁连山下的现象,但是,显示的俯冲深度很浅(30km)。横穿西昆仑-塔里木结合带的深地震反射剖面[75]显示了塔里木岩石圈下部南倾及西昆仑山下部北倾的强反射结构同时存在的特征,高锐等[75]认为西昆仑山下部北倾的强反射结构可延伸到100km深度,代表了在青藏高原西南缘的印度岩石圈俯冲板片;而本文中所引用的叶城-狮泉河天然地震层析剖面揭示了西昆仑及其两侧在更深尺度(400km)范围的地幔结构,在该剖面中清晰地显示了南塔里木高速异常带为塔里木岩石圈向南陆内俯冲于西昆仑山之下400km的"化石"残片。笔者还认为在乌图美仁-若羌剖面中,东塔里木高速异常带可能代表了塔里木地块岩石圈向南东陆内俯冲的"化石"残片,而不是Wittlinger等(1998)所认为的位于楔形阿尔金高速异常体下部的岩石圈板片[39];因为无论大洋还是大陆岩石圈俯冲板片一般都由高速异常体组成[34,35,52,57]。

3.1.3 岩石圈-地幔剪切带与"右旋隆升"的新机制

根据青藏高原大型走滑断裂研究已提出青藏高原"右旋隆升"的新机制[33],新的地震层析资料表明青藏高原新生代活动的主要走滑断裂大部分为超岩石圈或地幔剪切带,因此可以认为高原"右旋隆升"的机制发生在超岩石圈-地幔的范围。笔者认为在青藏高原腹地的上地幔剪切波各向异性方向自西往东从EW-NE-SE-NNE-SSW的转化是与"右旋隆升"的观点相吻合的。

3.1.4 青藏高原腹地深部的热结构及伸展体制

位于青藏高原腹地100km深度以下的巨型地幔羽与可可西里火山作用有成因联系,表明青藏高原腹地深部具有热结构,青藏高原南缘的陆内超深俯冲与北缘的陆内浅俯冲对高原产生南北向挤压及东西向拉伸,深部挤压环境导致物质熔融和地幔羽的形成,以及物质在地幔中的向东运动,浅部东西向拉伸环境造成南北向裂谷及腹地的火山喷发。

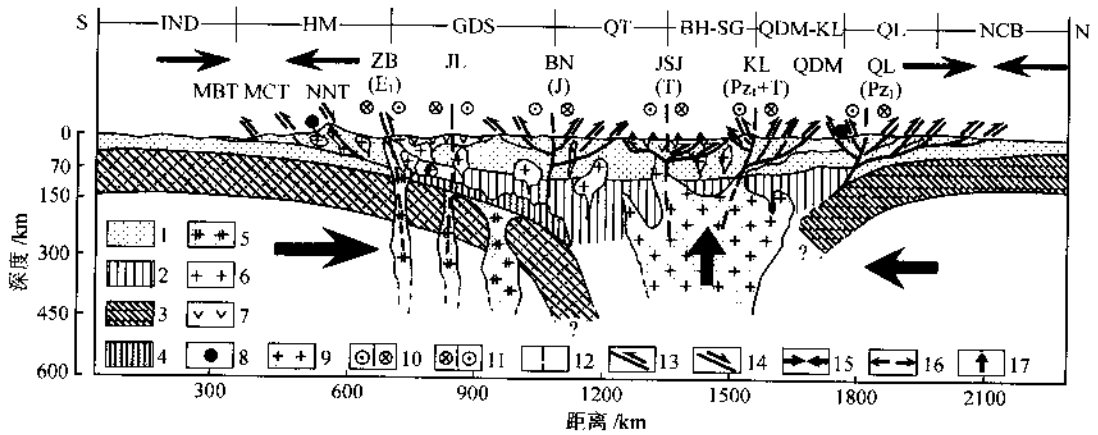

图8 青藏高原隆升的碰撞动力学模式

Fig.8 Collision dynamic model for the uplift of the Qinghai-Tibet Plateau

1—大陆地壳;2—青藏高原岩石圈地幔;3—俯冲大陆的岩石圈地幔;4—翻转的印度俯冲板片在上部的局部熔融层;5—翻转的印度俯冲板片在深部的局部熔融;6—花岗岩;7—火山岩;8—超高压变质柯石英;9—地幔羽;10—左行走滑断裂;11—右行走滑断裂;12—地幔剪切带;13—逆冲断裂;14—正断裂;15—挤压作用;16—拉张作用;17—上升作用

Xu Zhiqin(1999)[41]曾提出青藏高原隆升的"周缘陆内俯冲及内部地幔底辟"的碰撞动力学机制模型。在此基础上,根据新的地震层析资料及地震反射资料,提出了新的模式(图8),新模式可归结为:"青藏高原南部印度岩石圈板片的陆内超深俯冲,北缘克拉通的陆内深俯冲,腹地深地幔羽构造,超岩石圈范围的'右旋隆升'及物质向东挤出。"

4 结论和讨论

长期以来,由于青藏高原深部结构只限于岩石圈范围内讨论,因此对青藏高原碰撞动力学的深部背景的认识受到很大制约。通过横穿青藏高原的4条天然地震层析剖面的横波分裂、三维走时及转换波的资料处理,提供了地震各向异性、地震速度层及400km深度以上的速度图像,揭示了青藏高原地幔结构及物理性质,归结如下:

(1)青藏高原各地体的厚度及地壳平均地震波速度特征反映了各地体的物质组成及结构差异,表明地体拼合的特征。

(2)400km深度范围内的速度图像揭示了青藏高原腹地深部以大型低速异常体为特征的地幔羽的存在,以及通过热通道与可可西里地表大面积分布的新生代碱性火山作用有成因联系。

(3)伸入300km以下的5条垂向低速异常代表高原内部大型超岩石圈-地幔剪切带,伴随局部熔融及高热物质的组成。青藏高原的"右旋上隆"的机制发生在超岩石圈-地幔的范围内。

(4)青藏高原内部的南阿尔金、库地-康西瓦、东昆仑-金沙江和班公湖-怒江高速异常带分别代表了地体拼合的地质历史过程中保留的加里东、古特提斯和中特提斯大洋岩石圈"化石"残片,显示了岩石圈俯冲极性及"拆沉"特征。

(5)巨厚的印度岩石圈板片往北缓倾延伸,直达雅鲁藏布江以北400km的唐古拉山之下。

(6)进一步揭示了青藏高原北部周缘克拉通向南陆内俯冲的特征。

(7)提出青藏高原隆升的新模式为:"青藏高原南部印度岩石圈板片的陆内超深俯冲,北缘克拉通的陆内深俯冲,腹地深地幔羽构造,超岩石圈范围的"右旋隆升"及物质向东挤出。"

本研究是在中法青藏高原地质-地球物理第二轮合作(1994～2001)基础上进行的,曾得到国土资源部(原地质矿产部)重点基础项目"东昆仑造山带的构造演化","祁连山-阿尔金山地质演化及岩石圈剪切作用"[编号9501106],国土资源部科技专项"青藏高原演化与资源"的课题"地体边界和岩石圈断裂对青藏高原形成的贡献"[编号2001010201]及国家自然科学基金重点项目"祁连造山带的组成及造山过程"[编号49732070]的支持。成文过程中与杨文采、高锐研究员、曾令森博士及加拿大达霍西大学Robinson P.教授进行了有益的讨论。

参 考 文 献

[1] XIAO Xuchang, CHEN Guoming, ZHU Zhizhi. Geological and tectonic significance for the Paleo-ophiolites of the Qilian mountains[J]. Acta Geologica Sinica, 1978(4): 281～295 (in Chinese). [肖序常, 陈国铭, 朱志直. 祁连山古蛇绿岩的地质构造意义[J]. 地质学报, 1978(4): 281～295.]

[2] ZUO Guochao, LIU Jichen. Early-Paleozoic tectonic evolution of the North Qilian[J]. Geologica Science, 1987 (1): 14～24 (in Chinese). [左国朝, 刘寄陈. 北祁连早古生代大地构造演化[J]. 地质科学, 1987 (1): 14～24.]

[3] XU Zhiqin, ZHANG Jianxi, LI Haibing. Architecture and orogeny of the Northern Qinling Orogenic Belt, Northwestern China[J]. Journal of the Geological Society of China, 2000, 43 (1): 125～141.

[4] LIU Liang, CHE Zicheng, WANG Yan. Features of the Altun high-press metamorphic belt and it's tectonic significance [J]. Acta Petrologica Sinica, 1999, 15: 57～64 (in Chinese). [刘良, 车自成, 王焰. 阿尔金高压变质带的特征及其构造意义[J]. 岩石学报, 1999, 15: 57～64.]

[5] PAN Yusheng. Tectonic characteristics and evolution of the West Kunlun mountains[J]. Geologica Sinica, 1990, 25 (3): 224～232 (in Chinese). [潘裕生. 西昆仑山构造特征与演化[J]. 地质科学, 1990, 25 (3): 224～232.]

[6] DING Daogui, WANG Daoxuan, LIU Weixin, *et al*. The West Kunlun Orogenic Belt and Basin[M]. Beijing: Geological Publishing House, 1996. 1～230 (in Chinese). [丁道桂, 王道轩, 刘伟新, 等. 西昆仑造山带与盆地[M]. 北京: 地质出版社, 1996. 1～230.]

[7] MATTE P H, TAPPONNIER P, ARNAUD N B, *et al*. Tectonics of Western Tibet, between the Tarim and the Indus [J]. Earth and Planetary Science Letters, 1996, 142: 311～330.

[8] XIAO Xuchang, LI Tingdong. Tectonic Evolution and Uplift of Qinghai-Tibet Plateau[M]. Guangzhou: Guangzhou Science and Tecnology Press, 2000. 1～313 (in Chinese). [肖序常, 李廷栋. 青藏高原的构造演化与隆升机制[M]. 广州: 广东科技出版社, 2000. 1～313.]

[9] ZHANG Qi, ZHOU Guoqing. Ophiolites of China[M]. Beijing: Scientific Press, 2001. 1～182 (in Chinese). [张旗, 周国庆. 中国蛇绿岩[M]. 北京: 科学出版社, 2001. 1～182.]

[10] JIANG Chunfa, YANG Jingsui, FENG Binggui, *et al*. Opening-Closing Tectonics of Kunlun Mountains[M]. Beijing: Geological Publishing House, 1992. 1～224 (in Chinese). [姜春发, 杨经绥, 冯秉贵, 等. 昆仑开合构造[M]. 北京: 地质出版社, 1992. 1～224.]

[11] XU Zhiqin, HOU Liwei, WANG Zongxiu. Orogenic Processes of the Songpan-Ganze Orogenic Belt of China[M]. Beijing: Geological Publishing House, 1992. 1～190 (in Chinese). [许志琴, 侯立玮, 王宗秀. 中国松潘-甘孜造山带的造山过程[M]. 北京: 地质出版社, 1992. 1～190.]

[12] YANG J S, ROBINSON P T, JIANG C F, *et al*. Ophiolites of the Kunlun Mountains, China and their tectonic implications[J]. Tectonophysics, 1996, 258: 215～231.

[13] ZHONG Dalai, WU Genyao, JI Jianqing. Discovery of the ophiolites at Southeastern Yunnan[J]. Chinese Science Bulletin, 1998, 43: 1365～1370 (in Chinese). [钟大赉, 吴根耀, 季建清. 滇东南发现蛇绿岩[J]. 科学通报, 1998, 43: 1365～1370.]

[14] NICOLAS A, GIRARDEAU J, DUPRE B, *et al*. The Xigaze ophiolite (Tibet): A peculiar oceanic lithosphere[J]. Nature, 1981, 294: 414～417.

[15] WANG Xibin, BAO Peisheng, CHEN Keqiao. Ophiolites of Tibet[J]. Regional Geology of China, 1987 (3): 248～256 (in Chinese). [王希斌, 鲍佩声, 陈克樵. 西藏蛇绿岩[J]. 中国区域地质, 1987 (3): 248～256.]

[16] TAPPONNIER P, MOLNAR P. Active faulting and tectonics in China[J]. J Geophys Res, 1977, 82: 930～1095.

[17] PELTZER G, TAPPONNIER P. Formation and evolution of strike slip faults, rifts, and basins during the India-Asia collision: An experimental approach[J]. Journal of Geophysical Research, 1988, 93 (12): 1508～15117.

[18] AVOUAC J P, TAPPONNIER P. Kinematic model of active deformation in central Asia[J]. Geophys Res Lett, 1993, 20: 895～898.

[19] XU Zhiqin, YANG Jingsui, XU Qiang, *et al*. Mesozoic crustal evolution and dynamics of the east Kunlun-Taggula composite mountain chains[A]. Proc 30th Int'l, Geol Congr[C], 1997, 7: 7～20.

[20] XU Zhiqin, ZHANG Jianxin, XU Huifen, *et al*. Ductile Shear Zones of Main Continental Mountain Chains of China and Their Dynamics[M]. Beijing: Geological Publishing House, 1997. 1～294 (in Chinese). [许志琴, 张建新, 徐惠芬, 等. 中国主要大陆山链韧性剪切带及动力学[M]. 北京: 地质出版社, 1997. 1～294.]

[21] XU Zhiqin, QI Xuxiang, LIU Fulai, *et al*. The Kangxiwar Caledonian khondalite series in West Kunlun, China, and its geological significances[J]. International Geological Review, 2004 (in press).

[22] XU Zhiqin, LI Haibing, CHEN Wen, *et al*. A large ductile sinistral strike-slip shear zone and its movement timing in the South Qilian Mountains, Western China[J]. Acta Geologica Sinica, 2002, 76 (2): 183～194.

[23] CUI Junwen, TANG Zhemin, DENG Jinfu, *et al*. Altyn Tagh Fault System[M]. Beijing: Geological Publishing House, 1999. 1～249 (in Chinese). [崔军文,唐哲民,邓晋福,等. 阿尔金断裂系[M]. 北京:地质出版社, 1999. 1～249.]

[24] LI Haibing, YANG Jingsui, XU Zhiqin, *et al*. Geological and geochronogy evidences of Indosinian strike-slipping for the Altyn Tagh Fault[J]. Chinese Science Bulletin, 2001, 46 (16): 1333～1338 (in Chinese). [李海兵,杨经绥,许志琴,等. 阿尔金断裂带印支期走滑活动的地质及年代学证据[J]. 科学通报, 2001, 46 (16): 1333～1338.]

[25] XU Zhiqin, LI Haibing, YANG Jingsui, *et al*. A large transpression zone at the south margin of the East Kunlun Mountains and oblique subduction[J]. Acta Geologica Sinica, 2001, 75 (2): 156～164 (in Chinese). [许志琴,李海兵,杨经绥,等. 东昆仑山南缘大型转换挤压构造带和斜向俯冲作用[J]. 地质学报, 2001, 75 (2): 156～164.]

[26] SEARLE M P. Geology and Tectonics of the Karakoram Mountains[M]. Chichester: J. Wiley & sons, 1991. 1～358.

[27] MURPHY M A, AN Yin, KAPP P, *et al*. Southward propagation of the Karakoram fault system, southwest Tibet: *Timing and magnitude of slip*[J]. *Geology*, 2000, 28: 451～454.

[28] ROGER F. Dations et Tracage des Granitoides Associes a la Chaine de Songpan Garze (West Sichuan, China) Par les Methods U/ Pb, Rb/Sr et Sm/ Nd[D]. These de doctorat, Montpellier II, 1994. 1～200.

[29] TAPPONNIER P. The Ailao Shan/Red River metamorphic belt: Tertiary left lateral hear between Indochina and South China[J]. Nature, 1990, 343: 431～437.

[30] XU Zhiqin. Large shear zones in the main orogenic belts, China[J]. Episodes, 1995, 18: 41～43.

[31] TAPPONNIER P, PELTZER G, LE DAIN A Y. Propagating extrusion tectonics in Asia: New insights from simple experiments with plasticine[J]. Geology, 1982, 10: 611～616.

[32] TAPPONNIER P, XU Zhiqin, ROGER F, *et al*. Oblique stepwise rise and growth of the Tibet Plateau[J]. Sciences, 2001, 294: 1671～1677.

[33] ARGAND E. La tectonique de l'Asie[A]. C R Cong Geol Int[C]. Liege, XIII Sess., Fasc.1, 1922. 171～372.

[34] MOLNAR R, TAPPONNIER P. Cenozoic tectonics of Asia: Effects of a continental collision[J]. Science, 1975, 189: 419～426.

[35] BIGWAARD H, SJAKMAN W. Closing the gap between regional and global travel tomography[J]. J Geoph Res, 1998, 103: 30055～30078.

[36] Van der VOO R, SPAKMAN W, BIJWAAD H. Mesozoic subducted slabs under Siberia[J]. Nature, 1999, 397: 246～249.

[37] WILTTLINGER G, MASSON F, POUPINET G, *et al*. Seismic tomography of northern Tibet and Kunlun: Evidence for crustal blocks and mantle velocity contrasts[J]. EPSL, 1996, 139: 263～279.

[38] XUE Guangqi, JIANG Mei, SU Heping, *et al*. Tomographic study on the tectonics in the depth of Yecheng-Shiquanhe of Tibetan Plateau[J]. Science in China (Series D), 2004, 34 (4): 329～334 (in Chinese). [薛光琦,姜枚,宿和平,等. 利用层析成像研究青藏高原叶城—狮泉河地区深部构造[J]. 中国科学(D), 2004, 34 (4): 329～334.]

[39] WILTTLINGER G, TAPPONNIER P, POUPINET G, *et al*. Tomographic evidence for localized lithospheric shear along the Altun fault[J]. Science, 1998, 282: 74～76.

[40] XU Zhiqin, JIANG Mei, YANG Jingsui. Tectonophysical process at depth for the uplift of the northern part of the Qinghai-Tibet plateau: Illustrated by the geological and geophysical comprehensive profile from Golmud to the Tanggula mountains, Qinghai Province, China[J]. Acta Geologica Sinica, 1996, 70(3): 195～206 (in Chinese). [许志琴,姜枚,杨经绥. 青藏高原北部隆升的深部构造物理作用:格尔木-唐古拉山地质与地球物理综合剖面的解析[J]. 地质学报, 1996, 70 (3): 195～206.]

[41] XU Z Q, JIANG M, YANG J S. Mantle diapir inward intracontinental subduction: A discuss on the mechanism of uplift of the Qinghai-Tibet plateau[J]. Geological Society of America, Special Paper, 1999, 328: 19～31.

[42] XUE Guangqi, QIAN Hui, JIANG Mei, *et al*. Studies on the velocity structure of crust-upper mantle beneath Northeast Qinghai, China[J]. Acta Geoscientica Sinica, 2003, 24 (1): 19～26 (in Chinese). [薛光琦,钱辉,姜枚,等. 青海东北部天然地震探测与岩石圈深部特征[J]. 地球学报, 2003,24 (1): 19～26.]

[43] JIANG Mei, LÜ Qingtian, SHI Danian, *et al*. The study on the structure of crust and upper mantle with natural earthquakes in central Tibetan Plateau[J]. Acta Geophysica Sinica, 1996, 39 (4): 470~481 (in Chinese). [姜枚,吕庆田,史大年,等.用天然地震探测青藏高原中部地壳、上地幔结构[J].地球物理学报,1996,39(4):470~481.]

[44] JIANG Mei, XU Zhiqin, HIRN A, *et al*. Teleseismic anisotropy and corresponding features of upper mantle in Tibet Plateau and its Neighboring areas[J]. Acta Geoscientia Sinica, 2001, 22 (2): 111~116 (in Chinese). [姜枚,许志琴,HIRRN A,等.青藏高原及其部分邻区地震各向异性和上地幔特征[J].地球学报,2001,22 (2):111~116.]

[45] HIRN A, JIANG M, SAPIN M, DIAZ J, *et al*. Seismic anisotropy as an indicator of mantle flow beneath the Himalayas and Tibet[J]. Nature, 1995, 375: 571~574.

[46] DONG Yingjun, XUE Guangqi, MA Kaiyi. Studies on share wave anisotropy beneath Altyn-fault system and its adjacent area[J]. Progress in Geophysics, 1999, 14 (4): 58~63 (in Chinese). [董英君,薛光琦,马开义.阿尔金断裂带各向异性研究[J].地球物理学报,1999,14 (4):58~63.]

[47] JIANG M, QIAN H, SU H P. Teleseismic anisotropy and its features in the upper mantle beneath the Tibet plateau and neighboring areas[J]. Metallogenic implications Global Tectonics and Metallogeny, 2003, 8(1~4): 1~2.

[48] DENG Wanming. The Quaternary volcanic petrology and geochemistry in the Northern Tibet-A preliminary study[J]. Acta Geologica Sinica, 1978, 2: 148~162.

[49] DENG Wanming. Cenozoic volcanism and intraplate subduction in northern margin of the Tibet plateau [J]. Journal of Geochemistry, 1991, 10: 140~152.

[50] MOLNAR P. A review of geophysical constraints on the deep structure of the Tibetan Plateau, the Himalaya and the Karakoram, and their tectonic implications[J]. Phil Trans R Soc Lond, 1988, A326: 33~88.

[51] CONDIE K C. What is a superplume[A]? Superplume International Workshop Abstract[C]. Tokyo, Japan, Jan.28~31. 2002. 20~21.

[52] GRAND S P, Van der HILST R D, WIDIYANTORO S, *et al*. Global seismic tomography: A snapshot of convection in the Earth[J]. Geol Soc Am Today, 1997, 7(4): 1~7.

[53] RITSEMA J H J, HEIJST V, WOODHOUSE J H. Complex shear velocity structure beneath African and Iceland [J]. Science, 1999, 286: 1925~1928.

[54] RITSEMA J, NI S, HELMBERGER D V, *et al*. Evidence for strong shear velocity reductions and velocity gradients in the lower mantle beneath Africa [J]. Geophysical Research Letters, 1998, 25: 4245~4248.

[55] RITSEMA J. Structure of the African superplume [A]. Superplume International Workshop Abstract[C]. Tokyo, Japan, Jan. 28~31. 2002. 37~39.

[56] XU Zhiqin, YANG Jingsui, ZHANG Jianxin, *et al*. A comparison between the tectonic units on the two sides of the Altun sinistral strike-slip fault and the mechanism of lithospheric shearing[J]. Acta Geologica Sinica, 1999, 73 (3): 193~205 (in Chinese). [许志琴,杨经绥,张建新,等.阿尔金断裂两侧构造单元的对比及岩石圈剪切机制[J].地质学报,1999,73 (3):193~205.]

[57] Van der HILST R D, WIDIYANTORO S, ENGDAHL E R. Evidence for deep mantle circulation from global tomography[J]. Nature, 1997, 386: 578~584.

[58] CHEMENDA A I, BURG J P, MATTAUER M. Evolutionary model of the Himalaya-Tibet system: Geopoem based on new modeling[J]. Earth and Planetary Science Letters, 2000, 174: 397~409.

[59] XU Zhiqin, ZHAO Zhixing, YANG Jingsui, *et al*. Tectonics beneath plates and mantle dynamics [J]. Geological Bulletin of China, 2003, 22 (3): 149~159 (in Chinese). [许志琴,赵志兴,杨经绥,等.板块下的构造及地幔动力学[J].地质通报,2003,22 (3):149~159.]

[60] POWELL C Mc A, CONAGHAN P J. Plate tectonics and the Himalayas [J]. Earth and Planetary Science Letters, 1973, 20: 1~12.

[61] BEGNOUL N, BARAZANGI M, ISACKS B L. Lithospheric structure of Tibet and western north America: mechanisms of uplift and a comparative study[J]. Journal of Geophysical Research, 1993, 98: 1997~2016.

[62] TENG J W, ZHANG Z J, WANG G J, *et al*. A new model for deep-seated dynamics and continent-continent collision of Himalaya orogenic belt[J]. Chinese Journal of Geophysics, 1999, 42 (4): 481~493 (in Chinese). [滕吉文,张中

杰,王光杰,等. 喜马拉雅碰撞造山带的深层动力学过程与陆-陆碰撞新模型[J]. 地球物理学报, 1999, 42 (4): 481~493.]

[63] COWARD M P, BUTLER R W H. Thrust tectonics and the deep structure of the Pakistan Himalaya [J]. Geology, 1985, 13: 417~420.

[64] COWARD M P, BUTLER R W H, CHAMBERS A F, *et al*. Folding and imbrication of the Indian crust during Himalayan collision[J]. Phil Trans R Soc Lond, 1988, A326: 89~116.

[65] MATTAUER M. Intracontinental subduction, crust mantle decollement and crustal stacking wedge in the Himalaya and other collision belts[J]. Spec Publ J Geol Soc London, 1986, 19: 37~50.

[66] ZHAO W L, MOEGAN W J. Uplift of the Tibetan Plateau[JJ]. Tectonics, 1985(4): 359~369.

[67] CENG R S, DING Z F, WU Q J. Crustal Structures of Himalaya-Qilianshan and continent-continent collision process [J]. Chinese Journal of Geophysics, 1998, 41 (1): 49~60 (in Chinese). [曾融生,丁志峰,吴庆举. 喜马拉雅-祁连山地壳构造与大陆-大陆碰撞过程[J]. 地球物理学报, 1998, 41 (1): 49~60.]

[68] KOSAREV G, KIND R, SOBOLOV S V, *et al*. Seismic evidence for a detached Indian lithospheric mantle beneath Tibet[J]. Science, 1999, 283: 1306~1309.

[69] KANEKO Y, YAMAMOTO H, KATAYAMA I, *et al*. Coesite inclusions and prograde compositional zonation of zircons in Himalayan gneisses, NW Himalaya, Pakistan: Evidence from SHRIMP-dating of coesite-bearing zircon [A]. Abstract of UHPM Workshop. Fluid/Slab/Mantle Interactions and Ultrahigh-P Minerals[C]. Tokyo: Waseda University, 2001. 121~123.

[70] SACHAN H K, MUKHERJEE B K, OGASAWARA Y, *et al*. Discovery of Coesite from Indian Him Mantle Interactions and Ultrahigh-P Minerals[C]. Tokyo: Waseda University, 2001. 124~128.

[71] O'BRIEN P J, ZOTV N, LAW R, *et al*. Coesite in Himalayan eclogite and implications for models of India-Asia collision [J]. Geology, 2001, 29: 435~438.

[72] WU Xuanzhi, WU Chunling, LU Jie. Research on the fine crustal structure of the northern Qilian-Hexi corridor by deep seismic reflection [J]. Acta Geophysica Sinica, 1995, 38 (Suppl II): 29~35 (in Chinese). [吴宣志,吴春玲,卢杰. 利用深地震反射研究北祁连-河西走廊地壳细结构[J]. 地球物理学报, 1995, 38 (增刊 II): 29~35.]

[73] GAO Rui, CHENG Xiangzhou, DING Qian. Preliminary geodynamic model of Golmud-Ejin Qi geoscience transect[J]. Acta Geophysica Sinica, 1995, 38 (Suppl II): 3~14 (in Chinese). [高锐,成湘洲,丁谦. 格尔木-额济纳旗地学断面地球动力学模型初探[J]. 地球物理学报, 1995, 38 (增刊 II): 3~14.]

[74] GAO Rui, CHENG Xiangzhou, WU Gongjian. Lithospheric structure and geodynamic model of the Golmud-Ejin Qi transect in northern Tibet [J]. Geological Society of America, Special Paper, 1999, 28: 9~17.

[75] GAO Rui, XIAO Xuchang, LIU Xun, *et al*. Detail lithospheric structure of the contact zone of West Kunlun and Tarim evealed by deep seismic reflection profile along the Xinjiang Geotransect [J]. Acta Geoscientia Sinica, 2001, 22 (6): 547~552 (in Chinese). [高锐,肖序常,刘训,等. 新疆地学断面深地震反射剖面揭示的西昆仑-塔里木结合带岩石圈细结构[J]. 地球学报, 2001, 22 (6): 547~552.]

Mantle structure of Qinghai-Tibet Plateau: Mantle plume, mantle shear zone and delamination of lithospheric slab

XU Zhi-qin[1] JIANG Mei[1,2] YANG Jing-sui[1] XUE Guang-qi[1,2] SU He-ping[1]
LI Hai-bing[1] CUI Jun-wen[1] WU Cai-lai[1] LIANG Feng-hua[1]
(1. Key Laboratory of Continental Dynamics, Institute of Geology, CAGS, Beijing 100037, China; 2. Institute of Mineral Resources, CAGS, Beijing 100037, China)

Abstract By using four seismic tomographic profiles of nearly 8000km long across the Qinghai-Tibet Plateau, we obtained the crustal and mantle velocity images and seismic wave anisotropy over the depth down to 400km, which revealed significant characteristics of the crust and mantle structure in the region. The mantle velocity images indicate the presence of a mantle plume characterized by a large low-velocity anomalous body beneath the interior of the Qinghai-Tibet Plateau; this feature shows its genetic relationship to the widespread Hoh-Xil Cenozoic potassic and alkaline volcanism through a thermal channel. The Altyn Tagh, Kangxiwa, Jinshajiang, Jiali and Yaluzangbu strike-slip faults extend downward to the depth of 300～400km, which demonstrate the characteristics of a vertical low-velocity anomalous zone composed of high temperature material and the existence of large-scale translithospheric or mantle shear zones. The discontinuous anomalous high-velocity zones under the Kangxiwa, East Kunlun-Jinsha River, Bangong Lake-Nu River and Yaluzangbu sutures are tentatively interpreted as the "fossil" slab remnants of Caledonian, Paleo-Tethyan and Meso-Tethyan oceanic lithosphere preserved during the terrane amalgamation and collision; they formed several slab remnants separating the anomalous low-velocity zones, and can be the geophysical evidence for "delamination". The Indian lithospheric slab, which is marked by a gigantic, discontinuous anomalous high-velocity zone, was subducted gently northward to a depth of 300～400km beneath the Tanggula Mountains. Based on the new tomographic data across the Himalaya and Tibet plateau, we proposed a new collisional model for the uplift of the Tibet plateau, which involves the "roll over" of the subducted Indian lithospheric slab beneath the south of the Tibetan Plateau, the southward intracontinental subduction of the cratonic lithosphere in the northern margin of the plateau, the upwelling of the deep mantle plume in the interior of the plateau, and the "dextral uplift" of the plateau within the limits of the deep mantle, as well as the motion and the extrusion of material toward the east and the northeast.

Key words Qinghai-Tibet Plateau seismic tomographic profile mantle plume mantle shear zones delamination of lithospheric slab

板块下的构造及地幔动力学[0]

许志琴[1]　赵志新[1]　杨经绥[1]　袁学诚[2]　姜　枚[1]
(1. 中国地质科学院地质研究所大陆动力学实验室　北京　100037;
2. 国土资源部高咨中心　北京　100812)

摘　要　最新的全球地幔地震层析资料揭示了岩石圈板片可以俯冲到核幔边界,超地幔羽可以从核幔边界上升到地壳上部形成热点。在大陆板块汇聚边界,地幔地震层析图像不仅显示了岩石圈板片的超深俯冲,还保存了拆沉的岩石圈"化石"残片的重要信息。从地幔深部所获取的新资料为全地幔"单层对流"的新模式提供了依据。在介绍上述全球构造研究新动向的基础上,本文强调了研究岩石圈板块必须了解板块下的构造,探索岩石圈板块的驱动力应该从"岩石圈动力学"升华到"地幔动力学",并提出了大陆板块汇聚边界地幔动力学研究的新思考。

关键词　板块下的构造　超深俯冲　核幔边界　超地幔羽　地幔动力学
中图分类号:P541　**文献标识码**:A　**文章编号**:1671　2552(2003)03－0149　11

板块理论被公认为20世纪自然科学领域的五大成就之一,该理论的提出是一次地学革命,因为它重新调整了人们对地球动力学的认识。

根据板块观点,板块之间不断发生水平位移,它们的离散和分开形成了大洋,它们的汇聚与碰撞又形成山脉。研究表明,在地质历史中板块聚敛速度是很快的,东太平洋与美洲大陆之间的洋陆聚敛速度为10cm/a,西太平洋板块和亚洲大陆之间达10～17cm/a,而印度板块俯冲于欧亚板块之下的陆陆聚敛速度达5cm/a[1]。当板块汇聚和对接时,一个板块俯冲于欧亚板块之下,并使俯冲带及其板块边缘两侧的地壳发生强烈挤压和褶皱,形成碰撞造山带。研究还表明,许多板块的俯冲首先从"洋内俯冲"开始,然后经过大洋板块插入大陆板块之下的"洋陆俯冲",最后是一个大陆板块俯冲到另一大陆板块下面的"陆陆俯冲"[1,2]。

基于此,一个重要问题便引申出来,板块本身究竟能插入到地幔多大深度?

根据沿俯冲带的地震震源中心位置与深度资料,地学家们曾认为板块只插入地球内部数百公里深度(不超过600～700km),即板块可产生向下数百公里深度的俯冲作用;同时进一步认为随深度增加,温度和压力值增大,岩石圈板块会变软,降低了下插的能干性,而消失在软流圈中。但是,最近以Grandt[3],R.V.der Voo[4],Van der Hilst[5],Widiyantoro[6],Bigwaard[7]和Kendall,J.M[8]等为首的科学家通过对最新全球地震层析资料揭示的地幔中地震波速变化的研究,认为有的板块可以俯冲到过去不可想象的核幔边界(2891km深),从

[0] 地质通报,2003年第22卷第3期。
收稿日期:2002－12－30;修订日期:2003－03－05。
作者简介:许志琴(1941－),女,留法博士,研究员,中国科学院院士,从事大地构造学及构造地质学研究。

而提出了新的假设。

随之，另一个重要问题提了出来，地球内部究竟存在什么样的物质运动方式？

长期以来，地学家们用地球内部的对流来解释地球热历史、地球内部物质成分及分异过程。最初的板块观点认为，地球表面板块运动的几何学是简单的，板块的水平位移使冷板块插入热地幔中，又因为大洋中脊的热物质上升而得以补偿，曾提出"双层对流"模式。"双层对流"是由上地幔中的小对流环与下地幔的大对流环组成的，两个对流体系是独立的，中间为410～660km深度的过渡带所分开，因为在理论上过渡带上、下的地幔流变学存在差异。但最新的全球地震层析资料揭示了板块可俯冲到过去不可想象的深度，这对于"双层对流"模式无疑是一种挑战。

最近，Mattauer[9,10]强调最新的全球地震层析资料使地学家们重新考虑板块插入地幔及重新认识山脉的形成，提出研究地幔动力学具有重要意义。

本文通过最近几年来国际上已发表的全球最新的深部地震层析资料，介绍地幔层析、岩石圈板片的超深俯冲、超地幔羽的研究进展以及新的"地幔对流"观点和"板块下构造"的新假设、新模式，进而强调从"岩石圈动力学"到"地幔动力学"的地学研究新阶段已经到来。

1 地幔层析及岩石圈板片的超深俯冲

地壳与地幔的分界面为莫霍面，地幔又可分为上地幔(650km以上)及下地幔(650～2891km)，下地幔与地核的边界通常称为"D"层。进入地幔后地震波速度突然增大到8.1km/s，在莫霍面至150km深度的上地幔中，地震波速度变化不大，但到150～250km深度速度变低(P波速度为7.4km/s，S波速度为4.2km/s)，称为古登堡低速层(地幔软流层)。该层在全球普遍存在，又可称软流圈。在深度410～660km过渡带处，由于相变地震波速度突然增大；650km以下的地震波速度缓慢增大[11]。

地震层析的原理相当于医学上的"CT"，根据与俯冲相关的毕尼奥夫带的深源地震位置及形状，可以直接推测出俯冲板片下沉体的深度。但是深度加大时"CT"的追踪则失效，因此，许多研究都停留在上、下地幔界线附近的俯冲板片的行为上。在此处深部地震活动停止，并出现明显的不连续面，推测可能标志其物质化学相的变化，这种变化大大阻止了物质在上、下地幔之间的流动。因而，上、下地幔的界线似乎成了岩石圈俯冲板片继续往下插入的禁区。那么这些板片在660km之下的地幔中命运究竟如何？

最新的全球地震层析图像[5]包含了地幔地震构造的高分辨的P波和S波模型。两种模型是通过体波资料获得的，但数据的类型、选取和处理过程是不同的。P波模型运用国际地震中心的走时数据绘制了P波速度在地幔中的三维变化[5]，S波模型通过多次波动的剪切波资料绘制了地幔中的剪切波速的变化。这两种模型虽然是运用不同的反演技术和不同的数据组合而分别得到的，但它们对整个地幔中的许多大小规模的构造，甚至短波长的构造显示了相当的一致性(图1)。

特别是在板块汇聚边界，利用体波分辨的下地幔高波速异常为线型窄长构造，发现它们中的大部分可往上一直到达地壳表面俯冲带位置，往下追踪到核幔边界"D"层，展现了从地表俯冲带经中地幔一直到核幔边界的由高速体组成的超深俯冲图景。

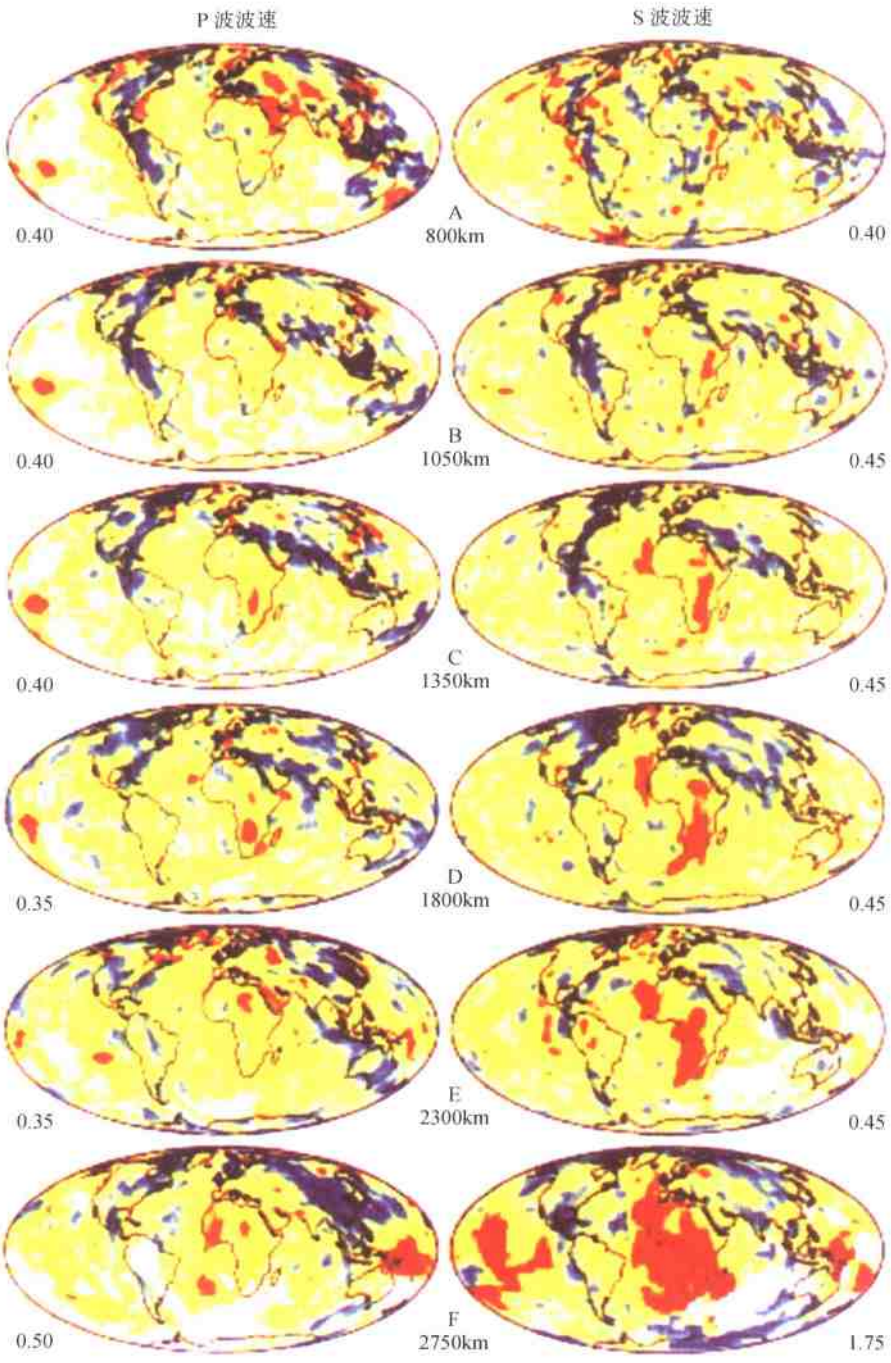

图 1　全球 P 波和 S 波对比模式

(据 R. D. Van der Hilst 等,1997[5])

Fig. 1　Comparative model of global P waves and S waves

显示通过下地幔不同深度(800km、1050km、1350km、1800km、2300km、2750km)P 波和 S 波地震波速的变化,两边的数字是平均波速不同百分比中的最大异常,蓝色代表高波速,红色代表低波速

在最新的全球高分辨 P 波和 S 波的地震层析图像(图 1)中,在北美洲法拉隆板块(Farallon)、南欧亚大陆的特提斯板块、西太平洋板块(Izangi 和 Kula)、西北太平洋板块[12]及太平洋 Tonga 板块[13]660km 之下都出现了线性高速异常体,异常体与上地幔板片相连接,并有一部分往下延伸到下地幔下部[13]。

下地幔最底部的地震构造与中地幔不同,无明显的线性特征。这可以解释为地幔最深处粘度的增加引起下沉板块的横向模糊图像;但是,核幔边界的高速异常区依然存在,可以解释为俯冲岩石圈的最后栖息地。

下面通过全球两个新的 P 波速和 S 波速在不同地幔深度的高分辨地幔层析图像以及地幔层析剖面的分析,来了解北美洲、南欧亚大陆及西伯利亚等板块汇聚边界的中下地幔构造模式。

1.1 北美洲的中下地幔构造

在不同地幔深度 P 波速和 S 波速高分辨地幔层析图像中,P 波速和 S 波速的两个模型几乎完全一致。在北美洲东部的下地幔上部的 800km 深度,高速异常带在平面上沿走向从 30°S 延伸到 50°N;在下地幔中部(1050～1350km),高速异常带往北继续延伸到 Hudson 湾的西岸和北阿拉斯加。在北美洲南部,P 波速和 S 波速两个模式均显示高速异常带在 1300km 的深度终止,但在下地幔下部(1800～2300km)显示了简单线性构造的扩散(图 2)。

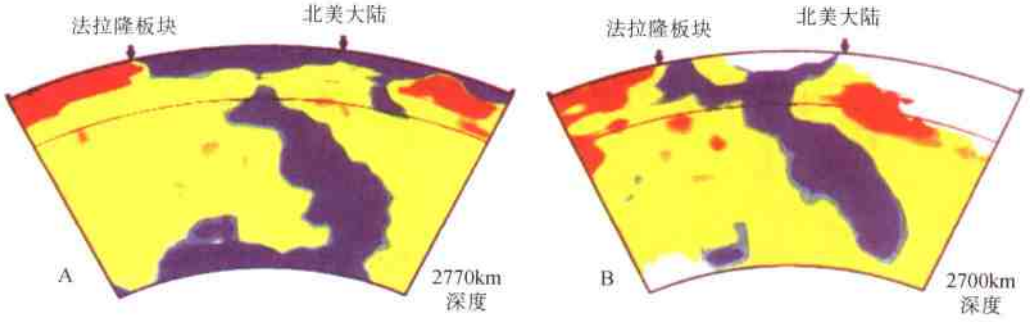

图 2 通过北美洲南部地幔中 P 波(A)和 S 波(B)波速变化剖面

(据 Grandt, S. P. 等,1997[3])

Fig. 2 Section of P—wave(A) and S—wave(B) velocity variations penetrating through the mantle beneath southern North America

图像显示了从地表至核幔边界不同深度相对全球平均波速的波速变化,蓝色代表高于平均波速,红色代表低于平均波速。穿过整个地幔的大的蓝色板状异常可能代表过去 100Ma 中俯冲下沉的法拉隆板块。S 波与 P 波模型在转换带(400～600km)及地幔底部的构造的不同是由于两种研究的数据采集不同

横穿北美洲南部的地幔层析剖面[3]的端点位于 30.1°N,117.1°W 和 30.2°N,56.4°W,揭示了太平洋东侧的法拉隆大洋板块与北美洲板块的洋陆板块汇聚边界从地球表面至核幔边界的 P 波速地震层析图像,记录了由高速异常体组成的法拉隆大洋岩石圈板片在 50～100Ma 期间从北美洲南部海沟表面下插到下地幔的历史。很明显,高速异常体越过了 660km 的上、下地幔的过渡带直至核幔边界,并在上述不同地幔深度的高分辨地幔层析图像中显示了纵向的连续性。Grandt 等[3]认为,北美洲下面的高速异常体的底部是 50Ma 俯

冲的板片前缘,利用板片在上地幔下沉速率 10cm/a,可推测板片在下地幔的下沉速率大约为 1～1.5cm/a。板片下沉速率的减小意味着俯冲阻力随深度的增加,这与粘度随深度增加一致,或者与 660km 深处吸热相的改变有关。法拉隆大洋板块的俯冲与大西洋的打开有关[7]。

上述表明,北美洲的中下地幔构造的地震图像显示了法拉隆大洋岩石圈板片超深俯冲的特征。

1.2　南欧亚大陆的中下地幔构造

在欧亚大陆南部存在一条近 EW 向往东又转为 NW-SE 向的特提斯构造带,从南欧地中海、阿尔卑斯往东经喜马拉雅延至印度尼西亚,长达 15000km,为北面的欧亚板块与南面的非洲板块、阿拉伯板块及印度-澳大利亚板块碰撞的产物。在 P 波速和 S 波速的高分辨地幔层析图像(图 1)中,该带的 S 波和 P 波模型中的高速异常带表现出复杂性:下地幔上部的高速异常带在 1800km 以下显示了该带在平面上的逐渐连续;在 1200～1800km 之间高速异常带从地中海一直到印度尼西亚完全连接;1800km 之下高速异常带只在 S 波速的地幔层析图像中有断续显示。

通过印度、西藏及邻近的印度洋下面的西喜马拉雅地幔层析剖面[4](图 3),揭示了不同深度的一些高速异常体的存在。在北东阿富汗的兴都库什地区上地幔 600km 范围内,高速异常板片向北倾斜并与印度板块岩石圈连接;在北巴基斯坦,同样的高速异常板片显示了"翻转构造",即印度板片高速异常体从地表往北下插,向下变成直立,最后在深部 600～800km 深度又往南翻转,表明印度板片以"翻转"几何形态俯冲至地幔深度;往东及南东的尼泊尔附近 450km 以下的高速异常体与兴都库什俯冲板片相连接,但与 350km 以上的岩石圈板片是分开的。这些异常体可以解释为板块碰撞之后大印度板块与亚洲板块汇聚过程中拆离的印度次大陆的岩石圈残片。

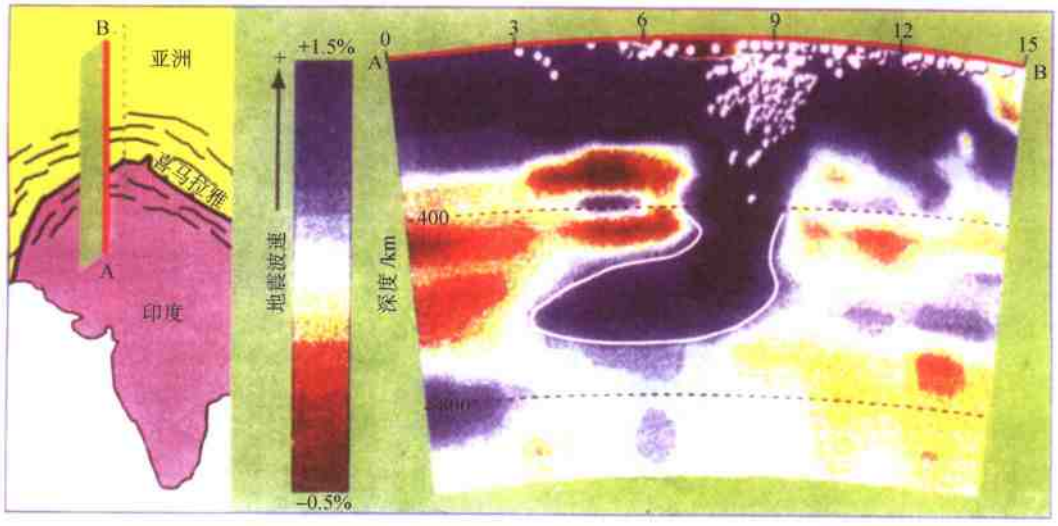

图 3　西喜马拉雅 1000km 深度范围内地震层析剖面

(据 H. Bigwaard,1998[7];Grandt,S. P. 等,1997[3])

Fig. 3　Seismic tomographic section in the 1000km depth range below the western Himalayas

蓝色代表高于平均波速,红色代表低于平均波速。图像显示了印度岩石圈板块呈"翻转构造"几何学插入下地幔中

在印度次大陆下面1000～2300km的下地幔深度范围内，还出现4个与浅部高速异常体析离的高速异常体，有的甚至掉到核幔边界的深度。这些异常体在纵向上形成3条平行于WNW-ESE方向延伸的带。R.V.der Voo等[4]认为，这些下地幔的高速异常体可解释为新特提斯洋封闭、两大陆碰撞后印度大陆俯冲岩石圈下部拆沉的大洋岩石圈残片(图4)，其中南面的Ⅱ、Ⅲ两个异常体代表新特提斯洋岩石圈残片，Ⅳ代表将拆沉的印度大陆俯冲岩石圈，位于北面的Ⅰ可能代表了中特提斯洋岩石圈残片。西喜马拉雅地震层析剖面不仅证明了拆沉构造的假设，而且反映了在大洋岩石圈板片拆沉之前存在大洋岩石圈超深俯冲。

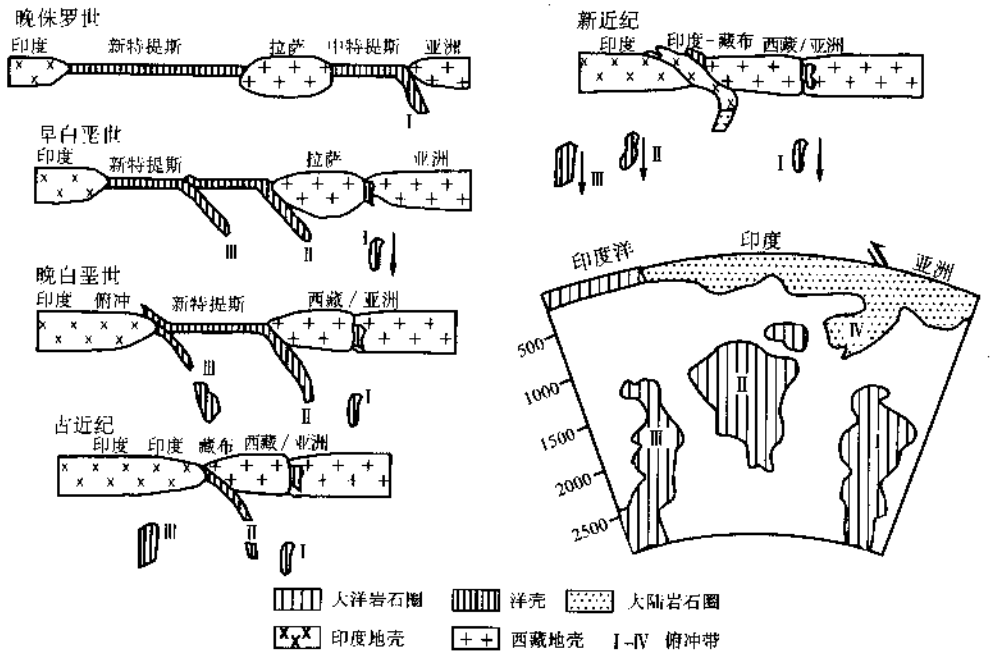

图4 通过印度洋、印度和西藏的地幔(2500km深度范围内)地震层析示意剖面(下图)及特提斯演化模式(上图)

(据R.V.der Voo, 1999[4])

Fig.4 Seismic tomographic section crossing mantle (in the 2500km depth range) beneath the Indian, India and Tibet (below, Fig.) and evolution model for Tethyan (upper Fig.)

Ⅰ代表中特提斯洋岩石圈残片，Ⅱ、Ⅲ为新特提斯洋岩石圈残片，Ⅳ代表将拆沉的印度大陆岩石圈

1.3 西伯利亚的中下地幔构造

位于亚洲东北部西伯利亚地区的蒙古-鄂霍次克-弗霍扬次克缝合带是早白垩世前西伯利亚板块与蒙古-北中国板块碰撞所保存的蒙古-鄂霍次克侏罗纪大洋岩石圈的记录。

在地壳中，蒙古-鄂霍次克-科里亚克缝合带从贝加尔湖以北经鄂霍次克海到达科里亚克山脉，长达4000km。近来R.Van der Voo等[14]的研究表明，通过蒙古-鄂霍次克-科里亚克缝合带的P波速在地壳及上地幔中有显示，在面波中也有表现。西伯利亚地区新的地震层析资料获得了西伯利亚的中下地幔构造的图像(图5)。在1200km深度，高分辨的高速异常(M)无论在垂向上还是在水平方向上都十分清晰；在大于1500km深度，高速异常带在平

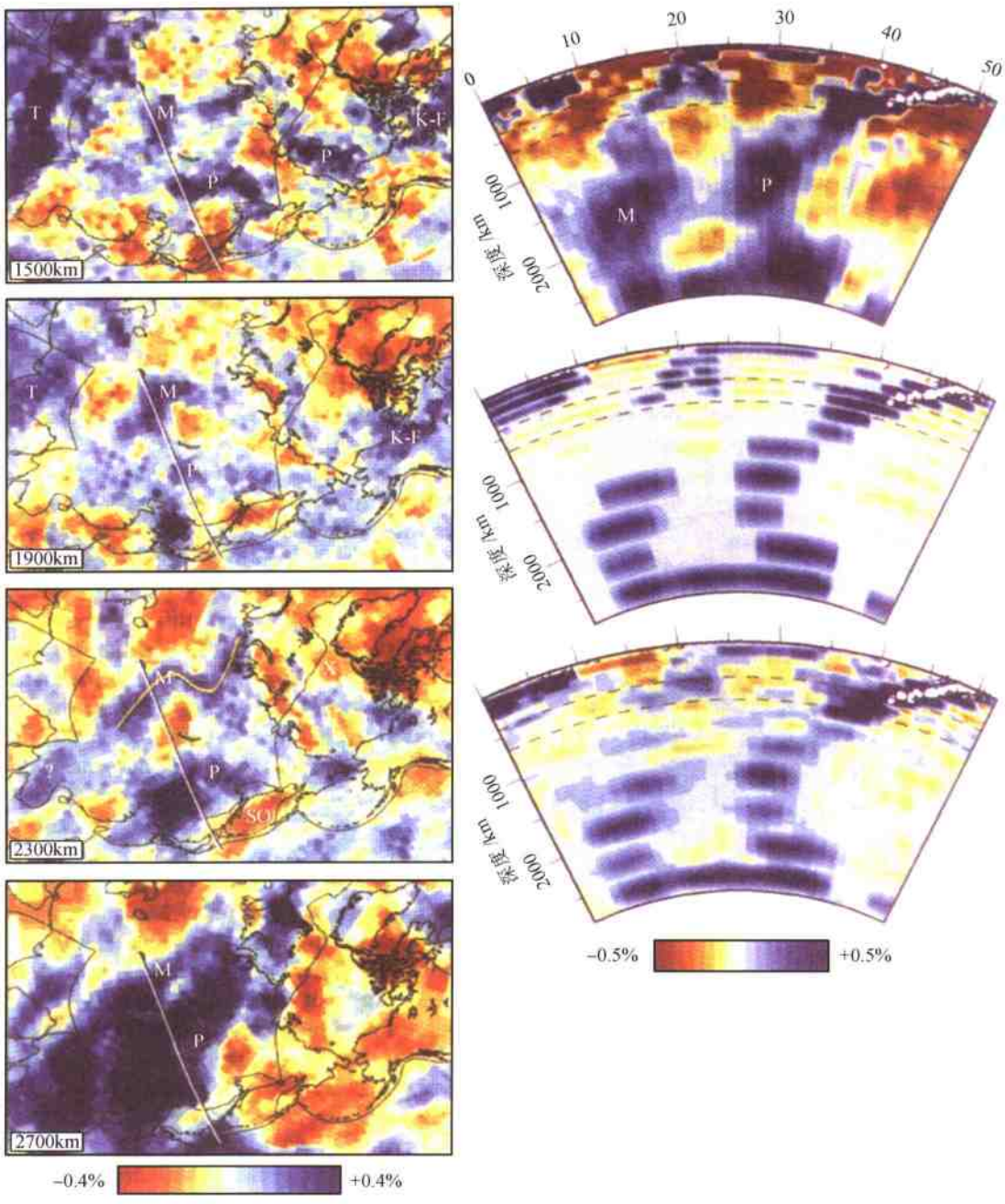

图 5　西伯利亚深地幔地震层析 P 波速异常模型(左图)及剖面(右图)

(据 R. Van der Voo 等,1999[14])

Fig. 5　Tomographic P-wave velocity anomaly patterns(left) and cross-section through tomographic model (right) in the deep mantle under Siberia

(左图)西伯利亚下面 1500～2700km 之间深地幔中 4 个不同深度地震层析 P 波速异常模型。M 代表西伯利亚蒙古-鄂霍次克-科里亚克缝合带下面的 P 波高速异常;P 代表日本下面的西太平洋高速异常;T—特提斯带高速异常;K-F—库拉-法拉隆板块;b—贝加尔湖;SO—鄂霍次克海;X—北极。(右图)上图:横穿西伯利亚的地震层析 P 波速异常剖面;M 代表西伯利亚蒙古-鄂霍次克-科里亚克缝合带下面的 P 波高速异常;P 代表日本下面的西太平洋高速异常;白点代表西太平洋毕尼奥夫带的地震位置;中图:剖面的全地幔蛋糕模型的模拟输入;下图:反演分析的结果

面上形成“弯钩”形，从蒙古的西北部往北，一直到西伯利亚的北极海岸；1900～2300km 深度，高速异常带在平面上往西位移；在 2300km 深度，平面上呈现“Z”形特点。在西伯利亚地区地震层析的不同深度平面图中，还明显显示了蒙古-鄂霍次克-科里亚克高速异常带(M)东部的日本下面的西太平洋高速异常带(P)的存在，它代表了在现代太平洋板块往西垂直俯冲到核幔边界的地球物理证据。

在横穿西伯利亚的地震层析剖面(图 5)中，同时展现了蒙古-鄂霍次克-科里亚克高速异常带(M)及其东部的西太平洋高速异常带(P)。在 650km 深度，可见 M 高速异常带往西插入转换带；在 650～1400km 之间，M 高速异常带断缺或不清晰；在 1500km 以下的深度，M 和 P 都具有高分辨的异常特征，在西伯利亚下面的深地幔高波速异常与在其他地区(东、西太平洋及欧亚南部等)所见相同。西伯利亚深地幔高波速异常(M)与东部的西太平洋高速异常带(P)的几何形态在下地幔下部都发生向东翻转，与喜马拉雅下面的高速异常体的特征十分相似。M 和 P 在核幔边界连接，构成了巨大的俯冲板片的“墓地”。

研究表明[14]，西伯利亚之下的高速异常带与新生代的俯冲无关。它代表了蒙古-鄂霍次克侏罗纪大洋岩石圈的记录。西伯利亚下的高速异常带分成上、下两段，在转换带至 1400km 缺失，1500km 以下的高速异常体部分可能代表了“拆沉”的大洋岩石圈的“化石”残片。这种巨大的拆沉可能是两大板块碰撞及大陆增生的标志。值得提出的是，蒙古-鄂霍次克侏罗纪大洋岩石圈俯冲发生在 150Ma 之前，今天，我们还能通过新的地震层析资料发现它的信息，是值得注意的事情。

2 地震层析与超地幔羽

Roger Larson 在 1991 年根据西南太平洋下面大型地幔上涌特点，提出“超地幔羽”的观点。由于地幔中放射性热的丢失，比地核冷得快，造成从地核到下地幔的热传导，形成热边界“D”层。热边界层的不稳定性使热的、上浮的地幔呈圆柱状上升，形成“超地幔羽”。超地幔羽把地球内部 10%的热量通过上涌流带到地表，成为补充俯冲的被动回返流。超地幔羽由 3 部分组成：蘑头、蘑尾及上涌流。实验和数值模拟显示了超地幔羽呈蘑菇状。地幔羽由于较周围地幔的粘度低而往上流动，使“蘑头”直径可增大到 1000km 以上，并不断从细圆柱状的“蘑尾”中吸收新的物质。在地幔中的其他浅部边界也可以形成小的地幔羽[15]。

近来，高分辨的全球地震波速度层析结果不仅表明在俯冲区的高速俯冲板片可以直接透入下地幔底部的核幔边界“D”层，而几深部热的低速异常体也可以从核幔边界“D”层往上横跨 660km 不连续面到达全球地表热点[3]，如东非、冰岛、卡那利群岛、黄石和大洋群岛之下的热点[16-18](图 1)。

非洲的超地幔羽是由最近提出的地震层析 S20RTS 模型(图 6)证实的[16-18]。S20RTS 模型是指 20°剪切波模型，是综合了 1980～1998 年大于 5 级地震的面波震相波速、体波走时和自由振荡分裂测量的地震数字宽频记录而确定的。S20RTS 模型的剖面首先显示了非洲的低剪切波速异常带被北美、南美、南极、东亚和印度洋下面的高剪切波速带围绕，揭示了非洲大陆下面的低速异常体有一个复杂的三维形态，非洲的低速异常体覆盖了靠近非洲西部的大西洋东南部之下核幔边界的广大区域(4000km×2000km)，它与中非、西北非和南印度下面的低剪切波速的异常区相连接。非洲的低速异常带在中地幔(1350～2350km)深度变窄，并且往东

及北东方向聚中在核幔边界以上较高的部位。垂直的 S20RTS 剖面表明,至少从 2000km 到上地幔范围内的低波速异常是连续的,异常从南非下面的核幔边界延至东非裂谷的上地幔,说明异常从非洲西南往东及北东方向倾斜上延,这种倾斜在 2000km 处发生侧向错位(图 6)。

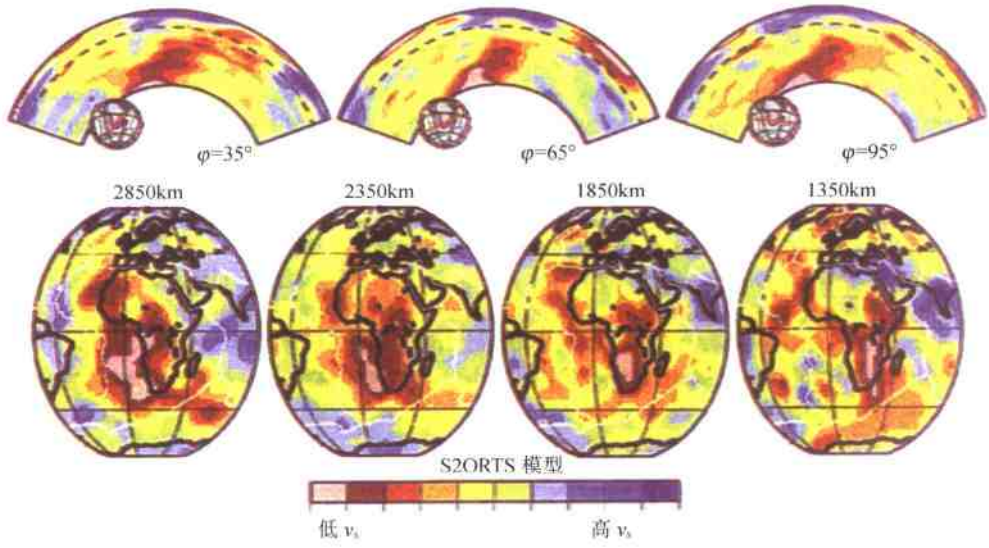

图 6　通过 S20RTS 模型的垂直及水平剖面

(据 Ritsema, J. ,2002[18])

Fig. 6　Vertical and horizontal sections across the S20RTS model

蓝色与红色分别代表高速及低速异常,白线代表板块边界

低速异常体代表了热的低密度物质,因此,可用大规模的热上涌流来解释东非超地幔羽。在地幔羽底部热上涌流的形态是复杂的,并且上涌的方向往东及北东方向偏移,这可能是冈瓦纳大陆分裂致使非洲板块向北东方向迁移的结果。

据推测,与板块离散边界有关的热点(火山中心)下面存在悬浮着的狭窄的地幔羽状物,热流是由地幔羽传导的,其热流量约为地球总热量的 12%,可与地核发射的热量相比,而且与地幔底部热边界层的超地幔羽一致。这些地幔羽状物可能是来自核幔边界朝地幔羽所提供的热物质的部分熔融的产物[19]。

3　地幔"双层对流"到"单层对流"模式

地球内部的"对流"首先是 Fisher(1881)提出来的,地幔对流的提出者是 Holmes(1929),Hess 的海底扩张假设(1962)是以 Holmes 的地幔对流为基础的。

板块运动的主要动力来自地幔对流。最早提出的"被动对流"论认为,板块是由地幔对流运载而运动的。由于"被动对流论"存在许多不完善的方面,很快就被"主动对流"论所代替。"主动对流"指对流在海岭上升,在海沟消失,俯冲体由于高密度而具有牵引拖力的动力作用而往下俯冲。但"主动对流"对地幔对流的具体动力学过程有不同说法:一种认为地幔

对流限于软流层以上的部分，其热能是由下地幔的中间层经热传导供给的；另一种提出“双层对流”模式，认为对流分别在上、下地幔两层中沿水平方向流动进行，上下对流圈是分开的，因为在650km深度存在的不连续面可能是物质的分隔界面。

Silver P. G. 等[20]在1988年曾提出双层和单层混合地幔模式，认为下地幔的结构比上地幔致密，但并没有致密到冷却的状态，高密度的俯冲体并没有穿过660km的过渡层而进入下地幔里面去，有可能在进入下地幔时只作短暂停留，高密度俯冲体就被高温熔化变成浮体，而又被返回到上地幔。这一解释与600～700km。Benioff中的深源地震分布结果相一致。

Davies G. F.（1992）[21]曾认为，在大陆板块汇聚边界的俯冲板片向地幔俯冲时，由于过渡带粘性增加，俯冲板片在660km过渡带可能发生局部的扭结，而继续进入较深部位时，由于下地幔的粘度的稳定增加而受到压力或热力，使之弯曲形变及坍塌。

新的板块汇聚边界地震层析结果支持了Davies G. F. 的推测，不仅揭示板块大规模整体运动使俯冲板块穿过上下地幔过渡层，并穿透地幔到达核幔边界；另一方面，导致火山热点的上涌超地幔羽从地幔底部的相对弱的热边界层（D层）直接升起，因而形成了全地幔的深循环。板块汇聚边缘的深部俯冲板片穿透地幔到达核幔边界的观察结果还表明，下地幔流动虽然距上地幔很远，但不可能单独构成对流系统，一定与上地幔流动有关。

在新的地幔地震层析结果揭示全地幔对流的基础上，Mattauer（1999）[9]提出了“单层地幔对流”模式，用图7示意了“单层地幔对流”模式与“双层地幔对流”模式的区别，表示了东太平洋板块及西太平洋板块分别往东及往西俯冲到美洲和亚洲大陆下面的地幔底部，由于

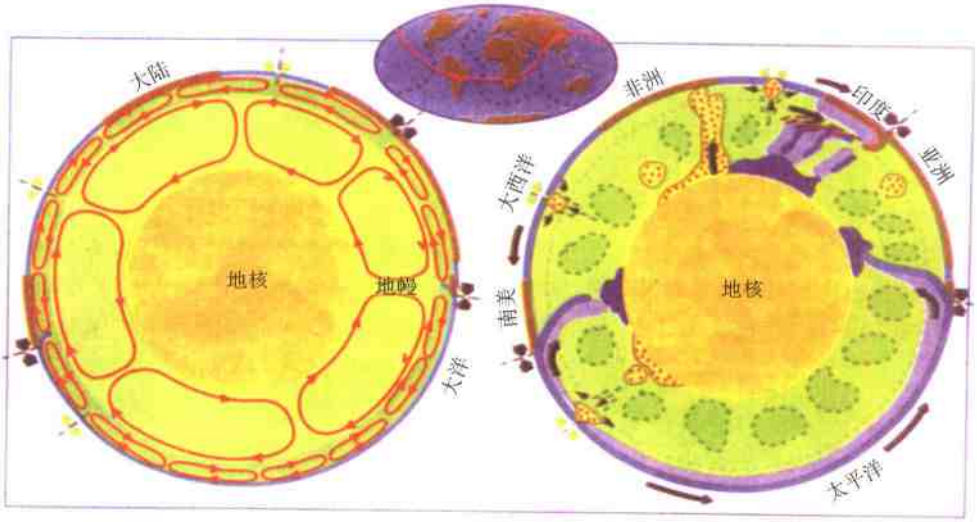

图7　地幔的对流模式
（据Mattauer, M.，1999[9]）
Fig. 7　Mantle convection model

左图为双层对流模式，分为两部分：由上地幔的小对流环与下地幔的大对流环组成，是两个对流体系；右图为单层对流模式：表现了太平洋岩石圈板片往东及往西分别俯冲在美洲和亚洲大陆之下，抵达核幔边界，形成“墓地”，印度次大陆岩石圈板片呈翻转几何学俯冲在亚洲大陆之下，下面有若干拆沉的岩石圈残片；东非、大西洋及东太平洋位置上有从核幔边界形成的超地幔羽上升到地表。假设整个中下地幔的对流由无数小对流环运载。褐色代表大陆地壳，蓝色代表大洋地壳，紫色代表厚度变化的上地幔，核幔边界附近带有十字的深蓝色地域为俯冲岩石圈的“墓地”，红点域代表热的地幔羽，绿色虚线圈代表下地幔中的对流环

地幔最深处粘度的增加引起下沉板块的横向模糊,核幔边界的高速异常区成了俯冲岩石圈的"墓地";印度次大陆及邻近地区下面的上中地幔内显示了俯冲岩石圈的翻转构造,1000km以下的中下地幔中保存了拆沉的特提斯大洋俯冲岩石圈残余板片,它们也与核幔边界的高速异常区组成的"墓地"相连;在非洲和亚洲大陆内部以及太平洋,印度洋和大西洋板块中的热点与地幔羽有关,有的与来自核幔边界的超地幔羽有关。假设下地幔中的对流通过大量的小对流环运载来完成。

模式中以地幔底部的低波速热边界层为能源发源地的超地幔柱首先上涌到扩张中心,地幔羽在上升时会拖曳着周围的物质,在穿过板块时由于板块规模水平运动使幔羽发生垂向偏移。同时地幔对流可以产生与观测结果相匹配的板块速度,板块在形成地幔对流结构和决定上升和下涌的主要位置方面起着决定性作用。由于热量向地表传导,板块随年龄增加而增厚,这个浅层过程至少使来自地幔的85%的热量失去了,这也是对流过程的一个很强的约束。它说明板块是地幔对流的整体,构成整个系统的主要驱动来自热边界层。这些在地幔中穿过660km过渡带的对流形成了全地幔的对流特征,即全地幔对流与构造板块运动的动力学过程[9]。

4 板块下的构造及地幔动力学

传统板块理论立足于岩石圈,板块运动指岩石圈板块在软流圈上的运动。新的研究表明,研究板块构造只考虑岩石圈的尺度及岩石圈动力学已远远不够了。全球地震层析新资料为我们揭示了岩石圈板片可以从地球表面俯冲到核幔边界,超地幔羽也可以从核幔边界直接上涌到地壳表层并导致大量热点的产生;同时,全球范围内地幔中地震波高速异常和低速异常的连续出现,表明物质可以从上往下或者从下往上穿过660km的不连续带。这一发现进一步证实了660km边界可以抵抗但并不能阻止大规模物质从上地幔进入下地幔,反之亦然。因此,研究板块的运动力必须考虑整个地幔的动力学背景。

现代板块构造研究展示了地球上的两大巨型板块汇聚边界:环太平洋和欧亚大陆南部的特提斯。前者是太平洋板块俯冲于美洲大陆板块(东面)及亚洲大陆板块(西面)之下的"洋陆俯冲"产物;后者是欧亚大陆板块与非洲板块、阿拉伯板块、印度-澳大利亚板块汇聚的结果,其中西段板块(欧亚大陆板块与非洲、阿拉伯及印度板块之间)已经碰撞,为"陆陆碰撞"及"陆陆俯冲"的产物,东南段板块(欧亚大陆板块与澳大利亚板块之间)尚未碰撞,印度与澳大利亚之间的印度洋正往北东方向俯冲于印度尼西亚岛弧之下,为"洋陆俯冲"的产物。

地幔地震层析资料揭示了洋陆板块汇聚边界及大陆板块汇聚边界的俯冲板片抵达核幔边界的超深俯冲的证据,特别是大陆板块汇聚边界的地幔构造的显示,为我们研究大陆板块汇聚边界的深部状态提供了更多的思考。

(1)印度和欧亚板块碰撞及青藏高原形成的研究一直是地学界关注的热点。自Argand E.(1924)[22]提出印度板块往北俯冲在欧亚大陆之下的观点以来,地球物理的探测不断提供了岩石圈范围内的俯冲证据[22-27]。喜马拉雅下面新的地幔地震层析资料,显示了在中上地幔范围内印度克拉通的岩石圈俯冲板片的几何形态呈上部往北、中部直立往下及下部往南翻转的特殊的超深俯冲形式[4,7]。这种超深俯冲的几何形式是如何形成的?反映了地幔中物质运动的什么特点?对两个大陆的碰撞造山及青藏高原的形成起了什么作用?

(2)喜马拉雅的地幔地震层析图像,揭示中下地幔范围内保存了若干高速异常体板片。R.V.der Voo 等(1999)[4]把它们当做特提斯大洋岩石圈或者拆沉的印度次大陆岩石圈的"化石"残片。这说明地幔层析资料支持了侏罗纪—白垩纪时期印度北面特提斯大洋及岩石圈超深俯冲的观点,而且提供了拆沉作用的地震层析的证据;无独有偶,西伯利亚下面的地幔地震层析图像不仅揭示了蒙古-鄂霍次克-科里亚克高速异常带的存在,也支持了西伯利亚和蒙古-北中国板块之间的蒙古-鄂霍次克侏罗纪大洋岩石圈的超深俯冲及拆沉的认识[14]。

通过大陆板块汇聚带的地幔地震层析资料,我们可以寻找与新生代俯冲无关的古俯冲残片(侏罗纪—白垩纪)并捕捉拆沉的证据。这一贡献给予我们重要的启示:拆沉作用与大陆增生的关系是什么?三叠纪时期(或更老)的岩石圈超深俯冲(大陆和大洋)及拆沉的证据能否在地幔地震层析资料中保存?

(3)岩石圈板片可以俯冲到地幔深部,一部分成为拆沉的"化石"残片,一部分在碰撞的过程中折返上来,折返上来的板片保存了大量的幔动力学的信息,包括超高压变质作用、超高压矿物相的转换、超高压矿物流变学、流体及熔融作用、壳-幔作用及地幔中的物质循环等。因此,我们可以通过地球物理以外的各种地质手段来研究超高压变质带,发现超深地幔矿物及超深俯冲的证据,探究汇聚板块边界的地幔动力学。

经过深俯冲在地幔中遨游的超高压变质带主要分布在碰撞造山带中。中国的大别-苏鲁超高压变质带是世界上最大的超高压变质带,是研究板块汇聚边界地幔动力学的最佳地区之一。

(4)实际上,太平洋板块俯冲和印度与欧亚板块的碰撞只是反映了从"洋陆俯冲"到"陆陆俯冲"的板块运动演化过程,因而两类汇聚边界的地幔地震层析是不同演化阶段的记录。

岩石圈的超深俯冲、超地幔羽及全地幔对流的揭示是对传统的板块构造有关对流、俯冲及驱动力的基本模型的挑战。核幔边界既是高速深俯冲异常板片的"墓地"又是低速异常体(超地幔羽)的发源地的新观点给予人们新的启示:板块下的全地幔运动是研究岩石圈板块运动之根本,研究板块下的构造必将从岩石圈动力学拓展到地幔动力学。

参 考 文 献

[1] Mattauer M. La formation des chaines de montaghes[J]. Science (Edition francaise de Scientific American), 1981, (46):40~56.

[2] Mattauer M. Monts et Merveilles Beaute's et richesses de la geologie[A]. In: Hermann ed. Teaurs des Sciences et des Arts [C]. 1989.

[3] Grandt S P, *et al*. Global Seismic Tomography: a Snapshot of Convection in the Earth[J]. Nature, 1997, 386: 578~584.

[4] R Van der Voo, *et al*. Tethyan Subducted Slabs under India [J]. Earth plan. Sc. Lett., 1999, 171: 7~20.

[5] Van der Hilst R D, Widiyantoro S, Engdahl E R. Evidence for Deep Mantle Circulation from Global Tomography [J]. Nature, 1997, 386: 578~584.

[6] Widiyantoro S, Van der Hilst R D. The slab of subducted lithosphere beneath the Sunda arc, Indonesia [J]. Science, 1996, 271: 1566~1570.

[7] Bigwaard H, Sjakman Win. Closing the Gap between Regional and Global Travel Tomography[J]. Journ. Geoph. Res., 1998, 103: 30055~30078.

[8] Kendall, J. M. & Silver, P. G. Constraints from seismic anisotropy on the nature of the lowermost mantle. Nature, 1996, 381:409～412.

[9] Mattauer M. Seismique et tectonique [J]. La Science, 1999, (265) :28～31.

[10] Mattauer M. La tectonique sous les plaques[J]. Science (Edition francaise de Scientific American), 2002, (295):70～75.

[11] Kamiya S, Miyatake T, Hirahara K. How deep can we see the high velocity anomalies beneath the Japan islands? [J]. Geophys. Res. Lett., 1988, 15:828～831.

[12] Van der Hilst R D. Complex morphology of subducted lithosphere in the mantle beneath the Tonga trench [J]. Nature, 1995, 374:154～157.

[13] 曾融生,陈运泰. 探索地球内部的奥秘[M]. 北京:清华大学出版社,暨南大学出版社,2002.120.

[14] Van der Voo R, Spakman W, Bijwaad H. Mesozoic subducted slabs under Siberia[J]. Nature, 1999, (397): 246～249.

[15] Condie K C. What is a superplume? [A]. In: Superplume International Workshop Abstract[C]. Tokyo, Japan, 2002.20～21.

[16] Ritsema J, Ni S, Helmberger D V, *et al*. Evidence for strong shear velocity reductions and velocity gradients in the lower mantle beneath Africa[J]. Geophysical Research Letters, 1998, 25: 4245～4248.

[17] Ritsema J, van Heijst H J, Woodhouse J H. Complex shear velocity structure beneath African and Iceland [J]. Science, 1999, 286:1925～1928.

[18] Ritsema J. Structure of the African superplume[A]. In: Superplume International Workshop Abstract[C]. Tokyo, Japan, 2002.37～39.

[19] Zhao Dapeng. A new tomography of the mantle: Slicing plumes and superplumes [A]. In: Superplume International Workshop Abstract[C]. Tokyo, Japan, 2002.24～27.

[20] Silver P G, Carlson R W, Olson P. Deep slabs, geochemical heterogeneity, and the large-scale structure of mantle convection: investigation of an enduring paradox: Ann. Rev. Earth Planet[J]. Sci., 1988, 16:477～541.

[21] Davies G F, Richards M A. Mantle convection[J]. J.Geol., 1992, 100:151～206.

[22] Argand E. La tectonique de l'Asie[C]. Proc. 13th Int. Geol.Congr. Brussels, 1924, 1: 171～372.

[23] Barazangi M, Ni J. Propagation characteristics of Pn beneath the Himalayan arc and Tibetan plateau: possible evidence for underthrusting of Indian continental lithosphere beneath Tibet [J]. Geology, 1982, 10: 179～185.

[24] Molnar P. A review of geophysical constraints on the deep structure of the Tibetan Plateau, the Himalaya and the Karakoram, and their tectonic implications[J]. Phil. Trans. R.Soc. Lond., 1988, A326: 33～88.

[25] Beghoul N, Barazangi M, Isacks B L. Lithospheric structure of Tibet and western north America: mechanisms of uplift and a comparative study[J]. Journal of Geophysical Research, 1993, 98:1997～2016.

[26] Hirn A, Jiang M, Diaz J, *et al*. Seismic anisotropy as an indicator of mantle flow beneath the Himalayas and Tibet [J]. Nature, 1995, 375:571～574.

[27] Zhao W, Nelson K D, Project INDEPTH Team. Deep seismic reflection evidence for continental underthrusting beneath S. Tibet[J]. Nature, 1993, 366:557～559.

Tectonics beneath plates and mantle dynamics

XU Zhiqin[1] ZHAO Zhixing[1] YANG Jingsui[1] YUAN Xuecheng[2] JIANG Mei[1]
(1. Laboratory of Continental Dynamics, Institute of Geology, Chinese Academy of Geological Sciences, Beijing 100037, China; 2. Senior Consulting Center, Ministry of Land and Resources, Beijing 100812, China)

Abstract The latest global mantle seismic tomographic data have revealed tectonics beneath plates: the lithospheric slab may be subducted to the core-mantle boundary and the superplume may rise from the core-mantle boundary to the upper crust to form a hot spot. The mantle "single-layer convection" model challenges the mantle "double-layer convection" model. Through the introduction of the aforesaid new hypothesis and new model, this paper emphasizes that to study the lithospheric plate is necessary to gain knowledge of the tectonics beneath the plate and that to explore the driving force of the lithospheric plate "lithosphere dynamics" should be sublimated into "mantle dynamics".

Key words tectonics beneath the plate superdeep subduction core-mantle boundary superplume mantle dynamics

A Large Ductile Sinistral Strike-Slip Shear Zone and Its Movement Timing in the South Qilian Mountains, Western China[1]

Xu Zhiqin Li Haibing Chen Wen Wu Cailai Yang Jingsui
Jin Xiaochi and Chen Fangyuan
(Institute of Geology, Chinese Academy of Geological Sciences, Beijing 100037)

Abstract There is a large ductile shear zone, 2km wide and more than 350km long, in the South Qilian Mountains, western China. It is composed of volcanic, granitic and calcareous mylonites. The microstructures of the ductile shear zone show nearly E-W extending subvertical foliation, horizontal and oblique stretching lineations, shearing sense from sinistral to oblique sinistral strike-slip from east to west, "Λ" type folds and abundant granitic veins. Measured lattice preferred orientations (LPOs) of the mylonitic and recrystallized quartz of the granitic mylonite in the west segment suggest a strong LPO characterized by the dominant slip systems $\{10\bar{1}0\}\langle c\rangle$ formed at high temperature (>650℃). K-feldspar of the mylonite shows an $^{39}Ar/^{40}Ar$ high-temperature plateau age of 243.3±1.3Ma, and biotite, 250.5±0.5Ma, which represent the formation age of the ductile shear zone. The $^{39}Ar/^{40}Ar$ plateau ages of 169.7±0.3Ma and 160.6±0.1Ma and the $^{39}Ar/^{40}Ar$ isochron ages of 166.99±2.37Ma and 160.6±0.1Ma of biotites in the mylonite represent the subsequent deformation age. These ages indicate that this ductile shear zone is similar to the Altun and South Kunlun sinistral ductile shear zones in its ages of movement, formation, reactivation and duration.

Key words Early Triassic ductile sinistral shear zone high-temperature LPO South Qilian

1 Geological Setting

The Qilian Caledonian orogenic belt is the result of the collision between the Alxa terrain, Qilian terrain and Qaidam-Kunlun terrain in the Caledonian period (Xu *et al*., 1999). During the Caledonian collision, a large number of granite masses (470～430Ma) (Xu *et al*., in press) were emplaced into the Precambrian metamorphic basement and the Early Palaeozoic low-grade metamorphosed and folded rock sequence in the Qilian area. Among the exposed granites, the largest one is the Qaidam granite (SHRIMP age 457Ma, Wu *et al*., 2001) in the South Qilian. The Middle-Upper Devonian molasse deposits unconformably overlie on the Lower Palaeozoic strata, which implies the termination of the Caledonian orogeny. Then, the South Qilian region underwent a local transgression during the post-orogenic period (Carboniferous-

[1] ACTA GEOLOGICA SINICA Vol. 76 No. 2 2002.

Triassic). During the Triassic, the Indosinian intercontinental orogeny overprinted the Caledonian orogeny and large strike-slip faults occurred around the Qilian, such as the Altun fault in the west and the South Kunlun fault in the south. Since the Mesozoic, the whole Qilian uplifted, and as a result, a high mountain chain formed and constituted a barrier during the Cenozoic at the northeastern edge of the Qinghai-Tibet Plateau.

This paper deals with a large ductile strike-slip shear zone, 2km wide and more than 350km long, which is situated in the northern part of the South Qilian Caledonian ultrahigh-pressure (UHP) metamorphic zone (Yang *et al.*, 1998; 2000; 2002). The Ordovician-Silurian low-grade metamorphic rocks, Carboniferous-Triassic marbles and clastic rocks, and Caledonian granites are mainly exposed on the northern side of the ductile shear zone, while the Proterozoic high-grade metamorphic basement rocks, Sinian-Ordovician limestone and sandstone, Upper Ordovician volcanic rock, Upper Devonian continental volcanic rocks, Carboniferous limestone, Lower-Middle Jurassic coal beds and the Cretaceous-Eocene red beds outcrop on the southern side. The narrow Carboniferous limestone slice stuffed in the east segment of this shear zone became mylonitic marbles due to intense deformation and metamorphism. Because of later movement, the tectonically superimposed slices composed of the Precambrian metamorphic basement and the Palaeozoic rocks were thrust southward over Mesozoic-Cenozoic sediments (Fig.1).

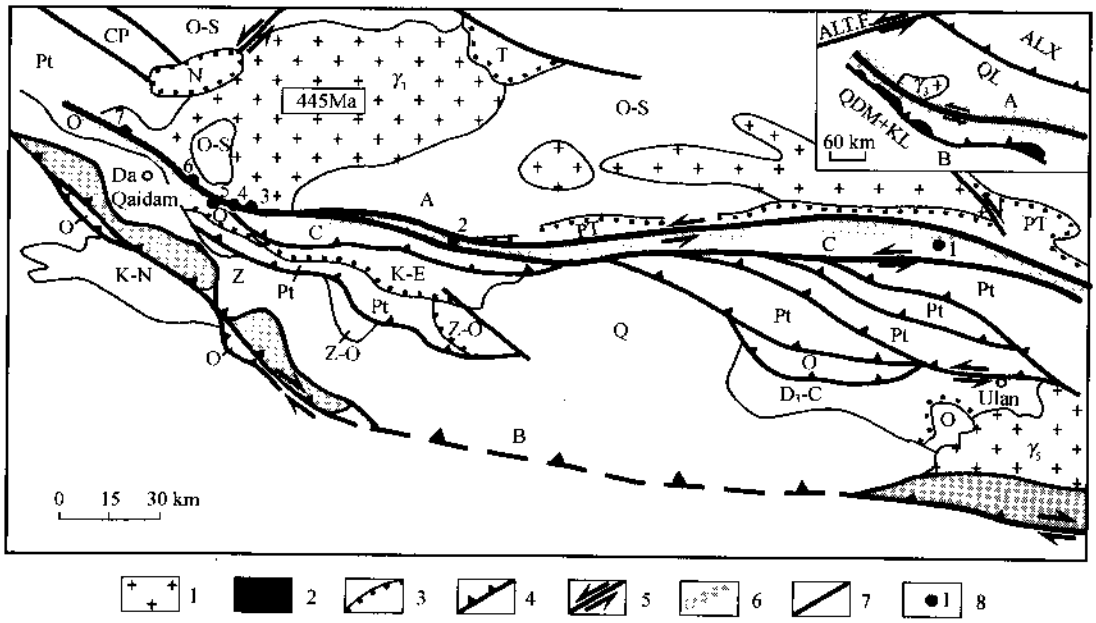

Fig. 1 Tectonic map of the Da Qaidam-Ulan area in the South Qilian.

1—Granite; 2—UHP (ultrahigh-pressure) metamorphic zone; 3—unconformity; 4—thrust; 5—strike-slip fault; 6—mylonitic zone; 7—fault; 8—observation locality.

A—South Qilian ductile sinistral strike-slip shear zone; B—South Qilian ultrahigh-pressure (UHP) metamorphic zone. ALX—Alxa terrain; QL—Qilian terrain; QDM + KL—Qaidam-Kunlun terrain; ALT.F. —Altun fault; γ_3—Caledonian granite; γ_5 Yanshanian granite; Pt—Proterozoic; Z—Sinian; Z-O—Sinian-Ordovician; O—Ordovician; O-S—Ordovician-Silurian; D_3-C—Upper Devonian-Carboniferous; C—Carboniferous; CP—Carboniferous-Permian; PT—Permian-Triassic; T—Triassic; K-E—Cretaceous-Eocene; K-N —Cretaceous-Neogene; N—Neogene; Q—Quaternary.

2 Microstructures of the South Qilian Ductile Sinistral Strike-slip Shear Zone

The South Qilian ductile sinistral strike-slip shear zone, about 2 km wide, was determined through microstructure observations and analysis of lattice preferred orientation (LPO) of quartz in the shear zone. There is a nearly E-W extending mylonite zone. The mylonitic zone composed of granitic mylonite and volcanic mylonite is located between the Qaidam granite and Late Ordovician intermediate-acid volcanic rocks, including tuff, gravel-bearing tuff, ignimbrite, thin-bedded marble and siliceous rocks in the western segment. A long, narrow Carboniferous mylonitic marble slice stuffed in the central-eastern segment of the shear zone with intense deformation and metamorphism is located between Ordovician-Silurian schists, Permian-Triassic strata and Carboniferous phillite and marble (Fig.2).

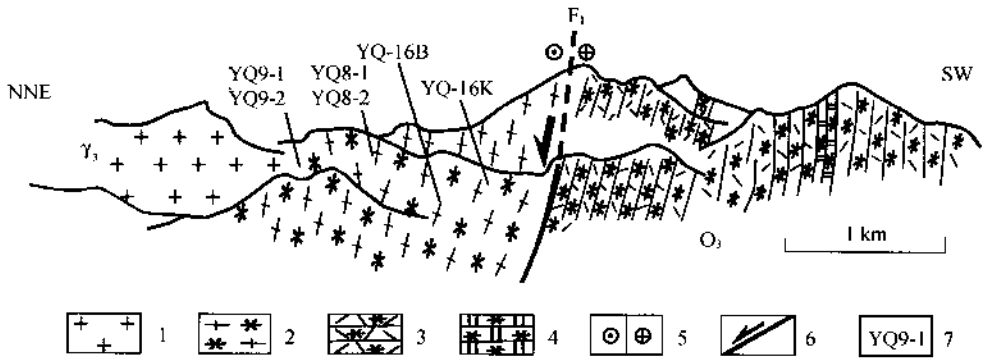

Fig.2 Structural profile of the northwestern part of the ductile shear zone (north of Da Qaidam) in the South Qilian Mountains.
1—Granite; 2—granitic mylonite; 3—volcanic mylonite; 4—mylonitic marble; 5—left-lateral shear; 6—normal fault; 7—sample numbers.

This mylonite zone is characterized mainly by subvertical foliation, subhorizontal-oblique stretching lineation and sinistral shearing strain. The stretching lineation developed on the foliation is shown by elongated volcanic gravels, elongated quartz aggregates, boudinage of granitic veins, extended and interrupted feldspar porphyroblasts and asymmetric pressure shadow structures. The stretching lineation from east to west in the shear zone changes from subhorizontal to oblique toward the west (Fig.3). The mullion structures (X stretching and Y = Z) developed in granitic mylonite in the western segment indicate a complex mechanism of "simple shear + contraction". A lot of "Λ" type folds (with hinges parallel to the stretching lineation) are developed. The clear sinistral indicators manifested by "σ" type and "δ" type feldspar and quartz porphyroblastic systems, S-C structure, mica-fishshaped muscovite and domino structures can be seen on the XZ plane [i.e. parallel to the stretching lineation (X), perpendicular to the foliation (XY)]. It is shown that the progressive evolution of the shearing sense is from sinistral strike-slip in the east to oblique sinistral strikeslip in the west of the mylonite (Fig.3 and 4).

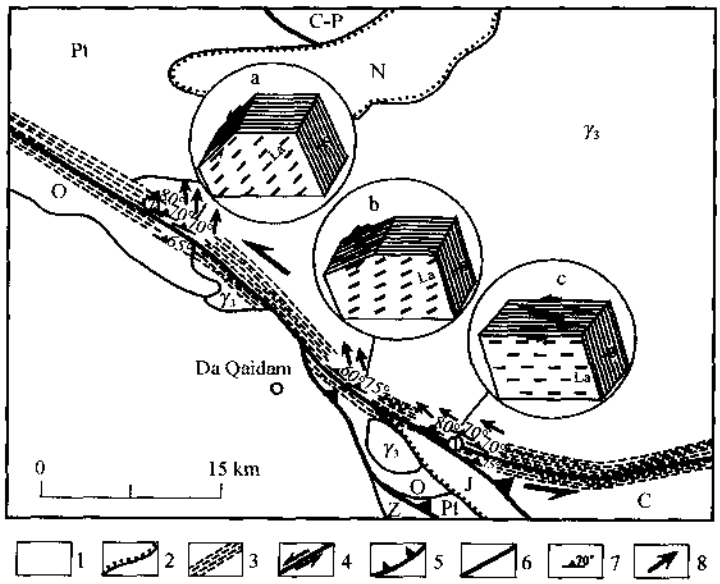

Fig. 3 Tectonic map of the western segment of the South Qilian ductile strike-slip shear zone.

1—Caledonian granite; 2—unconformity; 3—mylonite zone; 4—strike-slip fault; 5—thrust; 6—fault; 7—foliation; 8—stretching lineation. Pt—Proterozoic; Z—Sinian; O—Ordovician; C—Carboniferous; C-P—Carboniferous-Permian; J—Jurassic; N—Neogene; γ_3—Caledonian granite. La—stretching lineation; S—foliation; a, b and c indicate three-dimensional deformation patterns from the ESE to WNW side of the South Qilian ductile strike-slip shear zone. ①Locality of Samples SQX32, SQX34 and SQX36; ②Locality of Samples YQ8-1, YQ9-1 and YQ9-2.

3 Quartz LPO from Mylonite

Quartz constitutes an important part in the ductile shear zone of the middle crust. In the last two decades, experiment on deformation and dislocation slip of quartz has indicated that different intracrystal slip systems and LPO (fabric) patterns of quartz are formed at different temperatures. Especially the discovery of high-temperature LPO of quartz made the study of quartz LPO perfect (Carter *et al.*, 1964; Brunel and Maliakov, 1972; Boucher, 1977; Hara *et al.*, 1973; Mainprice *et al.*, 1986; He *et al.*, 1988; Xu *et al.*, 1997). Based on previous studies, Ji (1988) provided four types of quartz LPO patterns under non-coaxial shear strain: (Ⅰ) low-temperature basic LPO with slip system (0001) ⟨a⟩ formed at <400℃ and developed in lower greenschist facies; (Ⅱ) low to middle-temperature rhombic LPO with slip system $\{10\bar{1}\,\bar{1}\}$ ⟨a⟩ formed at 400～550℃ and developed in greenschist facies; (Ⅲ) middle-temperature prismatic LPO with slip system $\{10\bar{1}0\}$ ⟨a⟩ formed at 550～650℃ and developed in amphibolite facies; and (Ⅳ) hightemperature prismatic LPO with slip system $\{10\bar{1}0\}$ ⟨c⟩ formed at >650℃ and developed in granulite facies (Table 1). The studies indicate that the ductile shear zone accompanied with abundant granitic veins indicating partial melting in the shearing process may be formed at high temperature (>650℃) without high-grade metamorphism (Mainprice *et al.*, 1986; Okudaira *et al.*, 1995).

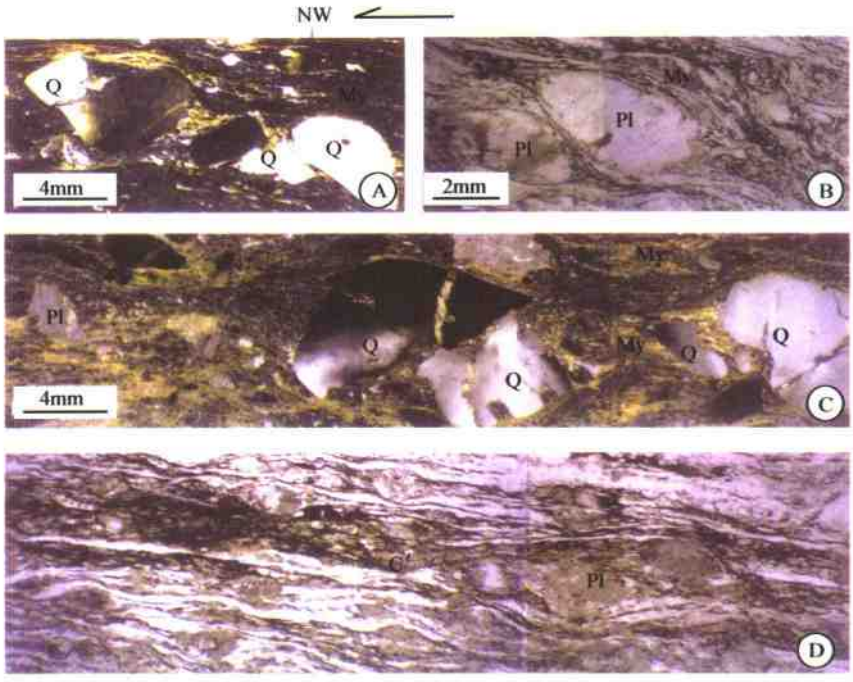

Fig. 4　Microphotographs of granitic mylonite on the XZ plane from the South Qilian ductile shear zone.

(A), (B) and (C) are from Samples YQ-16B, YQ-16K and YQ8-1 with steeply dipping foliation towards NE and oblique stretching lineation on the NW side of the mylonite zone, in which asymmetric porphyroclast system of quartz and feldspar indicates sinistral and normal slip sense of the mylonite zone; (D) is from Sample SQX36 with steeply dipping foliation towards NE and subhorizontal stretching lineation on the SE side of the mylonite zone, in which asymmetric porphyroclasts of quartz and feldspar, S-C structure as well as C′-shear layer foliation indicate sinistral sense of the mylonite zone.

Q—quartz; Pl—plagioclase; Kf—K-feldspar; Bi—biotite; C′—shear foliation.

Table1　LPO patterns and slip systems of no-coaxial shear strain under different temperatures (after Ji, 1988)

Type	Formation temperature	LPO pattern	Slip system	Metamorphic facies
Ⅰ	<400℃		(0001)〈a〉	Lower greenschist
Ⅱ	400～500℃		$\{10\bar{1}\,\bar{1}\}\langle a\rangle$	Greenschist
Ⅲ	550～650℃		$\{10\bar{1}0\}\langle a\rangle$	Amphibolite
Ⅳ	>650℃		$\{10\bar{1}0\}\langle c\rangle$	Granulite

When the LPOs of mylonitized quartz and recrystallized quartz from granitic mylonite with WNW-ESE strike in the western segment of the ductile shear zone were measured, the formation temperature conditions of different types of quartz in mylonite were determined and further

evidence was provided for the shearing sense.

3.1 Recrystallized quartz LPO from granitic veins in mylonite

Samples YQ8-1, YQ9-1 and YQ9-2 are from the north of Da Qaidam and SQX34, SQX35 and SQX36 are from the southeast of Da Qaidam. The quartz LPO was measured for the 〈C〉 axis of the rectangular and recrystallized quartz from granitic veins. Three types of recrystallized quartz LPO (Fig.4) were obtained: (1) low-temperature basic LPO, slip system (0001) 〈a〉, and 〈C〉 axis polarity near the Z axis; (2) middle-to lowtemperature rhombic fabric, slip system $\{10\bar{1}\,\bar{1}\}$ 〈a〉, and 〈C〉 axis polarity between the Z axis and X axis; (3) middle-temperature prismatic LPO, slip system $\{10\bar{1}0\}$ 〈a〉, and 〈C〉 axis polarity in the centre (Y axis). Therefore, the above LPO patterns indicate that the recrystallized quartzes from granitic veins in the mylonite were formed at middle- to low-temperatures (350～550℃) (Fig.5b and d).

Because Samples YQ8-1, YQ9-1 and YQ9-2 are characterized by oblique stretching lineation, it can be judged that the mylonite zone has an oblique sinistral strike-slip shear sense. But Samples SQX34, SQX35 and SQX36 are characterized by subhorizontal stretching lineation, which means that the mylonite zone has a sinistral strike-slip shear sense.

3.2 Mylonitized quartz LPO

Four types of mylonitized quartz LPOs from Samples YQ8-1 and YQ9-1 in the WNW segment of the fault and from SQX32, SQX34, SQX35 and SQX36 in the ESE segment of the fault were obtained. Among them, three LPOs are completely concordant with those of the above-mentioned recrystallized quartz, and only one LPO is different, i.e., $\{10\bar{1}0\}$ 〈c〉 LPO occurring near the axis X. It is indicated that mylonitized quartz was formed at high temperature (>650℃). All the mylonitized quartz LPOs show the oblique sinistral shear sense in the WNW and sinistral shear sense in the ESE (Fig.5a and c).

The above results show that the mylonitized quartz was first formed at high temperature (>650℃), and then evolved at middle temperature to low temperature (<400～650℃). In this process, the abundant granitic veins penetrated along the foliation, and also underwent shear deformation.

4 Age Data of the South Qilian Ductile Strike-slip Shear Zone

$^{39}Ar/^{40}Ar$ dating was carried out on biotite and Kfeldspar from two samples (YQ-16B and YQ-16K) of the granitic mylonite with steeply dipping stretching lineation in the NW segment (north of Da Qaidam) of the mylonite zone and biotite from two samples (SQX34, SQX35) of the granitic mylonite with subhorizontal stretching lineation in the SE segment (Dongdayangtouhe south of Da Qaidam). The obtained results and their interpretation are as follows.

4.1 $^{39}Ar/^{40}Ar$ age of biotite

(1) $^{39}Ar/^{40}Ar$ age of biotite from Sample YQ-16B

A flat $^{39}Ar/^{40}Ar$ age spectrum was obtained for biotite by incremental heating between 500

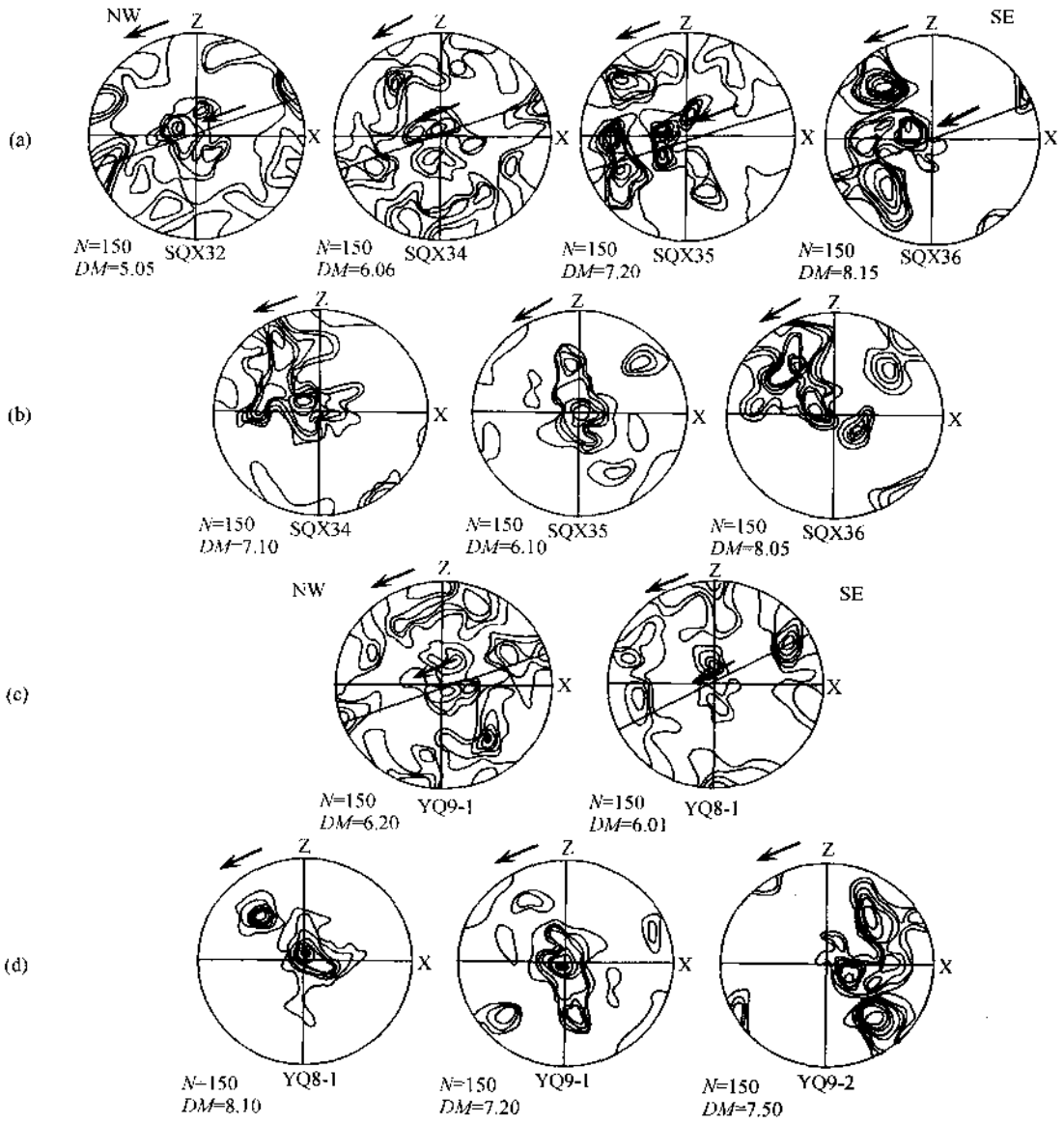

Fig.5 Quartz LPO of the granitic mylonite from the South Qilian ductile strike-slip shear zone.

Equal-area projection, lower hemisphere. Contours: 1, 2~3, 4~5, 6~7 and 8~9% by1%. Foliation (XY plane) is vertical and lineation (X) is from horizontal to oblique in this plane. N-number of measurements; DM-maximum density.

(a) and (b) show the quartz LPO patterns of the granitic mylonite from Samples SQX32, SQX34, SQX35 and SQX36 in the SE segment of the mylonite zone (north of Da Qaidam). XZ plane is an oblique plane parallel to the stretching lineation and perpendicular to the foliation. (a) shows (Ⅰ), (Ⅱ), (Ⅲ) and (Ⅳ) mylonitic quartz LPO; (b) shows (Ⅰ), (Ⅱ) and (Ⅲ) recrystallized quartz LPO. (c) and (d) show the quartz LPO of the granitic mylonite from Samples YQ8-1, YQ9-1 and YQ9-2 in the SE segment (Datouyanghe, south of Da Qaidam). XZ plane is parallel to stretching lineation and perpendicular to foliation. (c) shows (Ⅰ), (Ⅱ), (Ⅲ) and (Ⅳ) mylonitic quartz LPO; (d) shows (Ⅰ), (Ⅱ), (Ⅲ) and (Ⅳ) recrystallized quartz LPO.

and 1400℃ using the procedures outlined by Chen *et al*. (1998) (Table 2). The plateau age is 250.5±0.5Ma. The initial ratio of $^{40}Ar/^{36}Ar$ shows that there is no excess argon. Therefore it should represent the formation age of the transtensional ductile shear zone (Fig.6a).

Table 2 Data of step heating for YQ-16B (weight = 100.00mg, $J = 0.013453$)

T (℃)	$(^{40}Ar/^{39}Ar)_m$	$(^{36}Ar/^{39}Ar)_m$	$(^{37}Ar/^{39}Ar)_m$	F*	^{39}Ar(E-14 moles)	$\sum ^{39}Ar$	Age (Ma)
400	9.69070	0.00820	0.19760	7.26400	242.50	2.98	168.00±3.50
500	11.09640	0.00130	0.02770	10.70280	1058.00	16.02	242.70±2.80
600	11.31250	0.00050	0.01150	11.14700	1280.00	31.78	252.10±2.90
700	11.29090	0.00070	0.01410	11.08800	1038.00	44.58	250.80±2.90
800	11.76740	0.00230	0.09090	11.08270	215.00	47.23	250.70±3.00
900	11.89320	0.00230	0.14230	11.23040	309.00	51.04	253.80±3.00
1000	11.69040	0.00180	0.04980	11.14800	491.00	57.09	252.10±2.00
1100	11.23600	0.00080	0.12350	10.99200	1780.00	79.03	248.80±2.00
1200	11.08370	0.00070	0.15040	10.87260	812.00	89.03	246.30±2.80
1280	11.29250	0.00070	0.14400	11.09820	441.00	94.47	251.00±0.90
1350	11.27230	0.00090	0.10910	11.01210	224.00	97.33	249.20±2.90
1400	11.11110	0.00220	0.10860	10.45820	225.00	100.00	237.40±2.80

Average age= 246.38Ma; F is the ratio of radiogenic ^{40}Ar and ^{39}Ar. $F^* = {}^{40}Ar/{}^{39}Ar$.

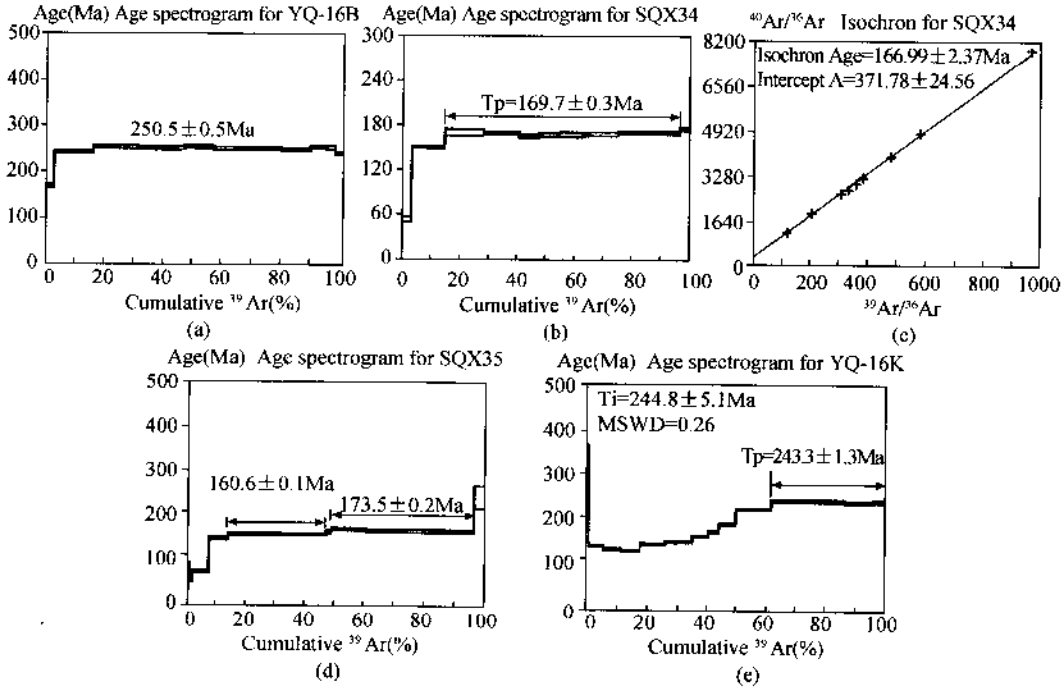

Fig.6 $^{39}Ar/^{40}Ar$ isochron ages and plateau ages of biotite and K-feldspar in the granitic mylonite from the transtensional ductile shear zone in the South Qilian Mrs.

(a) shows the $^{39}Ar/^{40}Ar$ plateau age of biotite from Sample YQ-16B; (b) shows the $^{39}Ar/^{40}Ar$ plateau age of biotite from Sample SQX34; (c)shows the $^{39}Ar/^{40}Ar$ isochron age of biotite from Sample SQX34; (d) shows the $^{39}Ar/^{40}Ar$ plateau age of biotite from Sample SQX35; (e) shows the $^{39}Ar/^{40}Ar$ plateau age of K-feldspar from Sample YQ-16K.

(2) $^{39}Ar/^{40}Ar$ age of biotite from Sample SQX34

A disturbed $^{39}Ar/^{40}Ar$ age spectrum was obtained for biotite (Table 3). The apparent ages be-

tween 600 and 1300℃ yield a plateau age of 169.7±0.3Ma (Fig.6b) for about 82% of the released ^{39}Ar, which is in concord with the age of 166.99±2.37 Ma obtained by the $^{39}Ar/^{36}Ar$～$^{40}Ar/^{36}Ar$ correlation diagram (Fig.6c).

Table 3 Data of step heating for SQX34 (weight = 95.70mg, J = 0.012405)

T (℃)	$(^{40}Ar/^{39}Ar)_m$	$(^{36}Ar/^{39}Ar)_m$	$(^{37}Ar/^{39}Ar)_m$	F*	^{39}Ar(E-14 moles)	$\sum ^{39}Ar$	Age (Ma)
400	27.70880	0.08560	0.07220	2.40220	268.77	3.41	52.90±3.50
500	10.60860	0.01230	0.03280	6.97840	894.20	14.75	149.80±1.50
600	8.90260	0.00320	0.01850	7.96020	1068.13	28.29	169.90±3.90
700	8.48990	0.00170	0.01400	7.98210	981.32	40.74	170.30±1.80
800	8.63730	0.00290	0.05300	7.76560	526.59	47.42	165.90±1.90
900	8.66300	0.00260	0.13040	7.90490	577.98	54.75	168.70±1.90
1000	8.70080	0.00280	0.11200	7.89130	642.16	62.89	168.50±2.30
1100	10.14580	0.00760	0.02220	7.91120	182.47	65.20	168.90±2.10
1200	8.56740	0.00210	0.05240	7.95780	820.47	75.60	169.80±1.70
1300	8.37230	0.00100	0.05590	8.06350	1647.04	96.49	171.90±1.70
1400	9.70200	0.00480	0.49350	8.31580	276.73	100.00	177.10±2.10

Average age = 163.85Ma; F is the ratio of radiogenic ^{40}Ar and ^{39}Ar. $F^* = {}^{40}Ar/^{39}Ar$.

(3) $^{39}Ar/^{40}Ar$ age of biotite from Sample SQX35

A disturbed age spectrum was obtained by dating the biotite extracted from Sample SQX35 (Table 4). This spectrum yields two plateau ages. The three lower temperature steps (620℃, 670℃ and 770℃) yield a plateau age of 160.6±0.1Ma. The four high-temperature steps yield a plateau age of 173.5 ±0.2Ma for about 48% of the released ^{39}Ar, which is in concord with the age of 160.6±0.1Ma obtained by the $^{39}Ar/^{36}Ar$～$^{40}Ar/^{36}Ar$ correlation diagram (Fig.6d).

Table 4 Data of step heating for SQX35 (weight = 100.45mg, J = 0.012405)

T (℃)	$(^{40}Ar/^{39}Ar)_m$	$(^{36}Ar/^{39}Ar)_m$	$(^{37}Ar/^{39}Ar)_m$	F*	^{39}Ar(E-14 moles)	$\sum ^{39}Ar$	Age (Ma)
350	40.72320	0.12560	0.56450	3.63270	20.99	0.65	79.50±55.20
350	41.35540	0.12720	0.35760	3.79600	14.35	1.10	83.00±11.60
430	14.20360	0.03820	0.52570	2.94740	40.38	2.35	64.80±11.80
510	7.77900	0.01480	0.70580	3.44220	179.84	7.92	75.40±3.70
570	9.50200	0.00880	0.25390	6.91720	215.36	14.59	148.50±2.40
620	9.50850	0.00680	0.13620	7.49040	251.83	22.40	160.30±3.00
670	9.09110	0.00530	0.05750	7.52840	310.60	32.03	161.10±2.40
770	8.67980	0.00400	0.07830	7.50320	497.72	47.45	160.50±1.60
930	15.23300	0.02520	0.49350	7.83300	67.04	49.53	167.30±3.70
1060	30.36350	0.07500	0.17450	8.19370	24.09	50.28	174.60±4.90
1210	9.68790	0.00530	0.61700	8.17870	390.38	62.37	174.30±2.10
1270	9.05920	0.00340	0.17030	8.07130	427.70	75.63	172.10±.2.80
1375	9.05180	0.00320	0.47570	8.12730	749.95	98.87	173.30±2.10
1450	26.95280	0.05300	9.47410	12.05530	36.36	100.00	251.40±24.40

Average age = 160.38Ma; F is the ratio of radiogenic ^{40}Ar and ^{39}Ar. $F^* = {}^{40}Ar/^{39}Ar$.

The lower-temperature plateau age of 160.6Ma is in good agreement with the plateau age of 166.99±2.37Ma and 167.0±2.4Ma obtained from Sample SQX34.

4.2 $^{39}Ar/^{40}Ar$ age of K-feldspar from Sample YQ-16K

The K-feldspar extracted from Sample YQ-16K was analysed by $^{39}Ar/^{40}Ar$ stepwise incremental heating dating (Table 5). The results yield a disturbed age spectrum (Fig.6e). Three high-temperature steps (1400℃, 1450℃ and 1490℃) yield a plateau age of 243.3±1.3Ma for about 38% ^{39}Ar released. This value is in agreement with the age of 244.8±5.1Ma (MSWD=0.26) obtained from the isochron diagram, with an intercept of 246.0Ma. Although radiogenic ^{40}Ar is easy to lose in K-feldspar in the site with higher activation energy, the K-feldspar can retain the earlier age information (Costa and Maluski, 1993; Harrison *et al*., 1991; Gerald and Harrison, 1993; Lovera *et al*., 1993). In fact, the high-temperature plateau age of 243.3Ma is in concord with the plateau age of 250.5±0.5Ma obtained from the biotite of Sample YQ-16B.

Table 5 Data of step heating for YQ-16K (weight=103.00 mg, J=0.013251)

T (℃)	$(^{40}Ar/^{39}Ar)_m$	$(^{36}Ar/^{39}Ar)_m$	$(^{37}Ar/^{39}Ar)_m$	F*	^{39}Ar(E-14 moles)	$\sum ^{39}Ar$	Age (Ma)
400	21.17720	0.01530	0.30240	16.53590	82.40	1.06	357.40±6.30
500	6.82190	0.00180	0.06270	5.30120	397.00	6.20	144.70±1.80
600	6.50890	0.00200	0.04870	5.99060	409.50	11.51	137.80±1.80
700	6.12500	0.00110	0.04670	5.78510	480.00	17.72	133.20±1.00
800	6.91110	0.00160	0.07930	6.45130	641.00	26.02	147.90±1.80
900	7.12850	0.00140	0.10890	6.70990	700.00	35.08	153.60±1.90
1000	7.77640	0.00150	0.06240	7.34080	407.00	40.25	167.50±2.00
1100	8.39290	0.00210	0.03630	7.75760	280.00	43.97	176.50±2.20
1200	9.14350	0.00230	0.02350	8.45650	432.00	49.57	191.60±2.30
1300	10.49150	0.00160	0.07750	10.01920	936.00	61.68	224.90±2.70
1400	11.14500	0.00060	0.07290	10.96270	1920.00	88.54	244.70±2.80
1450	11.17400	0.00130	0.25670	10.79260	707.00	95.69	241.10±2.80
1490	11.41140	0.00180	0.88730	10.94490	333.00	100.00	244.30±2.90

Average age=199.61Ma; F is the ratio of radiogenic ^{40}Ar and ^{39}Ar. F*=$^{40}Ar/^{39}Ar$.

These two ages represent the formation age of the transtensional ductile shear zone. The ages of 173~167Ma at the lower-temperature steps in the K-feldspar $^{39}Ar/^{40}Ar$ age spectrum can represent the age information of the post-thermo-tectonic events.

5 Conclusions and Discussion

(1) Studies have shown that the South Qilian ductile shear zone has the characteristics of sinistral strike-slip shearing in the eastern segment and oblique sinistral strike-slip shearing in the western segment.

(2) The LPOs of quartz in the mylonite of the western segment show that the mylonite

zone was firstly formed at high temperature (>650℃) and then evolved at middle temperature to low temperature (<400~650℃). In this process, abundant granitic veins penetrated along the foliation, and also underwent shear deformation. High-temperature prismatic fabric with $\{10\bar{1}0\}\langle c\rangle$ slip system is developed in the granodioritic mylonite from the Mozitan-Xiaotian ductile shear zone at the northern edge of the Dabie Mountains and the amphibolitic mylonite from the Dalian detachment ductile shear zone in the Liaodong terrain, East China. It is noticed that the veins were related to partial melting marked by abundant granitic veins caused by shear heating in the shear zone (Xu *et al.*, 1997).

(3) Age data show that the $^{39}Ar/^{40}Ar$ high-temperature plateau age of 243.3±1.3Ma of the K-feldspar (Sample YQ-16K) is similar to that of 250.5±0.5Ma of the biotite (Sample YQ-16K) from the mylonite. Applying the multi-domain theory, several researchers have suggested that the most retentive diffusion domain in the feldspars had a closure temperature close to or even higher than that of biotites. Similar ages of biotites and feldspars in this sample further support this idea. It is suggested that the formation age of the transtentional ductile shear zone is about 240~250Ma. The $^{39}Ar/^{40}Ar$ plateau ages of 169.7±0.3Ma (Sample SQX34) and 160.6+0.1Ma(Sample SQX35) and the $^{39}Ar/^{40}Ar$ isochron ages of 166.99±2.37Ma (Sample SQX34) and 160.6±0.1Ma (Sample SQX35) from biotite of the mylonite represent the subsequent deformation age. The formation age of 240~250Ma is shown in the NW segment and the subsequent deformation age of 160~170Ma is mainly shown in the SE segment of the mylonite zone. Therefore, we may infer that this zone may have formed firstly in the NW segment during 240~250Ma; consequently the movement from NW to SE made this ductile shear zone completely formed during 160~170Ma.

(4) The South Qilian ductile sinistral shear zone is situated on the eastern side of the Altun strike-slip fault. The study on the Altun fault zone shows that the Altun ductile sinistral strike-slip shear zone striking ENE 70° was formed at 223~244Ma as suggested by SHIRMP dating of zircon from the granitic mylonite (Li *et al.*, 2001) and the subsequent movement event happened at 140~163Ma (Arnaud *et al.*, 1995) and 120~86Ma (Li *et al.*, 2001). The South Kunlun ductile sinistral shear zone with E-W strike on the eastern side of the Altun fault zone and the southern side of the South Qilian ductile sinistral shear zone began at 240~220Ma, and there were subsequent reactivations at 150~140Ma and 120~100Ma (Xu *et al.*, 1997; 2001; Li *et al.*, 1996a, 1996b; Chen *et al.*, 1998). Therefore, from the formation age and reactivation age of the South Qilian ductile shear zone it can be inferred that the formation and reactivation of the ductile strike-slip shear zone in the southern Qilian Mountains probably were related to those of the Altun ductile sinistral shear zone (Fig.7).

Acknowledgements

The research was financially supported by the key project of the National Natural Science Foundation of China, "Composition and Orogenic Process of Qilian Mountain" (Project No.

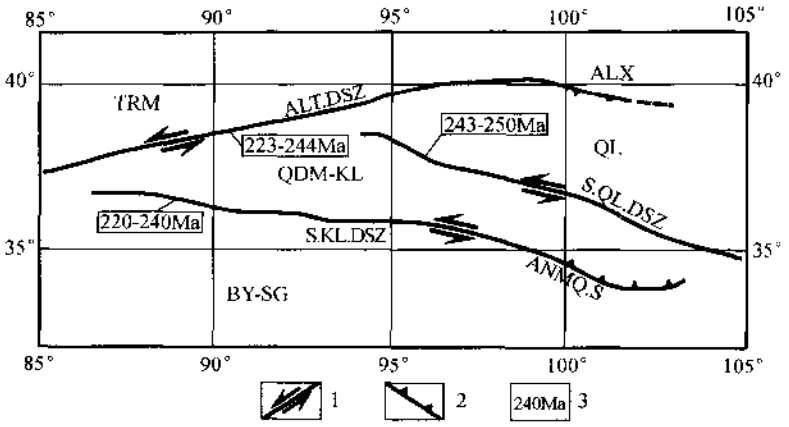

Fig. 7 Early Indosinian large ductile strike-slip shear zones in the northern part of the Qinghai-Tibet plateau. 1—Ductile sinistral strike-slip fault; 2- ductile trust; 3—formation age of ductile sinistral strike-slip fault. TRM—Tarim terrain; ALX—Alxa terrain; QL—Qilian terrain; QDM-KL—Qaidam-Kunlun terrain ; BY-SG—Bayan Har-Songpan-Garze terrain. ALT. DSZ—Altun ductile shear zone; S. QL. DSZ—South Qilian ductile shear zone; S. KL. DSZ—South Kunlun ductile shear zone.

4973020), the key project of the former Ministry of Geology and Mineral Resources, "The Basic Framework and Lithosphere Shearing of Qilian-Altun Mountains" (1996～2000) and the project of the Key Fundamental Research, Development and Planning (No. G 1998040800).

Manuscript received Oct. 2001
accepted Feb. 2002
edited by Xie Guanglian

References

Arnaud, N., Brunel, M., Malavielle, J., Scharer, U., Chen Wen and Tapponnier, P., 1995. Age and regime of deformation on the eastern Kunlun fault. In: Symposium on Uplift, Deformation and Deep Structure of Northern Tibet, La Grande Motte, France, Setp. 21～22, 1995, 1.

Brunel, M., and Maliakov, Y., 1972. Utilisation de l'orientation préférentielle du quartz comme marqueur de la déformation hercynienne dans le granite prehercynien du Mendic (Massif Central français). C. R. Ac. Sc., Paris, 2627～2630.

Boucher, J. L., 1977. Le quartz *et al* cinématique des zones ductiles. These, A l'U. E. R, des Sciences de la Nature de l'Universite de Nantes.

Carter, N. L., Christie, J. M., and Griggs, D. T., 1964. Experimental deformation and recrystallization of quartz. J. Geol., 72:687～733.

Chen Wen, Shen Jie, Zhang Sihong and Arnaud, N., 1998. Use of the laser probe $^{40}Ar/^{39}Ar$ and conventional $^{40}Ar/^{39}Ar$ technique dating for ages of the multi-tectonic events from South Kunlun shear zone (northern Tibetan plateau). Acta Geoscientia Sinica, 19 (Sup.): 68～75. (in Chinese with English abstract)

Costa, S., and Maluski, H., 1993. Use of the ^{39}Ar-^{40}Ar-stepwise heating method for dating mylonite zones: An example from the St. Barthelemy Massif (northern Pyrenees, France). Chem. Geol., 72: 127～144.

Gerald, J. D. F., and Harrison, T. M., 1993. Argon diffusion domain in K-felspar I: microstructures in MH－10. Contrib. Mineral. Petrol., 113: 367～380.

Hara, I., Takeda, K., and Kimura, T., 1973. Preferred lattice orientation of quartz in shear deformation. J. Sci. Hiroshima Univ., 7 (1): 1～11.

Harrison, T. M., Lovera, O. M., and Heizler, M. T., 1991. ^{39}Ar-^{40}Ar results for alkali felspar containing diffusion domains with differing activation energy, Geochim. Cosmochim. Acta, 55:1435～1448.

He Yongnian, Ling Chuanyong and Shi Lanbing, 1988. Basic on Tectono-petrology. Beijing: Geological Publishing House, 62～87 (in Chinese with English abstract).

Ji Shaochen, 1988. Tectonic siguificance of partial melting (1)Experiment study on transition of deformation mechanism. Acta Geoscientia Sinica, 4:347～356 (in Chinese with English abstract).

Li Haibing, Xu Zhiqin and Chen Wen, 1996a. Deformational features and tectonic evolution of the south Kunlun strike-slip shear zone, East Kunlun Mountains. Acta Geoscientia Sinica, Special Issue, 16～21.

Li Haibing, Xu Zhiqin and Chen Wen, 1996b. Southern margin strike-slip fault zone of East Kunlun Mountains: an Important consequence of Intracontinental Deformation. Continental Dynamics. 1 (2): 146～155.

Li Haibing, Yang Jingsui, Xu Zhiqin, Wu Cailai, Wan Yusheng, Shi Rendeng, Liou, J. G., Tapponnier, P., and Ireland, T. R., 2001. Geological and geochrological evidences for Indosinianstrike-slip of the Altyn Tagh fault zone. Chinese Science Bulletin, 46(16): 1333～1338 (in Chinese with English abstract).

Lovera, O. M., Heizler, M. T., and Harrison, T. M., 1993. Argon diffusion domains in K-felspar II: kinetic properties of MH－10. Contrib. Mineral Petrol. 113: 381～393.

Mainprice, D., Bouchez, T.-L., Blumenfeld, P., and Tubia, J. M., 1986. Dominant c slip in naturally deformed quartz: implications for dramatic plastic softening at high temperature. Geology, 14:819～822.

Okudaira, T., Takeshita, T., Hara, I., and Ando, J., 1995. A new estimate of the conditions for transition from basal ⟨a⟩ to prism ⟨c⟩ slip in naturally deformed quartz. Tectonophysics, 250:31～46.

Wu Cailai, Yang Jingsui, Ireland, T., Wooden, J., Li Haibing, Wan Yusheng and Shi Rendeng, 2001. Zircon SHRIMP ages of Aolaoshan granite from the south margin of Qilianshan and geological significance. Acta Petrologica Sinica, 17 (2):215～221 (in Chinese with English abstract).

Xu Zhiqin, Zhang Jianxin, Xu Huifen *et al*., 1997. Large Ductile Shear Zones and Their Dynamics in the Major Continental Chains of China. Beijing: Geological Publishing House, 294(in Chinese with English abstract).

Xu Zhiqin, Yang Jingsui, Zhang Jianxin, Jiang Mei, Li Haibing and Cui Junwen, 1999. Comparison between the tectonic units on the two sides of the Aityn Tagh sinistral strike-slip fault and the mechanism of lithospheric shearing. Acta Geologica Sinica, 73 (3): 193～05 (in Chinese with English abstract).

Xu Zhiqin, Li Haibing, Yang Jingsui and Chen Wen, 2001. A large transpression zone at the south margin of the East Kunlun Mountains and oblique subduction. Acta Geologica Sinica, 75(2): 156～164.

Xu Zhiqin, Yang Jingsui, Zhang Jianxin, Li Haibing, Wu Cailai, Wan Yusheng *et al*. Geological Evolution and Lithospheric Shearing of the Qilian Shan-Altun Shah. Beijing: Geological Publishing House (in press, in Chinese with English abstract).

Yang Jingsui, Xu Zhiqin, Li Haibing, Wu, Cailai, Cui Junwen, Zhang Jianxin and Chen Wen, 1998. Discovery of eclogite at northern margin of Qaidam basin, NW China. Chinese Science Bulletin, 43: 1755～1760.

Yang Jingsui, Xu Zhiqin, Li Haibing, Zhang Jianxin, Wu Cailai and Shi Rendeng, 2000. A Caledonian convergent border along the Qilian terraine, NW China: Evidence from eclogite, garnetperidotite, ophiolite, and S-type granite. Journal of the Geological Society of China, 43(1): 142～160.

Yang Jingsui, Xu Zhiqin, Song Shuguang, Zhang Jianxin, Wu Cailai, Shi Rendeng, Li Haibing, Brunel, M., and Tapponier, P., 2002. Subduction of continental crust in the Early Palaeozoic North Qaidam ultrahigh-pressure metamorphic belt, NW China: Evidence from the discovery of coesite in the belt. Acta Geologica Sinica, 76(1): 63～68.

About the first author

XU Zhiqin Female; academician of the Chinese Academy of Sciences. Research fields: tectonics and microstructure. Engaged in research on the tectonics of the Qinghai-Tibet plateau since 1981. At present her research includes the project on the tectonics of the Qinghai-Tibet plateau and the project on ultrahigh-pressure metamorphic belt and the Chinese Continental Scientific Drilling Project (CCSD). Tel: (86) 1068329504, E-mail: xuzhiqin@ccsd.org.cn

Geological and chronological evidence of Indo-Chinese strike-slip movement in the Altyn Tagh fault zone[*]

Li Haibing[1] Yang Jingsui[1] Xu Zhiqin[1] Wu Cailai[1] Wan Yusheng[1]
Shi Rendeng[1] Juhn G. Liou[2] P. Tapponnier[3] & Trevor R. Ireland[2]
(1. Institute of Geology, Chinese Academy of Geological Sciences, Beijing 100037, China;
2. Department of Geological & Environmental Sciences, Stanford
University, Stanford, CA 94305—2115, USA;
3. Institut de Physique du Globe, 4 Place Jussieu, 75252 Paris Cedex 05, France)

Abstract A set of granitic and amphibole mylonite are exposed in the Altyn Tagh fault zone. The preliminary study shows that these rocks are the product of the syntectonic anatexis in the process of the left-lat-eral strike-slip shear, and are the result of the ductile transpression. There are two types of zircon sorted from the mylonite formed with synshear anatexis. Among them, one is the anatectic long columnar zircon and another is the residual metamorphic sub-rounded columnar zircon. Two groups of age for single zircon measured by ion microprobe (SHRIMP) are obtained: one is 461 ~ 547Ma for the sub-rounded columnar residual metamorphic zircon, and the other is 239 ~ 244Ma for the long-columnar anatectic zircon. This type of zircon is directionally spread in rock, and the long axis direction of its crystal is identical to that of stretching lineation, representing the direction of tectonic stress in the process of the strike-slip. ^{40}Ar-^{39}Ar age of the directional growth hornblende in the same mylonite sample measured is 223 ~ 226Ma. The above geological and chronological data prove that the syntectonic anatexis occurred during Indo-Chinese Epoch, showing that the strong strike-slip movement occurred in the Altyn Tagh fault zone at least as early as Indo-Chinese Epoch.

Keywords Altyn Tagh fault zone, syntectonic anatexis, mylonite, zircon directional spread, U-Pb SHRIMP age, Ar-Ar age.

The Altyn Tagh fault zone is located in the northern edge of the Qinghai-Tibet Plateau, and is a large NNE-strike fault system within the Asia continent. Its formation age and geological process, especially the relationship with plateau uplift, has been a hotspot of studying the Qinghai-Tibet Plateau both at home and abroad. A relatively common recognition is that the Altyn Tagh fault zone is a large-scale left-lateral strike-slip fault since Cenozoic[1,2]. However, some research workers think that the Altyn Tagh fault zone had activated before Cenozoic, such as in Early Paleozoic[4], Variscan Periodt[3], Jurassic[5], Late Cretaceous[6], etc. This paper discusses the syntectonic anatexis occurring in the depth in the early movement of the Altyn

[*] Chinese Science Bulletin Vol. 47 No. 1 January 2002.

Tagh fault zone by discovering mylonite in the Xorkol area of the middle segment of the Altyn Tagh fault zone and studying the petrology, micro-tectonic geology and isotope chronology of the mylonized rock, and discusses the formation age of the Altyn Tagh fault zone by studying U-Pb SHRIMP and ^{40}Ar-^{39}Ar chronology of the newly formed syntectonic anatexis minerals.

1 Fundamental geological characteristics of the Aerjin strike-slip ductile shear zone

Recently, we have discovered a ductile shear zone in Tashidaban Group[7] of Middle Proterzoic in the Xorkol area of the middle segment of the Altyn Tagh fault zone. The shear zone, 100～500m wide, as zonal distribution, is completely controlled by the Altyn Tagh fault zone. The rocks in the shear zone are composed of granitic and amphibole mylonite. The metamorphic degree of the rocks reaches amphibolite facies. In general, the bedding plane strike of the rocks is steep NE70°(nearly vertical), which is identical to that of the Altyn Tagh fault zone(Fig. 1), but the stretching lineation constructed by the directional spread of hornblende is nearly horizontal. The shear stress is relatively developed within the zone, such as shear fold, S-C structure and nonsymmetrical mortar system. They all show that there are left-lateral shear characteristics. It can be seen on the YZ-plane of mylonite that there is compressional deformation characteristic along the direction of Z-axis, and there is stretching along Y-axis, showing that this ductile shear zone not only has strike-slip but also compression, therefore it is a typical ductile transpressional shear zone[8]. It can be seen under a microscope that ductile-brittle deformation is superimposed on the ductile deformation. Both of them have left-lateral shear characteristics. On the other hand, at the sides along the present the Altyn Tagh fault zone, there are thrust faults and "X-shape" faults that are near parallel to the Altyn Tagh fault zone(Fig. 1), showing that there is compression in the process of left-lateral brittle strike-slip, and it has the characteristics of the late brittle transpression. Moreover, it can be seen in the field that the brittle fractures(left-lateral)are superimposed on the ductile deformation zone. The above shows that ductile, ductile-brittle, brittle deformation fabrics were formed in the process of the integrated left-lateral transpression, and they have integrated distribution characteristic, so that the mylonite can be considered as the product of the early deep ductile deformation of the Altyn Tagh fault zone. It was uplifted to the surface in the late strike-slip process because of the thickening of the crust and the increase of geothermal gradient by transpression, and anatexis occurred under the condition of fluid coming-in[9,10].

2 Syntectonic anatexis

The recrystallized hornblende aggregate, being banded spread, has obvious nebula-like characteristics in the rock of the ductile shear zone, and the basement and vein can be obviously distinguished , or amphibole and granitic bandings were constructed , showing that there are

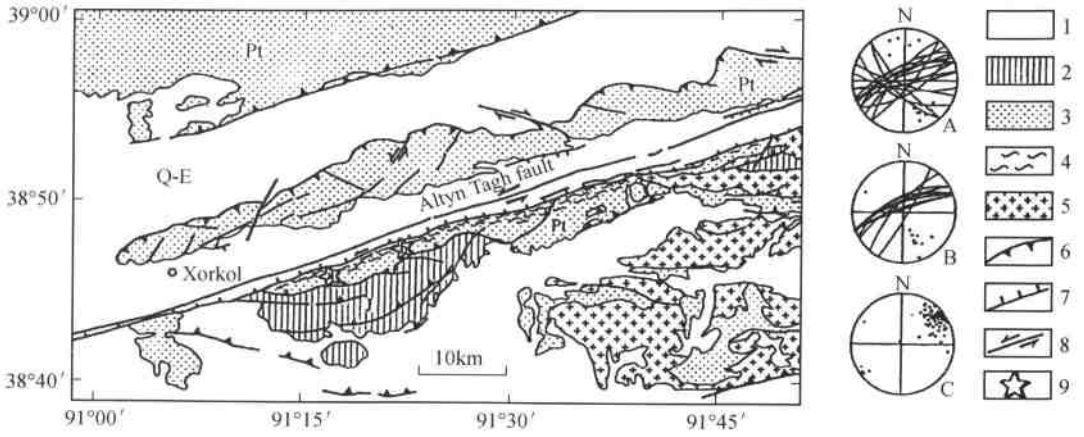

Fig.1 Geological sketch of Xorkol area in the middle segment of the Altyn Tagh fault zone. Map A and Map B in the lower part of the geological sketch are the sciagraphs of the foliation planes of the sampling point a and b; Map C is the sciagraph of stretching lineation. 1—Cenozoic; 2—Jurassic; 3—Middle Proterzoic(?); 4—mylonite zone; 5—granite; 6—thrust fault; 7—normal fault; 8—strike-slip fault; 9—sampling location.

anatexis characteristics. But the hornblende is directly spread, thus constructing near horizontal stretching lineation. It can be observed under a microscope that anatectic (magmatic) long columnar zircon is directionally spread too(Fig.2), the direction of its long axis is identical to that of stretching lineation, showing that anatexis is affected by shearing. Amphibole and granitic bandings are developed within the shear zone. Although their scale and size are different, their strike is identical to that of the Altyn Tagh fault zone. They were mylonized, but all the micro-tectonics indicate that there are left-lateral shear characteristics, reflecting that

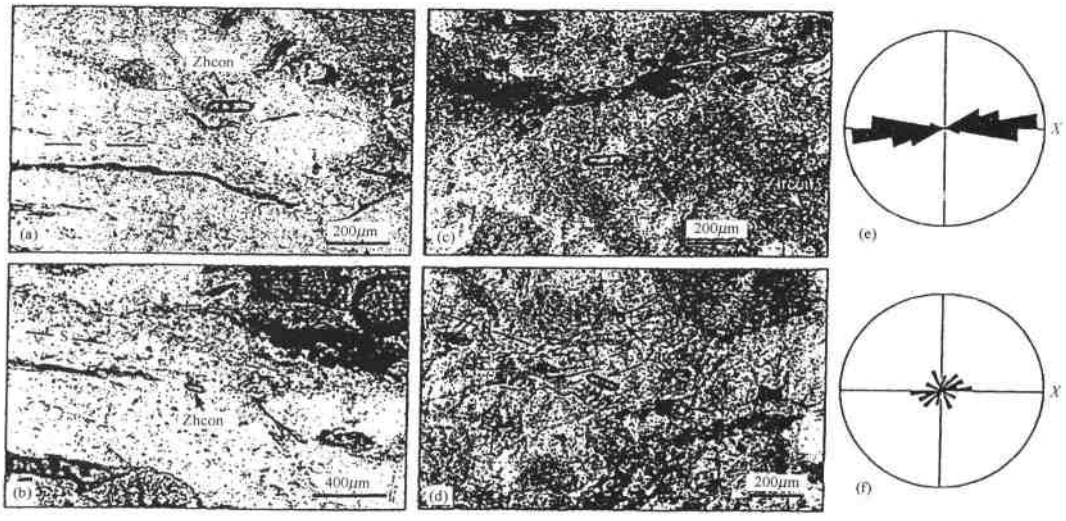

Fig.2 The microscopic fabric of zircon in the mylonized rock(micrograph of XZ plane under single polar).

they are the product formed under the same strike-slip shearing. These bandings are obviously controlled by the shear zone in the spatial distribution. Granitic bandings and massifs occurred isolatedly and unrootedly , but plane bedding within the mylonized granitic banding is identical to the occurrence of the outer mylonite plane bedding. Some bandings generated folds, and penetrated into granitic banding along the cleavage of axial plane(plane bedding of mylonite), showing that granitic bandings occurred in the successive deformation of strike-slip shear. In mylonite, Axis *C* fabrics of quartz show that they have left-lateral shear characteristics. In general, they are mainly the middle and low temperature basal fabric, but they also have the characteristics of high temperature ($>$ 600℃) prismatic plane fabric. It shows that at the beginning of the early strike-slip anatexis there is the characteristic of high temperature shearing, but there is the characteristic of middle temperature shearing in the process of the late uplifting. This is identical to the fact that arkosic bandings are developed in the thin sections, and some plagioclase has plastic deformation characteristic with left-lateral shear stress, showing that they have high temperature deformation. Furthermore, after we calculated the geological thermometer and manometer of plagioclase-hornblende mineral pair[11,12], the result achieved is that its formation temperature is 580～640℃ ; $P = 430 \sim 650$ kPa, and there are more hydrous minerals like hornblende and biotite formed under the shearing of shear zone, showing that there are much more fluid in the process of shear, therefore it can be considered that this temperature basically reached the magmatic melting temperature in the condition of enough fluid penetration. According to the relationship of the crystal form of zircon (in the form of prismatic face and pramidal face) with magmatic crystallization temperature[13], it is concluded that the type of long columnar anatectic(magmatic)zircon sorted from mylonite by statistics(in the rock, the direction of zircon's long axis is identical to that of stretching lineation)belong to G1, P1, and P2, and the corresponding crystallization temperature is 600 ～ 700℃ . The temperature is basically identical to that of the calculated mineral pairs, that of quartz *C* axis fabric and that of the plastic deformation of plagioclase. This shows not only the temperature of anatexis, but also the anatexis associated with shearing.

The above characteristics reflect the feature of syntectonic anatexis, i.e. the shearing, mylonization and anatexis occurred basically in the same period.

S represents foliation plane, (a), (b), (c), and(d)show that the zircon with long columnar crystal form is directionally spread, and the long axis of the crystal is parallel to foliation plane (S). In the lower part at the right side of(b)and at upper part of(d), the crystal form of zircon is weakly rounded, and its long axis has no direction. (e)is the rose map of the long axial spread direction of the long columnar zircon(42 grains of zircon), and the distribution of its long axial has obvious direction, which is identical to that of stretching lineation. (f)is the rose map of the long axial spread direction of the weakly rounded zircon(30 grains of zircon), and its long axis has no direction. (e)and(f)were made according to the statistics of zircon in the rock thin section(XZ plane).

3 Research of zircon U-Pb SHRIMP

(i) Characteristic of zircon. Three samples were collected from the syn-shear anatectic rock. Zircon was sorted respectively from No. Ⅰ Sample the granitic mylonite(S99－6), from No. Ⅱ Sample the amphibole mylonite(S99－9) and from No. Ⅲ Sample the amphibole mylonite(S99－25). Two types of zircon (long columnar and sub-rounded columnar) can be clearly distinguished for the sorted zircon under a binocular. The transparence of these two types of zircon is relatively good, with no color or light aubergine.

According to the observation in the thin section of XZ planes of 6 different specimens under a microscope, 72 grains of zircon were found, 42 of them belong to the long columnar zircon whose long axis is directional spread, and another 30 grains belong to the sub-rounded columnar zircon whose long axis is not directional spread (Fig.2). The characteristics of the zircon with better long columnar crystal form (this type of zircon is mainly developed in the mylonized granitic rock or in granitic mylonite) are that the grain is relatively large, the main crystal plane is flat and clear, and the edge of crystal is straight. It is shown under a microscope that this type of zircon is directionally spread in rock, and the growth direction of its crystal long axis is basically identical to that of stretching lineation (Fig.2), showing that it is the newly formed mineral in the process of shearing. On the cathodo-luminescence map of zircon, the zoning and residual inner core cannot be found, and only the stripes along the direction of prismatic face are found. In general, they are relatively homogeneous (Fig.3), and Th/U value is relatively high, showing that the zircon has the characteristic of anatectic (magmatic) origin[14]. The crystallization age of zircon not only represents that of anatexis, but also represents that of the strike-slip shear.

The second type of zircon, i.e. sub-rounded columnar zircon, its main characteristic is that the grain is relatively small, multi-crystal plane (multifaceted) is developed and has no direction. On the cathodo-lumine-scence map of zircon, the zoning and residual inner core can be found (Fig.3), some has elliptical residual core. Obviously, there are two growth parts, one is the core and the other is the outer part overgrowing on the core. This type of zircon displays that Th/U value is relatively low, showing that the zircon has the characteristic of metamorphic origin[14]. This can be the residual of the syntectonic anatectic mass of the early-metamorphosed product.

(ii) Chronology of zircon U-Pb SHRIMP. The chronological determination using the zircon U-Pb SHRIMP method for 14 grains from 3 mynolite samples (No. S99－6, No. S99－9 and No. S99－25) was carried out and completed in the Ion Microprobe Laboratory of Stanford University, USA. The results are seen in Figs. 3 and 4. In total, the values from 15 points were completed. The obtained age of zircon can be mainly divided into two groups: the age of group A is 461～547Ma, being the age of the sub-rounded columnar zircon with the characteristic of metamorphic origin (Fig.3), and the age of group B is 239～244Ma, being the age of the long

columnar zircon with the characteristic of anatectic(magmatic)origin(Fig.3).

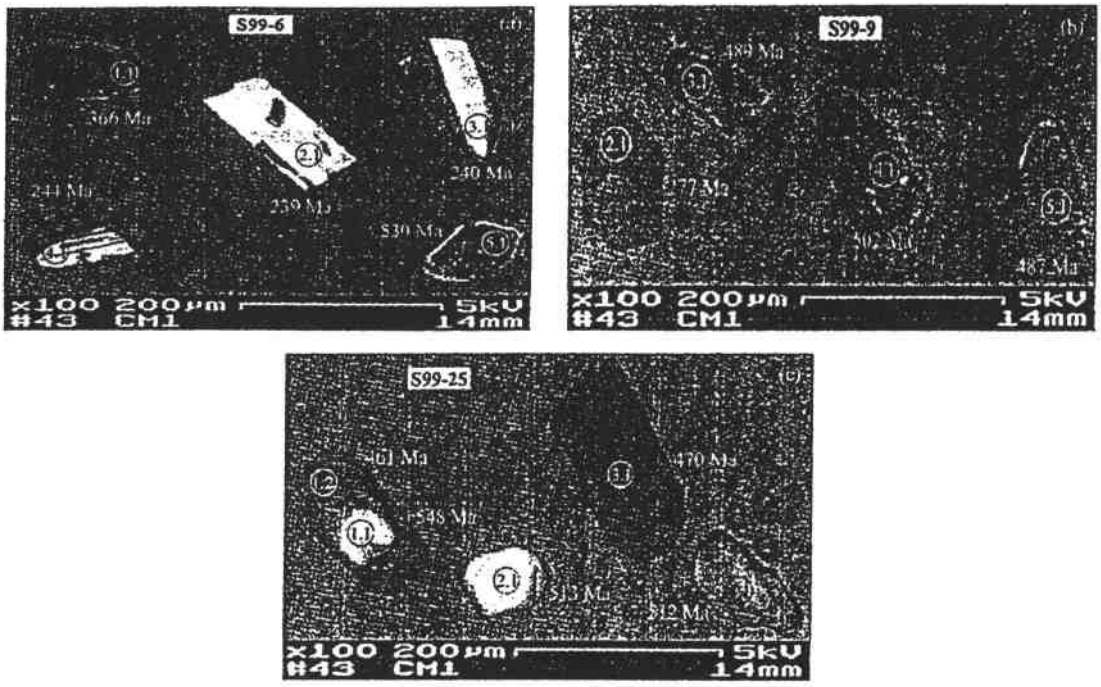

Fig.3 Cathodo-luminescence map of zircon and acquisition area of SHRIMP age.

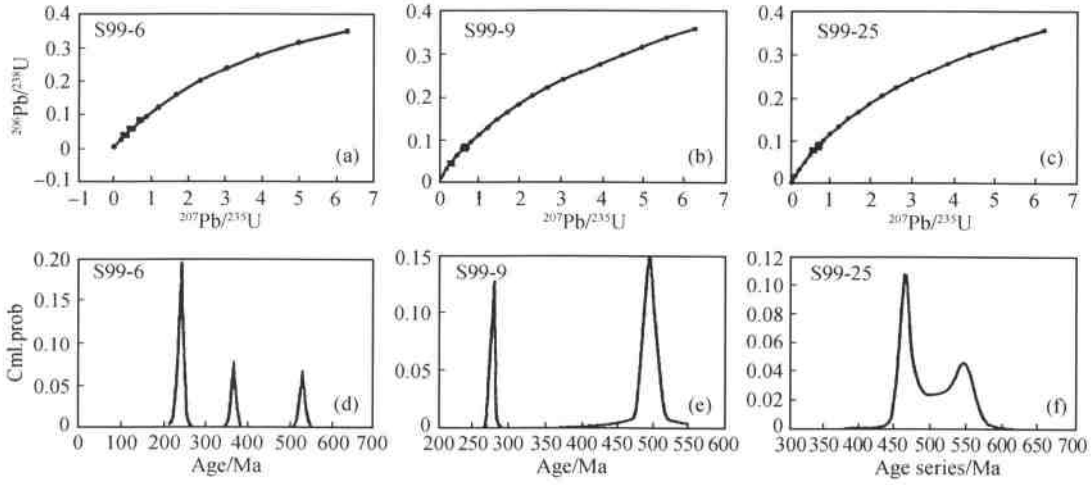

Fig.4 SHRIMP concordancy diagram of zircon U-Pb(a, b, c)and cumlative probability chart of SHRIMP U-Pb age(d, e, f).

In addition, 366Ma(the analytical point is S99－6－1.1), it has no geological significance because this age represents the mixed age between the core and outer overgrowth part. S99－6, S99－9, S99－25 are the numbers of samples, circle represents the areas hit by ion

microprobe. No. 2, 3, and 4 zircons from Sample S699 − 6 are the zircons with long columnar crystal form but their interiors have no zoning and residual core, therefore, they belong to the anatectic(magmatic) zircon. Zoning and inner core were found in the interior of other zircon (Fig. 3).

4 Ar-Ar isotope assaying

Also, hornblende was sorted from the mylonite sample S99 − 9 for the chronological determination by the ^{40}Ar-^{39}Ar method. The hornblende is directionally spread and the direction is identical to that of stretching lineation, also belongs to the product of syntectonic anatexis. ^{40}Ar-^{39}Ar isotope assaying was completed in the Isotope Laboratory of Institute of Geology, the Chinese Academy of Geological Sciences. The result is seen in Table 1 and Fig. 5.

Table 1 ^{40}Ar-^{39}Ar data of phase warming-up of hornblende of mylonite(S99 − 9) from the Altyn Tagh fault zone

Temp./℃	$(^{40}Ar/^{39}Ar)_m$	$(^{36}Ar/^{39}Ar)_m$	$(^{37}Ar/^{39}Ar)_m$	$(^{40}Ar^*/^{39}Ar)_m$	^{39}Ar ($\times 10^{-14}$, mol)	^{39}Ar(%) accumulative percentage	Age/Ma(2σ)
Hornblende in mylonite m = 137.00mg, J = 0.013453							
500	21.01170	0.03310	3.39000	11.50510	51.00	2.67	259.60 ± 11.10
600	16.13240	0.03480	2.97010	6.05640	29.00	4.19	141.30 ± 12.00
700	15.88040	0.02990	2.33950	7.21950	30.00	5.76	167.20 ± 10.30
800	16.58540	0.03200	3.61580	7.39880	33.00	7.49	171.20 ± 10.90
900	16.46820	0.02670	6.77320	9.10500	49.00	10.05	208.40 ± 9.20
1000	13.29550	0.01140	4.46430	10.28610	88.00	14.66	233.80 ± 4.70
1100	10.95920	0.00340	4.06810	10.28440	417.00	36.49	233.80 ± 3.00
1200	10.65570	0.00270	4.00300	10.15000	366.00	55.65	231.10 ± 2.90
1300	10.28950	0.00260	4.01780	9.82360	380.00	75.55	223.90 ± 2.80
1400	10.29980	0.00320	4.33430	9.68680	467.00	100.00	221.00 ± 2.80

Near unanimous age was obtained for hornblende from mylonite. The obtained integral age of ^{39}Ar release of 5 temperature phases is(222.6 ± 2.9)Ma(Table 1 and Fig. 5), reflecting that the intercept of $^{40}Ar/^{36}Ar$ on isochron is 333.77 ± 47.01, which is bigger than the value (295.5) of ideal atmosphere, and the obtained isochron age is(225.59 ± 4.63) Ma, which is identical to the integral age. This age is identical to that of long columnar zircon.

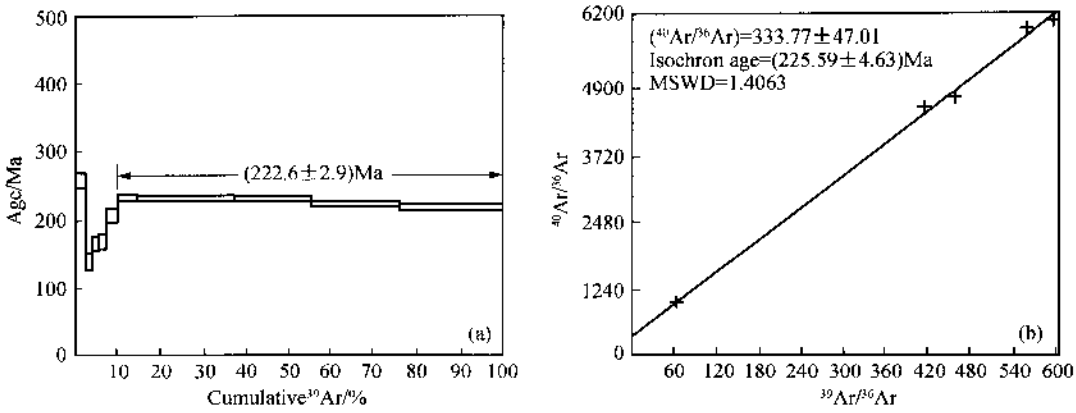

Fig. 5 Age spectrum(a)and isochron diagram(b)of hornblende from amphibole mylonite.

5 Discussion and significance

(i)461 ~ 547Ma is the age of the early metamorphism. 461 ~ 547Ma obtained from the sub-rounded columnar zircon can be considered as that of metamorphism of the rock, there is no relationship with the strike-slip shearing of the Altyn Tagh fault zone, but it is basically identical to the recent research result[15,16] that the Early Paleozoic orogenesis exists in the Altun and Qilianshan structural belt. It can represent the result of the Early Paleozoic collision. It can be seen in Fig. 3(c)that there were at least two periods of metamorphism during 461 ~ 547Ma. The age of the inner core S99 - 25 ~ 1.1 of the same grain of zircon is 547Ma, the age of the outer growth part S99 - 25 ~ 1.2 is 461Ma, the difference of the ages between the core and the growth part is 85Ma, which may reflect the age of two periods of metamorphism. Further discussion should be made on its significance.

(ii)223 ~ 244Ma is the age of the strike-slip movement In the Altyn Tagh fault zone. It is considered that 239 ~ 244Ma obtained from the long columnar zircon is the age of the occurrenoe of the anatectic melting, also shall represent that of the strike-slip shear activities. 223 ~ 226Ma(^{40}Ar-^{39}Ar)of the directional growth hornblende is basically identical to the SHRIMP U-Pb age of anatectic zircon(long columnar directional growth), showing that strong ductile strike-slip activities that were accompanied with anatectic melting occurred in the Altyn Tagh fault zone at the beginning of Indo-Chinese Epoch. This is basically identical to the formation age 220 ~ 240Ma[17] of the East Kunlun strike-slip fault zone. That means that during the Indo-Chinese Epoch relatively strong left-lateral strike-slip happened on the Western Tarim Massif and the eastern massif, while slant collision and strike-slip occurred between the Bayankala Massif and the East Kunlun Massif.

Arnaud *et al*.[6] made the chronological determination of Rb/Sr and biotite ^{40}Ar-^{39}Ar for the mylonized granite and schist with arkosic pudding exposed in the Altyn Tagh fault zone, and a set of age data(140 ± 2Ma ~ 162.9 ± 3.7Ma) was obtained. Liu *et al*.[6] made ^{40}Ar-^{39}Ar

chronological determination on laser micro-area for muscovite and biotite of the syntectonic newly formed minerals from the Jurassic strata and mylonized granite exposed in the fault zone, and a set of age data (92 ~ 89Ma) was obtained. We think that these two sets of age may represent the age of the Altyn Tagh fault zone reactivation. It is worth noting that also these two periods of strong left-lateral strike-slip movement exist since the Indo-Chinese Epoch in the East Kunlun strike-slip fault zone[17], therefore it shall belong to the reactivation in the whole deformation evolution of the fault. By this token, the formation age and reactivation time of the Altyn Tagh fault zone are very identical to those of the East Kunlun strike-slip fault. What a role they played in the formation of plateau is another new subject for us to study.

Acknowledgements We wish to thank Dr. Song Shuguang, Prof. Zhang Jianxin, Prof. Liu Fulai, Prof. Chen Wen and Dr. Meng Fancong for assistance, and academician Shen Qihan for constructive opinion. The work was supported by the National Key Basic Research Project (Grant No. G1998040800) and Sino-France Collaborative Project of "Altun Shan-Qilianshan" Tectonic Evolution and Lithosphere Shearing.

References

[1] Tapponnier, P., Peltzer, G, Armijo, R., On the mechanics of the collision between India and Asia (eds. Coward, M.P., Ries, A.C.), Collision Tectonics, Geological Society of London Special Publish, 1986, 115~157.

[2] Ge Xiaohong, Zhang Meisheng, Liu Yongjiang *et al*., Scientific problems and research thinking of Altyn Tagh Fault research, Modern Geology(in Chinese), 1998, 12(3): 295.

[3] Cui Junwen, Tang Zhiming, Deng Jinfu *et al*., Altyn Tagh Fault System(in Chinese), Beijing Geological Publishing House, 1999.

[4] Zhang Zhitao, Geological feature of Altyn Tagh Fault, Publication of Xi'an Institute of Geology and Mineral Resources, Chinese Academy of Geological Sciences (in Chinese), Beijing: Geological Publishing House, 1985, 9: 20.

[5] Arnaud, N., Delville, N., Montel, J.M. *et al*., Paleozoic to Cenozoic deformation along the Altyn Tagh fault in the Altun Shan massif area, Eastern Qilian Shan, NE Tibet, China: American Geophysical Union Annual Meeting Abstracts. 1999, F1018.

[6] Liu Yongjiang, Ye huiwen, Ge Xiaohong *et al*., $^{40}Ar/^{39}Ar$ age of laser micro-area of deformed rock of Altyn Tagh Fault Chinese, Science Bulletin(in Chinese), 2000, 45(19): 2101.

[7] Xinjiang Geological Bureau, Regional Geological Investigation Report of the People's Republic of China, Xorkol Sheet(1:200,000)(in Chinese), 1981.

[8] Krantz, R.W., The transpressional strain model applied to strike-slip, oblique-convergent and oblique-divergent deformation, Journal of Structural Geology, 1995, 17(8): 1125.

[9] Brown, M., Averkin, Y.A., McLellan, E.L. *et al*., Melt segregation in migmatites, Journal of Geophysical Research, 1995, 100: 15655.

[10] Druguet, E., Hutton, D.H.W., Syntectonic anatexis and magmatism in a mid-crustal transpressional shear zone: an example from the Hercynian rocks of the eastern Pyrenees, Journal of Structural Geology, 1998, 20(7): 905.

[11] Plyusnina, L.P., Geothermometry and Geobarometry of plagioclase-hornblende bearing assemblages, Contrib. Mineral. Petrol., 1982, 80: 140.

[12] Hollister, L.S., Grissom, G.C., Peters, E.K. *et al.*, Confirmation of the empirical correlation of Al in hornblende with pressure of solidification of calc-alkaline plutons, Am. Mineral., 1987, 72: 231.

[13] Pupin, J.P., Zircon and granite petrology, Contribution to Mineralogy and Petrology, 1980, 73: 207.

[14] Robb, L.J., Armstrong, R.A., Waters, D.J., The history of granulite-facies metamorphism and crustal growth from single zircon U-Pb geochronology: Namaqualand, South Africa, Journal of Petrology, 1999, 40(12): 1747.

[15] Yang Jingsui, Xu Zhiqin, Li Haibing *et al.*, Discovery of eclogite at northern margin of Qaidam Basin, NW China, Chinese Science Bulletin, 1998, 43(20): 1755.

[16] Zhang Jianxin, Zhang Zeming, Xu Zhiqin *et al.*, The ages of U-Pb and Sm-Nd for eclogite from the western segment of Altyn Tagh tectonic belt. Chinese Science Bulletin, 1999, 44(24): 2256.

[17] Li, H.B., Xu, Z.Q., Chen, W., Southern margin strike-slip fault zone of East Kunlun mountains: an important consequence of intracontinental deformation, Continental Dynamics, 1996, 1(2): 146.

Oblique Stepwise Rise and Growth of the Tibet Plateau[●]

Paul Tapponnier[1] Xu Zhiqin[2] Françoise Roger[1] Bertrand Meyer[1]
Nicolas Arnaud[3] Gérard Wittlinger[4] Yang Jingsui[2]
(1 Institut de Physique du Globe, 4 Place Jussieu, 75252 Paris, France;
2 Ministry of Lands and Resources, Baiwanzhuang Rd, 100037 Beijing , China;
3 Universite Blaise Pascal, 5 rue Kessler, 63000 Clermont Ferrand, France;
4 EOST, Université Louis Pasteur; 5 rue Descartes 67084 Strasbourg, France)

Two end member models of how the high elevations in Tibet formed are (i) continuous thickening and widespread viscous flow of the crust and mantle of the entire plateau and (ii) time-dependent, localized shear between coherent lithospheric blocks. Recent studies of Cenozoic deformation, magmatism, and seismic structure lend support to the latter. Since India collided with Asia ~55 million years ago, the rise of the high Tibetan plateau likely occurred in three main steps, by successive growth and uplift of 300-to 500-kilometer-wide crustal thrust-wedges. The crust thickened, while the mantle, decoupled beneath gently dipping shear zones, did not. Sediment infilling, bathtub-like, of dammed intermontane basins formed flat high plains at each step. The existence of magmatic belts younging northward implies that slabs of Asian mantle subducted one after another under ranges north of the Himalayas. Subduction was oblique and accompanied by extrusion along the left lateral strike-slip faults that slice Tibet's east side. These mechanisms, akin to plate tectonics hidden by thickening crust, with slip-partitioning, account for the dominant growth of the Tibet Plateau toward the east and northeast.

Tibet is Earth's largest and highest plateau, with a flat interior disrupted by active normal faulting(1 ~ 6) (Fig.1) .How such topography formed and is maintained has profound implications on the mechanics of continental deformation. Within the framework of India's collision with Asia, several models have addressed the question. One class of models focuses on today's uniform height(3), and on the extensional faulting, interpreted to indicate collapse of the plateau since the mid-Miocene(7)or earlier(8). The entire lithosphere is assumed to have thickened as a thin viscous sheet, with broadly distributed shortening of both crust and mantle having absorbed plate convergence(9, 10). Tibet as a whole is then inferred to have risen

● Science Vol 294 23 November 2001.

significantly above its current altitude (~5000m), as its crust buoyantly rebounded because of removal of part of its thickened lithospheric mantle, which triggered extension and volcanism(9~11). This "soft Tibet" model, however, ignores the half-dozen large strike-slip faults that border or slice the plateau, some of them at least as long as California's San Andreas fault(12), (Fig.1). The existence of such first-order tectonic features and their association with the high topography, which is unlikely to be coincidental, thus remains to be explained.

Evidence from geological, geochronological, and seismic studies now shows that these fault zones, far from being shallow and late(and hence minor)side effects of thickening(9, 10), have been key in controlling the growth of the Tibetan highlands from the start. Such studies also indicate little or no sign of lithospheric removal or surface rebound. Here, we review these recent findings and discuss an alternative model for the rise of topography north of the Himalayas that reconciles the two most prominent facets of Tertiary Asian tectonics: strike-slip extrusion and plateau building.

Strain and Faulting in Tibet

In Tibet, upthrust basement is only exposed along a few ranges (Gangdese, Tanggula, Kunlun, Altyn Tagh, and Qilian Shan) (Figs. 1 and 2) separated by large basins. Older, wide basins trend ~EW to NW-SE, parallel to the ranges. Younger, narrow ones trend NS. The youngest basins in southern Tibet and Yunnan are rifts due to ongoing, roughly EW extension (1, 2, 12) (Fig. 1). The total amount of extension related to the active normal faults of Tibet is quite small. As deduced from structural relief, it is at most a few tens of kilometers($\leqslant$40km), less than 3% strain across the~1200-km-long stretch of the plateau cut by the faults(~80 to 92E) (1, 2, 10). Most of the Tibetan rifts are filled with Plio-Quaternary conglomerates, and cut at high-angle older~EW basins with Miocene deposits(1, 2). Only the Thakkola and Yadong-Gulu grabens may have developed earlier(13, 14), probably in connection with strike-slip along the Karakorum and Jiali faults, respectively (Fig. 1). Overall, the extension regime thus postdates the Miocene, and the corresponding amount of crustal thinning since is less than 2km, negligible at the scale of the collision zone(1, 2). Six of the young NS trending rifts(Fig. 1) extend across the Zangbo suture into the Greater Himalayas(1, 2, 4~6), a region underlain by flexed Indian-plate mantle (15 ~ 17), beneath which lithospheric thinning did not occur. Extension in southern Tibet is thus most simply interpreted to result from a combination of dextral slip-partitioning and divergent thrusting along the MFT(1, 2, 18). The shortening rate predicted from this interpretation is consistent with that measured across the Himalayas [~2cm/year; (19, 20)], which corroborates the small amount of extension across the southern plateau. More subdued normal faulting in northern Tibet seems to result also from strike-slip movement, particularly near the splaying SW ends of the sinistral(leftlateral)Kunlun and Altyn Tagh faults(1, 2, 4~6, 21~23). In Yunnan, Pliocene-Quaternary extension is associated with bookshelf faulting due to horizontal shear(1, 2, 12, 24~27), and occurs below 3000m above sea

level(a. s. l.). Thus, neither the kinematics and altitude, nor the timing and amount of normal faulting require a model in which extension might be driven by gravity collapse, itself triggered by wholesale rebound of a buoyant plateau to elevations ≥1km higher than 5000m in the Eocene or Mid-Miocene(7～10). Rather, the evidence at hand makes it likely that much more recent, if diachronous, extension in different areas was unrelated to large uplift increments(14, 18, 28～30). The coincidence of high topography with active normal faulting between about 28° and 36° N merely implies a large vertical stress that enhances rifting(1, 2, 4～6).

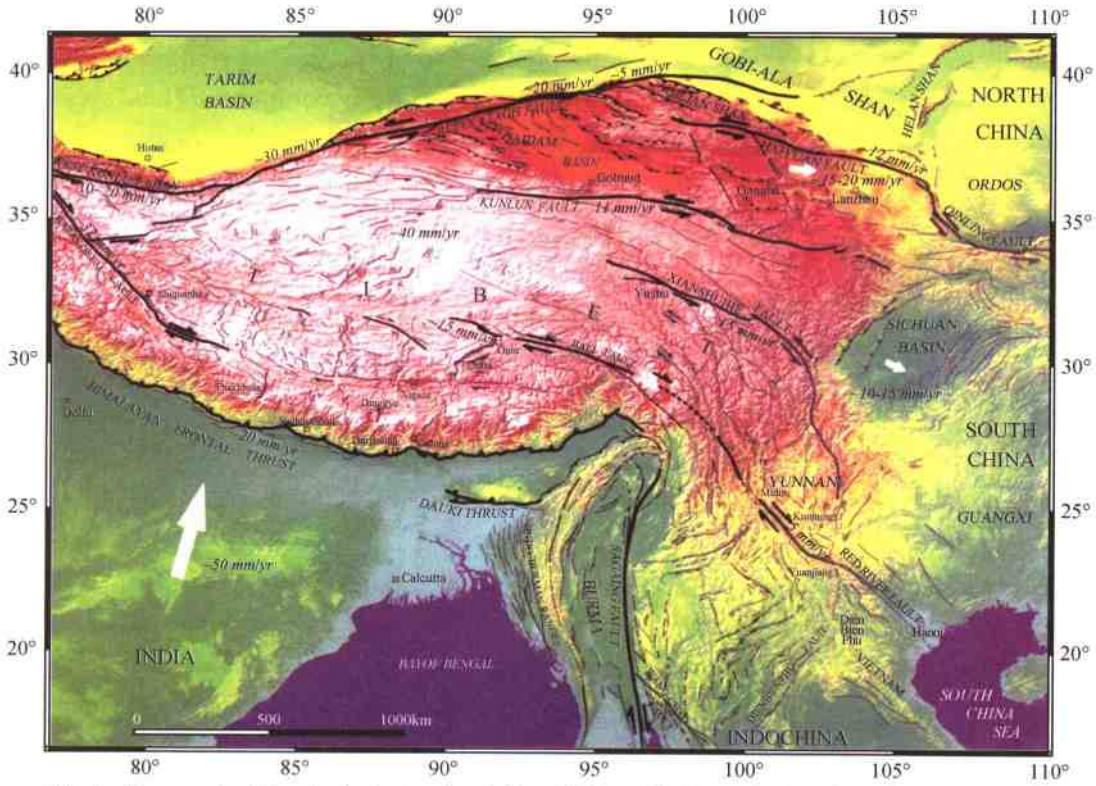

Fig. 1 Topography(3) and principal active faults of Tibet and adjacent regions(1, 2, 4, 12, 21～27, 53, 54, 56, 57, 99). Bold lines are faults that slip at 5mm/year or more. Bold numbers indicate rates where known. Thin lines, slower slipping faults. Dashed thin lines, inferred faults. Dotted lines, recent or growing folds. White arrows indicate motions of India, central Tibet, northeasternmost Tibet, and Sichuan relative to Siberia(56, 57, 94, 100).

The great flatness of broad areas on the plateau has been taken to indicate a deficit of Tertiary shortening. But there is now ample field evidence to support the conclusion long derived from paleomagnetic inclination differences(31, 32) that the amount of convergence absorbed since the Eocene by thrusts and strike-slip faults north and east of the Indus-Zangbo suture was large(～2000km). North of the Kunlun Fault, in the Qaidam basin and Qilian Shan (Fig. 2), mass balance estimates and retrodeformed sections across areas with predominantly

Neogene deposits show at least 150 to 200km of crustal shortening by thrusting in the last ~10 million years ago(Ma)(28~30). In the central part of the plateau, between the Kunlun and Tanggula ranges(Fenghuo Shan and Hohxil basin, Fig. 2), the strong folding, over a distance of~300km, of Paleogene red beds unconformably capped by more gently warped Neogene sandstones(33~37) implies a similar amount of earlier shortening. Comparable thrusting and folding affects the Eocene sandstones of the Lunpola and Baingoin basins(Fig. 2) south of the Tanggula range(33~37). Early-Middle Tertiary shortening also caused strong folding and thrusting of the Cretaceous - Paleocene red beds of the Chuxiong, Simao, and Lanping basins of

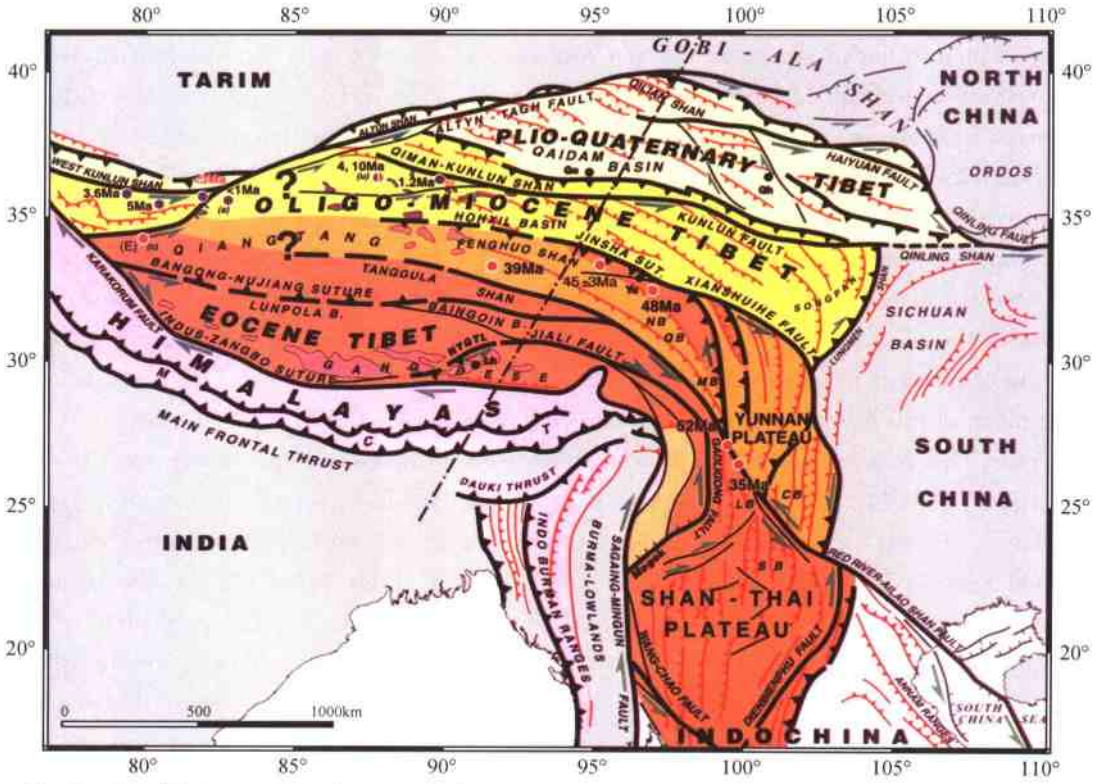

Fig. 2 Simplified map of major tectonic boundaries and Tertiary faults in Tibet, modified from(21, 22, 24~27, 40, 41, 51, 90). Bold black lines are major faults and localized shear zones (megathrust or strike-slip) with largest finite offsets, which may extend into lithospheric mantle. Dashed where uncertain. Thin red lines are crustal thrusts. Red and violet circles are Eocene and Plio-Quaternary magmatic centers, respectively, in central Tibet(80~83, 90). Corresponding numbers are ages discussed in text. Patches with deep pink and violet shades schematize other areas with Eocene-Early Miocene and Late Miocene-Quaternary lavas, respectively(84~86). Orange to pale yellow shades represent inferred ages of principal plateau-building epochs at expense of Asian crust(24~26, 28~30). Light pink shade south of Zangbo suture and west of Shan plateau indicates thickened Indian crust. Dashed line shows location of section in Fig. 3. Lh, Lhasa. Go, Golmud. Gh, Gonghe. Yu, Yushu. (a) Achikule, (j) Jingyu, (u) Ulugh Mustagh, (c) Changerchar, (E) Eocene. NB, QB, MB, LB, CB, SB, Nangqen, Qamdo, Markham, Lanping, Chuxiong, and Simao basins. MCT, Main central thrust.

Yunnan(24～26), and of the Nangqen and Qamdo-Markham basins south of Yushu in eastern Tibet(Fig.2). At the southern edge of the Lhasa block, the Gangdese thrust alone appears to have absorbed more than 40km of Oligocene shortening(38, 39), and much of the folding of the Cretaceous sandstones and limestones north of the Gangdese and in NW Tibet may postdate 55Ma(40, 41). Burial by less deformed Cenozoic sediments in the undrained interior of the plateau, or erosional unroofing, leaving mostly pre-Cenozoic rocks in the east, make it difficult to estimate collision-driven crustal shortening with precision. But there is little reason to doubt that it was enough in most places (～50%) to raise the average elevation of Tibet to that presently observed.

Tertiary offsets on the two largest strike-slip faults of Tibet are now documented to exceed those of plate boundaries such as the San Andreas and Alpine Faults. For the Red River-Ailao Shan shear zone (Fig.2), four independent lines of evidence-the 8° paleolatitude difference observed in Cretaceous red beds on either side(42), the reconstruction of seafloorspreading in the South-China Sea(43), the concordant displacements of several Mesozoic geological markers, among which the Cretaceous granite belt along South China's rim (24～26), and the diachronous cooling of the exhumed Ailao Shan high-grade mylonitic gneisses (44)-show that the sinistral offset is most likely 700±200km(24～26). The ages of magnetic chrons(32 to 16Ma)in the sea, a pull-apart basin at the end of the shear zone(43), and of crystallization and cooling of minerals in melts along the zone(35 to 15Ma)(24～26, 44～46)coincide, indicating that much of this offset accrued between the late Eocene and early Miocene at a rate of 3.5 to 4 cm/year. This rate is corroborated by the linear decrease in cooling ages along the Ailao Shan (～4 cm/year)(44). Sinistral shear was in large part coeval with transpressive thrusting and folding in the red-bed basins of Yunnan and SE Tibet, and both deformation regimes likely started before 35Ma(24～26, 45～47). On the Altyn Tagh Fault(Fig.2), the separation between piercing points of the Early Paleozoic suture in the Altun and Qilian Shan(48, 49), at 93° and 96.5°E respectively, testifies to ～300km of sinistral offset. To the south, displaced facies transitions of Bajocian deposits in the Qaidam and Tarim Basins suggest that the post-Jurassic offset between 86° and 91°E is greater(400±60km)(50). Yet farther south, the offset of the Permian granitoids of the eastern and western Kunlun reaches 500 to 600km(40, 41, 51). The concordant offset of a Cretaceous shear-zone found along the southern edge of the Kunlun implies that this largest displacement postdates ～100Ma(52). The 3±0.5 cm/year, 110 to 5 ka, left-slip rate derived from ^{14}C and ^{10}Be-^{26}Al cosmogenic dating of offset terrace risers and glacial moraines (53, 54) along the central segment of the fault (Fig.1), further suggests that 500 to 600km of offset on that segment could have accrued in the last 14 to 24 million years. The eastward decrease in total offset is consistent with propagation of the fault toward the Northeast(28～30). Cumulative offsets on the other large sinistral faults of Tibet (Haiyuan, Kunlun, Xianshui He)(Figs.1 and 2)remain debatable but reach or exceed 100km (27, 55～57).

Ongoing studies thus indicate that thrusting and sinistral strike-slip faulting have been

dominant and equivalent crustal deformation processes in Tibet. The total transpressive shortening taken up by such faults, which appear to have been active during most of the collision span, dwarfs by more than one order of magnitude the total extension across the recent, short-lived normal faults. Comparing the amounts and timing of strain related to either thus shows that the buildup of largescale Tibetan topography probably had little to do with buoyant rebound and extension at any epoch. Moreover, it is hard to see how gravity-induced outward spreading of a thin, viscous lithospheric sheet might have driven strike-slip motion and overthrusting at the edges of the plateau (8 ~ 10, 27, 58). Rather than being a small Plio-Quaternary addition to the collision process, strike-slip faulting began early on, ~15Ma or less after the onset of continental impact. Besides, the activation of the large strike-slip faults, which appear to have propagated eastward (29, 30, 43), was diachronous, starting earlier in the south than in the north (24 ~ 26, 56, 57). The age of strongly folded detrital sediments younger than ~100Ma also decreases northward across the plateau (28 ~ 30, 33 ~ 37).

Crust and Mantle Tomography

Seismic studies now provide more information on the bulk velocity structure of the crust and mantle beneath the Tibet plateau. Anisotropic inversion of Raleigh-and Love-wave phase-velocities (59) shows that, between depths of 100 and 300km, the mantle is faster, hence colder, under Tibet than under adjacent regions (Fig. 3), corroborating previous inferences (60 ~ 62). The surface-wave data consequently imply, contrary to local, teleseismic P-wave tomograms along the Golmud-Lhasa profile (Fig. 1) (63), which yield only relative velocity contrasts, that low velocities are mostly restricted to the thick crust of the high plateau (59, 60). The origin of the inefficient propagation of high frequency Sn-waves and of the slower Pn-wave velocity between the Tanggula and Kunlun ranges (64) may thus also lie at a shallower level (< 100km) than hitherto thought. Widespread lower crustal partial melting (65), however, is not required by low velocities. That there might be little such melting, if any, is suggested both by the low V_p/V_s and Poisson's ratios derived from simulated annealing inversion of teleseismic radial receiver functions along the Gonghe-Yushu profile (66) (Fig. 1), and by the presence of anhydrous crustal xenoliths in the Pliocene shoshonites of Qiangtang (67) (Fig. 2).

Large changes in mantle structure are seen at major crustal boundaries. Beneath the central Altyn Tagh Fault near 91°E, teleseismic tomography reveals a steep, 40-km-wide, low-P-wave velocity anomaly-up to − 8% relative to adjacent regions-in the crust and mantle down to 140km depth, aligned with the surface trace of the fault (68). This anomaly is best interpreted to outline a deep, narrow, transpressive shear-zone (68), comparable to that now partly exhumed along the Red River. Teleseismic S-wave splitting across the anomaly shows both an increase in delay times of up to 1.3 s, indicative of mantle anisotropy, and a sharp 40° swing of the fast polarization direction in less than 40km, compatible with sinistral drag (69). Both observations argue for localized shear in the continental lithospheric mantle along the Altyn Tagh Fault,

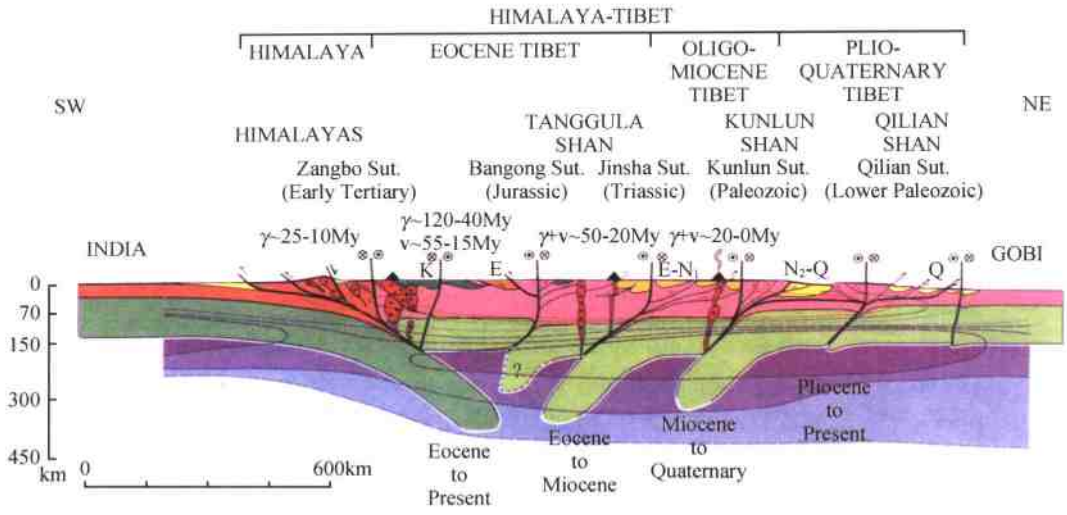

Fig. 3 Schematic lithospheric section of Cenozoic evolution of Himalaya-Tibet orogen. Shades of green represent subducted Indian and Asian lithospheric mantle. Shades of red and pink, Indian and Asian crust, or intrusives. Yellow and dark green shades, ages of sedimentary basins. Relative importance of sedimentary fills is portrayed, but thicknesses are not to scale. Dashed contours(5 % intervals) and shades of blue in mantle show variation of $L=\rho V_s^2$ with depth (V_s, shear wave velocity), after(59).

rather than for uniform, widespread anisotropic flow beneath Tibet(70). Changes in anisotropy across the Karakorum-Jiali fault zone(1,2)(Fig. 1) have been similarly interpreted to reflect deep-seated shear(71).

Taken together, such results are not consistent with the tenets of the soft Tibet paradigm (9,10,58, 70). First, localized transpressive shear-zones reaching the base of the lithosphere, such as the Altyn Tagh or Red-River Ailao-Shan ought to be little different from plate boundaries, as expected from their great length(>1500km), fast rates(2. 5 to 4 cm/year), and large total offsets(≥500km)(21,22,24～26,48～54). Second, if Tibet's mantle is colder than that of adjacent cratons, upwelling of hot asthenosphere could not have taken place beneath the plateau(Fig. 3). It is thus unlikely that convective removal of thickened lithospheric mantle occurred since the Eocene. Third, and consequently, it is also unlikely that such cold mantle might result from thickening of the lithosphere. For if such a process had taken place, given Tibetan Moho depths(up to 70 to 80km)(66,72,73), and usually accepted crustal and mantle densities(10,72,73), the average elevation of the plateau, which appears to be isostatically compensated(10,74), would be appreciably less than 5000m(10). Therefore, allowing for smear due to the low resolution(>350km) of surface-wave tomography, inward subduction of lithospheric mantle slabs beneath Tibet(59) seems to be a more plausible way to account for the high surface-wave velocities observed below 100km. In short, the crust most likely thickened while the mantle did not, and such thickening must have been decoupled from a more plate-like behavior of the lithosphere underneath(Fig. 3). The inward-dipping interfaces recently imaged by teleseismic receiver functions below about 100km along the Passcal-Indepth-Gedepth

transect(75)support this interpretation.

Ongoing Rise of NE Tibet

Nowhere does active overthrusting spread over a greater surface area(~500,000km^2)than in the NE corner of Tibet. To the south and north, this broad region of coeval mountain building is limited by the Kunlun and Altyn Tagh-Haiyuan fault systems, respectively(Figs. 1 and 2). All the large, 200-to 600-km-long, parallel(N120°E)mountain ranges in between, from the Qiman to the Qilian Shan, appear to grow as ramp anticlines of crustal scale, and most north-facing range -fronts are bounded by active thrusts (28 ~ 30) . Cumulative regional shortening perpendicular to such thrusts(N30°E)appears to have taken place at more than 1.5crn/year in the last 10Ma(28~30). This rate is only slightly less than that across the Himalayas(19, 20), and comparable to the post-glacial sinistral slip-rates of the Kunlun, Haiyuan, and northern Altyn Tagh faults(>1 and 2cm/a, respectively)(21, 22, 54, 56, 57).

Within the active realm of the collision zone, this region displays telling features. First, there is everywhere an intimate link between the sinistral faults and the generally north-vergent thrusts. Active thrusts along the southern edge of the Qaidam basin(76), most of them hidden beneath anticlines folding the about 8-km-thick upper-Miocene to Quaternary sedimentary cover (28 ~ 30) parallel the Kunlun fault for about 1000km along strike. This attests to large-scale slip-partitioning, as along oblique subduction zones(Figs. 1 and 2). Thrusts south of the Altyn Tagh fault splay from it at an angle of about 40°, forming a horsetail of grand scale, and seem to young eastward(28 ~ 30). This suggests that they developed south of the termination of the fault as it propagated northeastward across the Precambrian-Lower Paleozoic Tarim-Qaidam and Gobi-Ala Shan platforms(28 ~ 30). Present-day slip-rates sum where the thrusts merge with the fault(28~30, 77), as at FFT triple junctions. Such connected thrusting and strike-slip faulting are thus complementary facets of the same deformation process. Mountain building south of the fault results from the slip decrease along it. Rather than postdate crustal thickening (78, 79), strike-slip faulting governs the geometry of thrusting, and participates in driving it.

Second, the main ranges, which typically culminate at elevations between 5500 and 6000m, ~ 2000m lower than Tibet's southern rim, enclose high, flat, 30-to 200-km-wide basins, most of which are undrained. The largest is the Qaidam basin, ~2700m a.s.l.(Fig. 1). Smaller intermontane basins north of the Qaidam reach elevations in excess of 3000m. Such high sedimentary flats seem to start as foreland basins, evolve into piggy-backs, and finally become captive of the surrounding relief, as their outwashes are cut off by tectonic uplift of the boundary ranges. At that stage, upstream catchments fill the basins, potentially up to their mountain rims. Such "bathtub infilling" (28 ~ 30), at work in the Qaidam since the Upper-Miocene, accounts for the exceptionally thick fluvio-lacustrine sedimentary sequence of that age. Basin infill is thus an integral part of the crustal thickening and elevation increase process. Not only does it store mass inside the mountains, slowing down the efficiency of

outbound erosion, but it smoothes out regional relief and, together with the unusually broad areal extent of coeval thrusting(28～30, 76), shapes NE Tibet into a broad plateau of uniform height rather than into a higher, narrower, jagged mountain barrier. Hence, at its present size of half a million square kilometers and 3.5-to 4-km average elevation, this northeasternmost corner of the collision highlands provides the best model of a small, still actively growing and rising, Tibet plateau.

Finally, most of the parallel ranges between the basins are less than 40km wide. They are bounded by segmented thrust faults that slip at only a few millimeters per year. The thrust segments are but a few tens of kilometers long. Such scales and rates imply that the thrusts do not reach into the mantle (28～30, 76, 77). Size notwithstanding, the overall geometry of faulting and folding is identical to that typical of foreland fold and thrust belts, in which the shortened sedimentary cover is decoupled from the underthrust basement. The Plio-Quaternary shortening and progressive "plateau rise" of this part of Tibet(Figs. 1 and 2)is thus most simply interpreted to reflect the continuing growth of a thick-skinned, crustal accretionary wedge, decoupled from the mantle underneath on a gently south-dipping décollement, probably located near the base of the ductile lowercrust(28～30). Hence, in keeping with inferences derived from seismological evidence, probably only the crust thickens, whereas the mantle does not. Given the minimum amount of shortening between the Gobi and Kunlun range, it is likely that the lithospheric mantle of NE Tibet subducts obliquely southwestfwards beneath that range to about 200-to 300-km depth(28～30), consistent with sinistral slip-partitioning along the range (Figs. 2 and 3).

Diachronous Cenozoic Magmatism

A fraction of Tibet's magmatism, notably volcanism, occurred after India's initial impact onto Asia, mostly inward of the north and south rims of the high plateau(Figs. 2 and 3)(55). It was neither widespread and voluminous, nor synchronous (Fig. 2). The volcanism is characterized by high K lavas (shoshonites, latites) and calc-alkaline dacites, trachytes, and rhyolites(80～86). The petrology of the rocks implies that the magmas come from partial melting of the subcontinental lithospheric mantle and, to a lesser degree, the crust(80～86), but not from strictly asthenospheric or mantle plume sources. The most recent volcanism(≤20Ma), with K/Ar and Ar/Ar ages mostly between 14 and 8Ma (80～84), forms a patchy belt stretching along the Kunlun mountains between 78°and 93°E. Plio-Quaternary volcanic centers (Fig. 2) are located just south of the Kunlun range. The youngest edifices are closest to the main, northern branches of the Kunlun and Altyn Tagh faults, and two fields(Jingyu Hu, 36° 20N and 89°45E, Achikule, 35°40N and 81°30E, ～5000m a.s.l.; Figs. 1 and 2)have vents untouched by glacial erosion that likely formed in the last 15,000 years. At Ulugh Muztagh, 4-Ma-old rhyolitic tuffs are associated with 10-Ma-old, anatectic granites(82～84). The location of recent volcanoes relative to the strike-slip faults is similar to that observed along oblique

subduction zones(87), but volcanism reaches farther south where the faults splay southeastward into rifts(1, 2, 21, 22).

Along the southern edge of the plateau, postcollisional and earlier magmatic episodes overlap(Figs. 2 and 3). U/Pb ages of calkalcaline granitoids in the Gangdese range from 120 to 40Ma [e.g., (11, 45, 46, 88, 89)]. Volcanism is younger, starting with the Lingzizong ignimbrites at 55Ma, which probably reflect continental welding(e.g., 40, 47), and reaching into the Late Miocene, with most Ar/Ar ages between 26 and 15Ma(85, 86). There has been no volcanism south of the Zangbo suture and Karakorum fault. Overall, magmatism along Tibet's south rim has been more abundant and longer-lived than in the north. This supports the usually accepted view that unabated subduction of the Indian lithosphere beneath Tibet provided a lasting source of melts north of the suture(Figs. 2 and 3).

Other Tertiary magmatic rocks—calkalcaline granitoids and cogenetic rhyodacites—are found along the summits of the Tanggula range, which stands halfway and highest between the Kunlun and Gangdese mountain belts(90). These rocks, which have U/Pb and Ar/Ar ages of 39 to 48Ma, are much younger than the Triassic and Cretaceous plutons that mark the Mesozoic welding of the central Tibetan collage. But they are roughly coeval with deformed granites with U/Pb ages of 35 to 52Ma(45, 46) at the west end of the Ailao Shan shear zone and with Paleogene volcanic rocks at the western tip of northern Qiangtang(Changerchar)(Fig. 2)and in the central Pamirs. Together, such Eocene calcalkaline rocks thus mark a third postcollisional magmatic belt cutting the interior of the plateau in half from 80 to 100°E(90).

The localization of Cenozoic calkalcaline magmatism along three distinct belts of different ages, following the three principal topographic ranges north of the Zangbo suture(Gangdese, Tanggula, Kunlun), roughly parallel to the Himalayas, is more consistent with melt sources related to subduction beneath the ranges(28～30, 67, 80, 81, 90)(Fig. 3)than with wholesale convective thinning of the lithospheric mantle. The process operating since the Miocene along and north of the Kunlun edge of the high plateau appears to have had an earlier, Eocene-Oligocene equivalent along the Tanggula range(Fig. 3), which may have marked at the time the northern boundary of a smaller plateau.

That the growth of central and southern Tibet occurred in distinct stages by mechanisms similar to that now observed in NE Tibet is further supported by structural and kinematic evidence. The relation between the Kunlun fault and the thrusts that cut and fold the Eocene-Oligocene red beds south of the Kunlun range(33～37, 55)is comparable to that of the Plio-Quaternary thrusts that splay southeastward at～40° from the Altyn Tagh Fault(Fig. 2)(28～30). A similar transpressive geometry is observed for thrusts and folds—now trending roughly NS—in the older, Cretaceous-Eocene red beds southwest of the—now SE-striking—Red River (24～26) and Xianshui He(27) faults(Fig. 2). This relationship implies that, between the Paleogene and Miocene, the large strike-slip faults of central and southeastern Tibet played a role analogous to that of the Altyn Tagh and Kunlun faults in the more recent growth of NE Tibet. West of 97° E, the Kunlun, Xianshui He, and Red River faults roughly follow the

ultramafic rock girdles that mark the Kunlun-Anyemaqen, Jinsha, and Bangong-Nujiang sutures, respectively. This geometry suggests that the three faults reactivated the three weakest lithospheric cuts in the Tibetan collage, along which shear in the mantle could develop into oblique subduction.

Throughout the collision process, therefore, after India's impact onto Asia about 55Ma ago, the same mechanism, coupling sinistral strike-slip faulting and accretionary thrust-wedge growth in the crust with oblique lithospheric mantle subduction deeper down, may have repeated itself, step after step toward the north, leading to the successive rise of three plateaus (Figs.1 to 3). Soon after impact, the Bangong, then the Jinsha sutures would have been reactivated as mantle megathrusts, near the northern edge of a zone of high relief that grew eastward while escaping in this same direction. The Tanggula, then the Fengguo ranges, and the Red-River, then the Xianshuihe shear-zones would have formed at that time, coevally with transpressive folding and thrusting (24～26) and infilling of intervening basins in southern Tibet, southern Sichuan, Yunnan, and the ShanThai plateau (Fig.2). The southern and northeastern limits of this early Tibet plateau probably followed the Zangbo and Jinsha sutures, respectively, because Eocene Palmacea are not found in between (91). Later, in the Oligocene and Miocene, oblique growth and extrusion of the central plateau, between the Tanggula and Kunlun Shan, would have superseded the earlier relief rise in the south (26, 29) (Figs.2 and 3). Asian lithospheric mantle would have started to subduct southward along the Kunlun-Anyemaqen suture. The Kunlun fault would have propagated eastward (29), and the Hoxhil-basin and Songpan wedges would have become incorporated into the highlands. Resumed uplift of the Lungmen Shan (92) and folding of the Paleozoic-Mesozoic sediment cover of the South China craton, all the way to eastern Sichuan and Guangxi (93), were likely coeval with that second plateau growth phase. The third phase of areal growth and rise, still in progress, probably started in the Late Miocene, with branches of the Altyn Tagh fault propagating past and around the Qilian Shan to the Haiyuan Fault (28～30, 56, 57), shifting the plateau rim to the edge of the Gobi and circumventing the Qaidam and Gonghe basins (Figs.1 to 3).

Summary and Discussion

Although the three-phase Tibet growth model presented here remains conjectural, it brings many large-scale features of Tibet's Tertiary history, structure, and topography into a consistent framework. Oblique subduction of Asian lithospheric mantle is a mechanism that can viably coinvolve extrusion and crustal thickening. It can account for markedly asymmetric growth of relief toward the east, and for large amounts of both localized sinistral shear and coeval, distributed crustal thickening. Sequential, northward reactivation of sutures as India penetrated into Asia is what the opposite, southward vergence of Phanerozoic welding (48, 88) leads to expect (29). The resulting, stepwise, diachronous rise of the Tibetan highlands accounts for the differences in present-day relief and tectonic regimes (Fig.1). The highest, flattest, and

smoothest part of Tibet(3) is the central, Oligo-Miocene plateau, mature but still sheltered, especially in the west, from headward erosion. It lies between the immature, stillgrowing NE plateau and the early SE plateau, now more deeply dissected. The most vigorously rising thrust-ranges along the eastern rim of Tibet lie north of the Kunlun fault(28～30). Shortening along the Lungmen Shan, by contrast, is now modest, despite continuing erosional unroofing(92, 94). Farther south, the edge of the Yunnan plateau has become a site of tectonic inversion, with small-scale, extensional bookshelf faulting, and with normal faults reactivating early Tertiary thrusts(24～26, 95). That, unlike the Altyn Tagh fault, the large strike-slip faults of eastern Tibet seem to die out westward into the least explored part of the plateau(Fig. 2)is also easily accounted for. Their western stretches were probably cut off and superseded by more northerly faults, then smothered by basin infilling, as were early thrusts in the plateau interior. That the longest, fastest slipping shear zones form barriers to recent thrust or normal faults(Figs. 1 and 2)supports the inference that these zones extend deep into the lithospheric mantle. Conversely, the slower-slipping thrust or normal faults that cross neither the Red River, Kunlun, and Altyn Tagh Faults, nor the Bangong and Zangbo sutures, probably do not extend beneath the décollements that likely underlie much of the thickened crust of Tibet.

The stepwise growth scenario requires that a form of hidden Plate Tectonics has been operating beneath the deforming Asian crust. It seems unlikely that the mantle of Tibet ever behaved as a fluid, and that thickening of a viscous sheet coinvolving crust and mantle ever provided enough buoyancy to drive subsequent deformation(9, 10, 58). Instead, boundary forces along the Himalayas and the eastern edge of the Asian plate resulted in stresses sufficient to reactivate weakly welded sutures and to shear anew the Asian lithosphere along narrow zones, isolating coherent mantle blocks(40, 41, 51). Successive, oblique mantle subduction zones were thus created(28～30, 96), leading to the growth of crustal accretionary wedges, decoupled from the mantle in the weak lower crust. Subduction of Asian mantle slabs, once initiated, may have played a dynamic, feedback role in maintaining the continued growth and rise of the plateau. Tectonic damming of catchments and basin infill also played a key role in storing debris and slowing outbound erosion. Along major block boundaries, coeval crustal deformation was partitioned between steep strike-slip shear zones and gently dipping décollements, both chief elements of longlasting collision. That the mantle part-initially $>75\%$-of the lithosphere did not thicken may explain why two-dimensional, analog-model experiments have been the only ones to predict successfully the existence of such first-order Asian tectonic structures as the Red River and Altyn Tagh faults(40, 41, 51). Finally, a stepwise rise of different parts of Tibet makes postulated links between climate changes and tectonics(10) more plausible. Different stages of growth of the plateau could have contributed to trigger or enhance different climatic effects at different times, with thresholds in surface area being at least as important as height in shifting atmospheric circulation patterns(97, 98).

The main tenets of this model require testing. None of the postulated mantle subduction zones has yet been convincingly imaged. Regional paleo-elevations and uplift histories are mostly

unknown. Three phases of growth may be discerned, but the boundaries of early accretionary wedges within the plateau, particularly in the west, remain uncertain. Deformation ages in eastern Tibet, western Sichuan, and northern Yunnan are also poorly known (27, 90, 92). Whether large Tertiary basins existed in eastern Songpan is unclear, although stronger glacial and fluvial erosion in this most humid part of the plateau could have abraded them out in the last 10 million years. The dips of resumed Tertiary subductions along Tibet's southern sutures remain questionable (90). But the mechanism at the core of the stepwise growth scenario provides an alternative to the soft Tibet model that does not leave out first-order features of the time-dependent rise of the plateau. What makes the behavior of the continental lithosphere singular is probably less some overall, fluid-like weakness than structural contrasts in rheology and the ease with which large-scale shear zones localize and propagate.

References and Notes

[1] R. Armijo, P. Tapponnier, J. L. Mercier, H. Tong-Lin, J. Geophys. Res. 91, 13803(1986).

[2] R. Armijo, P. Tapponnier, T. Han, J. Geophys. Res. 94, 2787(1989).

[3] E. Fielding, B. Isacks, M. Barazangi, C. C. Duncan, Geology 22, 163(1994).

[4] P. Molnar, P. Tapponnier, J. Geophys. Res 83, 5361 (1978).

[5] P. Tapponnier *et al.*, Nature 294, 410(1981).

[6] P. Molnar, H. Lyon-Caen, Geophys. J. Int. 99, 123 (1989).

[7] M. Coleman, K. Hodges, Nature 374, 49(1995).

[8] S. L Chung *et al.*, Nature 394, 769(1998).

[9] P. C. England, G. A. Houseman, J. Geophys. Res. 94, 17561(1989).

[10] P. Molnar, P. England, J. Martinod, Rev. Geophys. 31, 357(1993).

[11] T. M. Harrison, P. Copeland, W. S. F. Kidd, A. Yin, Science 255, 1663(1992).

[12] P. Tapponnier, P. Molnar, J. Geophys. Res. 82, 2905 (1977).

[13] T. M. Harrison, P. Copeland, W. S. F. Kidd, O. M. Lovera, Tectonics 14, 658(1995).

[14] C. N. Garzione *et al.*, Geology 28, 339(2000).

[15] H. Lyon-Caen, P. Molnar, Geophys. Res. Lett. 11, 1251(1984).

[16] W. Zhao *et al.*, Nature 366, 557(1993).

[17] L. Ratschbacher, W. Frisch, G. Liu, C. Ghen, J. Geophys. Res. 99, 19917(1994).

[18] R. McCaffrey, J. Nabelek, Geology 26, 691(1998).

[19] J. Lavé, J. p. Avouac, J. Geophys. Res. 105, 5735 (2000).

[20] R. Bilham, K. Larson, J. Freymuller, Nature 386, 61 (1997).

[21] J. Van der Woerd *et al.*, Geology 26, 695(1998).

[22] J. Van der Woerd *et al.*, Geophys. Res. Lett. 27, 2353 (2000).

[23] A. Yin *et al.*, Geology 27, 787(1999).

[24] P. H. Leloup *et al.*, Tectonophysics 251, 3(1995).

[25] R. Lacassin *et al.*, Tectonics 15, 605(1996).

[26] R. Lacassin *et al.*, J. Geophys. Res. 102, 10013 (1997).

[27] E. Wang *et al.*, Geol. Soc. Am. Spec. Paper 327, 1～108(1998).

[28] P. Tapponnier *et al.*, Earth Planet. Sci. Lett. 97, 382 (1990).
[29] B. Meyer *et al.*, Geophys. J. Int. 135, 1 (1998).
[30] F. Metivier, Y. Gaudemer, P. Tapponnier, B. Meyer, Tectonics 17, 823 (1998).
[31] J. Achache *et al.*, J. Geophys. Res. 89, 10311 (1984).
[32] J. Besse, V. Courtillot, J. P. Pozzi, M. Westphal, Y. X. Zhou, Nature 311, 621 (1984).
[33] C. Chang, *et al.*, Nature 323, 501 (1986).
[34] W. S. F. Kidd *et al.*, Philos. Trans. R. Soc. London 327, 287 (1988).
[35] M. P. Coward *et al.*, Philos. Trans. R. Soc. London 327, 307 (1988).
[36] Z. Liu, C. Wang Sediment. Geol., in press.
[37] ——, H. Yi, J. Sediment. Res., in press.
[38] A. Yin *et al.*, J. Geophys. Res. 99, 18175 (1994).
[39] A. Yin *et al.*, Geology 27, 787 (1999).
[40] P. Tapponnier, G. Peltzer, R. Armijo, Geol. Soc. Spec. Publ. 19, 115 (1986).
[41] P. Matte *et al.*, Earth Planet. Sci. Lett., 142, 311 (1996).
[42] Z. Yang, J. Besse, Earth Planet. Sci. Lett. 117, 525 (1993).
[43] A. Briais, P. Patriat, P. Tapponnier, J. Geophys. Res. 98, 6299 (1993).
[44] T. M. Harrison *et al.*, in Tectonic Evolution of Asia, A. Yin and T. M. Harrison, Eds. (Cambridge Univ. Press, New York, 1996), pp. 208～226.
[45] U. Schärer *et al.*, Earth Planet. Sci. Lett. 97, 65 (1990).
[46] L. S. Zhang, U. Schärer, Contrib. Mineral Petrol. 134, 67 (1999).
[47] J. J. Jaëger, V. Courtillot, P. Tapponnier, Geology 17, 316 (1987).
[48] Z. Xu, in 15th Himalaya-Karakoram-Tibet Workshop, Chengdu, 21 to 24 April 2000, Earth Sciences Frontiers (China Univ. of Geosciences, Beijing, 2000), Vol. 7, p. 231.
[49] E. Sobel, N. Arnaud, Tectonics 18, 64 (1999).
[50] B. D. Ritts, U. Biffi, G. S. A. Bull. 112, 61 (2000).
[51] G. Peltzer, P. Tapponnier, J. Geophys. Res. 93, 15085 (1988).
[52] N. Arnaud *et al.*, in preparation.
[53] A.-S. Mériaux *et al.*, EOS Trans. (AGU Fall meeting), 81, 1137 (2000).
[54] F. J. Ryerson *et al.*, EOS Trans. (AGU Fall meeting) 80, 1008 (1999).
[55] Geological Map of Qinghai-Xizang Plateau and Adjacent Areas (scale: 1/1, 500, 000) (Geology Publishing House, Beijing, 1988).
[56] Y. Gaudemer *et al.*, Geophys. J. Int. 120, 599 (1995).
[57] C. Lasserre *et al.*, J. Geophys. Res. 104, 17633 (1999).
[58] P. England, P. Molnar, Science 278, 647 (1997).
[59] D. Griot, J. P. Montagner, P. Tapponnier, J. Geophys. Res. 103, 21215 (1998).
[60] L. Bourjot, B. Romanowicz, Geophys. Res. Lett. 19, 881 (1992).
[61] J. Revenaugh, S. A. Sipkin, J Geophys. Res. 99, 21911 (1994).
[62] R. Zeng, Z. Ding, Q. Wu, Pure Appl Geophys. 145, 425 (1995).
[63] G. Wittlinger *et al.*, Earth Planet. Sci. Lett. 139, 263 (1996).
[64] D. McNamara, T. Owens, W. Walter, J. Geophys. Res. 100, 22215 (1995).
[65] T. J. Owens, G. Zandt, Nature 387, 37 (1997).
[66] G. Wittlinger *et al.*, in preparation.
[67] R. Hacker *et al.*, Science 287, 2463 (2000).

[68] G. Wittlinger *et al*., Science 282, 74(1998).
[69] G. Herquel *et al*., Geophys. Res. Lett. 26, 3225 (1999).
[70] W. E. Holt, Geology 28, 67(2000).
[71] W. C. Huang *et al*., J. Geophys. Res. 105, 27979 (2000).
[72] A. Hirn *et al*., Nature 307, 23(1984).
[73] A. Hirn *et al*., Nature 307. 25(1984).
[74] Y. Jin, M. K. McNutt, Y. Zhu, Nature 371, 669(1994).
[75] G. Kosarev *et al*., Science 283, 1306(1999).
[76] W. P. Chen, C. Y. Chen, J. L. Nabelek, Tectonophysics 305, 165(1999).
[77] J. Van der Woerd *et al*., Tectonics, in press.
[78] B. C. Burchfiel *et al*., Geology 17, 448(1989).
[79] E. Wang, Earth Planet. Sci. Lett. 150, 55(1997).
[80] W. Deng, Chin. J. Geochem. 10, 140(1991).
[81] N. O. Arnaud *et al*., Earth Planet. Sci. Lett. 111, 351 (1992).
[82] B. C. Burchfiel *et al*., Earth Planet. Sci. Lett. 94, 57 (1989).
[83] S. Turner *et al*., J. Petrol. 37, 45(1996).
[84] J. Yang, Z. Xu, W. Bai, R. Zhao, Contin. Geodyn. 2, 1 (1997).
[85] C. Coulon, H. Maluski, C. Bollinger, S. Wang, Earth Planet. Sci. Lett. 79, 281(1986).
[86] C. Miller *et al*., J. Petrol. 40, 1399(1999).
[87] K. Sieh, D. Natawidjaja, J. Geophys. Res. 105, 28295 (2000).
[88] C. J. Allègre *et al*., Nature 307, 17(1984).
[89] F. Debon, P. Le Fort, S. M. F. Sheppard, J. Sonet, J. Petrol. 27, 219(1986).
[90] F. Roger *et al*., Terra Nova 12, 102(2000).
[91] T. Li, Tectonophysics 260, 45(1996).
[92] D. Arne *et al*., Tectonophysics 280, 239(1997).
[93] D. Yuan, 1st International Conference on Geomorphology, Manchester, 15 to 21 September 1985.
[94] R. King *et al*., Geology 25, 1279(1997).
[95] F. Wu, P. Wang, Geology 16, 153(1988).
[96] M. Mattauer, J. Geol. Soc. London Spec. Publ. 19, 37 (1986).
[97] G. Ramstein, F. Fluteau, J. Besse, S. Joussaume, Nature 386, 788(1997).
[98] F. Fluteau, G. Ramstein, J. Besse, J. Geophys. Res. 104, 11995(1999).
[99] A. Replumaz, R. Lacassin, P. Tapponnier, P. H. Leloup, J. Geophys. Res. 106, 819(2001).
[100] J. P. Avouac, P. Tapponnier, Geophys. Res. Lett. 20, 895(1993).
[101] The concepts presented here benefited from work and discussions with R. Armijo, J. P. Avouac, J. Besse, L. Bourjot, M. Brunel, Y. Chen, J. P. Cogné, V. Courtillot, Y. Gaudemer, S. Gilder, D. A. Griot, G. King, R. Lacassin, C. Lasserre, P. H. Leloup, B. Liu, Q. Liu, X. Liu, J. Malavieille, M. Mattauer, F. Metivier, A. S. Meriaux, J. P. Montagner, G. Peltzer, G. Poupinet, A. Replumaz, F. J. Ryerson, J. Van der Woerd, X. Xu, Z. Yang, among others. The many field trips to most parts of Tibet over the years were unfailingly supported by Institut National des Sciences de l' Univers (CNRS, Paris), and their logistics, by the Ministry of Lands and Resources, the National Science Foundation of China, Academia Sinica and the Seismological Bureau of China(Beijing). P. T. is grateful to the California Institute of Technology, where part of this paper was written while he was on sabbatical as visiting professor. A. C. Morillon is responsible for the quality of the figures. This is Institut de Physique du Globe de Paris contribution No. 1778.

青藏高原北部东昆仑-羌塘地区的岩石圈结构及岩石圈剪切断层❶

许志琴[1]　杨经绥[1]　姜　枚[1]　袁学诚[3]
李海兵[1]　薛光琦[2]　钱　辉[2]
(1. 中国地质科学院地质研究所　北京　100037; 2. 中国地质科学院矿产资源研究所　北京　100037; 3. 国土资源部中国地质调查局发展中心　北京　100035)

摘　要　通过横穿青藏高原北部东昆仑-羌塘地区的格尔木-唐古拉山口(西段)和共和-玉树(东段)两条天然地震探测剖面的综合研究,揭示东昆仑-羌塘地区岩石圈结构的如下特征:①地壳厚度自南往北由 70～75km 减小至 55～60km,西段厚度变化幅度(10km)较东段(20km)小;②地壳具高速与低速转换界面相间组成的层状结构,东段中地壳为透镜状低速层;③在 150km 深度范围内岩石圈的物理状态具高速体和低速体相间特征;④岩石圈结构不连续性表明地体边界及地体内部存在 150～250km 深度的 3 条主要的岩石圈剪切断层带:昆南-阿尼玛卿岩石圈剪切断裂带、金沙江岩石圈剪切断裂带和鲜水河岩石圈剪切断裂带。推测青藏高原北部存在岩石圈规模的向东挤出作用。

关键词　青藏高原北部　天然地震探测　岩石圈结构　岩石圈剪切断层

55Ma 以来,印度板块与欧亚大陆碰撞过程被看作是青藏高原隆升的主因,随着青藏高原研究的重点从南部的碰撞边界往北部扩展及深入,青藏北部岩石圈探测的新成果不断出现,为高原研究提供了新的深部信息。

自 1996 年以来,中国地质科学院地质研究所与法国宇宙科学院共同合作在青藏高原北部东昆仑-羌塘地区之西段格尔木-唐古拉山口及东段共和-玉树公路沿线进行了天然地震观测[1～5],这些工作为原本研究程度很差的该区深部岩石圈结构综合分析提供了研究基础。天然地震探测剖面主要横越了东昆仑和巴颜喀拉地体,西剖面往南还深入羌塘地体,东剖面往北深入了柴达木及祁连地体南缘(图 1)。研究区的主要构造单元有祁连地体、昆北-柴达木地体、昆南地体和巴颜喀拉-松甘地体及羌塘地体。祁连地体和昆北-柴达木地体之间的边界为新发现的 490～500Ma 形成的祁连南缘加里东俯冲杂岩带(或缝合带)[6,7],昆北-柴达木地体和昆南地体之间的边界为昆中缝合带(尚有争议)[8],昆南地体与巴颜喀拉-松甘地体之间的边界为昆南走滑断裂(西段)和阿尼玛卿缝合带(东段)[9～14],巴颜喀拉-松甘地体和羌塘地体之间的边界为金沙江走滑断裂(西段)与金沙江缝合带(东段)[5,11,12]。祁连地体为加里东造山带,东昆仑(包括昆北及昆南)是加里东与印支叠覆造山带,巴颜喀拉-松甘

❶ 中国科学(D 辑),2001 年第 31 卷增刊。
2001－02－12 收稿,2001－07－19 收修改稿。
国家重点基础研究发展规划(G1998040800)和国土资源部中法合作(9501106)项目资助。

地体为印支造山带和羌塘地体为印支与燕山叠置造山带[11]。研究表明,南祁连加里东缝合带与阿尼玛卿印支缝合带具有往北俯冲的剪切指向,而金沙江印支缝合带具有往南俯冲的剪切指向[15]。

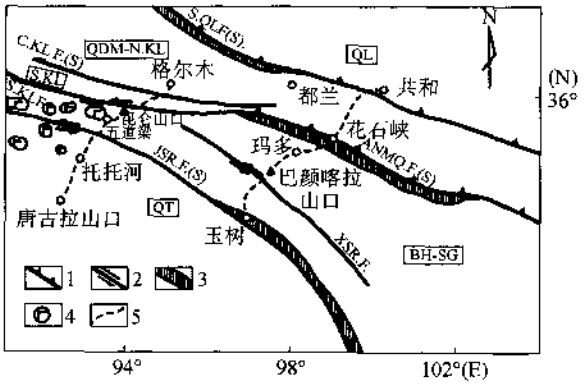

图 1 东昆仑-羌塘地区天然地震探测剖面位置图

1—逆冲断层;2—左行走滑断层;3—缝合带;4—新生代火山岩;5—天然地震探测剖面;QL—祁连地体;QDM-N.KL—柴达木-昆北地体;S.KL—昆南地体;BH-SG—巴颜喀拉-松潘甘孜地体;QT—羌塘地体;S.QLF.(S)—祁连南缘断裂(缝合带);C.KLF.(S)—昆中断裂(缝合带);S.KL F.—昆南断裂;ANMQ. F.(S)—阿尼玛卿断裂(缝合带);JSR F.(S)—金沙江断裂(缝合带);XSR.F.—鲜水河断裂

自早古生代至中生代末,上述地体自北往南逐渐碰撞及拼合,使陆壳不断增生,形成了劳亚大陆南部的复合地体,直至 55Ma 期间与印度板块发生一次更为重要的碰撞事件。55Ma 以来青藏高原发生大范围抬升,研究区伴随隆升的主要新生代构造事件表现为:①可可西里的碱性火山岩喷发;②伸展作用形成的南北向裂谷;③逆冲作用使祁连山往北叠置在酒泉盆地上,往南叠置在柴达木盆地上,使东昆仑山往北叠置在柴达木盆地上;④大型走滑断裂的活动,昆南左行走滑断裂的走滑速率为 7~11.5mm/a,鲜水河左行走滑断裂的走滑速率为 10~16mm/a,阿尔金左行走滑断裂的走滑速率为 10~16mm/a[16]。

利用横穿青藏高原北部东昆仑-羌塘地区的格尔木-唐古拉山口(西部)和共和-玉树(东部)两条天然地震探测剖面的资料[1-5],结合新的地质研究成果,揭示岩石圈结构层状性和不连续性,综合分析地质历史中岩石圈演化的追踪信息与现代岩石圈结构的表现进行新的解析是本文的主要目的。

1 岩石圈结构推断

1.1 东昆仑-唐古拉地区西段格尔木-唐古拉山口天然地震探测剖面

格尔木-唐古拉山口的地震层析和接收函数反演剖面通过的地点,自北往南为格尔木—昆仑山口—五道梁—托托河—唐古拉山口,剖面推测东昆仑-唐古拉地区西段的岩石圈结构有如下主要特征(图 1,2):①具高速与低速转换界面相间的地壳层状结构,浅部存在由两条往北缓倾的断层(25km 的深度)组成的逆冲叠复构造,莫霍面自南往北深度由 70km 减小为

60km(图 2);②在150km 以上的岩石圈范围内,昆北-柴达木地体由低速体组成,昆南地体和巴颜喀拉地体均由高速体组成,羌塘地体由低速体组成。昆南地体往北插入昆北-柴达木地体之下,昆南地体和巴颜喀拉地体之间的界线——昆南走滑断裂带在图 2 中表现明显不连续性,在地震层析剖面(图 3)中,表现为由低速物质组成、深 200km 垂向产出的岩石圈断裂带。羌塘地体与巴颜喀拉地体之间的金沙江断裂带为深达 150km 垂向产出的岩石圈断裂带;③位于巴颜喀拉地体西段及羌塘地体北部的可可西里地区之下,深度 200～360km 相当于软流圈处,存在 600km 宽和 200km 厚的大型低速异常体,已推测与可可西里新生代碱性火山岩的喷发有关(图 3)[17,18]。

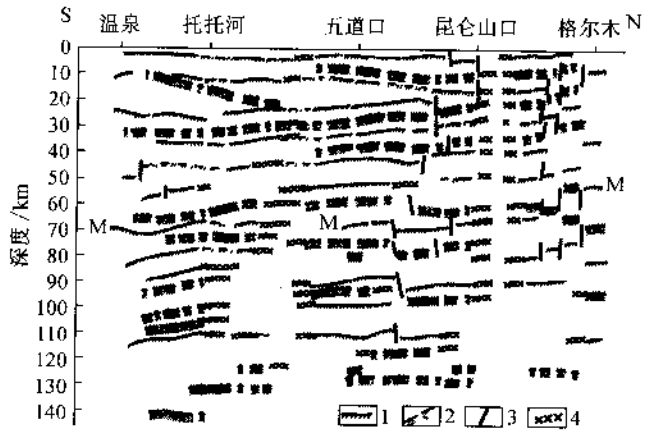

图 2　东昆仑-羌塘地区西段格尔木-唐古拉山口接收函数反演剖面的构造解释

1—高速转换界面;2—低速转换界面;3—推测断层;4—不连续面;M—为莫霍面

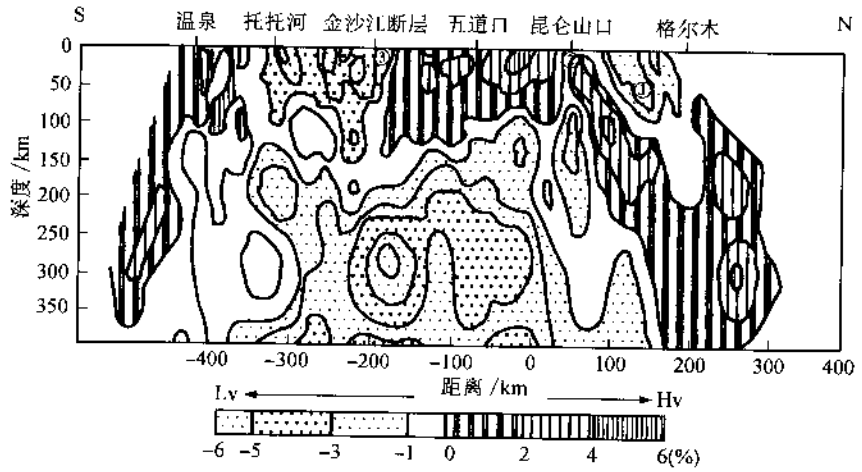

图 3　东昆仑-羌塘地区西段格尔木-唐古拉山口天然地震探测剖面图

Hv:高速;Lv:低速[1,5].①昆中岩石圈剪切断裂;②昆南岩石圈剪切断层;③金沙江岩石圈剪切断裂

1.2 东昆仑-唐古拉地区东段共和-玉树天然地震探测剖面

共和-玉树的地震层析和接收函数反演剖面及广角反射剖面所通过的地点，自北往南为共和—花石峡—玛多—巴颜喀拉山口—鲜水河断裂—玉树，对该地区东段的岩石圈结构可作如下地质解析：①地壳厚度自南往北由 75km 减少至 55km，具南厚北薄特征。②地壳结构根据 S 波波速大小可划分 4 层：上地壳(0～20km)为 3.0～3.7km/s，中地壳(20～35km)为 2.3～3.0km/s，下地壳(35～55km)为 3.2～3.9km/s，壳幔过渡层(55～70km)为 4.0～4.3km/s，上地幔波速为＞4.3km/s(图 4)。③中地壳由透镜状低速层组成，低速透镜体位于共和、花石峡以北及巴颜喀拉山口-鲜水河断裂之下部 18～30km(图 4)。共和位于祁连南缘加里东俯冲杂岩带上，沿带的锡铁山 ZK 3606 井、大柴旦红参 1 井和哈参 1 井均具较高热流值质(分别为54，41和38mW/m^2)[19]，可作为此条构造边界现代再活动的证据。共和

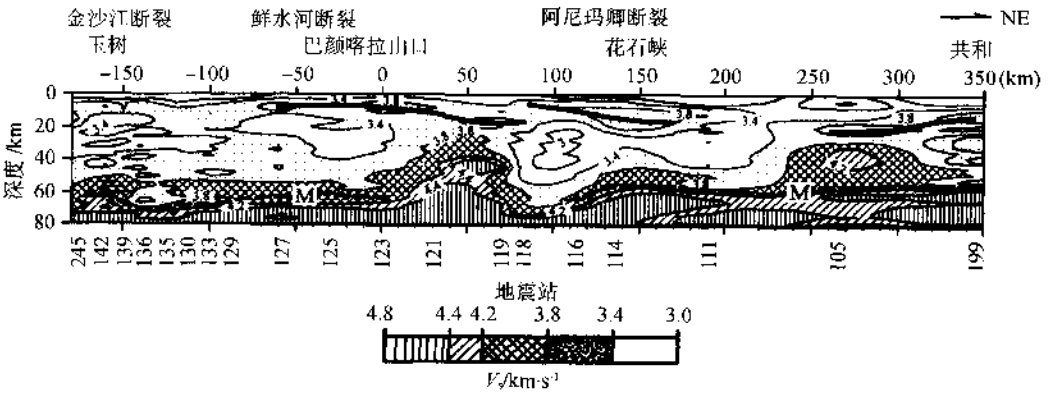

图 4 东昆仑—羌塘地区东段共和—玉树接收函数反演剖面的构造解释
M 为莫霍面，粗实线条为断层

盆地是晚新生代晚期的断陷盆地，受控南、北两条正向走滑断层，因此共和低速透镜体的出现导致古构造的活化及现代断陷盆地的形成。花石峡地区的地表地质显示了印支期火山岩浆结构及新生代拉分盆地的特征，花石峡以东的沙柳河 ZK 502 井热流测试获得 78mW/m^2 高热流密度值，因此推测花石峡中地壳低速透镜体可能反映印支期以来伸展背景，同时与地壳高热流有成因联系。而巴颜喀拉山口-鲜水河断裂深部的中地壳低速透镜体，可能与地壳大量的燕山期花岗岩浆活动有关。④地震层析剖面揭示了 400km 深度范围内岩石圈总体结构为北部往北倾斜、南部往南倾斜呈“八”字形的特征。北部的祁连地体由低速物质组成，昆南地体以高速物质为主，阿尼玛卿带的深部结构显示了高速体向北的插入，巴颜喀拉地体北部表现为低速带往北倾伏于昆南高速体之下，巴颜喀拉南部则表现为高速体往南插入低速体组成的羌塘地体之下(图 5)[18]。

2 岩石圈断裂解析

上述两条天然地震探测剖面明显地反映了岩石圈结构的不连续性及地体边界岩石圈断裂的特征及延深状况。主要有3条地体边界和地体内部的岩石圈剪切断裂带：昆南-阿尼

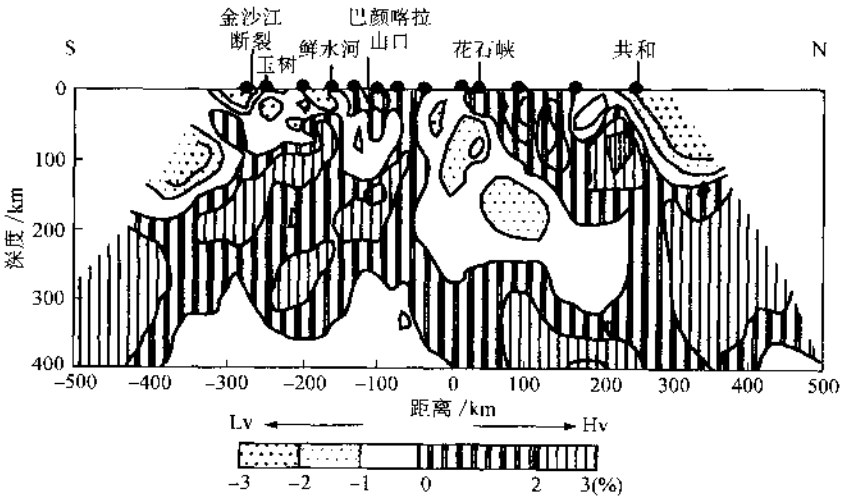

图 5　东昆仑-羌塘地区东段共和-玉树天然地震探测剖面

Hv:高速;Lv:低速[1,5]

玛卿岩石圈剪切断裂带、金沙江岩石圈剪切断裂带和鲜水河岩石圈剪切断裂带,推测昆中断裂带(缝合带)为岩石圈剪切断裂带。

2.1　岩石圈剪切断裂

(1)昆南-阿尼玛卿岩石圈剪切断裂。昆南-阿尼玛卿断裂的详细地质研究已表明了该断裂可分为东、西两段:西段为近东西向的昆南断裂,由 2km 宽的糜棱岩组成,面理直立,发育水平拉伸线理及"A"型剪切褶皱,具明显的左行剪切应变特征。沿断裂及断裂北侧发育同构造花岗岩体,同位素年代测定表明剪切走滑运动于 240～200Ma 开始,150～140Ma 以及 120～100Ma 又有强烈剪切活动,新第三纪(20Ma)时仍有韧性剪切作用影响[13],至今还具左行走滑活动性质(脆性为主)并伴随地震活动。东段为北西至南东向的阿尼玛卿断裂带,系印支期古俯冲带及缝合带,由一系列自北东往南西逆冲断裂构成[12]。新生代以来断裂性质转化为左行走滑活动。格尔木-唐古拉山口西剖面(图 3)揭示了昆南断裂为垂向的岩石圈剪切断裂,往下延伸达 250km,带中的低速带可能是使地壳熔融的高温物质,是印支期以来花岗岩浆活动的源区。共和-玉树东剖面(图 5)的花石峡地点,揭示了阿尼玛卿逆冲断裂系为低速体与高速体的界线,并以中等倾角往北斜向插入 200km 深处。

(2)金沙江岩石圈剪切断裂。金沙江断裂带位于巴颜喀拉-松甘地体和羌塘地体之间,根据金沙江断裂东段(松潘-甘孜造山带西缘)古特提斯蛇绿岩、混杂堆积及板块体制的研究,表明松潘-甘孜地体往南西俯冲于羌塘地体之下以及金沙江断裂东段具缝合带性质[18]。但金沙江断裂西段(玉树以西)缝合带性质不清,糜棱岩带及 200Ma 左右同构造花岗岩的存在反映了金沙江断裂西段为印支期形成的韧性左行走滑断裂[19]。格尔木-唐古拉山口(西部)剖面,揭示了金沙江断裂带西段为垂直延伸至 150km 的岩石圈剪切断裂;共和-玉树东剖面,揭示了金沙江断裂带东段为往南西插入 150km 深度的岩石圈剪切断裂。

(3)鲜水河岩石圈剪切断裂。鲜水河断裂带位于巴颜喀拉-松甘地体内部,巴颜喀拉-松甘地体西段由高速物质组成,共和-玉树东剖面揭示了巴颜喀拉-松甘地体东段较复杂,可分

为三部分：南部和北部段为低速体，中部由高速物质组成。北西至南东向的鲜水河断裂位于中部与南部的交界处，形成于20Ma[20]，是一条左行走滑的活动断裂，走滑速率为10～16mm/a[16]。东剖面显示了鲜水河断裂为垂直延伸至120km的岩石圈剪切断裂。

(4)昆中岩石圈剪切断裂，长期以来把昆中断裂带(缝合带)当作昆北-柴达木地体与昆南地体的边界。格尔木-唐古拉山口天然地震探测剖面所提供深部物理状态表明，昆北-柴达木地体由低速物质组成，昆南地体由高速物质组成，昆中断裂为明显的物质界面及构造界面。组成昆南地体的高速高密物质往北斜向延伸至200km深度，构成一条往北陡倾的岩石圈剪切断裂，提供了昆中断裂带可能为古俯冲带和昆中缝合带存在及其产状的地球物理证据。

2.2 岩石圈范围内的向东挤出作用

穿越研究区西端阿尔金山的乌图美仁-花土沟-塔什大坂-若羌天然地震探测剖面，已揭示了现代走滑速率为10～30mm/a的阿尔金走滑断裂是一条深达250km的岩石圈剪切断裂[21]。结合本项研究成果表明，青藏高原北部一些重要的线在地表大多为大型走滑断裂，在深部为岩石圈剪切断裂。Tapponnier等人[22]曾提出印度板块楔向北俯冲造成欧亚板块向东挤出的假说，根据青藏高原北部岩石圈剪切断裂的确定，可以认为青藏高原北部的向东挤出作用起码是岩石圈范围的。

3 结论与讨论

(1)东昆仑-唐古拉地区的地壳厚度自南往北由70～75km减小为55～60km，西段厚度变化幅度(10km)较东段(20km)小；地壳具"多层"结构，地壳上部显现叠复岩片构造；东段中地壳为透镜状低速层。

(2)通过横穿青藏高原北部东昆仑-羌塘地区的格尔木-唐古拉山口(西段)和共和-玉树(东段)两条天然地震探测剖面的综合研究，获得该区100km深度内岩石圈结构的主要特征：各地体的物理状态表现为高速体和低速体相间的结构特征。昆北-柴达木地体由低速体组成、昆南地体由高速体组成、巴颜喀拉-松甘地体西段由高速体组成，东段较复杂，其北部和南部由低速体、中部由高速体物质组成；羌塘地体由低速体组成。巴颜喀拉地体西部(可可西里地区)深200～360km处存在与新生代火山作用有成因联系的大型低速异常体。

(3)天然地震探测还揭示了岩石圈结构的不连续性及岩石圈剪切断层的存在。东昆仑地体与巴颜喀拉地体之间的昆南-阿尼玛卿断裂带之西段的昆南左行走滑断裂带，为垂向延深250km的岩石圈剪切断裂，东段阿尼玛卿断裂带(缝合带)位于高、低速体之间的交界面上，为往北陡倾延深至250km的岩石圈剪切断裂。巴颜喀拉-松甘地体和羌塘地体之间的金沙江断裂带，同样具东西差异的特点：西段为垂向延深150km的岩石圈剪切断裂，东段为往南西陡倾延深至150km的岩石圈剪切断裂。推测昆南-阿尼玛卿岩石圈剪切断裂带与金沙江岩石圈剪切断裂带，均因循了地表印支期形成的断裂系统而产出。巴颜喀拉-松甘地体内部的新生代鲜水河断裂，也具有垂向延深120km岩石圈剪切断裂的特征。

(4)据青藏高原北部新生代大型走滑断裂的特征及其岩石圈剪切断裂性质的确定，可以认为青藏高原北部新生代以来的向东挤出作用起码是岩石圈范围的。

致谢 成文过程中曾向杨文采和赵志兴研究员讨教，表示感谢。

参 考 文 献

[1] Jiang M, Hirn A, Poupinet G. Tibetan Plateau seismic experiment: Design and preliminary results, 1992～1993. Global Tectonics and Metallogeny, 1995, 4: 199～201.

[2] 姜 枚, 吕庆田, 史大年, 等. 用天然地震探测青藏高原中部地壳、上地幔结构. 地球物理学报, 1996, 39(4): 476～482.

[3] Wittlinger G, Masson F, Poupinet G, *et al*. Seismic tomography of northern Tibet and Kunlun: Evidence for crustal blocks and mantle velocity contrasts. EPSL, 1996, 139: 263～279.

[4] Kind R, Kosarev G L, Patersen N V, *et al*. Receiver functions at stations of the German Region Seismic Network (GRSN). Geophys J Int, 1995, 121: 191～202.

[5] Xue G Q, Qian H, Jiang M, *et al*. Studies on the velocity structure of crust-upper mantle beneath the eastern Qinghai-Tibet Plateau using seismic tomography. Continental Dynamics, 1999, 4(2): 79～85.

[6] 杨经绥, 许志琴, 李海兵, 等. 我国西部柴北缘地区发现榴辉岩. 科学通报, 1998, 43(3): 1544～1549.

[7] 杨经绥, 许志琴, 宋述光, 等. 青海都兰榴辉岩的发现及对中国中央带内高压-超高压变质带研究的意义. 地质学报, 2000, 74(2): 156～168.

[8] 姜春发, 杨经绥, 冯秉贵, 等. 昆仑开合构造. 北京: 地质出版社, 1992.

[9] Yang J S, Robinson P T, Jiang C F, *et al*. Ophiolites of the Kunlun Mountains, China and their tectonic implication. Tectonophysics, 1996, 258: 215～231.

[10] Xu Z Q. Large shear zones in the main orogenic belts. China Episodes, 1995, 18: 41～43.

[11] Xu Z Q, Yang J S, Li H B, *et al*. Mesozoc Crustal Evolution and Dynamics of the East Kunlun-Tanggula Composite Mountain Chains. In: Proceedings of the 30th International Geological Congress. Vol. 7. Orogenic Belts Geological Mapping. Utrecht: VSP, 1997. 7～20.

[12] Xu Z Q, Jiang M, Ang J S, *et al*. Mantle diapir and inward intracontinental subduction: A discussion on the mechanism of uplift of the Qinghai-Tibet Plateau. In: Macfarlane A, Sorkabi R B, Quade J, eds. Himalaya and Tibet: Mountain Roots to Mountain Tops: Boulder, Colorado. Geological Society of America Special Paper, 1999, 328: 19～31.

[13] Li H B, Xu Z Q, Chen W. Southern margin strike-slip fault zone of East Kunlun Mountains: An important consequence of intracontinental deformation. Continental Dynamics, 1996, 1(2): 146～155.

[14] 许志琴, 杨经绥, 陈方远. 阿尼玛卿缝合带及"俯冲-碰撞"动力学. 见: 张旗主编. 蛇绿岩与地球动力学研究. 北京: 地质出版社, 1996.

[15] 钱 辉, 姜 枚, 薛光琦, 等. 天然地震接受函数揭示的青藏高原东部地壳结构. 地震学报, 2001, 24(1): 103～108.

[16] Peltzer G, Tapponnier P. Formation and evolution of strike-slip faults, rifts and basins during the India-Asia Collision: An experimental approoach. Journal of Geophysical Research, 1988, 93: 15085～15117.

[17] Yang J S, Xu Z Q, Bai W J, *et al*. Cenozoic volcanism on the Qinghai-Tibet Plateau and its genesis. Continental Dynamics, 1997, 2: 1～11.

[18] 许志琴, 姜 枚, 杨经绥, 等. 青藏高原北部隆升的深部构造物理作用. 地质学报, 1996, 70(3): 195～206.

[19] 崔军文, 唐哲民, 邓晋福, 等. 见: 许志琴, 侯立玮, 王宗秀, 等. 阿尔金断裂系. 北京: 地质出版社, 2000.

[20] 许志琴, 侯立玮, 王宗秀, 等. 中国松潘甘孜造山带的造山过程. 北京: 地质出版社, 1996.

[21] 许志琴, 杨经绥, 姜 枚, 等. 阿尔金断裂两侧构造单元的对比及岩石圈剪切机制. 地质学报, 1999, 73(3): 193～205.

[22] Tapponnier P, Peltzer G, Le Dain A Y. Propagating extrusion tectonics in Asia: New insights from simple experiments with plasticine. Geology, 1982, 10: 611～616.

Deep structure and lithospheric shear faults in the East Kunlun-Qiangtang region, northern Tibetan Plateau[●]

Xu Zhiqin[1] Yang Jingsui[1] Jiang Mei[1] Li Haibing[1]
Xue Guangqi[2] Yuan Xuecheng[3] & Qian Hui[2]
(1. Institute of Geology, Chinese Academy of Geological Sciences, Beijing 100037, China;
2. Institute of Mineral Resources, Chinese Academy of Geological Sciences, Beijing 100037, China; 3. Bureau of Geological Survey, Ministry of Land and Resources of China, Beijing 100035, China)

Abstract An integrated study of earthquake seismic tomography in the Golmud-Tanggula Pass (west) and Gonghe-Yushu (east) with profiles traversing the East Kunlun-Qiangtang region of the northern Tibetan Plateau shows that the deep structure of the study region has the following characteristics: (1) from south to north the crustal thickness decreases from 70～75km to 55～66km, and the variation range of thickness (10km) in the western part is smaller than that in the eastern part (20km); (2) the crust has a sandwich-like structure and the middle crust has a lens-shaped low-velocity layer; (3) above 150km in depth, the physical states of various terranes are marked by alternation of high-velocity and low-velocity bodies; and (4) the discontinuity of the lithospheric structure reveals the existence of three lithospheric shear faults on the the East Kunlun-Qiangtang region——the South Kunlun-A' nyêmaqên lithospheric shear fault, the Jinsha River lithospheric shear fault and the Xianshui River lithospheric shear fault. It is inferred that the easternward extrusion of northern Tibetan Plateau occurred in the lithospheric range.

Key words northern Tibetan Plateau, earthquake-excited tomography detection, lithospheric structure, lithospheric shear fault.

1 Background

The collision between the Indian plate and Eurasian continent since 55Ma has been considered as a main cause for the uplift of the Tibetan Plateau. With the extension and the deepening of the focus of study on the plateau from south (the collision boundary) to north, new achievements have been scored steadily in the lithospheric probe under the northern part of the plateau, thus furnishing new deep-seated information for the study of the plateau.

Since 1996 the Institute of Geology of the Chinese Academy of Geological Sciences and Le Centre National de la Recherche Scientifique de la Republique Française have cooperated to carry out earthquake-excited tomography observations along the Golmud-Tanggula Pass Highway in the western part and the Gonghe-Yushu Highway in the eastern part of the East Kunlun-Qiangtang region on the northern Tibetan Plateau[1～5]. The work has provided a basis for

● SCIENCE IN CHINA (Series D) Vol. 44 Supp. December 2001.

an integrated analysis of the originally poorly studied lithospheric structure in the region(Fig.1).

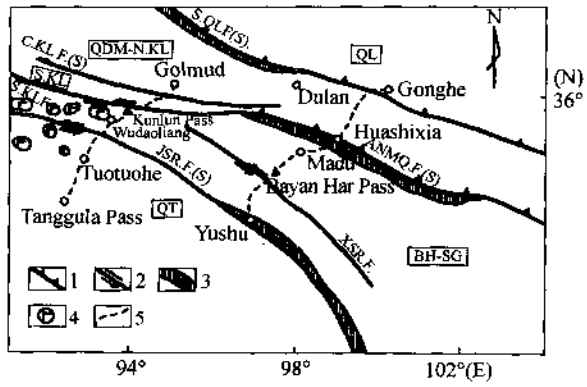

Fig.1 Location map of the earthquake-excited tomography profiles in the East Kunlun-Qiangtang region, northern Tibetan Plateau.

1—Thrust; 2—left-lateral strike-slip fault; 3—suture zone; 4—cenozoic volcanic rocks; 5—earthquake-excited tomography profile. QL—Qilian terrane; QDM-NKL—Qaidam-North Kunlun terrane; BH-SG—Bayan Har-Songpan-Garzê terrane; QT—Qiangtang terrane; SQL F.(S)—South Qilianern fault(suture zone); CKL F.(S)—Central Kunlun fault(suture zone); SKL F.—South Kunlun fault; ANMQ F.(S)—A'nyêmaqên fault(suture zone); XSR F—Xianshui River fault.

The seismic profiles mainly run across the East Kunlun and Bayan Har terranes. The western profile also runs southward into the Qiangtang terrane, and the eastern profile goes northward into the Qaidam terrane and the southern margins of the Qilian terrane. The major tectonic units of the studied region include the Qilian terrane, North Kunlun-Qaidam terrane, South Kunlun terrane, Bayan Har-Songpan-Garzê terrane and Qiangtang terrane. The boundary between the Qilian terrane and North Kunlun-Qaidam terrane is the newly discovered Caledonian Qilian southern-margin subduction complex zone (or suture zone) formed 490 ~ 500Ma ago[6,7], that between the North Kunlun-Qaidam terrane and South Kunlun terrane is the Central Kunlun suture zone[8], (which is controversial), that between the South Kunlun terrane and Bayan Har-Songpan-Garzê terrane is the South Kunlun strike-slip fault (western segment) and A'nyêmaqên suture zone (eastern segment)[9~13], and that between the Bayan Har-Songpan-Garzê terrane and Qiangtang terrane is the Jinsha River strike-slip fault (western segment) and the Jinsha River suture zone (eastern segment)[5,11,12]. The Qilian terrane is a Caledonian mountain chain, the East Kunlun (including the North and South Kunlun terranes) is a Caledonian and Indosinian superimposed mountain chain, the Bayan Har-Songpan-Garzê is an Indosinian mountain chain, and the Qiangtang terrane is an Indosinian and Yanshanian superimposed mountain chain[11]. The shear senses show northward subduction of the Caledonian South Qilian suture zone and Indosinian A'nyêmaqên suture zone and southward subduction of the Indosinian Jinsha River suture zone[14].

From the Early Paleozoic to the end of the Mesozoic, these terranes gradually collided and were amalgamated with each other from north to south; as a result continental crust was accreted steadily, thus forming a composite terrane in southern Laurasia. A more important

collision event occurred between the composite terrane and the Indian plate 55Ma ago. Since that time the Tibetan Plateau has been uplifted over vast areas. The major Cenozoic tectonic event accompanying the uplift in the study region included: (1) eruption of alkaline volcanic rocks in Hoh Xil; (2) formation of north-south-trending rifts by extension; (3) thrusting of the Qilian and east Kunlun Mountains over the basins; and (4) activity of large strike-slip faults, as exemplified by the South Kunlun strike-slip fault, Xianshui River strike-slip fault and Altyn Tagh strike-slip fault whose strike-slip rates were 7 ～ 11.5mm/a, 10 ～ 16mm/a and 10 ～ 30mm/a respectively[15].

The main purpose of this paper is to reveal the layering and discontinuity of the lithospheric structure based on data from the Golmud-Tanggula Pass (west) and Gonghe-Yushu (east) earthquake-excited tomography detection profiles traversing the East Kunlun-Qiangtang area of the northern Tibetan Plateau, combined with new geological research results. We give a new interpretation of the lithospheric structure through an integrated analysis of the information of the lithospheric evolution traced in the geological history and the manifestations of the contemporaneous lithospheric structure.

2 Lithospheric inverstigation

2.1 Golmud-Tanggula Pass seismic tomographic profile across the western part of the East Kunlun-Qiangtang region

The stations passed by the seismic tomographic and receiver function inversion profile from Golmud to Tanggula are Golmud, Kunlun Pass, Wudaoliang, Tuotuo River and Tanggula Pass. The lithospheric structure in the western part of the East Kunlun-Tanggula area may be deduced as follows.

(1) The lithosphere has a sandwich-like structure and the Moho depth decreases from 70km in the north to 60km in the south (Fig. 2).

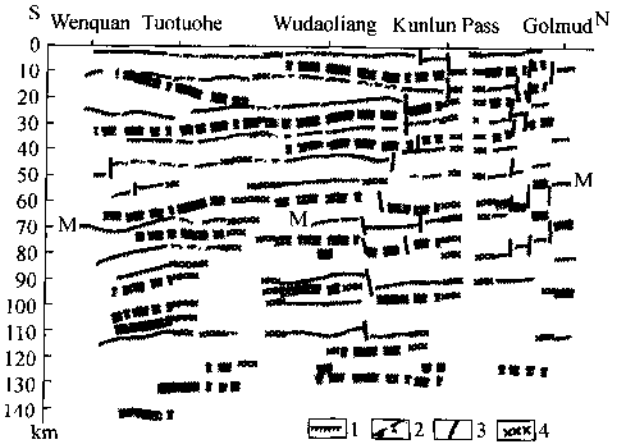

Fig. 2 Crustal profile of Golmud-Tanggula inferred from receiver function analysis.
1—High velocity transform contact plan; 2—low-velocity transform contact plan; 3—inferred fault; 4—discontinued zone.

(2)Above 150km in depth, the North Kunlun-Qaidam terrane is composed of low-velocity bodies and the south Kunlun terrane high-velocity bodies, with the latter penetrating northward beneath the former; the Qiangtang terrane is made up of low-velocity bodies.

(3)There exists a 250-km-wide and 160-km-thick low-velocity anomaly body in a zone equivalent to the asthenosphere at depths of 200～360km beneath the Hoh Xil in the western segment of the Bayan Har terrane and the northern part of the Qiangtang terrane, which is inferred to have been related to the eruption of Cenozoic alkaline volcanic rocks(Fig.3)[16,17].

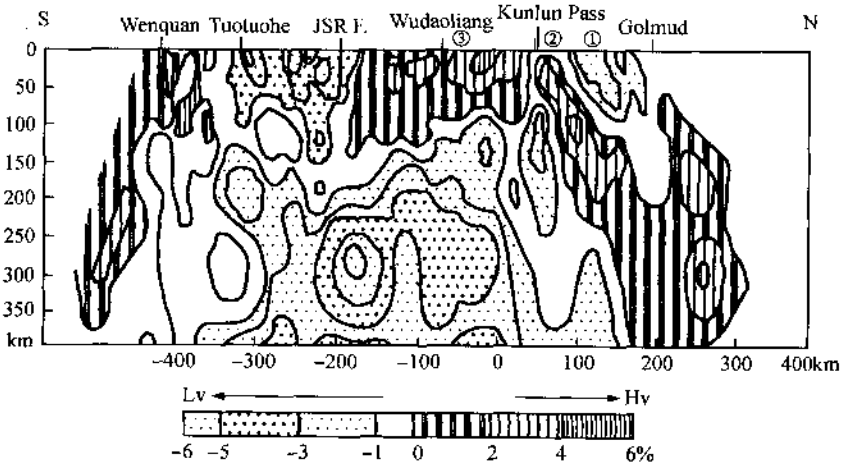

Fig.3 Golmud-Tanggula Pass seismic tomographic profile across the western part of the East Kunlun-Qiangtang region[1,5]. Hv, High-velocity; Lv, low-velocity.
①Central Kunlun lithospheric faults; ②South Kunlun lithospheric faults; ③Jinshuhe lithospheric fault.

2.2 Gonghe-Yushu seismic tomographic profile across the East Kunlun-Qiangtang region

The stations passed by the seismic tomographic and receiver function inversion profile and wide-angle reflection profile from Gonghe to Yushu are Gonghe, Huashixia, Madoi, Bayan Har Pass, the Xianshui River fault and Yushu. The following geological interpretation may be given to the lithospheric structure of the eastern part of the area(Fig.4).

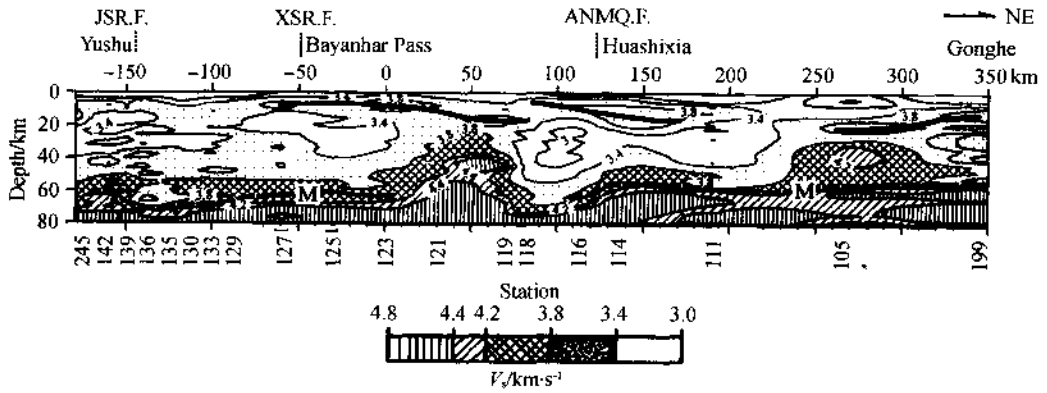

Fig.4 Crustal profile of Gonghe-Yushu inferred from receiver function analysis. The legend on the right denotes the S-wave velocities; M denotes the Moho; the thick broken line along the mid-crust low-velocity zone represents a possible detachment zone; the thick solid lines in the upper part denote faults.

(1)From south to north the crustal thickness decreases from 75 to 55km, showing the feature of being thick in the south and thin in the north[18].

(2)According to the S-wave velocities the crust may consist of four layers: an upper crust (0～20km) with wave velocity 3.0～3.7 km/s, a middle crust(20～35km) with wave velocity 2.3～3.0km/s, a lower crust(35～55km) with wave velocity 3.2～3.9km/s and a crust-mantle transition layer(55～70km) with wave velocity 4.0～4.3km/s and upper-mantle wave velocity >4.3km/s[18].

(3) The middle crust is composed of a lens-shaped low-velocity layer. The low-velocity lenses are located at 18～30km below Gonghe, north of Huashixia and the Bayan Har-Xianshui River fault. The wide-angle reflection and seismic Tomographic profiles both show the gently north-dipping stacked thrusts reaching a depth of 25km[18](Fig.4).

The surface geology of north Huashixia shows the features of the structure of Indosinian volcanic magma and a Cenozoic pull-apart basin. Testing of the thermal flow from the Shaliuhe ZK 502 well gave a thermal flow density of 78mW/m^2. Therefore, it is deduced that the low-velocity lens in the middle crust might reflect the background of extension and transtension since the Indosinian and have a genetic relation to the high thermal flow in the crust. Gonghe is located in a Caledonian subduction complex zone on the southern margin of Qilian, and the Xitieshan ZK 3606 well and Hongcan 1 and Hacan 1 wells of Da Qaidam all have higher thermal flow values(54, 41 and 38mW/m^2 respectively)[19], which may serve as the evidence for the modern reactivation of this tectonic boundary. The Gonghe Basin is a late Late Cenozoic down-faulted basin, bounded by two normal strike-slip faults lying on the north and south respectively; therefore, the occurrence of the low-velocity lens led to reactivation of paleostructure and formation of the modern down-faulted basin. The mid-crustal low-velocity hens in the deep part of the Bayan Pass-Xianshui River fault might be related to substantial Yanshanian granitic magmatism in the crust.

(4)The seismic tomographic profile has revealed that the lithosphere at a depth of 400km generally displays a "八"-shaped structure, with its northern part dipping to the north and its southern part dipping to the south. The Qilian terrane at northern Gonghe is composed of low-velocity material, but the Qaidam-South Kunlun terrane dominantly high-velocity material. The deep structure of the A' nyêmaqên zone suggests northward penetration of a high-velocity body. The northern part in the Bayan Har terrane shows northward underthrusting of a low-velocity zone beneath the South Kunlun high-velocity body, while the southern part in the Bayan Har terrane shows southward underthrusting of a high-velocity beneath the Qiangtang terrane composed of a low-velocity body[18](Fig.5).

3 Lithospheric faults

The above-mentioned two seismic profiles obviously show the discontinuity of the lithospheric structure and the characteristics and downward extension of lithospheric shear

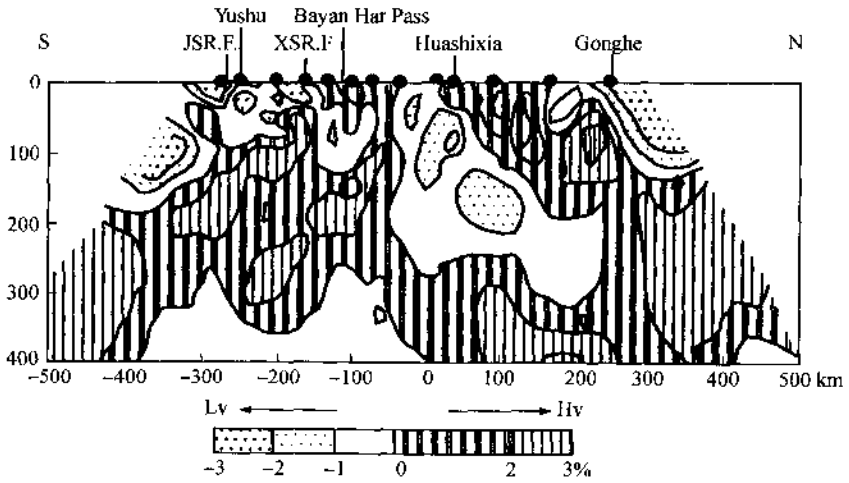

Fig.5 Gonghe-Yushu seismic tomographic profile across the eastern part of the East Kunlun-Qiangtang region[15]. Hv, High-velocity; Lv, low-velocity[1,5].

faults on terrane boundaries. There are mainly three lithospheric strike-slip faults and three lithospheric thrusts, they are: the South Kunlun lithospheric strike-slip fault, Jinsha River (western segment) lithospheric strike-slip fault and Xianshui River lithospheric strike-slip fault, and the South Qilian lithospheric thrust-Central Kunlun lithospheric thrust, A' nyêmaqên lithospheric fault and Jinsha River (eastern segment) lithospheric fault (Figs.3 and 5).

3.1 Identification of lithospheric faults

3.1.1 Nature of the South Kunlun-A' nyêmaqên fault zone as a lithospharic fault. Intensive geological study of the South Kunlun-A' nyêmaqên fault zone suggests that this fault zone may be divided into the eastern and western segments. The western segment is the nearly E-W-trending South Kunlun fault zone, composed of 2-km-wide mylonite with upright foliation, horizontal stretching lineation and "A"-type shear folds, displaying distinct characteristics of left-lateral shear strain. Syntectonic granite bodies are developed along the fault and on its northern side. Isotopic age dating suggests the following: the shear strike-slip motion started 240～200Ma ago; at 150～140Ma and 120～100Ma strong shear activities occurred again; during the Neogene (20Ma) ductile shear still had some effect[13]; and at present the fault still shows the left-lateral strike-slip nature (mainly brittle), accompanied by seismicity. The Golmud-Tanggula Pass profile (west) (Fig.3) reveals that this fault is a lithospheric strike-slip fault, which extends a vertically downward up to 250 km. The low-velocity body in the fault zone might be high-temperature material derived by melting of the crust and constitute a source region of granitic magmatism since the Indosinian. The eastern segment is the NW-SE-trending A' nyêmaqên fault zone, which is an Indosinian subduction zone as well as a suture zone and comprises a series of southwest-verging thrust faults[12]. The Huashixia station at the Gonghe-Yushu profile (east) (Fig.5) reveals that A' nyêmaqên fault zone represents the boundary

between the low-velocity body and high-velocity body and the dipping steeply northward lithospheric fault to a depth of 200 km.

3.1.2 Nature of the Jinsha River fault zone(suture zone)as a lithospheric fault. The Jinsha River fault zone lies between the Bayan Har-Songpan-Garzê terrane and Qiangtang terrane. Based on studies of the ophiolites, mélanges and plate mechanism in the eastern segment of the fault zone(the western margin of the Songpan-Garzê orogenic belt), we suggest that the Songpan-Garzê terrane was subducted southwestward beneath the Qiangtang terrane and that the eastern segment of the Jinsha River fault has the nature of a suture zone[11]. It is not yet clear whether the western segment (west of Yushu) of the fault has the nature of a suture zone. The existence of a mylonite zone and ca. 200Ma syntectonic granite implies that the western segment of the fault is a ductile left-lateral strike-slip fault formed in the Indosinian[11]. The Gonghe-Yushu profile(east) has revealed that the western segment of the fault is a lithospheric strike-slip fault, extending vertically down to a depth of 150km. The eastern segment of the fault is a lithospheric thrust, penetrating to a depth of 150km.

3.1.3 Nature of the Xianshui River fault zone as a lithospheric fault. The western part of the Bayan Har-Songpan-Garzê terrane consists of high-velocity material. Its eastern part is relatively complex and may be subdivided into three segments: the northern, southern(Hv) and central segments(Lv). The NW-SE-trending Xianshui River fault is the boundary between the central and southern segments. This fault, which originated 20Ma ago[20], is a left-lateral strike-slip active one with a strike-slip rate of 10～16mm/a. The eastern profile shows that the Xianshui River fault is a lithospheric shear fault, extending vertically down to a depth of 120km.

3.1.4 Nature of the Central Kunlun fault zone(suture zone)as a lithospheric fault. Disputes have long existed about whether the Central Kunlun fault zone in the central East Kunlun is a suture zone. The physical state revealed by the earthquake-excited tomography detection profile indicates that with the Central Kunlun fault as the boundary North Kunlun-Qaidam is composed of low-velocity material, but South Kunlun high-velocity material; so it is apparently a material interface as well as a tectonic interface. Besides, the physical state of North Kunlun is the same as that of Qaidam, but on the ground surface the North Kunlun unit, consisting of metamorphic basement and volumetric granite (which should be high-velocity, high-density material) is utterly different from the Qaidam Basin (low-velocity, low-density material). Therefore, we deduce that the North Kunlun unit might be rootless and that its lower part is composed of low-velocity, low-density material. The high-velocity, high-density material making up the South Kunlun unit extends downward to a depth of 200km, forming a steeply north-dipping high-velocity zone, which provides geophysical evidence that the Central Kunlun fault might exist as an ancient subduction zone and the Central Kunlun fault.

3.2 Eastward extrusion in the lithospheric range

It has been revealed that the Altun-Tagh fault with a strike-slip rate of 10～30mm/a is also a lithospheric fault, extending vertically downward to a depth of 250km using the Wutumeiren-Ruqian tomographic profile across the Altun Mountain[21] at the western edge of

the area under study. Thus, we suggest that on the northern Tibetan Plateau, the large faults on the surface are in fact lithospheric shear faults at the depth. Tapponnier has supposed the hypothese about the eastward extrusion of the Eurasia plate caused by the northward subduction of the Indian wedge[22]. We infer that the eastward extrusion on the northern Qinghai-Tibetan Plateau occurred in the lithospheric range.

4 Conclusions and discussion

An integrated study of the Golmud-Tanggula Pass (west) and Gonghe-Yushu (east) earthquake-excited tomography detection profiles traversing the East Kunlun-Qiangtang region of the northern Tibetan Plateau, shows that the deep-seated structure of the study region has the following characteristics:

(1) From south to north the crustal thickness decreases from 70～75km to 55～66km, and the variation range of thickness (10km) in the western part is smaller than that (20km) in the eastern part; the crust has a sandwich-like structure and the mid-crustal lens-shaped low-velocity layer may be a detachment layer.

(2) Physical states of various terranes are marked by the alternation of high-velocity and low-velocity material: the North Kunlun-Qaidam terrane is composed of low-velocity material, the South Kunlun terrane high-velocity material and the western part of the Bayan Har-Songpan-Garzê high-velocity material; whereas the eastern part of the Bayan Har-Songpan-Garzê is relatively complex, composed of low-velocity material in the northern and southern sectors and high-velocity material in the central sector; the Qiangtang terrane is composed of high-velocity material; a low-velocity body exists at depths of 200～360km in the western part of the Bayan Har terrane (Hoh Xil area) which is related to the Cenozoic volcanism;

(3) Earthquake-exicited tomographic detection has also revealed the discontinuity of the lithospheric structure and the existence of lithospheric shear faults on the study area, which follow the occurrences of the faults system on the surface formed in the Indosinian. The South Kunlun left-lateral strike-slip fault zone——the western segment of the South Kunlun-A'nyêmaqên fault zone is a lithospheric shear fault with a downward extension of 250km; the NW-SE-trending A'nyêmaqên suture zone——the eastern segment of the fault zone is a lithospheric shear fault steeply northward to a depth of 250km. In the Indosinian Jinsha River suture zone, the western segment is a lithospheric fault extending vertically down to a depth of 150km and the eastern segment of the fault is a lithospheric fault penetrating southwestward to a depth of 150km. The Xianshui River fault in the interior of the Bayan Har-Songpan-Garzê terrane also has the features of a lithospheric shear fault extending vertically down to depth of 120 km.

(4) According to the characteristics of the Cenozoic large-scale strike-slip faults and the identification of lithospheric shear faults of the northern Qinghai-Tibetan Plateau, we conclude that the eastward extrusion at the northern Tibetan Plateau is at least within the range of

lithosphere.

Acknowledgements We express our gratitude to Prof. Yang Wencai and Zhao Zhixin for their useful discussions with us on the paper. This work was jointly supported by the State Key Basic Research and Development Project (Grant No. G1998040800) and the Chinese-French cooperative projects "The Mechanism for Shortening of the Lithosphere in the East Kunlun and Adjacent Regions" and "Tectonic Evolution and Lithospheric Shear Faults of the Altyn and Qilian Mountains"(Grant No. 9501106).

References

[1] Jiang, M., Hirn, A. and Poupinet, G. Tibetan plateau seismic experiment: Design and Preliminary results, 1992～1993, Global Tectonics and Metallogy, 1995, 4: 199～201.

[2] Jiang, M., Lu, Q. T., Shi, D. N. *et al*., The crust and upper mantle structure of central Tibet plateau using seismic data, Acta Seismologica Sinica, 1996, 39(4): 476～482.

[3] Wittlinger, G, Masson, F., Poupinet, G. *et al*., Seismic tomography of northern Tibet and Kunlun: Evidence for crustal blocks and mantle velocity contrasts, EPSL, 1996, 139: 263～279.

[4] Kind, R., Kosarev, G L., Paterson, N. V. *et al*., Receiver junctions at stations of the German Region Seismic Network (GRSN), Geophys. J. Int., 1995, 121: 191～202.

[5] Xue Guagqi, Qian Hui, Jiang Mei *et al*., Studies on the velocity structure of crust-upper mantle beneath the eastern Qinghai-Tibet Plateau using seismic tomography, Continental Dynamics, 1999, 4(2): 79～85.

[6] Yang Jingsui, Xu Zhiqin, Li Haibing *et al*., Finding of the eclogites in the northern boundary of Qaidam, W. China, Chin. Sci. Bull., 1998, 43(14): 1544～1549.

[7] Yang Jingsui, Xu Zhiqin, Song Shuguang *et al*., Discovery of Eclogite in Dulan, Qinghai, and its significance for studying the HP-UHP metamorphic belt along the central orogenic belt of China, Acta Geol. Sin. (in Chinese), 2000, 74(2): 156～168.

[8] Jiang Chunfa, Yang Jingsui, Feng Binggui *et al*., Kunlun Opening-Closing Structure(in Chinese), Beijing: Geological Publishing House, 1992.

[9] Yang, J. S., Robinson, P. T., Jiang, C. E *et al*., Ophiolites of the Kunlun Mountains, China and their tectonic implication, Tectonophysics, 1996, 258: 215～231.

[10] Xu Zhiqin, Large shear zones in the main orogenic belts, China, Episodes, 1995, 18: 41～43.

[11] Xu Zhiqin, Yang Jingsui, Li Haibing *et al*, Mesozoic crustal evolution and dynamics of the East Kunlun-Tanggula composite mountain chains, Proceedings of the 30th International Geological Congress, Volume 7, Orogenic Belts Geological Mapping, 1997b, 7～20, Utrecht: VSP. 19.

[12] Xu Zhiqin, Jiang Mei, Yang Jingsui *et al*., Mantle diapirism and inward intracontinental subduction: A discussion on the mechanism of uplift of the Qinghai-Tibet Plateau (eds. A. Macfarlane, R. B. Sorkabi, J. Quade), Himalaya and Tibet: Mountain Roots to Mountain Tops, Geological Society of America Special Paper, 1999, 328: 19～31.

[13] Li Haibing, Xu Zhiqin, Chen Wen. Southern marginal strike-slip fault zone of the East Kunlun Mountains: an important consequence of intracontinental deformation, Continental Dynamics, 1996, 1(2): 146～155.

[14] Xu Zhiqin, Yang Jingsui, Chen Fangyuan, A' nyêmaqên suture zone and subduction-collision dynamics (ed. Zhang Qi), Ophiolites and Geodynamic Research (in Chinese with English abstract), Beijing: Geological Publishing House, 1996.

[15] Qian Hui, Jian Mei, Xue Guangqi *et al*., Crustal structures on the eastern Qinghai-Tibet Plateau revealed from receiver function inversion profiles, Acta Seismologica Sinica, 2001, 24, 1: 103～108.

[16] Pelzer, G, Tapponnier, P., Formation and evolution of strike-slip faults, rifts and basins during the India-Asia collision: an experimental approach, J. Geophys. Research, 1988, 93: 15085～15117.

[17] Yang Jingsui, Xu Zhiqin, Bai Wenji *et al*., Cenozoic volcanism on the Qinghai-Tibet Plateau and its genesis, Continental Dynamics, 1997, 2(1): 1～11.

[18] Xu Zhiqin, Jiang Mei, Yang Jingsui *et al*., Deep tectonophysical process of the uplift of the northern Qinghai-Tibet plateau: Evidence from the integrated geological-geophysical profile from Golmud to the Tanggula Mountains, Qinghai Province, China, Acta Geol. Sin., 1996, 70(3): 195～206.

[19] Cui Junwen, Tang Zhemin, Deng Jinfu *et al*., The Altyn Tagh FaultSystem (in Chinese), Beijing: Geological Publishing House, 2000.

[20] Xu Zhiqin, Hou Liwei, Wang Zongxiu *et al*., Orogenic Process of the Songpan-Garzê Orogenic Belt (in Chinese), Beijing: Geological Publishing House, 1996.

[21] Xu Zhiqin, Yang Jingsui, Zhang Jianxin *et al*., A Comparison between the Tectonic Units on the Two Sides of the Altyn Tagh Sinistral Strike-slip Fault and the Mechanism of Lithospheric Shearing, Acta Geol. Sin. (in Chinese), 1999, 73(3): 193～205.

[22] Tapponnier, P., Peltzer, G., Le Dain, A. Y., Propagating extrusion tectonics in Asia: New insights from simple experiments with plasticine, Geology, 1982, 10: 611～616.

青藏高原北部的碰撞造山及深部动力学[1]

——中法地学合作研究新进展

许志琴　杨经绥　姜　枚

（中国地质科学院地质研究所　北京）

摘　要　本文展示了中法 1995～2000 年青藏高原北部地学研究的如下主要新进展：①完成 8000km 长的青藏高原北部及中部天然地震岩石圈探测剖面，确定若干条岩石圈断裂，发现与新生代火山喷发有关的青藏高原中部深处的低速、低密度体，塔里木地块俯冲于阿尔金山之下；②提出阿尔金断裂形成于 220～240Ma 和左行平移 400km 的科学依据及确定其新生代变形量；③确定祁连南缘 350km 长的高压-超高压变质带，提出其可能代表早古生代时期北中国板块与扬子板块之间西部界线的新认识；④根据加里东期蛇绿岩、花岗岩及俯冲杂岩带的新发现，初步建立了古碰撞造山格架；⑤提出高原隆升的“地幔底辟和内向陆内俯冲”的新假设。

关键词　青藏高原北部　岩石圈结构　碰撞造山　深部动力学

近 20 年来，青藏高原一直作为固体地球科学领域的“重头戏”受到国内外地学家高度重视，并取得众所瞩目的研究成果。如果说八十年代人们把注意力集中在青藏高原南部印度板块与欧亚板块碰撞造成的近程效应的话，那么九十年代，青藏高原的研究已向北部转移，把研究和探索两大板块碰撞的远程效应作为主要目标。一些地质学家认为，青藏高原北部的研究已成为解决青藏整体隆升问题的最后关键。实际上青藏高原北部研究意义远非如此，因为青藏高原作为亚洲大陆最后拼合体，是在一系列地体从早古生代开始自北往南会聚拼合直至 55Ma 与印度板块的碰撞，然后经历了地球历史最壮观的隆升事件而成为今天之景观。研究青藏北部还面临重塑中国西部古亚洲构造体制的困难，因为古老构造体系受到后期强烈的改造及错位。研究表明，青藏高原北部隆升及其所引起的三维变形还对先存的基础及构造有很大的依附性及继承性，因此要了解高原北部的今天，必须认识它的过去。中法地质及地球物理探测的最新成果还为我们考虑青藏高原周围克拉通对高原的影响以及高原腹地大量新生代碱性火山岩的喷发与深部热驱动有关的可能性。可以认为来自高原南部印度板块与欧亚板块的碰撞已并非高原隆升的唯一驱动力。因此，采用多学科研究青藏高原北部物质组成、构造演化及岩石圈尺度的结构及动力学成为中法青藏高原北部合作研究（1995 年至今）的科学目标。

---

[1] 地球学报，2001 年第 22 卷第 1 期。
责任编辑：宫月萱。
第一作者：许志琴，女，构造地质专业，中国科学院院士，留法博士，中国地质科学院地质研究所所长，长期从事青藏高原地学研究，“九五”期间为青藏北部中法地学合作项目、国家基金重点项目“祁连造山带的组成及造山过程”（49732020）及国土资源部重点基础项目“阿尔金山-祁连山构造演化及岩石圈剪切作用”（9501106）的首席科学家。

1 青藏高原北部岩石圈三维结构的初步揭示

中法地球物理学家在青藏高原北部及相邻地域共同开展的新的天然地震岩石圈探测剖面，共8000km，先后完成西藏定日-唐古拉(青藏南部)，唐古拉山口-青海格尔木(青藏北部西段)，青海若羌-新疆茫崖(穿越阿尔金山)，新疆克拉玛依-库车(穿越天山)和青海共和-玉树(青藏北部东段)剖面(Jiang *et al*., 1995, 1996; Wittlinger *et al*., 1996; Xue *et al*., 1999; Qian *et al*., 2000)，布置便携地震台站超过300台次(图1)。其主要成果：①揭示了高

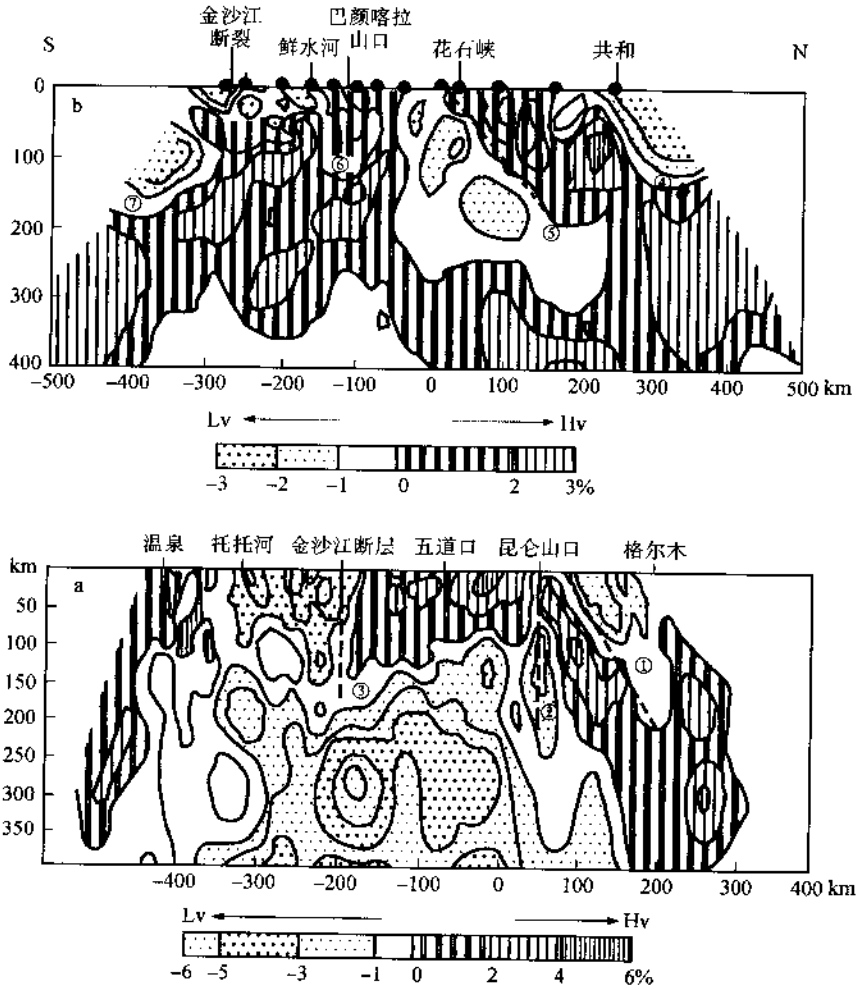

图1 穿越青藏高原北部及中部的地震层析剖面

Fig.1 Seismic tomographic cross-sections of the Northern Qinghia-Tibet Plateau

a—格尔木-唐古拉山地震层析剖面；b—共和-玉树地震层析剖面。Hv—高速体，Lv—低速体

①昆中岩石圈逆冲断裂；②昆南岩石圈走滑断裂；③玉树岩石圈走滑断裂；④祁连南缘岩石圈逆冲断裂；⑤阿尼玛卿岩石圈逆冲断裂；⑥鲜水河岩石圈走滑断裂；⑦金沙江岩石圈逆冲断裂

原北部和中部东昆仑-羌塘地区地壳厚度自南往北由 70～75km，减小为 60～55km，西部厚度变化幅度较东部小，各地体岩石圈的物理状态表现为高速体与低速体相间的结构特征，岩石圈具"多明治"层圈结构并存在中地壳透镜状低速层；②发现岩石圈的不连续性及岩石圈剪切断层的存在，确定了阿尔金左行走滑断层，昆南左行走滑断层，阿尼玛卿缝合带及金沙江缝合带等均为深入地下 150～200km 的岩石圈剪切断层，按类型又分为岩石圈平移断层及岩石圈逆冲断层；③发现了与可可西里新生代火山活动有成因联系的深部 200～360km 的大型低速低密度异常体；④印度板块岩石圈地幔往北以中等倾角插入喜马拉雅山下部，不超过雅鲁藏布江缝合带；⑤塔里木地体以低缓角度往南俯冲于由高速体组成的阿尔金山之下。

2　确定青藏北部祁连南缘 350km 长的高压-超高压变质带

在青藏高原北部祁连山南缘发现一条 350km 长(大柴旦—锡铁山—都兰)的高压-超高压榴辉岩带，研究表明，榴辉岩形成的压力大于 2.5GPa，温度大于 700℃，形成及折返时代为 500～400Ma(杨经绥等，1998；张建新等，1999；许志琴等，1999)，并与石榴石橄榄岩(杨建军等，1994)、蛇绿岩共生。提出 400～500Ma 期间北中国板块与扬子板块之间可能存在一条长 4000km 的巨型中央高压-超高压变质带(苏鲁-大别-秦岭-祁连南缘-阿尔金山)，(杨经绥，2000)，这些重要发现及认识不仅有利于青藏高原北部构造格架的建立及中国西部古亚洲体系的重塑，对解决早古生代中国南北板块汇聚动力学有重要意义(图 2)。

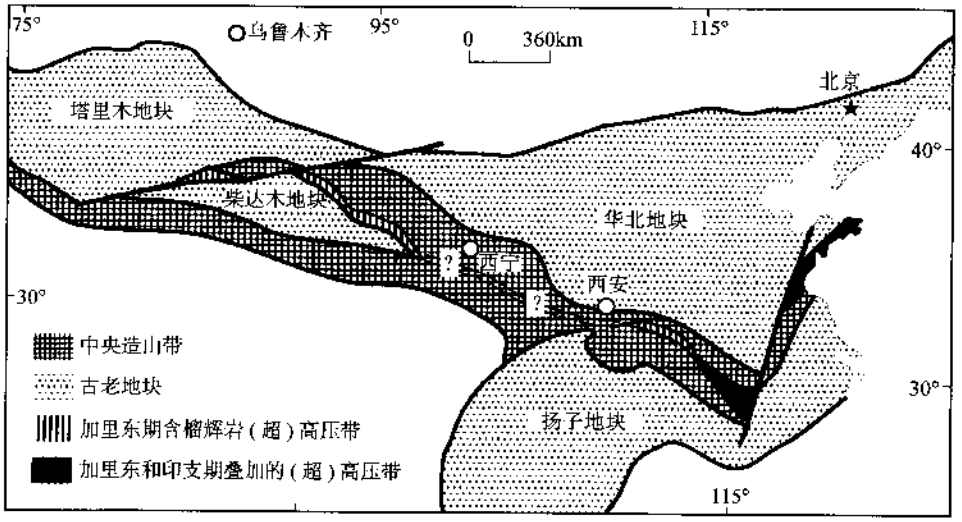

图 2　横贯中国中部巨型高压超高压变质带位置图

Fig. 2　Distribntion of a large high and ultrahigh-pressure metamorphic belt in the Central China Orogenic Belt

3 祁连山的西延及阿尔金断裂巨大平移

阿尔金断裂位于青藏高原西北部边界，也是中亚最大的平移断层，其平移量及形成时代问题在地学界争议已久。由于祁连山西段被阿尔金断裂所截，祁连山西延问题成了重塑中国西部古亚洲体制的关键。在前人研究基础上，通过阿尔金断裂两侧祁连山与阿尔金山前寒武系变质基底，下古生代盖层、缝合带及碰撞花岗岩的对比，特别是祁连南缘超高压变质带与南阿尔金超高压变质带(刘良等，1996；张建新等，1999)在榴辉岩产出、围岩、地球化学特征、原岩恢复、形成温压条件及形成折返时代的对比，表明阿尔金山与祁连山一样为加里东造山带，阿尔金山是祁连山的西延部分；获得阿尔金主断裂两侧左行平移 400km 的科学依据(许志琴等，2000)(图 3)。

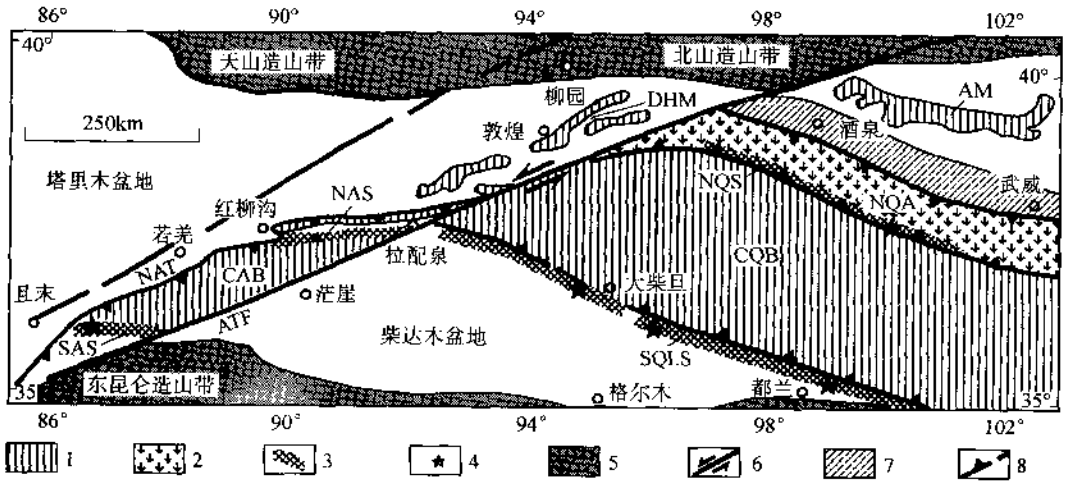

图 3 阿尔金断裂两侧构造单元对比图

Fig.3 Comparison between tectonic units of both sides along the Altun Tagh fault

1—前寒武变质基底；2—加里东火山岛弧带；3—俯冲杂岩带；4—榴辉岩；5—相邻造山带；6—左行走滑断裂；7—弧后盆地及被动大陆边缘；8—逆冲断裂

AM—阿拉善地块；DHM—敦煌地块；NQA—北祁连火山岛弧带；NQS—北祁连缝合带；CQB—祁连地块；SQLS—南祁连缝合带；NAS—北阿尔金缝合带；CAB—阿尔金地块；SAS—南阿尔金缝合带；NAT—北阿尔金逆冲断裂；ATF—阿尔金断裂

发现了沿阿尔金断裂中段(索尔库里)及东段(当今山口)的糜棱岩带，并应用离子探针及 Ar-Ar 测年手段，判断断裂形成时代为 220～240Ma，与法国科学家认为断裂形成于新生代显然不同(李海兵，2000)[1]。

[1] Li Haibing, Yang Jingsui, Xu Zhiqin, Wu Cailai, Wan Yusheng, Shi Rendeng, Juhn G., Liou P. Tapponnier, Trevor R. Ireland. 2000. Abstract. International Symposium on Geoscience of the Northern Qinghai-Tibet Plateau. 52～57.

4 青藏高原北部的古碰撞造山的基本格架与模式

青藏高原北部基本构造格架为"三山一盆",即阿尔金山、祁连山、东昆仑山与柴达木盆地。

(1)基本地体单元的划分:阿拉善-敦煌地体、北祁连-北阿尔金下古生代缝合带、祁连-阿尔金地体、南祁连-南阿尔金下古生代缝合带、柴达木-东昆仑地体、东昆仑南缘古特提斯缝合带及走滑断裂。

(2)测定了阿尔金山-祁连山中大量加里东碰撞花岗岩(420～490Ma)[1] 及前震旦纪变质基底加里东期再活化事件的年代。

(3)确定了东昆仑加里东-印支叠复造山带性质及大量印支期花岗岩存在[2]。

(4)确定了印支期以来形成的新的"挤压转换型"[3] 及"伸展转换型"的造山构造造型。

(5)厘定了华力西期右行平移作用及印支期左行平移作用形成的大型韧性走滑剪切带,表明地体或块体之间的相对运动与斜向碰撞、俯冲作用有关。

(6)初步建立了青藏高原北部碰撞造山模式。

5 新生代三维变形的定量研究

中法科学家运用新的测量技术,获得青藏高原北部新生代以来某些的汇聚及走滑速率。

(1)阿尔金断裂西段走滑速率为每年20mm,中段走滑速率为每年30mm,东段肃北以西走滑量22.5mm/a,肃北以东为17mm/a,其中被党河南北逆冲断层吸收的逆冲量5mm/a,被肃北盆地吸收的伸展量为3mm/a,中段索尔库里走滑断陷谷地(长宽比大于50)的形成表明了走滑量转换为伸展量。

(2)东昆仑南缘断层自印支期以来总走滑断裂距110km,走滑速率为11～16mm/a(Li *et al*., 1996);海原断裂走滑速率为8～16mm/a。

6 可可西里火山岩及其深源包体研究

可可西里地区新生代鲸鱼湖火山群、雄鹰台火山群和双泉子火山群属橄榄安粗岩系列;辉石岩包体被岩浆捕获,是地幔低度部分熔融的辉石岩浆形成。可可西里地区的火山活动时间从中新世到更新世(15.47～0.69Ma)。通过计算122个辉石温度、压力,结果表明,辉石形成的压力为3～6GPa(平均4.6GPa),温度为1100～1400℃(平均约1250℃),推测岩浆的来源深度大于150km。

---

[1] 吴才来等.2001.祁连南缘嗷唠山花岗岩SHRIMP锆石年龄及其地质意义.岩石学报,待刊。

[2] 许志琴,姜枚,杨经绥等.1997.东昆仑-唐古拉地区地壳演化、深部构造及大陆动力学(研究报告)。

[3] 许志琴,李海兵,杨经绥,陈文.2001.青藏高原北部"东昆仑南缘"印支转换挤压构造带及其动力学.地质学报,待刊。

7 探索高原隆升新机制

综合新的地质与地球物理成果，认为印度板块俯冲并非是高原隆升的唯一驱动，高原周缘克拉通作用及深部热驱动是高原隆升不可忽视的地内因素。提出探讨青藏高原隆升的"周缘内向的陆内俯冲及腹地地幔底辟"的新机制(许志琴等，1996，1999；Xu *et al*.，1999)，目前对此机制正在不断验证。

参 考 文 献

许志琴，姜枚，杨经绥等．1996．青藏高原北部隆升的深部构造物理作用．地质学报，70(3)：195～206．

许志琴，杨经绥，姜枚等．1999．大陆俯冲作用及青藏高原周缘造山带的崛起．地学前缘，6(3)：139～151．

许志琴，杨经绥，张建新等．1999．阿尔金断裂两侧构造单元的对比及岩石圈剪切机制．地质学报，73(3)：193～205．

刘 良，车自成，罗金海等．1996．阿尔金山西段榴辉岩的确定及地质意义．科学通报，41(14)：1485～1488．

吴才来等，2001．青藏高原北缘火山岩中辉石岩包体研究．地球学报，22(1)：61～66．

杨建军，朱 红，邓晋福，周天祯，赖绍聪．1994．柴达木北缘石榴石橄榄岩的发现及其意义．岩石矿物学杂志，13(2)：97～105．

杨经绥，许志琴，李海兵等．1998．我国西部柴北缘地区发现榴辉岩．科学通报，43：1544～1548．

杨经绥，许志琴，宋述光等．2000．青海都兰榴辉岩的发现及对中国中央造山带内高压-超高压变质带研究的意义．地质学报，74：156～168．

张建新，张泽明，许志琴等．1999．阿尔金构造带西段榴辉岩的 Sm-Nd 及 U-Pb 年龄．科学通报，44：1109～1112．

张建新，杨经绥，许志琴等．2000．柴北缘榴辉岩的峰期和退变质年龄：来自 U-Pb 及 Ar-Ar 同位素测定的证据．地球化学，29(3)：217～222．

G Wittlinger *et al*..1996. Seismic tomography of northern Tibet and Kunlun: Evidence for crustal blocks and mantle velocity contrasts. EPSL, 139: 263～279.

Jiang M, Him A, Poupinet G. 1995. Tibetan Plateau Seismic Experiment: Design and Preliminary Results. Global Tectonics and Metallogeny, (4): 199～201.

Jiang M, *et al*..1996. The Study on the structure of crust and upper mantle with natural earthquakes in central Tibetan plateau. Chinese journal of geophysics, 39(4).

Li Haibing, Xu Zhiqin and Chen Wen. 1996. Southern Margin StrikeSlip Fault Zone of East Kunlun Mountains: an Important conseguence of Intracontinental Deformation. Continental Dynamics. 1 (2): 146～155.

Qian Hui *et al*..2000. The Crust structure in the eastern Tibet infered from teleseismic receiver function. Acta, Seism. Sinica.

Xue Guangqi *et al*..1999. Studies on the velocity structure of crust-upper mantle beneath the eastern Qinghai-Tibet Plateau using seismic tomography, continental Dynamics. 4(2): 79～85.

Xu Zhiqin *et al*..1999. Mantle diapir and inward intracontinental subduction: A discussion on the mechanism of uplift of the Qinghai-Tibet Plateau. In Macfarlane, A., Sorkabi, R.B., and Quade, J., eds; Himalaya and Tibet: Mountain Roots to Mountain Tops: Boulder, Colorado, Geological Society of America Special Paper 328, 19～31.

Collision-Orogeny of the Northern Qinghai-Tibet Plateau and Its Deep Dynamics

Xu Zhiqin Yang Jingsui Jiang Mei
(Institute of Geology, CAGS, Beijing)

Abstract The paper reported the main new progresses on the northern Qinghai-Tibet plateau made by the Sino-France team during 1995～2000. They are: ①completed total 8000km long natural seismic profiles cross the northern boundary and central part of the plateau, identified several deep-cut lithospheric faults and low velocity and low density bodies under the central part of the plateau related to Cenozoic volcanic eruption, the Tarim block subducted beneath the Altun Mts; ②found the evidence that the Altyn Tagh fault formed in 220～240Ma and at least 400km sinistral offset since, and determined quantitatively deformation in Cenozoic; ③discovered 350km long high-ultrahigh pressure metamorphic belt in the south border of the Qilian terrane, which brobably represented the Early Paleozoic boundary between the North China and Yangtze plates; ④according to new discoveries of caledonian ophiolite, granite are subducted complex established paleo-collision orogenic framework of northern Qinghai-Tibet plateau; ⑤proposed a new model . "Mantle diapir and inward intracontinental subduction", to explain the uplift of the Qinghai-Tibet Plateau.

Key words Northern Qilian-Tibet plateau lithosphere structure collision orogen deep dynamics

Tectonic significance of early Paleozoic high-pressure rocks in Altun-Qaidam-Qilian Mountains, northwest China[●]

Jingsui Yang[1] Zhiqin Xu[1] Jianxin Zhang[1]
Ching-Yen Chu[2] Ruyuan Zhang[2] Juln-Guang Liou[2]
(1. Institute of Geology, Chinese Academy of Geological Sciences, 26 Baiwanzhuang Road, Beijing, 100037, China; 2. Department of Geological and Environmental Sciences, Stanford University, Stanford, California 94205-2115, USA)

Abstract Several early Paleozoic eclogite-bearing very high-pressure(P)belts have been recognized in Alpine-type orogens in the north Qiadam Mountains, the Altun Mountains, and the Beishan Mountains of northwest China. These eclogitic rocks together with minor garnet peridotites occur as blocks or lenses in amphibolite facies gneissic terranes of continental affinity, and have been subjected to extensive retrogression. On the basis of mineral chemistries and phase assemblages, peak P-temperature(T) conditions were estimated as follows: for the north Qaidam eclogites, $T = 720 \pm 120$℃ and $P > 22$kbar and for garnet peridotites, 720～850℃ and 25kbar; for the Altun eclogites, $T = 730 \sim 810$℃ and $P > 15$kbar; and for the Beishan eclogites, $T = 700 \sim 800$℃ and $P = 16 \sim 18$kbar. U-Pb and Ar-Ar isotopic determinations for the north Qaidam eclogite gave a peak metamorphic age of 495 ± 6Ma and a retrograde age of 470～480Ma. Sm-Nd and U-Pb isotopic data indicate that the peak metamorphic age of the Altun eclogite is 500～504Ma. Zircon separates from the Beishan eclogites provide a U-Pb upper intercept at 861 ± 50Ma and a lower intercept at 440 ± 50Ma. Similarities in the modes of occurrence, mineral parageneses, P-T estimates, and radiometric dates of eclogites suggest that the Altun very high P belt can be correlated with that of north Qaidam, whereas the Beishan belt may have been displaced to the north of the Alxa massif. These Alpine-type eclogite-bearing orogens were resulted from continental subduction and collision; they are different from the blueschist-and ophiolite-bearing Pacific-type orogen of the northern Qilian, where an early Paleozoic calc-alkaline volcanic arc was well developed due to northward subduction of the Qillan oceanic lithosphere. The disposition of several recognized Pacific-and Alpine-type orogens supports the hypothesis of 400km of left-lateral displacement on the Altyn Tagh fault. A preliminary model for early Paleozoic tectonic evolution involving subduction, accretion, and collision for the formation and emplacement of both Alpineand Pacific-type orogenic belts in the vicinity of the Altun-Qaidam-Qilian Mountains is proposed.

● Geological Society of America Memoir 194 2001.
Yang, J.S., *et al.*, 2001, Tectonic significance of early Paleozoic high-pressure rocks in Altun-Qaidam-Qilian Mountains, northwest China, *in* Hendrix, M.S., and Davis G.A., eds., Paleozoic and Mesozoic tectonic evolution of central Asia: From continental assembly to intracontinental deformation: Boulder, Colorado, Geological Society of America Memoir 194, p.151～170.

Introduction

Eclogite and garnet peridotite constitute a volumetrically minor component in orogenic belts, but provide invaluable information about orogenic processes; two distinct eclogite types have been recognized in the high pressure- temperature(P-T)belts of China(e.g., Liou *et al*., 1989). Coesite-bearing Alpinetype eclogite in the Dabie-Sulu ultrahigh-P belt is associated with garnet peridotite, occurs as blocks, lenses, or layers in paragneiss, is retrograded to amphibolite, and has distinctly high P-T peak metamorphic conditions; $P > 25$ kbar and $T > 700$℃ (Q. Wang *et al*., 1992; Liou *et al*., 1994, 1996; Coleman and Wang, 1995; X. Wang *et al*., 1995). In contrast, Pacifictype high-P eclogite is associated with ophiolite, blueschist, and prehnite-pumpellyite facies rocks in the Qilian Mountains(Wu *et al*., 1993; Wu and Tian, 1994), is overprinted by blueschistgreenschist facies assemblages, and has peak metamorphic P-T conditions < 14kbar and < 500℃. As described in detail by Maruyama *et al*. (1996), such contrasting high P-T belts reflect different tectonic settings in terms of protoliths, subduction, and exhumation(e.g., Ernst and Liou, 1995).

Several newly discovered very high P eclogites in the vicinity of the Altun-Qaidam-Qilian Mountains are intercalated with continental sequences of sedimentary and igneous origin, and are indicative of continental subduction and/or collision. These Alpine-type eclogites are enclosed in similar country-rock gneisses, share analogous decompression P-T paths, and may have been formed in different parts of a similar or the same tectonic unit. Their occurrences can be used to constrain suture geometry and to determine the magnitude of slip along the Altyn Tagh fault, one of the largest strike-slip fault systems in the world.

The Altun-Qaidam-Qilian region shown in Figure 1 at the northern border of the Qinghai-Tibet Plateau is bounded by the Qaidam basin to the south, the Tarim basin to the west, and the Sino-Korean craton to the east. This region includes several orogenic belts. For example, the Qilian orogen, >300km wide, extends from the Altyn Tagh fault southeastward for ～1000km to the Qinling-Dabie orogen, and forms a major geographictectonic boundary between north and south China. The north Qilian early Paleozoic orogen has been regarded as one of the best exposed orogenic belts in the world(e.g., Xu *et al*., 1994; Feng and He, 1996) and contains Pacific-type margin petrotectonic assemblages, including lawsonite-bearing high-P belts and ophiolitic sequences(e.g., Wu *et al*., 1993; Wu and Tian, 1994). However, the petrotectonic assemblages of the southern border between the central Qilian block and the Qaidam basin are not well known, and their correlation across the Altyn Tagh fault to the west has not been investigated. Recent findings of eclogites and garnet peridotites in an Alpine-type collision belt along the northern border of the Qaidam basin(e.g., Yang *et al*., 1994, 1998) and the findings of similar eclogite in the Altun Mountains(e.g., Che *et al*., 1995a, 1995b; Hanson *et al*., 1995) and the Beishan Mountains(Mei *et al*., 1998) provide new data for the petrotectonic evolution of northwestern China.

The purposes of this chapter are to characterize the petrochemical and geochronological features of these very high P eclogites, garnet peridotites, and their enclosing gneissic rocks from both the north Qaidam and the Altun Mountains, and to document their significance regarding the regional tectonics. These data are compared and contrasted with analogous data from Pacific-type high-P rocks of the north Qilian terrane. A Paleozoic tectonic evolution scenario involving subduction, accretion, and collision involving the formation and emplacement of both Alpine-and Pacific-type orogenic belts in the AltunQaidam-Qilian Mountains is proposed.

Regional Geologic Setting

A number of intracontinental orogens separate several major Precambrian cratons and record magmatic and metamorphic events associated with subduction, collision, and subsequent tectonic movements of the cratonic blocks as eastern Eurasia was assembled. The broad Qilian orogen on the southern borders of the Sino-Korean craton (Fig. 1) extends eastward for ~ 1000km and is connected with the Qinling-Tongbai-Dabie Mountains; its west end merges with the Altun Mountains. Bounded on the south by the Qaidam basin and on the northwest by the Altyn Tagh fault system , these remote , arid mountains comprise a series of west - northwest -

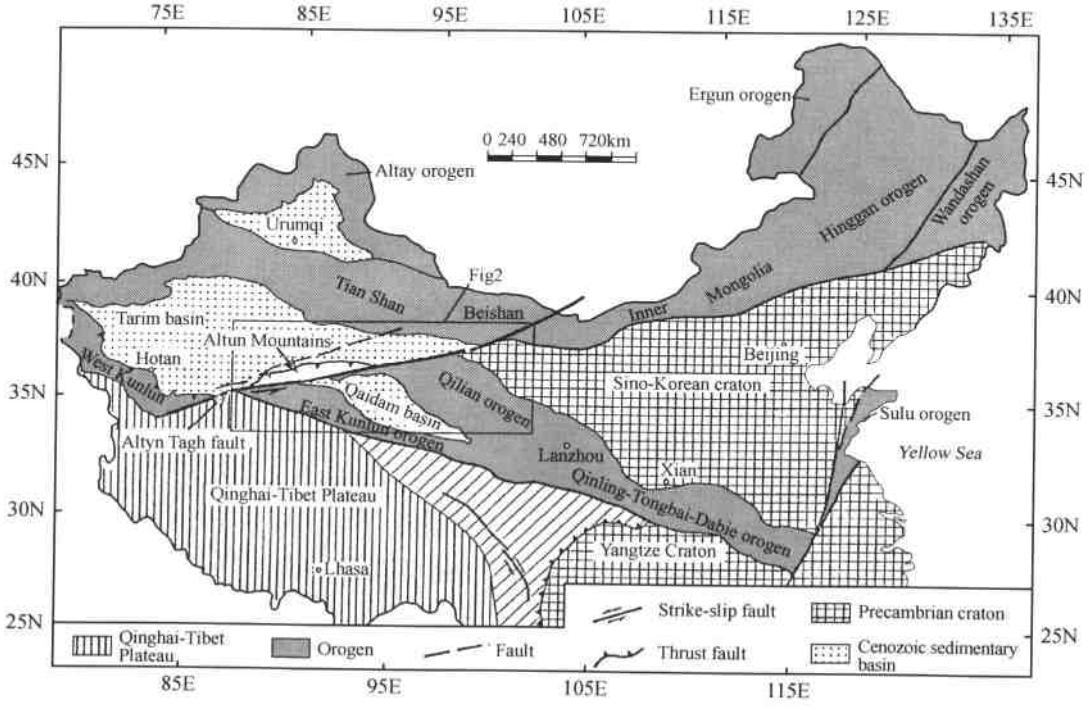

Fig. 1 Regional tectonics of China showing distribution of Sino-Korean, Tarim, and Yangtze cratons, several major intracratonal mountain belts, and location of Figure 2. This map is modified after Ma *et al*. (1996).

trending subparallel tectonic units. Between cratons, several microcontinental blocks, including the Qaidam block and the central Qilian block, and early Paleozoic metamorphic belts are present in the regions between the Tarim and Qaidam basins and the Sino-Korean craton. The Qilian and adjacent orogens contain distinctive lithotectonic assemblages, suggesting early Paleozoic convergence, including subduction of oceanic lithosphere and continent-continent collision. High *P-T* rocks in these orogens therefore are useful in probing the various stages of plate interactions around the margins of the paleo-Eurasian continent.

On the basis of recent geologic mapping and detailed study of lithotectonic characteristics in the Qilian-Qaidam region (e.g., Bureau of Geology and Mineral Resources of Qinghai Province [BGMQ], 1991; Xu *et al*., 1994; Chen *et al*., 1995), several fault-bounded major tectonic units have been recognized (Fig. 2). From north to south, they are① the Alxa massif, ②the north Qilian arc, ③the north Qilian subduction complex, ④the central Qilian block, ⑤ the north Qaidam subduction complex, and⑥the Qaidam block (approximately coincident with the Qaidam basin in Fig. 2). These units can be correlated with those in the Altun Mountains (Table 1), assuming 400km of left-lateral displacement for the Altyn Tagh fault (Yue and Liou, 1999).

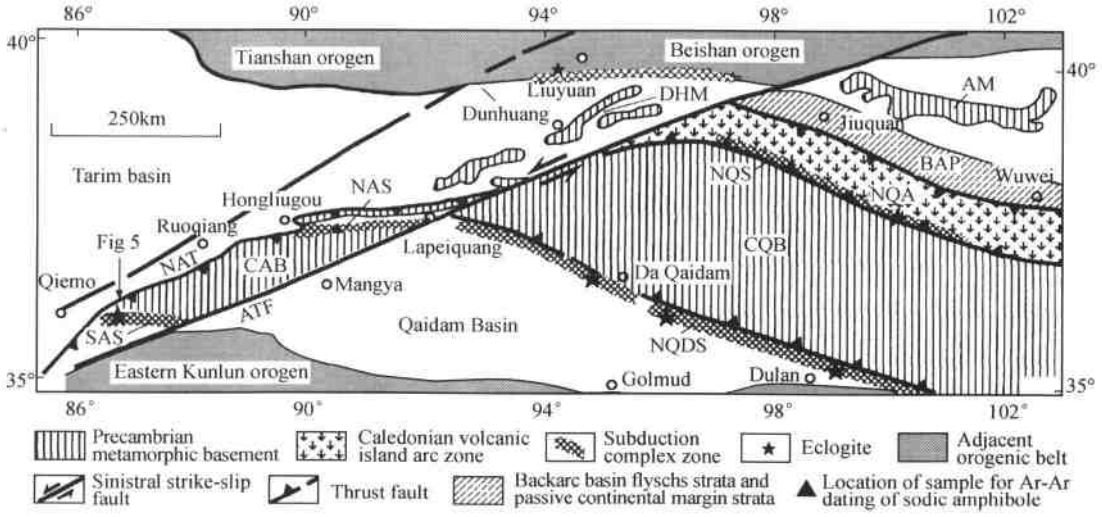

Fig. 2 Tectonic sketch map of Altun-Qilian region and locations of newly discovered eclogites in Altun, north Qaidam, and Beishan areas, modified after Bureau of Geology and Mineral Resources of Gansu Province (BGM) (1989), BGM of Qinghai Province (1991), BGM of Xinjiang Uygur Autonomous Region (1993), Che *et al*. (1995a), Yang *et al*. (1998), and Yue and Liou (1999).

Abbreviations: NAT—north Altun thrust; ATF—Altyn Tagh sinistral strike-slip fault; DHM—Dunhuang massif, NAS—north Altun subduction complex; CAB—central Altun block; SAS—south Altun subduction complex; AM—Alxa massif; BAP—backarc basin flysch strata and passive continental margin strata; NQA—north Qilian arc; NQS—north Qilian subduction complex; CQB—central Qilian block; NQDS—north Qaldarn subduction complex.

Table 1 Correlation Between Tectonic Units on Both Sides of the Altyn Tagh Fault

Qilian-North Qaidam Mountains		Altun Mountains	
Tectonic units	Petrotectonic assemblages	Tectonic units	Petrotectonic assemblages
Alxa Massif	Ar_3(?)-Pt_1, gneiss, graphite-bearing marble, amphibolite, migmatite	Dunhuang massif	Ar-Pt_1, amphibolite, granulite, marble, migmatite
Northern Qilian arc	O_{1-2} calc-alkalic volcanics	?	?
Northern Qilian subduction complex	Ophiolite and ophiolitic melange, blueschist(440～462Ma), eclogite	Northern Altun subduction complex	Ophiolite, ophiolitic melange, sodic-amphibole-bearing metabasalt(457Ma)
Central Qilian block	Amphibolite, marble, migmatite, pelitic schist, felsic gneiss	Central Altun block	Marble, quartz-mica schist, amphibole schist, migmatite, felsic gneiss
North Qaidam subduction complex	Early Paleozoic garnet-peridotite, eclogite (495Ma), felsic gneiss	South Altun subduction complex	Early Paleozoic eclogite(500～504Ma), amphibolite, felsic gneiss

Abbreviations: Ar_3, Late Archean; Pt_1, Early Proterozoic; O_{1-2}, Early-Middle Ordovician.

References: Bureau of Geological and Mineral Resources of Gansu Province, 1989; Bureau of Geological and Mineral Resources of Qinghai Province, 1991; Liu and Wang, 1993; Wu *et al*., 1993; Xia *et al*, 1995; Che and Sun, 1996.

The Altun Mountains extend northeast for～800km, are between the Tarim and Qaidam basins and the Kunlun orogen, and are bounded on the northwest by strands of the north Altyn Tagh fault system and on the south by the left-lateral strike-slip Altyn Tagh fault(Fig.2), The extent and displacement of the Altyn Tagh fault are still poorly known, partly because the region is extremely remote and only limited geologic data are available(for a summary of recent studies, see Yue and Liou, 1999). Major lithologic units within the Altun Mountains include the Dunhuang massif and the Early Proterozoic Altun Group, separated by two subduction complexes(Fig.2). The regional geology of the Altun Mountains has been significantly modified by large Cenozoic displacement of the Altyn Tagh fault system due to tectonic extrusion during the Eurasia-India continent collision(Tapponnier and Molnar, 1977). Major lithotectonic units across and bordering the Altyn Tagh fault are described in the next section. Analytical details and uncertainties for age determination using Ar-Ar, U-Pb, and Nd-Sm isotopic systematics are described, respectively, in Chen *et al*.(1996), Lu and Li(1991), and Z. Zhang *et al*.(1999).

Description of Main Tectonic Units

Alxa-Dunhuang massif

The western margin of the Sino-Korean craton, named the Alxa massif(Fig.2), consists mainly of an Early Proterozoic metamorphic complex including a variety of gneiss, schist, graphitebearing marble, amphibolite, and migmatite. These basement rocks were intruded by granite at 1719 ± 50Ma and gabbro at 1365 ± 50Ma(Liu and Wang, 1993). The Longshou fault separates this basement complex from a 60～100-km-wide belt of Cambrian to Silurian passive margin strata in the Qilian Mountains to the south(Wu *et al*., 1993; Wu and Tian, 1994). The sedimentary strata include Cambrian marginal clastics and minor platform carbonate rocks,

overlain by Ordovician sandstone, shale, quartzite, and limestone with thin flows of andesite and rhyolite and pyroclastics, which are in turn overlain by Upper Silurian molasse.

In the Altun Mountains, the Archean basement of the Dunhung massif (Fig.2) includes high-grade amphibolite, granulite, and migmatite; Sm-Nd dating of these rocks yielded an age of 2789 ± 110Ma (Che and Sun, 1996). The Paleozoic passive margin sequence is not well preserved.

North Qilian arc

The northern Qilian arc (Fig.2) terrane extends for more than 300km and is about 50～100km wide; it consists of rhyolite, dacite, and andesitic flows and volcaniclastic strata. These volcanics have geochemical characteristics of the calc-alkalic series and yield U-Pb ages of 466～495Ma (Xu *et al*., 1997; Zhang *et al*., 1997). Backarc basin (Fig.2) flysch strata overlying a 454～469Ma ophiolitic sequence (Xia *et al*., 1995) were developed to the north of the island arc complex. A thin molasse deposit of Middle to Late Silurian age represents the closure of the backarc basin resulting from the collision of the Qilian arc and the Alxa massif, whereas an overlying thick Devonian nonmarine molasse sequence was developed due to final collision of the Alxa massif with the central Qilian block (Zuo and Liu, 1987) (described in the following).

North Qilian-North Altun subduction complex

The north Qilian subduction (Fig.2) complex is composed largely of ophiolite and ophiolitic melange, and has been divided into southern high-grade and northern low-grade blueschist belts (Zhang and Liou, 1987; Wu *et al*., 1993; Wu and Tian, 1994). The ophiolitic sequence consists of harzburgitic ultramafics, cumulate gabbro, pillow basalt, and radiolarian chert of Late Cambrian to Early Ordovician age (Xiao *et al*., 1978; Zhang and Xu, 1995; Feng and He, 1996); these in turn are overlain by pelagic to semipelagic flysch deposits and limestone. Blueschist and eclogite are widespread; they occur as tectonic blocks in serpentinite matrix and are respectively overprinted by greenschist facies and epidote amphibolite facies assemblages. Radiometric age determinations by U-Pb and Ar-Ar systematics yield consistent ages of 440～462Ma for blueschist-eclogite facies metamorphism and 410～420Ma for the greenschist facies overprint (Wu *et al*., 1993; Xu *et al*., 1994; Zhang *et al*., 1997). The disposition of an early Paleozoic high *P-T* belt and nearly coeval island arc and backarc basin sequences successively northward suggests a northward subduction of the Qilianoceanic lithosphere.

The northern Altun subduction (Fig.2) complex crops out discontinuously along the northeastern edge of the Altun Mountains between Hongliugou and Ruoqiang. Ultramafics, cumulate gabbro, pillow lava, and radiolarian chert occur as blocks in ophiolitic melange. Transitional blueschist-greenschist with sodic amphiboles has been described in the Lapeiquang area of Ruoqiang (BGMQ, 1991). We obtained a ^{39}Ar-^{40}Ar plateau age of 457 ± 0.7Ma for sodic amphibole from metabasalt in the Hongliugou area of Ruoqiang (Fig.3) (also see Sobel and Arnaud, 1999). This preliminary age for blueschist facies metamorphism and the nature of ophiolitic assemblages suggest that the northern Altun complex can be correlated with

the ophiolitic and high P-T rocks of the northern Qilian complex. However, the distribution, nature, and age of the Altun subduction complex remain to be investigated.

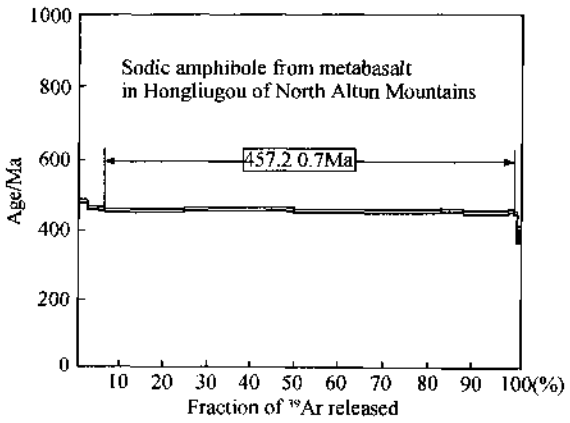

Fig. 3 ^{39}Ar-^{40}Ar plateau spectra for sodic amphibole from metabasalt in Hongliugou area of Ruoqiang, Altun Mountains.

Qilian-Altun block

The central Qilian block(Fig.2)is equivalent to the Early Proterozoic Huangyuan Group (BGMQ, 1991)and comprises mainly Precambrian metamorphic basement consisting of gneiss, low-to high-grade amphibolite, migmatite, marble, and pelitic schist(Wu *et al.*, 1993; Wu and Tian, 1994). The basement rocks are unconformably overlain by upper Paleozoic shallow-marine sedimentary strata. Zircons from migmatitic gneiss give a U-Pb age of 2469 ± 110Ma(Wang and Chen, 1987), whereas K-Ar amphibole and biotite ages and Rb-Sr whole-rock ages cluster around about 1700～1600Ma. These basement rocks are intruded by 1416 ± 50Ma granite and 874 ± 50Ma diorite. This terrane has been considered to be a fragment of a much larger continent that rifted to form the Tarim, Qaidam, and Alxa massifs(Wu *et al.*, 1993).

The central Altun block(Fig.2)is equivalent to the Early Proterozoic Altun Group(Bureau of Geology and Mineral Resources of Xinjiang Uygur Autonomous Region [BGMX], 1993)and consists of low-grade amphibolite facies marble, quartzmica schist, amphibole schist, migmatite, and felsic gneiss. Radiometric dating of these basement rocks has not been done.

North Qaidam-south Altun subduction complex

The north Qaidam Mountains along the northeastern rim of the Qaidam basin have long been considered to be exposed Qaidam basement(BGMQ, 1991). Recent discovery of high-P garnet peridotite(Yang *et al.*, 1994)and eclogite(Yang *et al.*, 1998)within deformed gneiss of the Early Proterozoic Dakandaban Group led to establishment of a new subduction complex unit in the north Qaidam Mountains(Figs.2 and 4). The Early Proterozoic Dakendaban Group occurs throughout the range, and consists of various amphibolite facies lithologies including felsic gneiss, quartz schist, garnet-bearing gneiss, amphibolite, and minor eclogite and garnet peridotite. Details of the high P-T rocks are described in a later section.

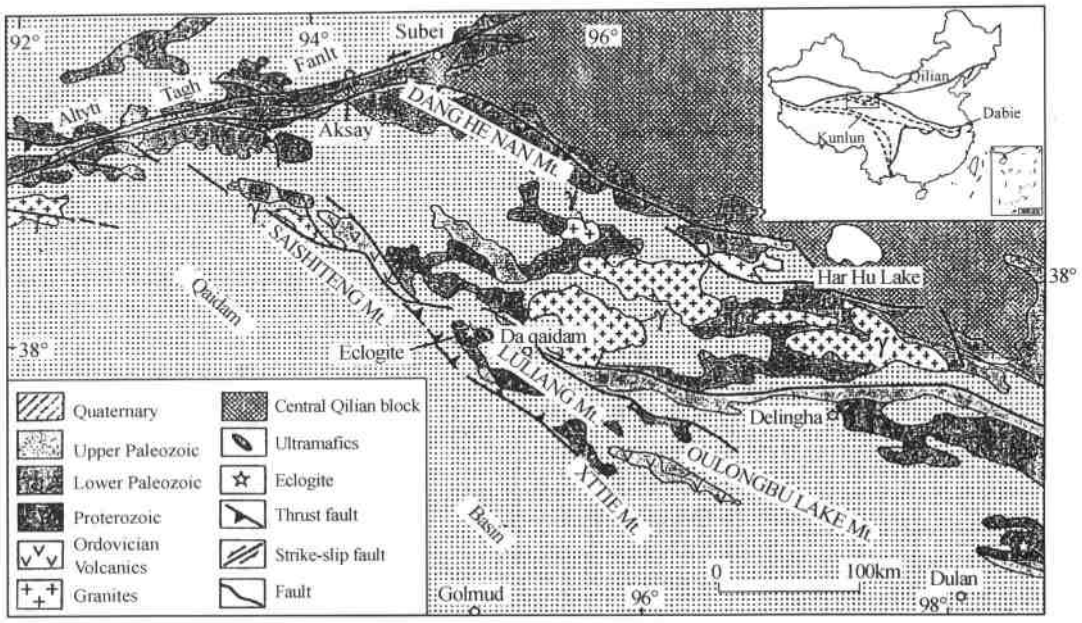

Fig.4 Schematic geologic map of northern Qaidam region, showing distribution of eclogite, ultramafics(including garnet peridotite), and postcollisional granite in northern Qaidam Mountains. γ—Paleozoic and Mesozoic granite.

A similar eclogite-bearing high *P-T* belt about 200km long was identified by Che *et al*, (1995a, 1995b) on the southern margin of the Altun Mountains. Eclogitic cobbles of various sizes were discovered as detritus in Pleistocene conglomerates and as boulders in modern stream channels within the foothills near Qiemo (Hanson *et al*., 1995). Che *et al*. (1995a, 1995b) described eclogite lenses and blocks as garnet-quartz-clinopyroxenite within an Early Proterozoic mylonitized amphibolite, amphibole schist, garnetbearing granitic gneiss, and muscovite-quartz schist sequence. Our reconnaissance study in the vicinity of the approximately northsouth-trending stream channel (Jianggalesayi Creek) yielded the occurrence of eclogitic lenses in strongly deformed granitic gneisses(see Fig.5). Consistent lithologies, *P-T* estimates, and timing of eclogite facies metamorphism described in a later section led us to correlate the eclogite-bearing South Altun complex(Fig.2) with the north Qaidam subduction complex, as shown in Fig.2.

Qaidam block

Similar to the Tarim block, the basement of the Qaidam basin has been considered as part of a rigid, stable, Precambrian craton (BGMQ, 1991). However, extensive geological and geophysical studies indicate that the Qaidam basement is a complex of accreted tectonic fold belts (Wang and Coward, 1990). Basement units consist of a Paleozoic fold belt in the southwest, and a Proterozoic to Paleozoic complex in the northeast, based on the published borehole, geophysical, and field data from the surrounding mountains(BGMQ, 1991).

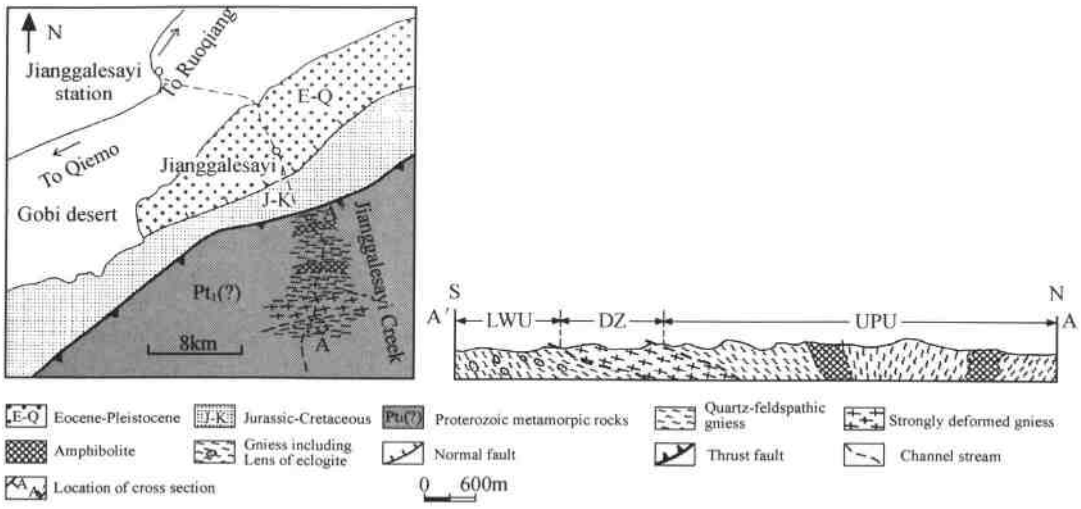

Fig. 5 Geological sketch map and cross section for occurrences of eclogite and amphibolite in strongly deformed felsic gneisses in Altun Mountains.
LWU—lower lithotectonic unit; DZ—decollement zone; UPU—upper lithotectonic unit.

Early Paleozoic high-Pressure Metamorphic rocks

Several high *P-T* rocks have been identified in the Altunnorth Qaidam-Qilian regions. Petrotectonic characteristics, including index assemblages, *P-T* estimates, and metamorphic ages of these high *P-T* rocks, are described in the following. Representative compositions of the analyzed garnet and omphacite from these eclogitic rocks are listed in Table 2 and plotted in Figure 6. The eclogite and garnet peridotite from these regions consitute < 10 vol% of the lithic section but preserve the best very high *P* record. Quartzofeldspathic gneisses are volumetrically predominant rock types and occur as country rocks for many very high-*P* eclogites and garnet peridotites. They contain abundant quartz, albitic plagioclase, phengitic mica, and K-feldspar together with biotite, hornblende, clinozoisite, minor garnet, and other accessory phases such as zircon, rutile, topaz, and tourmaline. Such mineral assemblages are stable over a broad *P-T* range, and appear to have been thoroughly reequilibriated under retrograde conditions. Hence, gneissic rocks lack a clear record of the peak very high-*P* event: this lack led to an early hypothesis that eclogites and country rocks were metamorphosed separately, under different *P-T* regimes, and were subsequently juxtaposed by faulting. According to this hypothesis, the extent of very high *P* metamorphism was no larger than eclogite boudins and lenses now exposed at the surface, which usually measure no more than a few meters in length and thickness.

However, many new observations from the study of country rocks in very high *P* terranes worldwide indicate that country rocks and eclogites are not all fault bounded, and that many contacts retained structural coherence throughout subduction, metamorphism, and exhumation.

Table 2 Representative Compositions of Garnet and Omphacite From the Altun, Beishan, and da Qaidam Eclogites

Rocks	Altun eclogite						Beishan eclogite*			Da Qaidam eclogite					
Minerals	Grt	Grt	Grt	Grt	Omp	Omp	Grt	Grt	Omp	Grt-R	Grt-M	Grt-C	Omp	Omp	Omp
SiO_2	39.32	40.65	39.29	40.65	54.36	55.85	39.57	39.47	56.02	39.32	37.52	38.71	55.72	54.61	54.79
TiO_2	0.03	0.00	0.08	0.04	0.12	0.17	0.00	0.26	0.26	0.01	0.13	0.08	0.08	0.07	0.04
Al_2O_3	21.78	21.92	22.63	22.74	8.67	8.81	21.38	20.83	7.57	22.83	22.36	21.46	10.48	9.38	8.43
Cr_2O_3	0.04	0.06	0.04	0.03	0.00	0.05	0.00	0.00	0.00	0.01	0.07	0.00	0.00	0.00	0.01
FeO	20.74	20.13	21.63	19.30	6.04	4.89	24.58	23.64	6.69	22.09	21.39	23.03	2.65	3.03	3.71
MnO	0.38	0.35	0.43	0.37	0.02	0.00	0.50	0.55	0.10	0.42	0.40	0.54	0.00	0.04	0.02
MgO	7.24	6.88	7.81	8.10	9.20	9.40	5.55	4.84	9.35	7.72	6.01	4.35	10.16	10.45	10.00
CaO	10.46	9.81	9.36	9.79	15.80	15.39	7.67	9.44	14.88	8.46	11.28	10.80	15.37	16.09	16.29
Na_2O	0.00	0.02	0.00	0.05	5.26	5.12	0.02	0.00	4.65	0.03	0.03	0.04	6.25	5.74	5.18
K_2O	0.00	0.00	0.00	0.00	0.00	0.00	0.10	0.02	0.00	0.00	0.00	0.00	0.00	0.00	0.00
Total	99.98	99.76	100.98	101.04	99.47	99.69	100.41	99.61	100.36	100.88	99.12	99.01	100.71	99.41	98.47
Si	3.01	3.11	2.97	3.05	1.97	2.01	3.04	3.06	2.01	2.98	2.91	3.04	0.95	1.95	1.99
Ti	0.00	0.00	0.01	0.00	0.00	0.01	0.00	0.02	0.01	0.00	0.01	0.01	0.00	0.00	0.00
Al	1.96	1.98	2.01	2.01	0.37	0.37	1.94	1.90	0.32	2.04	2.04	1.98	0.43	0.39	0.36
Cr	0.00	0.00	0.00	0.00	0.00	0.00	0.00	0.00	0.00	0.00	0.00	0.00	0.00	0.00	0.00
Fe	1.33	1.29	1.24	1.29	0.18	0.15	1.58	1.54	0.20	1.40	1.39	1.52	0.08	0.09	1.01
Mn	0.03	0.02	0.03	0.02	0.00	0.00	0.03	0.04	0.00	0.03	0.03	0.04	0.00	0.00	0.00
Mg	0.83	0.79	0.88	0.91	0.50	0.51	0.64	0.56	0.51	0.87	0.69	0.51	0.53	0.56	0.54
Ca	0.86	0.81	0.76	0.79	0.61	0.60	0.63	0.79	0.57	0.69	0.94	0.91	0.58	0.61	0.63
Na	0.00	0.00	0.00	0.01	0.37	0.36	0.01	0.00	0.32	0.00	0.01	0.01	0.43	0.40	0.36
K	0.00	0.00	0.00	0.00	0.00	0.00	0.00	0.00	0.00	0.00	0.00	0.00	0.00	0.00	0.00

Note: C—core; M—middle; R—rim; Grt—garnet; Omp—omphacite.

* Data from Mei *et al*., 1998.

Mineralogical indicators of very high P metamorphism have now been found in a number of country rocks, including gneiss, quartzite, and marble. For example, tiny coesite inclusions have been reported from other collisional belts in zircons from felsic gneisses, in dolomite and garnet from calc-silicate rocks and dolomite-bearing eclogite, and in garnet and jadeite from jadeite-bearing quartzite. Hence, the in-situ model has been accepted(for details, see Liou *et al*., 1996; Chopin and Schertl, 1999; Carswell et al., 1999). Several newly discovered very high P terranes in northwestern China described in this chapter require detailed study of the country rocks in order to address this issue.

Qilian Pacific-type eclogite and blueschist

Reported occurrences of prehnite + pumpellyite-and lawsonite-bearing blueschist and jadeite-bearing blueschist + eclogite record the likely existence of parallel subduction zone complexes in the north Qilian, i.e., lower grade blueschist on the north, and higher grade blueschist + glaucophane-bearing eclogite on the south(Wu *et al*., 1993; Wu and Tian, 1994; Tian and Wu, 1994). These high P-T rocks have been extensively investigated since the first description of sodic amphibole by Xiao *et al*. (1974). The northern low-grade blueschist belt

occurs in an Early to Middle Ordovician ophiolite complex, whereas the southern eclogite-bearing high-grade blueschist belt occurs in a Middle Cambrian ophiolitic complex. Pacific-type eclogites of the southern high P-T belt occur as tectonic blocks and have distinctly different compositions of garnet(Alm_{53-77} Gro_{11-37} Pyr_{4-13} Spe_{2-3}) and omphacite(Jd_{27-41}) compared to those from Alpine-type eclogites described here (Fig. 6). The P-T estimates for the northern low-grade blueschist are 150 ~ 250℃ and 4 ~ 7 kbar, whereas those for the high-grade blueschist are $T > 380$℃ and $P = 6 \sim 7$kbar; both P-T estimates are similar to those for classic Franciscan Pacific-type blueschists (Ernst, 1971). Both Qilian high P-T belts are associated with graywacke, ophiolitic rocks, and deep-sea chert with radiolarian fossils of Early Ordovician age (Xiao *et al.*, 1978); the closure of intervening oceanic-crust-capped basins prior to aregenerating collisional events seems plausible. Preliminary radiometric data suggest that the more northerly suture zone may have closed during the Silurian, whereas the more southerly belt was the site of lithospheric underflow and concomitant high-P recrystallization and arc volcanism in Cambrian-Ordovician time (ca. 443 ~ 462Ma) (Wu *et al.*, 1993; Wu and Tian, 1994; Zhang *et al.*, 1997).

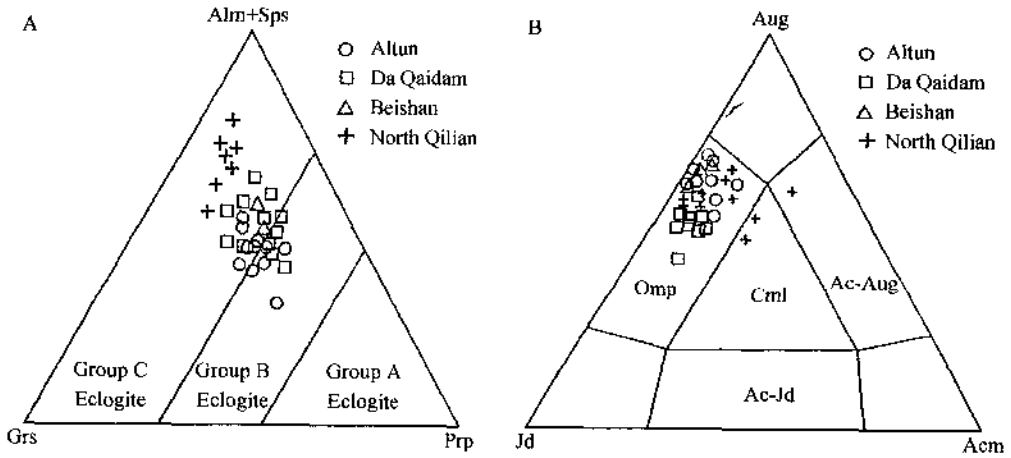

Fig. 6 Compositional plots for (A) garnet, and (B) clinopyroxenes in eclogites from Altun, Da Qaidam, Beishan, and north Qilian areas. Analytical error is within size of symbol.

North Qaidam eclogite

Mode of occurrence. More than 20 eclogite blocks have been described in the Dakendaban Group from an area ~40km northwest of the town of Da Qaidam (Yang *et al.*, 1998; Fig. 4). The eclogite occurs as pods, to 40 ~ 50m long and 20 ~ 30m wide, but most less than 20m × 10m (Fig. 7A), in garnet-bearing felsic gneiss consisting mainly of plagioclase and quartz, with minor muscovite (5% ~ 10% by volume) and garnet (1% ~ 2%). Eclogite pods are boudinaged, and are parallel to the regional foliation. Some are massive *et al.* are extensively retrograded to garnet-amphibolite, which also occurs as blocks or layers concordant with the foliation of country-rock gneiss. Eclogite is best exposed in the Luliang Mountains near Da Qaidam (Fig. 4).

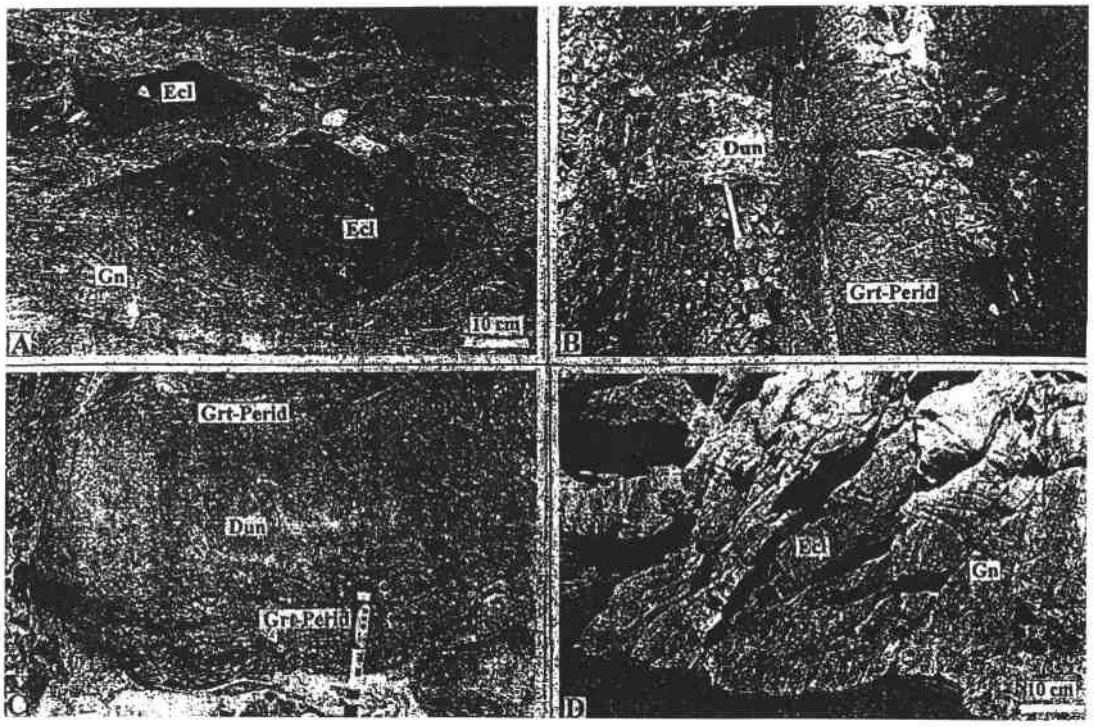

Fig.7 Field views showing occurrence of eclogite and garnet peridotite in Altun and north Qaidam Mountains. A: Eclogite(Ecl)lenses within felsic gneiss(Gn)in north Qaidam Mountains. B, C: Garnet peridotite(Grt-Perid)and dunite(Dun)occurring as blocks in gneiss of the Dakendaban Group in north Qaidam Mountains. D: Eclogite lens within felsic gneiss in Altun Mountains.

Mineral parageneses and pressure-temperature estimates. Eclogites with various degrees of retrogression are medium to fine grained, and consist mainly of garnet and omphacite(each 40～50 vol%), with minor amphibole, phengite, quartz, titanite, and rutile(Fig.8, A-C). Garnets are euhedral, even grained, and mostly 1～2mm in size; some contain minor inclusions of quartz, omphacite, phengite, and rutile, and are replaced by symplectic amphibole + plagioclase (Fig.8C). Analyzed garnets ($Alm_{44-62}Gr_{15-33}Py_{12-30}$) are plotted within the compositional fields of group C and B garnets of Coleman *et al*. (1965)(Fig.6A); they have compositions similar to those of eclogitc garnets in the gneisses from the Altun Mountains described here, but differ considerably from group C eclogitic garnets in the Qilian Mountains(Wu *et al*., 1993). Microprobe analyses of omphacite yield 37%～46% jadeite (Jd)and 50%～57% augite(Aug), and plot within the omphacite compositional region(Fig.6B).

Fine-grained phengite(<5 vol%)occurs as oriented laths of 0.2～1mm size in the matrix (Fig.8C)or as fine-grained inclusions in garnet, and is in textural equilibrium with omphacite and garnet. Some late-formed tabular muscovite flakes are coarse grained(to 2～5mm size)and randomly oriented in eclogite. Analyzed phengite varies in Si content from 6.6 to 6.9, Mg from 0.6 to 0.8, and Fe from 0.21 to 0.25 atoms/formula unit based on a stoichiometry of 22

oxygen atoms, belonging to a typical high-pressure phase(Liu *et al*., 1997).

As a result of varying degrees of retrograde metamorphism, hornblende and plagioclase occur as various grain sizes of symplectite around omphacite grain margins(Fig.8C). Fine-to medium-grained euhedral amphiboles are in textural equilibrium with omphacite and garnet, and were likely formed during eclogite-stage recrystallization. However, both coarse grained amphiboles with fine-grained garnet and omphacite inclusions, and amphiboles along garnet fractures and symplectic amphiboles are retrograde. Eclogitic amphiboles contain a considerable amount of the glaucophane component, whereas retrograde amphiboles are either pargasite or hornblende.

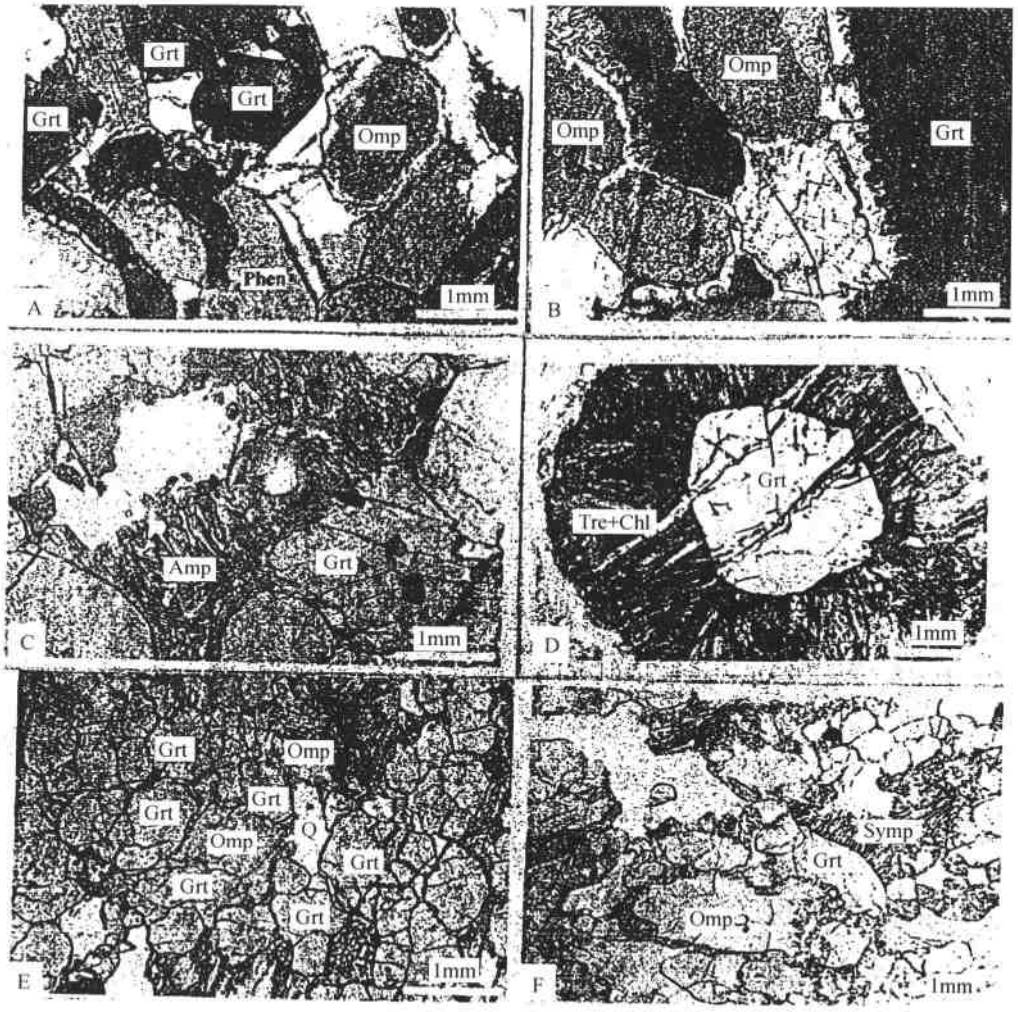

Fig.8 Photomicrographs of eclogite and garnet peridotite in Altun and north Qaidam Mountains.

A, B: Eclogite from north Qaidam Mountains showing granoblastic garnet(Grt) and omphacite(Omp) with phengite(Phen) (cross polarizers). C: Eclogite from north Qaidam Mountains showing amphibole(Amp) riming garnet (plain polarized light). D: Tremolite + chlorite(Tre + Chl) kelyphite rim around garnet of garnet peridotite from north Qaidam Mountains (plain polarized light). E: Eclogite from Altun Mountains showing granoblastic garnet and omphacite with quartz(Q) (plain polarized light); F: Eclogite from Altun Mountains showing fine-grained symplectite(Symp) of clinopyroxene(+ amphibole) and plagioclase after omphacite(plain polarized light).

On the basis of mineral chemistries and phase assemblages, peak P-T conditions of these rocks are estimated to be about 720 ± 120℃ and >22kbar(Yang *et al*., 1998)(Fig.9). Using the phengite-garnet-omphacite geobarometer described by Carswell *et al*. (1997), some of these eclogitic rocks have P estimates to 33kbar. On the basis of these preliminary data, Yang *et al*. (1998, 2000)concluded that these eclogites and garnet peridotites in the north Qaidam terrane are similar to ultrahigh P rocks in the Dabie-Sulu terrane in terms of occurrence, rock type, country-rock gneiss, and P-T conditions. The north Qaidam Mountains may be a coherent, very high P metamorphic terrane, constituting one of the major tectonic boundaries of the north Tibetan Plateau. These very high P(>22kbar)rocks are the first ever recognized in this region.

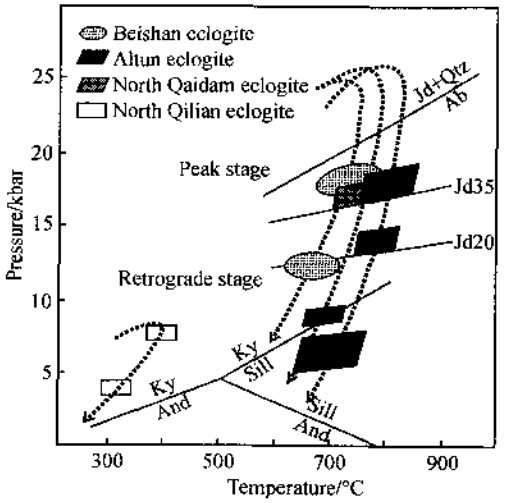

Fig.9 Pressure-temperature(P-T) diagram showing P-T estimates for peak and retrograde metamorphism of eclogites from Da Qaidam, Altun, Beishan, and north Qilian. Size of boxes and circles plotted in this figure correspond to uncertainty of P-T estimates.

Age of metamorphism. U-Pb concordia plot of zircons from an eclogite sample yield metamorphic ages of 494.6 ± 6.5Ma, as shown in Figure 10A. Phengite separates from eclogites gave an $^{40}Ar/^{39}Ar$ platcau age of 467 ± 1Ma and an isochron age of 466 ± 5Ma(Fig.11); these data represent the cooling age of the eclogite during exhumation. In addition, muscovite from the country-rock gneiss yields a disturbed, saddleshaped age spectrum, indicating the presence of excess argon. No meaningful plateau can be defined (Fig.11). The central portion of six contiguous steps, corresponding to more than 90% of the total ^{39}Ar released, define a linear array on the isochron diagram($^{40}Ar/^{36}Ar$ vs. $^{39}Ar/^{36}Ar$). Although the linear relationship is not apparent, the data imply an isochron age of 477.7 ± 17.7 Ma with a trapped $^{40}Ar/^{36}Ar$ ratio of 1012 ± 425 (Fig.11), which is significantly higher than the atmospheric value of 295.5, suggesting the existence of excess argon in the mineral. Nevertheless, the isochron age of the muscovite(477.7 ± 17.7 Ma)is in good agreement with that of phengite in the eclogite sample

within the uncertainty. The consistent age data for both eclogites and their country rocks suggest that basaltic protoliths together with supracrustal rocks of the continental lithosphere were subducted and recrystallized ca. 495Ma and subsequently exhumed to mid-crustal level by ca. 466Ma.

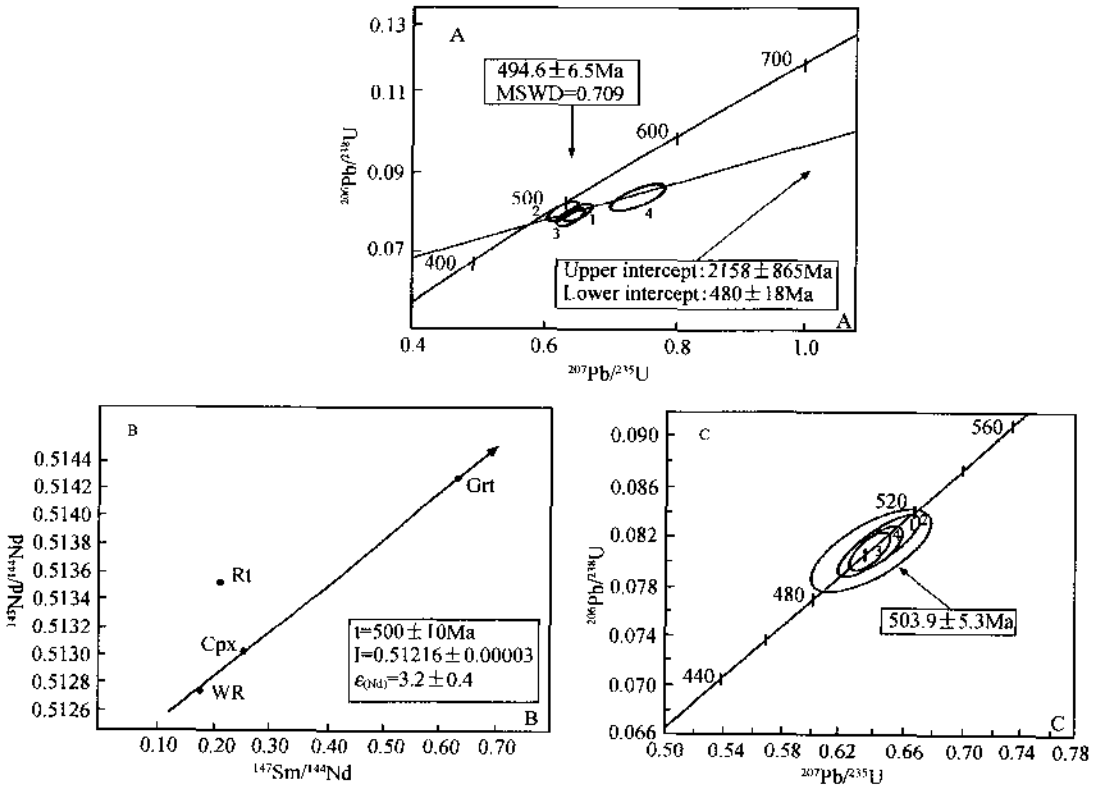

Fig. 10 U-Pb concordia diagram of zircons and whole-rock-mineral Sm-Nd isochron diagram for eclogites from Qaidam and Altun Mountains. A: Eclogite sample from Da Qaidam of north Qaidam Mountains. B, C: Eclogite samples from Altun Mountains. MSWD—mean square of weighted deviates.

North Qaidam garnet peridotite and associated ultramafic rocks

Various ultramafic rocks, including garnet-bearing and garnet-free peridotite, pyroxenite, and dunite occur as lenses and blocks ranging from a few meters to more than 100 meters long in gneisses of the Dakendaban Group (Yang *et al.*, 1994, 1998) (Fig. 7, B and C). These ultramafic rocks are extensively serpentinized, particularly along fractures or near contacts with country rocks. Some outcrops display compositional bands parallel to the regional foliation. Thus far, eclogitic rocks have not been found within these ultramafic rocks.

Garnet-free peridotite and dunite are dominant, and consist mainly of olivine (80 ~ 95 vol%) with subordinate orthopyroxene (5% ~ 15%), clinopyroxene (< 5%), chromite (< 1%), and minor sulfide. Garnet peridotite is characterized by porphyroblastic texture; porphyroblastic (2 ~ 3 cm) garnets (5 ~ 10 vol%; $Pyr_{73-68}Alm_{20-15}Gro_{8-6}Uva_{2-5}Sps_{1-0.5}$) are set in a fine-

grained (<0.2 cm) matrix of olivine(Fo_{89-90}), orthopyroxene(En_{85-91}; 1.37wt% Al_2O_3), and clinopyroxene. Some garnets contain inclusions of chromite and have a wide kelyphitic rim (Fig.8F); many have been entirely replaced by chlorite and amphibole.

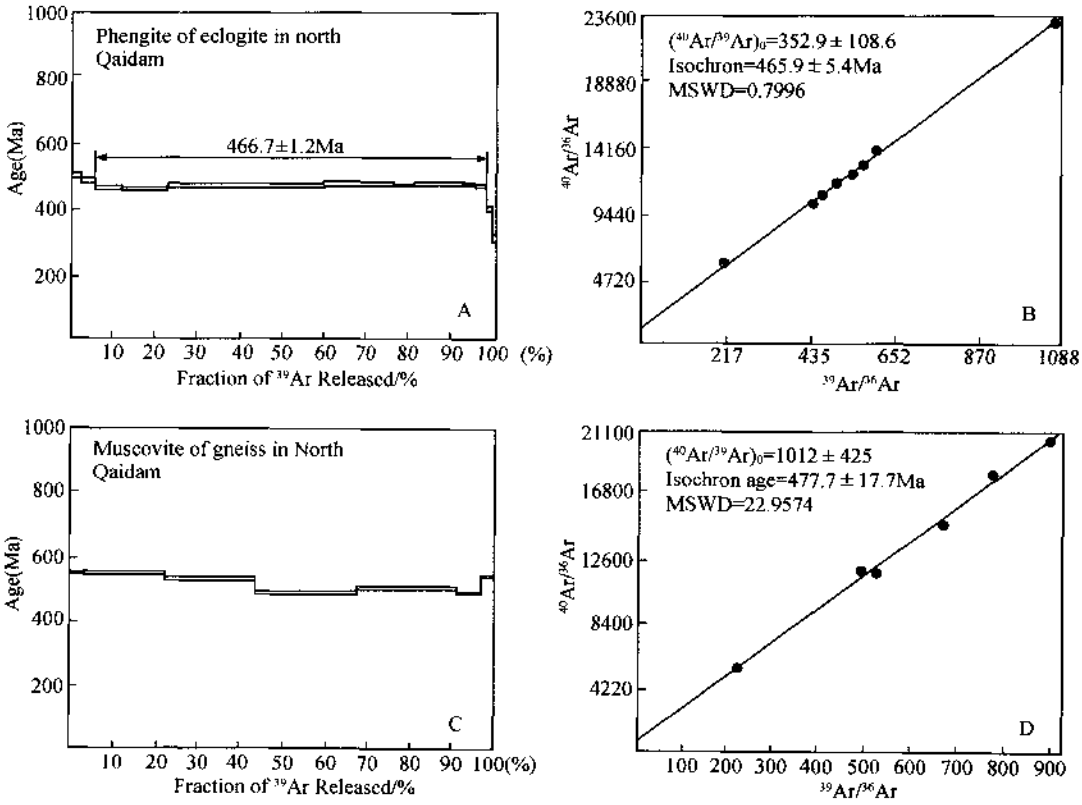

Fig. 11 Ar-Ar age spectra and isochron of white micas from eclogite and granitic gneiss from north Qaidam Mountains. MSWD—mean square of weighted deviates.

Garnet-pyroxenite is significantly retrograded and contains more clinopyroxene than orthopyroxene; exsolution lamellae of orthopyroxene from clinopyroxene are common. Garnets have thick kelyphitic rims; most clinopyroxenes are replaced by amphiboles. In some samples, retrograded amphibole (to 50 vol%) and phlogopite (to 10 vol%) are dominant.

Equilibrium *P-T* conditions for recrystallization of the garnet-peridotite were calculated, using the garnet-orthopyroxene-olivine geobarometry (Stroh, 1976) and the garnet-olivine thermometry (Neill and Wood, 1979), as 837℃ and to 25kbar (Yang *et al.*, 2000). This estimate is consistent with other estimates of 720～850℃ and 25kbar by Yang *et al.* (1994) for garnet peridotite from this area. A K-Ar age of 490Ma was obtained for phlogopite from garnet peridotite. Because phlogopite occurs as a retrograde phase, Yang *et al.* (1994) concluded that the peak metamorphic age of garnet peridotite should be >490Ma. This suggestion is consistent with the age of 495Ma for eclogites from this high *P-T* belt.

Altun eclogitic and gneissic rocks

Mode of occurrence. Eclogite occurs as lenticular blocks or layers, tens of centimeters to a few meters long, and a few centimeters to a few meters wide(Fig.7D); they are concordant with the structural trends of the enclosing country-rock gneisses, which include mainly granitic gneiss and schist, and minor marble, calc-silicates, and amphibolite(Pig.5). Granitic gneisses are foliated and mylonitized, and contain quartz, K-feldspar, plagioclase, biotite, green amphibole, opaque minerals, and chlorite. In the mylonitic rocks, fractured and deformed K-feldspar porphyroblasts(3～10mm) are surrounded by a matrix of quartz, plagioclase, and biotite with well-developed pressure shadows. Both green amphibole and biotite are partially replaced by chlorite. Stretched quartz, biotite, and chlorite define the regional foliation. Some gneisses contain kyanite, indicating high-pressure recrystallization. Margins of eclogite lenses are strongly retrograded to garnet-amphibolite or amphibole schist. Less-deformed amphibolite blocks(2～5m long) also occur; these amphibolite blocks and layers appear to be retrograde products of eclogite.

Mineral parageneses and pressure-temperature estimates. Altun eclogites are partially to strongly retrograded, and contain medium-to coarse-grained omphacite, garnet, phengite, and quartz and fine-grained rutile(Fig.8, E and F). Omphacites ($Jd_{34-45}Aug_{56-63}Acm_{0.1-3.4}$) (Fig.6)are fractured, coarse grained (1.1～2.6mm), and are surrounded by symplectite rims of clinopyroxene with relatively low Jd components(Jd_{21-25}) + plagioclase(An_{10-20})(Fig. 8B). Garnets(0.45～0.88mm) contain inclusions of quartz, omphacite, and rutile in the core. Most garnets are fractured and have rather uniform compositions ($Al_{43-49}Py_{24-28}Gr_{27-33}Sps_1$) (Fig.6). However, garnets of strongly retrograded eclogite and amphibolite have lower almandine and pyrope and higher grossular components than those from less retrograded eclogite. Rutile is rimmed by ilmenite.

Strongly retrograded eclogite is characterized by the total absence of omphacite and a well-preserved granoblastic texture. Widespread retrogression includes the replacement of omphacite by symplectitic intergrowth of clinopyroxene(Jd_{10}) + plagioclase(An_{10}) + minor pargasitic amphibole, rutile by ilmenite, garnet by amphibole-plagioclase kelyphite, and by the growth of matrix biotite and Ca-amphibole. With advanced retrogression, garnet-amphibolite occurs and contains porphyroblastic garnet(～1mm) replaced by green amphibole, quartz, plagioclase, and chlorite. Matrix green amphiboles are elongate and wrap around relict garnets; this and quartz and ilmenite define the rock foliation.

Three distinct stages of metamorphic recrystallization were identified in the eclogites. Mineral assemblages and Fe-Mg distributions between garnet and omphacite yield T =730～810℃ and P>15kbar for eclogite facies metamorphism(J. Zhang, *et al*., 1999). P-T estimates of 660～830℃ and 14～18.5kbar were obtained by Ches *et al*. (1995a, 1995 b). Decompression is indicated by the breakdown of omphacite to symplectites of less sodic clinopyroxene(Jd_{21-25}) and plagioclase(An_{11-16}), followed by symplectites consisting of worm-like plagioclase + green amphibole intergrowths. The second-stage assemblage is represented by

pargasitic amphibole, plagioclase (An_{21-38}), quartz, ilmenite, and clinopyroxene ($Jd < 5$). Such amphibolite facies parageneses are most common in country-rock gneiss and garnet amphibolite. The amphibole-plagioclase geothermometer of Blundy and Holland (1990) was employed for the coarseto medium-grained amphibole and fine-to medium-grained plagioclase, and yields $T = 700 \pm 75$℃ at $P = 5$kbar; the pressure estimate was obtained by Al-in-hornblende(Schmidt, 1992)for felsic gneiss that contains two feldspars + quartz + amphibole + ilmenite. A late-stage greenschist facies overprint is indicated by the occurrence of biotite, chlorite, albite, and titanite in both eclogite and country rocks.

Age of metamorphism. Eclogite of the Altun Mountains has been recently dated by two independent methods as shown in Figure 10(J. Zhsng *et al*., 1999). A Sm-Nd mineral isochron for eclogitic garnet, omphacite, and the whole rock yields an age of 500 ± 10Ma, whereas an U-Pb isochron for zircon separates from eclogite gives an overlapping age of 504 ± 5Ma. A similar Sm-Nd mineralisochron age of 519Ma was obtained for mylonitized amphibolite from this belt (Lin *et al*., 1996). Muscovite and biotite from Altun gneisses and schists yield $^{40}Ar/^{39}Ar$ ages of 430 ± 20Ma, whereas $^{40}Ar/^{39}Ar$ age of 575 ± 20Ma for phengite from eclogite-associated metapelite was interpreted to overestimate the age of high-P metamorphism(Sobel and Arnaud, 1999). Thus, the south Altun high-P terrane involves eclogite-bearing granitic gneiss with consistent 500～504Ma U-Pb and Sm-Nd ages, and represents an early Paleozoic subduction complex similar to that in the northern Qaidam basin.

Beishan Alpine-type eclogite

Numerous eclogitic blocks and lenses enclosed within granitic gneisses were discovered in a southern belt of the Beishan orogen(see Fig.1 for location)(Mei *et al*., 1998). The largest extends for 500m and is 100m wide, larger than most eclogitic bodies described herein. These eclogitic lenses are concordant with foliation of country rocks, and are in a belt consisting mainly of granitic gneisses together with quartz schist, marble, amphibolite, and garnet peridotite. Details of the garnet peridotite have not been described. The eclogite contains equal amount of garnet($Alm_{50-55}Grs_{22-29}Pyr_{19-22}Sps_{1-2}$)and omphacite($Jd_{31-35}$), and minor rutile and retrograded phases including amphibole, ilmenite, and quartz. Garnet is well preserved and has only thin taramitic amphibole rims; some garnet grains contain inclusions of quartz aggregates and exhibit radial fractures around the inclusions. Mei *et al*. (1998)suggested that these textures were related to retrograded coesite developed during exhumation of the eclogitic rocks, and coesite was a stable phase of peak eclogite facies metamorphism. Omphacite shows various degrees of symplectite replacement of clinopyroxene (Jd_{17}) + amphibole + plagioclase (An_{13}); rutille is rimmed by ilmenite. Three distinct stages of metamorphic recrystallization were identified: peak eclogite, retrograded amphibolite, and later greenschist facies overprints. The P-T estimates yield peak stage recrystallization at 700～800℃ and 16～18 kbar, and amphibolite stage at 650℃ and 10～12 kbar. A U-Pb concordia plot of several zircon separates from granitic gneiss yields protolith ages of 1756～2056Ma and metamorphic ages of 467 + 50Ma. Zircon separates from eclogite provides a U-Pb upper intercept at 861 ± 50Ma and

a lower intercept at 440 ± 50Ma(H. Mei, 1999, personal commun.). Mineral parageneses, *P-T* estimates, and the possible occurrence of coesite together with petrotectonic assemblages of granitic gneiss, quartz schist, and marble as country rocks for eclogites and garnet peridotite blocks suggest A-type subduction of Early Proterozoic supracrustal rocks and an early Paleozoic continental collision.

Tectonic Correlation and Discussion

Significance of Pacific-and Alpine-type subduction complexes

High-pressure eclogites, represented by the Franciscan Complex of western California, are products of Pacific-type subduction and are associated with blueschist and epidote amphibolite of oceanic affinity (Ernst *et al.*, 1994; Ernst and Liou, 1995). Ultrahigh-*P* coesite-and/or microdiamond-bearing eclogites in the Dabie-Sulu terrane of east-central China are products of Alpine-type intracontinental collision, and are associated with gneiss, paraschist, and marble of continental affinity. Petrotectonic studies of eclogites and associated rocks establish the pressure-temperature-time(*P-T-t*) path, which can be used to interpret the crustal evolution, including subduction, collision, and exhumation. Moreover, these high-*P* and ultrahigh-*P* eclogites and associated garnet peridotites rarely crop out in subduction complexes, which generally occur in linear zones. These high-and ultrahigh-*P* metamorphic belts provide useful constraints in regional tectonic studies.

The north Qilian subduction complex, and its lawsonitebearing blueschist and low-T eclogite associated with ophiolitic melange and graywacke, is similar to many Pacific-type subduction orogens around the circum-Pacific(see Maruyama *et al.*, 1996). This complex has been intensively investigated (e.g., Wu *et al.*, 1993; Wu and Tian, 1994; Tian and Wu, 1994) and is characterized by the occurrence of coeval calc-alkalic volcanics due to the inferred northward early Paleozoic subduction of the Qilian oceanic lithosphere.

Several newly documented eclogite terranes in the north Qaidam, the Altun Mountains, and the Beishan are within major continental collision belts in northwest China, extending several hundred kilometers or more, and are confined to Alpinetype orogens. They share common lithologic and geochronologic characteristics. ① These terranes have been considered to be Precambrian basement because they occur mainly within amphibolite facies gneiss, schist, migmatite, marble, amphibolite, and serpentinized ultramafics at the margins of continental blocks(Bureau of Geology and Mineral Resources of Gansu Province [BGMG], 1989; Bureau of Geology and Mineral Resources of Qinghai Province [BGMQ], 1991). ②Very high *P* records occur in minor but significant rocks—eclogite and garnet peridotite—included as pods and slabs within quartzofeldspathic gneissic units. The occurrence of inclusions of coesite pseudomorphs has been suggested, but they have not been positively identified. However, independent estimates using various thermobarometers indicate eclogite facies recrystallization took place at $P > 20$ kbar, and some estimates are > 30 kbar(J. Yang, 1999, personal comun.). ③Eclogites

and peridotites have been subjected to various extents of retrograde metamorphism, first under amphibolite facies, and later under greenschist facies conditions. ④ Protolith lithologies have continental and subcontinental geochemical and petrological characteristics, including granitic gneiss, aluminous pelite, minor quartzite, marble, and mafic-ultramafics, and have Proterozoic isotopic ages. ⑤ Coeval calc-alkalic volcanic and plutonic rocks do not occur, whereas postcollisional or late-stage granitic plutons are common in some occurrences. These features are similar to many ultrahigh-P terranes, including the Dabie-Sulu belt (Liou *et al*., 1996; Ernst and Liou, 1999; Liou, 1999). Trace ultrahigh-P minerals would be best preserved in strong containers such as zircon or garnet in eclogite and their enclosing gneiss, and will be the subject of future research (Liou *et al*., 1998). Such coesite-bearing (ultrahigh P) or coesite-free (very high P) Alpine-type terranes. have resulted from deep subduction of continental lithosphere prior to continent collision.

U-Pb data for zircon separates and Sm-Nd isochrons of minerals from very high P eclogitic rocks (Fig. 10) indicate that the peak eclogite facies metamorphism occurred ca. 495～504Ma in the south Altun and north Qaidam eclogites. The $^{40}Ar/^{39}Ar$ plateau ages of amphibole and phengitic mica from these eclogitic rocks are 460～470Ma (Fig. 11), which probably represents the timing of exhumation and overprinting of retrograde recrystallization. However, the Qilian high P-T blueschists and eclogites have a peak metamorphic age of 443 ～ 462Ma and a retrograde age of 410～420Ma (Wu *et al*., 1993; Wu and Tian, 1994; Zhang *et al*., 1997). These data suggest that the subduction and collision of the Qaidam block with the central Qilian block occurred prior to the convergence of the Qilian ocean beneath the margins of the Alxa massif.

Nature of the Altyn Tagh fault

The Altyn Tagh fault truncates and bounds many orogenic belts, including the Beishan, Altun, Kunlun, and Qilian Mountains (Fig. 2). This fault has been investigated extensively; understanding its evolution is essential for an accurate reconstruction of northwestern China (see Yue and Liou, 1999, for a summary). The proposed total left-lateral displacements by realigning critical petrotectonic assemblages on both sides of the fault range from 200 to 1200km (Peltzer and Tapponnier, 1988; Ge *et al*., 1991; Yue and Liou, 1999).

The Altyn Tagh fault was identified as a key element of the escape tectonics model for the Eurasia-India continentcontinent collision (Tapponnier and Molnar, 1977; Peltzer and Tapponnier, 1988). Zhou and Graham (1996) proposed a wedge extrusion model and suggested that: ①the Altun Mountains at the tip and southern edge of the wedge are part of the west Kunlun Mountains, and ② the Beishan and Qilian Mountains belong to the same orogenic belt. Yue and Liou (1999) proposed a two-stage evolution for the Altyn Tagh fault, which continues northeast to the inactive Alxa-east Mongolia fault: according to them, this continuous fault slipped about 400km, and separated the Beishan orogen from the Inner Mongolia orogen, beginning in the Oligocene and continuing until the middle Miocene. The Alxa-east Mongolia fault then became inactive, and the displacement was compensated for by the shortening of the

Qilian Mountains and the Qaidam basin from the middle Miocene to the present. This model indicates that①the Altun and Qilian Mountains are part of the same belt, and②the Beishan and Inner Mongolia orogens belong to the same late Paleozoic subduction and/or collision complex.

The similarities in the occurrences, associated country rocks, P-T estimates, and age data for the very high P eclogitic rocks in both the Altun and north Qaidam Mountains described herein attest to the plausibility of the correlation proposed by Yue and Liou(1999). Moreover, identification of the north Altun subduction complex, which has an ophiolitic melange and a transitional blueschist-greenschist assemblage of ca. 457Ma, as being equivalent to the north Qilian Pacific-type subduction complex provides another piecing point for the AltynTagh fault. More geochronologic data are required for the high-P lithologies and their host rocks to test this hypothesis.

However, as shown in Figure 2, several tectonic units of the Qilian Mountains have not been identified in the Altun Mountains, including passive margin deposits at the southern margin of the Dunhuang massif, and the early Paleozoic island arc and its associated backarc basin deposit. Moreover, the central Altun terrane is much narrower than its equivalent in the central Qilian terrane. Such differences could be due in part to the different width for identical units along their strike and in part to the significant displacement along the Altyn Tagh fault system. Moreover, despite of the tectonic significance of the Altyn Tagh fault, the magnitude and direction of displacement along this fault are still poorly constrained, partly because there have only been limited field mapping and petrotectonic studies done in the Altun Mountains. The different models for the Altyn Tagh fault result from the lack of definitive geological data.

Occurrence of the Beishan very high pressure belt

According to Yue and Liou(1999), the Beishan orogen could be correlated with the Inner Mongolia orogen to the east of the Altyn Tagh fault; details of such correlation are documented in Yue *et al*. (this volume). The occurrence of the early Paleozoic, eclogite-bearing, A-type subduction complex as a suture between the Beishan terrane and the Dunhung massif leads to the question, what is the equivalent suture to the east, across the Altyn Tagh fault? The eclogite-bearing gneissic terrane is in a southern belt of the Beishan terrane, and on the northern margin of the Dunhuang massif. Its eastern extension may exist in the northern margin of the Alxa massif, but this is unsubstantiated. The Beishan very high P belt contains numerous eclogitic and ultramafic lenses enclosed within granitic gneiss, dolomitic marble, and garnet-bearing quartzite. However, regional geology, the distribution and the contact relation of this very high P belt with the adjacent tectonic units, the, age of eclogitic metamorphism, and the nature of ultramafics are not known. Therefore, speculation regarding its correlation eastward to Inner Mongolia or westward to the Tian Shan is premature.

Tectonic model

The Qilian-Qaidam-Altun region of northwest China is a remote mountainous and high plateau area where geological studies are limited compared to other orogens in central and east

China. We initiated a petrotectonic study of high-*P* metamorphic belts in this area, and our preliminary model for the tectonic evolution of the Qilan-Qaidam region is described in the following.

Fig. 12 illustrates a tectonic evolution model for the northern Qilian Mountains based on our field and geochronological data (Xu *et al.*, 1994, 1997; Zhang *et al.*, 1997) and results from Tian and Wu (1994). Our discussion does not include the Tian Shan eclogite belt because its study is still in an early stage. Major chronological events are summarized in the following.

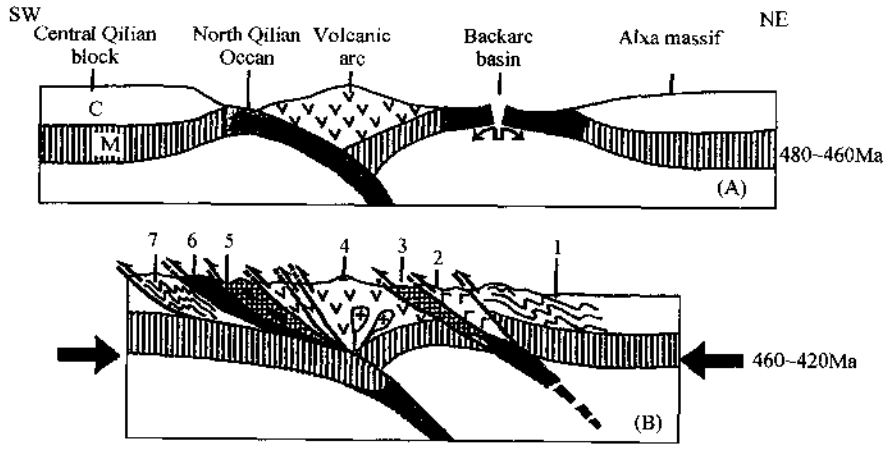

Fig. 12 A, B: Plate tectonic scenario for evolution of north Qilian during early Paleozoic time.
A: Northward subduction of north Qilian ocean resulting in formation of high-pressure (*P*) metamorphic rocks and volcanic arc. This was followed by rifting of backarc basin 460~480Ma. B: Closures of north Qilian ocean and backarc basin resulted in two different continent-arc collision zones. 1—Early Paleozoic fold belt of continental margin of Alxa massif. 2—Backarc volcanic rocks. 3—Northern high-*P* metamorphic zone. 4—North Qilian volcanic arc. 5—South high-*P* metamorphic zone. 6—Ophiolite zone. 7—Early Paleozoic fold belt of central Qilian block C—crust, M—mantle.

1. Three Precambrian continental fragments for the Alxa massif, central Qilian, and Qaidam basin could have rifted from a single continent (e.g., Wu *et al.*, 1993) or might represent independent microcontinents (e.g., Z.M. Zhang *et al.*, 1984). For example, the central Qilian terrane rifted from the Alxa massif in Late Proterozoic time, and created a north Qilian ocean; the oceanic crust subsequently was obducted to form the Zhulongguan late Sinian ophiolitic suite (e.g., Tian and Wu, 1994). Although similar lithologies occur in the basement complex and overlying strata of these massifs, available data, particularly those from the Qaidam basin, do not support such a suggestion.

2. An Alpine-type convergent margin, including possible northward subduction of the Qaidam continental lithosphere beneath the Qilian terrane, may have occurred in Cambrian Ordovician time (ca. 500Ma). Available microstructural analyses of rocks from the Qaidam Mountains exclude southward subduction (Xu *et al.*, 1999). During this period of time, a north Qilian ocean may have widely separated the Qilian terrane to the south and the Alxa massif and

the Sino-Korean craton to the north.

3. The disposition of major lithologic units in the Qilian Mountains suggests two distinct stages of tectonic evolution, as shown in Fig. 12: (a) subduction stage at 500～440Ma, and a collision stage at 440～400Ma. The nearly coeval occurrence of the north Qilian arc complex (466 to ca. 495Ma, Xu *et al.*, 1997; Zhang *et al.*, 1997) to the north and the Pacific-type high *P-T* complex (440～462Ma, Wu *et al.*, 1993; Xu *et al.*, 1994) to the south and kinematic data of Xu *et al.* (1994) suggest northward subduction of the north Qilian oceanic lithosphere ca. 500～440Ma. Calcalkaline volcanic activity extended to the transition region of the Alxa massif. During this period of time, the Qilian ophiolite (454～469Ma, Xia *et al.*, 1995) was emplaced and a backarc basin was formed to the north of the north Qilian arc complex.

The collision stage (440～400Ma) included two parts; the closure of the north Qilian ocean to the south, and that of the backarc basin to the north of the north Qilian arc complex. The former resulted in the collision of the central Qilian block and the north Qilian volcanic arc ca. 440Ma, whereas the latter resulted in the collision between the north Qilian volcanic arc with the Alxa massif after 410Ma. The collision time was determined on the basis of greenschist facies retrograded ages of 410～420Ma for blueschists from the southern high *P-T* belt (Xu *et al.*, 1994; Zhang *et al.*, 1997) and Ar-Ar data (443 ± 3Ma) for phengite from a Qilian eclogite in an ophiolite melange (Wu *et al.*, 1993). A possible southward subduction of the backarc oceanic lithosphere has been suggested to have occurred in the Silurian (409Ma) to form the low-grade lawsonite-bearing blueschist zone (e.g., Tian and Wu, 1994), and flysh strata were deposited in the backarc basin.

A thin Devonian molasse, which contains blueschist pebbles derived from the south, and unconformably overlies the folded early Paleozoic sequence, represents the collision of the north Qilian arc and the Alxa massif after 410Ma. This suggestion is consistent with the deposition of passive-margin strata within the transition region along the southern margin of the Alxa massif, and the younger age of the low-grade blueschist compared with the southern eclogite-bearing epidote-blueschist zone.

4. Amalgamation of the united Qilian-Qaidam terrane with the north Qilian arc and Alxa massif may have occurred in Devonian time, when a widespread, thick, nonmarine molasse was deposited in the Qilian-Qaidam regions.

5. The Altyn Tagh fault-east Mongolia fault system may have begun around Oligocene time as a result of the Cenozoic collision between the Indian and Asian continents. This megafault system displaced all early Paleozoic tectonic units of the Qilian-Qaidam regions from the Altun Mountains northeastward for～400 ± 50km (Yue and Liou, 1999).

The proposed chronological sequence for tectonic evolution for this area is consistent with the petrological and geochronological data of major lithologic units, including both Pacific-and Alpine-type subduction complexes described herein. Further petrotectonic and geochronologic studies of basement, ophiolite, arc volcanics, and subduction-zone complexes in these remote regions are necessary to refine this new tectonic model.

Conclusions

Several Pacific-type and Alpine-type high P-T metamorphic belts of early Paleozoic age occur in the Qilian-north Qaidam-Altun blocks. The Pacific type was documented in the north Qilian block and is regarded as the result of subduction of oceanic crust. The peak high-P metamorphism occurred at 440～462Ma, at $T>380$℃ and $P=6\sim7$ kbat, and the exhumation occurred at 410 ～ 420Ma. The Alpine type occurs in the north Qaidam and south Altun Mountains, and is regarded as the result of continental subduction having a peak metamorphic age of 495 ～ 504Ma, and higher pressure ($P>22$ kbar) and temperature (720 ± 120℃), suggesting deeper subduction than that of the north Qilian blueschist belt.

According to the similarities in many aspects between the blocks on opposite sides of the Altyn Tagh fault, including disposition of lithological units, occurrence of both Pacificand Alpine-type high P-T belts, P-T conditions, and ages of formation and exhumation, it is suggested that 400km of leftlateral displacement has occurred along the Altyn Tagh fault (Xu *et al*., 1999).

Acknowledgments

This paper was prepared by a joint effort of a Stanford Chinese Academic Geologic Science cooperative project supported by National Science Foundation grant EAR～9814468, and the Stanford China Industrial Affiliates Program, and was supported by the National Natural Science Foundation (49732070)and the National Key Project for Basic Research on the Tibetan Plateau(G1998040800). We thank Lin Liang and Mei Hualing, respectively, for information regarding Altun and Beishan eclogites, and Gary Ernst, Edmund Chang, and Yongjun Yue for useful discussions. The manuscript was critically reviewed and materially improved by Gary Ernst, X.C. Xiao, Shige Maruyama, Edward Sobel, Hakon Austrheim, and Marc Hendrix. We thank these individuals and institutions for their support and assistance.

References cited

Blundy, J.D., and Holland, T.J.B., 1990, Calcic amphibole equilibria and a new amphibole-plagioclase geothermometer: Contributions to Mineralogy and Petrology, v.104, p.208～224.

Bureau of Geology and Mineral Resources of Gansu Province(BGMG), 1989, Regional geology of Gansu Province: Beijing, Geological Publishing House, p.1～35(in Chinese with English abstract).

Bureau of Geology and Mineral Resources of Qinghai Province(BGMQ), 1991, Regional geology of Qinghai Province: Beijing, Geological Publishing House, 661 p.(in Chinese with English abstract).

Bureau of Geology and Mineral Resources of Xinjiang Uygur Autonomous Region, 1993, Regional geology of Xinjiang Uygur Autonomous Region: Beijing, Geological Publishing House, 841 p.(in Chinese with English abstract).

Carswell, D.A., O'Brien, PJ., Wilson, R.N., and Zhai, M., 1997, Thermobarometry of phengite-bearing eclogites in the Dabie Mountains of central China: Journal of Metamorphic Geology, v.15, p.239～252.

Carswell, D.A., Cuthbert, S. J., and Krough Ravna, E. J., 1999, Ultrahighpressure metamorphism in the Western Gneiss Region of the Norwwegian Caledonides: International Geology Review, v.41, p.955～966.

Che, Z., and Sun, Y., 1996, The age of the Altun granulite facies complex and the basement of the Tarim basin: Regional Geology of China, v.56, p.51～57(in Chinese with English abstract).

Che, Z., Liu, L., Liu, H., and Luo, J., 1995a, The discovery and occurrence of high-pressure metapelitic rocks from Altun Mountain area, Xinjiang Autonomous Region: Chinese Science Bulletin, v.40, p.1298～1300(in Chinese with English abstract).

Che, Z., Liu, L., Wang, Y., and Luo, J., 1995b, Metamorphic evolution and tectonics: Exhumation geodynamics of ultra-high-pressure and highpressure metamorphic rocks in Altun: Chinese Science Bulletin, v.40, p.131～133(in Chinese with English abstract).

Chen, B.W., Wang, Y.B., and Zuo, G.C., 1995, Terrain subdivision of the Northern Qinghai-Xizang Plateau and tectonic evolution: Acta Geophysica Sinica, v, 38, p.113～128(in Chinese with English abstract).

Chen, W., Li, H.B., Xu, Z.Q., Arnaud, N., Han, D., and Shen, J., 1996, Using the laser microprobe $^{40}Ar/^{39}Ar$ dating technique and $^{40}Ar/^{39}Ar$ stepwise incrimental heating technique to date the ages of Xidatan shear zone: Acta Geoscientia Sinica, special issue, p.228～232.

Chopin, C., and Schertl, H.P., 1999, The UHP unit in the Dora-Maira Massif, western Alps: International Geology Review, v.41, p.765～780.

Coleman, R.G., and Wang, X., 1995, Overview of the geology and tectonics of UHPM: *in* Coleman, R.G., and Wang, X., eds., Ultrahigh pressure metamorphism: Cambridge, Cambridge University Press, p.1～32.

Coleman, R.G., Lee, D.E., Beatty, L.B, and Brannock, W.W., 1965, Eclogitec and eclogites: Their differences and similarities: Geological Society of America Bulletin, v.76, p.483～508.

Ernst, W.G., 1971, Do mineral parageneses reflect unusually high-pressure conditions of Franciscan metamorphism?: American Journai of Science, v.270, p.81～108.

Ernst, W.G., and Liou, J.G., 1995, Contrasting plate tectonic styles of the Qinling-Dabie-Sulu and Franciscan metamorphic belts: Geology, v.23, p.353～356.

Ernst, W.G., and Liou, J.G., 1999, Overview of UHP metamorphism and tectonics in well-studied collisional orogens: International Geology Review, v.41, p.477～493.

Ernst, W.G., Liou, J.G., and Hacker, B.R., 1994, Petrotectonic significance of high-and ultrahigh-pressure metamorphic belts: Inferences for subduction-zone histories: International Geology Review, v.36, p.213～237.

Feng, Y. M., and He, S.P., 1996, Geotectonics and orogeny of the Qilian Mountains, China: Beijing, Geological Publishing House, 135 p.(in Chinese with English abstract).

Ge, X.H., Duan, J., Li, C., Yang, H., and Tian, Y., 1991, A new recognization of the Altun fault zone and geotectonic pattern of Northwest China: International Geological Correlation Programme Project 321; Proceedings of first international symposium on Gondwana dispersion and Asian accretion; geological evolution of eastern Tethys: Beijing, Geological Publishing House, p.125～128.

Hanson, A, Chang, E., Zhou, D., Ritts, B., Sobel, E., Graham, S., Chu, C., Liu, J., Zhang.R., and Liou, J.G., 1995, Discovery of eclogite blocks in the Altun Mountains, SE Tarim basin, NW China [abs.]: Eos (Transactions, American Geophysical Union), v.76, p.S283.

Liou, J.G., 1999, Petrotectonic summary of less-intensively studied UHP regions: International Geology Review, v.41, p.571～586.

Liou, J.G., Wang, X., Coleman, R.G., Zhang, Z.M., and Maruyama, S., 1989, Blueschists in major suture zones of China: Tectonics, v.8, p.609～619.

Liou, J.G., Zhang, R, and Ernst, W.G., 1994, An introduction to ultrahighpressure metamorphism: The Island Arc, v.3, p.1～24.

Liou, J.G., Zhang, R.Y., Wang, X.M., Eide, E.A., Ernst, W.G., and Maruyama, S., 1996, Metamorphism and tectonics of high-P and ultrahigh-*P* belts in the Dabie-Sulu region, eastern central China, *in* Yin, A., and Harrison, M.T., eds., Tectonic development of Asia: Rubey Volume 13: Cambridge, Cambridge University Press, p.300～344.

Liou, J.G., Zhang, R., Ernst, W.G., Rumble, D., and Maruyama, S., 1998, High pressure minerals from deeply subducted metamorphic rocks, *in* Mao, H.K., and Hemley, R.J., eds., Ultrahigh pressure mineralogy: American Mineralogical Society Reviews in Mineralogy, v.37, p.33～96.

Liu, L., Ce, Z.C., Luo, J.H., Wang, Y., and Gao, Z.J., 1996, Identification of the eclogite at the west part of Altyn Tagh Mountains and its geological implications: Chinese Science Bulletin, v.41, p.1485～1488(in Chinese with English abstract).

Liu, L., Che, Z.C., Luo, J.H., Wang, Y., and Gao, Z.J., 1997, Recognition and implication of eclogite in the western Altun Mountains, Xinjiang: Chinese Science Bulletin, v.42, p.931～934(in Chinese with English abstract).

Liu, X.Y., and Wang, Q., 1993, Tectonics of the Longshoushan ancient rift and Hexi Corridor: Chinese Academy of Geological Sciences Bulletin, v.27, p.1～14(in Chinese with English abstract).

Lu, S.N., and Li, H.M., 1991, A precise U-Pb single zircon age determination for volcanics of Dahongyu formation, Changcheng System in Jixian: Chinese Academy of Geological Sciences Bulletin, v.22, p.137～146 (in Chinese with English abstract).

Ma, L., Ding, X., and Fan, B., 1996, Geological map of China: Beijing. Geological Publishing House, scale 1: 12000000.

Maruyama, S., Liou, J.G., and Terabayashi, M., 1996, Blueschists and eclogites of the world and their exhumation: International Geological Review, v.38, p.485～594.

Mei, H.L., Yu, H.F., Li Q., Lu, S.N., Li, H.M., Zuo, Y.C., Zuo, G.C., Ye, D.J., and Liu, J.C., 1998, First discovery of eclogite and Paleo-Proterozoic granitic rock in the Beishan region, Gansu province, China: Chinese Science Bulletin, v.43, p.2105～2111(in Chinese with English abstract).

Neill, H.S.C., and Wood, B.J., 1979, An experimental study of Fe-Mg partitioning between garnet and olivine and its calibration as a geothermometer: Contributions to Mineralogy and Petrology, v.70, p.59～70.

Peltzer, G., and Tapponnier, P.G., 1988, Formation and evolution of strike-slip faults, rifts, and basins during the India-Asia collision. An experimental approach: Journal of Geophysical Research, v.93, p.15085～15117.

Schmidt, M.W., 1992, Amphibole composition in tonalite as a function of pressure: An experimental calibration of the Al-in-hornblende barometer. Contributions to Mineralogy and Petrology, v.110, p.304～310.

Sobel, E.R., and Arnaud, N., 1999, A possible middle Paleozoic suture in the Altyn Tagh NW China: Tectonics, v.18, p.64～74.

Stroh, J. M., 1976, Solubility of alumina in orthopyroxene plus spinel as a geobarometer in complex system: Application to spinel-bearing Alpine type peridotite: Contributions to Mineralogy and Petrology, v.54, p.173～188.

Tapponnier, P.G., and Molnar, P., 1977, Active faulting and tectonics in China: Journal of Geophysical Research, v;82, p.2905～2930.

Tian, B., and Wu, H., 1994, Geochemistry of the two blueschist belts and implications for the early Paleozoic

tectonic evolution of the north Qilian Mountains, China, *in* Wu, H., *et al*., eds., Very low grade metamorphism: Mechanisms and geological applications: Beijing, Seismological Press, p.92～116.

Wang, Q., and Coward, M.P., 1990, The Chaidam Basin, NW China: Formation and hydrocarbon potential: Journal of Petroleum Geology, v.13, p.93～112.

Wang, Q., Nishidai, T., and Coward, M.P., 1992, The Tarim basin, NW China: Formation and aspects of petroleum geology: Journal of Petroleum Geology, v.15, p.5～34.

Wang, X., Zhang, R., and Liou, J.G., 1995, Ultrahigh pressure metamorphic terrane in eastern central China, *in* Coleman, R.G. and Wang, X., eds., Ultrahigh pressure metamorphism: Cambridge, Cambridge University Press, p.356～390.

Wang, Y.S., and Chen, J.N., 1987, Metamorphic zones and metamorphism in Qinghai Province and its adjacent areas: Beijing, Geological Publishing House, p.42～56(in Chinese with English abstract).

Wu, H., and Tian, B., 1994, New achievements on the study of the lowtemperature metamorphism in north Qilian Mountains: Discovery of lawsonite in southern high-grade blueschist belt and metamorphism of ophiolite in Yushigou, Qilian County, China, *in* Wu, H., *et al*., eds., Very low grade metamorphism: Mechanisms and geological applications: Beijing, Seismological Press, p.156～167.

Wu, H., Feng, Y., and Song, S., 1993, Metamorphism and deformation of blueschist belts and their tectonic implications, north Qilian Mountains, China: Journal of Metamorphic Geology, v.11, p.523～536.

Xia, L.Q., Xia, Z.C., and Xu, X.Y, 1995, Dynamics of tectono-volcanomagmatic evolution from north Qilian Mountains, China: Northwest Geosciences, v.16, p.1～28(in Chinese with English abstract).

Xiao, X.C., Chen, G.M., and Zhu, Z.Z., 1974, Some knowledge about the paleo-plate tectonics of the Qilian Mountains: Geological Science and Technology, v.3, p.73～78(in Chinese with English abstract).

Xiao, X.C., Chen, G.M., and Zhu, Z.Z., 1978, A preliminary study on the tectonics of ancient ophiolites in the Qilian Mountains, Northwest China: Acta Geologica Sinica, v.52, p.287～295(in Chinese with English abstract).

Xu, Z.Q., Xu, H.F., Zhang.J.X., and Li, H.B., , 1994, The Zoulang Nanshan Caledonian subduction complex in the Northern Qilian Mountains and its dynamics: Acta Geologica Sinica, v.68, p.225～241(in Chinese with English abstract).

Xu, Z.Q., Zhang, J.X., and Xu, H.F., 1997, Ductile shear zones in the main continental mountain chains of China and their dynamics: Beijing. Geological Publishing House, p.71～108(in Chinese).

Xu, Z.Q., Yang.J.S., Zhang.J.X., Jiang.M., Li, H.B., and Cui, J.W., 1999, A comparison between the tectonic units on the sides of the Altun sinistral strike-slip fault and the mechanism of lithospheric shearing: Acta Geologica Sinica, v.73, p.193～205(in Chinese with English abstract).

Yang, J.J., Zhu, H., Deng, J.F., Zhou, T.Z., and Lai, S.C., 1994, Discovery of garnet-peridotite at the northern margin of the Qaidam basin and its significance: Acta Petrologica et Mineralogica, v.13, p.97～105 (in Chinese with English abstract).

Yang, J.S., Xu, Z.Q., Li, H.B., Wu, C.L., Cui, J.W., Zhang, J.X., and Chen, W., 1998, Discovery of eclogite at northern margin of Qaidam basin, NW China: Chinese Science Bulletin, v.43, p.1755～1760(in Chinese with English abstract).

Yang, J.S., Xu, Z.Q., Li, H.B., Wu, C.L., Zhang, J.X., and Shi, R.D., 2000, A Caledonian convergent border along the southern margin of the Qilian terrane, NW China: Evidence from eclogite, garnet-peridotite, ophiolite, and S-type granite: Geological Society of China Journal, v.43, p.142～164.

Discovery of coesite in the North Qaidam Early Palaeozoic ultrahigh pressure(UHP) metamorphic belt, NW China[●]

Jingsui Yang[a, *] Zhiqin Xu[a] Shuguang Song[a] Jianxin Zhang[a]
Cailai Wu[a] Rendeng Shi[a] Haibing Li[a] Maurice Brunel[b]
([a] Institute of Geology, Chinese Academy of Geological Science, Beijing, China;
[b] Department of Earth Sciences, University of Montpellier-2, Montpellier, France)
Received 8 October 2001; accepted 15 October 2001
Communicated by Paul Tapponnier

Abstract Coesite and graphite were discovered as inclusions in zircon separates from pelitic gneiss associated with a large eclogite body in the North Qaidam UHP terrane. This finding suggests UHP metamorphism at pressures below the diamond stability field. This supports previous indirect UHP evidences, such as polycrystalline quartz inclusions in eclogitic garnet, quartz lamellae in omphacite and *P-T* estimates for both eclogite and garnet peridotite. The U/Pb and Sm/Nd isotopic ages from the North Qaidam eclogite indicated that continental subduction occurred in Early Palaeozoic, most probably in relation with the collision between the Sino-Korean and Yangtze plates. © 2001 Académie des sciences / Éditions scientifiques et médicales Elsevier SAS.

UHP metamorphism / coesite/eclogite / Qinghai-Tibet plateau / North Qaidam Mt

Résumé-Découverte de coésite dans la ceinture métamorphique UHP d'âge Paléozoïque inférieur du Nord-Qaidam, Chine nord-occidentale. De la coésite et du graphiet ont été identifiés en inclusion dans des zircons de gneiss pélitiques associés à un massif d'éclogite des terrains métamorphiques de très haute pression des chaînons montagneux du Nord du Qaidam, dans le Nord-Est du plateau du Tibet en Chine. Cette découverte suggère un métamorphisme de type UHP dans des conditions de pression inférieures au champ de stabilité du diamant et conforte les observations antérieures de quartz polycristallin en inclusion dans des grenats éclogitiques, de lamelles d'exsolution de quartz dans de l'omphacite et les données *P*, *T* préliminaires sur les éclogites et les péridotites. Las âges U/Pb et Sm/Nd des éclogites du Nord-Qaldam indiquent

● C. R. Acad. Sci. Paris, Sciences de la Terre et des planètes / Earth and Planetary Sciences 333(2001)719–724.

S1251-8050(01)01718 9/FLA.
Géomatériaux / Geomaterials.
(Pétrologie/Petrology).
Correspondence and reprints.
* E-mail address: yangjsui@public.bta.net.cn(J. Yang).

qu' une subduction continentale s' est développée au Paléozoïque inférieur, probablement en relaton avec la collision des cratons Sino-Koréen et du Yangze. © 2001 Académie des sciences / Éditions scientifiques et médicales Elsevier SAS.

métamorphisme UHP/coésite/éclogite/plateau du Qinghai-Tibet/Nord-Qaidam

1 Introduction

The North Qaidam Mountain is located at the northeastern marginal area of the Qinghai-Tibet plateau, and is the western segment of the southern border of the Qilian terrane(Fig. 1). This border extends about 600km long from north of Dulan to the east to the Altyn Tagh fault to the west. In this region, eclogites were discovered first in Da Qaidam [18], then in Xitieshan [25] and north of Dulan [18, 25], constituting a remarkable highultrahigh pressure(UHP) metamorphic belt at least 350km long. This belt most likely connects westward to the eclogites in the South Altun terrane [7, 15, 17], and probably eastward to the eclogites in East Qingling [3], Xiongdian [4, 23] and North Dabie [14, 16], thus representing an ancient border between the North China and South China plates [21].

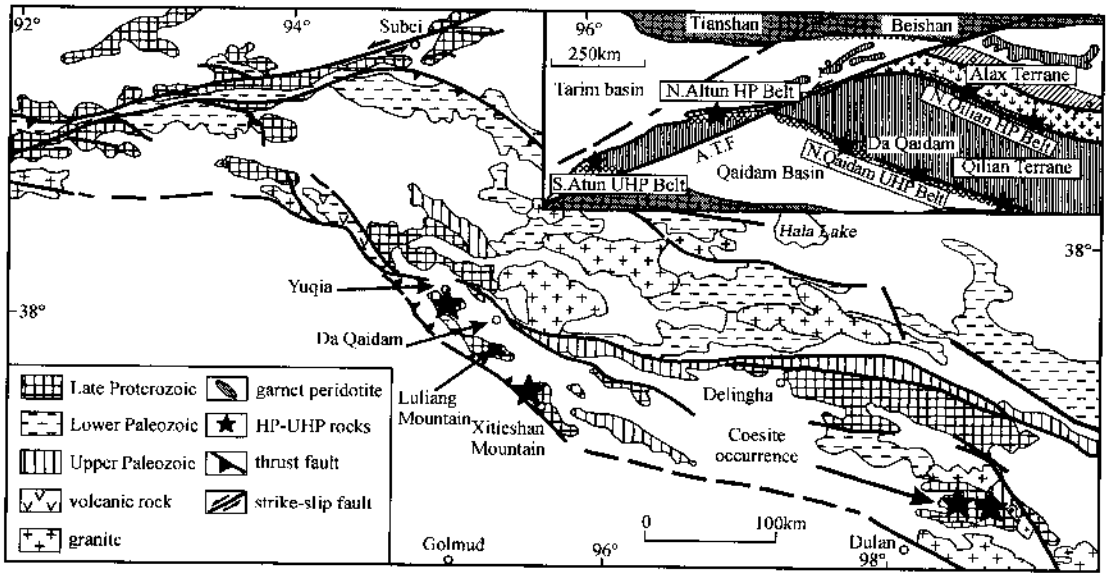

Fig. 1 Geological map of the Da Qaidam region, southern margin of the Qilian terrane (modification based on the geological map of the Qinghai-Tibet plateau and neighbouring area, scale 1:1 500000, Chendu Institute of Geology and Mineral Resources(China), 1988).

Figure 1. Carte géologique schématique de la région de Da Qaidam, limite sud du terrain des Qilan Shan(d' après la carte géologique du plateau Qinghai-Tibet et des régions voisines, au 1:1 500000e, Institut de géologie et des ressources minérales de Chengdu(Chine), 1988, modifiée).

Early reports of pseudomorph of coesite in eclogitic garnet and quartz lamellae in omphacite as well as *P-T* estimates for both eclogite and garnet peridotite suggested that the North Qaidam UHP terrane may have been recrystallized at pressure above the coesite stability field [21]. However, this was not well established since no typical UHP minerals had yet been found in this terrane. This paper will report the new discovery of coesite from the North Qaidam UHP belt.

2 Main characteristics of the North Qaidam HP-UHP metamorphic belt

The North Qaidam UHP belt is located at the northern margin of the Qaidam basin and extends at least 350km from Da Qaidam to the west, through Xitieshan to North of Dulan to the east (figure 1). Large amounts of eclogite and some garnet peridotite occur in the belt as tectonic boudins, mostly in the Proterozoic sequence [13, 20]. Most eclogite blocks are less than 20m × 10m in size, but may reach sizes of 100m × 50m. The Proterozoic sequence consists of gneiss, schist, quartzite, marble and basaltic volcanic rocks. The eclogite blocks occur in gneiss palegrey in colour and consisting mainly of plagioclase and quartz, and minor muscovite(5% ～ 10% in vol.) and garnet (1% ～ 2%). Some Early Palaeozoic granite intrusions were also reported within the sequence [15].

Eclogites have varied mineral assemblages and chemical compositions from place to place.

In Da Qaidam, eclogites are fresh and metamorphic peak mineral assemblage is garnet (Grt) + omphacite (Omp) + phengite (Phe) (Si = 3.3 ～ 3.45) + rutile (Rut). The garnets consist mainly of 44% ～62% almandine(Aim), 15% ～33% grossular(Grs) and 12% ～30% pyrope(Prp). Omphacites contain 37% ～46% of jadeite(Jd). Two types of phengite were recognized. The metamorphic peak conditions of eclogite metamorphism occurred at about 722 ± 123℃ and $P > 2.2$ GPa [18]. Using the Phe-Grt-Omp geobarometer and Grt-Omp geothermometer [2], some of the Da Qaidam eclogite rocks have $P = 2.8$ GPa and $T = 730$℃.

The eclogites in Xitieshan have largely been retrograded, and metamorphic peak minerals are Grt + Omp + Rut, without phengite. Garnets have cores (Prp47 ～ 50Alm28 ～ 31Grs 17 ～ 22) and retrograded mantles (Prp38 ～ 45Alm28 ～ 38Grs20 ～ 23), with their rims replaced by clinopyroxene (Cpx) + plagioclase (Pl) or amphibole (Am) + Pl. The eclogites were mostly replaced by Grt-granulite and Grt-amphibolite, and their country rocks are sillimanite gneiss and granitic gneiss. In general, garnets in the Xitieshan eclogites have higher Pyr content than elsewhere in the metamorphic belt, but omphacites have lower (22% ～ 26%) Jd content. A transition from eclogite to Grt-granulite, Grt-amphibolite and Pl-amphibolite can be observed in some large eclogite bodies. The peak metamorphic conditions of the eclogite are: $T = 770$ ～ 830℃ and $P > 14$ kbar [26]. However, the exsolved needles of quartz observed in omphacite may suggest UHP metamorphic conditions [1, 11, 27].

The eclogite belt in the Dulan region can be subdivided into two belts, the North and South Eclogite belts of Dulan (NEBD and SEBD, respectively). The eclogites in SEBD consist mainly

of Grt + Omp + kyanite(Ky) + Rut + zoisite(Zo). The garnets contain relatively lower(38% ~ 54%)Alm, higher(19% ~ 37%)Prp and constant(21% ~ 24%)Grs. Omphacites contain 24% ~ 38% Jd. *P-T* conditions of the eclogite in the SEDB are estimated to be about 856 ~ 896℃ and $P \geqslant 1.6 \sim 1.8$ GPa [19]. Kyanite is a typical mineral in UHP metamorphic belts throughout the world(e.g., in the eclogite of the Dabie UHP metamorphic belt, Wang *et al*. [12] suggested peak metamorphic pressure in excess of 2.7 ~ 2.9 GPa). The NEBD eclogites consist mainly of Grt + Omp + Phe (Si = 3.45) + Ru. The garnets contain relatively higher (41% ~ 58%) Alm, lower (10% ~ 27%) Pyr and widely varying (13% ~ 38%) Gro. The omphacites are stretched or broken, with 23% ~ 37% Jd. Based on current mineral chemistries and phase assemblages, peak *P-T* conditions of these rocks are estimated to be about $T = 624 \sim 735$℃ and $P = 20 \sim 26$ kbar[19].

In addition, several lines of evidence including pseudomorph of coesite in eclogitic garnet and quartz lamellae in omphacite suggest that the North Qaidam UHP terrane may have reached, pressure above the coesite stability field [19].

3 Discovery of coesite inclusions in zircon

Coesite and micro-diamond as typical UHP minerals rarely survive retrogression in the rocks groundmass but can resist as inclusions in garnet and omphacite, especially in zircon [5, 9, 10, 22].

Coesite was found as inclusions in zircon separates from pelitic gneisses associated with a large eclogite body in the NEBD(Fig. 2). The gneisses have been intensely deformed and consist of garnet(~ 5%) + muscovite(30%) + biotite(< 10%) + quartz (> 50%) + sphene(few), which is obviously a retrograde mineral assemblage. The garnets are elongated and rotated, and muscovite occurs as narrow leaves, while biotite formed after garnet. No peak metamorphic minerals remained in the rocks. Zircons from the gneiss are sub-rounded [6], and some have relic cores of previous ones. They were separated by crushing, sieving, magnetic and heavy liquid in Tianjin Institute of Geology and Mineralogy. Detailed UHP mineral searching was carried out using laser Raman microspectroscopy(JASCO NRS-2000)at the Tokyo Institute of Technology [5]. Many types of mineral inclusions have been found, including coesite, graphite, phengite, garnet, rutile, quartz, apatite and calcite. Coesite inclusions are few micrometres in size, and occur at the rim or mantle of the garnet grains(Fig. 2). Graphite inclusions are commonly seen with the same size as coesite.

Thus, it is proposed that the peak pressure of the metamorphism of the North Qaidam HP-UHP terrane was below the diamond stability field($2.8 \leqslant P < 3.5$Gpa). This conclusion is consistent with other UHP evidence, including polycrystalline Kfeldspar, quartz inclusion in eclogitic garnet and quartz lamellae in omphacite.

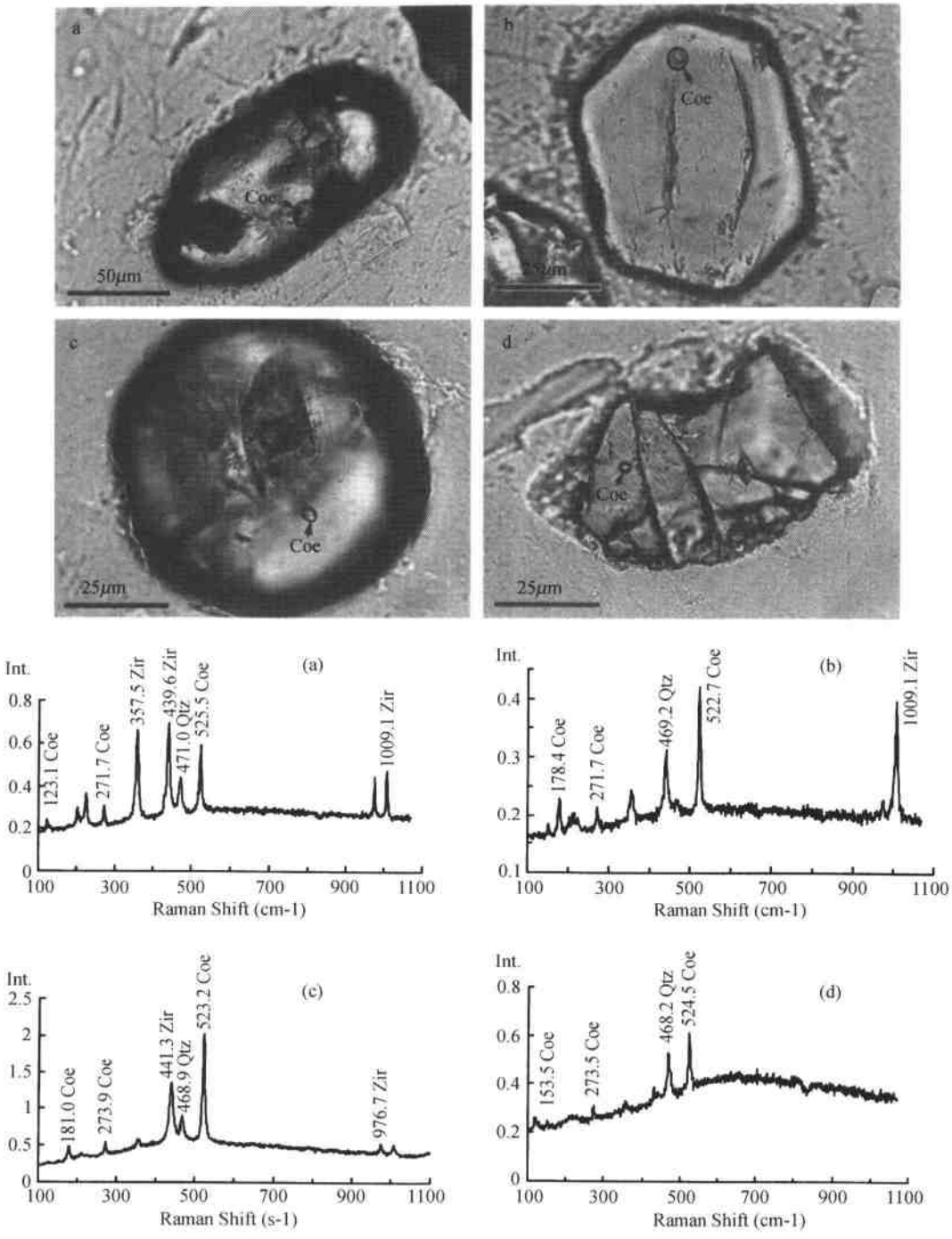

Fig.2 Microscopic images and Raman spectra of coesite inclusions in zircon from pelitic gneiss associated with large eclogite body in North Dulan, east section of the North Qaidam UHP belt.

Fig.2. Images microscopiques et spectres Raman des inclusions de coésite dans les zircons des gneiss pélitiques associés aux massifs éclogitiques du Nord de Dulan, section orientale de la ceinture UHP du Nord Qaidam.

4 Tectonic implications

The discovery of coesite and graphite inclusions in zircons from paragneisses surrounding the eclogite indicates the existence of an UHP metamorphic belt and continental collision in the region. The zircons from the eclogite give a SHRIMP U/Pb formation age of 494.6 ± 6.5Ma, which represents the peak metamorphic age of eclogitic facies. The phengite produced an Ar-Ar plateau age of 466.7 ± 1.2Ma, which may represent the cooling age of the eclogite during exhumation [25]. In addition, the muscovites from the gneiss, the country rock of the eclogite, yield a plateau age of 478.3Ma. These data suggest that the collision took place 495Ma ago, while exhumation was delayed until 466Ma. This is similar to the 504Ma subduction ages from the eclogite in the Altun mountains[24]. Apart from the North Qaidam mountains, eclogites of Early Palaeozoic age were also reported from the North Qingling[3] and Tongbai regions [14], as well as from North Dabie[4, 23]. We propose that an Early Palaeozoic UHP belt developed along the Central Orogenic belt of China from North Qaidam through North Qingling, to North Dabie(Fig.3). This belt possibly extends westward to the Kokchetav UHPM belt in Kazakhstan[8].

Acknowledgements. We thank Shige Maruyama and his colleagues for using the Laser Raman Spectroscopy in the Institute of Toknjo Technology, Louie Liou and Gary Ernst of Stanford University for useful discussion and Joe Wooden for SHRIMP U-Pb dating. The research was supported by the National Natural Science Foundation of China(grant 49732070) and was carried out under the auspices of the Chinese National Key Project for Basic Research

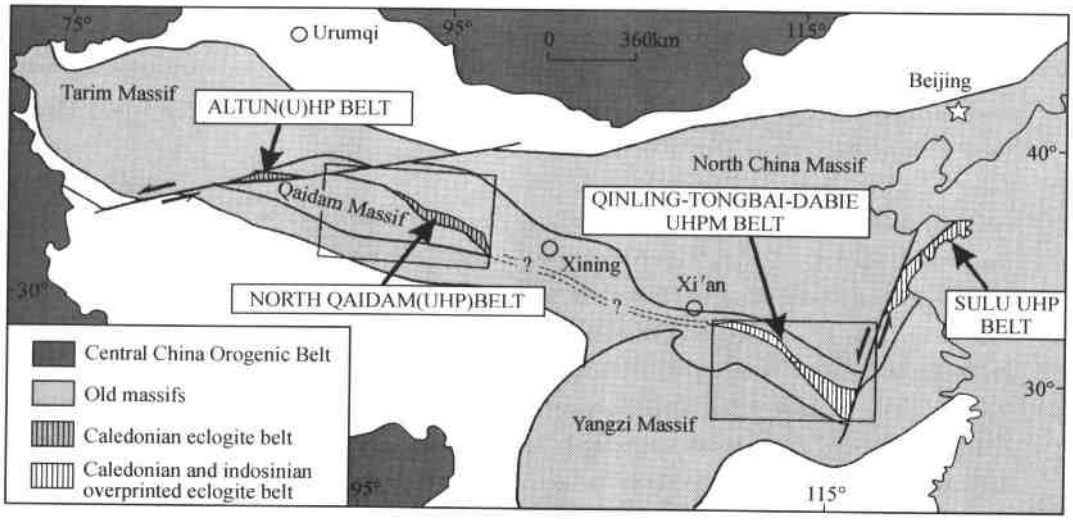

Fig.3 Possible extension of the North Qaidam UHP belt connecting to eclogites in East Qingling, Tongbo, and perhaps in Dabieshan.

Fig.3. Extension géographique possible de la ceinture métamorphique de UHP du Nord Qaidam, en continuité avec les éclogites des Qinling orientales, Tongbo et, peut-être, Dabieshan.

on Tibetan Plateau (G1998040805). We thank Nicolas Arnaud and Paul Tapponnier for thorough reviews.

References

[1] Carswell D.A., O'Brien P.J., Wilson R.N. *et al*., Thermobarometry of the phengite-bearing eclogites in the Dabie Mountains of the central China [J], J. Metamorph. Geol. 15(2)(1997)239～252.

[2] Carswell D.A., Zhang R.Y., Petrographic characteristics and metamorphic evolution of ultrahigh-pressure eclogites in platecollision belts, Int. Geol. Rev. 41(1999)781～798.

[3] Hu N., Xu B., Zhao D., Geochemical characteristics of eclogites and the related rocks from the northern Qinling Orogenic Belt, J. Xian College of Geology 19(1)(1997)7～13(in Chinese with English abstract).

[4] Jian P., Yang W., Li Z., Zhou H., Isotopic geochronological evidence for the Caledonian Xiongdian eclogite in the western Dabie Mountains, China, Acta Geol. Sin. 71(2)(1997)133～141(in Chinese with English abstract).

[5] Katayama I., Zayachkovsky A.A., Maruyama S., Prograde pressure-temperature records from inclusions in zircons from ultrahigh-pressure-high-temperature rocks of the Kokchetav Massif, northern Kazakhstan, The Island Arc 9(2000) 417～427.

[6] Liu F., Xu Z., Yang J., Maruyama S., Liou J.G., Katayama I., Masago, Mineral inclusions and evidence of ultrahigh-pressure metamorphism from zircons in gneisses in pre-pilot hole(CCSD－PP2) of Chinese Continental Scientific Drilling Project, North Jiangsu, China, Chin. Sci. Bull. 46 (2001) 241 ～ 246 (in Chinese).

[7] Liu L., Che Z., Luojinhai, Determination of eclogite in western Altyn and its geological significance, Chin. Sci. Bull. 41(1996)1485～1488.

[8] Maruyama S., Parkinson C.D., Overview of the geology, petrology and tectonic framework of the HP-UHPM Kokchetav Massif, Kazahkstan, The Island Arc 9 (2000)439～455.

[9] Sobolev N.V., Shatsky V.S., Vavilov M.A., Inclusions of diamonds, coesite and co-existing minerals in zircons and garnets from metamorphic rocks of Kokchetav massif northern Kazakhstan, USSR, in: Proc. 29th Int. Geol. Congr., Vol. 2, 1992, p. 599.

[10] Tabata H., Yamauchi K., Maruyama S., Liou J.G., Tracing the extent of ultrahigh-pressure metamorphic terrane: a mineralinclusion study of zircons in Gneisses from the Dabie Mountains, in: Harker B., Liou J.G. (Eds.), When Continents Collide: Geodynamics and Geochemistry of Ultrahigh-Pressure Rocks, Kluwer Academic Publishers, 1998, pp. 261～273.

[11] Tsai C.-O., Liou J.G., Eclogite-facies relics and inferred ultrahigh-pressure metamorphism in the North Dabie Complex, central-eastern China, Am. Mineral. 85(2000)1～8.

[12] Wang X., Liu J., Liou J.G., Zhou G. and Anonymous, High-pressure metamorphic kyanite-bearing schists from the SW Dabie Mountains, central China, Geological Society of America, Cordilleran Section, 89th Annual Meeting, and Rocky Mountain Section, 46th Annual Meeting, Vol. 25, p. 160.

[13] Wang Y., Chen J., Metamorphic zones and metamorphism in Qinghai Province and its adjacent areas, Geological Publishing House, Beijing, 1987, pp. 213～220(in Chinese with English abstract).

[14] Wei C., Wu Y., Ni Y., Chen B., Wang S., Eclogites and their geological implications in Tongbai Region, Henan Province, Chin. Sci. Bull. 44(1999)1882～1885.

[15] Wu C., Yang J., Trevor I., Joe W., Li H., Wan Y., Shi R., Zircon SHRIMP ages of Aolaoshan granite

from the south margin of Qilianahan and its geological significance, Acta Pet. Sin. 17(2)(2001)215～221.

[16] Xu S., Su W., Liu Y., Wang R., Jiang L., Wu W., Discovery of eclogites and their petrographic features in the North Dabieshan, Chin. Sci. Bull. 44(1999)1452～1456.

[17] Xu Z., Yang J., Zhang J., Jiang M., Li H., Cui J., A comparison between the tectonic units on the two sides of the Altun sinistral strike-slip fault and the mechanism of lithospheric Shearing, Acta Geol. Sin. 73(3)(1999)193～205(in Chinese with English abstract).

[18] Yang J.S., Xu Z.Q., Li H., Wu C., Cui J., Zhang J.X., Chen W., Discovery of eclogite at northern margin of Qaidam Basin, NW China, Chin. Sci. Bull. 43(1998)1755～1760.

[19] Yang J.S., Song S., Wu C., Shi R., Jalivet M., North Qaidam ultrahigh pressure metamorphic(UHPM) belt on the northeastern Qinghai-Tibet plateau and its eastward extension, Earth Sci. Frontiers 7(Suppl.)(2000)241～242.

[20] Yang J.S., Xu Z.Q., Song S., Wu C., Shi R., Zhang J., Wan Y., Li H., Jin X., Jalivet M., Discovery of eclogite in Dulan, Qinghai Province and its significance for the HP-UHP metamorphic belt along the central orogenic belt of China, Acta Geol. Sin. 74(2000)156～168(in Chinese with English abstract).

[21] Yang J.S., Xu Z.Q., Li H.B., Wu C.L., Zhang J.X., Shi R.D., An Early Paleozoic convergent border at the southern margin of the Qilian terrain, NW China: evidence from the eclogite, garnet peridotite and ophiolite, J. Geol. Soc. China 43(2000)142～164.

[22] Ye K., Yao Y., , Katayama I., , Cong B., Wang Q., Maruyama S *Large areal extent of ultrahigh pressure* terrane of East China new implications from coesite and omphacite inclusions in zirce of granitic gneiss, in: Carswell D.A.(Ed.), Ultrahigh pressur metamorphic rocks, Vol.52, Elsevier, Amsterdam, 2000, pp.157～164.

[23] Zhang J., Zhu X., Du J., Zhang Y., Petrography and *retrometa* morphism of the eclogite in Dabie Mountains, Hebei Dizhi Xueyna Xuebao-J. Hebei College of Geology 18(Suppl.)(1995)54～57.

[24] Zhang J., Zhang Z., Xu Z., Yang J., Cui J., The ages of UPb and Sm-Nd for eclogite from the western segment of the northerr Qaidam motmtains, western China, in: Int. Symp. on Geoscience of the Northern Qingai-Tibetan Plateau(abstract), Bejing, China, pp 142～147.

[25] Zhang J., Yang J., Xu Z., Wan Y., Meng F., Li H., Shi R., Song S., Two contrasting eclogite types in the western segment of the northern Qaidam mountains, western China (abstract), in: Int. Symp. Geoscience of the Northern Qingai-Tibetan Plateau, Bejing, China, 2000, pp.142～147.

[26] Zhang J., Yang J., Xu Z., Wan Y., Meng F., Li H., Shi R., Song S., Two contrasting eclogite types in the western segment of the northern Qaidam Mountains, northern Qinghai-Tibet Plateau, in: Grasemann B., Stuewe K. (Eds.), Special abstract issues, 16th Himalaya-Karakorum-Tibet workshop, Vol.19, Pergamon, Oxford, p.81.

[27] Zhang R.Y., Liou J.G., Ultrahigh-pressure metamorphism of the Sulu terrane, eastern China: a prospective view, Cont. Dynam. 3(1998)32～53.

Architecture and Orogeny of the Northern Qilian Orogenic belt, Northwestern China[1]

XU Zhiqin ZHANG Jianxin and LI Haibing
(Institute of Geology, CAGS, Beijing)

Abstract The northern Qilian orogenic belt lying between the southwestern part of the Sino-Korea plate (Alashan block) and Central-southern Qilian microterrane is a highly linear Caledonian subduction-collision orogenic belt. Since early Paleozoic period, it has experienced a lengthy geological evolution from opening of the Qilian oceanic basin, through northward subduction of oceanic crust and arc-continent collision during the Caledonian and an intracontinental convergence during the post-Caledonian orogeny stage, to the final uplift and re-orogeny in Cenozoic era. Macroscopic and microscopic studies reveal that the architecture formed during orogenic stages can be divided into early deep ductile and late shallow brittle deformation regimes. The former system constitutes the basic architecture of the northern Qilian orogenic belt. The Tuoleishan ophiolitic nappe was resulted from intraoceanic shearing and ocean lithosphere-mantle obduction onto the Central-southern Qilian microterrane during the northward subduction of the Qilian ocean. The overriding slices in Zoulangnanshan subduction complex were resulted from underplating and high-pressure metamorphism occurred at the orogenic root during the Caledonian subduction-collision stage. A large-scale ductile strike-slip shear zone and a transpressional zone were developed along the southern margin of the northern Qilian orogenic belt during Variscan post-orogenic oblique collision. Small-scale extensional shear zones were formed and followed by the emplacement of post-orogenic granitoids.

The shallow brittle strain is characterized by thrust and strikeslip, reflecting the post-orogenic transpression from Devonian to Cretaceous periods. The Cenozoic re-orogeny led to rising of the Qilian mountains. Formation of piedmont thrust fault system was associated with the southwestward intracontinental underthrust of the Alashan block. The Altyn sinistral strike-slip fault probably had pushed the Precambrian metamorphic series of the Central-southern Qilian microterrane northward onto the Ordovician volcanic island arc zone of the northern Qilian mountains during Cenozoic era.

Key words architecture, deformation regime, orogeny, dynamics, northern Qilian orogenic belt

Introduction

The northern Qilian orogenic belt lies between the southwestern part of the Sino-Korea plate(Alashan block)and the Central-southern Qilian microterrane. It is characterized by having developed lower Palaeozoic ophiolite suites, subduction-accretionary complexes, high-pressure

[1] Journal of the Geological Society of China.
Vol.43, No.1, P.125~141, 10 Figs., February, 2000.

metamorphic zones, volcanic arcs, and back-arc basins(Fig. 1 a). Strata were strongly folded and metamorphosed, and the Devonian molasse unconformably overlie the Caledonian deformed strata(Wang and Liu, 1976; Xiao *et al*., 1978; Wu, 1980; Zuo, 1986; Zuo and Liu, 1987; Xia *et al*., 1991, 1996; Xu *et al*., 1994; Feng and He, 1996).

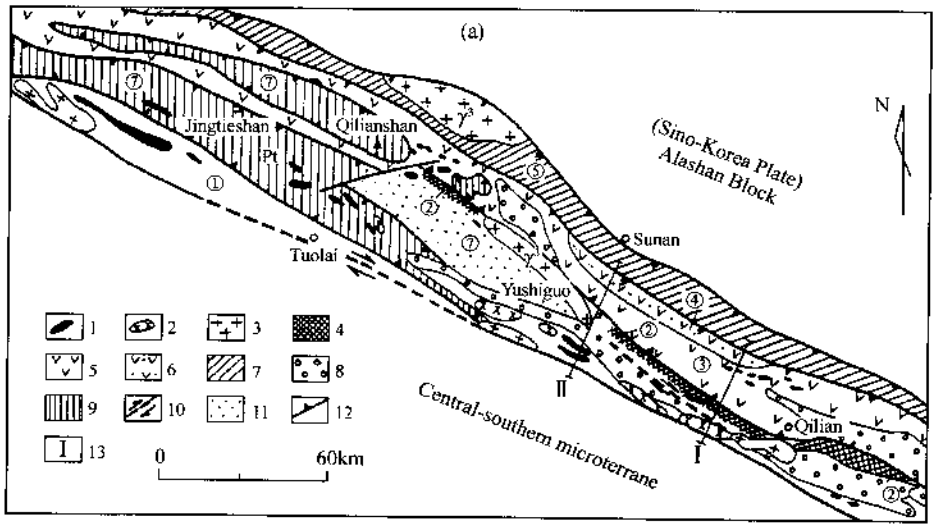

Fig. 1 (a)Tectonic Sketch-map of the northern Qilian orogenic belt.

1—ultramafic rock; 2— gabbro-diabase; 3—granitoids; 4—subduction complex zone; 5—island arc volcanic rock; 6—back-arc volcanic rock; 7—Silurian remnant ocean basin; 8—Devonian molasse and Carboniferous-Triassic intramontane basin; 9—Precambrian metamorphic terrane; 10—strikeslip shear zone; 11—Cretaceous-Tertiary terrigenous basin; 12—thrust; 13—location of crosssection.

Based on detailed studies on marine volcanic rocks of the northern Qilian mountains, Xia *et al*. (1996) proposed that rifting took place at the southwestern margin of the Sino-Korea plate and further splitted into a limited ocean during Neoproterozoic to Cambrian period (639 ~ 514Ma), then the oceanic crust subducted northward and formed a trench-arc-basin system (486~445Ma). On the basis of petrotectonic research for the Qilian orogenic belt, Xu *et al*. (1994) divided the orogenic belt into seven tectonic units as follows: ① Tuoleishan ophiolite zone(Cambrian-early Ordovician); ② Subduction-accretionary complex zone along the south slope of Zoulangnanshan(early Ordovician-late Ordovician); ③ Zoulangnanshan palaeovolcanic island arc zone(Ordovician); ④ back-arc basin along the northern slope of Zoulangnanshan (middle Ordovician to late Ordovician); ⑤ Silurian remnant ocean basin; ⑥ post-Caledonian orogenic molasse and intramontane basin; ⑦ Jingtieshan Precambrian metamorphic nappe mass.

This paper will expound architectures of the northem Qilian orogenic belt and reconstruct the orogenic stages on the basis of macroscopic and microscopic studies on a series of structural profiles.

The Architecture of the Northern Qilian Orogenic Belt

The architecture of the northern Qilian orogenic belt is composed of ductile and brittle deformation systems. In the course of orogenic evolution, the former deformation was transformed into the latter. Two sections across the middle part of the belt show general structural features of its long geological history of evolution (Fig. 1 b). The ductile shear zone with the NNE-SSW sense was formed during the Caledonian orogenic stage, while the large scale ductile strike-slip structures were formed during the Variscan post-orogeny. Moreover, the shallow brittle deformation occurred after Mesozoic.

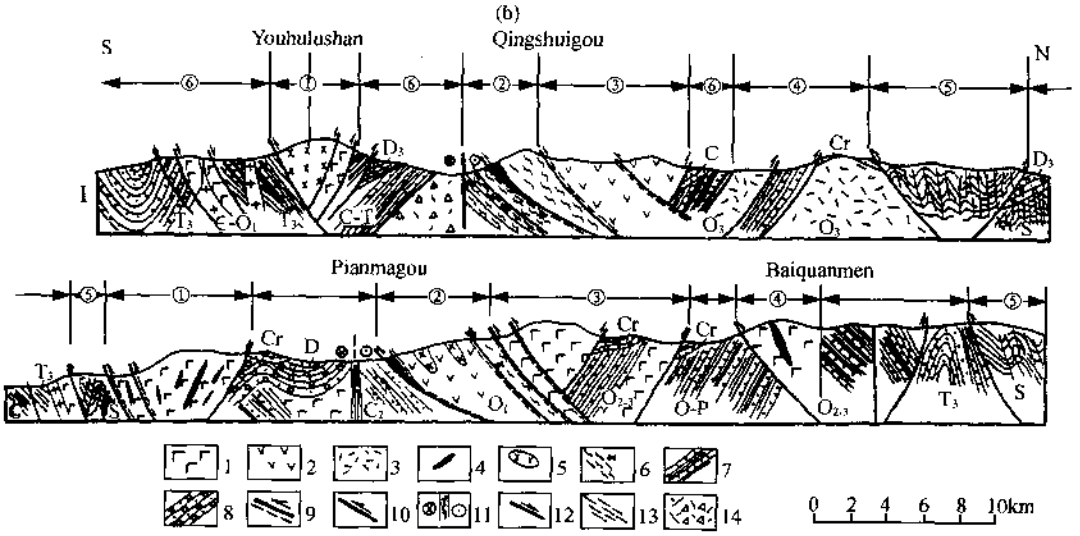

Fig. 1 (b) Tectonic cross-sections across the northern Qilian orogenic belt.

I: Youhulushan-Qingshuigou section; II: Bianmagou-Baiquanmen section.

1—basic volcanic rock. 2— intermediate volcanic rock. 3—intermediate-felsic volcanic rock. 4—serpentinite. 5—gabbro. 6—high-pressure metamorphic zone. 7—sandstone and shale. 8—conglomerate. 9—ductile thrust shear zone. 10—thrust fault. 11—ductile dextral strike-slip shear zone. 12—Normal fault, 13—cleavage. 14—volcanic breccia. ① Tuoleishan ophiolite zone; ② subduction accretionary complex zone; ③ Zoulangnanshan volcanic island arc zone; ④ back-arc basin; ⑤ Silurian remnant basin; ⑥ post-orogenic molasse and intramontane basin.

(1) Ductile deformation regime

The deep ductile deformation regime was developed mainly in the southern part of the orogenic belt. Ductile nappe mass of the Tuoleishan ophiolite zone is a result of intraoceanic shearing and obduction of oceanic slices during northward subduction of the Qilian oceanic crust (Xu *et al.*, 1994). Ductile overthrust imbricate rock slices composed of subduction complex along the southern slope of Zoulangnanshan represent underplating related to the Caledonian plate subduction at the root of the orogenic belt (Xu *et al.*, 1997). Ductile dextral strike-slip

shear zone at the southern margin of the orogenic belt indicates a Variscan relative movement between the orogenic belt and the Central-southern Qilian microterrane(Xu *et al*., 1997). The transpressional zone on the southern border of the subduction complex zone is a product of transformation from thrusting to strike-slipping. Ductile extensiona l zone was developed locally and related to emplacement of orogenic granitoids.

(A)The Tuoleishan ophiolitic nappe structure

The Tuoleishan ophiolitic zone was developed along the southern margin of the northern Qilian orogenic belt. It is mainly composed of ultramafic rocks(serpentinized harzburgite and dunite), mafic rocks(cumulative gabbro and diabase), pillow basalt and radiolaria-bearing clastic rocks of abyssal and bathyal facies, probably formed at an oceanic ridge during the spreading (Xiao *et al*., 1978, Bao, 1989, Xia *et al*., 1996; Feng and He, 1996). Slices of this oceanic ridge ophiolite formed an allocthonous mass overlying an autochthon which is composed of Precambrian metamorphic rocks, Caledonian granitoids, and early Paleozoic continental slope sediments on the passive margin of the Central-southern Qilian microterrane. The ophiolitic nappe masses include two thrust nappe slices: an upper ultramafic-mafic slice and a lower volcanic rock slice (Fig.2). The former is subdivided into the following four tectonically superimposing units. They are from top to bottom(a)upper ophiolitic melange unit, (b)lower ophiolitic melange unit, (c)spinel-bearing and chromite-bearing ultramafic rock unit, and(d) gabbro unit(Fig.2). They were all thrust to overlie the autochthon unit(e in Fig.2). Matrix of the ophiolitic melanges is serpentine schists, while exotic blocks consist of metagabbro-diabases, crystalline limestones, metavolcanic rocks, and peridotites. The nappe masses are foliated with NNE-SSW-trending stretching lineations. Boundaries between the slices are ductile shear zones. Rotational strain indicates that the shear sense is from north to south.

The ophiolitic nappe masses may have resulted from the southward obduction of the oceanic lithosphere during the early Caledonian orogeny. It is inferred that there was intraoceanic shearing during the northward oceanic subduction. Due to the plate collision in the late Caledonian orogeny and the following continental convergence, the nappe masses were superimposed again on postorogenic granitoids and Permo-Carboniferous Terrigenous sedimentary rocks.

(B)Ductile overthrust imbricate slices in the subduction complex

The subducton complex along the south slope of Zoulangnanshan is composed of highpressure metamorphic zone (garnet-bearing glaucophane schists, glaucophane-bearing mylonites), lenticular ultramafic rocks, gabbro and eclogite blocks(Wu *et al*., 1993)(Fig. 3). The protoliths of high-pressure glaucophane schists are basic and intermediate-basic volcanic rocks, gabbros and supracrustal clastic rocks, and carbonate rocks(Wu *et al*., 1993; Xu *et al*., 1994). It was shown that crustal materials from the forearc accretionary wedge and volcanic arc with the ophiolitic masses on the hanging wall of subduction zone were evidently carried down to the depth by the downgoing slab and formed the root of the orogenic belt(Wu *et al*., 1993; Xu *et al*., 1994; Shen *et al*., 1997).

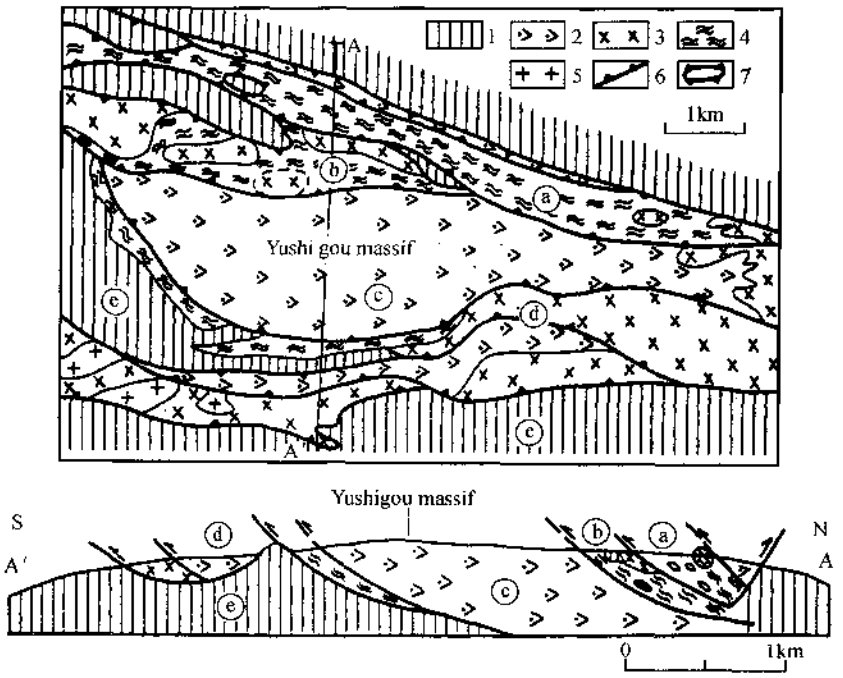

Fig.2 *The tectonic map and section for ultramafic rocks in Yushigou.*
(after BGMRQP, 1979, and Feng and He, 1996, slightly revised).
ⓐupper ophiolitic melange unit; ⓑlower ophiolitic melange unit; ⓒspinel-bearing and chromite-bearing ultramafic rock unit; ⓓgabbro unit; ⓔautochthon unit. 1—autochthon; 2—ultramafic rock; 3—mafic rock; 4—ophiolitic melange; 5—granitoid; 6—ductile thrust; 7—tectonic window.

The ductile overthrust imbricate slices with NWW-SEE trending in the subduction complex were formed under a high-pressure metamorphic condition. The accretionary volcanic units in association with the high-pressure metamorphic zones were formed during the step-back in underthrusting (Xu *et al.*, 1994). They are separated by the ductile thrust shear zones in which the gently-dipping foliations (or mylonitic foliation), transverse stretching lineations (NNE-SSW trending), and A-type shear folds with a shear sense from NNE to SSW were all well-developed. Preferred oriented quartz in the glaucophane schist belongs to basal and rhombohedral fabrics which were formed under low to medium temperature condition (350℃ ～ 450℃) and reflects a shear sense from NNE to SSW (Fig 4). The finite strain measurement of meta-volcanic pebbles (Flinn index k = 1.2) indicates a simple shear mechanism (Fig 4). Pressure-temperature studies and isotopic dating on the mineral assemblage of the glaucophane schist yielded a P-T-*t* path which indicates that the rocks of subduction complex first underwent a low-temperature and low-pressure metamorphic period (less than 15km), followed by a high-pressure and lowtemperature metamorphic period (P = 6.5kb, T = 400℃, 20～25km at depth) and a high-pressure peak-metamorphic period (P = 7.5kb, T = 300℃, about 30km at depth at 448～462Ma), then retrograded, and finally exhumated to the earth surface during the collision stage at 400～412Ma (Wu *et al.*, 1993; Zhang, 1989; Zhang *et al.*, 1989; Xu *et al.*, 1997).

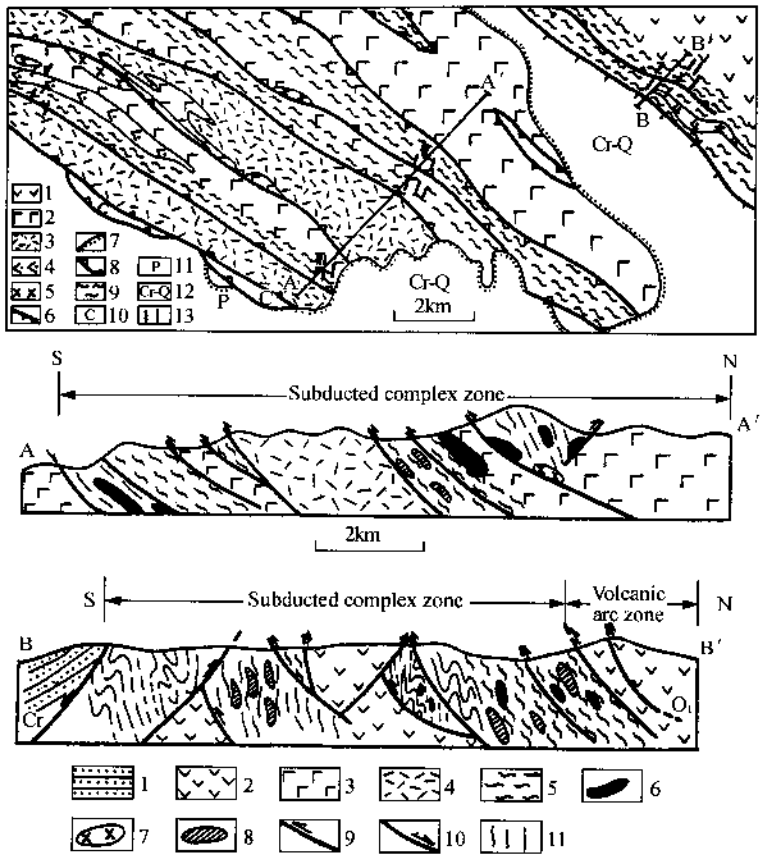

Fig.3 Tectonic sketch-map and tectonic sections of the subduction complex along the southern slope of Zoulangnanshan.

Tectonic sketch-map: 1—intermediate-basic volcanic rock; 2—basic volcanic rock; 3—intermediate-felsic volcanic rock and tuff; 4—ultramafic rock; 5—gabbro; 6 normal fault; 7—unconformity; 8—thrust; 9—glaucophane schist, 10—Carboniferous; 11—Permian; 12—Cretaceous-Quaternary, 13—stretching lineations sections; Sections: (A-A') Xialiugou section of the northern Qilian(B-B') Yu'ergou section of the northern Qilian; 1—sandstone; 2—intermediate-basic volcanic rock, 3—basic volcanic rock; 4—Intermediate-felsic volcanic rock and tuff; 5—glaucophane schist; 6—ultramafic rock; 7—gabbro-diabase; 8—allochthonous unit; 9—thrust; 10—normal fault; 11—glaucophane-bearing greenschist.

(C)Ductile strike-slip shear zone

The ductile strike-slip shear zone lying between the northern Qilian orogenic belt and the Central-southern Qilian microterrane is the greatest strike-slip shear zone in the Qilian orogenic belt. It formed a 2km-wide shear zone between the Ordovician volcanic rocks and the Neoproterozoic metamorphic rocks (Fig.5). The shear zone consist mainly of garnetiferous phyllonites and garnetiferous mica schists with approximately vertical foliation. Horizontal stretching lineations defined by garnet pressure shadow, stretching kyanite, and boudinage reflect strike-slip nature. A great deal of microstructures, such as £ \ -type and £ _-type porphyroclastic system , S - C structures , and shear folds , indicate that the sense of shear is

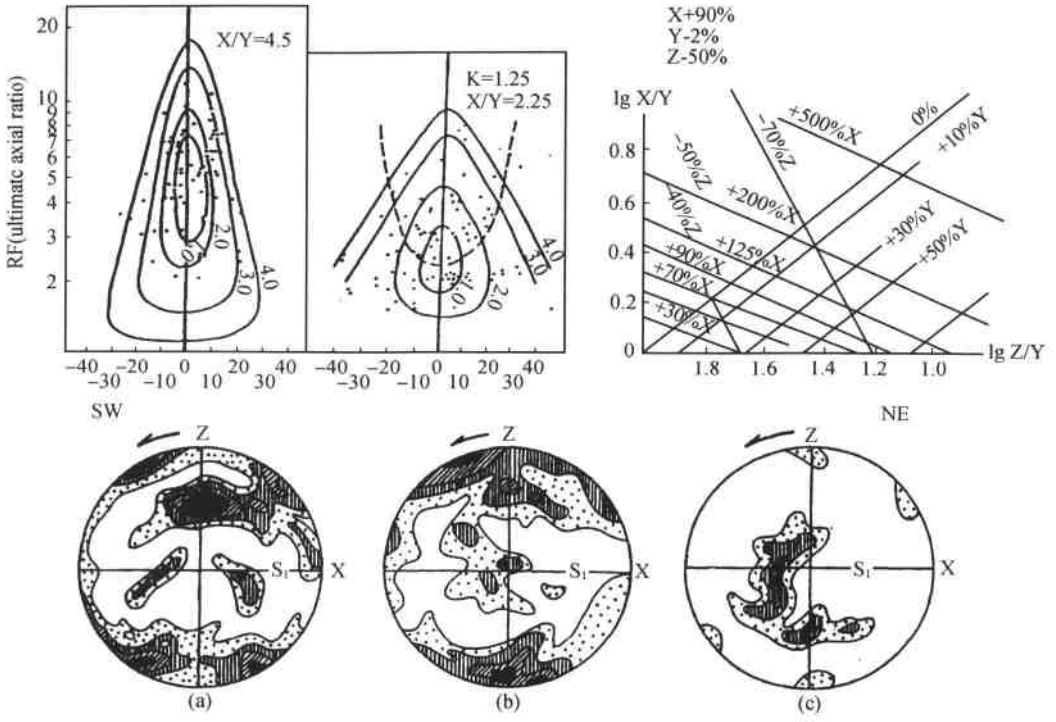

Fig.4 The results of finite strain measurement of deformed pebbles and quartz c-axis fabrics in the blueschists from subduction-accretionary zone.

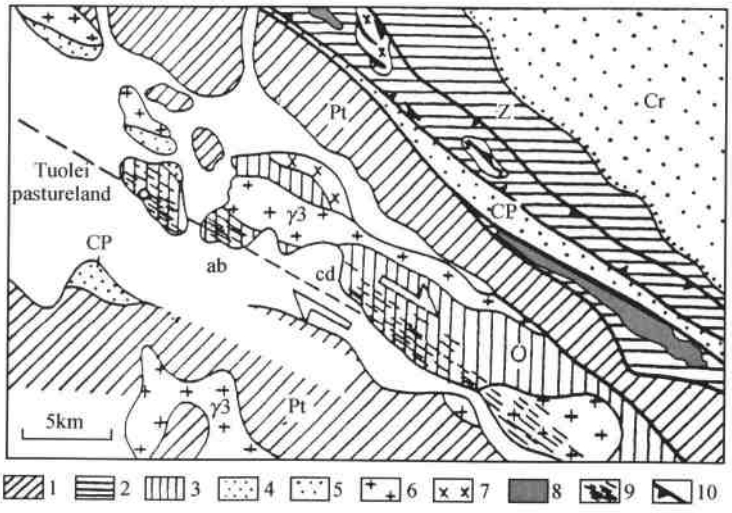

Fig.5 Geological sketch-map of the Tuolei pastureland area, northern Qilian mountains.

1—early-Proterozoic high-grade metamorphic rock; 2—Sinian low-grade metamorphic rock; 3—Ordovician volcanic rock; 4—Permo-Caboniferous Terrigenous sedimentary rock; 5—Cretaceous Terrigenous sedimemtary rock; 6—granitoid; 7—gabbro; 8 — ultramafic rock ; 9 — ductile shear zone ; 10 — thrust fault . Pt : Proterozoic ; Z : Sinian ; O : Ordovician ; CP : Permo-Caboniferous; Cr: Cretaceous; γ3 :Caledonian granitoids.

dextral. Sheath folds were developed in the central part of the shear zone. Its closed direction indicates the same shear sense. The preferred orientations of quartz grains include high temperature prismatic < c > fabrics (more than 650℃), moderate-temperature rhombic fabrics (greater than 450℃) and low-temperature (350℃) basal fabrics. This illustrates that the shear zone was evolved from high-temperature to low-temperature stage (Xu *et al*., 1997).

This shear zone was resulted from the post-collisional orogeny during early Variscan. This is evidenced by its cutting Caledonian granitoids, being covered unconformably by Carboniferous strata, an Ar-Ar plateau age of 361.5 ± 3.7Ma, and an isochron age of 359.2 ± 4.05Ma shown by the constituent biotite (Xu *et al*., 1997).

(D) Ductile transpressional zone

Series of ductile transpressional zones are found in the southern part of the northern Qilian orogenic belt. A ductile transpressional zone is a ductile shear zone which developed at a deep crust level with both thrust and strike-slip features. It is composed of mylonites or high-strain rocks with steep foliations and oblique stretching lineations. Therefore, remarkable rotation strain can be found on the two sections perpendicular to the foliations.

The Heihe EW-trending ductile transpressional zone lying in the southern side of subduction complex zone was developed in the Ordovician volcanic breccia zone with a width of 500m. Pebbles were intensively stretched, fractured and then filled by calcite. On the northward steeply-dipping foliations, stretched pebbles intersect the horizontal plane at angles of 50°～60°. North-south thrust shearing is displayed on the vertical section and dextral strike-slip shearing on the horizontal section (Fig. 6). These features show superimposition of thrusting and strike-slipping, which caused a change in deformation mechanism from simple shear to flattening and produced a contraction strain along y-axis.

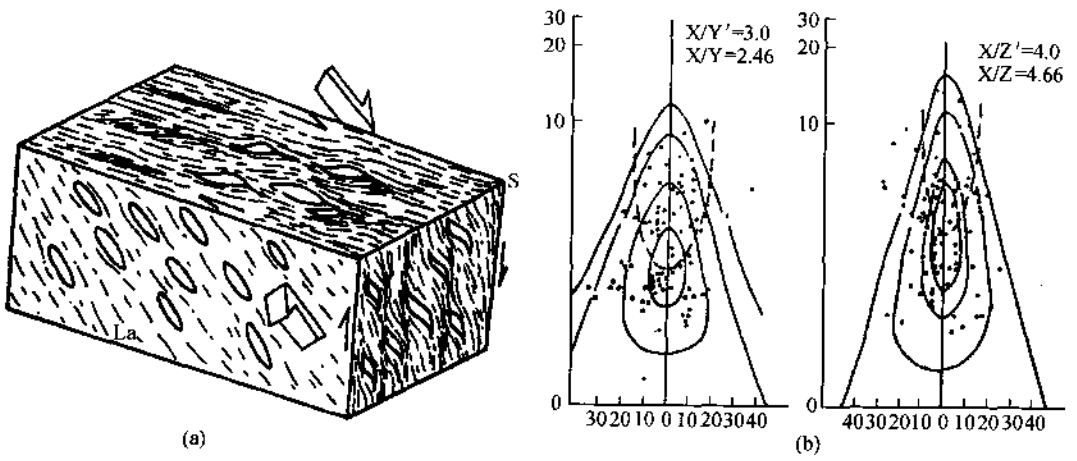

Fig. 6 The finite strain analyses of deformed pebbles in Heihe ductile transpressional zone.
(a) Stereographic sketch-diagram of metavolcanic breccia; La: stretching lineation, S: foliation.
(b) the results of finite strain measurements.

(E)Post-orogenic ductile extensional shear zone

A post-orogenic ductile extensional shear zone in the central-western segment of the northern Qilian orogenic belt is related closely to the emplacement of post-orogenic granitoids. It is commonly found around the margins of granitoids. For example, a granitoid mylonitic zone is present at the SE margin of the Niuxinshan granitoids near Qilian County(Fig. 7). Stretching lineations defined by the oriented K-feldspar augens and hornblende grains on the mylonitic foliation plunge toward SE. Asymmetrical feldspar augens and asymmetrical folds of granitoid veins reflect a normal shear movement from NW towards SE. Granitoid mylonites show hightemperature ductile deformation features. Feldspars in the mylonites display intracrystalline deformation features of wavy extinction, subgrains, and dynamic recrystallization. Moreover, myrmekite appears on the edge of K-feldspar pophyroclasts, but quartz lacks intracrystalline deformation and displays annealing and re-crystallization phenomena. These features suggest that the formation of the high-temperature ductile extensional shear zone is related to the emplacement and uplift of the granitoids. The annealing and re-crystallization in mylonite indicates the continued high-temperature effect of the granitoids(Xu *et al*., 1997).

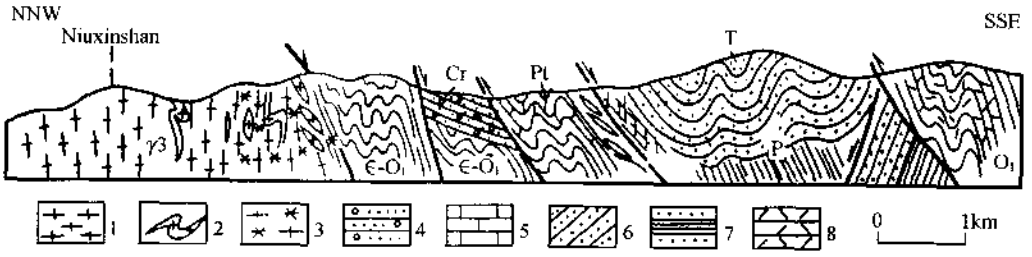

Fig. 7 The section of ductile extensional shear zone on the eastern side of Niuxinshan granitoids.
1—deformed granitoid, 2—granitoid vein, 3—mylonite, 4—conglomerate, 5—limestone, 6—sandstone, 7—sandstone and shale, 8—tuff.

(2)Brittle deformation regime

The deep ductile deformation formed during Caledonian and Variscan periods was redeformed by brittle structures during exhumation and uplift. It is manifested in the following features: (a) reactivation of the ductile strike-slip fault generated pull-apart basins, which were filled by post-orogenic terrigenous sediments, (b) thrust slices(i.e. crustal accretionary wedge) were formed in the Mesozoic and Cenozoic Jiuquan basin, on the northern margin of the northern Qilian Mountains, (c) due to further compression, brittle thrusts, back-thrusts, and brittle strikeslip faults were formed within the orogenic belt, and (d) the Precambrian metamorphic blocks exposed in the western segment of the northern Qilian Mountains are the allocthons in the Zoulangnanshan volcanic island arc zone. It is inferred that they are the nappe masses or extrusion bodies transported from the Central-southern Qilian microterrane to the present site by the northward overthrusting associated with the Altyn sinistral strike-slip fault.

(A)Piedmont thrust slices of the northern Qilian Mountains

The Jiuquan basin on the northern margin of the northern Qilian Mountains is a successional piedmont basin. It consists of Carboniferous-Permian, Jurassic-Cretaceous, Neogene, and Quaternary terrigenous sediments, as thick as 2000m. There are records of three compressional events, which resulted in three unconformities between Permian and Jurassic, Cretaceous and Neogene, and Neogene and Quaternary respectively. Piedmont thrust faults cut the Caledonian rock formations and the terrigenous sedimentary rocks on the edge of the basin, and formed "under-superimposition type" thrust sequence with northward direction. Based on estimation of balance profile of the thrust fault system, the eastern part differs from the western part in their deformation intensity. Shortening of the western part is 41km (shortening ratio 34.8%) while that of eastern part is 8.95km (shortening ratio 7.96%). The crustal structure of the northern Qilian-Hexi corridor, shown in a deep seismic reflection profile (Wu *et al.*, 1995), indicates that the piedmont fault zone of the northern Qilian inclines to the south and consists of listric-type thrusts. A reflection zone shown here may be a decollement zone with depths of about 10～12km (Fig. 8).

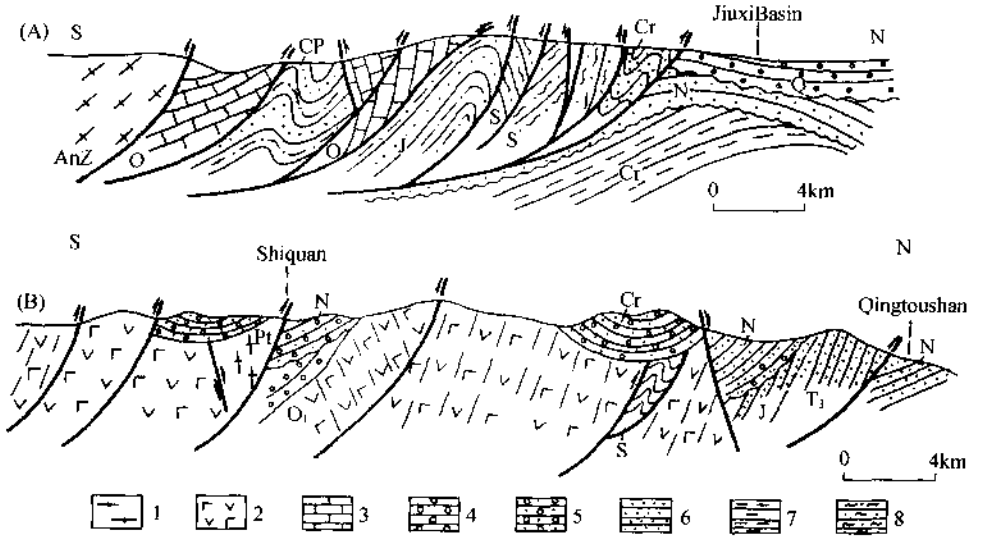

Fig. 8 Tectonic profiles across the northern margin of the northern Qilian Mountains.

(A) The section interpreted by seismic reflection profile for Jiuxi basin. (B) Qingtoushan-Shiquan tectonic section. 1—gneiss; 2—volcanic rock; 3—limestone; 4—conglomerate; 5—sandstones and conglomerate; 6—sandstone; 7—shale; 8—schist. AnZ: Pre-Sinian; O: Ordovician; S: Silurian; CP: Permo-Cahoniferous; Cr: Cretaceous; N: Neogence; Pt: Proterozoic; J: Jurassic; Q: Quaternary.

(B)Jingtieshan extrusion mass and Qilianshan nappe mass

In the western part of the orogenic belt, there occur two large Precambrian metamorphic masses, namely Jingtieshan and Qilianshan, each more than thousends of square kilometers, in the region of the Caledonian trench-arc system. They are long stripes in shape and are parallel to

the orogenic belt and lithologically very similar to the rocks of the Central-southern Qilian microterrane. Field observation shows that the contact between the two masses and the underlying Ordovician volcanic sequence is a low-angle thrust fault. Based on this contact relation, it is inferred that the two masses are allocthonous and were tranported to the present site from the Central-southern Qilian microterrane by the northward low-angle thrust in association with sinistral strike-slip motion of the Altyn fault during the uplift of the said microterrane. Further field studies reveal that the basal plane of the Qilian mass is a gentlydipping low-angle plane, suggesting that it is probably a nappe mass. In contrast, the boundary thrust fault plane of the Jingtieshan mass has a relatively steep angle of 50°～60°, suggesting that it is more likely an extrusion mass.

Orogeny and Plate Dynamics

(1) Architecture and orogenic stage

The formation and evolution of the northern Qilian orogenic belt underwent four stages: epi-orogeny, main orogeny, post-orogeny, and re-orogeny. The formation of deformation regimes of this belt is a combination of deformation, imbrication, and transpression of rock masses from different depths during the whole orogenic process.

(A) Epi-orogenic stage in early Caledonian.

Through the intraoceanic shearing and northward subduction of the Paleo-Qilian ocean lithosphere(522～495Ma), an arc-trench-basin system(486～438Ma) was formed on the leading edge of active continental margin of the southwest part of the Sino-Korea plate(Alashan block) (Fig. 9). Embryonic volcanic island-arc chains were first formed in early Ordovician. Then, a shear system was formed in the subduction complex in the forearc region, followed by formation of the back-arc basin(middle Ordovician-late Ordovician). During the late stage of the epi-orogeny, remnant basins filled with Silurian flysch were formed between back-arc basin and southwest margin of the Sino-Korea plate(Alashan block).

(B) Main orogenic stage in the late Caledonian.

The paleo-Qilian oceanic basin, back-arc basins and remnant basins were closed gradually in this stage. In the mean time, the Central-southern Qilian microterrane collided with the volcanic island arc of Zoulangnanshan along the leading edge of the Alashan block to form Caledonian fold mountain system with crustal shortening and thickening accompanied by the intrusions of the Caledonian granitoids(Fig. 9). The appearance of the Devonian molasse basin marked the end of the Caledonian main orogeny. The deformation structures of this stage overwhelmed the whole collisional orogenic belt. But, during the subsequent post-orogeny and re-orogeny, denudation has completely eroded away the shallow-level brittle structures and has exposed the medium-and deep-level ductile structures in the belt. The ductile structural system was formed during the late Caledonian main orogenic stage by (a) emplacement, thrusting and orogenesis of the ophiolitic zone, (b) accretionary orogenesis of the forearc region before plate collision and

formation of imbricated slices of the subduction complex, (c) compressional orogenesis in the volcanic arc under the coaxial symmetrical compressional stress in NNE-SSW direction, and (d) thrusting orogenesis in the back-arc region.

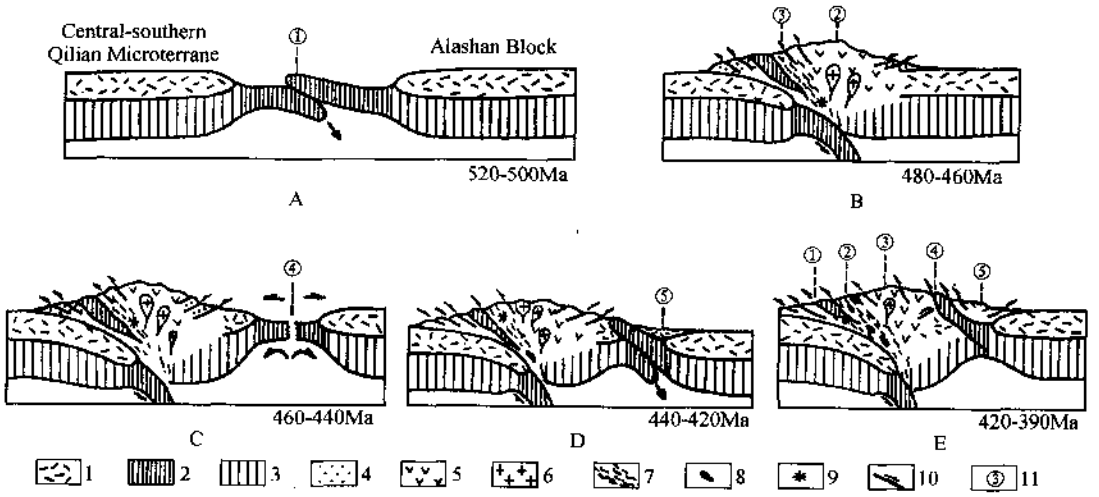

Fig. 9 Epi-orogenic stage, main orogenic stage, and orogenic evolution model during Caledonian period. 1—continental crust; 2—ocean lithosphere; 3—continental lithospheric mantle; 4—subduction complex; 5—arc volcanic rock; 6—arc granitoid; 7—high-pressure metamorphic zone; 8—ultramafic rock; 9—blueschist; 10—thrust fault; 11—tectonic unit. ①palaeo-Qilian ocean, ②volcanic island arc, ③subduction-accretionary complex, ④back-arc basin, ⑤Silurian remnant basin.

(C) Post-orogenic stage (Variscan to Mesozoic).

This was intracontinental orogenic stage, and was characterized by formation of the Devonian-Cretaceous intramontane and piedmont basins along with uplift of the major mountain belt. Ductile deformation was changed to ductile-brittle and brittle deformation during this stage. The main expressions are: (a) formation of the ductile strike-slip shear zone and transpressional zone (350Ma); (b) formation of terrigenous pull-apart basins related to the strike-slip fault; (c) high-femperature and low-pressure normal ductile shear zone accompanied by emplacement of the postorogenic granitoids; and (d) ductile structures formed in the main orogenic stage was reactivated and tranformed into ductile-brittle and brittle as well as small-scale ductile (or brittleductile) normal shear zone which formed at the back of the ductile thrust structure.

(D) Re-orogenic stage (Cenozoic).

The northern Qilian mountains have been involved in the uplift of the Qinghai-Tibetan plateau. The piedmont crustal accretionary wedge composed of the thrust imbricated slices was formed along the northern margin of the northern Qilian mountains and along the southern margin of the Central-south Qilian microterrane as a radial symmetric type on the whole. According to the calculaton by Avouac and Peltzer (1995), present horizontal shortening

rate of the Qilian mountains reaches 15mm/y, only 3mm/y less than that(18mm/y)of eastern Himalaya. This shows that there was intensive compression in Cenozoic. In addition, the sinistral strike-slip movement of the Altyn fault affected intensively the Qilian orogenic belt and might have thrust two Precambrian metamorphic slabs from the Central-southern Qilian microterrane onto the northern Qilian Mountains as two nappe masses.

(2)deformation system and plate dynamic analyses

Deformation system not only can display the basic architecture of various orogenic processes, but also provide the important information for plate kinematics and dynamics through the synthetic studies on its microstructures.

(A)Deep ductile thrust-nappe system and the dynamics of plate subduction and collision.

The deep ductile thrust-nappe system was formed during the Caledonian collisional orogenic stage mainly in the ophiolitic zone and subduction complex zone. Microstructural features of the transverse stretching lineations and rotational strain in the deep ductile thrust-nappe system are the best criteria to judge the relative motion of plates.

In this system of the subduction complex zone, transverse stretching lineations with NNE-SSW direction are perpendicular to the trending of the chains and is a direct evidence for shearing vector of the plate convergence. A great deal of rotational strain criteria indicate a shearing sense from NNE to SSW and show the subduction of the Central-southern Qilian microterrane under the Sino-Korea plate.

In addition, the studies on the P-T path of the high-pressure metamorphic zone in the subduction complex zone indicate that the formation depth of the high-pressure zone was greater than 30km under the conditions of 7.5kb and 300～400℃. The subduction complex zone at the root of the orogenic belt began to exhume at 420Ma(Xu *et al*., 1997)

(B)Ductile strike-slip system and oblique collision

The large-scale dextral strike-slip shear zone, formed along the southern margin of the orogenic belt during early Variscan, indicates that the orogenic belt moved laterally eastward relative to the Central-southern Qilian microterrane. In the meantime, the plate convergence transformed from NNE-SSW to NE-SW and was oblique to the strike of the mountain range. Therefore, it can be inferred that the large-scale dextral strike-slip shear zone was formed by the above oblique collision.

(C)Piedmont crustal accretionary wedge and intracontinental underthrusting

The piedmont crustal accretionary wedge of the orogenic belt, which is composed of the thrust imbricated slices, has been formed during the re-orogeny of the northern Qilian mountain since Cenozoic. On the basis of a deep seismic reflection profile of the crustal structure of the northern Qilian-Hexi corridor(Fig. 10)(Wu *et al*., 1995), formation of the piedmont crustal thrust wedges was related to the southwestward insertion of the Sino-Korea plate into the Qilian Mountains at a low-angle. This kind of intracontinental overthrust or underthrust caused the shortening and uplift of the northern margin of the Qinghai-Tibetan plateau.

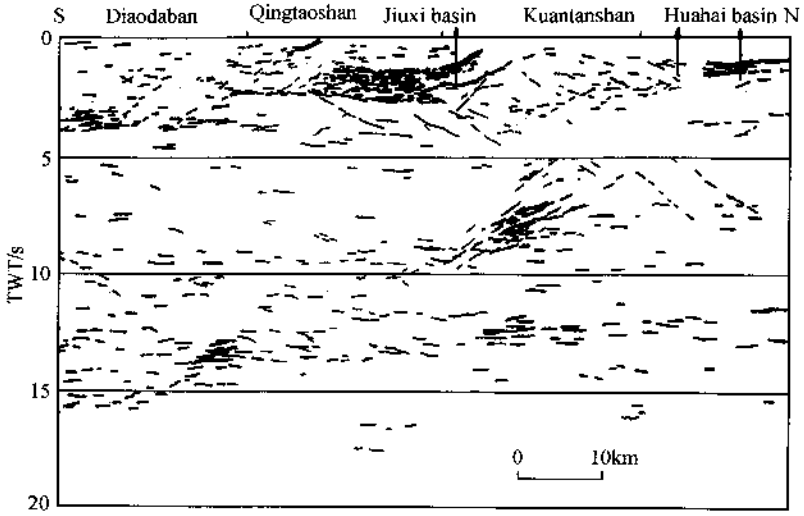

Fig. 10 Deep seismic reflection profile of the northern Qilian-Hexi Corridor(Wu *et al*., 1995).

Acknowledgments

This study was supported by National Natural Science Foundation of China(49732027)and under the auspices of the National Project of China (G1998040800). We thank Profs. Y.M.Feng and L.Q.Xia for providing some valuable data.

References

Avouac, J.P. and Peltzer, G. (1995) Kinematic model of active deformation in central Asia, from Thesis De DOCTORAT DE L'UNIVERSITE PARIS VII.

Bao, P. and Wang, X. (1989) Some new ideas on the genesis of the Dadao Erji Chromite deposit: Mineral Deposits, 8, 3~18.

Feng Y.M. and He, S.P. (1996) Geotectonics and orogeny of the Qilian mountains, China : Geological Publishing House, 40~42. (in Chinese with English abstract)

Jones, R.R. and Geoff Tanner, P.W. (1995) Strain partitioning in transpression zones: J. Struc. Geol., 17, 793~802.

Shen, K., Xu, Zh.Q. and Xu, H.F. *et al*., (1996) Fluid inclusions of HP/LP metamorphic rocks in north Qilian orogenic zone: Continental Dynamics, 1, 134~145.

Wang Q. and Liu X.Y. (1976) Palaeo-oceanographical crust in Qilian Shan area, western China and its geotectonic significance: Scientia Geologica Sinica, 11, 42~55. (in Chinese with English abstract).

Wu, H.Q. (1980) The glaucophane-schists of eastern Qinling and northern Qilian mountains in China: Acta Geologica Sinica, 54, 195~207. (in Chinese with English abstract).

Wu, H.Q., Feng, Y.M. Huo, Y.G., and Song, S.G. (1993) Metamorphism and deformation of blueschist belts and their tectonic implications, North Qilian Mountains, China: J. Metamorphic Geol., 11, 523~536.

Wu, X.Zh., Wu, Ch.L., Lu, J. and Wu, J. (1995) Research on the fine crustal structure of the northern Qilian-

Hexi corridor by deep seismic reflection: Acta geophysica Sinica, 38 (Suppl. Ⅱ), 29～35. (in Chinese with English abstract).

Xia, L.Q., Xia, Z.Ch. and Xu, X.Y. (1996) The petrogenesis of marine igneous rocks: Geological Publishing House, 153P. (in Chinese).

Xiao, X.Ch., Chen, G.M. and Zhu, Zh.Zh. (1978) The geologic-tectonic significance of ophiolite in Qilian mountains: Acta Geologica Sinica, 52, 287～295. (in Chinese with English abstract).

Xu, Zh.Q. (1995) Large shear zones in the main orogenic belts of China: Episodes, 18, 41～43.

Xu, Zh.Q., Xu, H.F. and Zhang, J.X. *et al*. (1994) The Zoulangnanshan Caledonian subductive complex in the northern Qilian mountains and its dynamics: Acta Geologica Sinica, 68, 1～15. (in Chinese with English abstract).

Xu, Zh.Q., Zhang, J.X., Xu, H.F., Wang, Z.S., Li, H.B., Yang, T.N., Qiu, X.P., Zeng, L.S., Sen, K., and Chen, W. (1997) Ductile shear zones in the main continental mountain chains of China and their dynamics: Geological Publishing House. 294P. (in Chinese with English abstract).

Zhang, J.X., Xu, Zh.Q. and Chen, W. (1997) The exploration to the time of subduction accretionary complex / volcanic arc in the central sector of northern Qilian: Petrology and Mineralogy, 16, 112～119. (in Chinese with English abstract).

Zhang, Zh.M. (1989) High pressure-low temperature metamorphism in North Qilian, China. In The Expolation for Geological Science of China (eds., Cui, G.Zh. and Shi, B.H.), Publishing House of Beijing University, 273～295. (in Chinese with English abstract).

Zuo, G.Ch. (1986) The early Paleozoic collision and suture in the northern Qilian region. Collected Works for Structure of the Northern Plates of China: Geological Publishing House, 27～35. (in Chinese with English abstract).

Zuo, G.Ch. and Liu G.Ch. (1987) The evolution of tectonics of early Paleozoic in North Qilian Range, China: Scienta Geologica Sinica, 1, 14～24. (in Chinese with English abstract)

中国西北部北祁连造山带的构造格架及造山作用

许志琴 张建新 李海兵

(中国地质科学院地质研究所)

摘 要 位于中朝板块西南部和中-南祁连地体之间的北祁连造山带是一条线性很强的典型加里东碰撞造山带。它的形成及演化经历了早古生代早期以来的祁连洋盆的开启、消减、洋壳向北俯冲、"陆-陆"碰撞,以及后造山阶段的陆内会聚和新生代以来最后隆升崛起的地质过程。通过宏观与微观研究,揭示了形成于北祁连造山带造山过程的构造体制可划分为早期深层韧性变形体系和浅层脆性变形体系。

深部韧性构造系统构成了造山带基本构造格架,其中托莱山蛇绿岩推覆体为祁连洋盆消减过程中洋内剪切至大洋岩石圈俯冲阶段产物;走廊南山俯冲杂岩带中的叠置岩片是加里东期板块俯冲和碰撞过程中造山带根部的板底垫托作用及高压变质作用的反映。北祁连造山带南缘大型韧性平移剪切带以及两侧的挤压转换带形成于华力西期后造山斜向碰撞作用背景之下,伴

随后造山花岗岩侵位形成小型伸展型剪切带。

以逆冲及走滑为特征的浅层脆性应变反应了后造山阶段(泥盆纪至白垩纪)的挤压转换作用的存在。新生代的再造山作用使北祁连山体最后崛起。山前逆冲断裂系的形成与阿拉善地块向西南方向陆内俯冲有关。阿尔金左行平移作用可能使中-南祁连地块的古老变质系往北推移在北祁连奥陶系火山岛弧带之上。

关键词 构造格架 变形体系 造山作用 动力学

阿尔金断裂两侧构造单元的对比及岩石圈剪切机制[1]

许志琴　杨经绥　张建新　姜　枚　李海兵　崔军文
（中国地质科学院地质研究所　北京　100037）

摘　要　中亚最大的阿尔金走滑断裂系构成了青藏高原的北部边界，阿尔金北缘断裂及阿尔金左行走滑断裂（阿尔金主断裂）所夹持的阿尔金地体自北往南由敦煌地块、北阿尔金加里东俯冲杂岩带、中阿尔金地块及南阿尔金加里东俯冲-碰撞杂岩带组成，研究表明这些单元分别可与阿尔金主断裂带东侧的阿拉善地块、北祁连俯冲杂岩带、中-南祁连地块及柴达木北缘加里东俯冲-碰撞杂岩带相对比。特别通过南阿尔金与柴达木北缘榴辉岩带的详细对比，发现它们具有相似的地质背景、产状、矿物组合、岩石地球化学、原岩特征、温度压力条件、退变质作用和围岩特征以及非常接近的峰期变质时代（500～503Ma 和 495Ma），可能构成了中国又一条被巨型走滑断裂所切割的高压-超高压变质带（?），并为阿尔金断裂带左行走滑 400km 的确定提供了科学依据。天然地震探测剖面显示阿尔金主断裂由近直立低速低密度的物质组成，与低角度向南倾的阿尔金北缘断裂之间夹持由高速高密度组成的阿尔金地体。阿尔金北缘断裂与阿尔金主断裂在 80km 深度处交汇，并继续向南陡倾下插到 150km，反映出塔里木地块向南陆内俯冲于阿尔金山及柴达木盆地之下。代表上地幔物质剪切流动矢量的高强度各向异性，显示了剪切作用可抵达上地幔，阿尔金断裂的岩石圈剪切作用可能与塔里木地块往南俯冲有关。

关键词　左行走滑　俯冲-碰撞杂岩带　构造单元对比　岩石圈剪切断裂　陆内俯冲

阿尔金断裂带位于青藏高原北部边缘，为亚洲大陆内部巨型的 NEE 向断裂体系，它以具有巨大左行走滑位移和非常醒目的线性特征而引起中外地质学家的注目，断裂的东北端切割祁连造山带及阿拉善地块，西南端插入昆仑造山带，把塔里木地块和柴达木地块分隔开来，一些重要的构造线（如高压变质岩和蛇绿岩等）至阿尔金断裂带均突然终止，或被改变方向。其动力学意义可与中国东部的郯庐断裂系以及美国西部的圣安德列斯断裂相媲美。不少学者将之纳入青藏高原隆升及演化的统一地球动力学体系，并认为阿尔金断裂的研究是解决青藏高原隆升和动力学问题的关键所在[1～4]。

然而，长期以来，人们的注意力主要集中在对阿尔金断裂的巨型走滑断裂系的研究[2,5～12]，而对阿尔金断裂系所夹持的古地质体的研究涉及较少，尤其是很少把它们与相邻的构造单元特别是祁连造山带联系起来。近年来，一些学者开始注意到对阿尔金断裂系

---

[1] 地质学报，1999 年第 73 卷第 3 期。
注：本文为原地质矿产部“九五”重点基础项目（编号 9501106）、国家自然科学基金重点项目（编号 49732027）和国家“973”项目成果。
本文 1999 年 6 月收到，7 月改回，任希飞编辑。

所夹持的蛇绿岩、高压变质岩及前寒武纪基底变质岩的研究[13~20]；少数学者已开始注意到阿尔金断裂系两侧地质体的相似性，并进行初步的对比[21~25]。葛肖虹等[24,25]根据区域对比认为：柴达木盆地(地块)对应于南塔里木盆地(地块)；祁连山对应于塔里木中部(其中北祁连对应于满加尔拗陷，中祁连对应于塔中隆起)；北塔里木地块对应于阿拉善地块。根据几年来我们对阿尔金和祁连山进行的地质及地球物理研究，认为阿尔金断裂带不仅仅是一个巨型断裂系，也是一个经历过多期复杂地质演化历史，由不同层次、不同时期和形成于不同构造环境地质体所组成的造山带，并与相邻造山带有着密不可分的关系。在阿尔金山中，存在近 EW 向(NWW-SEE)和 NEE-SWW 两个方向的构造线。前者主要由一些古老地质体所组成，如蛇绿岩、俯冲杂岩、中深变质岩石等，记录了阿尔金主断裂活动之前的地质演化历史，与祁连山及柴达木北缘可以对比；而后者切割了前者，与阿尔金左行走滑活动有关。横穿阿尔金山的地震探测也显示，阿尔金断裂带的深部物质主要由两部分所组成，一部分为低速低密度的物质，其上地幔具有 NEE 向各向异性；另一部分为被低速低密度物质所围绕的由高速高密度物质所组成的阿尔金地体，具有近 EW 向的各向异性。本文通过对阿尔金山与祁连山及柴达木北缘的构造单元对比，特别是最近分别在南阿尔金和柴达木北缘所发现的榴辉岩的详细对比，来确定阿尔金断裂可能的最大走滑量；结合深部地震探测，探讨现今阿尔金断裂带的特征、性质及形成机制。

1 阿尔金地体的基本组成及与祁连山-柴达木北缘的对比

阿尔金地体主要是指阿尔金北缘逆冲断裂和阿尔金南缘走滑断裂(即阿尔金主断裂)之间的地区，它主要由不同时代的近 EW 向分布的古地质体所组成(图 1)，并与两侧的边界断裂有一定的交角。这些古地质体从北向南包括：

(1)敦煌地块　分布在阿尔金构造带东北边缘(北塔里木南缘)，主要由 Ar-Pt_1 敦煌群和米兰群角闪岩相-麻粒岩相的变质杂岩所组成，其形成时代为 2460～2789Ma[14,26,27]，这套岩石被认为是塔里木地块古老变质基底的一部分。

(2)北阿尔金俯冲杂岩带　主要分布在红柳沟-拉配泉一带，与北部的太古代米兰群和南部的中新元古代岩石为断层接触。由浅变质的火山岩、火山碎屑岩及碎屑岩所组成，并伴生具蛇绿岩特征的超基性岩(蛇纹岩)、辉长岩和基性熔岩[28]，并在红柳沟发现有代表洋脊扩张的基性岩墙群，在拉配泉等地还具有保存较好的枕状玄武岩。这些岩石的变质程度以浅变质的低绿片岩相-绿片岩相为主，局部地段发现有含蓝闪石的绿片岩❶及高压泥质岩的存在[13,29]。变基性火山岩中的角闪岩的 Ar-Ar 测定获得 457Ma 的年龄❷。

(3)中阿尔金地块　主要由古元古界(?)阿尔金群及中、新元古界的长城系，蓟县系，青白口系和震旦系所组成。阿尔金群长期以来被认为是以角闪岩相为主的变质杂岩，并作为塔里木变质基底的一部分[26]。中新元古代的岩石主要由浅变质的稳定的大陆边缘环境的碎屑岩、碳酸盐岩所组成，夹少量火山岩，与北部的北阿尔金俯冲杂岩带为断层接触关系。其中碳酸盐岩中含有叠层石化石，并作为其时代的主要依据。

---

❶ 青海省地质局. 1:20 万俄博梁地质报告. 1991.

❷ 张建新. 阿尔金构造带西段加里东期山根的初步研究. 中国地质科学院博士论文, 1998.

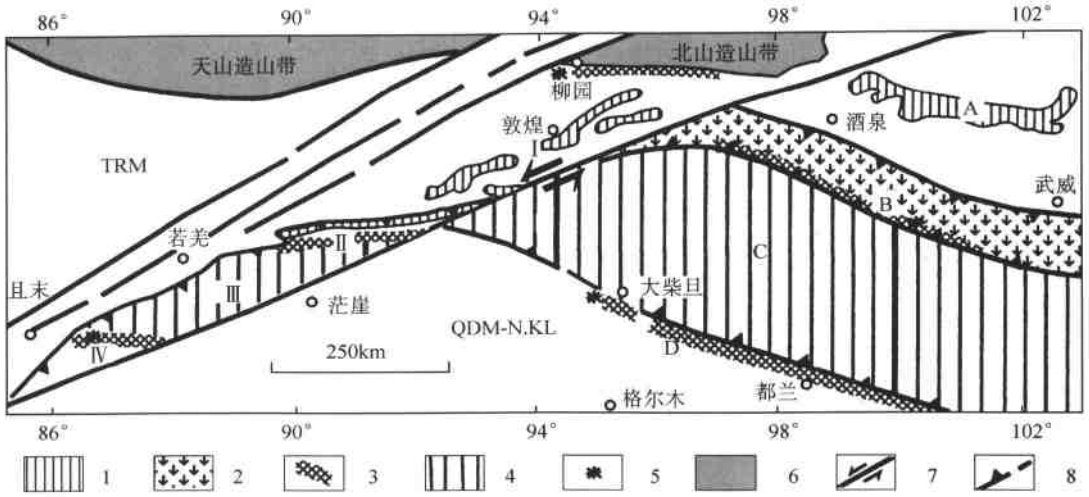

图 1 阿尔金地体与祁连-柴达木北缘构造单元对比图

(原始资料据文献[15, 18, 27, 32, 33])

Fig. 1 Map showing the tectonic units comparison between Altun terrane and Qilian-northern Qaidam

(original data from references[15, 18, 27, 32, 33])

1—前寒武纪变质基底;2—加里东期火山岛弧带;3—俯冲及碰撞杂岩带;4—中-南阿尔金及中祁连地块;5—榴辉岩;6—相邻造山带;7—左行走滑断裂;8—逆冲断裂;Ⅰ—敦煌地块;Ⅱ—北阿尔金俯冲杂岩带;Ⅲ—中阿尔金地块;Ⅳ—南阿尔金俯冲-碰撞杂岩带;A—阿拉善地块;B—北祁连俯冲杂岩带;C—中南祁连地块;D—柴达木北缘俯冲-碰撞杂岩带;TRM—塔里木地块;QDM—N. KL—柴达木-昆北地块

1—Precambrian metamorphic basement; 2—Caledonian volcanic island arc zone; 3—subduction and collision complex zone; 4—central Altun and central Qilian block; 5—eclogite; 6—adjacent orogenic belt; 7—sinistral strike-slip fault; 8—thrust fault; Ⅰ—Dunhuang block; Ⅱ—northern Altun subduction complex zone; Ⅲ—central Altun block; Ⅳ—southern Altunsubduction-collision complex zone; A—Alxa block; B—northern Qilian subduction complex zone; C—central-southern Qilian block; D—northern Qaidam subduction-collisional complex zone; TRM—Tarim massif; QDM—N. KI-Qaidam-northern Kunlun massif

(4)西南阿尔金俯冲-碰撞杂岩带 近年来在阿尔金的西南部原定为阿尔金群中发现有高压榴辉岩[15,18]及具有孔兹岩系特征的麻粒岩相岩石,初步确定其变质峰期时代为 450～500Ma[18,19]。因此,在阿尔金构造带的南侧可能存在一条加里东期的俯冲-碰撞杂岩带,这些榴辉岩及麻粒岩相岩石可能就是其山根岩石的出露部分。

以上 4 个不同时代构造单元由近 EW 向的剪切带(断裂)为边界,新生代以来重新活动,显示出活动构造特征。

阿尔金地体中的这 4 个地质单元可分别与阿尔金断裂东侧的阿拉善地块、北祁连俯冲杂岩带、中南祁连地块及柴达木北缘俯冲-碰撞杂岩带对比(表 1)。

阿拉善地块主要由阿拉善群和龙首山群所组成,为一套中深变质的变沉积岩及变火山岩,其岩石组合与敦煌地块非常相似,这套岩石被年龄为 1719Ma 的花岗岩侵入,显示其时代应为古元古代[30]。

北祁连俯冲杂岩带主要由蛇绿岩、蛇绿混杂岩和高压蓝片岩所组成,蛇绿岩的时代为早寒武世-奥陶纪,一些学者认为还可能有代表早期裂谷作用的新元古代的蛇绿岩[31];高压

表 1 阿尔金山和祁连山及邻区构造单元对比

Table1 The comparison of tectonic units between Altun, Qilian and adjacent area

祁连山及邻区	阿尔金山
阿拉善地块	敦煌地块
阿拉善地块南大陆边缘	不明显
北祁连加里东火山岛弧带	?
北祁连俯冲杂岩带	北阿尔金俯冲杂岩带
祁连地块	阿尔金地块
柴达木北缘俯冲-杂岩带	南阿尔金俯冲-碰撞杂岩带

蓝片岩的时代为 440～460Ma[32-34]。

中南祁连地块，主要由前寒武纪变质基底岩石所组成，古元古代岩石被称之为熊源群、化隆群等，由角闪岩相为主的变质岩石所组成；中新元古代岩石被称之为党河群（相当于长城系）和托莱南山群（相当于蓟县-青白口系），由浅变质的碳酸盐岩、碎屑岩夹火山岩所组成[35]。

最近，在柴达木盆地北缘，在原定为古元古界达肯达坂群中发现有榴辉岩和石榴橄榄岩[36,37]，本文的研究显示其榴辉岩的时代为加里东期，因此，它们组成了柴达木北缘加里东俯冲-碰撞杂岩带，可能为加里东造山带山根岩石。

这些不同时代和性质的构造单元呈 NWW 向分布，与阿尔金山中不同构造单元的边界相似，主要以韧性剪切带及断层为边界，它们在新生代又重新活动。

以上阿尔金山和祁连山及相邻区域 4 个不同单元的对比显示，它们具有明显的相似性。当然，由于沿走向的变化以及研究程度（特别是阿尔金地区）较低，阿尔金两侧地质体的对比还不是一一对应，如在北祁连发育的加里东期的火山岛弧及弧后盆地带，在阿尔金山中还没有发现；在阿拉善地块南侧的早古生代大陆边缘建造在阿尔金山中也不明显。

2 南阿尔金及柴达木北缘俯冲-碰撞杂岩带的对比——又一条被巨型走滑断裂切割的高压-超高压变质带(?)

在中国东部的郯庐断裂两侧，分布有著名的大别-苏鲁高压-超高压变质带，构成世界上最大规模的高压-超高压变质带，并被许多学者作为郯庐断裂巨大左行位移的证据之一[38,39]。近年来，在中国西北部的阿尔金山南部及柴达木盆地的北缘，也先后发现有分布在长英质片麻岩中的榴辉岩[15,37]，它们位于亚洲大陆最大的走滑断裂——阿尔金断裂的两侧。研究表明这两处的榴辉岩在野外产状、围岩特征、岩石及矿物组合、形成的 *PT* 条件、地球化学及原岩特征以及它们的形成时代均非常相似。因此，我们认为阿尔金榴辉岩和柴达木北缘榴辉岩可能同为加里东期陆壳俯冲及碰撞造山作用的产物，很可能是继大别-苏鲁高压-超高压变质带之后，在中国发现的又一条被巨型走滑断裂所切割的高压-超高压变质带(?)。

2.1 阿尔金南段榴辉岩的基本特征及形成时代

2.1.1 榴辉岩的地质背景及产状

阿尔金南段的榴辉岩分布在且末的江尕勒萨依沟-玉石矿沟一带[18]，呈透镜状或布丁

状产于原认为是古元古界阿尔金群的片麻岩之中[26],其透镜体的长轴与片麻岩的片麻理走向一致。这些片麻岩主要包括含石榴石的长英质片麻岩、含石榴石的斜长角闪片麻岩等,片麻理的走向为90°～120°,总体上显示出角闪岩相的矿物组合,局部也可能达到高角闪岩相甚至麻粒岩相❶,还没有发现有高压矿物组合的残留。

2.1.2 榴辉岩的矿物学及岩石学特征

榴辉岩总体上呈等粒状,具有弱的拉伸线理和叶理,主要由绿辉石和石榴石定向排列所组成。峰期榴辉岩相的矿物组合为石榴石+绿辉石+金红石+多硅白云母+石英,电子探针成分分析显示绿辉石的硬玉分子含量为30～36mol%;大部分榴辉岩的石榴石较细(0.5～1.0mm),成分较均匀,不显示明显的成分环带,其端元分子为:Prp28～34, Alm35～42, Grs27～32, Sps0.8～1.3(本文出现的英文矿物代号均引自R.Kretz, 1983[40]),而少部分榴辉岩的石榴石颗粒较粗(>3mm),且具有明显的成分环带,其端元分子为:Prp17～40, Alm30～53, Grs22～31, Sps0.8～4.5。从核部到边部,MgO、CaO升高,MnO、FeO降低,显示出进变质生长环带的特征[41,42]。在最边部,石榴石MgO、CaO又有所减小,MnO和FeO则有升高的趋势,显示出退变质过程中形成的扩散环带特征。多硅白云母的硅原子数为3.49(基于11个氧原子)。

榴辉岩显示出明显的减压结构:一些绿辉石边部以形成低Na的单斜辉石(Jd为15%～20%(mol))和奥长石(An=10～20)组成的蠕虫状后成合晶为特征;多硅白云母的边部形成黑云母和奥长石(An=10～20)组成的后成合晶。石榴石的边部则多被角闪石和斜长石组成的次生边或冠状体所围绕。金红石则大多具有钛铁矿边。

稀土元素的球粒陨石标准化配分模式主要以轻稀土平坦和略富集为特征,没有明显的Eu异常或略具正异常。显示具有"E"或"T"型MORB(过渡型洋脊拉斑玄武岩)的特征(图2(a))。少数样品显示出轻稀土亏损的特征。榴辉岩全岩的$^{147}Sm/^{144}Nd=0.1686$, $^{143}Nd/^{144}Nd=0.512704$, $\varepsilon_{Nd}(500Ma)=3.2$, $\varepsilon_{Nd}(0)=1.19$,为亏损地幔来源,可能受到地壳物质的轻度混染。

2.1.3 形成的温压条件

利用Grt-Cpx地质温度计,再根据Ab=Jd+Qtz的变质反应压力计,估算其榴辉岩峰期的$t=731～811℃$, $P>1.5GPa$。如果利用的Grt-Omp-Phe压力计和Grt-Omp温度计[43]和Ge0-Calc程序[44],得到的温压条件为$t=860℃$, $P=3.0GPa$(图3(a)),这种温压条件已在柯石英的稳定范围内,但到目前为止,还没有发现有柯石英的存在。在减压过程中,还经历了麻粒岩相($P=1.1～1.4GPa$, $t=750℃$)及角闪岩相($P=0.63～0.95GPa$, $t=619～738℃$)的变质作用,构成顺时针Pt轨迹❶。

2.1.4 榴辉岩的形成时代

选择新鲜退变质较弱的榴辉岩分别进行Sm-Nd全岩-矿物等时线和锆石的U-Pb年代学测定,其中测得全岩-石榴石-绿辉石的Sm-Nd等时线年龄为500±10Ma;4组锆石U-Pb同位素测定获得的表面年龄很好地落在一致线上,并得出其权重平均值为503.9±5.3Ma[18](图4(a))。两种方法获得的基本一致的年龄数据反映了榴辉岩的峰期变质时代。

❶ 张建新.阿尔金构造带西段加里东期山根的初步研究.中国地质科学院博士论文,1998.

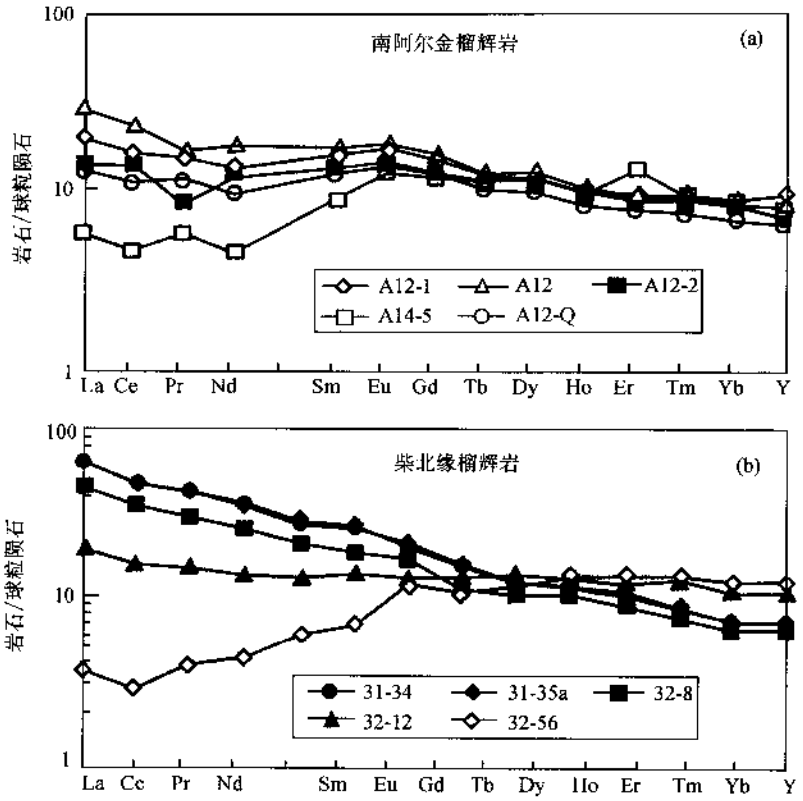

图 2 南阿尔金(a)及柴达木北缘(b)榴辉岩的稀土元素球粒陨石标准化图

Fig.2 The chondrite-normalized REE distribution pattern for the eclogites from southern Altun(a)and northern Qaidam(b)

除了榴辉岩外,在榴辉岩出露的南侧 30km 的吐拉一带还发现由富铝片麻岩和夹于片麻岩中的石榴角闪二辉麻粒岩所组成的孔兹岩系,其中石榴角闪二辉麻粒岩中保留有早期高压麻粒岩的特征❶,其 U-Pb 和 Ar-Ar 同位素测定显示其峰期变质时代为 447～462Ma[19],与榴辉岩一起构成了代表加里东山根的俯冲-碰撞杂岩带。

2.2 柴达木北缘榴辉岩的基本特征及形成时代

2.2.1 柴达木北缘榴辉岩的地质背景及产状

柴达木北缘榴辉岩发现于柴达木盆地北缘大柴旦镇西北的鱼卡河附近,1m 到数十米大小不等的榴辉岩块体呈透镜状分布于达肯大坂群(Pt_1(?))的含石榴石的片麻岩(片岩)之中[37]。榴辉岩透镜体的长轴平行于 NWW-SEE 走向的片麻理(片岩)围岩。围岩主要有含石榴石的花岗质片麻岩、斜长角闪质片麻岩、含石墨的片麻岩及石榴白云母石英片岩等,还没有发现高压矿物组合,它们长期以来被归为古元古代的达肯大坂群,作为柴达木地块的变质基底岩石[35],但缺少同位素证据。

❶ 张建新.阿尔金构造带西段加里东期山根的初步研究.中国地质科学院博士论文,1998.

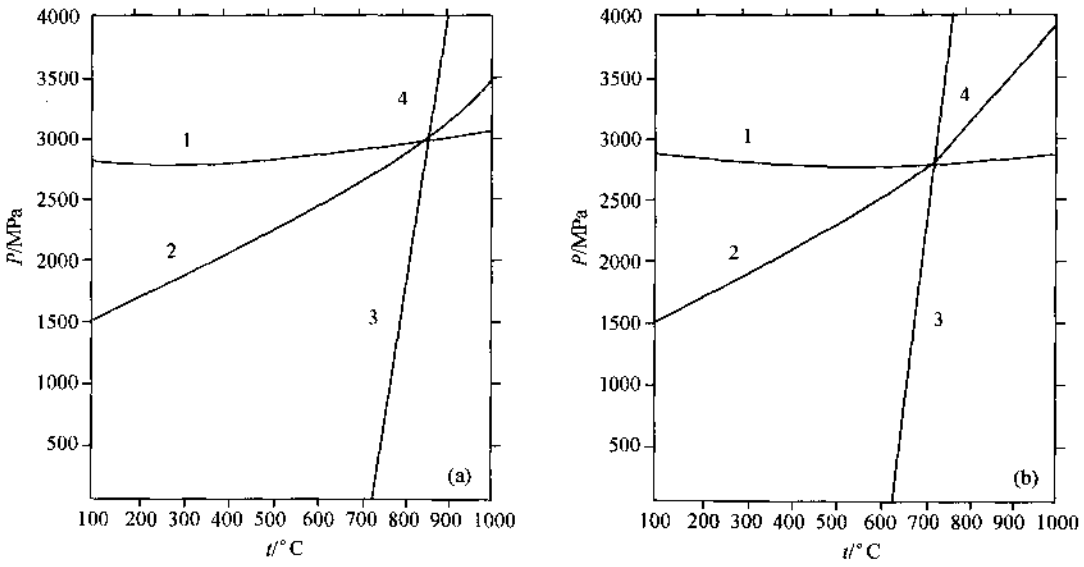

图 3 南阿尔金(a)及柴达木北缘(b)榴辉岩峰期的 P-t 条件

Fig.3 The P-t diagram showing peak metamorphic condition for southern Altun(a)and northern Qaidam

1、2、3、4 分别代表单变反应曲线(1, 2, 3 and 4 represent univariant reaction lines):

1:3Al-Cel + 2Grs + Prp = 3MS + 6Di; 2: Alm + 3Al-Cel + 2Grt = Ms + 3Hed + 6Di; 3: 3Di + Alm = 3Hed + Prp;

4: 2Alm + 3Al-Cel + 2Grs = Prp + 3Ms + 6Hed

Al-Cel:铝绿磷石,其它矿物缩写据 R. Kretz, 1983[39]

Al-Cel: Aluminium-Celedonite other abbreviations for minerals after Kretz(1983)[39]

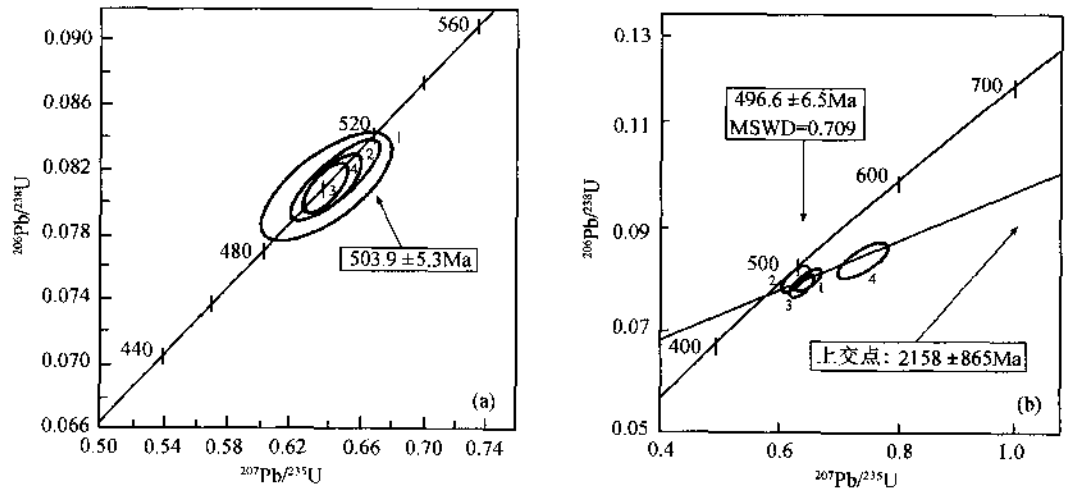

图 4 南阿尔金(a)及柴达木北缘(b)榴辉岩的锆石 U-Pb 测定结果

Fig.4 U-Pb analytical results of zircons for eclogites of southern Altun(a)and northern Qaidam(b)

2.2.2 岩石学及矿物学特征

保存较好的榴辉岩总体上呈等粒状，部分榴辉岩显示出由多硅白云母和绿辉石定向分布所组成的叶理和拉伸线理。峰期榴辉岩相的矿物组合为石榴石＋绿辉石＋金红石＋多硅白云母＋石英±黝帘石，具有少量退变质作用形成的角闪石和斜长石。绿辉石的硬玉分子含量为38mol%～41mol%；多硅白云母的硅原子数为3.35～3.49(基于11个氧原子)。一些榴辉岩中的石榴石成分变化较大，其端元组分为：Prp10～32，Alm39～56，Grs22～36，Sps0.6～9，具有明显的成分环带，从石榴石的核部到边部，MgO增加，CaO在略有增加后明显降低，而MnO和FeO则明显减小。这些特征显示出进变质生长环带的特征。在最边部的狭窄范围内，石榴石的MgO和CaO又有减小的趋势，MnO和FeO则有升高的趋势，是退变质过程中形成的扩散环带。总体上，虽然与阿尔金榴辉岩中石榴石的成分环带有所区别，但它们都具有进变质生长环带和最边部很窄范围的退变质扩散环带，显示它们在形成过程中具有类似热动力条件。

榴辉岩具有明显的减压结构，在绿辉石边部形成低Na的单斜辉石和斜长石组成的蠕虫状或毛发状后成合晶为特征；石榴石的边部则多被角闪石和斜长石组成的次生边或冠状体所围绕。金红石则大多具有钛铁矿的退变边。

与南阿尔金榴辉岩相似，柴达木北缘榴辉岩的稀土元素的球粒陨石标准化配分模式主要以轻稀土平坦、略富集和中度富集为特征，没有明显的Eu异常。显示具有“E”或“T”型MORB(过渡型洋脊拉斑玄武岩)的特征，LREE中度富集的稀土特征可能与榴辉岩的原岩受到地壳物质的混染有关。少数样品显示出轻稀土亏损的特征(图2(b))。榴辉岩全岩的$^{147}Sm/^{144}Nd=0.1687$，$^{143}Nd/^{144}Nd=0.512677$，$\varepsilon_{Nd}(500Ma)=2.6$，$\varepsilon_{Nd}(0)=0.65$，为亏损地幔来源，但可能受到地壳物质的混染。

2.2.3 形成的温压条件

杨经绥等[37]根据Grt-Cpx地质温度计和Ab＝Jd＋Qtz的变质反应压力计，估算其榴辉岩峰期的$t=722\pm123℃$，$P=2.2GPa$。我们进一步利用的Grt-Omp-Phe压力计和Grt-Omp温度计[43]和GeO-Calc程序[44]，得到的温压条件为$t=730℃$，$P=2.8GPa$(图3(b))。这种温压条件与分布在同一套达肯达坂群片麻岩中的石榴石橄榄岩的峰期变质温度相似[36]，已进入柯石英的稳定范围，但到目前为止，还没有发现有确切柯石英的存在。虽然李怀坤等[45]等报道了柴达木北缘榴辉岩中发现有柯石英，但从文中的照片和拉曼谱线来看，所确定柯石英的521峰值只是背景值。对其退变质的P-t条件还未估算，但从与阿尔金榴辉岩类似的减压结构和退变质矿物组合来看，应具有与阿尔金榴辉岩相似的退变条件和P-t轨迹。

2.2.4 峰期及折返年龄

选择保持较好的榴辉岩分别进行锆石的U-Pb和同位素Ar-Ar同位素测定，测定结果见表1和图4(b)和图5。从榴辉岩中选出的1、2、3号锆石具有较好的多晶面发育，表现出变质锆石的特征，其测定结果显示t_{206}，t_{207}，表面年龄在误差范围内一致，并大致落在一致线上，并得出$^{206}Pb/^{238}U$表面年龄统计权重平均值为494.6±18Ma，代表峰期榴辉岩相变质的年龄。4号锆石点远离一致线，得到古元古代的上交点年龄，可能与原岩受到古元古代地壳的混染有关，这与稀土元素和Nd同位素的结果一致。

同样样品榴辉岩的多硅白云母被分选出用于^{39}Ar-^{40}Ar年代学测定。测定结果获得的坪年龄为466.7±1.2Ma，等时线年龄为465.94Ma，此年龄值代表了榴辉岩在折返过程中

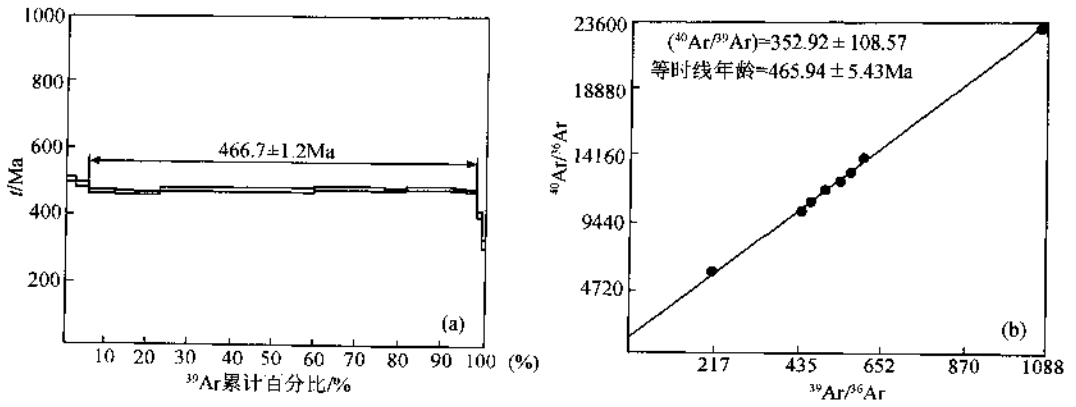

图 5 柴达木北缘榴辉岩多硅白云母的年龄谱(a)及等时线(b)

Fig.5 The age spectra(a) and isochron diagram(b) of phengite from eclogite of northern Qaidam

的冷却年龄。

除榴辉岩外,柴达木北缘还具有石榴橄榄岩、石榴辉石岩(高压麻粒岩?)等,虽然还缺少年代学证据,但从它们的岩石学特征及产出状态来看,是与榴辉岩一起构成了加里东期山根的俯冲-碰撞杂岩带。

2.3 南阿尔金-柴达木北缘加里东期俯冲-碰撞杂岩带——阿尔金左行平移 400km 的证据

由于榴辉岩特殊的产出环境,把它与邻区所出露的榴辉岩进行对比将具有重要的区域构造意义。就目前的资料,阿尔金构造带及邻区有 4 处发现有榴辉岩,除南阿尔金以外,其它 3 处分别是柴达木北缘大柴旦、北山柳园和北祁连中段[27,32,37]。北祁连的榴辉岩与高压蓝片岩和具有洋壳残片性质的蛇绿岩伴生,其形成温压为 $t = 340 \pm 10$℃, $P = 0.8 \pm 0.1$GPa[32],这是典型的 Franciscan 型的"冷"榴辉岩[46],显然与本文所讨论的榴辉岩不同。而柴达木北缘大柴旦榴辉岩和北山柳园的榴辉岩则与阿尔金西段的榴辉岩相似,它们均产在长英质片麻岩围岩中,其围岩均被定为是古元古代的、以角闪岩相变质作用为特征的岩石,其形成温度都大致在 700~800℃之间,压力大于 1.5GPa[27,37]。北山柳园的榴辉岩地质体分布在阿尔金主断层东段北侧的北山地区,敦煌地块的北侧,与阿尔金西段榴辉岩处于阿尔金主断裂同一侧,且相隔甚远,因此,很难把它与阿尔金南段的榴辉岩地质体联系起来,其区域构造意义有待于进一步的研究。柴达木北缘大柴旦榴辉岩地质体分布在阿尔金主断裂的东侧,通过以上分别对它们的讨论,可以看出这两处的榴辉岩的地质背景、产状、矿物组合、岩石地球化学及原岩特征、形成温压条件、退变质作用、围岩特征以及形成时代等均非常相似。因此,我们认为,阿尔金西段的榴辉岩和柴达木北缘的榴辉岩可能同为加里东期的大陆俯冲及陆-陆碰撞造山作用的产物,形成同一条俯冲-碰撞杂岩带,后来被阿尔金断裂的左行平移作用所切割,构成了继被郯庐断裂所切割的大别-苏鲁高压-超高压变质带后,在中国发现的又一条被[illegible]型走滑断裂所切割的高压-超高压变质带(?)。如按它们现在产状及分布特征,结合阿尔金及柴达木北缘-祁连地区其它地质体的对比研究,估计阿尔金断裂的位移大约在 400km 左右。

3 岩石圈剪切断裂及陆内俯冲作用

阿尔金走滑断裂带在平面上由一系列平行断裂组成，主断裂位于南侧，在地表宽 6～15km，长 1600km，总体为直线型，SW 端呈弧形[7]。阿尔金主断裂具明显的走滑性质，现代水系的被切割及沿主断裂大量地震活动显示其是一条至今仍在活动的走滑断裂。以走滑断裂为中心，出现两侧反向逆冲、在阿尔金断裂带北西侧为阿尔金北缘逆冲断裂，其后部发育同倾向的正断层，使山体明显垂向挤出。

最近中法乌图美仁-茫崖-若羌天然地震探测剖面提示了阿尔金主断裂是一条近直立的岩石圈断裂，延深达 100～140km[47]。阿尔金主断层的深部在地球物理场上显示宽为 40km 的低速带，由低速低密度物质组成，反映阿尔金主断层的深部可能为韧性的糜棱岩所组成，深部的韧性剪切加热使该剖面上的 100km 深度的等温面在断裂带中上拱至 70km 深处[48]，表示可能存在部分熔融作用。代表上地幔物质剪切流动矢量的 SKS 波各向异性强度大，且与断裂带的 NEE-SWW 向一致(图 6)，反映了该断裂带可延至上地幔，并在深部同样发生了剪切位移。

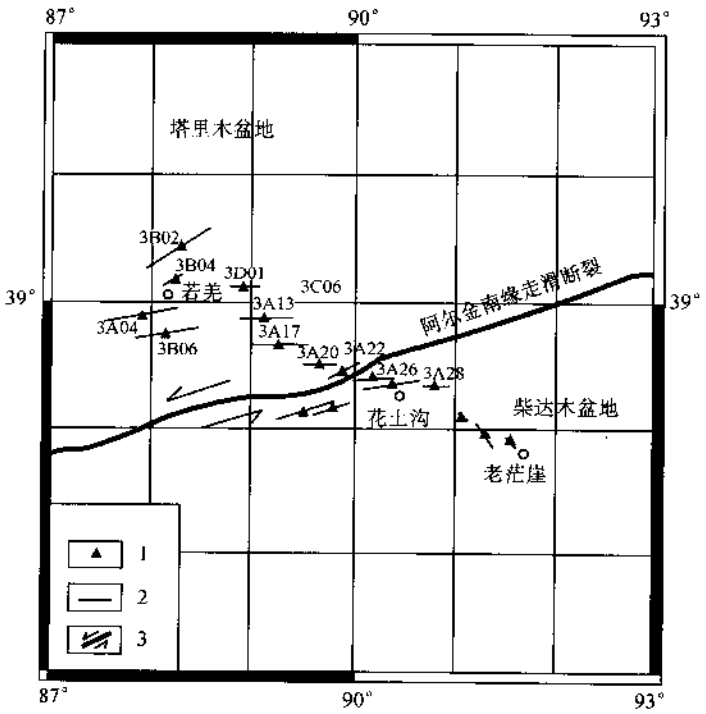

图 6 横穿阿尔金山的 SKS 波各相异性图

Fig.6 The anisotropy of SKS wave across the Altun Mountains

1—三分量台站；2—SKS 波各相异性的方向和强度(线段的长度代表强度的大小)；3—走滑断裂

1—3-component stations; 2—the direction and magnitude of anisotropy(the length of bars represents the magnitude of anisotropy); 3—strike-slip fault

天然地震探测还显示阿尔金山与塔里木盆地为界的阿尔金北缘逆冲断裂由向 SE 方向倾斜的低速层所组成，在 20km 深度左右宽度为 5km，它以 30°倾角向南东下插到 80km 深处，并与近直立的深达岩石圈地幔的阿尔金南缘走滑断裂(即阿尔金主断裂)交汇，在此深度其低速层的宽度增加到 15km。阿尔金北缘逆冲断裂与阿尔金主断裂交汇后，继续向南陡倾下插到 150km[48]，反映出塔里木地块向南陆内俯冲于阿尔金山及柴达木盆地之下。近 EW 向的各相异性矢量代表俯冲过程中上地幔物质的滑移方向。

由两条边界断裂所控制的以古地质体为特征的阿尔金地体在深部呈现宽 100km，深 50km 的高密度、高波速体，被低速低密度物质所围绕。

综合阿尔金的深部探测资料，结合其地表地质特征，得到图 7 所示的反映阿尔金现今性质及特征的模式，可以看出，阿尔金断裂带主要由阿尔金走滑主断裂和阿尔金北缘逆冲断裂及两者所夹的阿尔金楔形体(阿尔金地体)所组成。塔里木地块沿阿尔金北缘逆冲断裂陆内斜向俯冲于阿尔金之下，并在深部与阿尔金主断裂会合并继续以陡角度向南俯冲于柴达木盆地之下。

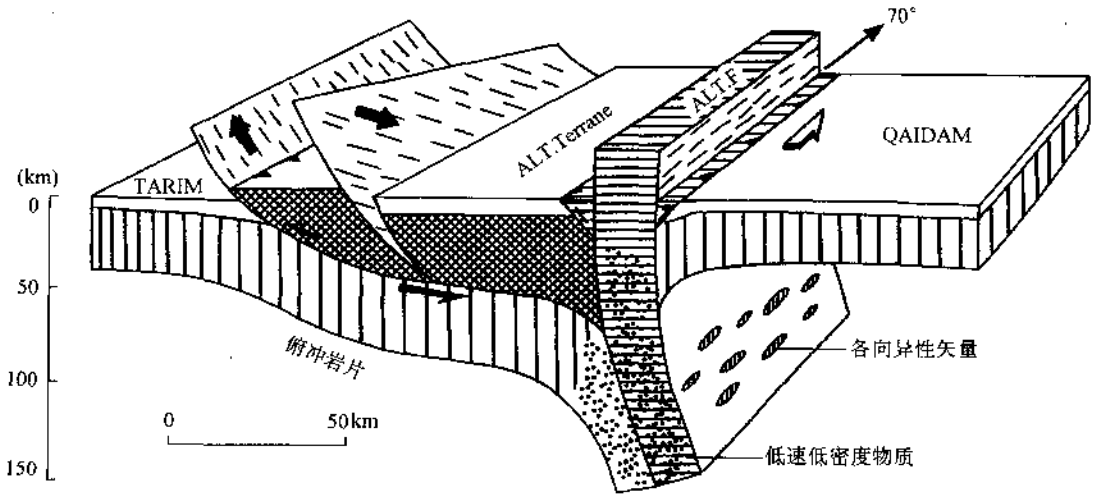

图 7　阿尔金断裂带的构造模式

Fig.7　Tectonic model of the Altun fault belt

TARIM—塔里木地块；ALT. Terrane—阿尔金地体；ALT. F—阿尔金主断裂；QAIDAM—柴达木地块

TARIM—Tarim block; ALT. Terrane—Altun terrane; ALT. F—Altun main fault; QAIDAM—Qaidam block

4　初步结论

(1)根据阿尔金主断裂两侧构造单元，特别是高压-超高压俯冲-碰撞杂岩带(?)的对比，获得阿尔金断裂左行平移 400km 的证据。

(2)阿尔金断裂为岩石圈剪切断裂，剪切作用可抵达上地幔，并伴随局部熔融作用，阿尔金岩石圈剪切作用可能与塔里木地块向南的俯冲作用有关。

(3)笔者曾提出青藏高原周缘内向陆内俯冲作用的动力学模式[49,50],在青藏高原北部得到进一步的验证。

参加野外工作的还有张泽明,吴才来,陈文,史仁灯等。肖序常院士仔细审阅了全文,并提出了宝贵意见。天津地质矿产研究所李惠民研究员在年代学研究方面给予很大的帮助及支持,中科院地质所王清晨研究员提供了 Ge0-Calc 程序,特此感谢!

参 考 文 献

[1] Tapponnier P, Molnar P. Slip-line field theory and large-scale continental tectonics. Nature, 1976, 264: 319～324.

[2] Peltzer G, Tapponnier P. Formation and evolution of strike-slip faults, rifts, and basins during the India-Asia collision: An experimental approach. Journal of Geophysical Research, 1988, 93(12): 15085～15117.

[3] Avouac J P, Peltzer G. Kinematic model of active deformation in central Asia. from these de Doctorat de L'Universite Paris, Ⅶ., 1995.

[4] 许志琴,崔军文,张建新. 大陆山链的变形构造动力学. 北京:冶金工业出版社,1996.

[5] 郑剑东. 阿尔金断裂带的几何学研究. 中国区域地质,1991,36:54～59.

[6] 崔军文,邓晋福,唐哲民. 青藏高原北缘变形构造动力学的一些新认识. 中国地质科学院院报,1994,29:145～146.

[7] 国家地震局"阿尔金活动断裂带"课题组. 阿尔金活动断裂带. 北京:地震出版社,1992.

[8] 丁国瑜. 阿尔金断裂的古地震与分段. 第四纪研究,1995,2:97～106.

[9] Zhou D, Graham S A. Extrusion of the Altyn Tagh wedge: A kinematic model for the Altyn Tagh and palinspastic reconstruction of north China. Geology, 1996, 24(5): 427～430.

[10] Wang E Q. Displacement and timing along the northern strand of the Altyn Tagh fault zone, northern Tibet. Earth Planet. Sci. Lett., 1997, 150: 55～64.

[11] 张建新,许志琴,崔军文. 一个韧性转换挤压带的变形分解作用——以阿尔金断裂带东段为例. 地质论评,1998,44(4): 348～356.

[12] 周勇,潘裕生. 阿尔金断裂早期走滑运动方向及其活动时间探讨. 地质论评,1999,45(1):1～9.

[13] 车自成,刘良,刘洪福. 阿尔金地区高压变质泥质岩石的发现及其产出环境. 科学通报,1995,40(14):1298～1300.

[14] 车自成,孙勇. 阿尔金麻粒岩相杂岩的时代及塔里木盆地的基底. 中国区域地质,1996,15(1):51～57.

[15] 刘良,车自成,罗金海等. 阿尔金山西段榴辉岩的确定及地质意义. 科学通报,1996,41(14):1485～1488.

[16] 刘良,车自成,王焰等. 阿尔金茫崖地区早古生代蛇绿岩的 Sm-Nd 等时线年龄证据. 科学通报,1998,43(8):880～883.

[17] 郭召杰,张志诚,王建军. 阿尔金北缘蛇绿岩的 Sm-Nd 等时线年龄及其大地构造意义. 科学通报,1998,43(18):1981～1984.

[18] 张建新,张泽明,许志琴,杨经绥,崔军文. 阿尔金构造带西段榴辉岩的 Sm-Nd 及 U-Pb 年龄——阿尔金中加里东期山根存在的证据. 科学通报,1999,44(10):1109～1112.

[19] 张建新,张泽明,许志琴,杨经绥,崔军文. 阿尔金西段孔兹岩系的发现及岩石学、同位素年代学初步研究. 中国科学 D 辑,1999,29(3):245－251.

[20] Sobel E R, Arnaud N. A possible middle Paleozoic suture in the Altyn Tagh, NW China. Tectonics, 1999, 18(1): 64～74.

[21] 葛肖虹,段吉业,李才等. 阿尔金断裂与西北大地构造格局的新认识. 见:肖庆辉等主编. 地球科学进展. 武汉:中国地质大学出版社,1996,9～18.

[22] 车自成,良,刘洪福,罗金海. 阿尔金断裂系的组成及相关中生代含油气盆地的成因特征. 中国区域地质,1998,17(4):377～384.

[23] 崔军文,唐哲民,邓晋福,岳永军,孟令顺,余钦范等. 阿尔金断褶系. 北京:地质出版社,1999.

[24] 葛肖虹,张梅生,刘永江. 阿尔金断裂研究的科学问题与研究思路. 现代地质,1998,12(3):295～301.

[25] 葛肖虹,刘俊来．北祁连造山带的形成与背景．地学前缘,1999,6(4):223～230.
[26] 新疆维吾尔自治区地质矿产局．新疆维吾尔自治区区域地质志．北京:地质出版社,1993.
[27] 梅华林,于海峰等,甘肃北山地区首次发现榴辉岩和古元古花岗质岩石．科学通报,1988,43(19):2103～2111.
[28] 潘桂棠,焦淑沛,徐耀荣,王培生,向天秀．阿尔金山新生代构造及造山性质．见:青藏高原地质文集(15)．北京:地质出版社,1984.113～119.
[29] 刘良,车自成,王焰,罗金海,陈丹玲．阿尔金高压变质带的特征及其构造意义．岩石学报,1999,15(1):57～64.
[30] 刘雪亚,王荃．龙首山古裂谷带及河西走廊的大地构造．中国地质科学院院报．1998,27～28:1～14.
[31] 夏林圻,夏祖春,徐学义．北祁连山的构造-火山-岩浆演化动力学．西北地质,1995,16:1～28.
[32] Wu H Q, Feng Y M, Song S G. Metamorphism and deformation of blueschist belt and their tectonic implications, North Qilian Mountains. J. Metamorphic Geol., 1993, 11:523～526.
[33] 许志琴,徐惠芬,张建新等．北祁连走廊南山加里东俯冲杂岩地体及动力学．地质学报,1994,(1):1～14.
[34] 张建新,许志琴,陈文等．北祁连中段俯冲增生杂岩/火山弧的时代探讨．岩石矿物学杂志,1997,(2):112～119.
[35] 青海省地质矿产局．青海省区域地质志．北京:地质出版社,1991.
[36] 杨建军,朱红,邓晋福,周天祯,赖绍聪．柴达木北缘石榴石橄榄岩的发现及其意义．岩石矿物学杂志,1994,13(2):97～105.
[37] 杨经绥,许志琴,李海兵等,柴北缘地区榴辉岩的发现及潜在的地质意义．科学通报,1998.43(14).
[38] Xu J, Zhu G, Tong W, Cui K, Liu Q. Formation and evolution of the Tancheng-Lujiang wrench fault system: a major shear system to the northwest of the Pacific Ocean: Tectonophysics, 1987, 134:273～310.
[39] Wang X, Liou J G. The large displacement of the Tanlu fault: evidence from the distribution of coesite-bearing eclogite belt in eastern China: EOS, Trans. Am. Geophs. Union, 1989, 70:1312～1313.
[40] Kretz R. Symbols for rock- forming minerals. Am. Mineral., 1983, 68:277～279.
[41] Jamtveit B. Metamophic evolution of the Eiksunddal eclogite complex, Western Norway, and some tectonic implications. Contrib. Mineral. Petrol., 1987, 95:82～99.
[42] O'Brien P J. Garnet zoning and reaction textures in overprinted eclogites, Bonemian Massif, Eruopean Variscides: A record of their thermal history during exhumation. Lithos, 1997, 41:119～133.
[43] Caswell D A, O'Brien P J, Wilson R N, Zhai M. Thermobarometry of the phengite-bearing eclogites in the Dabie Mountains of the central China. Journal of Metamorphic Geology, 1997, 15(2):239～252.
[44] Brown T H, Berman R G, Perkins E H. Ge0-Calc: Software packege for calculation and display of pressure-temperature-compositoin phase diagrams using an IBM or compatiable personal computer. Computer Geosci., 1988, 14:279～289.
[45] 李怀坤,陆松年,赵凤清,于海峰．柴达木盆地北缘鱼卡河柯石英榴辉岩的确定及其意义．现代地质,1999,13(1):43～50.
[46] Ernst W G, Liou J G, Hacker B R. Petrotectonic significance of high-and ultrahigh-pressure metamorphic belts: inferences for subduction-zone histories. International Geology Review, 1994, 36:213～237.
[47] 姜枚,许志琴,薛光琦,史大年．青海茫崖-新疆若羌地震探测剖面及其深部构造的研究．地质学报,1999,73(2):153～161.
[48] Wittinger G, Tapponnier P, Poupinet G, Jiang M, Shi T N, Herquel G, Masson F. Tomographic evidence for localized lithospheric shear along the Altun fault. Scince, 1998, 282:74～76.
[49] 许志琴,杨经绥,姜枚,李海兵．大陆俯冲作用及青藏高原周缘造山带的崛起．地学前缘,1999(3):139～151.
[50] Xu Z Z, Jiang M, Yang J S. *et al*. Mantle diapir inward intracontinental subduction: A discuss on the mechanism of uplift of the Qinghai-Tibet plateau. Geological Society of America, Special Paper328, 1999, 19～31.

A Comparison between the Tectonic Units on the Two Sides of the Altun Sinistral Strike-slip Fault and the Mechanism of Lithospheric Shearing

Xu Zhiqin Yang Jingsui Zhang Jianxin Jiang Mei Li Haibing and Cui Junwen
(Institute of Geology, Chinese Academy of Geological Sciences, Beijing, 100037)

Abstract The Altun strike-slip fault is the largest strike-slip fault in Asia and defines the northern boundary of the Qinghai-Tibet Plateau. The Altun terrane, bounded by the north Altun thrust fault and the Altun strike-slip fault on the south, consists of Dunhuang massif, northern Altun Caledonian subduction complex, central Altun massif and southern Altun subduction-collision complex from north to south. Our studies indicate that these tectonic units correspond to the Alxa block, northern Qilian subduction complex, central Qilian block and northern Qaidam subduction-collision zone respectively on the two sides of the Altun strike-slip fault. Especially, the eclogites in the southern Altun and northern Qaidam show strong similarities in geological setting, occurrence, mineral assemblage, geochemical and protolith feature, *P-t* condition of formation, retrograde metamorphism, associated country rock and almost consistent metamorphic age. This suggests the HP-UHP(?)metamorphic zone displaced by a large strike-slip fault be similar to the case of the Dabie-Sulu HP-UHP metamorphic zone which was truncated by the Tanlu sinistral strike-slip fault, and the offsets along the Altun sinistral strike-slip fault is about 400km.

A seismic tomographic section across the Altun Mountains, established by the natural earthquake experiment, indicates a steep low-velocity anomaly beneath and along the Altun strike-slip fault, and a high-velocity anomaly(implying dense material)beneath the Altun terrane located between the southern Altun strike-slip fault and the northern gently-dipping thrust fault. The two faults may meet at a depth of 80km, then continue to underthrust steeply southward to 150km, suggesting that Tarim block has been underthrusted southward beneath the Altun Mountains and the Qaidam block. The large magnitude of anisotropy represents the existence of shearing of upper mantle along Altun strike-slip fault, while the lithospheric shearing may be attributed to the southward subduction of the Tarim block.

Key words sinistral strike-slip subduction-collision complex comparison between tectonic units lithospheric shearing fault intracontinental subduction

大陆俯冲作用及青藏高原周缘造山带的崛起❶

许志琴　杨经绥　姜　枚　李海兵
(中国地质科学院地质研究所　北京　100037)

摘　要　青藏高原周缘造山带于新生代时崛起。周缘造山带中古老变质地体的折返与3种挤出作用方式有关:喜马拉雅"逆冲-伸展"型挤出、祁连山"反向逆冲"型挤出和阿尔金"逆冲-转换"型挤出。据地质与地球物理综合研究推测,造山带的折返与周缘大陆岩石圈向内的俯冲作用有关:印度板块岩石圈向北俯冲至雅鲁藏布江缝合带下约200km处,西伯利亚板块往南低角度插入祁连山40km以下,塔里木地块沿阿尔金北缘逆冲断层呈铲式往南俯冲于阿尔金山下100km处,扬子地块呈楔入体插入青藏高原东部中地壳下面。是否存在扬子地块往西运动及大陆俯冲作用尚待探究。

关键词　大陆俯冲作用　青藏高原周缘造山带　隆升　折返　CLC　P542

1　关于青藏高原隆升驱动力的思考

青藏高原是具特殊地貌景观的正在快速隆升的大陆块体,其周缘高峻陡峭的地形构成一堵与外界隔绝的屏障,高原的内部却是广阔而又平坦的地域。研究表明,印度板块和欧亚板块自55Ma前碰撞以来,板块之间的作用从未终止,强大的陆内会聚塑造了喜马拉雅造山带及中亚地区的巨型变形域[1~6]。巨型变形域的范围南起喜马拉雅前陆盆地,北抵天山和祁连山,东至龙门山、锦屏山,达几百万平方公里(图1)。

印度板块与欧亚板块碰撞以来,青藏高原开始大范围抬升,周缘剧烈崛起。在高原及其周缘显示曾发生过如下构造事件:①高原南部喜马拉雅前陆逆冲叠覆体(即地壳增生楔)形成;②高原南部物质向南东挤出,形成大规模挤压转换带;③高原腹地伸展形成南北向裂谷,并伴随产生碱性火山作用;④高原北部的挤压作用形成后陆逆冲带及阿尔金走滑逆冲带的形成;⑤高原东部的挤压作用形成龙门山逆冲带。

高原隆升机制的探究可以追溯到20年代。自Argand(1924)[7]首先提出青藏高原隆升机制的俯冲模式以来,许多地质学家把注意力集中在青藏高原南缘的陆-陆碰撞作用上。有

---

❶　地学前缘,1999年9月,第6卷第3期。
收稿日期:1999-02-08。
作者简介:许志琴,女,1941年生,研究员,博士生导师,中国科学院院士,构造地质学专业。长期从事青藏高原及造山带的研究。
本文系国家自然科学基金资助项目(编号:49732070)及原地质矿产部中法合作项目成果。

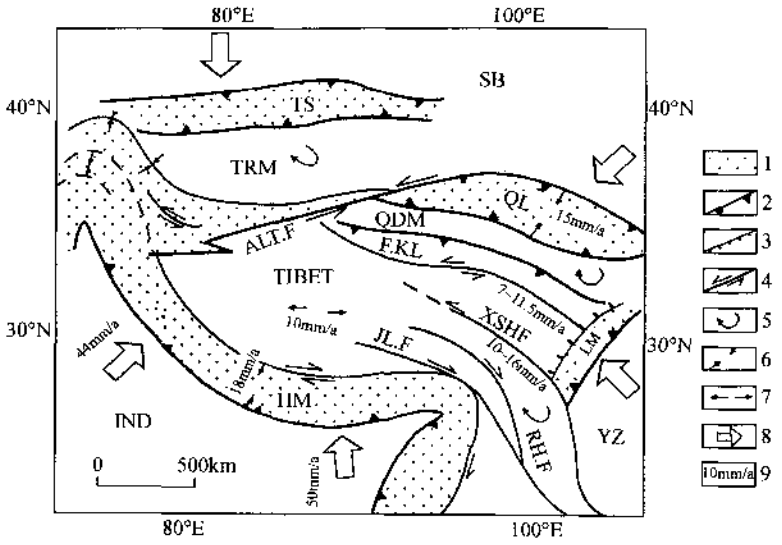

图 1　青藏高原及周围造山带构造平面示意图

(据 Avouac, 1991, 修改)

Fig. 1　Tectonic sketch map of the Qinghai-Tibet Plateau and its marginal orogenic belts

1—周缘造山带；2—逆冲断层；3—正断层；4—平移断层；5—块体旋转；6—板块会聚；7—板块伸展；8—板块运动方向；9—块体位移速度；TIBET—青藏高原；IND—印度板块；YZ—扬子板块；SB—西伯利亚板块；HM—喜马拉雅山；LM—龙门山；E.KL—东昆仑山；QL—祁连山；TS—天山；QDM—柴达木盆地；TRM—塔里木盆地；ALT.F—阿尔金断裂；XSH.F—鲜水河断裂；RH.F—红河断裂；JL.F—嘉黎断裂

人认为印度板块以低角度往北大规模俯冲于青藏高原下，形成双层地壳，而后由于重力均衡造成高原隆升[3,8,9]；青藏高原岩石圈的缩短与加厚和印度、欧亚板块碰撞同时发生[10~12]。另一些学者则认为，印度板块岩石圈往北深深地俯冲于青藏高原之下[13~15]。Tapponnier 等人[16]用印度板块楔往北俯冲造成欧亚板块向东挤出，来解释印度和欧亚板块碰撞所形成的陆内变形远程效应。随着研究的深入，某些学者还提出了青藏高原的高度是由于地幔的拆沉作用[17]或软流圈中的对流作用造成的[18]。也有一些学者开始注意到高原北部可能存在往南的大陆俯冲作用[15,19,20]。

笔者认为，青藏高原是巨型复合体，在地质历史过程中，不仅存在地体的多次拼合及镶嵌，还应考虑新生代隆升过程中的多因素驱动力。

青藏高原巨型变形域的变形强度并非自南往北由强变弱，而是由强应变带及弥散变形域相间组成变形图案。强应变带主要分布于高原周缘(喜马拉雅、阿尔金、祁连山和龙门山)及高原内部的古缝合带及其两侧，强应变带之间则为弥散变形域(即大面积弱变形域)。弥散变形特征为宽缓褶皱，表层破裂及断裂。因此，只考虑来自印度板块一个方面的驱动作用已远远不够了，特别是现代喜马拉雅会聚速率为 18mm/a[21,22]，而祁连山会聚速率已达 16mm/a[21,22]，表明不可忽视来自北部的驱动力。至于青藏高原东缘龙门山逆冲带的形成，是否反映存在东部驱动力则值得思考。

对高原内部驱动力的思考基于以下事实：高原腹地伸展作用伴有大量高热裂谷生成及新生代火山岩喷发，它与地球物理资料所显示的深部 Sn 波衰竭与低速体存在有否内在联

系？为此，笔者提出用多因素驱动力来解释高原隆升的新模式，即高原腹地的隆升与地幔底辟有关，而周缘的隆升与周围克拉通插入高原之下的大陆俯冲作用有关[23]。这一思路摆脱了把高原南部的俯冲当作惟一驱动力的束缚(图 2)。

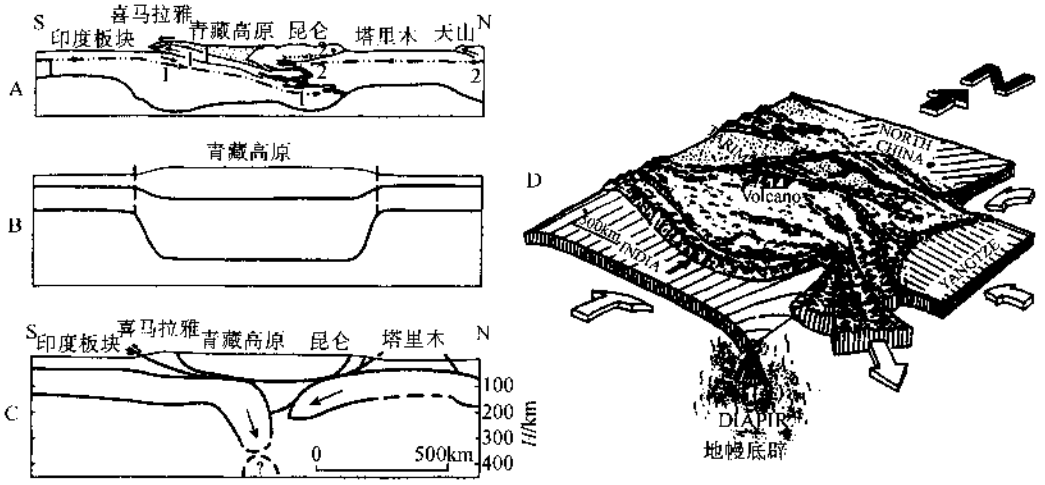

图 2 青藏高原隆升机制的几种假设

Fig.2 Models for explaining the mechanism of the uplift of the Qinghai-Tibet Plateau

A—印度板块俯冲到青藏高原下的模式(Argand, 1924)；B—重力均衡造成的隆升模式(England and Houseman, 1988)；C—双向陆内俯冲模式(Mattauer, 1986)；D—青藏高原腹地地幔底辟及周缘陆内俯冲模式(许志琴等, 1996)

本文将重点讨论青藏高原周缘造山带的形成机制，探究周缘克拉通与青藏高原之间的相互作用及制约关系。

2 青藏高原周缘造山带中古老变质体的上隆、向上挤出作用

青藏高原周缘的造山带是新生代崛起的，南面为喜马拉雅山，北面为祁连山，东面为龙门山，西面为阿尔金山。在这些山链中，都出露有古老变质地体。研究表明，它们都是 55Ma 以来，甚至 20Ma 以来快速上隆的，与向上挤出作用有关。

2.1 喜马拉雅山中高喜马拉雅变质地体的折返

现代板块运动研究表明，55Ma 以来，印度板块与欧亚板块间的会聚速率在西喜马拉雅和帕米尔为(44±5)mm/a，在东喜马拉雅为(50±2)mm/a[24]；西喜马拉雅的滑移矢量为 SW 向，缩短距离近 500km；东喜马拉雅的滑移矢量为 SE 向，缩短距离近 1000km[11]。板块间的碰撞及会聚以挤压为主，构造造型以从印度斯河-雅鲁藏布江缝合带逐步往南扩展的逆冲叠覆作用为特征。因此，印度板块被动陆缘北部的变质基底及古生代至中生代的沉积盖层，均卷入碰撞边界南缘的地壳叠置增生楔中。增生楔由特提斯喜马拉雅、高喜马拉雅及低喜马拉雅构造带组成，构造带之间发育韧性逆冲断层。位于印度斯河-雅鲁藏布江缝合带内的主幔逆冲断裂(MMT)形成于 60～50Ma，位于特提斯喜马拉雅的北喜马拉雅逆冲断裂(NHT)

形成于 40Ma，位于高喜马拉雅与低喜马拉雅之间的主中逆断裂（MCT）形成于 20Ma，位于低喜马拉雅与希瓦利克前陆盆地之间的主边冲断裂（MBT）形成于 10Ma，希瓦利克盆地前缘的主前逆冲断层（MFT）的滑移开始于 2.1～1.6Ma[25]。

高喜马拉雅构造带是折返最快、抬升最高的地带，以出露前寒武纪深变质岩系为特征。对构造带前缘底盘的蓝晶石-夕线石片麻岩研究表明，其形成压力为 800～1000MPa，形成深度为 28～35km，形成时代为 30～21Ma。

在高喜马拉雅构造带北缘北喜马拉雅正断层（NHNF）的发现[15]，表明高喜马拉雅岩片顶部存在 NS 向拉伸，并与主中逆断层（MCT）形成时间相同（21～18Ma）。Chemanda[26,27]通过岩石圈板块的构造物理模拟实验表明，大陆俯冲作用可以造成这种正-逆断裂的耦合作用，并使高喜马拉雅变质地体呈楔状体以 1.4～2.1mm/a 快速[25]向上挤出，形成世界上最高的山链（图 3）。

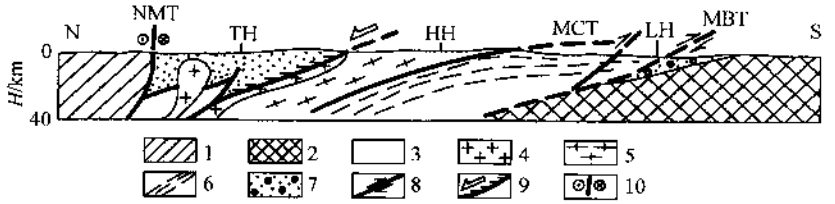

图 3　喜马拉雅造山带构造横剖面

（据 Mattauer, 1986）

Fig.3　Tectonic cross-section of the Himalayas orogenic belt

MMT—主幔逆断层；MCT—主中冲断层；MBT—主边冲断层；TH—特提斯-喜马拉雅构造带；HH—高喜马拉雅构造带；LH—低喜马拉雅构造带；1—欧亚板块；2—印度板块；3—印度俯冲板块上的沉积岩；4—地壳岩片上隆中产生的花岗岩；5—高级变质岩；6—低级变质岩；7—新生代磨拉石沉积；8—逆冲断层；9—正断层；10—右行平移断层

2.2　祁连山变质地体的上隆

祁连山为阿拉善地体、祁连地体及柴达木地体经加里东末期板块碰撞而形成的典型加里东造山带，而后又经历晚古生代至中生代后造山构造变动才进入新生代再造山阶段。根据祁连山北侧地球物理资料揭示，祁连山北缘发育有往北东逆冲的叠置岩片，前震旦纪变质岩系往北逆冲到早古生代复式岩片上，继而叠加在侏罗纪陆相煤层上。逆冲岩片前缘为由逆冲断层及正断层夹持的志留纪复理石挤出岩片，往北又逆冲到白垩纪陆相沉积岩系上（图 4A）。逆冲叠置岩片为祁连山山前地壳增生楔，整体叠覆在由白垩纪、新第三纪和第四纪沉积组成的酒泉盆地之上，并以山前滑脱断裂为界，反映叠覆岩片具有下叠式递进演化序列特点。

祁连山南缘发育有往南西逆冲的断裂系，使含超高压榴辉岩及石榴石橄榄岩的元古宙片麻岩逆冲到柴达木盆地新、老第三纪沉积层上，新、老第三纪地层又不整合覆盖在侏罗纪、白垩纪陆相沉积岩系之上（图 4B）。

上述研究表明，整个祁连山为双向逆冲断裂系所夹持的挤出体（图 4）。古老变质岩主要分布在祁连山中部，由古元古界煌源群长英质片麻岩、泥质片麻岩、片岩、钙硅酸盐岩、大

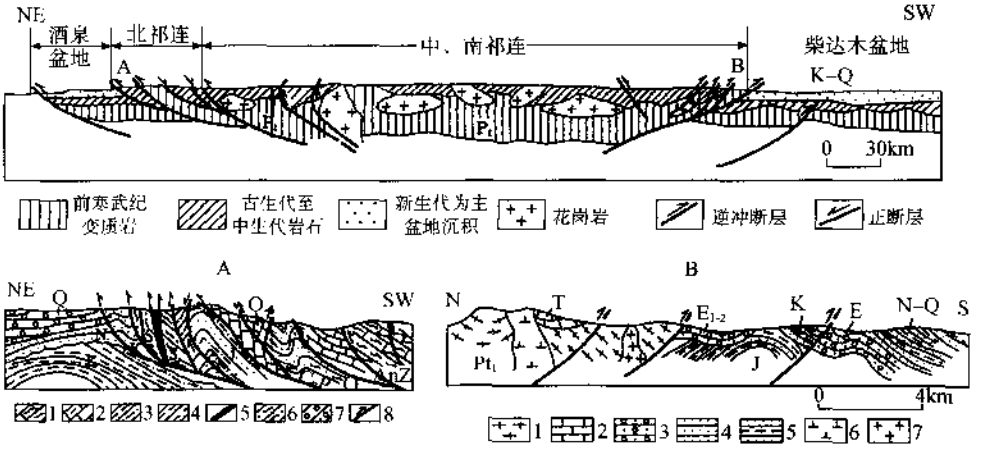

图 4 祁连造山带构造横剖面图

Fig.4 Tectonic cross-section of the Qilian orogenic belt

A—祁连山北缘逆冲构造剖面图:1—大理岩、片岩;2—泥灰岩、灰岩;3—泥岩、砂泥岩;4—煤层;5—超基性岩;6—千枚岩;7—砾岩、砂砾岩;8—逆冲断层。B—祁连山南缘柴北缘逆冲构造剖面图:1—片麻岩;2—结晶灰岩;3—砂砾岩;4—砂岩;5—砂泥岩;6—石英闪长岩;7—花岗岩

理岩、中-新元古界浅变质碎屑岩及碳酸盐岩组成。在北祁连西部祁连山主峰及镜铁山一带出露了与中祁连类同的古老变质岩系,被认为是中祁连变质基底受逆冲及正断层耦合作用而挤出的变质地体。

2.3 阿尔金山变质地体的折返

NE70°~80°方向的阿尔金山主体为前寒武纪变质岩系,并夹有早古生代板块体制的残体,阿尔金山东侧的柴达木盆地及西侧的塔里木盆地均为中、新生代陆相盆地。阿尔金山北西侧 Pt_{2-3}变质岩系逆冲到塔里木盆地第四纪水平砂砾层上,在第四系中还存在由于挤压造成的逆冲断层(F_1)。阿尔金东南侧与柴达木盆地的接触界限为阿尔金主干断层系(F_5),以左行走滑运动为主,往东伴有正断层活动。这条断层不仅切割新第三系,还切割全新统(Q_4),是一条活动断层。第四纪以来走滑断距至少 40~100m,强度分段性很明显,组成主干断裂系的两条走滑断层内,发育有小型拉分盆地,地貌上呈断谷,两侧为活动断层。在阿尔金山中还发育两条沿山脊走向的逆冲断层(F_2 和 F_3),F_3 位于塔什达坂北坡,被晚更新统(Q_3)覆盖,但切割并控制了新第三纪沉积盆地,故形成时间较早,使 Pt_{2-3}^1的片麻岩由南往北逆冲到震旦系灰岩上。F_4 断层位于 F_3 南侧,古元古界由南往北逆冲到 γ_3 花岗岩上(图 5)。因此阿尔金变质体的上隆时限大致为新第三纪-全新世,它是一个由北缘逆冲断层(F_1)和南缘走滑转换断层(带正向滑移性质)(F_5)所夹持的挤出体。

2.4 龙门山变质杂岩体的折返

青藏高原东部的松潘-甘孜造山带于三叠纪末褶皱成山,经历了侏罗纪以来的上隆,并在东侧形成由新生代逆冲带组成的龙门山地壳增生楔。龙门山逆冲带由一系列逆冲叠置岩片及飞来峰组成,并在西侧出现山前震旦纪彭灌杂岩、雅斯德杂岩及康定杂岩组成的变质地体。变质地体呈 NNE-SSW 走向,其后缘发育伸展型韧性正剪切带。在后龙门山伸展型韧性正剪切带北段(汶川一带),剪切带位于变质杂岩与呈强烈剪切应变特征的奥陶纪-志留纪

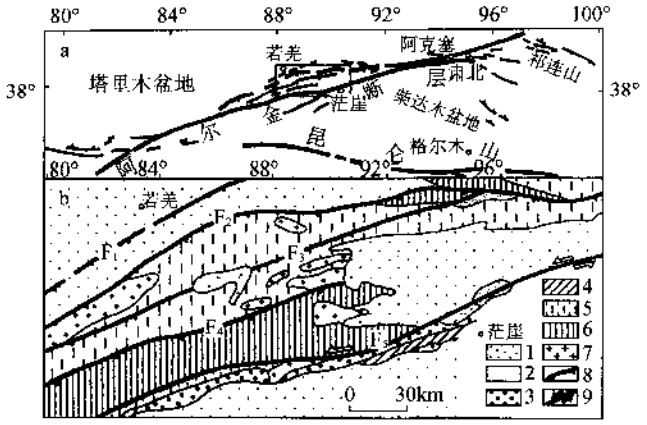

图 5　阿尔金山构造地质平面图

Fig. 5　Sketch geological map of the Altun Mountains

a 图为青藏高原北缘构造示意图，图内方框(b)为研究的阿尔金山位置图；b 图为阿尔金山构造平面图：1—第四系；2—新第三系；3—侏罗系；4—古生界；5—中、新元古界；6—古元古界；7—花岗岩；8—逆冲断层；9—走滑断层

浅变质岩系(绿片岩相)之间。劈理面朝 NW 陡倾，由石榴子石、黑云母、绿泥石、绢云母等矿物组成。面上发育由拉伸磁铁矿、黑云母以及由变斑晶(黑云母、石榴子石)压力影组成的陡倾拉伸线理。在 XZ 面上不对称的 σ 型及 δ 型变斑晶体系，显示了正向滑移的剪切指向。在石榴子石黑云母片岩中，重结晶石英的石英光轴优选方位表示重结晶石英的中低温(底面及菱面)组构及正向滑移指向，组构所代表的温度与高绿片岩相生成温度一致[28]。在中段(宝兴以西、雅斯德)，位于龙门山前陆逆冲楔"宝兴杂岩推覆体"以西的"雅斯德变质体"(由 Pt_3 变火山岩系及花岗闪长岩组成)与古生代浅变质地层之间为韧性正剪切带。韧性正剪切带由花岗质糜棱岩组成，宽约 30m，在糜棱岩中，以钾长石及钠长石为碎斑的不对称 σ 型碎斑体系，也指示正向滑移。在南段(康定一带)，龙门山前陆逆冲楔中康定变质杂岩体(Pt_3)呈南北向展布，其东缘逆冲在泥盆纪浅变质岩系之上，其西缘发育韧性正剪切带，使变质杂岩与震旦系、泥盆系接触。在变质杂岩及震旦系至奥陶系之间，存在糜棱岩带(康定跑马山)。糜棱岩中的 S-C 构造、δ 型石榴子石碎斑体系、长石结晶尾以及震旦系至奥陶系中白云质大理岩条带的拖曳褶皱，均指示自上而下的正向剪切滑移(图 6)。

龙门山-锦屏山西缘的韧性正剪切带与青藏高原东部松潘-甘孜地区新生代以来的伸展作用相伴随。伸展构造表现为深层变质核杂岩的形成及上隆、浅层正断层的发育，以及在重力作用下直立地层表部的膝折及肠形弯曲以及大型重力平卧褶皱的产生。

龙门山前缘逆冲带是由始新世及其以下时代地层组成。在北段，可见早侏罗世的砂砾岩不整合地盖在褶皱与断裂的地层上，表明印支运动的影响范围已达龙门山。龙门山的崛起应于渐新世开始，推测强烈的隆升发生在渐新世至中新世，可能延至早更新世。从龙门山彭灌变质杂岩和宝兴变质杂岩中获得的磷灰石裂变径迹年龄为 4.3～18.2Ma[29]。龙门山西部丹巴地区公差混合岩化片麻岩中，代表变质核杂岩快速冷却时间上限的角闪石与黑云母 ^{40}Ar-^{39}Ar 封闭温度年龄为 20Ma[28]，雪隆包变质核杂岩周围的角闪石年龄为 25～30Ma，表明青藏高原东部隆升、龙门山崛起及变质杂岩折返的主要时代为中新世。

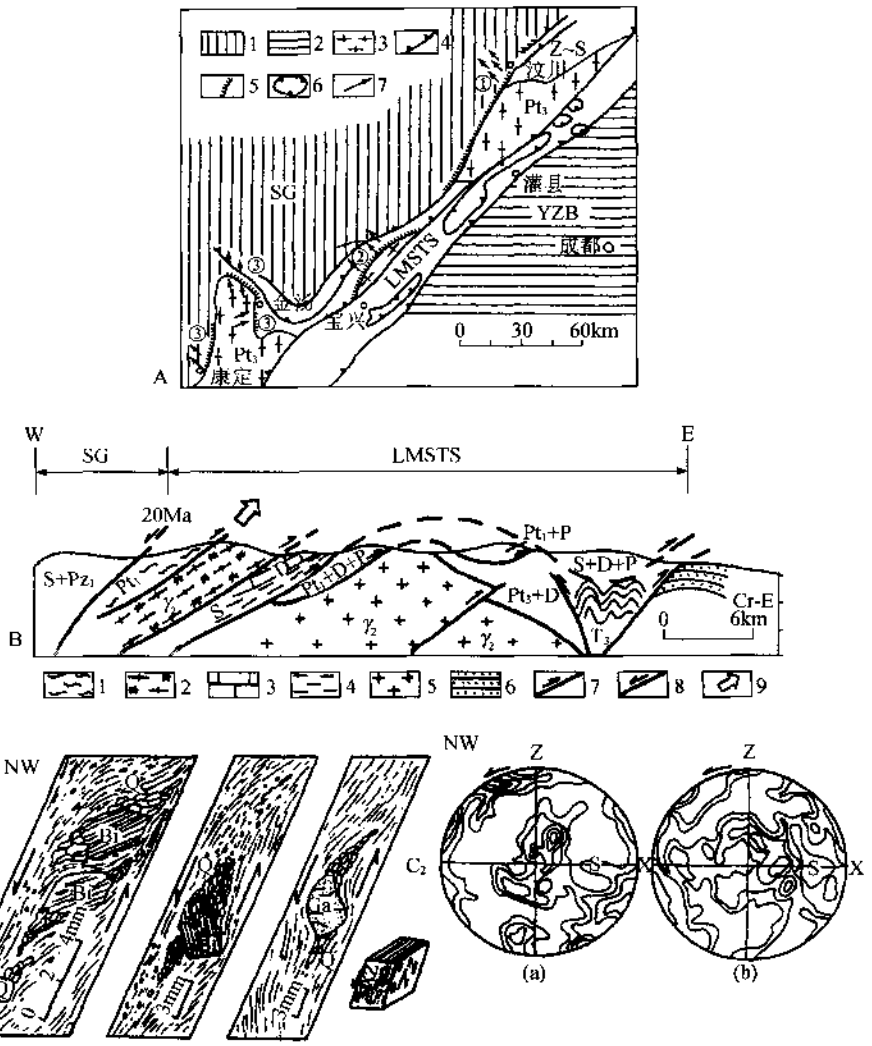

图 6 龙门山逆冲带构造图

Fig.6 Structure map of the Longmenshan thrust belt

A—龙门山逆冲带构造平面图;1—松潘-甘孜造山带(SG);2—扬子板块(YZB);3—变质杂岩体;4—逆冲断层;5—正断层;6—飞来峰;7—拉伸线理;B—龙门山逆冲带构造剖面图;1—绿片岩;2—糜棱岩化花岗片麻岩;3—灰岩;4—千枚岩;5—花岗岩;6—砂岩;7—逆冲断层;8—正断层;9—垂向挤出方向;C—后龙门山韧性正剪切带微构造图;C_1—正向滑移薄片素描;Bi—黑云母;Ga—石榴石;Q—石英;C_2—志留系片岩中石英优选 方位图(112～130 颗粒,下半球投影,等密线 1%～2%～3%～5%～7%)(引自许志琴等,1992)

综上所述,青藏高原周围造山带中,古老变质体是以垂向挤出方式上隆的,这是一种快速上隆的垂向挤出作用产物。垂向挤出作用的主要构造造型有 3 种:第一种是逆冲断层与正断层同时作用,使变质体快速挤出(喜马拉雅、龙门山);第二种是反向逆冲断层系作用,使变质体快速挤出(祁连山);第三种是逆冲断层与转换断层共同作用形成挤出体(阿尔金山)(图 7)。

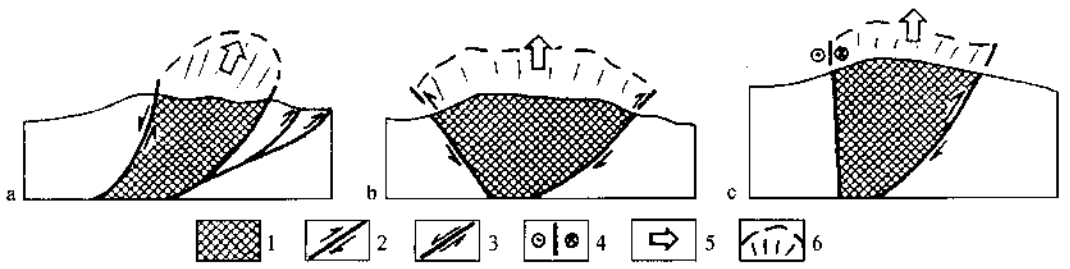

图 7　青藏高原周缘造山带古老变质体挤出方式

Fig.7　Three types of vertical extrusion of the old metamorphic complex at the marginal area of the Qinghai-Tibet Plateau

a—喜马拉雅型(逆冲断层+正断层);b—祁连山型(双向逆冲);c—阿尔金山型(逆冲断层+走滑断层)

1—古老变质体;2—逆冲断层;3—正断层;4—走滑断层;5—挤出方向;6—古老变质体被挤出的原轮廓

3　大陆俯冲作用与周围造山带的最后崛起

在大陆碰撞后,印度板块继续以 5cm/a 速率往北俯冲到青藏高原下,使青藏高原下面的地壳加厚至 70km,并使喜马拉雅造山带目前仍以 18mm/a 的会聚速度缩短[22]。高喜马拉雅变质体的向上挤出作用,与冷的印度板块大陆岩片往北深俯冲有直接成因联系[27]。

近年来地球物理探测新成果进一步揭示了印度板块往北俯冲的细节,同时对青藏高原四周的克拉通是否存在内向俯冲提供了进一步的证据。

(1)印度板块向北俯冲

印度板块岩石圈往北俯冲到喜马拉雅下的细节,已为愈来愈多的地球物理资料所揭示。

中法地球物理探测(格尔木-定日)的最新成果[30],❶(图 8A)为印度板块往北深深俯冲到青藏高原南部提供新证据:①据天然地震剪切波推测,代表上地幔物质活动方向的各向异性图,反映了以雅鲁藏布江缝合带为界,南部各向异性方向为 NNW-SSE 向,北部各向异性方向为近 E-W 向。这两种不同方向,分别代表印度板块往北俯冲并在雅鲁藏布江缝合带深处插下及青藏高原深部物质往东移动的方向;②地层层析资料反映出,以地震波高速体为代表的冷的印度板块岩石圈地幔,以中等倾角插入喜马拉雅之下约 150km 处,但没越过雅鲁藏布江。这一结果与各向异性的资料完全吻合,即高速带以上的喜马拉雅及藏北岩石圈由相对热的低速物质组成(图 8A)。

(2)塔里木地块往南俯冲到阿尔金山下

喜马拉雅北坡的帕米尔以具有大规模向北逆冲的断层为特征,活动的逆冲作用与深源地震相伴随。地震资料表明,北面塔里木地体岩石圈往南俯冲到喀喇昆仑山下 300km 深处[31],地壳增生楔以 2cm/a 速率会聚[18]。

最近中法乌图美仁-若羌的地震层析剖面成果[32](图 8B)反映出阿尔金山及其两侧(塔里木、柴达木盆地)深部结构具如下特征:①柴达木盆地西部以地震波相对低速为主,特别是

❶　地质矿产部成都地质矿产研究所.应用 GPS 技术监测滇中地壳形变(内部报告).1996.

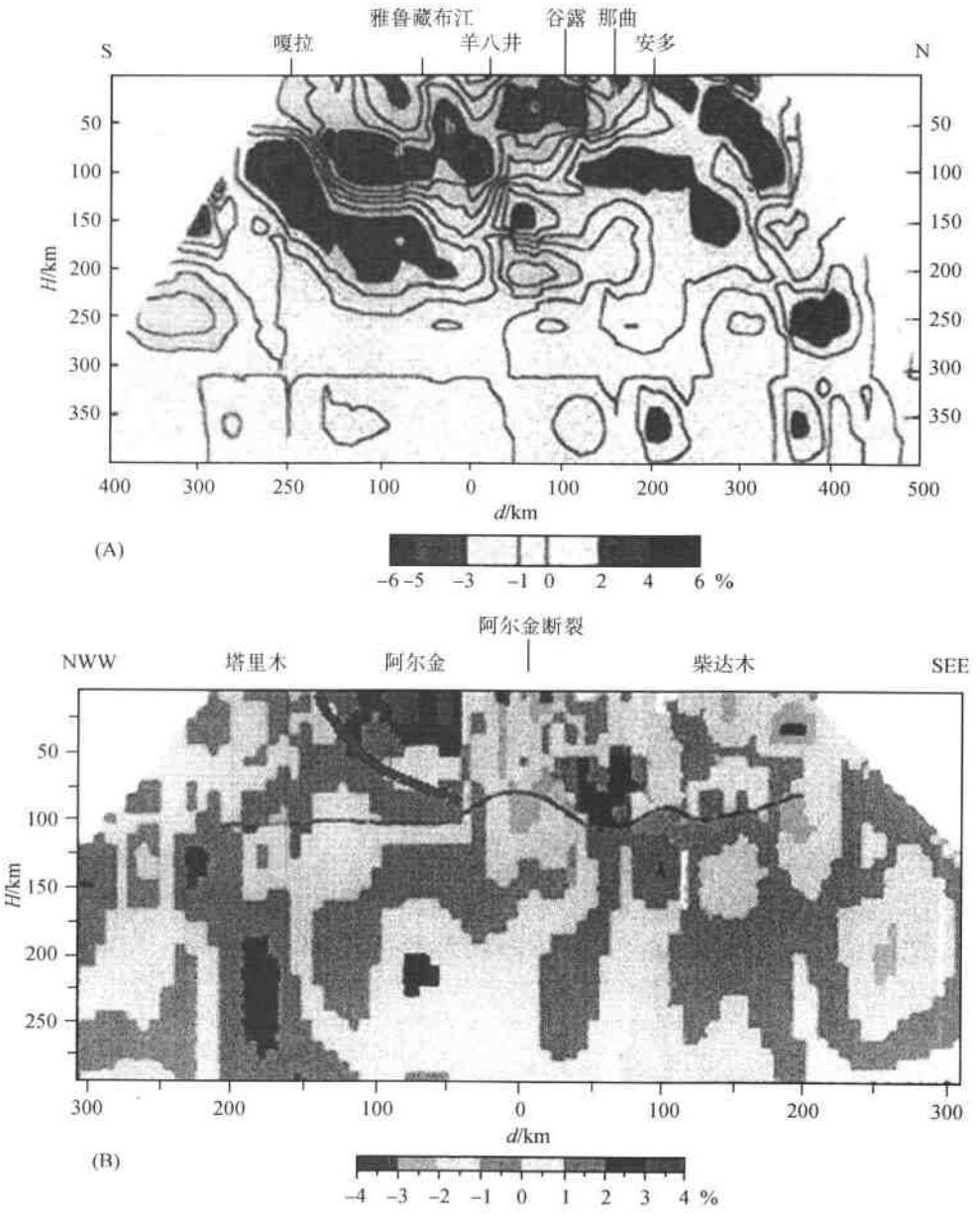

图 8　青藏高原南部及西北部陆内俯冲地球物理剖面

Fig.8　Seismic cross-sections of the southern and the northeastern Qinghai-Tibet Plateau, based on data from tomographic inversion

(A)青藏高原南部嘎拉-安多天然地震剖面(Jiang M, *et al*., 1995);
(B)青藏高原西北部乌图美仁-且末天然地震剖面(Wittlinger, *et al*., 1998)

阿尔金山部位出现宽 50km、深 150km 的低速体，整体向 SE 陡倾。因此，阿尔金山东部的柴达木地块具有较热的岩石圈及上地幔，热源可能来自 SE 面深部。②阿尔金山宽 200km，地震波以高速为主，特别是阿尔金山东部出现高强波速体，宽约 60 km，深达 80km，被夹于 F_4

与 F_3 断层之间。F_1 断层为阿尔金北缘逆冲断层(见图 8B),呈铲式下延到 100km 深处。③塔里木地块地震波以相对低速为主,并显示沿 F_1 断层往南俯冲的影像。因此,推测塔里木地块向南俯冲于阿尔金山之下。

(3)阿拉善地块向南俯冲到祁连山下

横穿柴达木后陆盆地及祁连山后陆逆冲带的格尔木-额济纳旗地学断面研究指出,祁连山往北、往南逆冲到河西走廊及柴达木盆地上。在 100km 长的北缘地震反射剖面[33](图 9A)中,可见北祁连及河西走廊的深部细结构:北祁连的前缘逆冲断层往南倾斜,呈铲式断面与祁连山下 10km 深处的滑脱带相连;在北部河西走廊中,一条大的北边界逆冲断层(NBT)以低角度(−20°)向南延伸至 100km 远,30km 深[34]。地震资料表明,该断裂为北部非地震区及南部震区的分界线。南区的天然地震分布在 NBT 以南 60～130km 处,震源深度不超过 30km[33],说明北中国板块往南是以低角度俯冲于祁连山下的(图 3)。

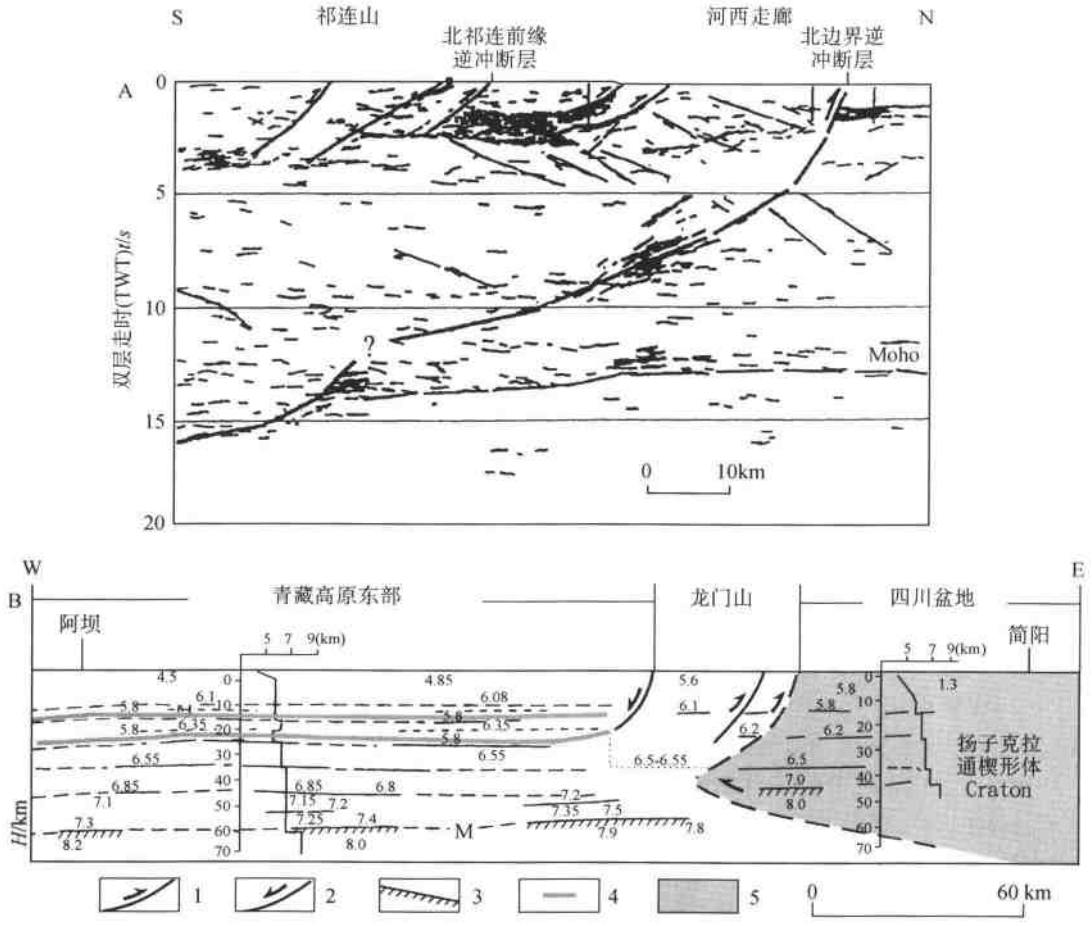

图 9 青藏高原北缘及东缘的地球物理剖面

Fig.9 Deep seismic profile of the northern and eastern Qinghai-Tibet Plateau

A—青藏高原北缘地震剖面(据吴宣志等,1995);B—青藏高原东缘花石峡-简阳地震剖面(据崔作舟等,1996);1—逆冲断层;2—正断层;3—莫氏面;4—低速层;5—扬子克拉通楔

(4)扬子地体与青藏高原的深部关系

NW-SE 向的阿坝-简阳地震剖面[35](图 9B)穿过高原东部、龙门山及四川盆地西缘，770km 长，剖面特征如下：①从东至西地壳厚度从 40km 增至 68km；②高原东缘下部 20km 深处，存在两条由低速层组成的滑脱带，它们与后龙门山正断层相连；③龙门山前缘逆冲带使龙门山叠置于四川盆地之上；④龙门山下 40km 深处，莫霍面被向东缓倾的逆断裂所切，扬子克拉通呈楔形体下插入龙门山下地壳中，形成"鳄鱼构造"。

Tapponnier 和 Molnar[16,36,37]强调以下观点，即印度大陆向北俯冲，使欧亚大陆内部的物质沿大型走滑断裂向东及东南侧向位移。由于受这种"大陆块体的逃逸模式"的影响，扬子地块处于被动后退的状态，并认为红河断层的左行平移运动造成南海的开裂。

张连生和钟大赉[38]根据 U-Pb 法对红河剪切带左行走滑运动进行了精细的年代学分析，确定这一运动时限为 25～20Ma，与南海张开时限吻合，并提出在太平洋板块加速俯冲下，南海作为主动盆地扩张，引起扬子地块在 35～20Ma 期间由 SE 向 NW 方向运动。这一看法与 Tapponnier 等[16,36,37,39]提出的观点针锋相对，即印度板块向北挤压作用造成印支地体向 SE 滑出。

在 1996 年美国凤凰城召开的 KHT 会议上，笔者展出青藏高原东部深部地球物理资料揭示的扬子地块影像，它们呈楔状体嵌入高原东部的中地壳下[35](图 9B)，反映出扬子地块往西具有大陆俯冲作用的特征[23]。

据 GPS 测量认为，目前龙门山及四川盆地之间无相对位移[40]。因此这种俯冲作用可能发生在大约 35～20Ma 期间，此问题尚待进一步探讨。

4 结语

(1)青藏高原南部的印度板块岩石圈地幔往北俯冲于喜马拉雅山下，没越过雅鲁藏布江，形成喜马拉雅前陆逆冲叠覆体。高喜马拉雅古老变质体的折返与前缘逆冲断裂、后缘正断层在 20Ma 时产生的垂向快速挤出作用有关，是印度板块往北向陆内俯冲的结果。

(2)青藏高原西北缘阿尔金山中的古老变质体上隆，与前缘逆冲断层、后缘左行转换断层所夹持的地质体挤出作用有关，主要驱动力来自塔里木地块向阿尔金高速体的俯冲。

(3)青藏高原北缘的祁连山以双向逆冲形式挤出，南北两侧地块俯冲到祁连山下。

(4)青藏高原东缘龙门山中的古老变质地体上隆方式与高喜马拉雅相似，折返年龄为 20Ma 左右，扬子地块相对青藏高原是否也存在陆内俯冲尚需进一步研究。

野外工作期间，得到了甘肃省地质矿产局、甘肃省地质矿产局地质科学研究所、青海省地质矿产局的支持和帮助。中法合作项目"阿尔金-祁连山地质演化及岩石圈剪切作用"和"东昆仑及邻区岩石圈缩短作用"由原地质矿产部资助，"祁连山造山带的组成及造山过程"项目由国家自然科学基金项目资助。图件由张晓卫、宋迎年、张淼清绘，文字由郜源红录入，在此一并致谢。

参 考 文 献

[1] Gansser A. Geology of the Himalayas: Interscience Publication. London: John, Wiley, Lith., 1964. 289.

[2] Dewery J, Bird J. Mountain belts and the new global tectonics. Journal of Geophysical Research, 1970, 75: 2625～2647.

[3] Powell C Mc A, Conaghan P J. Plate tectonics and the Himalayas. Earth and Planetary Science Letters, 1973, 20: 1～12.

[4] Powell C Mc A, Conaghan P J. Tectonics models of the Tibetan Plateau. Geology, 1975, 3: 727～732.

[5] Le Fort P. Manaslu leucogranite: a collisional signature of the Himalaya, a model for its genesis and emplacement. J Geophys Res, 1981, 86: 10, 545～568.

[6] Molnar P, Tapponnier P. Cenozoic tectonics of Asia: effects of a continental collision. Science, 1975, 74: 419～462.

[7] Argand E. La tectonique de l'Asie: international geological congress, 13th, Brussels, 1922. Reports, 1924, 1: 170～372.

[8] Barazangi M, Ni J. Propagation characteristics of Pn beneath the Himalayan arc and Tibetan plateau: possible evidence for underthrusting of Indian continental lithosphere beneath Tibet. Geology, 1982, 10: 179～185.

[9] Beghoul N, Barazangi M, Isacks B L. Lithospheric structure of Tibet and western north America: mechanisms of uplift and a comparative study. Journal of Geophysical Research, 1993, 98: 1997～2016.

[10] Dewey J, Burke K. Tibetan, Variscan and Precambrian basement reactivation: products of continental collision. Journal of Geology, 1973, 81: 683～692.

[11] Dewey J F, Cande S, Pitman W C. Tectonic evolution of the India/Eurasia collision zone. Eclogae Geol Helv, 1989, 82: 717～734.

[12] England P, Hdusemen G. Finite strain calculations of continental deformation 2. Comparison with the India-Asia collision zones. Journal of Geophysical Research, 1986, 91: 3664～3676.

[13] Coward M P, Butler R W H. Thrust tectonics and the deep structure of the Pakistan Himalaya. Geology, 1985, 13: 417～420.

[14] Coward M P, Butler R H, Chambers A F, *et al*. Folding and imbrication of the Indian crust during Himalayan collision. Phil Trans R Soc Lond, 1988, A326: 89～116.

[15] Mattauer M. Intracontinental subduction, crust mantle décollement and crustal stacking wedge in the Himalaya and other collision belts. Spec Publ J Geol Soc London, 1986, 19: 37～50.

[16] Tapponnier P, Molnar P. Active faulting and tectonics in China. J Geophys Res, 1977, 82: 930～2095.

[17] Zhao W L, Morgan W J. Uplift of the Tibetan Plateau. Tectonics, 1985, 4: 359～369.

[18] Molnar P. A review of geophysical constraints on the deep structure of the Tibetan Plateau, the Himalaya and the Karakoram, and their tectonic implications. Phil Trans R Soc Lond, 1988, A326: 33～88.

[19] 白文吉, 杨经绥. 青藏高原隆升的主因——大陆板内盆-山碰撞作用. 长春地质学院学报, 1987(2): 131～142.

[20] Matte Ph, Mattauer M, Olivet J M, *et al*. Continental subductions beneath Tibet and the Himalayan orogeny: a review. Terra Nova, 1997(9): 264～270.

[21] Avouac J P. Application des methods de morphologic quantitative a la Neotectonique. In: Model Cinematique Des Deformations Actives en Asia Centrale. These de Doctorat de l'Universite Paris, 1991. 50.

[22] Avouac J P, Tapponnier P. Kinematic model of active deformation in Central Asia. Geophys Res Lett, 1993, 20: 895～898.

[23] 许志琴, 姜枚, 杨经绥. 青藏高原北部隆升的深部构造物理作用. 地质学报, 1996, 70(3): 195～206.

[24] DeMets C, Gordon R G, Argus D F, *et al*. Current plate motions. Geophys J Int, 1990, 101: 425～478.

[25] Searle M P. Cooling history, erosion, exhumation, and Kinematics of the Himalaya-Karakoram-Tibet orogenic belt. In: An Yin, Harrison T M, eds. Tectonics of Asia. Cambridge: Cambridge Univ Press (Ruhey Volume), 1996. 110～137.

[26] Chemenda A I. Subduction, Insights from Physical Modeling. Dordrecht/Boston/London: Kluwer Academic Publishers, 1994. 193.

[27] Chemenda A I, Mattauer M, Malavieille J, *et al*. A mechanism for syn-collisional rock exhumation and associated normal faulting: results from physical modeling. Earth and Planetary Science Letters, 1995, 132: 225～232.

[28] 许志琴, 侯立玮, 王宗秀, 等. 中国松潘-甘孜造山带的造山过程. 北京: 地质出版社, 1992. 1～60.

[29] Hirn A, Jiang M, Diaz J, *et al*. Seismic anisotropy as an indicator of mantle flow beneath the Himalayas and Tibet. Na-

ture, 1995, 375: 571～574.
[30] Jiang M, Hirn A, Poupinet G. Tibetan Plateau Seismic Experiment: design and Preliminary Results, 1992～1993. Global Tectonics and Metallogeny, 1995, 4: 199～201.
[31] Fan G, Ni J F, wallace T C. Active tectonics of the Pamirs and Karakorum. J Geophys Res, 1994, (99): 7131～7160.
[32] Wittlinger G, Tapponnier P, Poupinet G, *et al*. Tomographic evidence for localized lithospheric shear along the Altyn Tagh fault. Science, 1998, 282: 74～76.
[33] 吴宣志, 吴春玲, 卢杰, 等. 利用深地震反射剖面研究北祁连-河西走廊地壳细结构. 地球物理学报, 1995, 38(增刊Ⅱ): 29～35.
[34] 高锐, 成湘洲, 丁谦. 格尔木-额济纳旗地学断面地球动力学模型初探. 地球物理学报, 1995, 38(增刊Ⅱ): 3～14.
[35] Cui Zuozhou, Chen Jiping Wu Ling. Altray-Taiwan GGT, Texture and Structure of Huashixia-Shaoyang Deep Crust. Beijing: Geological Publishing House, 1996, 192.
[36] Tapponnier P, Molnar P. Slip-line field theory and large scale continental tectonics. Nature, 1976, 264: 319～324.
[37] Tapponnier P, Molnar P. Active faulting and Cenozoic tectonics of the Tian Shan, Mongolia and Baykal regions. J Geophys Res, 1979, 84: 3425～3459.
[38] 张连生, 钟大赉. 从红河剪切带走滑运动看东亚大陆新生代构造. 地质科学, 1996, 31(4): 327～340.
[39] Peltzer G, Tapponnier P. Formation and evolution of strike-slip faults, rifts, and basins during the India-Asia Collision: an experimental approach. Journal of Geophysical Research, 1988, 93: 15085～15117.
[40] Royden L H, Burchfiel B C, King R W, *et al*. Surface deformation and lower crustal flow in eastern Tibet. Science, 1997, 276: 788～790.

CONTINENTAL SUBDUCTION AND UPLIFTING OF THE OROGENIC BELTS AT THE MARGIN OF THE QINGHAI-TIBET PLATEAU

Xu Zhiqin Yang Jingsui Jiang Mei Li Haibing
(Institute of Geology, Chinese Academy of Geological Sciences, Beijing, 100037)

Abstract The orogenic belts at the margin of the Qinghai-Tibet Plateau have already been uplifting since Cenozoic. The exhumation of the old metamorphic complex in these marginal orogenic belts is related to three types of extrusion: (1) "thrust-extension" related to extrusion of Himalayan type; (2) "opposite thrust" related to extrusion of Qilianshan type; (3) "thrust-transformation" related to extrusion of the Altun type. On the basis of geological and geophysical study, it is postulated that the exhumation of the orogenic belts is correlated to the inward-subduction of the continental lithosphere around the plateau, i.e. (1) the Indian plate subducted northward down to about 200km deep under the Yalung Zangbo suture zone; (2) The Siberian plate subducted southward at a low-angle down to 40km deep beneath the Qilianshan; (3) The Tarim terrain subducted along the northern marginal thrust fault of the Altun Mountain southward down to 100km deep under the Altun Mountain; (4) The Yangtze plate wedged into the middle crust of the eastern Qinghai-Tibet Plateau. However, further study is needed to verify the existence of westward movement of the Yangtze plate and that of the continental subduction.

Key words continental subduction the Qinghai-Tibet Plateau uplifting exhumation inversion

Mantle diapir and inward intracontinental subduction: A discussion on the mechanism of uplift of the Qinghai-Tibet Plateau[●]

Xu Zhiqin[1] Jiang Mei[2] Yang Jingsui[3] Zhao Guoguang[4]
Cui Junwen[5] Li Haibing[5] Lu Qingtian[6] Xue Guangqi[6]

(1. Institute of Geology, Chinese Academy of Geological Sciences, 26 Beiwanzhuang Road, Beijing 100037, China; 2. Institute of Mineral Resources, Chinese Academy of Geological Sciences, Beijing 100037, China; 3. Institute of Geology, Chinese Academy of Geological Sciences, 26 Beiwanzhuang Road, Beijing 100037, China; 4. Institute of Crustal Dynamics, State Seismological Bureau, Beijing, 100085, China; 5. Institute of Geology, Chinese Academy of Geological Sciences, 26 Beiwanzhuang Road, Beijing 100037, China; 6. Institute of Mineral Resources, Chinese Academy of Geological Sciences, Beijing 100037, China)

Abstract In this chapter, we account for the mechanism of uplift of the Qinghai-Tibet Plateau beyond the subduction model of the Himalayas, through studies of features of Cenozoic deformation and the accompanying geological events, with a combination of results from geophysical exploration and experiments at the interior and hinterland of the plateau. Extensive alkaline volcanic rocks of Cenozoic age in the interior of the plateau are shoshonitic and high-K, formed by the partial melting of the lower crust and upper mantle in an extensional tectonic setting. A seismic converted-waves study from Golmud to Wenquan further shows that the lithosphere at the northern interior of the plateau has a multisandwich structure and lithospheric faults with sinistral strike-slip sense. The large low-velocity anomaly at the depths from 210 to 360km beneath the Hoh Xil region, detected by seismic tomographic data, is interpreted to be a mantle diapir responsible for the genesis of the alkaline volcanic activity. A seismic reflection profile across the northern hinterland of the plateau shows that the North China craton was subducted southward beneath the Qilian Mountains. In the eastern hinterland, a wedge of the Yangtze craton embedded into the lower crust at the Longmenshan indicates that intracontinental subduction existed between the eastern Qinghai-Tibet Plateau and the Yangtze craton. The noncoaxial compression and oblique crustal shortening in the Qinghai-Tibet Plateau caused by northwest-southeast-trending compression at the northern margin and the south-north-trending compression at the southern margin are most likely responsible for the formation of strike-slip faults and

● Xu Zhiqin, Jiang Mei, Yang Jingsui, Zhao Guoguang, Cui Junwen, Li Haibing, Lu Qingtian, and Xue Guangqi, 1999, Mantle diapir and inward intracontinental subduction: A discussion on the mechanism of uplift of the Qinghai-Tibet Plateau, in Macfarlane, A., Sorkhabi, R. B., and Quade, J., eds., Himalaya and Tibet: Mountain Roots to Mountain Tops: Boulder, Colorado, Geological Society of America Special Paper 328.

rotation of blocks. We suggest a new model for the uplift of the Qinghai-Tibet Plateau: a mantle diapir in the interior and inward intracontinental subduction at the margin.

Introduction

After the collision between the Indian and Eurasian plates, extensive convergence has apparently caused the formation of the Himalaya orogenic belt and much of the observed Cenozoic deformation in Central Asia (Gansser, 1964; Dewey and Bird, 1970; Powell and Conaghan, 1973, 1975; Le Fort, 1975; Molnar and Tapponnier, 1975). This huge deformation domain ~ 2400km long and 1500km wide, extends northward from the foreland basin of the Himalayan orogen to the Tianshan-Qilian mountains, and earthward to the Longmenshan mountains. We named the deformation domain the Tethys-Himalaya orogenic composite(Xu *et al*., 1996). It is surrounded by the Indian, Yangtze, and North China cratons, and consists of four parts: the Himalayan foreland superimposed thrust zone, the interior of the Qinghai-Tibet Plateau, the Tarim-Qaidam hinterland basins, and the Tianshan-Qilianshan-Longmenshan hinterland thrust zone(Fig. 1). The interior of the Qinghai-Tibet Plateau includes four terrains: the Kunlun, Bayan Har, Qiangtang, and Gangdise terrains(Fig. 1).

Since Argand (1924) proposed the subduction model on the mechanism of uplift of the Qinghai-Tibet Plateau, a number of geologists have tried to address the role of continent-continent collision at the southern Qinghai-Tibet Plateau. For example, it is proposed that the Indian plate subducted beneath the Qinghai-Tibet Plateau at a low angle, which formed a two-layer crust and caused uplift of the plateau by gravity equilibrium (Barazangi and Ni, 1982; Beghoul *et al*., 1993). It has also been suggested that the lithospheric shortening and thickening of the Qinghai-Tibet Plateau occurred contemporaneously with the collision between the Indian and Eurasian plates(Dewey and Burke, 1973; England and Houseman, 1986). Different models of subduction and large-scale delamination were suggested to explain the uplift of the Qinghai-Tibet Plateau(Molnar and Deng, 1984; Zhao and Morgan, 1985; Zhao and Yuen, 1987; Mattews and Hirn, 1984; England and Houseman, 1986). Eastward extrusion of the Eurasian plate resulting from northward subduction of the Indian wedge was proposed by Tapponnier *et al*. (1982) to explain the formation of the huge deformation domain caused by the long-distance effect of the collision between the Indian and Eurasian plates. Some geologists considered that intracontinental subduction may also take place at the northern Qinghai-Tibet Plateau (Deng, 1978; Mattauer, 1992). Mattauer(1990) suggested a mantle diapir beneath the plateau as well.

We believe that the driving force for the uplift of the Qinghai-Tibet Plateau is complex and constrained by many factors, such as: ① complicated fabrics of the Tethys-Himalaya orogenic composite; ② the effect of the rigid cratons at the margins of the Qinghai-Tibet Plateau; and ③ direct deep factors of Cenozoic alkaline volcanic-magmatic activity, high heat flow and rifting at the interior of the Qinghai-Tibet Plateau.

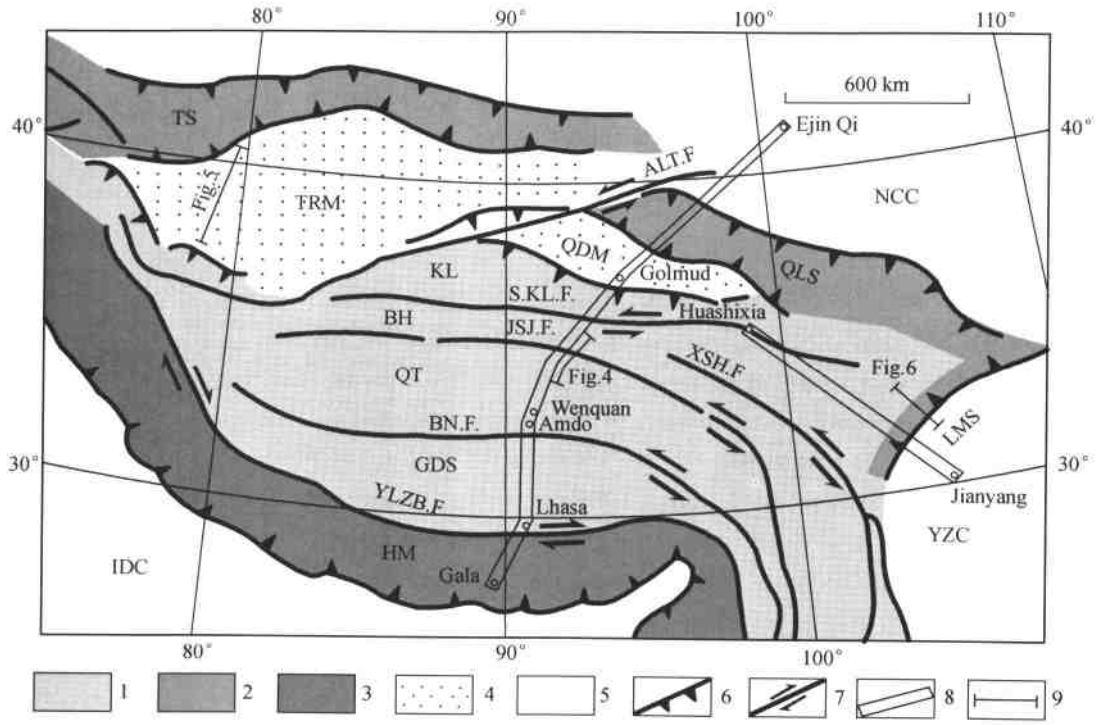

Fig. 1 Tectonic map of the Tethys-Himalaya orogenic composite (modified after Xu *et al.*, 1996), showing: 1—interior of the Qinghai-Tibet Plateau (QTP), including Kunlun (KL), Bayan Har (BH), Qiangtang (QT), and Gangdise (GDS) terrains; 2—Himalaya foreland superimposed thrust zone (HM); 3—Tarim (TRM)-Qaidam (QDM) hinterland basins; 4—Tianshan (TS)-Qilianshan (QLS)-Longmen-shan (LMS) hinterland thrust zones; 5—North China craton (NCC), Yangtze craton (YZC), and Indian craton (IDC); 6—thrust; 7—strike-slip faults: Altyn-Tagh fault (ALT.F), South Kunlun fault (S.KL.F), Jinshajiang fault (JSJ.F), Xianshuihe fault (XSH.F), Bangong-Nujiang fault (BN.F); Yarlung Zangbo Fault (YLZB.F); 8—geophysical profiles; 9—location of geological section.

However, until now most of the studies have mainly concentrated on the Himalayas, the southern interior of the plateau, and Karakoram, and not on the northern interior and hinterland of the plateau, e.g., the East Kunlun, Bayan Har, Qiangtang, Qaidam, and Qilian regions. Thus, we take account of the mechanism of the uplift of the Qinghai-Tibet Plateau, in particular the geodynamics of the formation of hinterland and interior of the plateau, through studies of features of Cenozoic deformation and the accompanying geological events at the interior and the hinterland of the Qinghai-Tibet Plateau; we also combine our results from geophysical experiments, including Sino-French geophysical exploration from Golmud to Gala in 1992～1995, and the geoscientific transects at the northern and eastern margins of the Qinghai-Tibet Plateau by Gao *et al.* (1995), and Cui *et al.* (1996), respectively.

Cenozoic Geological Events in the Interior of the Qinghai-Tibet Plateau

After the collision between Indian and Eurasian plates, the Qinghai-Tibet Plateau was sub-

jected to heterogeneous uplift during Cenozoic time. Available data indicate that extensive uplift of the Qinghai-Tibet Plateau occurred after Miocene and Pliocene time, especially after Pleistocene time(Xiao, 1995). We focus on sedimentation, magmatism, structural deformation, and other geological events accompanying the uplift within the plateau since Cenozoic time.

Formation of Eocene pull-apart basins and Quaternary rifting basins

There are a number of small continental Eocene-Oligocene basins filled with red lacustrine sandstone and mudstone having thicknesses to 2000m(Bureau of Geology and Mineral Resources of Qinghai Province, 1991), distributed along sinistral strike-slip faults that trend east-west in the northern Qinghai-Tibet Plateau(Tapponnier and Molnar, 1977). Most of the basins are rhombohedral in shape(plane geometry)(Fig.2). We consider that the formation of pull-apart basins is probably related to sinistral strike-slip movement. According to our study, the east-west-trending Dongqiao basin at the south of the Bangonghu-Nujiang fault is an Eocene-Oligocene basin developed on the Jurassic-Cretaceous folded strata. The Eocene sedimentary sequence is thicker in the west(1400m)and the north (1100m), and thinner in the east(1000m) and the south (100～200m). The sedimentary center was located at the northwest part of the basin and controlled by normal faults during Eocene time, and then moved to the center of the basin during Oligocene time. This implies that the Dongqiao basin was a pull-apart basin along the east-west-trending sinistral strikeslip fault during Eocene time.

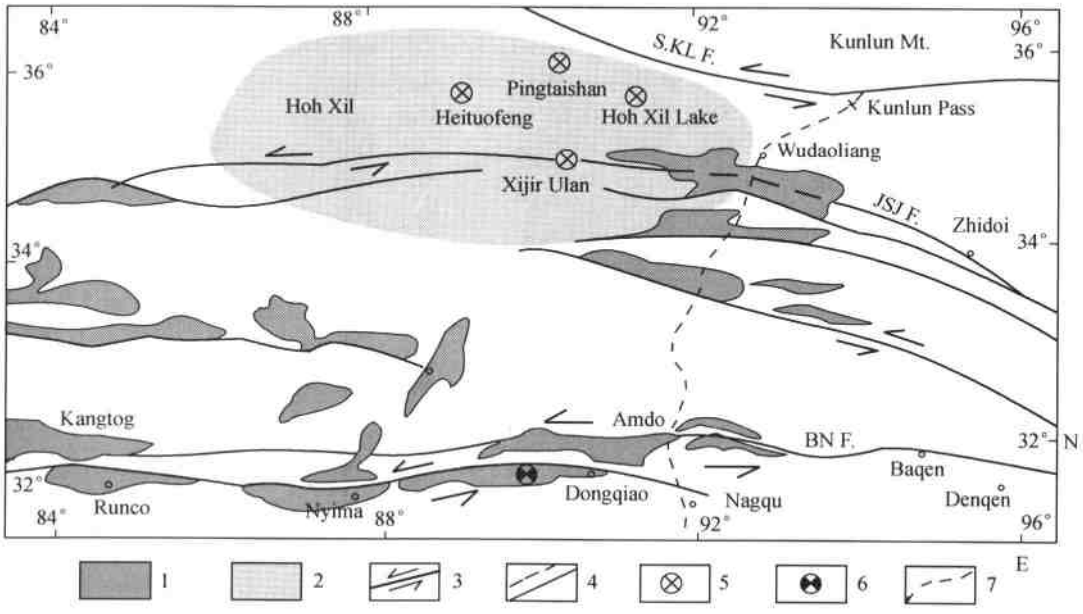

Fig.2 Geological map of the northern interior of the Qinghai-Tibet plateau, showing the distribution of Cenozoic alkaline volcanic rocks, Eocene-Oligocene sedimentary basins, and sinistral strike-slip faults. 1—Eocene-Oligocene sedimentary basin; 2—regions of Cenozoic alkaline volcanic rocks; 3—strike-slip fault; 4—fault and inferred fault; 5—sites of volcanics quoted in this chapter; 6—Eocene-Oligocene basins; 7—road.

North-south-trending Quaternary extensional systems are well developed within the southern interior of the plateau, where grabens bounded by normal faults control the distribution of Quaternary sedimentation, north-south-trending lakes, and large earthquakes, and form a rifting system(Tapponnier and Molnar, 1977; Peltzer and Tapponnier, 1988). The Quaternary rifting region in the southern plateau(Gangdise terrain) is characterized by remarkable variations of heat flow ranging from 66mW/m^2 to 364mW/m^2 and an abrupt change in heat-flow types, from pure conductive to conductive-convective transition within a short distance. The peak value in the former type may reach 140mW/m^2, whereas that in the latter exceeds 300mW/m^2. The heat-flow anomaly demonstrates an obviously shallow heat source(Shen, 1996).

Alkaline volcanic activity

There are some alkaline volcanic rocks of Cenozoic age in the northern interior of the plateau, mainly in the Hoh Xil region (Fig.2). Most of the volcanic rocks in Hoh Xil belong to a shoshonitic association(Fig.3), including latite, shoshonite, and trachyte(Deng, 1991; Deng *et al.*, 1996; Zhang and Zheng, 1994; Yang *et al.*, 1996; Xu *et al.*, 1996). The shoshonite at the Heituofeng-Pingtaishan-Hoh Xil Lake, north of Hoh Xil, is characterized by enrichment in K, large ion lithophile elements (LILE), and light rare earth elements(REE), and depletion in Nb and Ta(Deng *et al.*, 1996). A recent study on the shoshonite association at the Xijir Ulan Lake, at the center of Hoh Xil, by Yang *et al.* (1998) indicates that the SiO_2 content varied between 58 and 70 wt%, and TiO_2 and MgO increase with decreasing SiO_2. The rock has an initial $^{87}Sr/^{86}Sr$ ratio of 0.708 and $^{143}Nd/^{144}Nd$ ratio of 0.512, and almost constant Pb ratios ($^{206}Pb/^{204}Pb = 18.61 \sim 18.74$, $^{207}Pb/^{204}Pb = 15.62 \sim 15.77$, and $^{208}Pb/^{204}Pb = 38.72 \sim 39.10$). It is inferred that the shoshonitic magma originated by the partial melting of the lower crust or crust-mantle boundary material and are related to the heat flow of the K-rich materials due to magmatism in the mantle(Xu *et al.*, 1996). The olivine-bearing leucite and the alkaline basalt(Zhang and Zheng, 1994) discovered in Hoh Xil may be derived directly from partial melting of the mantle.

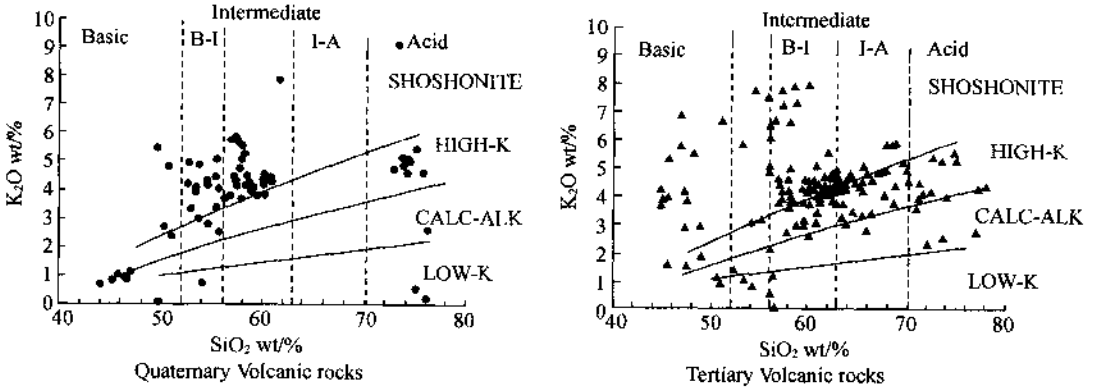

Fig.3 K_2O vs. SiO_2 plots show that most of the Quaternary and Tertiary volcanic rocks in the interior of the Qinghai-Tibet Plateau shoshonite association(after Yang *et al.*, in press).

The K-Ar method yielded ages of 7～56Ma for the volcanic rocks in Hoh Xil(Zhang and Zheng, 1994; Deng, 1991; Deng *et al*., 1996; Xu *et al*., 1996), and among them ages of 10～20Ma predominated. In addition, three new K-Ar ages(15.66, 14.05, and 33.37Ma)were obtained from samples at the Xijir Ulan Lake(Yang *et al*., 1998), and ages of 6.95～7.5Ma were obtained from samples in northern Hoh Xil(Deng *et al*., 1996).

Crustal shortening

The crustal deformation and shortening occur extensively in the northern and central interior of the plateau; in different parts of the region, they have different deformational forms and strengths and directions of stress.

1. In the Bayan Har-Qiangtang region at the central interior, crustal deformation is characterized by crustal shortening rather than faulting. The Eocene and Oligocene strata formed west-northwest-trending gentle concentric folds andare discordantly covered by Miocene sediments. The pre-Cenozoic strata in the region were thrust onto the Miocene strata along a high angle fault. A crustal shortening rate of 13% is inferred for the region (Xu and Cui, 1996) (Fig.4). These features, coupled with the development of east-west-trending sinistral strike-slip faults, suggest that the compressional stresses in the region were relatively weak, trended north-northeast, and the compression occurred mainly in two periods: between Oligocene and Miocene time, and between Miocene and Quaternary time.

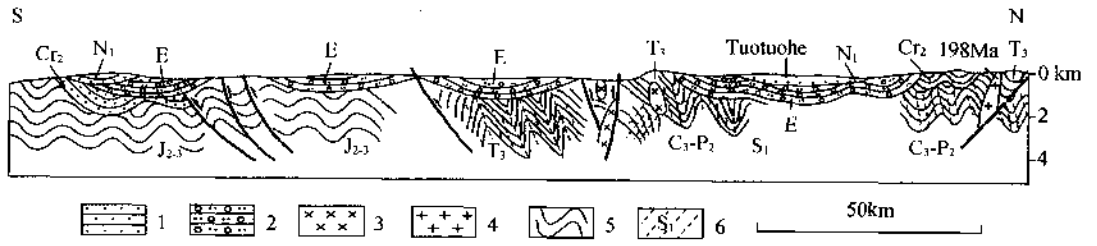

Fig.4 Geological cross-section of the Qiangtang region showing that the Miocene strata discordantly cover the gently folded Eocene strata. 1—Miocene strata; 2—Eocene strata; 3—gabbro; 4—granite; 5—folds; 6—cleavage. S_1—Lower Sillurian; C_3—Upper Carboniferous; P_2—Upper Permian; T_3—Upper Triassic; $J_{2\text{-}3}$—Middle and Upper Jurassic; K_2—Upper Cretaceous; E—Eogene; N_1—Miocene.

2. Because the Kunlun Mountains at the northern interior are mainly composed of lower Paleozoic folded basement and a large number of rigid granitic plutons, the crustal shortening is expressed by thrust faults. A series of west-northwest-striking ductile and brittle thrust faults have overthrust Proterozoic metamorphosed strata to the south-southwest onto Paleozoic, Mesozoic, and Cenozoic age strata, forming klippe and a stretching lineation trending 210°. In addition, there are some small north-northwest-striking dextral strike-slip faults and a few pull-apart basins of Oligocene age along these faults. The small dextral strike-slip faults cut off folded Mesozoic strata and displace some granitic bodies by less than 10km. These deformational features, coupled with the sinistral sense of the east-west-trending South Kunlun fault, indicate that the Kunlun terrain has undergone northeast-southwest commpression since Cenozoic time.

Strike-slip faulting

Large-scale shearing forces gave rise to the relative movement of the blocks in the northern plateau (Tapponnier and Molnar, 1977). The major strike-slip faults are described as follows (Fig.1).

1. The Altyn Tagh fault strikes 060°～070° and shows sinistral motion. The total displacement in Quaternary time is 39～50km, which was estimated from the horizontal offset of the Miocene basins at an average slip rate of 13～16.7mm/yr (Ge, 1992). Peltzer and Tapponier (1988) calculated that the displacement rate was～12 ± 2mm/yr in the western section and 15 ± 5mm/yr in the central section of the Altyn Tagh fault.

2. The South Kunlun fault zone consists of a series of sinistral faults, trending west-northwest for ～1600km. Along the fault zone there are a number of broad valleys, pull-apart basins, and push-up structures. The total ductile displacement along the fault zone since Triassic time is 110km, and in Quaternary time it is ～30km (Li *et al*., 1998). Kidd and Molnar (1988) proposed that the Holocene slip rate of the South Kunlun fault was between 10 and 20mm/yr, but more likely 13～15mm/yr. Detailed data of geomorphic offsets, evidence of paleo-earth-quakes in relation to the slip rates, and results of ^{14}C and thermoluminescence (TL) dating give estimated slip rates of 11.5mm/yr for the western, 9.5～11.5/mm for the central, and 7.0 mm/yr for the eastern sections of this fault (Zhao *et al*., 1996).

3. The Xianshuihe fault trends northwest-southeast in the eastern plateau and changes strike to north-south at the eastern margin of the plateau. The age of the Xianshuihe fault can be inferred by the ages of a syntectonic granite located at the southern end of the fault. This granite has an emplacement U-Pb age of 12.8 ± 1.4Ma and a cooling Rb-Sr age of 11.6 ± 0.4Ma (Calassou, 1994). The cumulative displacement by sinistral strike-slip movement is～80km (Xu *et al*., 1992). In a study of the regional history of late Quaternary fluviation and glaciation, Zhao *et al*. (1991) made geomorphic profiles and more than 80 measurements of ^{14}C and TL dating. The refined averages of left-lateral slip rates are 14 ± 2mm/yr, 2～5mm/yr, 10 ± 2mm/yr for the northwest, central, and southeast sections, respectively, in late Quaternary time.

The large strike-slip faults at the northern margin and central interior of the Qinghai-Tibet Plateau are therefore characterized by a sinistral sense, and, as a result of the faulting, blocks in the interior of the plateau have been rotated and extruded eastward or southeastward.

Cenozoic Deformation in the Hinterland of the Qinghai-Tibet Plateau

Tarim-Qaidam hinterland basins

The Tarim and Qaidam basins are located in the northern hinterland of the Qinghai-Tibet Plateau, and are separated by the Altyn Tagh fault. The basins contain Mesozoic-Cenozoic marine to continental facies sediments.

In the Qaidam basin, the sedimentary sequence is as thick as 6000m, and the basin is

characterized by high-angle thrust faults and west-northwest-trending folds (Fig.5). The folding in the basin migrated from the west to the center of the basin during Eocene and Holocene time (Xu *et al*., 1996). Both the southern and northern margins of the Qaidam basin are bounded by reverse faults. According to a magnetotelluric section (Zhang *et al*., 1992), the Qaidam basin plunged along the east-west-trending North Kunlun fault at its south margin at an intermediate angle southward beneath the Kunlun Mountains to a depth of 15km. At the northern margin of the basin, the Paleozoic and Proterozoic metamorphic rocks from the southern Qilianshan have been thrust southward onto the Cenozoic sediments of the basin. Xu *et al*. (1996) estimated that the crust of the Qaidam basin has shortened since Cenozoic time by at least 50～60km.

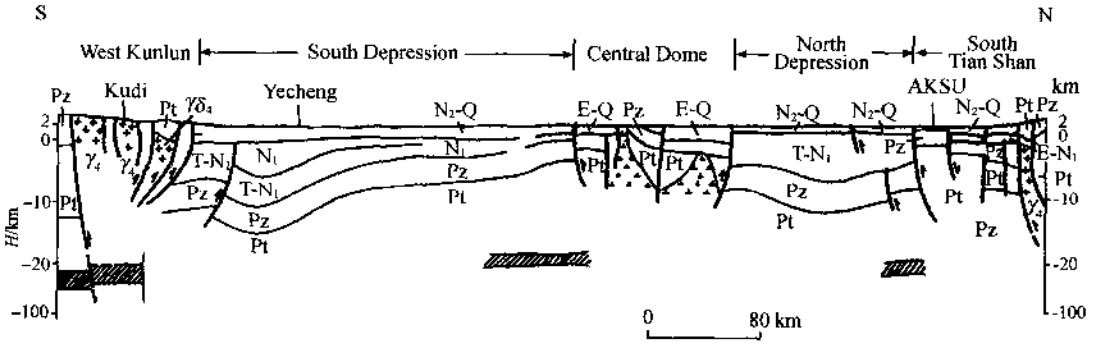

Fig.5 Geological cross-section of the Qaidam hinterland basin based on the magnetotelluric data (MT) (modified after Ding and Tang, 1996) showing tectonic units of the basin: north depression, central dome, and south depression; high-angle reverse faults, well developed in the basin, and marginal mountains thrusted on to the Tarim basin. Shaded parts represent low-resistant layers. Pz—Palaeozoic; Pt—Proterozoic; P—Permian; T—Triassic; N_1—*Miocene*; N_2—*Pliocene*; E—Eogene; Q—*Quaternary*. λ_4—Variscan granite; $\gamma\delta_4$—Variscan granodiorite.

To the west of the Altyn Tagh fault, there are two well-developed faulting depressions separated by a central dome in the Tarim basin; sediment thicknesses are as much as 6000m in the south and 9000m in the north. Symmetrical ramp faults are developed at both the northern and southern margins of the basin, suggesting that compression was transferred from the marginal mountains (South Tianshan and Karakoram) to the basin (Fig.5). The Tiekelike nappe at the northern Karakoram is displaced 70km northward by thrusting (Ding and Tang, 1996).

Hinterland thrust zone of the Tianshan-Qilianshan-Longmenshan

The Tianshan, Qilianshan, and Longmenshan thrust zones are at the northwestern, northeastern, and eastern margins, respectively, of the orogenic composite. The extensive convergence and deformation in Cenozoic time resulted in the overturned fan-like thrust system in the Tianshan-Qilianshan orogenic belt. As a result, the Tianshan was thrust southward onto the Tarim basin and northeastward onto the Junggar basin, whereas the Qilianshan was thrust southward onto the Qaidam basin and northward onto the Hexi corridor basin. The crustal shortening since 20Ma has been estimated to be～120km (Ding and Tang, 1996), and the

shortening rate is about 13mm/yr for the Tianshan and 15mm/yr for the Qilianshan during Holocene (Molnar and Deng, 1984; Avouac, 1991).

The northeast-southwest-trending Longmenshan thrust zone at the eastern margin of the plateau consists of a series of superimposed thrust sheets (Fig.6). The Proterozoic metamorphic complex at the front of the Longmenshan nappe has been overthrust eastward onto the continental Sichuan basin of Cretaceous-Eocene age. The lag ductile normal fault formed at 13～20Ma, as determined by $^{39}Ar/^{40}Ar$ dating of retrograde metamorphic biotite (Xu *et al.*, 1992; Calassou, 1994). The uplift of the Longmenshan Proterozoic metamorphic complex is considered to be closely related to the vertical extrusion caused by the formation of both the thrust and normal faults (Fig.6). This is similar to the uplift and exhumation of the High Himalaya metamorphic belt associated with the formation of the Main Central thrust and the south Tibetan detachment fault at 20Ma (Burg and Chen, 1984; Burchfiel and Royden, 1985; Mattauer and Brunel, 1989; Cui *et al.*, 1992; Chemenda *et al.*, 1995). Therefore, vertical extrusion is probably one of the most important factors related to the uplift of old metamorphic terrain in the orogenic belts and is the result of intracontinental subduction of lithospheric plate material (Chemenda, 1994).

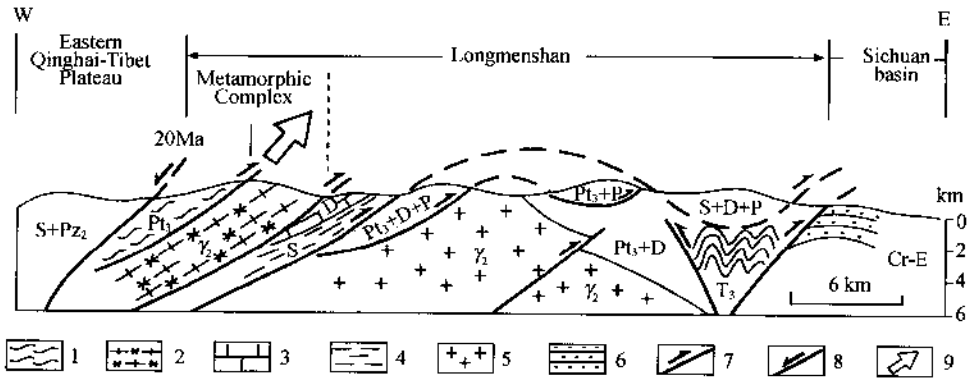

Fig.6 A tectonic cross-section of Longmenshan Mountains (modified after Xu *et al.*, 1992), displaying Longmen Shan thrusts and nappe structure. This section shows that the uplift of the upper Proterozoic metamorphic complex is related to vertical extrusion, which is caused by thrusts and normal faults. 1—Schist; 2—granitic mylonite; 3—limestone; 4—phyllite; 5—migmatited granite; 6—sandstone and conglomerate; 7—thrust; 8—normal fault; 9—vertical extrusion. Pz_2—upper Paleozoic; Pt_3—upper Proterozoic; S—Silurian; D—Devonian; P—Permian; T—Triassic; Cr—Cretaceous; E—Eogene; γ_2—Proterozoic granite.

In general, the hinterland of the Qinghai-Tibet Plateau has been subjected to extensive compression for at least 20Ma, and the compression direction is north-south at the Tianshan, northeast-southwest at the Qilianshan, and northwest-southeast at the Longmenshan. The Mesozoic and Cenozoic basins on the North China and Yangtze cratons at the margins of the Tethys-Himalaya orogenic composite have been embedded beneath the hinterland thrust zones. The compression at the hinterland thrust zones was stronger than that at the hinterland basins and the interior of the Qinghai-Tibet Plateau, but weaker than that at the Himalaya foreland

superimposed thrust zone, where the crustal shortening rate reached 18mm/yr in Holocene time (Molnar and Deng, 1984; Avouac, 1991). In addition, the rapid uplift and exhumation of the old metamorphic terrain at the margins of the Qinghai-Tibet Plateau is probably attributable to vertical extrusion, a result of intracontinental subduction. Thus the Qinghai-Tibet Plateau formed a particular topography, that is, high mountains at the margins and relatively flat in the interior of the plateau, as we see today.

Geophysical Investigation of the Interior and the Hinterland of the Qinghai-Tibet Plateau

The data quoted here are from the Sino-French natural earthquake experiment section (Golmud-Kunlun Pass-Wudaoliang-Tuotuohe through Amdo-Lhasa-Rikaze-Gala) at the interior and the foreland of the Qinghai-Tibet Plateau, carried out in 1992～1994, using 110 seismometers. In this project, properties of anisotropy of the lithospheric mantle from Golmud to Gala were measured based on the splitting features of SKS, PKS, and PS (converted) waves (Hirn *et al*., 1995; Shi *et al*., 1998). Velocity images down to 400km in depth were obtained by seismic tomography and the lithospheric structure from Golmud to Gala was mapped using converted phases from natural earthquakes (Jiang *et al*., 1995; Xu *et al*., 1996; Wittlinger *et al*., 1996).

Lithospheric structure of the northern Qinghai-Tibet Plateau

The lithospheric structure of the northern Qinghai-Tibet Plateau was obtained by earthquake converted wave experiments. The arrival times of the PS (converted waves) at the section from Golmud to Wenquen (Fig.7) show the following features.

1. The depth of the Moho changes from 70km to 60km from south to north.

2. There are three low-velocity layers dipping northward at a low angle within the upper 30km of crust in the region.

3. The 140-km-thick multisandwich structure of lithosphere consists of alternating high- and low-velocity layers. It is well accepted that the high-velocity and low-velocity layers represent the materials of high and low density, respectively. The low-velocity layer at the lower lithosphere may be explained by the properties of partial melting, high heat flow, and low rheologic strength (Xu *et al*., 1996).

4. The lithospheric faults (or zones of discontinuity) correspond to the northern marginal faults of the Kunlun Mountains, the South Kunlun fault and the Jinshajiang fault, and these are characterized by sinistral movement (Xu *et al*., 1996).

Seismic tomographic section transversing the northern Qinghai-Tibet Plateau and Himalayas

The seismic tomographic section of Golmud-Gala (Jiang *et al*., 1995; Hirn *et al*., 1995; Wittlinger *et al*., 1996) has provided velocity images to 400km in depth shown in Figures 8 and 9.

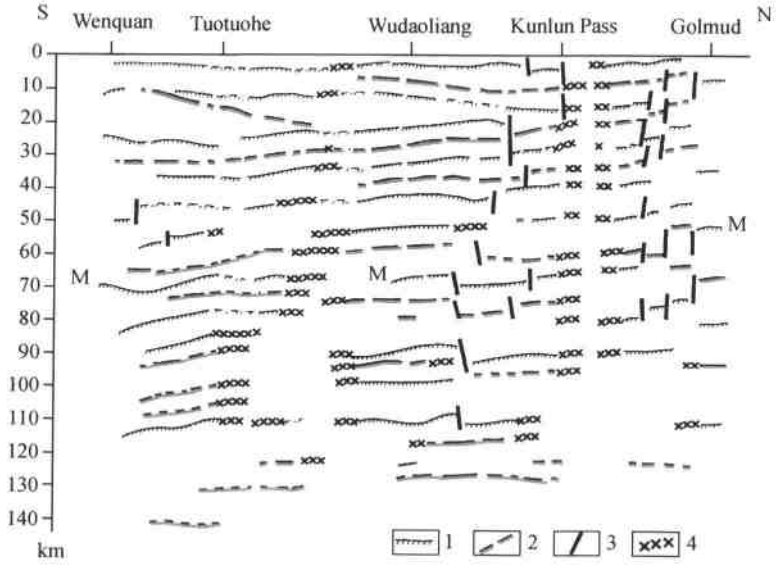

Fig. 7 An interpreted lithospheric structure profile from Golmud to Wenquan derived from the arrival time of PS converted waves, showing the multisandwich structure, which consists of alternating high-and low-velocity layers, and lithospheric faults. 1—converting interface of high velocity; 2—converting interface of low-velocity; 3—inferred fault; 4—zone of discontinuity.

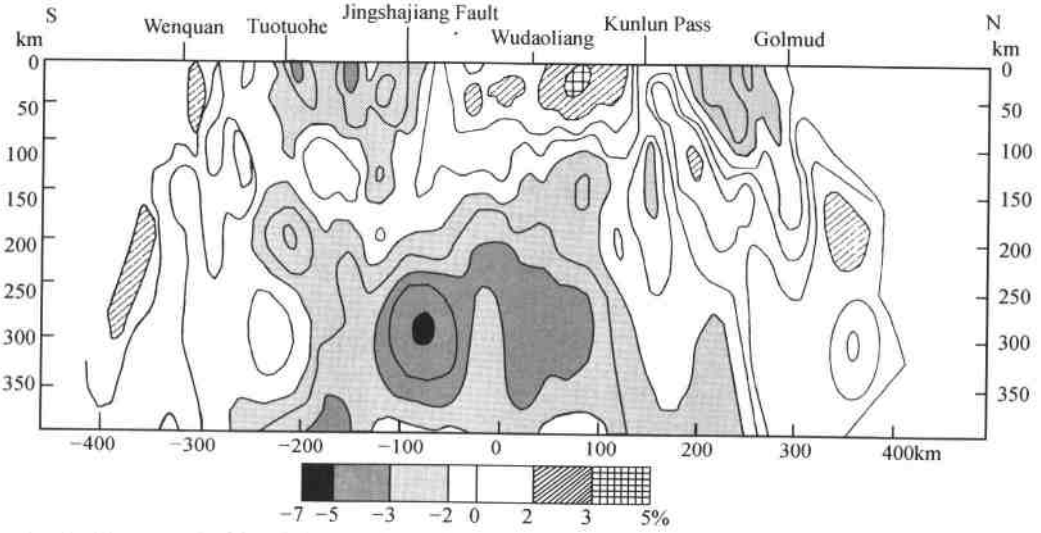

Fig. 8 A cross section from Golmud to Wenquan based on data from seismic tomographic inversion (after Jiang *et al.*, 1998), showing a large low-velocity anomaly from 200 to 360km depth beneath the Hoh Xil region. The lithosphere above 100km, north of the Jinshajiang fault, is high velocity, whereas it is low velocity south of the Jinshajiang fault. Units represent relative seismic velocity ratio (%).

Golmud-Wenquan seismic tomography section. The lithosphere above 100km in depth in the Bayan Hat terrain between the Kunlun Pass to the Jinshajing fault is of high velocity, and inferred to be cold, whereas in the northern Qiantang terrain between the Jinshajiang fault and

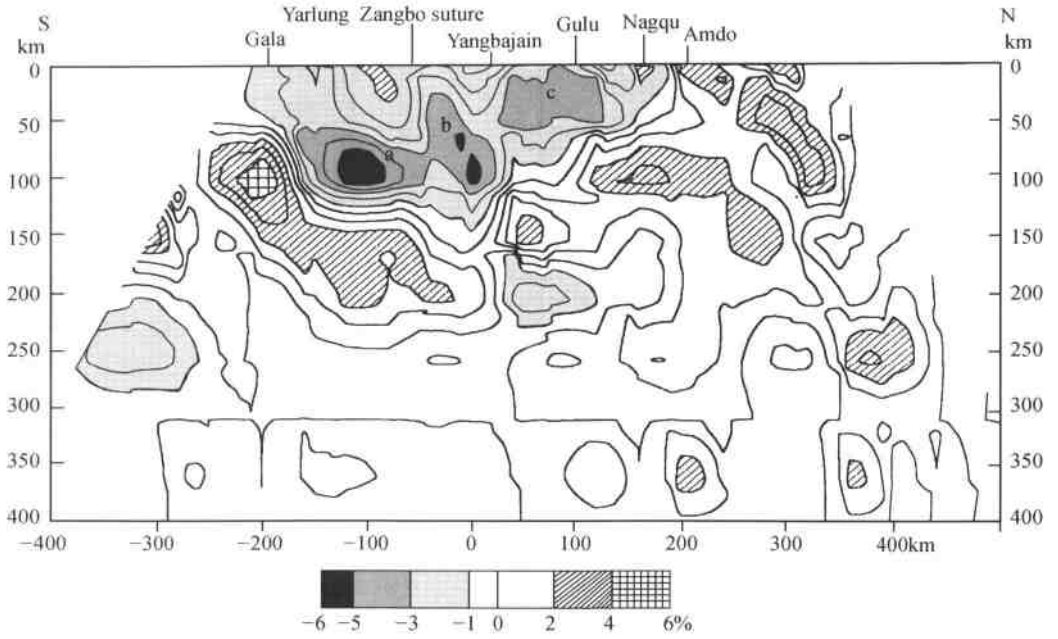

Fig.9 A cross section from Amdo to Gala based on data from seismic tomographic inversion shows a high-velocity zone plunging northward beneath the Himalayas 200km in depth at the south of Gala, and three low-velocity anomalies (a, b, c) from Gala to Nagqu above the high-velocity zone. Units represent relative seismic velocity ratio (%).

Tuotuohe it is low-velocity and inferred to be hot. Under the Hoh Xil region in the central part of the interior of the plateau, there is a large low-velocity anomaly between the depths of 200 and 360km. It is～250km long, 250km wide, and 160km thick. This low-velocity anomaly is inferred to be associated with high heat flow, high conductivity, and low creep strength, corresponding to the Cenozoic alkaline volcanic activity in the Hoh Xil region. The large low-velocity anomaly may indicate a mantle plume or mantle diapir (Xu *et al*., 1996; Wittlingen *et al*., 1996; Jiang *et al*., 1998), and the smaller low-velocity bodies located in the shallow region south of the Jinshajiang fault may correspond to a hotspot group (Xu *et al*., 1996).

Amdo-Gala seismic tomographic section. In this section, a high-velocity zone from the south of Gala plunges northward at an intermediate angle to 200km beneath the Himalayas, but not beyond the Yarlung Zangbo suture, and it is interpreted to be the result of the intracontinental subduction of the lithospheric mantle of the Indian plate under the Eurasian plate. Above this high-velocity zone, an obvious low-velocity anomaly zone (A in Fig.9) occurs at depths of 50 to 100km north of Gala, and probably formed in response to the subduction. The small northward-dipping low-velocity block (B in Fig.9) below the Yarlung Zangbo suture zone is explained as the result of partial melting produced by the continuous activity on this suture zone. The shallow (0－50km) low-velocity layer (C in Fig.9) from Yangbajain to Gala is considered to be related to the Quaternary rifting. There are two high-velocity bodies within the lower velocity section at depths from 80 to 150km in the mantle, which are located below the

low-velocity layer C (Fig.9) north of Yangbajain, and these are suggested to be evidence for delamination of the lithosphere (England and Houseman, 1989).

A comparison of the seismic tomography sections in Figures 8 and 9 shows that the low-velocity anomaly region beneath the southern plateau and Himalaya is at a shallow level (<100km), whereas the low-velocity anomaly region beneath the central interior (Hoh Xil region) of the plateau is at a deep level (200~300km). The low-velocity region in the southern part was related to intracontinental subduction caused by the collision of the Indian and Eurasian plates. Previous seismic data for the northern part indicated a Sn-poor zone (Barazangi and Ni, 1982), a poor high-velocity upper mantle cover, thinner lithosphere, high heat-flow values, and a low-velocity zone (Molnar and England, 1990), as well as a large-magnitude anisotropy, all of which represent upper mantle flow beneath the Hoh Xil region and are related to alkaline volcanic activity since 20Ma. However, the interpretation of the presence of a mantle diapir located in the upper part of the lower mantle can be considered as genetically related with these features.

Geophysical data from the hinterland of the Qinghai-Tibet Plateau: Explosive seismic profile from Huashixia to Jianyang at the eastern margin of the Qinghai-Tibet Plateau. The deep structure of the crust at the eastern margin of the Qinghai-Tibet Plateau and the nearby Yangtze craton was recently revealed by the Huashixia-Jianyang explosive seismic section (Fig.10) (Cui *et al*., 1996). The northwest-southeast-trending Huashixia-Jianyang section is about 770km long, and crosses the eastern margin of the Qinghai-Tibet Plateau, the Longmenshan, and the western Sichuan basin. The section shows the following features.

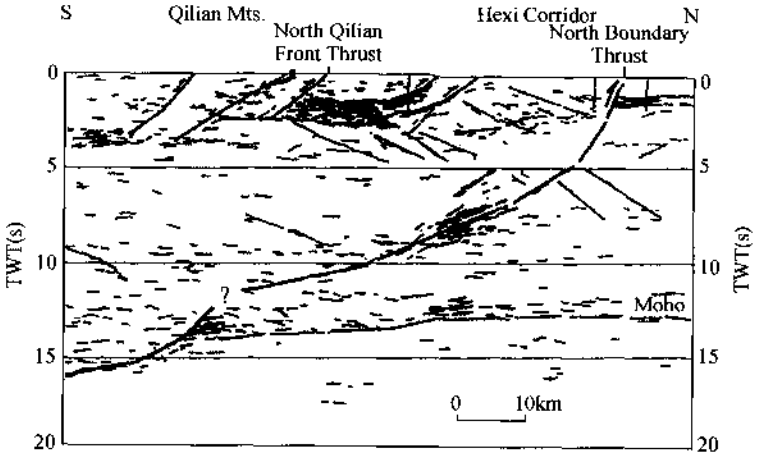

Fig.10 Explosive seismic profile from Jianyang to Aba (eastern section of Jianyang-Huashixia, after Cui *et al*., 1996), showing two low-velocity layers at 10 and 20km depth beneath the eastern Qinghai-Tibet Plateau. The Yangtze craton was embedded as a wedge into the lower crust of the Longmenshan forming a "crocodile" structure between the Longmenshan, and the Yangtze Craton.

1. The crustal thickness is progressively augmented from east to west, from 40km to 68km.

2. Two detachments composed of low-velocity materials at a depth of 20km beneath the eastern Qinghai-Tibet Plateau have been recognized, and are associated with the normal fault at the west of the Longmenshan Mountains.

3. Thrusts at the front of the Longmenshan Mountains caused the Longmenshan strata to overlap the Sichuan basin.

4. The Moho at 40km depth below the Longmenshan has been offset by a gently east dipping reverse fault. As a result, the Yangtze craton acted as a wedge and was embedded into the lower crust of the eastern Qinghai-Tibet Plateau (Cui *et al*., 1996).

Golmud-Ejin Qi geotransect at the northern margin of the Qinghai-Tibet Plateau. The Golmud-Ejin Qi geotransect (Fig.11) (Wu *et al*., 1995) shows that thrusting occurs at the both sides of the Qilian Mountains and, as a result, the Qilian mountains have been overthrust onto the Hexi corridor basin, and Qaidam basin. On the basis of the fine crustal structure of the northern Qilianshan and Hexi corridor obtained by the seismic reflection survey (Fig.11), it is apparent that the front thrust of north Qilianshan is dipping to the south, steeply at shallow levels and gently at deeper levels. This thrust fault connects with a low-angle decollement zone, represented by a reflection zone at the depth of ～10km beneath the Qilian mountains. In the north, the major North Boundary thrust in the Hexi corridor extends southward at a low angle (～20°) for 100km, reaching a depth of 30km beneath the Qilian mountains (Gao *et al*., 1995). This fault acts as a boundary between the seismic region to the south and the aseismic region to the north (Yan *et al*., 1979). Natural earthquake activity is distributed at 60～130km depth south of the North Boundary thrust and the focal depth is not deeper than 30km (Wu *et al*., 1995). Thus, it is inferred that the North China craton has been subducted southward beneath the Qilian mountains.

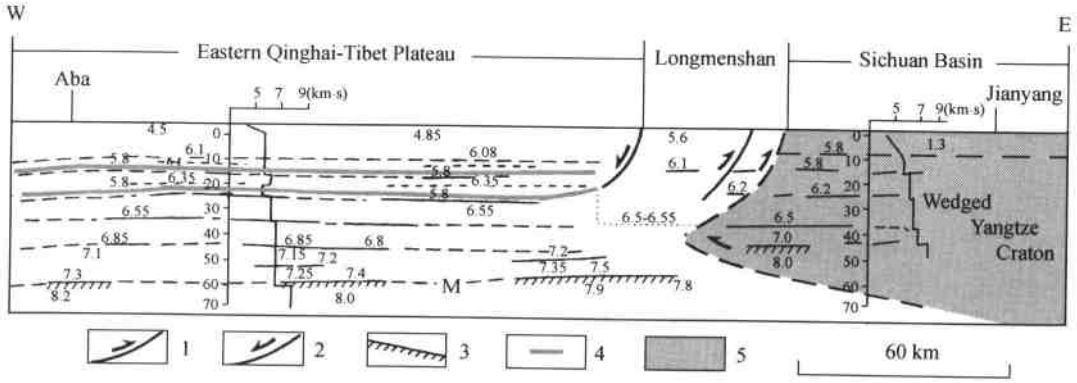

Fig.11 Deep seismic reflection profile from the northern Qilianshan Mountains to the Hexi corridor basin (after Wu *et al*., 1995), showing the North Qilian front thrust connected by a decollement zone represented by a reflection zone at 10km depth beneath the Qilianshan, and the North Boundary thrust in the Hexi corridor extending southward at a low angle to 30km depth beneath the Qilianshan. 1—Thrust fault; 2—normal fault; 3—Moho; 4—decollement zone; 5—wedged Yangtze craton.

Discussion on Mechanism of the Uplift of the Qinghai-Tibet Plateau

Several lines of evidence show that intracontinental deformation occurred in the Cenozoic time, particularly since 20Ma, after the collision between the Indian and Eurasian plates. Crustal deformation and geophysical properties of the interior and margin of the Qinghai-Tibet Plateau show significant differences during the Cenozoic geological events. Therefore, it is necessary to take the constraints on various factors, obtained from different sections and depths of the Qinghai-Tibet Plateau, into consideration.

Mantle diapir below the northern Qinghai-Tibet Plateau

The existence of the mantle diapir beneath the interior of the plateau suggests that it is an important dynamic source at depth. The genetic relationship between the mantle diapir and alkaline volcanic activities hints that the dynamic source is probably produced initially from a cohesive thermal flow, and the dynamic driving force probably originates from radioactivity and heat energy from the upper mantle. The thermal upflow moves horizontally along the lower part of lithosphere and forms an extensional setting. In contrast, along lithospheric faults, it flows up to the Earth's surface, and produces largescale volcanic eruptions in the Hoh Xil region. The thermal upflow in the mantle is probably the cause of the multisandwich structure in which high-and low-velocity layers alternate in the lithosphere around this region.

Inward subduction at the margins of the Qinghai-Tibet Plateau

That the Indian plate subducted northward beneath the Eurasian plate has been further confirmed by the Sino-American INDEPTH I seismic profile across the Himalayas (Zhao and Nelson, 1993; Zhao *et al*., 1996). The result of the Sino-French seismic tomographic profile shows that the Indian lithospheric mantle subducted northward at an intermediate angle to a depth of 220km beneath the Himalayas, but does not go beyond the Yarlung Zangbo suture. This is consistent with the results of the seismic anisotropy section, in which obvious different anisotropic directions are represented by flow of upper mantle on both sides of the Yarlung Zangbo suture (Jiang *et al*., 1995; Shi *et al*., 1998).

Some geologists have proposed that the volcanism of Hoh Xil, in the interior of the Qinghai-Tibet Plateau, is related to intracontinental subduction from the north, which would suggest that the Qaidam block and the Tarim block underlie the Kunlun mountains. However, we have not obtained any geophysical data to prove this. Instead, we propose that the North China craton plunged southwestward at a low angle beneath the Qilianshan. The intensive crustal shortening of the Qilianshan and earthquake activity since Cenozoic time support this hypothesis.

At the eastern margin of the Qinghai-Tibet Plateau, the lithospheric structure represented by the geoscientific transect data suggests the existence of intracontinental subduction between the eastern Qinghai-Tibet Plateau and the Yangtze craton. Thus, we propose a hypothesis of inward intracontinental subduction at the margins of the Qinghai-Tibet Plateau.

Significance of strike-slip faults

A number of sinistral strike-slip faults are in the interior of the Qinghai-Tibet Plateau, and these have been considered to be the result of collision between the Indian plate and the Eurasian plate (Tapponnier and Molnar, 1977; Molnar and England, 1990).

We suggest that noncoaxial compression and oblique crustal shortening in the Qinghai-Tibet Plateau, which are caused by northeast-southwest compression at the north margin and the south-north compression at the southern margin, are most likely responsible for the formation of sinistral strike-slip faults in the interior of the Qinghai-Tibet Plateau.

In conclusion, we suggest a new model to explain the mechanism of uplift of the Qinghai-Tibet Plateau, that is, a mantle diapir in the interior and inward subduction at the margins of the Qinghai-Tibet Plateau (Fig. 12). However, questions about ① the original relationship between a mantle diapir at the interior of the plateau and inward subduction at the margins of the plateau, and ② whether the inward subduction of the margin is active or passive remain.

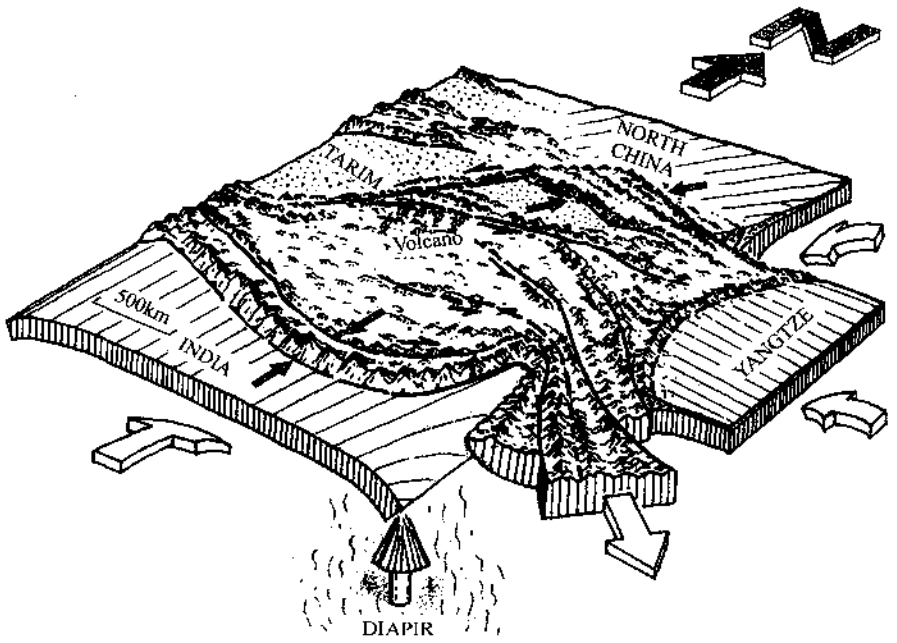

Fig. 12 A model of the Qinghai-Tibet Plateau shows a mantle diapir and deep thermal spreading beneath northern interior of the plateau, suggested to be responsible for the alkaline volcanic activity of in the region. Inward intracontinental subduction occurs at the south, east, and northeast margins of the plateau, as shown by the arrows. Strike-slip faults cause eastward or southeastward extrusion of the blocks under noncoaxial compression. The spear shows the direction of high heat flow from the mantle diapir.

Acknowledgments

We acknowledge strong and continuous support given by the Ministry of Geology and Mineral Resources of the People's Republic of China and the Institut National des Science l'Univers, Center National de la Recherche Scientifique of France during the previous East Kunlun (1992～1994) and undergoing Altyn-Qilianshan (1995～1998) collaborative projects between Chinese and French scientists. We thank A. M. Macfarlane, George Zandt, Yang Wencai, and an anonymous reader for thorough and constructive reviews.

REFERENCES CITED

Argand, E., 1924, La tectonique de l'Asie: International Geological Congress, 13th, Brussels, 1922, Reports, v. 1, p. 170～372.

Avouac, J. P. 1991, Application des methods de morphologie quantitative a la Neotectonique: Model Cinematique des deformations actives en Asia Centrale [Ph.D. thesis]: Paris, Universite Paris Ⅶ, 50p.

Barazangi, M., and Ni, J., 1982, Propagation characteristics of Pn beneath the Himalayan arc and Tibetan plateau: Possible evidence for underthrusting of Indian continental lithosphere beneath Tibet: Geology, v. 10, p. 179～185.

Begboul, N., Barazangi, M., and Isacks, B. L., 1993, Lithospheric structure of Tibet and western north America: Mechanisms of uplift and a comparative study: Journal of Geophysical Research, v. 98, p. 1997～2016.

Burchfiel, B. C., and Royden, L. H., 1985, North-south extension within the convergent Himalayan region: Geology, v. 13, p. 653～679.

Bureau of Geology and Mineral Resources of Qinghai Province, 1991, Regional Geology of Qinghai Province: Beijing, Geological Publishing House, p. 206～227.

Burg, J. P, and Chen, G. M., 1984, Tectonics and structural zonation of southern Tibet, China: Nature, v. 311, p. 219～223.

Calassou, S., 1994, Etude Tectonique d'une chaine de Decollement [thesis]: Universite de Montpellier Ⅱ-Sciences et Technigues du Langnedoc, 373 p.

Chemenda, A. I., 1994, Subduction, insights from physical modeling: Dordrecht, Kluwer Academic Publishers, 193 p.

Chemenda, A. I., Mattauer, M., Malavieille, J., and Bokun, A. N., 1995, A mechanism for syn-collisional rock exhumation and associated normal faulting: Results from physical modeling: Earth and Planetary Science Letters, v. 132, p. 225～232.

Cui Junwen, Zhu Hong, and Wu Chande, 1992, Yadong-Golmud GGT, Deformation and dynamics of the lithosphere in Qinghai-Xizang (Tibet) plateau: Beijing, Geological Publishing House, 164 p.

Cui Zuozhou, Chen Jiping, and Wu Ling, 1996, Altay-Taiwan GGT, texture and structure of Huashixia-Shaoyang deep crust: Beijing, Geological Publishing House, 192 p.

Deng Wanming, 1978, The Quaternary volcanic petrology and geochemistry in the Northern Tibet——A preliminary study: Acta Geologica Sinica, v. 2, p. 148～162.

Deng Wanming, 1991, Cenozoic volcanism and intraplate subduction in northern margin of the Tibet plateau: Journal of Geochemistry, v. 10, p. 140～152.

Deng Wenming, Zheng Xilan, and Yukio Matsumoto, 1996, Petrological characteristics and ages of Cenozoic volcanic rocks from the Hoh Xil Mts., Qinghai province: Acta Petrologica et Mineralogica, v. 15, p. 289～298.

Dewey, J., and Bird, J., 1970, Mountain belts and the new global tectonics: Journal of Geophysical Research, v. 75, p.

2625～2647.

Dewey, J., and Burke, K., 1973, Tibetan, Variscan and Precambrian basement reactivation: Products of continental collision: Journal of Geology, v. 81, p. 683～692.

Ding Daogui and Tang Liangjie, 1996, Formation and evolution of the Tarim basin: Hehai University Press House, 302 p.

England, P., and Houseman, G., 1986, Finite strain calculations of continental deformation. Comparison with the India-Asia collision zones: Journal of Geophysical Research, v. 91, p. 3664～3676.

England, P., and Houseman, G., 1989, Extension during continental convergence, with application to the Tibetan plateau: Journal of Geophysical Research, v. 94, p. 17561～17579.

Gansser, A., 1964, Geology of the Himalayas: London, Interscience Publication, John Wiley, 289 p.

Gao Rui, Cheng Xiangzhou, and Ding Qian, 1995, Preliminary geodynamic model of Golmud-Ejin Qi Geoscience transact: Acta Geophysica Sinica, v. 38, supplement Ⅱ, p. 3～14.

Ge Shumo, ed., 1992, The Altyn-Tagh active fault zone: Beijing, Seismological Press, 319 p.

Hirn, A., Jiang, M., Diaz, J., Nercessian, A., Lu, Q. T., Lepine, J. C., Shi, D. N., Sachpazi, M., Pandey, M. R., Ma, K., and Gallart, J., 1995, Seismic anisotropy as an indicator of mantle flow beneath the Himalayas and Tibet: Nature, v. 375, p. 571～574.

Jiang, M., Hirn, A., and Poupinet, G., 1995, Tibetan Plateau Seismic Experiment: Design and preliminary results, 1992～1993: Global Tectonics and Metallogeny, v. 4, p. 199～201.

Jiang Mei, Lu, Q. T., Shi, D. N., Xue, G. D., Poupinet, G., and Hirn, A., 1998 Research on crust-upper mantle structure under the central Tibetan plateau by means of teleseismic experiment: Acta Geophysica Sinica (in press).

Kidd, W. S. F., and Molnar, P., 1988, Quaternary and active faulting observed on the 1985 Academia Sinica-Royal Society Geotraverse of Tibet: Royal Society of London Philosophical Transactions, ser. A, v. 327, p. 337～363.

Le Fort, P., 1975, Himalayas-the collided range, present knowledge of the continental arc: American Journal of Science, v. 275A, p. 1～44.

Li Haibing, Xu Zhiqin, and Chen Wen, 1998, Important style of introcontinental deformation: The South Kunlun strike-slip fault zone in the East Kunlun Mts.: Continental Dynamics, v. 1, no. 2 (in press).

Mattauer, M., 1990, Arguments en faveur d'un diapir mantellique sous le plateau Tibetan: Science de la Terre, v. 310, p. 1695～1700.

Mattauer, M., 1992, Continental subductions and large strike-slip faults in Tibetan-Himalayan system [abs.], in International symposium on the Karakoram and Kunlun Mountains, Kashi, China, June 5～9, 1992: Paris, Inst. National. Sci. Univers., p. 2.

Mattauer, M., and Brunel, M., 1989, La faille normale Nord-Himalayenne (FNNH) consequence probable d'un diapirisme granitique: Paris, Académie des Sciences Comptes Rendus, v. 308, p. 1285～1289.

Mattews, D., and Hirn, A., 1984, Crust thickening in Himalayas and Caledinides: Nature, v. 308, p. 497～498.

Molnar, P., and Deng, Q. D., 1984, Faulting associated with large earthquakes and the average rate of deformation in central and eastern Asia: Journal of Geophysical Research, v. 89, p. 6203～6228.

Molnar, P., and England, P., 1990, S-wave residuals from earthquakes in the Tibetan and lateral variations in the upper mantle: Earth and Planetary Science Letters, v. 101, p. 68～77.

Molnar, P., and Tapponnier, P., 1975. Cenozoic tectonics of Asia: Effects of a continental collision: Science, v. 74, p. 419～462.

Peltzer, G., and Tapponnier, P., 1988, Formation and evolution of strike-slip faults, rifts, and basins during the India-Asia collision: An experimental approach: Journal of Geophysical Research, v. 93, p. 15085～15117.

Powell, C., and Conaghan, P. J., 1973, Plate tectonics and the Himalayas: Earth and Planetary Science Letters, v. 20, p. 1～12.

Powell, C., and Conaghan, P. J., 1975, Tectonics models of the Tibetan Plateau: Geology, v. 3, p. 727～732.

Shen Xianjie, 1996, Plate-kinematics origin of the N-S heterogeneity of the Tibetan crustal-mantle thermal structure and its dynamic implications: Continental Dynamics, v. 1, p. 38～48.

Shi Danian, GongYingjun, and Jiang Mei, 1998, Shear wave anisotropy beneath the Tibetan plateau: Global Tectonics and Metallogeny, v. 5 (in press).

Tapponnier, P., and Molnar, P., 1977, Active faulting and Cenozoic tectonics of China: Journal of Geophysical Research, v. 82, p. 2905～2930.

Tapponnier, P., Peltzer, G., and Le Dain, A. Y., 1982, Propagating extrusion tectonics in Asia: New insights from simple experiments with plasticine: Geology, v. 10, p. 611～616.

Wittlinger, C., Masson, F., Tappnnier, P., Jiang Mei, Herquel, G., and Achauer, U., 1996, Seismic tomography of northern Tibet and Kunlun: Evidence for crustal blocks and mantle velocity contrasts: Earth and Planetary Science Letters, v. 139, p. 263～279.

Wu Xuanzhi, Wu Chunling, Lu Jie, and Wu Jie, 1995, Research on the fine crustal structure of the northern Qilian-Hexi Corridor by deep seismic reflection: Acta Geophysica Sinica, v. 38, supplinent Ⅱ, p. 29～35.

Xiao Xuchang, 1995, Tectonic evolution and uplift of the Himalaya-Tibet plateau: 10th Himalaya-Karakoram-Tibet Workshop (Abstract volume); Eidgenössischen Technischen Hochschule Conference Center Monte Verita (Ascona), Canton Ticino Switzerland: p. 45～46.

Xu Zhiqin and Cui Junwen, 1996, Deformation and dynamics of continental mountain chains: Beijing, Metallurgic Publishing House, 246 p.

Xu Zhiqin, Hou Liwei, and Wang Zongxiu, 1992, Orogenic processes of the Songpan-Ganze orogenic belt of China: Beijing, Geological publishing House. 190 p.

Xu Zhiqin, Jiang Mei, and Yang Jingsui, 1996, Tectonophysical process at depth for the uplift of the northern part of the Qinghai-Tibet Plateau: Illustrated by the geological and geophysical comprehensive profile from Golmud to the Tanggula mountains, Qinghai Province, China: Acta Geologica Sinica, v. 70, p. 195～206.

Yan Jiaquan, Shi Zhenglian, Wang Suyun, and Huan Wenlin, 1979, The regional characteristics of present-day tectonic stress field in China and adjacent region: Acta Seismologica Sinica, v. 1, p. 9～24.

Yang, J.-S., Bai, W., and Hu X., 1996, Basin subduction model for the uplift of the Qinghai-Tibet Plateau: Evidence from the Cenozoic volcanism in Hoh Xil, North Tibet: International Geological Congress, 30th, Beijing, China, 4～14 August 1996, Abstracts v. 1, p. 205.

Yang Jingsui, Xu Zhiqin, Bai Wenji, and Zhao Rongli, 1998, Cenozoic volcanism on the Qinghai-Tibetan plateau and its genesis: Continental Geodynamics (in press).

Zhang, Q. R., Xie, M. Q., and Xue, C., 1992, Statistical analysis of the structural evolution of western Qaidam basin: Geological Society of Malaysia Newsletter, v. 18, p. 265～266.

Zhang Yifu and Zheng Jian kang, 1994, Geological overview in Hoh Xil, Qinghai and adjacent Areas: Beijing, Seismic Publishing House, 177 p.

Zhao Guoguang, Liu Dequang, Wei Wei, He Qunlu, and Su Gang, 1991, The late Quaternary slip rate and segmentation of the Xian Shuihe active fault zone, in Proceedings of the PRC-USA Bilateral Symposium on the Xianshuihe fault zone, Chengdu, China, October 1990: Beijing, Seismological Press, p. 41～57.

Zhao, W. J., and Nelson, K. D., 1993, Project INDEPTH Team, deep seismic reflection evidence for continental underthrusting beneath south Tibet: Nature, v. 366, p. 557～559.

Zhao Wenjin, Nelson, K. D., Che Jingkai, Brown, L. D., Xu Zhongxin, and Kuo. J.T., 1996, Deep seismic reflection in Himalaya region reveals the complexity of the crust and upper mantle structure: Acta Geophysica Sinica, v. 39, p. 615～628.

Zhao, W. L., and Morgan, W. J., 1985, Uplift of the Tibetan Plateau: Tectonics, v. 4, p. 359～369.

Zhao, W. L., and Yuen, D. A., 1987, Injection of Indian crust into Tibetan lower crust: A temperature-dependent viscous model: Tectonics, v. 6, p. 505～514.

Manuscript Accepted by the Society February 3, 1998.

The Formation of The Qinling Mountain Chain As The Backbone of China——Convergence, Collision and Intracontinental Subduction[1]

Xu Zhiqin Tang Yaoqing[2] Lu Yilun
(Institute of Geology, CAGS, Beijing, China;
Geological Bureau of Shaanxi Province, Xi'an, China)

The Qinling Mountain Chain including the Qinling, Dabie and Jiaonan Mountains, which streches latitudinally more than 1000km long and is viewed as a backbone of the mainland of China, was formed through convergence, and subsequent collision and intracontinental subduction of the South China plate (SCP) against the North China plate (NCP). Therefore, the Qinling Mountain Chain is of composite orogenic belts constituted by a narrow Palaeozoic belt to the north and a broader Indosinian one to the south. Furthermore, it was complicated by the truncation at its eastern extreme by the N-S striking Tanlu fault.

The northern Palaeozoic belt was formed during 450～330Ma, which is underlain by an ancient crystalline basement (2500Ma) and overlain unconformably both by Middle and Upper Proterozoic and lower Palaeozoic covers, with widespread fold and largescale nappe structures and ophiolitic slices found along its southern margin of the belt. The southern Indosinian belt is characterized by a double metamorphic basement composed of Lower to Middle Proterozoic high-grade metamorphic rocks (Dabie Group) and Upper Proterozoic low-grade metamorphic volcanic rocks. Formation of the folds developed within the Sinian to Triassic cover rocks is essentially caused by detachment appearing between these and the Upper Proterozoic rocks. Moreover, detachment occurred also between the low-grade metamorphic (Pt_3) and high-grade metamorphic (Pt_{1-2}) rocks. The Indosinian orogenis occurred mainly at a time span of 200～250Ma, but it started since the Late Hercynian locally along its northern margin. A large E-W-trending sinistral striking-slip fault exists between the northern and southern orogenic belts, which formed during 300～320Ma.

Generally, features of the Qinling Mountain Chain were ultimately caused by these large nappe, strike-slip and detachment.

---

[1] Progress in geosciences of China(1985～1988).
——Papers to 28th IGC.

[2] Participated in the study of the Qinling Mountains are also Mattauer, Matte, Tapponnier, Maluski Malavielle et Peltze from France, and Zhang Qingwen, Wang Yongming from China.

1 Nappe structure in the northern orogenic belt

Within this orogenic belt, fold structure involved with the cover is manifested by a feature of progressive evolution. For instances, the simple Jura-type concentric folds, with steep local cleavage, were formed in its north part, tight and overturned fold, with strong slaty cleavage, were developed in its central part, and the pennine-type fold nappe took place in its south part. In addition, three major ductile thrust zones are developed in the southern part, i.e. the intracrustal northern and central ductile thrust zones and the mantle-crustal southern thrust zone. The ductile thrust zones are commonly featured by gentle flow cleavage, A-type folds, mylonization and nearly N-S down-dip stretching lineation. The latter is particularly well developed in conglomerates and oolitic limestones. In the northern ductile nappe zone (NDT), the maximum stretching value (X:Z) of oolites in the Middle Cambrian oolitic limestones attains 50:1. The study of the finite and rotational strains and the quartz fabric analysis indicate a simple shear mechanism (Flinn parameter $K=1$) and southward shearing direction.

In the southern ductile zone (SDT), a large (20km×2km) ophiolitic massif, consisting mainly of mylonitized Cr-rich metamorphic peridotites (dunite and harzburgite), metagabbro and metavolcanic rocks, has been thrust onto the Lower Palaeozoic dome about 30km wide. This dome is composed of gneiss and marble which have subjected to early horizontal foliation, recumbent folds, ductile thrusts and strong migmatization. The existance of 40m wide of garnet-bearing amphibolite at the base of the ophiolitic allochtone can be seen as an important evidence for ocean floor obduction.

Study of preferred orientation and dislocation in olivine from harzburgite through electron microscope transmission observations indicates that high temperature (>1300℃) creep strain occurred within the upper mantle and subsequent superimposed low temperature strain (<800℃) happened in the process of ophiolitic obduction. Both of them are considered to be related to the southward thrusting. It is estimated that the slipping system of the olivine formed in the upper mantle along (010) [100], the value of paleostress deviation is 138MPa and strain rate is 6.14×10^{-14}/sec. The isotopic measurement of the central ductile thrust (CDT) has provided an age of 350Ma.

2 Indosinian folds and the detachment structures formed along the northern margin of the South China plate (SCP)

In the southern Indosinian belt, the development of folds in the Upper Sinian-Triassic sedimentary strata, about 10km thick in the eastern part and 15km thick to the western part, is related to detachments reccuring at various depths of the crust.

(1) Detachment between the Palaeozoic cover and the Upper Proterozoic metavolcanic basement: This structure is manifested by listric structures in the cover and shear strain in the

basement. The transition from the vertical fan-shaped cleavages in the upper part to the horizontal cleavage in the lower part throughout the folded sedimentary slab (Z_2-T_2) is progressive, forming a typical concave-upward listric structure as seen in the Rhine Variscan belt of Europe. The multi-level detachment structures and the imbricated arrangement of faults are developed mainly due to the difference in lithology of the cover.

The deformation and metamorphism between the basement and the cover show a continuously progressive evolution trend. The gentle foliation in the basement is parallel to the cleavage at the base of the cover; the direction of the stretching lineation (N0°E～N30°E) is very stable in a distance of 1500km long from east to west. The nearly horizontal mylonite zone, which is formed as a result of detachment, is distributed in the east side of the Tancheng-Lujing fault. In Zhanbaling area, underlain by the metavolcanic basement (Pt_3), the mylonite and the ultramylonite about 3km in thickness are characterized by S-C texture and σ-type or δ-type porphyroclastic systems. The strata from the metavolcanic basement through the Lower Palaeozoic cover were affected by the syntactonic deforamtion and metamorphism. The medium to high metamorphic zone has been found along the main detachment plane, where the glaucophane schist facies exists in west of the Tanlcheng-Lujiang fault and jadeite-bearing glaucophane schist to the east. According to rotational strains of minerals and preferred orientations of quartz, the shear sense is southward directed and the isotopic age for the detachment is of 210～230Ma.

(2) Deeper detachment structure between the low-grade metamorphic rocks (Pt_3) and the high-grade metamorphic rocks (Pt_{1-2}): On the basis of study of the multiepisodic deformation of the high-grade metamorphic Dabie Group (Pt_{1-2}) and the low-grade metamorphic Shusong Group, the detachment structure resulting from the first phase of deformation in the Dabie Mountain has been reconstructed. It shows that the foliation has been refolded, which is tilted northward in the northern part and southward in the southern part under the influence of uplifting of the Dabie Mountain. The stretching lineation with the direction of 150°～160°, A-type folds, the large-scale gentle mylonite zone with high temperature (>650℃) fabric of quartz in the Dabie Group (Pt_{1-2}) and the high pressure metamorphic zone composed of glatucophane-phengite-chronite in the lowst part of the Shusong Group, has been considered as principal evidences for the ductile detachment.

Magnificent Indosinian imbricate slabs have underthrust beneath the detachment zone due to subduction of the South China plate under the North China plate.

3 Sinistral strike-slip shear zone between the northern Palaeozoic and the southern Indosinian belts

A narrow transited zone lies between the two belts, which is composed of Lower Palaeozoic and Devonian flysch metasediments more than 4km thick, folded and thermometamorphosed at the Late Hercynain time, with the Middle Carboniferous terrestrial facies locally overlying conformably the Devonian successions. On its northern margin, there is a large duc-

tile strike-slip fault about 1000km in length, along which strongly mylonitized rocks about 2km wide consisting mainly of schists, gnisses, granites and diorites are developed, and they are characterized by vertical foliation, horizontal stretching lineation, S-C structures, mica fishes and asymmetrical por-phyroblast system indicating a left lateral movement.

4 Formation, evolution of the Qinling Mt. and their dynamics in view of plate tectonics

The Qinling Mountain Chain has been subjected to complicated processes of evolution since Palaeozoic time.

(1) Formation and evolution of the northern Palaeozoic belt: The belt was formed in Caledonian-Variscan time. Its evolution involved intracontinental deformation added with left lateral movement at different stages.

Caledonian stage: During the Early Palaeozoic, it seems that an ocean basin of several thousands kilometers wide existed between the NCP and the SCP, which is supported mainly by the paleomagnetic data. In addition, in the northern part of the ocean basin, passive continental margin and sedimental prism associated with normal faults were developed. It is considered that the first stage of convergence had led to the intraoceanic obduction conducted under condition of a high temperature creep strain in the upper mantle. Subsequently, the ophiolites were obducted southward onto the Qinling microplate simultaneously with the formation of the SDT, and were overprinted by low-temperature strain.

The presence of fragments of various crystalline rocks, including ultrabasic and basic rocks, as well as granites and siliceous rocks transported from the north, suggests that the transitional zone between the two belts may represent a molasse foredeep during the Caledonian orogenesis, and the closure of Palaeozoic oceanic basin may happen during the Middle to Upper Devonian.

Variscan stage: It involves the following major events:

a. At the beginning of Middle Devonian, the NCP, the Qinling microplate and the SCP began to collide with each other, subsequently, leading to intracontinental deformation; b. The large-scale southward thrusting, resulting simultaneously in rock metamorphism and formation of the central ductile thrust (CDT) (350～320Ma); c. The thrusting and migrating northward, leading to formation of the Northern ductile thrust (less than 350～320 Ma). d. The N-S contraction and migrating also northward under the influence of thrusting, leading to formation of radial structures; e. The emplacement of abundant Early Variscan granites in the Qinling microplate; f. Large-scale eastward movement of the SCP against the NCP since the beginning of Carboniferous (319Ma).

(2) Formation and evolution of the southern Indosinian belt: At Early Palaeozoic, the greatly varied thickness of the Early Palaeozoic sedimentary sequence, the presence of horst and graben pattern confined by the synsedimentary normal faults as well as the alkaline and paraka-

line volcanic activities in the southern belt can all be accounted for by the rifttype continental crust extension developed on the passive margin of the SCP.

The Late Palaeozoic-Early Triassic sediments as examplified by platform-type shallow-sea carbonates and clastic sediments, were accumulated at the northern margin of the SCP. The folds of cover (Sinian to Middle Triassic) are typical of Indosinian intracontinental structures. The existence of concave-upward listric structures in the cover and shearing strain in the metavolcanic rocks clearly indicates the occurrence of the largescale imbricated ductile detachments occurred between the cover and the basement. At the rear part of the detachment, the deformation prism may reached 20km thick, which can be used to interpret why high-pressure glaucophane mineral was formed. It is estimated that the crust was shortened and displaced at least 100km to the east and 150km to the west of the Tancheng-Lujiang fault.

Comparing the differences in the high-pressure metamorphic zones across the Tancheng-Lujiang fault, it is infered that the accretional prism caused by the detachment in the eastern part is thicker than that in the western part.

Althogh the occurrence of multi-level detachments and accretional prism structures in the crust at the northern margin of the SCP is related to the intracontinental subduction of the SCP underthrust beneath the NCP, it's assumed that the intracontinental subduction may cause the expansion of the Indosinian ocean which existed further away from the southern part of SCP.

Ductile Nappe-Shear Zones in the Himalayas and Their Dynamic Analysis●

Xu Zhiqin
(Institute of Geology, Chinese Academy of Geological Sciences)

The Himalayas, like the Alpes, are characterized by large scale nappe structures. These nappe structures occur as wide high-strain bands——ductile nappe-shear zones with strongly plastic flow and shear strain, since they lie at depth within the crust (more than 5～10km) (Mattauer, 1975; Brunel and Andrieux, 1980; Brunel, 1983; Xu, 1984).

In the Himalayan Chains, from north (the Yarlung Zangbo River) to south (Nepal) are developed several great ductile nappe-shear zones with a length of more than 1000km, extending in an E-W trend. According to their geotectonic position and formation conditions in processes of plate evolution, these ductile nappe-shear zones can be divided into three types (Fig.1):

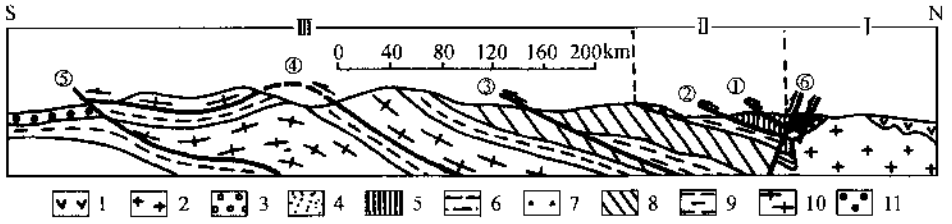

Fig.1 Sketch section of structures of the Himalayan Chains.

Ⅰ—Lhasa plate; Ⅱ—Yarlung Zangbo River suture; Ⅲ—Northern margin of the Indian plate
①Yarlung Zangbo River "intramantle" ductile nappe-shear zone; ②Yarlung Zangbo River "crust-mantle" ductile nappe-shear zone; ③Kangmar-Tingri "intracrust" ductile nappe-shear zone; ④Nepal "intracrust" ductile nappe-shear zone; ⑤Main boundary thrust; ⑥Yarlung Zangbo River thrust
1—Mesozoic volcanics; 2—Gangdise granites; 3—Eocene conglomerates; 4—Flysch deposits of the Xigaze Group (K_2); 5—Ophiolites; 6—Triassic-lower Jurassic flysch deposits; 7—Melanges; 8—Palaeozoic-Mesozoic neritic facies deposits; 9—Lower Palaeozoic schists; 10—Precambrian gneisses; 11—Miocene mollasse deposits.

1. The intramantle ductile nappe-shear zone (the Yarlung Zangbo River ophiolitic ductile shear zone) found within ophiolites, was formed during intraoceanic obduction taking place about 100Ma ago.

2. The crust-mantle ductile nappe-shear zone (the Yarlung Zangbo River ductile nappe-

● GEOLOGY OF THE HIMALAYAS——Papers on Geology.

shear zone) located between ophiolites of oceanic crust and the continental crust——the northern margin of the Indian plate, was produced about 80Ma ago when ophiolites of oceanic crust were obducted on the continental crust.

3. The intracrustal ductile nappe-shear zone (the Kangmar-Tingri and the Nepal ductile nappe-shear zones) is developed within the continental crust, and has been occurring because of continental collision and intracontinental subduction since 20Ma.

So occurrence of ductile nappe-shear zones has continued throughout all stages from the subduction of Neo-Tethys to the formation and evolution of the Himalayan Chains. Study of these zones must begin with microstructures, because they display plastic deformation of progressive evolution at depth within the crust, but not abruptly breaking plane. Information provided by microstructures is applicable research on crustal deformations of convergence zones and hence dynamical analysis of plates can be made. This is a new method of studying microstructure (10^{-8}cm) to global structure (10^{8}cm) (Mattauer and Mercier, 1980).

The Intramantle Ductile Nappe-shear Zone and Intraoceanic Obduction

The ophiolitic relics of the Neo-Tethyan oceanic crust are distributed discontinuously along the Yarlung Zangbo River suture zone and extend more than 1000km. The ophiolite suite underwent polytectonic disturbances after it had formed. Much of the suite hasn't retained sequences of the origin section, and the most major early tectonic motions are represented by the thrusting from north to south, its major evidences are given as follows:

1. The relatively lower strata of the ophiolite suite have been overthrust on the relatively upper ones. Even it can be observed that the complete ophiolite suite including pyrolites has been thrust on the radiolarian siliceous rocks of the upper most oceanic crust (e. g. Xigaze).

2. The principal boundary plane of nappestrutures is not a visible fracture plane, but consists of a series of northward-dipping foliations or flow cleavages with progressive evolution and permeability, on which have been recognized nearly NS stretching lineations perpendicular to the Himalayan Chains. These lineations are expressed in stretching of orthopyroxene and chrome-spire, sausage structure and rodding structure, and represent vectors of intraoceanic shearing.

3. Minerals forming ophiolites are characterized by strongly plastic flow deformations in shearing zones. For example, in ultrabasic rocks such as lherzolites and harzburgites, olivine shows torsion, undulose extinction, deformation lamination, Liiders line and structure recrystallization, orthopyroxene flattening, stretching cutting, latticed extinction, disolution, torsion and structure recrystallization, and chromespinel stretching; in gabbros, plagioclase is rotated; and in siliceous rocks, quartz displays stretching, flattening, rotation, deformation lamination, inclusion decoration and structure recrystallization.

4. Judging from mineral rotation, deformation, drag fold, etc. direction of napping is from north to south.

5. Olivine mylonites of the Alpes type are developed near the main plane of the shearing zone, possessing porphyroclastic texture, mylonitic structure and recrystallized matrix (Nicolas *et al.*, 1973). Olivine observed using decoration method and the transmission electron microscope possesses obvious dislocation structure of high-temperature (100) system which consists of (100) dislocation wall and [100] dislocation, and the slip system is (100) [100] or (OKL) [100]. From experiments of olivine deformation (Cater *et al.*), it is evident that this kind of the slip system has occurred at above 1000℃; and the low-temperature (<800℃) strain-slip zone is superimposed on (100) organization.

6. Fabric analyses of olivine in the peridotite from the Jyajya, Xigaze and Luobusha areas reveal that the olivine has two types of diagrams: (1) maximum of crystal axis Ng [100]; (2) maximum of Np [010] and Nm [001]. The maxima represent respectively high-temperature ([100] slip direction) and low-temperature ([010], [001] slip directions) deformations. From the relation between foliations and slip planes in Ng [100] maximum diagram, it is suggested that direction of shearing is from north to south (Fig.2, 3).

7. The transmission electron microscope technique has provided the new dynamic information of deformed minerals. From calculations of geometry of the olivine observed under the electron microscope, the dislocation density is $2.4 \times 10^8/cm^2$, the diameter (d) of subgrains is 5.6μ on average, the value of paleostress about 1.78kb (higher temperature in early stage) and 1.35kb (lower temperature in late stage). From the value of the stress obtained from subgrains, the strain rate is 9.7×10^{-14}/second.

8. Garnet which appears in greenschists (original rocks are thought to be volcanic rocks) beneath the peridotite nappe is a high-temperature strain mineral.

Above mentioned analyses suggest that with continuously northward shifting of the Indian continent, the Neo-Tethys ocean was subducted by intraocean shearing from north to south. The intraoceanic shearing would affect directly the upper mantle, so it is believed that the high-temperature flow mechanism (>1000℃) in the upper mantle might be a driving force at depth of subduction of the entire oceanic crust and close of both Indian plate and Xizang plate.

The intraoceanic shearing was first proposed by Nicolas (Nicolas, 1973), after he had studied the Lanzo ultrabasic massif of the Alpes Chains. Study of deformed structures of ophiolites in the Himalayas, has proved that this mechanism is of the same use in the Hamalayan Chains. This is pattern of the early evolution of mountain chain of obduction type different from that of the Andes of subduction type (Mattauer, 1980).

The Crust-Mantle Ductile Nappe-Shear Zone

The shear zone is located at the boundary between the ophiolitic zone and the northern margin of the Indian plate.

1. The shear zone is characterized by the development of the "A" type and isoclinal folds associated with subhorizontal flow cleavages and NS stretching lineations. Away from the main

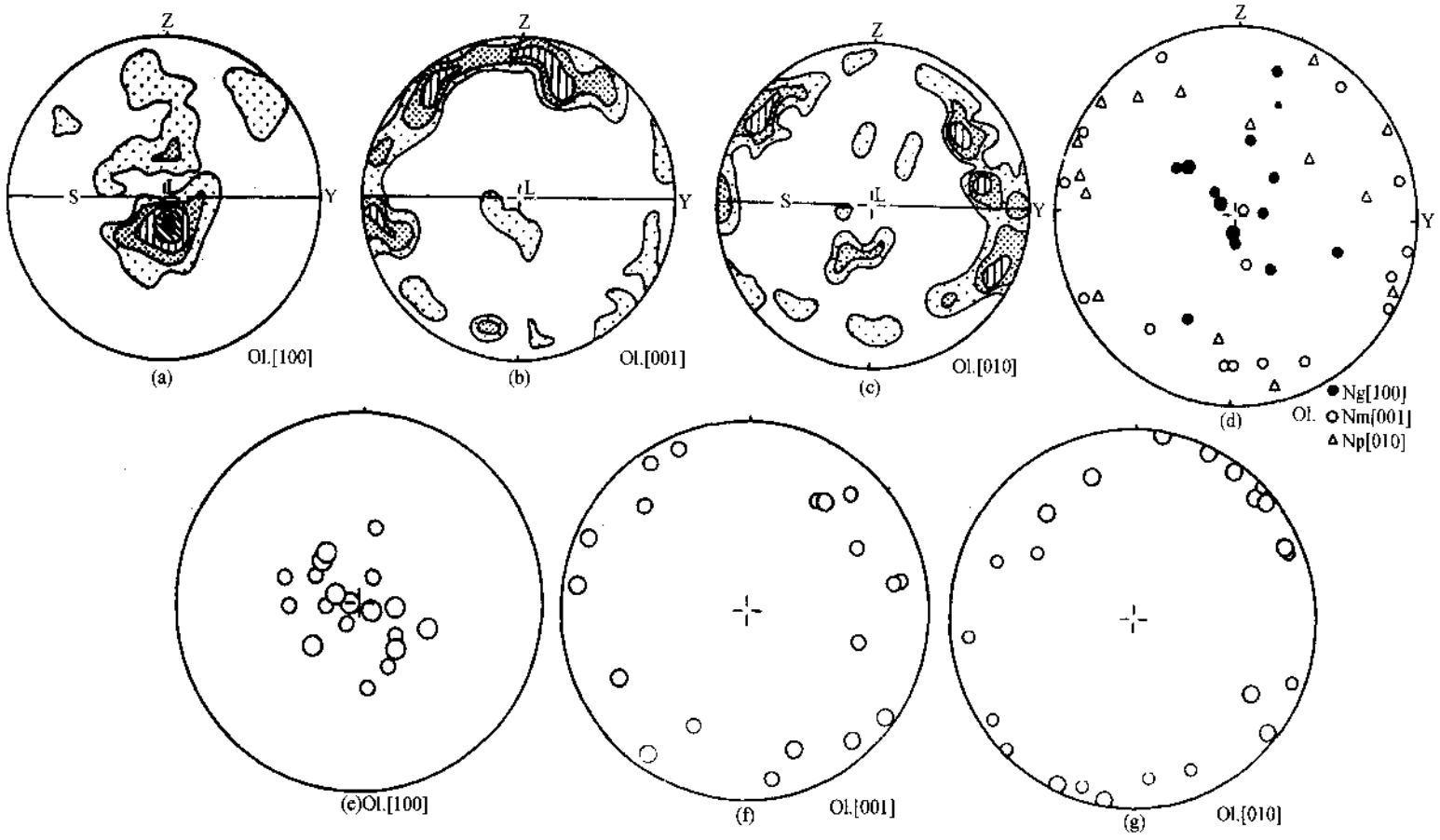

Fig.2　Olivine fabrics-diagram Ⅰ.

a, b, c—Western Jyajya lherzolites in the Yarlung Zangbo River, lower hemisphere projection, isodensity: 1%—3%—5%—7%—9%, Ng [100] maximum, Nm [001] and Np[010] no maximum; d—Xigaze lherzolites, X-ray fabric analysis, lower hemisphere projection, Ng [100] maximum, Nm [001] and Np [010] no maximum; e, f, g—Eastern Luobusha in the Yarlung Zangbo River, X-ray fabric, lower hemisphere projection, Ng [100] maximum, Nm [001] and Np [010] no maximum.

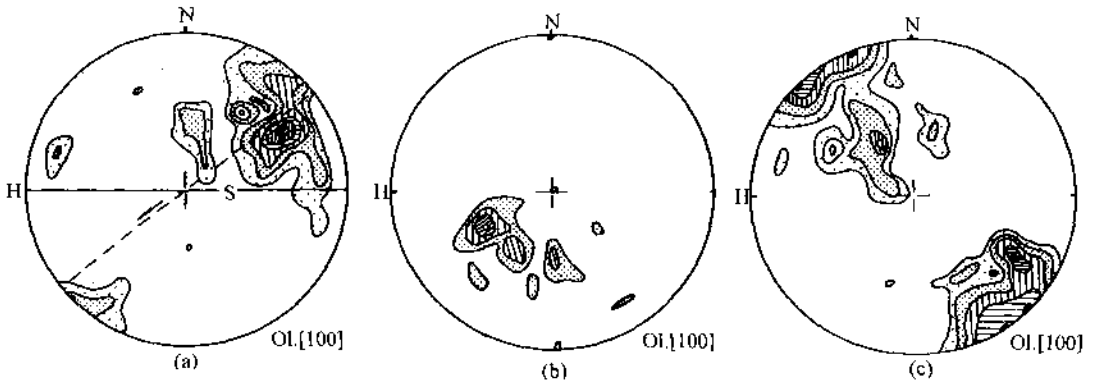

Fig.3 Olivine fabric-diagram Ⅱ.

Luobusha lherzolites, lower hemisphere projection, isodensity: 1%—2%—3%—4%—5%—6%, Ng [100], Nm [001] and Np [010] maximum.

boundary plane occur refraction cleavages (intergrowth of flow and fracture cleavages), fracture cleavages and the "B" type folds. S_2 flow cleavages produced during the late thrusting cut early S_{0-1}, suggesting that superposition of contraction strain emerged during collision to form vertical folds on microstructures related to thrusting.

2. Nearby the main shear plane is developed a quartz mylonite-phyllonite zone with rectangular bands composed of quartz aggregates, where quartz is elongated in the X direction (the direction of stretching lineations) and is recrystallized. Away from the main plane, there is progressive evolution of quartz structural recrystallization through recrystallization (stretching is not clear) to unrecrystallization (obvious rotational deformation), showing that the plastic deformation of the shear zone has undergone the three stages from cold deformation through hot deformation to structural recrystallization (Fig.4).

3. The quartz fabrics in the shear zone are divided into two types: the asymmetric fabric of the basal plane (0001) known as c-axis fabric, and the asymmetric fabric of $[10\bar{1}0]$ prismatic plane known as a-axis fabric. In the former case, the relationship between the (0001) plane and flow cleavage plane (S) indicates shearing from north to south and reflects low-temperature (<600℃) and high strain at the edge of the shear zone; In the latter group, $[10\bar{1}0]$ maximum direction is slip direction. Similarly, it suggests that shearing is from north to south, and reflects conditions of high-temperature (>800℃) in the central of the shear zone (Carter, 1971).

4. The finite strain calculation of the flattened and elongated cenophanians from the greenschists of late Jurassic to early Cretaceous in the shear zone has given X:Y:Z = 3.10:1.65:1.0, and the Flinne index (K = 1.39), indicating a simple shear mechanism, From the "Wood" diagram, the crust is elongated by 80% in the X-direction (N-S direction, that is, direction of stretching lineations) and shortened by 45% in the Z-direction (direction normal to cleavages).

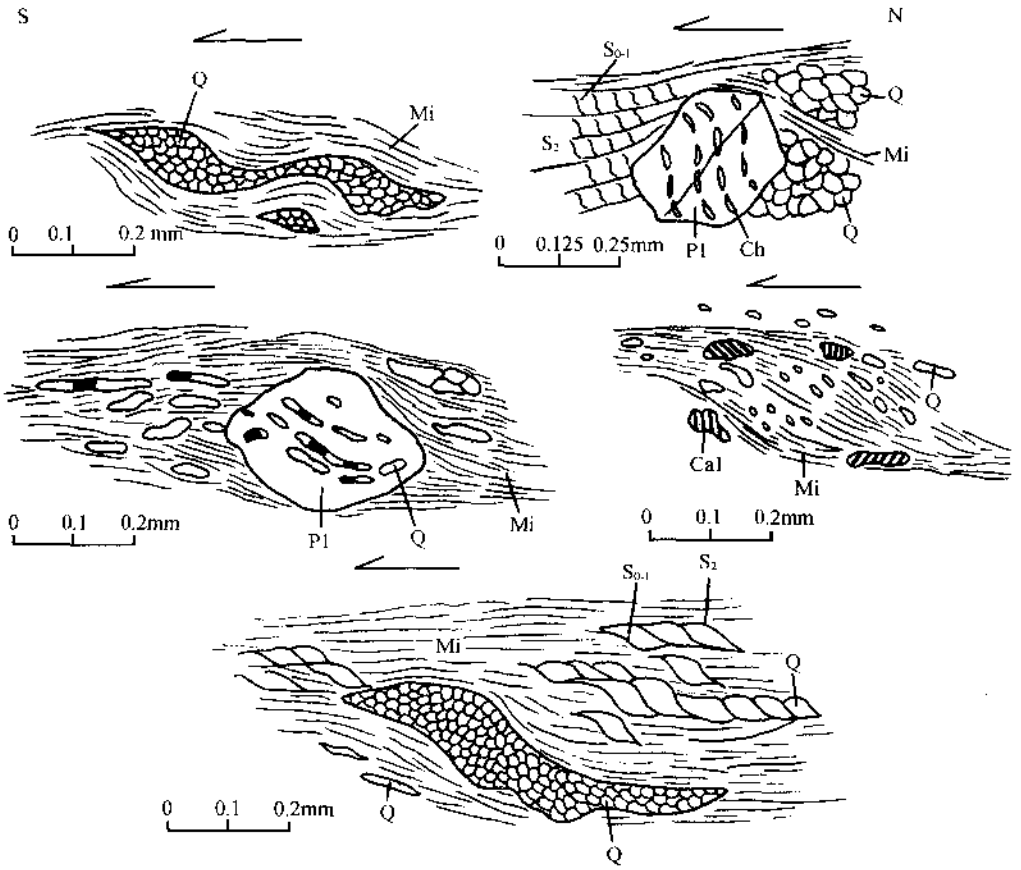

Fig.4 Rotational strain in crust-mantle ductile nappe-shear zone.

1—Rotation of quartz (Q) aggregates, surrounding by flow cleavages consisting of mica; 2—Rotation of chlorite (Ch) inclusions contained in plagioclase (Pl); 3—Rotation of structurally recrystallized quartz (Q); 4—Sigmoidalmica (Mi); 5—Quartz with trails; S_{0-1}—Being bedding and flow cleavages of first stage; S_2—Flow cleavages of second stage; above-mentioned rotation strain indicating shear direction from north to south.

5. A high pressure metamorphic belt is developed in the footwall (the southern side) of the main boundary plane of thrusting. It consists of the northern zone——glaucophaneschist zone and the southern zone——stilpnomelaniteschist zone (Xiao and Gao, 1984), This belt, being a product of thrusting under the conditions of low-temperature and high strain, is characterized by decreasing deformation and metamorphism from north to south.

As above mentioned, following the intraoceanic shearing, the oceanic crust was being subducted, thus leading ophiolites of the oceanic crust to obduct on the continental crust. Compared with the intraoceanic shearing, oceanic-continental obduction could occur in thermal conditions relatively shallow depth, lower temperature and higher strain. This process also was superimposed on the top wall (within ophiolites), which was influenced by early high strain, or say, high-temperature strain of olivine was superimposed by low-temperature strain.

The Intracrustal Ductile Nappe-Shear Zone, Related to Collision and Intracontinental Subduction

The ductile shear zone is located 100km south of the afore-said zones. Deformation features presenting in this shear zone are similar to those in the shear zones described above, earlier. The analyses of deformation extent of the quartz from deformed granites in the Mala Mountains show $X:Y:Z=3.1:1.12:1$ and Flinne index $K=1.33$, suggesting that the quartz has resulted from a simple shearing as well, On the basis of the deformation extent, it is estimated that the crust has been elongated by 65% in the X-direction and shortened by 40% in the Z-direction. The measurements of fabrics of the twinning plane (e plane) and the optical axis (c axis) of calcite in Permian marbles in Kargma are expressed by $\sigma_1=334°/6°$, $\sigma_2=65°/5°$, $\sigma_3=191°/82°$ which are in agreement with those determined according to Etchecopar's processing program (Etchecopar, 1984; Laurent, 1984), thus showing a southward shear movement (Fig.5, 6). Observations using a transmission electron microscope demonstrate that there are ultramicrostructures inside the calcite, such as twins, subgrains, misorientation dislocations, dislocation loops and liquid inclusions occurring along dislocations. The dislocation density (ρ) obtained from calculations is $6.2\times10^8/cm^2$, and palaeostress (6), estimated based upon ρ, is 168～181 bar (relatively lower). The strain rate ($\dot{\varepsilon}$) is $10^{-12}-10^{-13}$/sec.. Therefore, it can be estimated that the temperature of generation of the calcite ranges between 300℃ and 500℃.

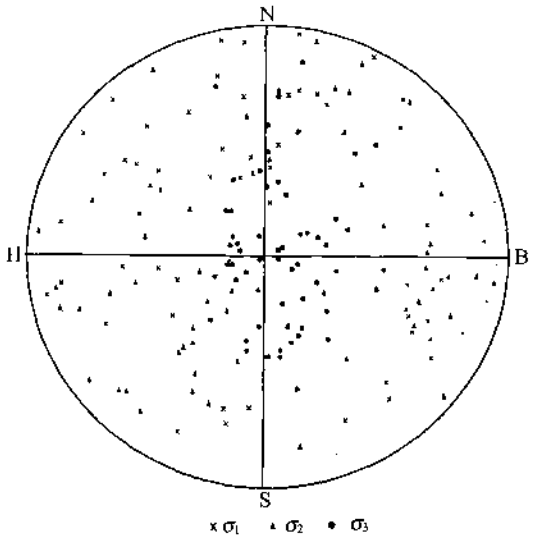

Fig.5 Calculations of calcite.

Permian marbles in Kangmar, lower hemisphere projection, σ_1—Main pressure stress axis; σ_2—Intermediate main stress axis; σ_3—Main tension stress axis.

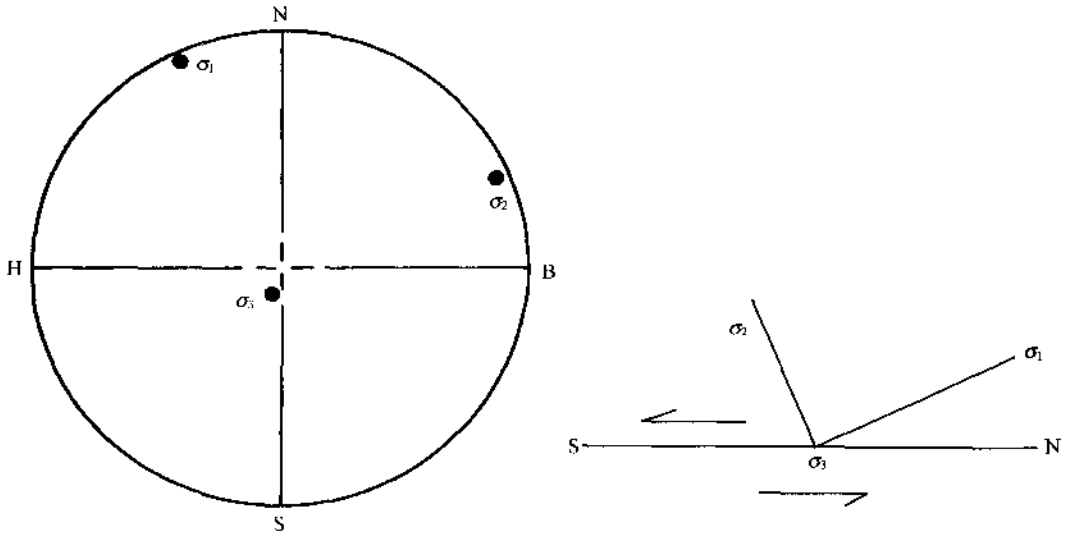

Fig.6 Shear direction identified on the basis of calcite stress field.

σ_1—Main pressure stress axis; σ_2—Intermediate stress axis; σ_3—Main tension stress axis; H—top; B—Base; N—North; S—South arrow showing shear direction.

Concluding Remarks

1. A series of ductile nappe-shear zones have been occurring in a continuous way during all stages of processes from the closure of Palaeotethys to the formation and evolution of the Himalayan Chains. The uplift of the Himalayas is mainly due to thrusting. The principal deformation mechanism is a simple shearing.

2. Intraoceanic shearing indentified on the basis of analyses of microstructure ophiolite and ultramicrostructures of pyrolite is considered to be the first stage of interaction between the Indian and Xizang plates. This is a relatively ideal model for the Paleotethys ocean being several km wide (in accordance with palaeomagnetic data) which was quickly closed during 20～40Ma.

3. The ductile nappe-shear zones are characterized by development from north to south, from old to young (about 100－20Ma) in age, from deep to shallow (intramantle→crust-mantle→intracrust) in depth, and from high to low (more than 1000℃ to 300～500℃) in temperature. Contraction strain related to the late thrusting has progressively been extending towards the outer side of the suture line because of deformation following collision of the large plates. Thus, superimposed migration from north to south is charateristics of the shear zones.

4. The microstructural analyses of minerals in the ductile nappe-shear zones show a stage from cold deformation to hot deformation and structural recrystallization. A great quantity of

shear heat could be produced in the late stage of formation of shear zones, giving rise to partial melting and generation of granitic magma (e. g. granitic zones in the Yarlung Zangbo River and Lhagoi Kangri). It is inferred that in crust at depth the shear zone is linked together with ductile decollement shear zone of low-velocity levels in crust-mantle and intracrust obained from data of geophysical sections (Mattauer, 1983). The low-velocity zones are thought to be the source places of heat flow, seismic activity and magmas, and they would provide possible conditions for large-scale slipping of rocks at both sides of the shear zones.

References

Brunel, M. and J. Andrieux, 1980. Sur un modele tectonique explicatif du métamorphisme"inverse" Himalayan. C. R. Acad Sc. Paris, t. 291, Ser. D, 509～612.

Brunel, M., 1983. Etude pétro-structurale des chevauchements ductiles en Himalaya (Nepal Oriental at Himalaya du Nordouest). Thèse, presentée à l' université de Paris Ⅵ pollr l' obtention de Docteur des Sciences.

Etchecopar, A., 1984. Etude des Etats de contrainte en tectonique cassante et simulations de déformations plastiques. (Thèse) présentée à l' université des Sciences et Techniques du Lanquecoc.

Laurent, Ph., 1984, Les mâcles de la calcite en tectonique (Thèse) présenteé à l' université des Sciences et Techniques du Lanquedoc.

Mattauer, M., 1975. Sur le mécanisme de formation dela schistosité dans l' Himalaya. Earth. Planet. Sci. Lett., 28, 144～154.

Mattauer, M., 1983. Subduction de lithosphere continentale decollement croute-menteau et chevauchement d' echelle crustale dans la chaine de collision Himalayenne. Comptes rendus de l' Academie de l' Academie des Science. Serie Ⅱ.

Mattauer, M. et J. L. Mercier, 1980. Mirotectonique et grande tectonique. Men. H. Ser. Soc. Geol. de France, No. 10.

Nicolas, A., F. Boudier and A. M. Boullier, 1973. Interprétation cinématique des déformations plastiques dans le Massif de Iherzolites de Lanzo (Alpes piémontaires). Tectonophysics 14, 143～171.

Nicolas, A., F. Boudier and A. M. Boullier, 1973. Mechanisms of flow in naturally and experimentally deformed peridotites. Am. Jour. Sci., 273, 853～876.

Xiao Xuchang and Gao Yanlin, 1984. Some new observations on the high P/T metamorphic belt along the southern boundary of Yarlung Zangbo ophiolite zone, Xizang (Tibet). (in Chinese) Himalaya Geology. Geol. Publ. House. Beijing.

Xu Zhiqin, 1984. Major deformation features of the Alpine chain and the Himalayan chain in the Alpine Cycle. (in Chinese) Bulletin of the Chinese Academy of Geological Sciences, (9).

阿尼玛卿缝合带及"俯冲-碰撞"动力学[1]

许志琴[2]　杨经绥　陈方远
（中国地质科学院地质研究所　北京　100037）

摘　要　东昆仑阿尼玛卿蛇绿岩为古特提斯洋盆的标志，根据火山岩空间分布及俯冲杂岩系的特征，进一步确定了古板块体制，提出阿尼玛卿山的形成及演化经历了洋内剪切、洋陆俯冲、大陆活动边缘增生体形成、地体碰撞及陆内逆冲推覆与平移造山的动力学过程。

关键词　阿尼玛卿　蛇绿岩　"俯冲-碰撞"动力学

延伸1200km以上的阿尼玛卿古特提斯缝合带位于青藏高原中部、东昆仑造山带之南缘，为东昆仑地体与松甘-巴颜喀拉地体的分界线。其东段（布青山-花石峡-下大武-玛沁-卡曲）为正向俯冲形成的NW-SE向俯冲杂岩带，西段（喀达坂—库赛湖北—西大滩—东大滩—布青山）为斜向俯冲形成的近东西向昆南左行平移韧性剪切带（含少量俯冲杂岩）。

1　阿尼玛卿蛇绿岩及洋内剪切作用

1.1　阿尼玛卿蛇绿岩

阿尼玛卿蛇绿岩带为古特提斯洋壳标志[1,2]，上百个基性及超基性岩体沿带断续分布，大部分位于东带，如布青山、下大武、玛积雪山和玛沁；少量位于西带，主要在木孜塔格[3]。根据下大武玄武岩的260Ma年龄[2]，放射虫硅质岩中含有孔虫化石：*Carposphaera* sp.，*Acanthosphaera* sp.，*Lithacarripe* sp.，*Tricolocapsa* sp.，*Dicolocapsa* sp.，*Cenellipsis* sp.以及蛇绿岩带两侧地块上均有P_1台地相含科化石的生物灰岩及碎屑岩的存在，可以认为蛇绿岩形成时代起始于P_2。

阿尼玛卿蛇绿岩由变质橄榄岩、辉长岩、玄武岩和放射虫硅质岩组成，平行区域构造线方向排列。在布青山、玛积雪山和玛沁一带均分布洋脊拉斑玄武岩。变质橄榄岩以方辉橄榄岩为主，有少量纯橄岩，普遍蛇纹石化及碳酸盐化，变质橄榄岩为高Mg型，MgO/(MgO+FeO*)值为0.81～0.87，铬尖晶石成分显示这套变质橄榄岩可与深海型橄榄岩相对比。层状辉长岩主要分布于玛积雪山一带，可见其堆积结构，伴生的有斜长花岗岩与辉长岩及堆积橄榄岩。在玛沁地区还发现宽20～30m的席状岩墙群岩块，化学成分表明其为拉斑玄武质[2]。席状岩墙群的发现可作为海底扩张的重要标志。

---

[1] 本文为中法东昆仑合作项目的成果。

[2] 许志琴，女，54岁，研究员，构造地质学专业。

1.2 大洋地幔岩幔源矿物的超微构造及洋内剪切作用

在玛沁—布青山一带的阿尼玛卿蛇绿岩橄榄岩块的下部均发现具三峰结构的橄榄糜棱岩带。橄榄石碎斑及重结晶橄榄石的位错构造研究表明，其具有的优选组构及位错构造与雅鲁藏布江蛇绿岩幔源矿物相类似(图 1)。

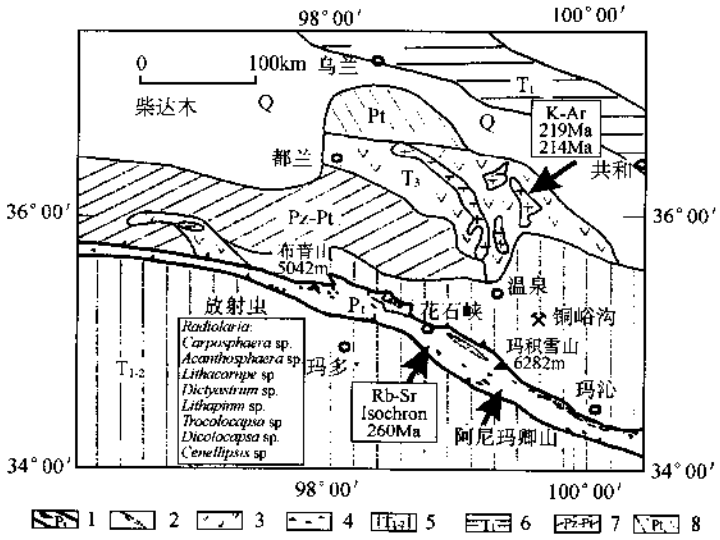

图 1 阿尼玛卿缝合带地质图

1—蛇绿岩带和超镁铁岩；2—石炭纪岩块；3—上三叠统；4—花岗闪长岩；5—下、中三叠统；6—下三叠统；7—古生界—元古宇；8—元古宇

①具橄榄石高温 Ng 组构；

②具高温(>1000℃)条件下形成的位错构造：亚晶粒、位错排，短歪扭位错、位错环及位错网络。位错滑移系为(010)100；

③具叠加于高温位错上的由长位错及位错缠结组成的低温高应变位错构造(~800℃)；

④估算大洋上地幔中流变参数古差异应力 192MPa，应变速率为 $8.73\times10-11/s$。

另外，根据橄榄岩块底部的橄榄糜棱岩及含石榴石角闪片岩的存在，也可以作为大洋地幔岩俯冲的一种标志。

上述研究表明了阿尼玛卿古特提斯洋的消减经历了洋内剪切引起的上地幔中高温稳态蠕变的作用，应速率较快(一般为 10－13/s～10－14/s)的原因可能与洋盆规模较小，消减速度快有关，这与变俯冲速度快、岛弧不发育的情况相吻合。

2 东昆仑主动大陆边缘、俯冲体制及俯冲杂岩系

东昆仑地体一侧(即北侧)为阿尼玛卿洋盆消减、洋壳往北俯冲于东昆仑之下形成的活动大陆边缘，这主要由该侧发育的岩浆-火山系列和"弧-沟-盆"俯冲体系的展布以及俯冲杂岩系的变形构造动力学所确定的。

2.1 火山岩的空间分布及俯冲体制

东昆仑主动大陆边缘的火山岩显示了较宽的成分区间,结合其空间展布,自南往北可将其归划为洋脊、岛弧、弧后盆地和碰撞四个构造背景成因的火山岩类型。其中洋脊玄武岩分布在布青山、玛积雪山和玛沁一带,岛弧钙碱性火山岩(T_1)主要出露于下大武至玛积雪山之间,岛弧面积小,发育不成熟,可能与洋盆小、俯冲时限短有关。岛弧以北分布了 T_{1-2} 含火山岩及滑塌沉积的池塘群复理石巨厚岩系,弧盆地范围很大,出露的已褶皱复理石岩层的最大宽度已超过 100km。根据其南部铜峪沟玄武岩形成于弧后盆地的环境分析,笔者认为池塘群复理石岩系有可能为弧后盆地与大陆边缘的沉积复合体。温泉以北的 T_3 陆相鄂拉山火山岩(伴生铜矿)则属于后碰撞型火山岩类型(图 2)。

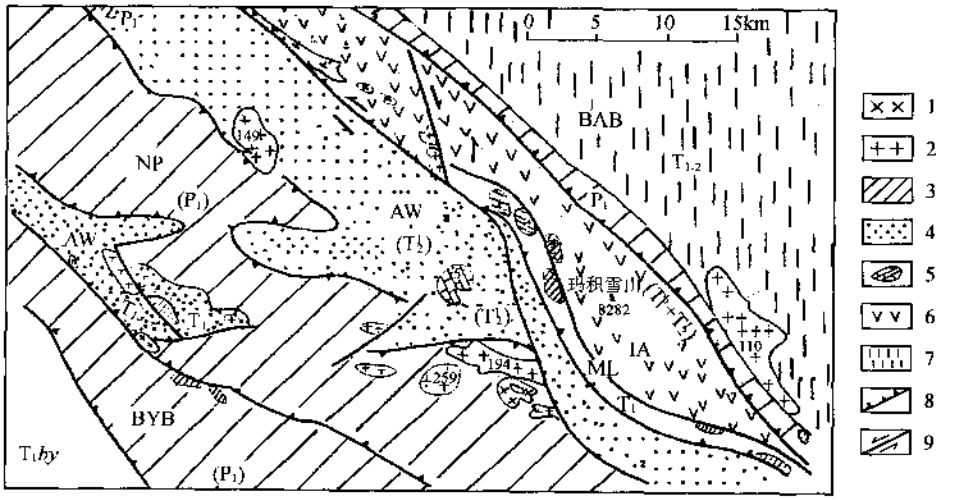

图 2 阿尼玛卿缝合带玛积雪山段的板块俯冲体系图

1—辉长岩;2—花岗岩;3—P_1 台地相沉积;4—弧前增生楔(T_{1-2});5—含外来灰岩块的复理石岩系(T_1);6—火山岩;7—弧后盆地沉积;8—逆冲断层;9—平移断层。BAB—弧后盆地;IA—岛弧;ML—混杂堆积;AW—弧前增生楔;NP—纳布;BYB—巴颜喀拉地块

印支期的花岗岩在缝合带以北的东昆仑地区属于安第斯类型,大部分花岗岩为高钾的钙碱性系列,少部分为低钾钙碱系列及拉斑系列。自南往北又可划分为岛弧型花岗岩、碰撞型花岗岩及大陆边缘岩浆弧类型。化学成分上在 SiO_2 为 60% 时,K_2O 含量自南往北渐增(1.34%～2.30%)。花岗岩类的成分极性表明洋盆位于三叠系花岗岩浆弧的南面以及俯冲带往北倾[4]。

2.2 俯冲杂岩系

阿尼玛卿俯冲杂岩系为古特提洋盆(P_2-T_2)存在并经洋内剪切、洋壳俯冲至板块缝合碰撞的表征,包括阿尼玛卿蛇绿岩(前已述)、混杂堆积、弧前增生楔及高应变滑脱带四个组成部分(图 3)。

2.2.1 阿尼玛卿混杂堆积

由超镁铁质岩、辉长岩及喷出岩组成的蛇绿岩残片呈不规则长条状及块状混杂体产于

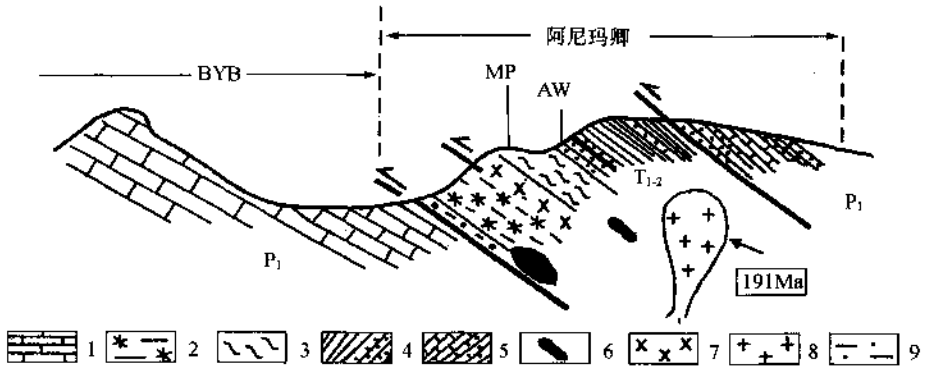

图 3　阿尼玛卿缝合带东段(玛沁马其强)构造剖面

1—灰岩;2—糜棱岩;3—含镁钠闪石绿片岩;4—复理石岩系;5—台地相碎屑岩及碳酸岩沉积;6—超基性岩;7—辉长岩;8—花岗岩;9—含石榴石角闪片岩;BYB—巴颜喀拉地块;AW—弧后增生楔;MP—中压变质带

中下三叠系砂板岩地层中;并见大量含化石的石炭纪与二叠纪的灰岩块、三叠纪浊积岩块作为外来岩块混杂其中。阿尼玛卿混杂堆积带从布青山往东一直到玛沁一带,规模大,标志明显。

2.2.2　弧前增生楔

主要发育于布青山-玛沁岛弧的西南侧,由 T_{1-2} 含浊流沉积的海相复理石岩系组成,以蛇绿岩带及高应变滑脱带为底面。

2.2.3　高应变俯冲滑脱带

弧前增生楔底面为高应变剪切带,其与蛇绿岩残片一起组成俯冲滑脱带。玛沁以南发育完好,下部为含石榴石角闪片岩,原岩为玄武质岩石;上部为安山质糜棱岩带,宽 200～300m,具密集叶理面。NE-SW 向拉伸线理、"A"型剪切褶皱和微构造特征显示了明显的剪切应变及向 SW 的剪切指向。糜棱岩带上部是含镁钠闪石的绿片岩带,为板块俯冲时形成的中压变质带,镁钠闪石定向排列(NE-SW 向),表示了剪切运动矢量。

3　阿尼玛卿构造演化及"俯冲-碰撞"动力学机制探讨

阿尼玛卿山的构造演化经历了以下进程:

(1) P_2 末期,古特提斯小洋盆开启;

(2) T_{1-2} 期间,洋内剪切作用与洋壳往北东方向俯冲于昆仑地体之下,在东段由于正向板块聚敛形成增生地体——大陆活动边缘的弧前增生楔,岛弧及弧后盆地,并进而形成印支期初始山链;

(3) T_3 阶段,昆仑与巴颜喀拉地体碰撞,变形向南北扩展,形成具向南造山指向的碰撞山链,西段由于斜向俯冲形成左行平移走滑带,伴随同构造花岗岩的侵入;

(4) 燕山期以来,东段巴颜喀拉地体继续向北东陆内俯冲,在仰冲板片一侧形成苦海、赛什唐及活勒吾大型推覆体(具向南指向),并在缝合带附近形成科帕式对称构造;西段两地体之间沿东西方向继续左行走滑,形成东-西大滩拉分盆地及同构造花岗岩浆的继续侵位。南侧形成一系列 NW-SE 向雁列褶皱山系。

参 考 文 献

姜春发,杨经绥,冯秉贵等,1992,昆仑开合构造,北京:地质出版社.

Molnar, P., Burchfiel, B.C., Zhao, Z. Y., *et al*., 1987, Geologic evolution of northern Tibet: results of an expedition to Ulugh Muztagh, Science, 235: 299～306.

Yang Jingsui, Xu Zhiqin, 1995, The A'nyemaqen ophiolite belt of east Kunlun Mts., NW China: Geology and Tectonic significance. Symposium on uplift, deformation and deep structure of northern Tibet. La Grande Motte-France September 21～22, 1995. 46.

Guo Zhengfu *et al*., 1995, Triassic Andes-type granitoid arc in the Eastern Kunhm Mountains, Qinghai Province, North-Western China. Symposium on uplift, deformation and deep Structure of northern Tibet. La Grande Motte-France, September 21～22, 1995, 11.

THE A'NYEMAQEN SUTURE BELT AND THE DYNAMICS IN SUBDUCTION AND COLLISION

Xu Zhiqin Yang Jingsui Cheng Fangyuang

(Institute of Geology, Chinese Academy of Geological Sciences, Beijing 100037)

Key words A'nyemaqen; Ophiolite; Subduction-collision dynamics

Mesozoic Crustal Evolution and Dynamics of the East Kunlun-Tanggula Composite Mountain Chains[1]

XU Zhiqin YANG Jingsui LI Haibing XU Qiang
CHEN Wen GUO Zhengfu
Institute of Geology, Chinese Academy of Geological Sciences, Beijing 100037, P.R. China

Abstract The East Kunlun-Tanggula Mesozoic composite mountain chains are composed of the Kunlun terrain (North Kunlun terrain and South Kunlun terrain), Bayan Har-Songpan-Garze terrain and the Qiangtang-Tang gula terrain. The Successive subduction and consumption of the Paleotethys and Neotethys led to the comergence and collision of the Kunlun, Bayan Har-Songpan-Garze, Tanggula-Qiangtang terrains and Gondwana and resulted in the Mesozoic orogenic process, forming the Paleotethyan and Neotethyan Composite imbrication mountain chain.

The Paleotethys (the Anymaqen and Jinshajiang Oceans) opened in the Paleozoic-Early Triassic, separating the kunlun, Bayan Har-Songpan-Garze and Tanggula-Qiangtang terrains. The Paleotethys Subducted during the Early to Late Triassic. The Anymaqen oean subducted northward under the Kunlun terrain, the Jinshajiang ocean subducted southward under the Qiangtang-Tanggula terrain, due to the difference of ocean subducted angle, the subduction system of differential tectonic environment are formed. The three terrains collidel at the and of the Triassic, forming the 500km-wide northern Indosinian orogenic belt. The Bangong-Nujing orean opened in the Jurassic, separating the Tanggula-Qiangtang terrain and Gondwana. The Tanggula-Qiangtangterrain collided with Gonduana at the and of the Jurassic, forming the southern Tanggula orogenic belt. The East Kunlun-Tanggula composite mountain chains formed. Since the Cretaceous, the Eart Kunlun-Tanggula region is in uplifting.

Key words Tethy Oceanic Basin, ophiolite, Subduction System, Orogeuic Process, Crustal Structure, Mesozoic, East Kunlun-Tanggula Composite Mountain Chains.

Introduction

Since the Late Paleozoic-Early Triassic, there occurred between Eurasia and Gondwana a series of important geologic events such as the opening of the Tethys oceanic basin and the splitting of continent, subduction, consumption and closing of oceanic crust, collision and convergence between continents, orogenic amalgamation, crustal shortening and thickening and the

[1] Proc. 30th Int'l Geol Congr., Vol 7, pp. 7-20 Xu Zhiqin, Ren Yufeng and Qiu Xiaoping(Eds.)©VSP 1997.

rotation of blocks. All these events have been recorded in the East Kunlun-Tanggula Mesozoic composite mountain chains, which provides the key evidences and geologic features to study the Mesozoic crustal evolution and dynamics.

Tethys Oceanic Basin and Ophiolite

The East Kunlun-Tanggula Mesozoic composite mountain chains are composed of the North Kunlun terrain, South Kunlun terrain, Bayan Har-Songpan-Garze terrain and the Qiangtang terrain. The Central suture zone between the North Kunlun and South Kunlun terrains is the product of the closing of the oceanic basin between the North China plate and South China plate and the collision of these two plates before the Late Devonian.

Since the Late Paleozoic, the successive opening of the Paleotethys and the Neotethys resulted in the splitting of Gondwana and southern Eurasia, which is primarily marked by the presence of ophiolite. There are four Tethyan ophiolite belts in the present Qinghai-Tibet plateau, the Paleotethyan Anymaqen belt(P_2-T_{1-2}), the Paleotethyan Jingshajiang belt (P_2-T_{1-2}), the Neotethyan Bangong-Nujiang belt (T-J_2) and the Neotethyan Yarlung Zangbo belt (K-E). The former three belts lie within the East Kunlun-Tanggula Mesozoic mountain chains, while the later is located at the boundary between the Gandise-Nyanqentangula terrain and the Indian continental block. The Anymaqen oceanic basin split the Yangtze continent from southern Eurasia and divided it further into the South Kunlun terrain and Bayan Har-Songpang-Garze terrain. This small "shear-type" oceanic basin together with the contemporary Jinshajiang oceanic basin to the south made the Bayan Har terrain as a continent bridge extending into the oceanic basin (Fig.1).

(1) Anymaqen ophiolite belt

The Anymaqen ophiolite belt, located in the southern margin of the Kunlun terrain, extends from Muztagh eastward to Maqin for about 1000km.

Jiang and Yang (1992) named it first and, based on the 260Ma age of the basalt in the Xidawu region of Maqin and the foraminifera in the radiolarian silicalite, determined that it began in the Late Permian. Recent studies [16] show there is mid-oceanic ridge basalt (MORB) all in the Buqinshan, Majixieshan and Maqin in the eastern section of the ophiolite belt with deep-sea Mg-rich metamorphosed periodic, bedded gabbro of cumulate texture, plagiogranite, gabbro and cumulate peridotite. The tholeiitic dyke swarms marking sea-floor spreading found in the Maqin region further demonstrate that the ophiolite suggests an oceanic basin. Because of dextral transformation in the western section, the outcrop of ophiolite has only been found in Muztagh[6]. This belt may extend eastward via Nanping and Kangxiang, and join the West Qinling Mianxian-Lueyang ophiolite belt [19] (Fig.2).

(2) Jingshajiang ophiolite belt

The Jingshajiang ophiolite belt is east-west striking between the Bayan Hat terrain and the Qiangtang terrain and north-south striking in the western margin of the Indosinian Songpan-

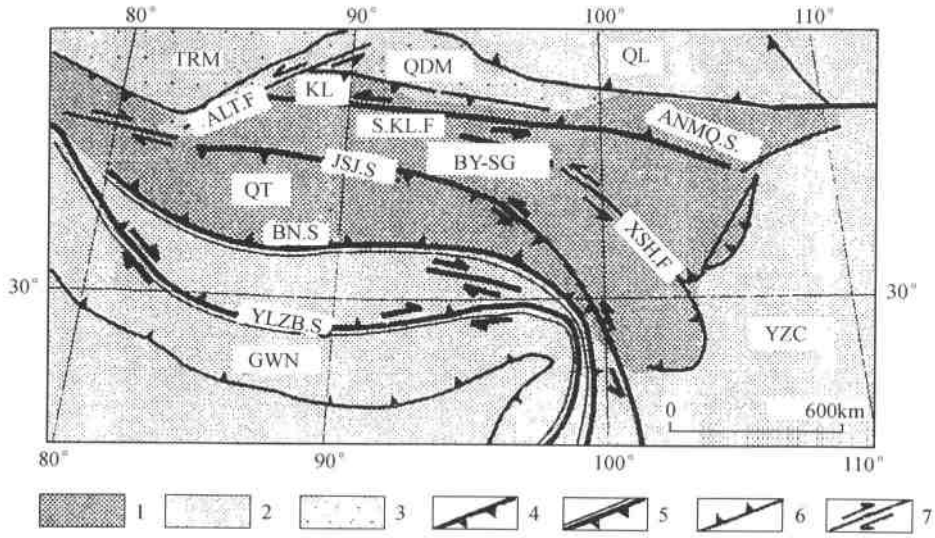

Fig. 1 Plate tectonic sketch of the East Kunlun-Tanggula Mesozoic composite mountain chains. 1—scope of Mesozic orogenic belts; 2—surrounding terrains; 3—Mesozoic-Cenozoic basins; 4—Paleotethyan sutures; 5—Neotethyan sutures; 6—thrusting faults; 7—strike-slip faults; E. KL—East Kunlun terrain; BY-SG—Bayan Har-Songpan-Garze terrain; QT—Qiangtang-Tanggula terrain; GWN—Gondwanaland; YZC—Yangtze craton; TRM—Tarim basin; QDM—Qaidam basin; QL—Qilian Mountains, S.KL.F—Southern Kunlum fault; XSH.F—Xianshuihe fault; ANMQ. S—Anymaqen suture; JSJ. S—Jinshajiang suture; NB. S—Bangong-Nujiang suture; YLZB.S—Yarlung Zangbo suture.

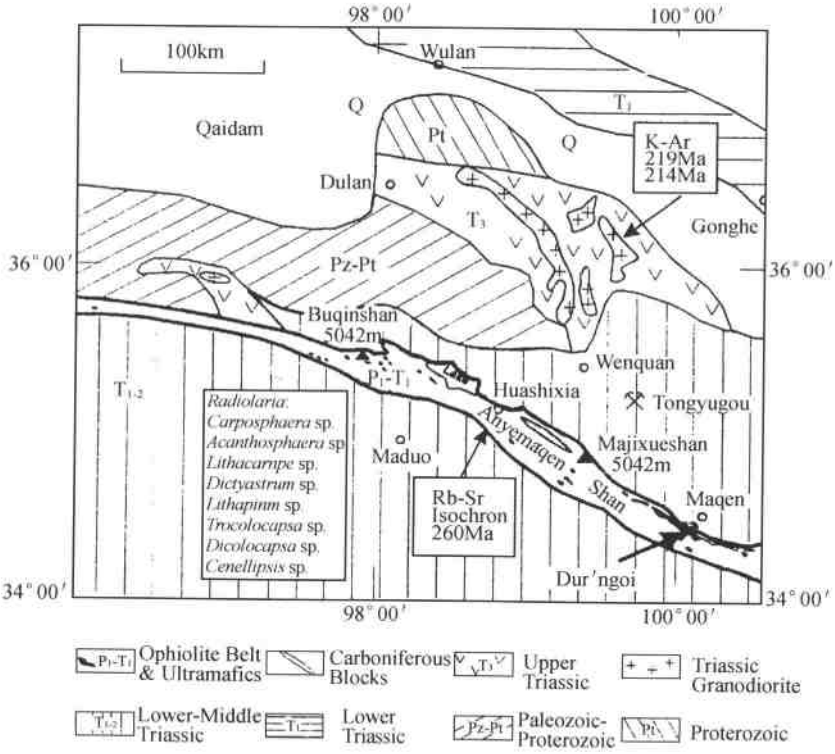

Fig. 2 Sketch geological map of the Anymaqen ophiolite belt.

Garze orogenic belt. The latter north-south striking section consists of the eastern Garze-Litang and western Ailoshan-Batang belts. The formation age of the ophiolite in the eastern belt is believed to be P_2-T_2, but that of the western belt is controversial (C-P_1,) [14] though it indisputably belongs to the Paleotethys. No outcrop of typical opiolite has been found in the considerably long western belt and our recent studies on the dismembered lherzolite, gabbro, pillow basalt and diabase swarms show that they are of marginal volcanic arc rather than oceanic crust [16, 17]. We believe that Andes-type oceanic crust subduction may have took place in the Yushu region [14,15] (Fig.3).

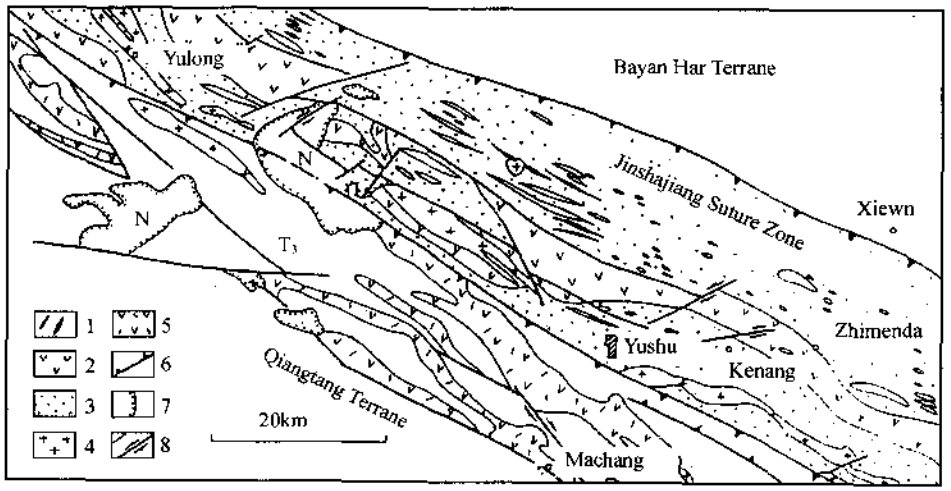

Fig.3 Sketch geological map of the Jinshajiang suture (Yushu region). 1—ultrabasic rock and gabbro; 2—epicontinental outer volcanic rock; 3—epicontinental deposit; 4—epicontinental granite; 5—epicontinental inner volcanic rock; 6—thrust fault; 7—unconformity; 8—strike-slip foult and fault.

(3) Bangong-Nujiang Ophiolite Belt

Starting from the Bangong Co in western Tibet through Gerze, Dongqiao and Denqen, turning southward, to Myanmar along the Nujiang River, this belt contains 80 ophiolite complexes. The ophiolites in the Bangong Co and Denqen are more or less complete, consisting of mantle peridotite, bedded gabbro, massive and pillow basalt and radiolarian silicalite. In addition there are cumulate complex and basic dyke swarms in Dongcuo and Jiangsuori. According to Bao Peisheng, the geochemistry of the basic lavas in the Bangong Co area shows that most of them were produced in the spreading environment of MORB. The Dongco ophiolite may have been formed in an extensional initial oceanic basin while the ophiolite in the Denqen area might belong to the island arc setting. Since the ophiolites were emplaced in the Lower-Middle Jurassic and older sequences, radiolarians in the silicalites are Jurassic of age [20] and the amphibole in the dynamo-thermal metamorphic aurora of the ophiolite gave age of Middle Jurassic (179Ma), they must have been formed in the Early Jurassic in a short development of oceanic crust [10] and were structurally emplaced in the Middle or Middle-Upper Jurassic.

Subduction Dynamics of the Tethys Oceanic Basin

Ocean consumption is realized via plate subduction and the studies on the time-space distribution of the plate regime of the Tethys and kinematics of the subduction rock complexes are indispensable to determining the plate subduction dynamics of the Tethys. Researches suggest that the Anymaqen oceanic crust subducted northward (Triassic), the Jinshajiang southward (Triassic) and the Bangong-Nujiang northward (Jurassic).

Subduction of the Anymaqen Oceanic basin and plate subduction regime of the East Kunlun terrain

A. Volcanic series in the active continental margin of the East Kunlun terrain

On one side of the East Kunlun terrain was the active continental margin resulting from the consumption of the Anymaqen oceanic basin and its northward subduction [3]. Recent studies show that the active margin had a more or less full range of composition and there occurred, from south to north, volcanic rocks formed in the environments of oceanic ridge, island arc, continental margin and collision zone [17], among which the oceanic ridge volcanic rocks occurred in the Buqinshan, Majixueshan and Maqin and the calc-alkaline island arc volcanic rocks (T_1) mainly in the area between Xiadawu and Majixueshan. The island arc had a small area and was immature probably because of the small size of the ocean basin and short-time subduction. North of the island arc there was an enormously thick flysch series of the Early-Middle Triassic age, containing volcanic rocks and olistostrome that represents the sedimentary complex of back-arc basin and continental margin. Among the volcanic rocks those in Tongyugou are basalt formed in back-arc basin and most of the others are the intermediate-acid volcanics rocks of the andesite-dacite-rhyolite assemblage. These volcanics rocks are mainly of the K-rich calc-alkaline series, (Fig.4) rich in Si, poor in Ti, rich in Al_2O_3, poor in CaO and having a lower content of Mg and Fe. REE analysis shows that their $(La/Yb)_N$ is relatively great and Eu anomaly low, suggesting the characteristics of continental margin arc associated with oceanic crust subduction. The contemporary granite belt is mainly of the K-rich calc-alkaline series and the geochemistry of its major elements and its REE and trace element geochemistry all show features of granites in the continental margin arc.

B. Subduction rock complex

The Anymaqen subduction rock complex is the product of the oceanic crust subduction of the Paleotethys and consists of the Anymaqen ophiolite, melange, fore-arc accretionary prism and high-strain detachment belt. The ophiolite relict composed of ultrabasic rocks, gabbro and tholeiite occur as irregular strips and blocks in the Lower-Middle Triassic sandy slates and which is mixed with exotic blocks of richly fossiliferous Carboniferous and Permian limestones and Triassic Turbidite. The Anymaqen melange belt runs from the Buqingshan Mts. to Maqin on a large scale and with obvious indication.

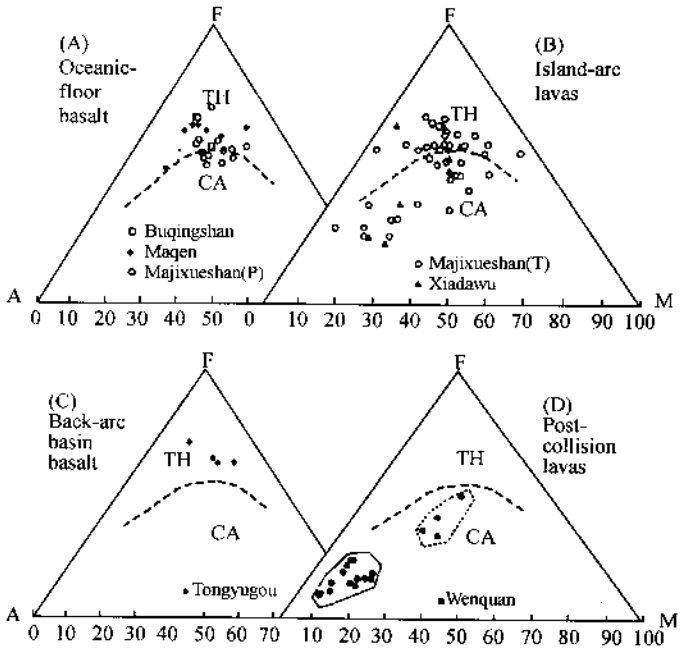

Fig.4 AFM diagram of 4 suites of volcanic rocks in the Anymaqen suture.

C. Soft Cushion of Accretionary melange on the passive margin of the Bayan Har-Songpan-Garze Terrain

During the spreading and gradual consumption of the Anymaqen and Jinshajiang oceanic basins (T_1-T_3^1), there formed vast area of sedimentary accumulation mainly of the Triassic flyschoid (the Bayan Har group and the Xikang group) on the Bayan Har continental bridge and the western passive margin of the Yangtze block. The lower part of the Triassic flyschoid series is a typical turbiditic sedimentation with the AB sequence and large olistostrome intercalation. The middle-upper part, mainly of flyschoid, is characterized by the central-outer fan facies and the sedimentary body shows an obvious southward drifting from bottom to top and enormous paleo-current data suggests southward and southeastward flowing. Trace element geochemistry demonstrates that the sedimentary basin was fairly deep and Sengor (1984) called the Triassic sediments in the Bayan Hat and Songpan-Garze region as a soft cushion of accretionary melange between the two continents. The data of the Sino-French natural earthquake topographic profile from Golmud to Wenquan show that this terrain is composed of high-velocity cold material in the upper 50km, thus the Bayan Har terrain has a structure of "soft cushion" and "hard basement".

Mesozoic Crustal Deformation and Orogenic Process

The successive subduction and consumption of the Paleotethys and Neotethys led to the convergence and collision of the Kunlun, Bayan Har-Songpan-Garze, Tanggula-Qiangtang ter-

rains and Gondwana and resulted in the Mesozoic orogenic process, forming the Paleotethyan and Neotethyan composite imbrication mountain chain.

The Mesozoic orogeny consists of two orogenic phases. The first is the Indosinian orogeny taking place at the end of the Triassic, equivalent to the Early Cimmerian orogeny [8, 9] of the (eastern) Tethys-Alps orogenic Belt, and was caused by the collisional convergence of the Kunlun, Bayan Har-Songpan-Garze and Tanggula-Qiangtang terrains, producing the Indosinian orogenic belt 500～600km wide associated with Indosinian granites to the north of the Kunlun-Tanggula range. The second is the Tanggula orogeny occurring at the end of the Jurassic, equivalent to the Late Cimmerian orogeny [8, 9]. The orogenic belt is in the south of the mountain range and was superimposed on the Indosinian orogenic belt. The Tanggula-Qiangtang terrain collided with Gondwana along the 300Km-wide Tanggula orogenic belt formed of active margin (the north side).

(1) Indosinian orogeny

The Indosinian orogeny had many complicated crustal deformation forms. The major constraints on the forms, intensity and mechanism of the deformation were ①the competency and thickness of the Caledonian sedimentary cover (Devonian-Triassic) and the paleo-position of the block; ②the distance from the Paleotethys suture and the subduction dynamics; ③the re-activity along the existing structural belts and ④the direction of the main stress.

(A) Indosinian crustal deformation of the Kunlun terrain

Because of the existence of the Qaidam block during the Early Carboniferous-Late Triassic, there formed around it marginal troughs and bays and thus the cover on the Kunlun terrain was thicker in the east than west and thicker in the south than the north (in the eastern section).

The folding in the western section is simple. In the lower cover (Carboniferous-Permian) there developed syn-cleavage folding with radiating thrust faults and in the upper cover there developed concentric fold. The axis of these folds turned from NW-SE striking in the west gradually to nearly E-W striking in the east, which was associated with the change to sinistral strike-slip of the Paleotethys suture on the southern margin of the Kunlun terrain.

The Indosinian deformation in the eastern section was more complex and there are the following deformation zones from south to north (Fig.5):

① The frontal subduction thrusting belt of Anymaqen: growing to the north of the Anymaqen subduction zone, it consists of a series of south-verging thrusting faults and nappes. The Indosinian movement (at the end of the Triassic) further reworked the Anymaqen subduction complex, the ophiolite, island arc volcanic rock, sediments in the forearc and backarc basins and the basement of platform facies (Lower Permian limestone) formed before the plate splitting being all involved in the thrusting.

② Backarc detachment north of Maqin: it developed in the flysch series of the Early-Middle Triassic backarc basin north of the Anymaqen subduction zone. The flysch series was slightly metamorphosed to the lower green schist facies and the strong folding and shearing suggest

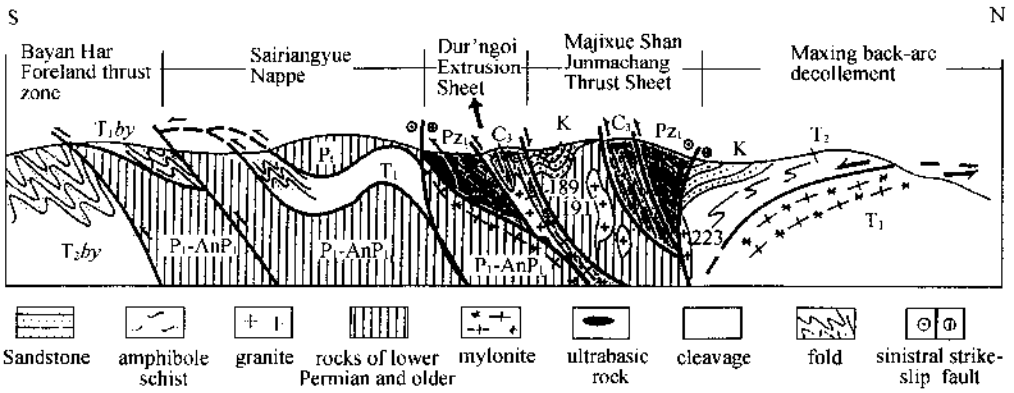

Fig.5 Comprehensive structural section of the Anymaqen suture.

the presence of a southward detachment, in which the flow foliage was further folded into gentle domes.

③ The central Kunlun thrusting nappe belt: Located in the Lower Paleozoic suture zone of the central Kunlun and to the south, it consists of a series of south-verging thrusting faults and nappes. The thrusting placed the Ordovician-Silurian metamorphic series over the Upper Paleozoic shallow-sea sedimentary rocks which in turn was placed on top of the Lower-Middle Triassic flysch series. There are two large nappes, the Kuhai and Tongyugou, to the south of the central Kunlun belt. Covered by the Jurassic-Cretaceous red beds, the Kuhai nappe is composed of Ordovician-Silurian metamorphic rocks over a ductile detachment under which are the Carboniferous, Permian and Lower-Middle Triassic sequences. This nappe was formed by subsequent intra-continent subduction along the previous structural zones(Fig.6).

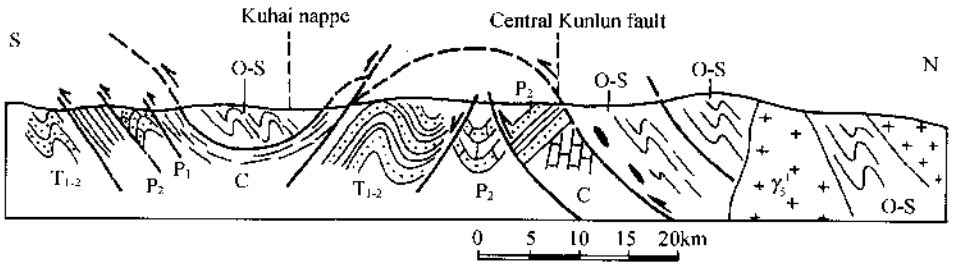

Fig.6 A section of the Kuhai thrust sheet in Wenquan, Central Kunlun Mnt.

④ The northern weak deformation belt: In the vast area from the central Kunlun suture northward to Gonghe, there developed non-foliage vertical concentric folds and reverse faults.

(B) Indosinian Crustal Deformation in the Bayan Har-Songpan-Garze Terrain

During the Indosinian plate converging, the Yangtze continental block subducted as a passive margin separately northward under the Kunlun terrain and southwestward under the Tanggula-Qiangtang terrain, forming the "Bayan Har-Songpan-Garze Terrain" of the "basin-

formed" geometry. Because the converging force at the end of the Triassic in the eastern (Songpan-Garze) section between the northern and southern plates was mainly in the N-S direction, there formed in the region between the Anymaqen belt southward and the Danba-Yajiang line the mainly E-W arcuate deep-and shallow-level detachment-thrust system, in the front of which there are stacking thrust sheets of pre-Triassic metamorphic series (Neoproterozoic-Triassic) and in the rear there occurred Indosinian syn-tectonic granite (181～199Ma) [1, 12]. In the southwest of the Songpan-Garze terrain and the Batang-Litang belt, the Indosinian crustal deformation is characterized by a series of eastward nappes, among which, the "Zhongza" nappe stacking on the Yidun arc came from the Qiangtang terrain to the west [12]. In the western (Bayan Har) section, because the plate converging at the end of the Late Triassic was mainly in the direction of NNE-SSW, the Bayan Har flysch series (Early-Late Triassic) was compressed into tight WNW-ESE steep folds with parallel cleavage which was regionally, arranged in the shape of fan. Along with the folding were low-grade metamorphism (lower green schist facies) and the development of numerous thrusting faults, among which, the Meiyaogou fault to the south of the South Kunlun fault is the greatest ductile reverse fault.

(C) Indosinian Crustal Deformation of the Tanggula-Qiangtang Terrain

The Indosinian deformation in the Qiangtang-Tanggula terrain got weaker southwards from the Jinshaiang suture. The deformation structure of the Jinshajiang suture is characterized by a series of large-scale thrusting shear belt indicated by the high-strain mylonitized rocks. The shearing vergence in the northern section is northward and that in the southern southward, forming a typical radial "Kober" structure cut by a series of Cenozoic strike-slip and thrusting faults. In the inner volcanic belt (the Batang Group of Upper Triassic) in the continental margin of the Qiangtang terrain south of the suture, there developed east-west folds with vertical cleavage.

(2) Tanggula Orogeny

The 500m-thick Middle-Upper Jurassic shallow sea-neritic sediments are the latest marine record on the uplifting. Because the Tanggula orogeny caused by the collision between the Tanggula-Qiangtang terrain and Gondwana at the end of the Jurassic deformed the Middle-Late Jurassic strata on the terrain, forming 300km-wide Alpine "Jura-type" concentric folds and thrusting faults, the crust was shortened about 35% (Fig.7).

Large-Scale Ductile Strike-Slipping and Block Rotating

The Anymaqen structural belt revealing the oceanic crust of the Paleotethys between the East Kunlun and the Bayan Har-Songpan-Garze terrains shows different features in the deformation model and mechanism in its different sections, the western section (west of the Buqingshan Mts.) characterized mainly by sinistral strike-slipping, the middle section (between the Buqingshan Mts. and Huashixia) by oblique thrusting and the eastern section (Huashixia-Maqin) by southward thrusting.

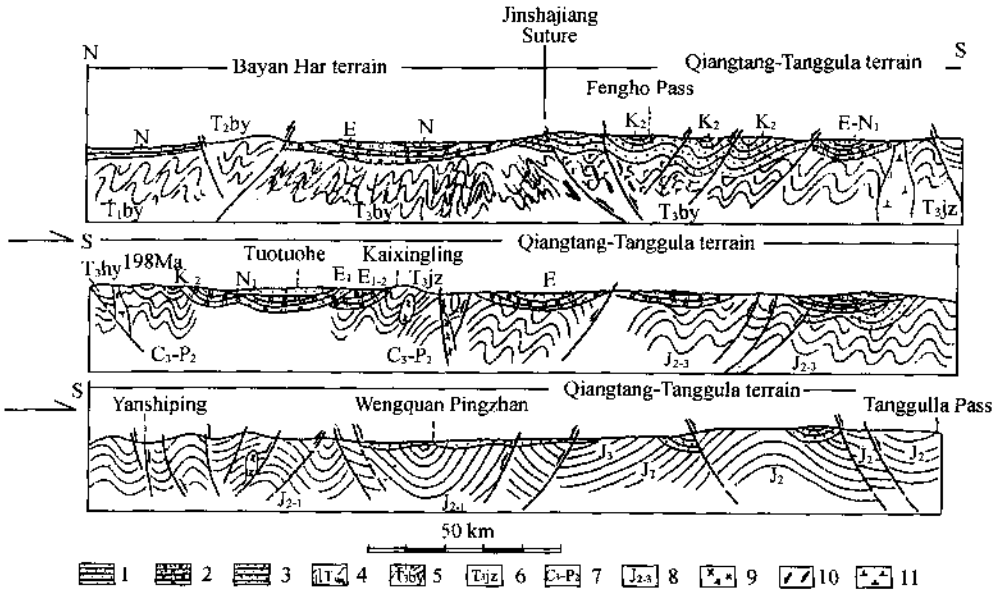

Fig.7 Bayan Har-Tanggula structrual section. 1—Neogene sediments; 2—Paleogene sediments; 3—Upper Cretaceous continental sediments; 4—Upper Triassic Bayan Har Group; 5—Upper Triassic Batang Group; 6—Upper Triassic Jizha-Group; 7—Upper Carboniferous-Upper Permian; 8—Middle-Upper Jurassic; 9—gabbro; 10—ultrabasic rock; 11—diorite.

The 5-6km-wide mylonite belt and high-shear strain rocks constitute the bulk of the middle-western section of the large-scale ductile shear zone. In the syn-tectonic granites associated with the shear zone, some are stripped and parallel with shear zone and the others occur to the north with their long axis striking N65°W, in the shape of spindle, water drop and ball oblique to the shear zone. In contrast, in association with the strike-slipping in the south are the fold bundles striking about N65°-60°W, sinistral en enchlon, in the Triassic Bayan Har flysch series, with no syn-tectonic granite (Fig.8).

(1) Characteristics of shearing strain and shearing mechanism

The rocks in the shear zone are mainly granitic mylonite, phyllonite, gneiss, micca schist, amphilole schist, etc. The foliation is nearly vertical, the streching lineation is horizontal and the rotation strain and the C-axis fabrics of quartz suggest sinistral strike-slipping. Subsequent brittle deformation superimposed on the ductile deformation and there developed breccia along the zone. Pull-apart basins, en-enchlon earthquake mound and pond and the displacement of river terrace all suggest sinistral strike-slipping.

Calculation of the rate of converging R (R = amount of converging/amount of strike-slipping) [7] reveals that the western section had a converging strike-slipping mechanism (R = 0.58) and the middle section had an oblique shortening mechanism (R = 1.09) and the main stress was in the direction of NNE-SSW [4,5].

(2) Strike-slipping and syn-tectonic granites

The granite in the strike - slipping zone and to the north are all syn - tectonic granites pro-

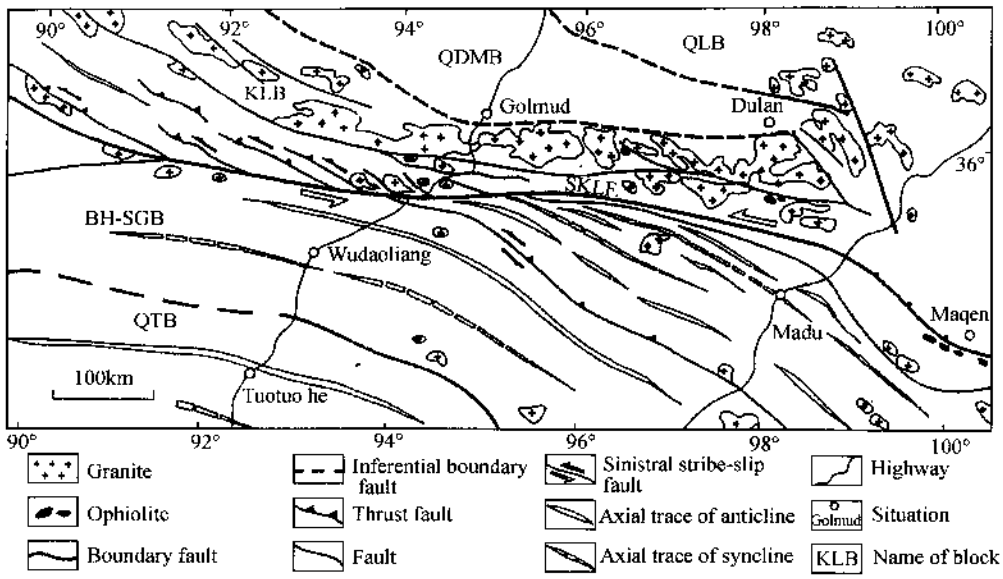

Fig.8 Strike-slip fault belt of the southern Kunlun and structural map of both sides, QLB—Qilian block; QDMB—Qai dam block; KLB—Kunlunblock; BH—SGB—Bayan Hat—Songpan Garze block; QTB—Qiang Tang block; SKLF—Sonthern Kunlun Fault.

duced by shearing. The main reasons are:

(A) As long strips, the granites show obvious, strong ductile flowing deformation and shearing and intruded the Early Paleozoic sandy slates and schists. The en-enchlon granites to the north have a geometry of converging toward the shear zone and vertical flowing plane parallel to their long axes and horizontal flowing structures. Deformation is stronger near the center and weaker beyond.

(B) There is obvious migmatization. The granites are transitional to their country rocks which also suggest sinistral strike-slipping.

(C) In the granites there are xenolith of the country rocks that had been sheared.

(D) Petrochemical analysis indicates that the granites have the features of crustal S-type granite, $\delta^{18}O>8‰$, initial $^{87}Sr/^{86}Sr$ ratio >0.708, HREE depleted, LREE enriched, Nb depleted among the trace elements, and Th enriched, resulting from intra-continental deformation.

(3) Age and displacement of the strike-slipping

Displacement of strike-slipping is calculated on the parameters of shearing strain in the shearing zone of different kinds. In the weak strain zone (3km wide) in the marginal portion of the displacement ductile shear zone, the shear angle Q (S∧C) averages 15°, shearing strain $(r)=2/tg2Q=3.5$, and the displacement is about 10km; In the strong strain zone (0.5～2km wide) in the central portion, $r=35$ and the displacement is about 70km.

Quantitization of the fold system in association with the strike-slipping gives the direction of shortening in the eastern section (in the vicinity of Huashixia) of the strike-slip fault as 30°～45°,

the shortening rate in the NE-SW direction 70% ～80% and that in E-W direction about 15%; and in the western section (at a point of the Kunlun Pass), the direction of shortening as 20°～30°, shorterning rate 60% [4, 5]. The ages (220～240Ma, 150～140Ma, 120～100Ma and 20Ma) of the syn-tectonic granites in association with the strike-slipping, which can basically represent the age of the strike-slipping, indicate that the ductile strike-slipping began in the Middle-Late Triassic and lasted until 20Ma, and since then it has been brittle strike-slipping.

Crustal Structure, Evolution and Dynamics in the Mesozoic

(1) Shape of the Mesozoic mountain chain and reconstruction of crustal structure

The East Kunlun, Bayan Har-Songpan-Garze and the Tanggula-Qiangtang terrains collided at the end of the Late Triassic and formed an integrated composite mountain chain, but they had their own shapes of mountain chain and features of crustal structure (Fig.9).

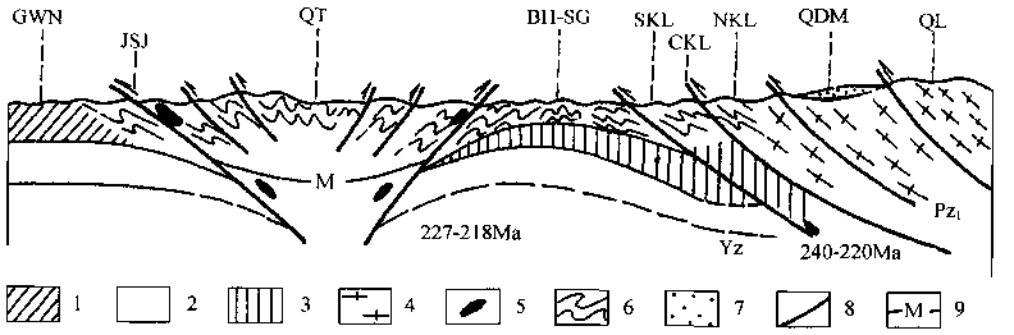

Fig.9 Generalized crustal section of the East Kunlun-Tanggula Mesozoic Composite Mountain Chains. 1—Gondwanaland; 2—manlle; 3—basement of Yangze block; 4—early-paleazoic folded belt; 5—Ulrra mafic rocks; 6—fold; 7—meso-cenozoic basin; 8—thrust; 9—infered Moho.

A. East Kunlun Mountain Chain

Because the subduction of the Anymaqen ocean and the subsequent collisional orogeny shortened and thickened the crust of the East Kunlun and resulted in the southward polarity, there formed thrust stacking mountain chain. There occurred in the terrain in succession subduction island arc volcanic rocks, granite, volcanic rocks and granites of continental margin, collision granites and post-orogeny volcanic rocks and granites, and all these show that the crust of the East Kunlun had a high geothermal gradient and was warm.

B. Bayan Har-Songpan-Garze mountain Chain

Since the enormously thick Triassic flysch series of the Bayan Har group and the Xikang group appeared as a "soft cushion" of passive margin on the hard basement (pre-Triassic) of the western margin of the Yangtze block, there formed a "soft cushion-hard basement" crustal

structure. Because of the divergent subduction of the Paleotethys (the Anymaqen and Jinshajiang oceans), the crust of the eastern (Songpan-Garze) section of the terrain had a "hetero-axis, bilateral" orogenic polarity (i.e. southward and eastward), forming "detachment-thrust" mountain chain [12], whereas that of the western section (the Bayan Har) had a "co-axis, bilateral" orogenic polarity (i.e. northward in the north and southward in the south). The strike-slipping in addition changed the mountain chain into "compression-transformation" type. Studies show that very little granite intruded into the upper soft cushion of the crust, in the lower hard basement, however, there occurred high-temperature ductile detachment shear zone and associated local melting in the crust, and thus it is postulated that the crust of the terrain in the Mesozoic was generally cool with warm, viscous low-velocity layers in the depth. The crust of Bayan Har had been consumed under the Kunlun and Qiangtang terrains in the early stage of the Indosinian subduction, gradually forming the crustal cumulate wedge.

C. Tanggula-Qiangtang Mesozoic mountain chain

The "co-axis, bilateral" subduction of the Jinshajiang Paleotethys ocean and the Bangong-Nujiang Neotethys ocean under the Tanggula-Qiangtang terrain produced the following features of the crust:

① The matching and superimposing of the Indosinian orogenic belt (the Late Triassic) in the north and the Tanggula orogenic belt (the Late Jurassic) in the south.

② The crust having a bilateral "Kober" structure (fan-shaped), shortened in the horizontal N-S direction and elongated and thickened vertically.

(2) Formation and evolution of composite mountain chains

Summarizing the above, we have the following stages of the Mesozoic crustal evolution of the East Kunlun-Tanggula Mesozoic composite mountain chain:

A. The Paleotethys (the Anymaqen and Jinshajiang oceans) opened in the the latest-Paleozoic-Early Triassic, separating the Kunlun, Bayan Har-Songpan-Garze and Tanggula-Qiangtang terrains. It is postulated that the Anymaqen ocean was a small shear oceanic basin.

B. The Paleotethys subducted during the Early to Late Triassic. The Anymaqen ocean subducted northward under the Kunlun terrain, forming the Anymaqen subduction system composed of the subduction rock complex, accretionary prism, island arc, back-arc basin and continental margin volcanic arc. On the passive margin of the Yangtze block there formed the "soft cushion" of accretionary rock complex consisting of the Early-Late Triassic flysch series. The Jinshajiang ocean subducted southwards at a larger angle under the Qiangtang-Tanggula terrain, resulting in an extension setting in the northern margin of the terrain and producing the Jinshajiang subduction system characterized by an Andes-type volcanic arc of active margin.

C. The three terrains collided at the end of the Triassic, forming the 500km-wide northern Indosinian orogenic belt.

D. The Bangong-Nujiang ocean opened in the Jurassic, separating the Tanggula-Qiangtang terrain and Gondwana.

E. The Tanggula-Qiangtang terrain collided with Gondwana at the end of the Jurassic,

forming the southern Tanggula orogenic belt. The East Kunlun-Tanggula composite mountain chains formed.

F. Since the Cretaceous, the East Kunlun-Tanggula region is in uplifting.

(3) The formation mechanism of the inverted triangular-shaped geometry of the Bayan Har-Songpan-Garze mountain chain

The inverted triangular-shaped geometry of the Bayan Har-Songpan-Garze mountain chain in the Kunlun-Tanggula composite mountain chain has provoked special attention. This mountain chain, which is called the geological Bermuda in China, had gone through the stages of the Indosinian orogeny, Yanshanian post-orogeny and the Cenozoic re-orogeny and had formed, in the Indosinian period, the embryonic form that was a long strip in the west and an inverted triangle in the east.

Studies have shown that the N-S converging between the northern and southern plates in the eastern section of the composite mountain chain formed the Indosinian South Qinling folding-decollement mountain chain and the Indosinian Songpan-Garze folding-decollement mountain chain [11～13], whereas in the western section, the (NE-SW) converging between the Qiangtang and East Kunlun terrains resulted in the large-scale South Kunlun strike-slip fault and made the material of Bayan Har terrain flow eastward and caused in the western margin of the Yangtze block nearly E-W compressing, that, together with the N-S converging, produced the nearly E-W arcuate Danba-Yajiang detachment-thrust system.

The NW-SE Xianshuihe strike-slip fault formed in 20Ma cut the Danba-Yajiang system with a sinistral displacement of 80km [12], resulting in the peculiar inverted triangular geometry in the eastern section of the Bayan Har-Songpan-Garze mountain chain.

References

[1] S.Calassou. Etude tectonique d'une chaine de decollement (Ouest Sichuan et East Tibet, China). These de doctorat, Montpellier Ⅱ. 1～169(1995).

[2] J. W. Cui, H.zhu, C.D.Wu *et al*. Deformation and dynamics of the lithosphere in Qinghai-Tibet plateau. Geological Publishing House, Beijing.(1992).

[3] C. F. Jiang, J.S.Yang, B. G. Fong *et al*. Opening-closing tectonics of Kunlun Mountains, Geological Publishing House, Beijing.(1992).

[4] H.B.Li, Z.Q. Xu and W.Chen. Deformational features and tectonic evolution of the South Kunlun strike-slip shear zone, East Kunlun Mountains, Aeta Geoscientia Sinica, Special issuc, . 16～ 21.(1996).

[5] H. B.Li. The Strike-slip tault at the Southern marg in of East Kun lun orogen and the accompanying granitic magma activity. Master dissertation, China University of Geology. 1～ 94(1996).

[6] P.Molnar, *et al*. Geologic evolution of Northern Tibet: results of an expe dition to Ulugh Muztagh. Science, 235, 299～305 (1987).

[7] R. W. Krantz. The transpressional strain strain model applied to strike-slipe, oblique-convergent and oblique-divergent deformation. J. Struct. Geol. 17, 1125～1137 (1995).

[8] A.M.C.Sengor, The Cimmeride orogenic system and the tectonics of Eurasia, The Geological Society of America, Spe-

cial Paper, 195, 82 (1984).

[9] A.M.C.Sengor. The Tethyside orogenic system: an introduction; in Sengor, A.M.C. (ed.), Tectonic Evolution of Tethyan Region, . 1～22.(1989).

[10] X.C.Xiao. Tectonic evolution and uplift of the Himalaya-Tibet plateau: 10th Himalaya-Karakoram-Tibet Workshop: ETH Conference Monte Verita (Ascona), Canton Ticino Switzerland. Abstract, pp. 45～46 (1995).

[11] Z.Q.Xu. Large shear zones in the main orogenic belts, China, Episodes, 18, 41～43.(1995).

[12] Z.Q.Xu, L.W.Hou, Z.X.Wang. Orogenic processes of the Songpan-Garze orogenic belt of China: Geological Publishing House, Beijing, 1～190.(1992).

[13] Z.Q.Xu and J.W.Cui. Deformation and dynamics of continental mountain chains: Metallurgic Publishing House, Beijing, 246.(1996).

[14] Z.Q.Xu, J.S.Yong and F.Y.Chen, The Anymaqen suture belt and the dynmics in subduction and collision. In: Study on ophiolites and Geodynamics, edited by Zhang Qi, Geological Publishing House, Beijing, China, 185～189.(1996).

[15] Z.Q.Xu, M.Jiang and J.S.Yang. Deep Tectonophysical Process of the Uplift of the Northern Qinghai-Tibet Plateau——Evidence from the Integrated Geological-Geophysic al Profile from Golmud to the Tanggula Mountains, Qinghai Province, China. ACTA GEOLOGICA SINICA 17, 1～14 (1997).

[16] J.S.Yang, P.T.Robinson, C.F.Jiang and Z.Q.Xu. Ophiolite of the Kunlun Mountains, China and their tectonic implications. Tectonophysics, 258, 215～231.(1996).

[17] J.S.Yang, X.H.Zheng, W.J.Bai and Y.F.Ren. A preliminary study on genesis of the Durngoi massive Cu-Co-Zn sulfide deposit hosted by the peridotite of A'nyemaqen ophiolite, Kunlun Mr., China, Proceedings for the 30th IGC. (in press).(1997).

[18] Y.F.Zhang amd J.K.Zheng. Geological overview in Hoh Xil, Qinghai and adjacent areas: Seismic Publishing House, Beijing, 177.(1994).

[19] G.Zhang, Z. Yu, Y. Sun *et al*. The major suture zone of the Qinling orogenic belt. Journal of Southeast Asian Earth Sciences. 3:63～76 (1989).

[20] N.W. Wang. On the Palaeobiogeography and Plate tectonics of Qinghai-Tibet Plateau. Bullein of the institvte of Geology, CAGS. Geological Publishing House, Beijing. 9:1～28 (1984).

韧性推覆剪切带及喜马拉雅山链的形成机制[1]

许志琴

1 概述

著名的雅鲁藏布江缝合带，作为东特提斯洋最终闭合及印度板块与西藏板块碰撞的直接产物，以保存较为完整的洋壳遗迹（蛇绿岩套）、复理石混杂岩带、高压变质带以及火山岛弧、弧前盆地复理石楔及陆缘山链磨拉石而确认无疑。那么，印度板块及拉萨板块究竟是以什么方式互相靠拢、碰撞，而最终形成举世瞩目的喜马拉雅山链呢？运用微观构造与宏观构造相结合的分析方法研究板块聚合带的地壳变形，从而对山链形成及大陆板块构造进行动力学解释，这是当今世界上研究大陆板块构造的新动向之一。

喜马拉雅山链的形成大致经历了100Ma历史，由于山链的不断上升、隆起及遭受剥蚀，因此我们可以看到从上构造层次至中、下构造层次丰姿多彩的构造形式及变形特征。和阿尔卑斯山链一样，在喜马拉雅山链中，存在着大规模的韧性剪切带，它是地壳深部塑性变形的重要形式，一般形成于地壳10km以下的深处，是具有强烈塑性流变及剪切应变特征的高应变带，宽度可达数公里（许志琴，1984）。

韧性剪切带按产状可分为推覆型、平移型及滑脱型等类型（许志琴，1984）。推覆型是指主界面比较平缓，近水平的韧性剪切带，它是逆掩断层在深部的表现，平移型是指主界面近于直立的韧性剪切带，它是平移断层在深部的表现；滑脱型与推覆型类似，但其主界面位于两种不同物性岩层之间。韧性剪切带在板块聚合及山链形成演化过程中起着重要作用，并直接提供了板块动力学分析的信息[2]。

在喜马拉雅山链中，自北（雅鲁藏布江）至南（尼泊尔），发育数条大规模近东西向展布的韧性推覆剪切带，按大地构造部位及形成条件可以分为雅鲁藏布江幔内型韧性推覆剪切带（发育在洋壳蛇绿岩内部）；雅鲁藏布江壳幔型韧性推覆剪切带（发育在洋壳与陆壳之间）；康马-定日壳内型韧性推覆剪切带及尼泊尔壳内型韧性推覆剪切带（Brunel, M., *et al*., 1980; Brunel, M., *et al*., 1983）它们分别是在印度板块与西藏板块相互作用及演化过程中的洋内剪切（100Ma），洋壳蛇绿岩仰冲（80Ma），大陆碰撞及陆内俯冲（40～20Ma至今）阶段形成的（图1）。

---

[1] 摘自：中华人民共和国地质矿产部地质专报，五、构造地质 地质力学，第7号喜马拉雅岩石圈构造演化总论，肖序常、李廷栋、李光岑、常承法、袁学诚等著，1988，地质出版社，121～140。

[2] 许志琴，1985，《显微构造与板块动力学，板块构造基本问题》，地震出版社。

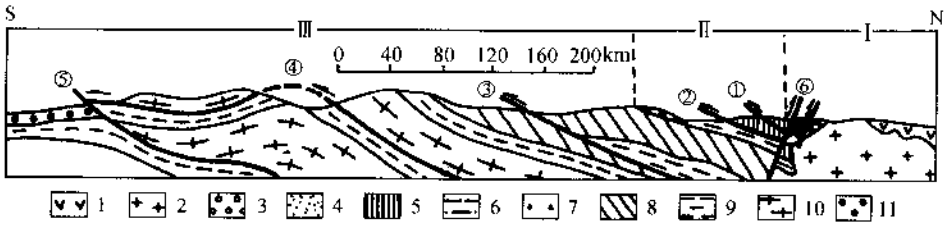

图 1 喜马拉雅山链构造示意剖面

Ⅰ—拉萨板块；Ⅱ—雅鲁藏布江缝合带；Ⅲ—印度板块北缘

①雅鲁藏布江幔内型韧性推覆剪切带；②雅鲁藏布江壳幔型韧性推覆剪切带；③康马—定日壳内型韧性推覆剪切带；④尼泊尔壳内型韧性推覆剪切带；⑤主边冲断层；⑥雅鲁藏布江冲断层

1—中生代火山岩；2—闪底斯花岗岩；3—始新世砾岩；4—日喀则群(K_2)复理石沉积；5—蛇绿岩；6—三叠系—下侏罗统复理石沉积；7—混杂堆积；8—古生代—中生代浅海相沉积；9—下古生代片岩；10—前寒武系片麻岩；11—中新世西瓦里克磨拉石沉积

本章通过喜马拉雅山链中韧性推覆剪切带的微观构造研究，来探讨板块动力学问题。

2 雅鲁藏布江幔内型韧性推覆剪切带

2.1 蛇绿岩带内的推覆构造

雅鲁藏布江缝合带的主体—蛇绿岩带是由超镁铁岩、堆积岩、席状岩床岩墙群、镁铁质火山熔岩及深海、半深海放射虫硅质岩组成(肖序常等，1980)。由于复杂的构造侵位及后期构造影响，使蛇绿岩套原始剖面层序被破坏，主要表现为一系列上冲岩片，作为外来岩块叠置在印度地台北缘特提斯喜马拉雅构造带以北的硅铝质原地岩块之上，形成大规模纳布(推覆)构造。

雅鲁藏布江西部萨嘎以东郭林淌剖面(图 2)表明蛇绿岩带内部的一系列叠瓦式逆掩关系：自北往南方辉橄榄岩逆掩于放射虫硅质岩之上，辉长岩逆掩于基性火山岩之上，基性火山岩又逆掩于放射虫硅质岩之上。在日喀则大竹卡还出现完整的蛇绿岩套(厚 3000m)逆掩于洋壳放射虫硅质岩上(图 3)。在蛇绿岩套方辉橄榄岩的下部还出现热动力变质石榴子石角闪片岩。

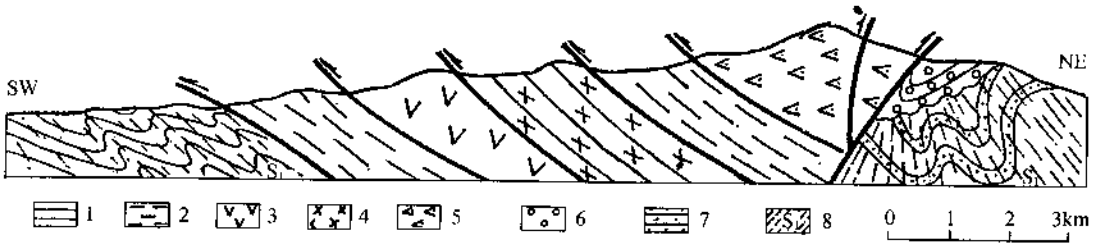

图 2 雅鲁藏布江西部萨嘎东郭林淌蛇绿岩构造剖面

1—三叠系—下侏罗统片岩；2—放射虫硅质岩；3—基性火山岩；4—辉长岩；5—方辉橄榄岩；6—柳曲组(始新世)砾岩；7—日喀则群(上白垩统)复理石沉积；8—流劈理

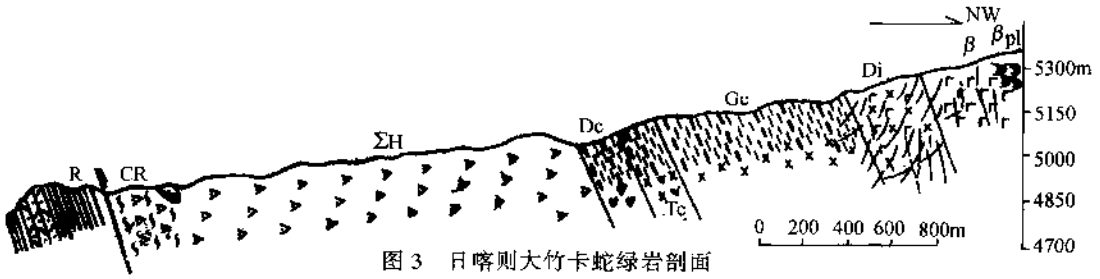

图 3 日喀则大竹卡蛇绿岩剖面

(据肖序常,1984)

βpl、β—枕状熔岩及拉斑玄武岩;Di—岩墙群及席状岩床;Gc—辉长堆积岩;Dc、Tc—橄长岩和易剥橄榄岩;ΣH—蛇绿岩化橄榄岩;CR—蛇绿岩化混杂岩;R—放射虫硅质页岩及燧石

微构造研究表明,这些推覆构造是位于深部递进演化的构造变形带。它并不具有明显的破裂面,而是以一定厚度范围内由强烈塑性流变及旋转应变蛇绿岩岩石组成的韧性推覆剪切带形式表现出来:

(1)普通发育叶理或流劈理,叶理面走向近东西,由于后期应变而重褶,在硅质岩内最明显;

(2)伴随同斜及近平卧褶皱;

(3)叶理面(或流劈理面)上发育明显拉伸线理,近南北向,垂直于喜马拉雅山链方向,它代表了剪切运动的矢量(Mattauer, M., 1975; Mattauer, M., *et al*. 1980)在方辉橄榄岩中拉伸线理表现为斜方辉石强烈拉伸甚至被截断,在放射虫硅质岩内表现为石英及石英集合体的拉伸。

2.2 矿物的塑性流变

大量蛇绿岩岩石薄片的显微构造观察(加加、昂仁、日喀则及罗布莎地区)表明了剪切带内蛇绿岩岩石矿物(包括幔源矿物)塑性流变的普遍性。以下列举幔源矿物(橄榄石及斜方辉石)的变形现象。

2.2.1 变形纹

在橄榄石晶体内发现一组极密集的条纹,据 X 光射线分析为一系列细小滑移面,由于位错作用造成的,常垂直于橄榄石拉长方向分布,变形纹宽度为 1～5mm,在斜方辉石中也可见到变形纹,宽度大约 10mm。

2.2.2 膝折(kink)及弯曲

在斜方辉石以及橄榄石组成的残碎斑晶中常发育(100)扭折带,表现为变形纹或介理面的弯曲及扭折,但未折断,这也是由于晶格位错作用造成的位移作用。

2.2.3 吕德尔线

在晶体中具装饰(固体及液态包体)的变形纹,可见二组共轭的,交角近 90°的吕德尔线。

2.2.4 不均匀消光

可分为波状消光、格子状消光及条带状消光三类。每个消光域实际上就是显微亚晶粒,是由于晶格位错引起的方位变化的结果。条带及格子状变形的出现表示应力较强。

2.2.5 多边化亚构造

为晶体内不同消光域的多边形亚晶粒组成的构造,一般是高温应变的结果。当应力进

一步增加，亚晶粒便脱离晶体，并重结晶。

2.2.6 残碎斑晶沿叶理面的压扁及沿拉伸方向 x 的拉伸截断。

2.3 蛇绿糜棱岩带

雅鲁藏布江蛇绿糜棱岩带的发现，可以作为韧性超覆剪切带存在的一个重要标志。

目前，对糜棱岩的研究表明，糜棱岩是韧性剪切应变、回复作用及重结晶作用，并伴有碎粒的破碎作用的产物，并发现糜棱岩的显微构造是随着剪切应变的递增而发育的。

糜棱岩带大致相当于缝合带中蛇绿岩带的位置，往往位于蛇绿岩内的逆冲面附近，约几米或几十米厚，由橄榄糜棱岩、辉长糜棱岩及硅质糜棱岩组成。根据基质含量及糜棱质粒径(Sibson, R.H)，糜棱岩又分为初糜棱岩、糜棱岩及超糜棱岩。

橄榄糜棱岩是包含有叶理及线理的岩石，拉伸线理是通过斜方辉石及橄榄石沿 x 方向的拉伸而显示出来。在大量重结晶基质中嵌有应变的残碎斑晶(橄榄石及斜方辉石)，碎斑的边界港湾状，直径 1～7mm，平均 5mm；基质中又包括中粒(直径平均 45μm)、微粒(直径平均 6μm)的橄榄石颗粒，所以形成明显的三峰结构。基质中重结晶的橄榄石为多边形，由三角点相连，交角 120°，残碎斑晶伴有旋转变形。上述显微构造的特征很类似于阿尔卑斯山脉的瑞士-阿拉米绿泥石橄榄糜棱岩，故可称作阿尔卑斯型橄榄糜棱岩。残碎斑状结构出现表明橄榄糜棱岩形成于上地幔流变状态下(Boudier, F., *et al*., 1980; Nicolas, A., *et al*., 1972)。

2.4 橄榄石的组构分析

目前，地质学家公认橄榄岩来自于上地幔。对幔源矿物特别是橄榄石的组构分析，是研究上地幔流变机制的重要方面之一。

雅鲁藏布江橄榄糜棱岩(加加、日喀则及罗布莎[1] 等处)的组构(x 光及费氏台)具明显的 Ng[100]极密，滑移系为(010)[100]。据 Ng 滑移向与叶理面之间的关系，可推断剪切方向自北往南(图 4)。

实验证明(Carter, N.L., *et al*., 1961; Carter, N.L., *et al*., 1964; Nicolas, A., *et al*., 1973)，橄榄石滑移系随温度(t)、围压(σ)及应变速率($\dot{\varepsilon}$)而变化。在围压 15×10^8Pa，应变速率 $\dot{\varepsilon}=7.8\times10^{-5}$/s 下，温度 $t>1200\sim1300$℃时，滑移系为(010)[100]；$t=1000\sim1200$℃时，滑移系为{okl}[100]；$t<900\sim1000$℃，滑移系为{110}[001]。可以看出[100]滑移向只可能是高温应变的结果。因此上述组构表明橄榄石只经受了高温(>1000℃)应变。

2.5 橄榄石的超微构造及滑移系与应变参数测定

地质证据表明大多数富镁橄榄石(纯橄岩及橄榄岩)作为玄武岩浆的外源碎屑和阿尔卑斯型侵入岩而从地幔转移到地壳，因此可以通过橄榄石超微构造的研究(在透射电镜下观察)来了解上地幔流变(固态流动)的信息。由于在上地幔高温塑性流变中，橄榄石晶体内形成位错构造，并且不会被后期低温应变所消除，因此为我们提供了研究的可能。

选择加加、日喀则及罗布莎二辉橄榄岩中橄榄石残碎斑晶，运用双枪离子减薄器制成小于 1000 埃(Å)厚度的薄晶试样，在 EM-400 型，100 千伏(kV)电压的透射电子显微镜下，对橄榄石晶体进行超微构造的观察，并进行滑移系及应变参数(差异应力 σ，应变速率 $\dot{\varepsilon}$ 等)的测定(图 5)。

橄榄石的超微构造。在橄榄石中可见到反映高温(>1000℃)及低温(<800℃)应变的两

[1] 罗布莎橄榄石组构资料据崔军文。

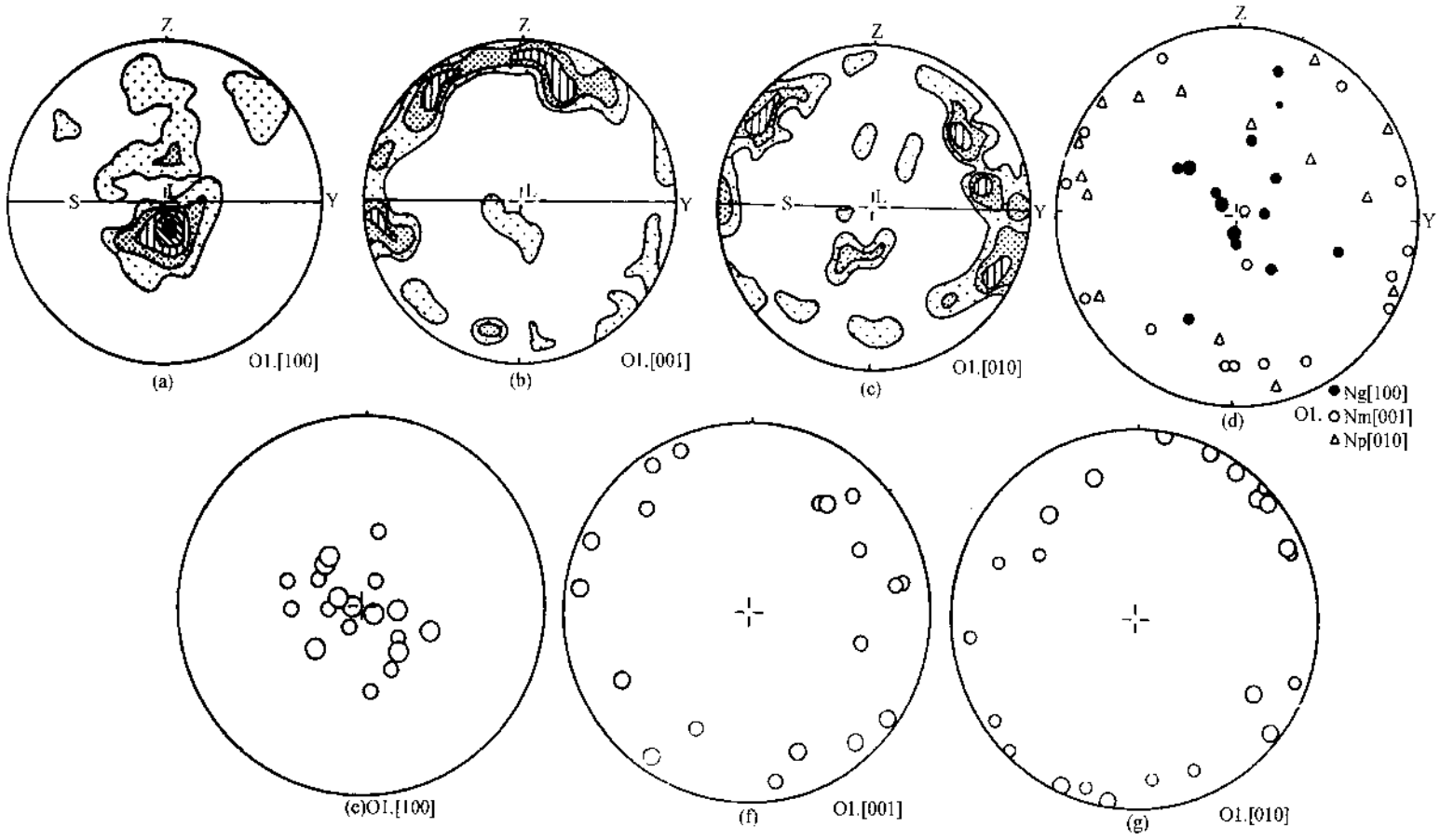

图 4　橄榄石组构图 I

(a)、(b)、(c)雅鲁藏布江西加加方辉橄榄岩，下半球投影、等密线：1%—3%—5%—7%—9%，Ng[100]呈极密，Nm[001]及 Np[010]不呈极密，(d)日喀则方辉橄榄岩，x 光组构分析，下半球投影，Ng[100]呈极密，Nm[001]及 Np[010]不呈极密；(e)、(f)、(g)雅鲁藏布江东罗布莎，x 光组构分析，下半球投影，Ng[100]极密，Nm[001]及 Np[010]不呈极密

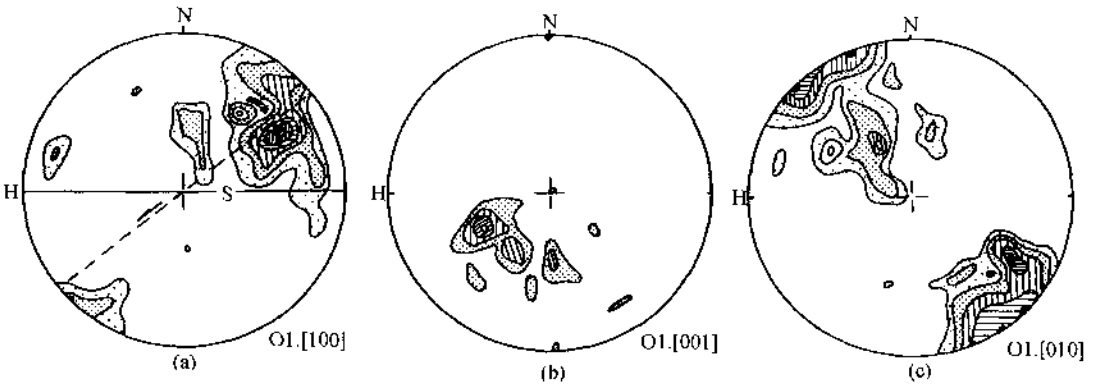

图 5　橄榄石组构图Ⅱ

罗布莎方辉橄榄岩，下半球投影，等密线：1%—2%—3%—4%—5%—6%；Ng[100]、Nm[001]及 Np[010]均呈极密

种类型的超微构造。

2.5.1　高温应变的超微构造

表现为以(100)体系的亚晶粒为主要特征的位错构造。亚晶粒在显微镜下表现为不同的消光域，但人们看不清其边界细节。通过缀饰法及透射电子显微镜可观察到其边界是由一系列平行、短直的刃位错排列而成的位错壁。亚晶粒一般呈长条形，直径宽度约 4～10μm，组成位错壁的刃位错线与位错壁交角 38°～55°，平均 45°(20 条位错壁统计)，位错壁或平直或稍有弯曲。此外位错环及沿位错线发育液态包体装饰，也是高温应变标志。

用缀饰法处理的橄榄石晶体(SA_{11}，加加，XZ 面)的位错构造，与 Guequan(1979)提出的橄榄石六种位错构造中的高温位错吻合，即滑移系为(001)[100]或(okl)[100]。

2.5.2　低温应变的超微构造

表现为自由位错切割了高温应变的亚晶粒位错壁，计算位错密度 $\rho=\frac{n}{S}$(n 为位错线数，S 为面积)，获得 $2.42\times10^8/cm^2$。

滑移系的计算主要根据透射电镜所获得电子衍射花样(图像)，橄榄石衍射花样的几何图形基本分两种类型：矩形及平行四边形。衍射花样中心至邻近衍射斑点的距离 R_1(R_2、R_3)与晶体面间距之间关系可运用公式 $Y=\frac{L\lambda}{R}$(Lλ 为透射电镜常数，10kV 时为 16.65Åmm)，而 d(面间距)$=\frac{1}{\sqrt{(\frac{h}{a})^2+(\frac{k}{b})^2+(\frac{1}{c})^2}}$，(其中晶胞参数 a = 4.76Å，b = 10.21Å，c = 5.98Å)。如 d_{001} = 5.98Å，d_{100} = 4.76Å，d_{010} = 10.21Å，d_{110} = 4.31Å，d_{011} = 5.16Å，d_{111} = 3.50Å。计算结果表明，对于高温应变的橄榄石来说，位错攀移的方向(即垂直于位错壁方向)为[100]，位错壁内位错线的方向有[221]、[101]、[010]。滑移系为(010)[100]为主。

计算低温应变的滑移方向为[111]、[001]及[010]。

2.5.3　应变参数的计算

应变参数主要指差异应力(σ)及应变速率($\dot{\varepsilon}$)

(1)差异应力(σ):主要根据 σ 与位错密度(ρ)、亚晶粒直径(d)的简化公式来计算❶。据日喀则方辉橄榄岩橄榄石透射电镜图像计算位错密度(ρ)为 $2.25\times10^{8}/cm^{2}$,差异应力值(σ)平均为 1.35×10^{8}Pa;缀饰法计算亚晶粒直径(d)平均为 5.6 微米,差异应力值(σ)为 1.78×10^{8}Pa。后者(亚晶粒)计算结果可能代表高温应变的差异应力值,而前者(位错密度)计算结果可能代表后期叠加的低温应变的差异应力值。

(2)应变速率($\dot{\varepsilon}$):可根据下列的蠕变公式(Goetze)来计算应变速率($\dot{\varepsilon}$)(当 $\sigma<2\times10^{8}$Pa 时):

$$\dot{\varepsilon}=70\sigma\cdot\exp\left(\frac{-122\times4.1868\text{kJ/mol}}{RT}\right)$$

($R=1.987\times4.1868\text{kJ}^{-1}\cdot\text{mol}^{-1}$,T 为绝对温度)

在高温应变(≥1100℃)下,利用亚晶粒计算的应力值来求应变速率,获得 $\dot{\varepsilon}=9.8\times10^{-14}$/s,表明与上地幔中稳态蠕变的速率相当($10^{-15}\sim10^{-13}$/s, Nicolas, 1976)

2.6 幔内型韧性推覆剪切带的动力学:洋内剪切作用

蛇绿岩带内一系列以推覆形式所表现出来的高应变带(韧性推覆剪切带)以发育 A 型平卧及同斜褶皱,明显流劈理或叶理,近南北向拉伸线理,矿物的塑性流变和旋转应变及蛇绿糜棱岩等为特征。它究竟形成于怎样的一个大地构造环境及热动力条件呢?微观构造提供了以下十分有用的依据:

(1)韧性推覆剪切带的存在表明其形成于地壳的深部。因为只有较高的温、压条件才能使蛇绿岩甚至上地幔岩这样坚硬岩石具高韧性。

(2)完整蛇绿岩剖面推覆在洋壳上部,表明剪切作用在洋内进行,并影响到洋壳下部的上地幔,这样才致使上地幔推覆至洋壳硅质岩之上。蛇绿岩中拉伸线理代表洋内剪切运动的矢量,而其中上地幔岩中拉伸线理则可能是在上地幔中滑移的结果。

(3)橄榄石中普遍发育的亚晶粒反映了高温应变,方辉橄榄岩所具明显的碎斑结构是上地幔蠕变的典型构造,橄榄石的高温滑移系(001)[100]的存在,及高应力、高应变速率更有力地证实了它是上地幔流变机制的产物。

微观构造分析表明了蛇绿岩内发育的韧性推覆剪切带是由于大陆碰撞之前的洋内剪切作用造成的。这种剪切作用使洋壳之一侧插入另一侧洋壳下部上地幔之中。而且只有这样,才有可能出现在橄榄石中我们所见到的代表上地幔流变的高温超微构造的现象。因而笔者把此种类型的韧性推覆剪切带称为幔内型。洋内剪切作用的提出(Nicolas *et al.*, 1972; Bard, J.P., 1980)是板块构造学说关于板块运动方式的一种发展。很长时期以来,板块碰撞前的运动方式被看作为只是洋壳顺利俯冲到陆壳之下,研究表明(Mattauer, M., 1981)这是安第斯山链,即俯冲型山链形成前板块运动方式。而阿尔卑斯、喜马拉雅以及欧洲的华力西山链等在山链形成前都经历了洋内仰冲(剪切)作用,故称之为仰冲型山链。笔者通过实际资料证实了这种洋内作用存在于印度板块与拉萨板块逐渐靠拢,即新特提斯洋逐渐消减过程中,大约自 100Ma 左右开始。

---

❶ 利用位错密度计算差异应力 σ 的简化公式:
$\sigma=9\times10^{-5}\rho^{0.5}$(Goetze, 1975)
利用亚颗粒计算 σ 简化公式:
$\sigma=10d^{-1}$(Durham, 1977)

3 雅鲁藏布江壳幔型韧性推覆剪切带

雅鲁藏布江壳幔型韧性推覆剪切带主界面位于幔内型韧性推覆剪切带之南侧，蛇绿岩带及印度地台北缘的陆壳间，后前叠置了雅鲁藏布江缝合带。缝合带之南侧(印度地台北缘)曾被命名为特提斯喜马拉雅构造带，由古生代及早三叠系浅海相沉积，中、上三叠系复理石沉积和侏罗系—白垩系的浅海相沉积地层组成，古生代地层不整合在前寒武系高喜马拉雅深变质岩系(聂拉木群)之上。近缝合带的古生代及三叠系至下白垩统地层(可达 20km 之远)均卷入韧性推覆剪切带范围。

3.1 变形特征

剪切带特别主界面附近，发育近水平流劈理(Mattauer, M., 1975)及 A 型褶皱，劈理面上普遍发育近南北向拉伸线理，如在昂仁错南的 T_3 和 J_3—K_1 片岩中发育一系列褶皱轴平行于拉伸线理方向(10°～30°)的 A 型褶皱(Mattauer, M., *et al*., 1980)(图 6)，而在刚、柔性层互层或远离主界面部位，则发育轴面北倾，枢纽弯曲 290°～310°的 B 型褶皱，与拉伸线理方向垂直，并可清楚看到由流劈理(片岩中)及破劈理(砂岩中)所组成的折射劈理(图 6)及布丁构造。

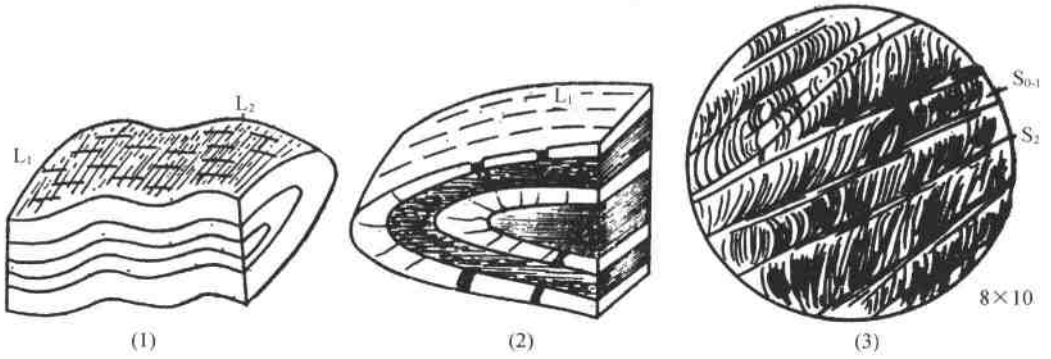

图 6 壳幔型韧性推覆剪切带中褶皱

(1)A 型褶皱及叠加应变；(2)B 型褶皱及折射劈理；(3)折劈理(S_2 切 S_{0-1})；L_1—拉伸线理；L_2—细褶纹线理(T_3—J_1 片岩；当丁拉)

上述两种类型的褶皱都可以看作是相同剪切机制所造成的(Mattauer, M., 1975; Mattauer, M., *et al*. 1980)。对于第一种类型 A 型褶皱，我们可用两种方式来解释：或者原先褶皱是平行剪切方向，在演化过程中继续保持平行；或者原先是垂直(或斜交)于剪切方向，后来又重新定向。重新定向的褶皱代表了强烈的剪切应变。第二类褶皱 B 型，具弯曲枢纽，变形程度较弱，演化较慢，保持垂直于运动方向，实应是剪切应变的初期阶段。两类褶皱形成表明构造部位及岩性是变形的函数。

拉伸线理是剪切带中明显的构造，其方向与蛇绿岩内一样，为近南北向(350°～30°)，在区域上很稳定。拉伸线理最主要表现形式是矿物拉伸，窗棂构造及杆状构造，还常与刚性层的布丁构造相伴随，布丁轴垂直于拉伸线理方向。拉伸线理的明显程度与所处构造部位(远离剪切带主界面的不明显)、岩性及后期叠加有关。

随剪切作用的加剧，在较柔性层内可形成第二期近水平流劈理(S_2)，切割了早期的S_{n-1}称之为折劈理(图 6)。

3.2　剪切带内石英及动力学

石英是一种对应变反映十分灵敏的矿物，因此它可以保存变形的信息。随着石英变形实验的进展，我们可以通过石英组构及微构造的分析来对剪切带进行动力学分析(Boullier, A.M., et al., 1978; Boucher, J.L., 1977; Boucher, J.L., *et al*., 1981)。

3.2.1　石英的塑性流变及剪切应变

在剪切带的不同部位，石英变形特征不同(图版Ⅳ)剪切带外部石英，变形微弱，弱波状消光，少量拉长压扁，颗粒边部有港湾状弯曲，旋转变形不明显。

剪切带内部石英，具明显的拉长及压扁，强烈的塑性流变使矿物显"浆屑状"，波状消光，变形纹，在 XZ 切面上可见明显的旋转应变；如带尾巴的石英集合体被流劈理所包围，石英颗粒内绿泥石及金红石包体的旋转，石英及云母组成显微韧性断层等都指示了剪切运动方向自北往南。

剪切带中心部位石英，具有强烈构造重结晶现象，石英颗粒常呈矩形，沿 X 方向拉伸，颗粒内具波状消光及变形纹，并见矩形石英小颗粒呈"S"形旋转，表示了构造重结晶作用是在自北往南剪切作用下发生的。构造重结晶作用与静态重结晶作用不同之处在于前者是构造与热同时参与的作用，而后者是纯粹热事件的反应。剪切带中心构造重结晶石英的普遍存在，反映了随着剪切作用加强而产生剪切热的作用，而这种作用又掩盖了早期在剪切带中心部位强大剪切应变所形成的显微构造特征。

在剪切带中心部位还发育石英糜棱岩-千糜岩带，是高温高应变的结果，石英糜棱岩中的剪切应变指示了向南的剪切运动方向。

从剪切带边部至中心，石英显微构造特征反映了剪切带塑性变形经历了冷变形→热变形→构造重结晶的过程。

3.2.2　石英组构分析

剪切带内石英具两种类型的组构(图 7)：

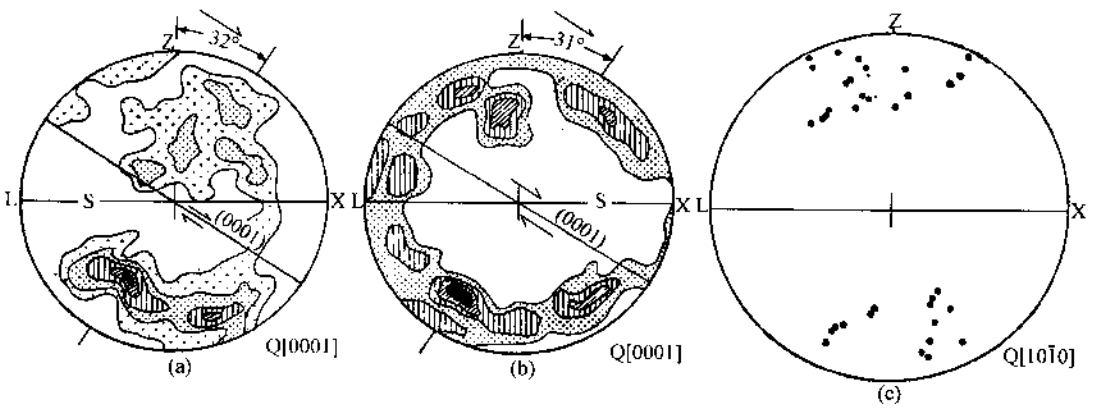

图 7　石英组构图

(样品采自萨迦郭林淌以南)

(a)，(b)为Ⅰ类(0001)不对称底面型组构，其中 a. 等密线 2—4—6—8—10%，197 石英颗粒；b. 等密线 2—4—6—8%，200 个石英颗粒；(c)为Ⅱ类|10$\bar{1}$0|不对称柱面型组构(x 光)

(1)(0001)不对称底面型组构(或 c 轴组构),位于剪切带内部,采用当丁拉地区三叠系石英岩进行 XZ 面上石英颗粒费氏台组构测定,获得明显光轴(c)轴极密及环带,与 X 轴呈明显不对称,(0001)面与流劈理面(S)的关系指示了剪切运动方向自北往南,光轴 c 与 z 轴夹角(即劈理面 S 与光轴面(0001)的夹角)为 31°~32°。

(2)$\{10\bar{1}0\}$柱面不对称组构(或 m 轴组构),位于剪切带中心部位,通过石英糜棱岩中石英颗粒 x 光组构分析获得此类组构,表明了滑移方向为 m 轴。

不同类型的石英组构类型反映了不同的温度条件(Carter, 1971),(0001)底面组构代表形成于 350℃以下的温度,显示了剪切滑移的特征,是高应变作用的反映;而$\{10\bar{1}0\}$柱面组构类型代表形成于 600℃以上的温度,m 轴与 X 方向近于垂直,表明高温条件下,由于原子扩散产生垂直滑移方向的位错攀移(沿 m 轴攀移)。这与剪切带中心具剪切热作用的认识是吻合的。

3.3 有限应变分析

有限应变分析是确定应变椭球体类型及变形机制的一种有效方法。弗林(Flinn, 1962)曾根据弗林指数 $K=\dfrac{\frac{X}{Y}-1}{\frac{Y}{X}-1}$的大小来确定应变椭球体类型:K = 0,扁球型;0 < K < 1,压扁型;K = 1,剪切型;∞ < K < 1,收缩型;K = ∞,长球型。所以弗林图解实际上反映了应变椭球体三个主轴(X、Y、Z)的关系。

我们利用原始均匀而且是球形的变形化石——圆球虫(Cenophanian)作为有限应变计算的标志。在剪切带主界面以南的绿片岩(J_3—K_1)中还保存了压扁拉伸的圆球虫,在 XY 及 XZ 面上计算应变主轴,获得 X/Y/Z = 3.10/1.65/1,K = 1.39(图 8)。再据伍德(Wood)图解,获得地壳沿 x 方向拉伸为 80%,沿 Z 方向缩短 42%,沿 y 方向变形很小,这表明属于剪切型机制,由于 XZ 面上可见明显的旋转变形特点,所以应为简单剪切机制。

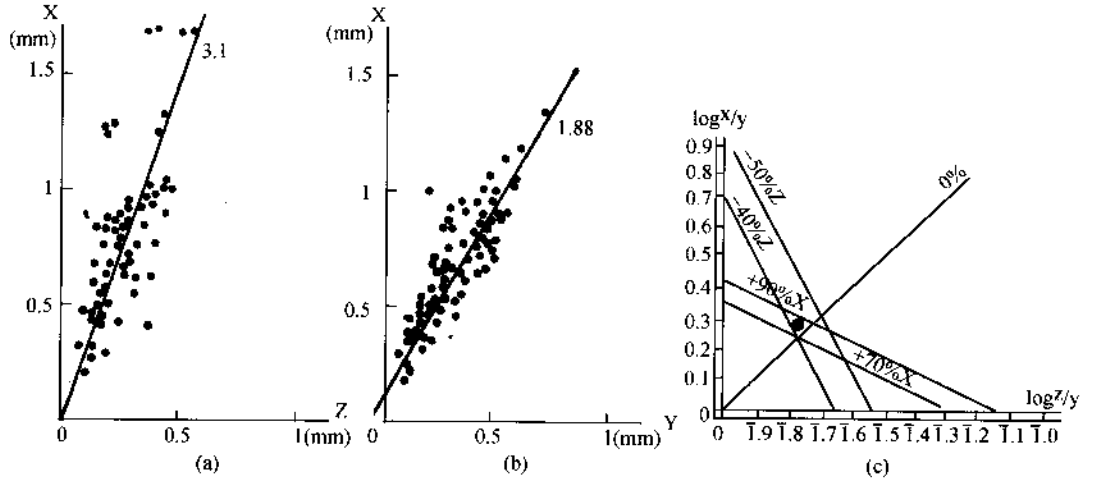

图 8 变形圆球虫的有限应变分析

(a)、(b)变形圆球虫的弗林图解,(a)为 XY 面上 61 个圆球虫测量,(b)为 XZ 面上 73 个圆球虫测量;(c)变形圆球虫的伍德(Wood)图解

3.4 高压变质带

雅鲁藏布江蛇绿岩带以南高压变质带的发现(肖序常等,1982)不仅为西藏板块构造研究提供了有益的依据,而且也有助于分析韧性超覆剪切带中变形及变质作用的关系。

高压变质带包括了北侧的蓝片岩带,以蓝闪石类、文石、硬玉、黑硬绿石、硬柱石、绿纤石等矿物组合为特征;南侧绿片岩带,以出现硬绿泥石等矿物为特征。变质作用的前沿可达吉隆—萨迦—曲松一带。

变质程度自北往南从强到弱,压力从高到低的变化是与变形作用从强至弱变化趋势相一致的。高压变质带可以作为蛇绿岩仰冲于印度陆台北缘陆壳之上的产物。

3.5 蛇绿岩仰冲作用

随着洋内剪切作用的继续,洋壳不断消减,两侧板块逐渐靠拢,致使洋壳之一侧仰冲于另一侧板块边缘,造成了蛇绿岩的仰冲作用。由于这种作用发生在洋陆之间,因此热动力条件与洋内剪切作用相比,应属于低温高应变作用。以下依据表明了这种作用发生在喜马拉雅山链开始形成之时:

(1)雅鲁藏布江壳幔型韧性推覆剪切带的特征表明,和洋壳剪切作用一样,是简单剪切机制的产物。

(2)方辉橄榄岩中橄榄石组构及透射电子显微镜分析表明,低温高应变作用叠加于高温低应变作用(地幔流变)之上,是洋壳蛇绿岩仰冲上陆的结果。

(3)高压变质带反映了低温高应变变质作用伴随变形作用产生。

(4)石英动力学分析表明仰冲作用过程又使剪切带矿物(石英)从低温向高温转化,这同样又反映在橄榄石低温高应变的位错构造出现液态包体的装饰。并且沿主界面形成石英千糜岩带。

(5)变质矿物(角闪石)同位素测试年代为 89Ma[1]。

4 康马—定日壳内型韧性推覆剪切带

4.1 变形特征

剪切带位于壳幔型韧性剪切带以南 100km 的康马—定日一带,呈东西向展布。古生代、中生代地层及花岗岩体(如康马岩体、马拉山岩体)均卷入剪切运动之中,变形特征与上述剪切带类同,具 A 型平卧或同斜褶皱、近南北向拉伸线理及近水平流劈理;而远离剪切带中心,拉伸线理及劈理渐弱,褶皱渐变为 B 型。

4.2 有限应变分析

利用马拉石变形花岗岩中变形石英颗粒进行有限应变分析(图 9),获得 X/Y/Z=2.27/1.45/1,弗林指数 K=1.26,伍德图表计算结果:地壳沿 X 方向拉伸 55%,沿 Z 方向缩短小于 40%,沿 Y 方向不变,同样表明是简单剪切机制产物。

4.3 方解石的组构分析与剪切带的应力场

为确定本剪切带所处的应力场,进而判断剪切运动的方向,笔者采用了方解石组构测定与艾切戈巴(Etchecoper)方解石电算法相结合的方法。

[1] 王希斌等,西藏蛇绿岩,印刷中。

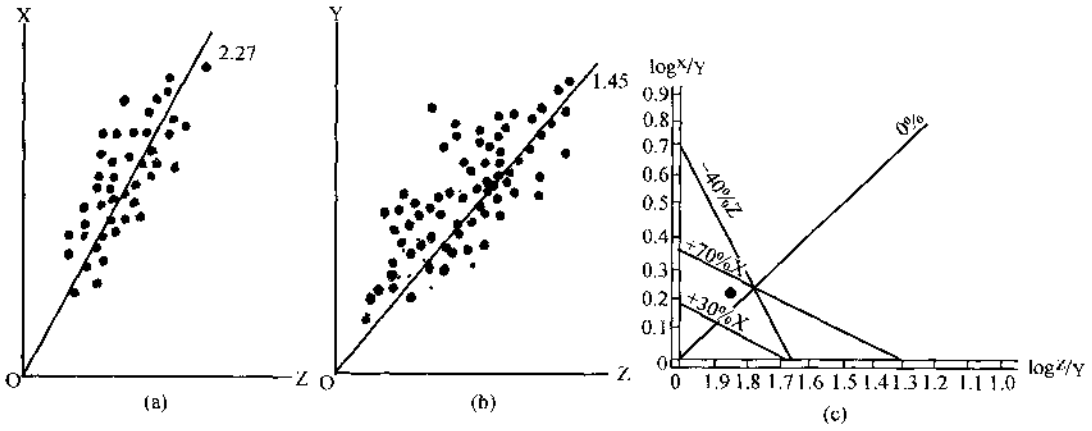

图 9　马拉山花岗岩变形石英有限应变分析

(a)、(b)为弗林图解;(c)为伍德图解

我们知道,在三方晶系方解石的结晶要素中,方解石 c 轴[0001]的优选方法及双晶面-e 面$|01\bar{1}2|$具有动力学意义。因为方解石的实验表明,有效应力状态与晶间滑动有关,对于一个给定的方解石颗粒来说,可能最有效地发动沿 e_1 的双晶滑动的唯一压应力方向与 e 面夹角为 45°,与[0001]面夹角为 71°,拉张应力方向与 e 面夹角也为 45°,与[0001]面夹角为 45°。

标本选自剪切带康马二叠系大理岩,劈理产状 55°NW∠23°,拉伸线理方向为 164°,在 XY、XZ 及 YZ 面上各测三十三个方解石颗粒的双晶 c_1、e_2、e_3 光轴 c(已知其中二个要素,便可通过作图求其它要素),然后运用艾切戈巴(Etchecopar)方解石电算法获得应力场:σ_1 = 334°/6°,σ_2 = 65°/5°,σ_3 = 191°/82°(图 10),表示剪切运动方向往南(图 11)。

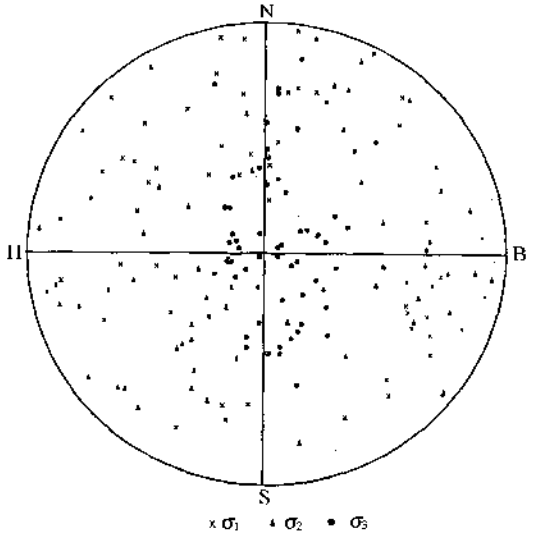

图 10　方解石电算结果

康马二叠系大理岩,下半球投影,σ_1—主压应力轴,σ_2—中间应力轴,σ_3—主张应力轴

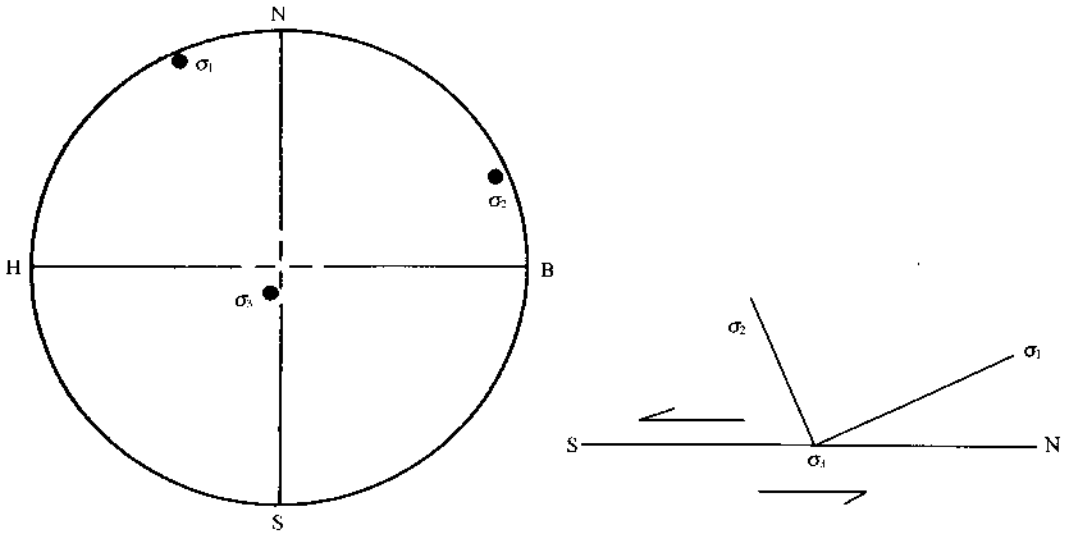

图 11　据方解石应力场判断剪切方向

σ_1—主压应力轴；σ_2—中间应力轴；σ_3—主张应力轴；H—顶面；B—底面；N—北；S-南，箭头指示剪切方向

4.4　方解石的透射电镜观察及动力学分析

作为显微构造研究的最新技术——透射电子显微术，是把岩石及矿物的变形与晶格构造相结合起来，研究变形本质及进行热动力条件分析的有效方法。将上述二叠系大理岩中方解石颗粒经离子轰击制成七个薄晶试样，在 200 千伏的 JEM-200 型透射电子显微镜下观察，实验目的是观察与剪切带塑性变形有关的亚构造，确定塑性变形阶段及计算变形参数。

4.4.1　方解石的超微构造

(1)位错线及位错环。由于热历史及变形史通常使一个完整晶体结构产生缺陷，位错是一种线的缺陷，为晶格滑移区与未滑移区之间的界限。在方解石晶体中普遍存在位错构造，位错线短，呈歪扭状，并出现圆形或拉长的位错环。通过交叉法及一般法测量的位错及位错环密度平均为 $10^8\sim10^9/cm^2$($6.66\times10^8/cm^2$，$6.85\times10^8/cm^2$，$5.6\times10^8/cm^2$，$2.73\times10^8/cm^2$，$5.79\times10^8/cm^2$)。此外可观察到由于位错相互作用所形成的位错壁(由一系列平行位错线组成)、位错堆积，位错堆积被位错壁所切割。

(2)亚颗粒。亚颗粒边部是由位错壁组成，不同亚晶粒在光学显微镜下表现为不同的消光域。方解石晶体内亚晶粒呈长条形，亚晶粒宽度(d)大约为 0.18～1,3μm。

(3)液态包体。作为一种装饰，液态包体沿位错线分布，呈拉长状，最大包体面积约 $0.6\mu m^2$，最小为 $0.02\mu m^2$。

(4)微双晶。微双晶的宽度为 0.06～0.26μm，其切割了位错环。

4.4.2　变形参数的计算

与变形有关的物理参数主要有差异应力(σ)及应变速率($\dot{\varepsilon}$)。

(1)差异应力的估算

我们可采用位错密度及亚晶粒直径与差异应力有关的公式来进行差异应力的估算。

位错密度(ρ)与差异应力(σ)的关系可用以下公式表示：

$$\rho = K\left(\frac{\sigma}{\mu}\right)^n \text{(Weertman, 1970)}$$

其中，μ = 剪切模量，方解石为 0.25mb，n 及 K 为常数，是据 Schmid, S.M., Boland, T.N. 及 Polerson;M.S.(1977)实验计算而获得(图 12)。据位错密度-应力对数图，计算了 K 的平均值(采用 $n=1$, $n=3$)，获得 $n=1$ 时，$K=8.5\times10^2$；$n=3$ 时，$K=3.5\times10^{-9}$(表 1)，因此，我们可以根据 ρ、K 及 n 来计算 σ(表 2)，差异应力值：$137\times10^5\text{Pa}<\sigma>182\times10^5\text{Pa}$。

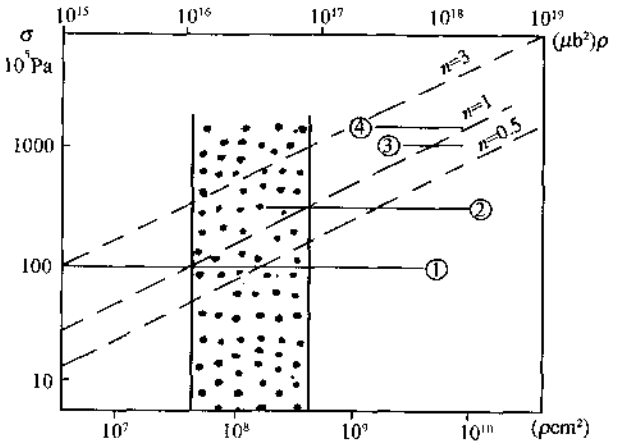

图 12　位错密度-应力对数图

(Schmid, S.M. 1977)

表 1　据图 15 计算的 k 值

线	应力($\times10^5$Pa)	k	
		$n=1$	$n=3$
①	100	2.5×10^2	1.56×10^{-9}
②	500	6.0×10^2	1.52×10^{-8}
③	1000	1.56×10^3	1.0×10^{-10}
④	1200	1.0×10^3	3.9×10^{-11}
平均值 km		8.5×10^2	3.5×10^{-9}

表 2　差异应力计算结果

	照片号码	位错密度$(\text{cm})^2$	差异应力 σ($\times10^5$Pa)	
			$n=1$	$n=3$
1	7098	3.69×10^8	108	118
2	7100－7102	5.79×10^8	170	137
3	7257	6.85×10^8	201	145
4	7259	2.73×10^8	80	107
5	7261	5.6×10^8	165	136
6	7262	6.66×10^8	196	144
7	7298	1.07×10^9	314	168
8	7311	1.11×10^9	326	170
9	7315	3.62×10^8	106.5	117
10	7868	5.17×10^8	152	132
平均值		6.2×10^8	181.8	137.4

(据位错密度)

(2)应变速率($\dot{\varepsilon}$)的估算

根据蠕变实验得到的蠕变公式:

$\dot{\varepsilon} = A\exp(-\frac{Q}{RT})\sigma^n$ 可应用各种矿物的塑性变形中。其中 A 与 n 为实验常数,Q 为活动能,R 为理想气体常数,下为绝对温度。对于方解石来说,我们采用 $A = 4.7\times10^{-2}$(Dorn 常数),$Q = 70\times4.1868\text{kJ}\cdot\text{mol}^{-1}$,$R = 1.9872\times4.1868\text{kJ}^{-1}$,$\text{mole}^{-1}$,$T = 573\sim873$℃(因为 $10^8/\text{cm}^2$ 的位错密度存在中级变质碳酸岩中,温度为 300～600℃,据 Barber, D. J., (1976), n=3 或 5。

当 σ=137b 及 182b 时,

$$n=3,\sigma=137\times10^5\text{Pa},\dot{\varepsilon}=2.0\times10^{-15}\text{sec}^{-1};$$
$$\sigma=182\times10^5\text{Pa},\dot{\varepsilon}=4.6\times10^{-15}\text{sec}^{-1};$$
$$n=4,\sigma=137\times10^5\text{Pa},\dot{\varepsilon}=3.7\times10^{-11}\text{sec}^{-1};$$
$$\sigma=182\times10^5\text{Pa},\dot{\varepsilon}=1.5\times10^{-10}\text{sec}^{-1}。$$
$$2.0\times10^{-15}<\dot{\varepsilon}<1.5\times10^{-10}(\text{sec}^{-1})$$

我们获得平均应变速率约 $10^{-12}\sim10^{-13}\text{sec}^{-1}$。

4.4.3 讨论

为研究本区大理岩形成的热动力条件,首先对比阿尔卑斯贝赫杰纳(Bergell)地区三叠系大理岩。Barber, D.J. 和 Wenk, H.R.(1976)在研究该大理岩中方解石显微构造、变质程度及温度之间关系时发现,在低级变质的碳酸盐岩中,位错密度大约 $10^8\sim10^9/\text{cm}^2$,发育直线形位错,显微双晶及位错缠结,形成温度为 50～200℃;在中级变质的碳酸盐岩中,位错密度小于 $2\times10^9/\text{cm}^2$,以发育亚晶粒为主要特征,形成温度为 300～600℃;在高级变质的碳酸盐岩中,位错密度较低,大约 $10^7/\text{cm}^2$,以亚晶粒及气孔发育为特征,形成温度大约 800℃。喜马拉雅山链中的康马二叠系大理岩内方解石的超微构造特征:扭歪位错、圆形位错环、位错壁及亚晶粒的大量出现说明塑性变形的回复阶段占主要地位,这是高温低应变的阶段,液态包体的出现归因于温度上升的静止一幕,但新颗粒及核结作用缺失及液态包体少量存在表明静态重结晶阶段不是主要的。因此,我们认为所研究的大理岩应相当于阿尔卑斯贝赫杰纳大理岩的中级变质相,是在低应变(150～180×10^5Pa),温度大约 300～500℃的条件下形成的。

康马-定日壳内型韧性推覆剪切带及南面的尼泊尔韧性推覆剪切带的存在(推覆距离达 100km)表明陆壳内完全有可能发生大规模的滑移,正如玛托耶教授指出的(1984),俯冲作用可以在陆壳内继续进行。

5 喜马拉雅山链的形成机制探讨

5.1 变形机制

和阿尔卑斯山链一样,大规模推覆构造(韧性推覆剪切带)是喜马拉雅山链的最主要变形构造特征(许志琴,1984)。根据微构造研究表明喜马拉雅板块聚合带主要经历了两期重要变形阶段:第一阶段表现为在简单剪切机制(K≥1)作用下形成的韧性推覆剪切带,伴随大规模流劈理、南北向拉伸线理及 A 型平卧褶皱,剪切运动方向自北往南;第二阶段是在收缩机制下形成的东西向褶皱,伴随直立或放射状劈理。第一阶段的变形是主要的,它贯穿在

拉萨板块与印度板块相对运动的全过程中，韧性推覆剪切带从幔内型→壳幔型→壳内型发展表明剪切应变从北往南，从洋内至陆内迁移，时代从老至新（100～20Ma 迄今），由深至浅，温度从高到低（大于 1000℃至 300～500℃），应力从大至小（$2-3\times10^8$ 帕至几百 $\times10^8$ 帕。韧性推覆剪切带内矿物显微构造分析表明存在从冷变热至热变形及构造重结晶阶段，说明剪切带形成后期可产生大量剪切热，以致出现石英{$10\bar{1}0$}柱面组构及糜棱岩带。据 Fleitout, L. 和 Froidevaux, C., 1980）对剪切热的研究，认为如果剪切带经受了几个 $\times10^8$ 帕的应力，那么变形结果便会产生大量热，随时间的延续，可在剪切带主界面附近出现 900K 温度的岩浆深溶作用，雅鲁藏布江、拉轨岗日及尼泊尔花岗岩带可能就是更深处剪切热的产物。同时可以推测，剪切带在地壳深部相当于地球物理剖面资料所提供的低速层，它是热流及岩浆的孕育带，也为剪切带的大规模滑移提供了可能的条件。收缩作用是在板块碰撞后（K_2 后）开始的，收缩应变也不断从缝合带向外侧扩展，故存在迁移性，并叠加于早期应变之上。

在喜马拉雅山链形成过程中，简单剪切机制是最重要的，它可以把岩石向南推覆至 100km 之外（尼泊尔），造成地壳大规模缩短及叠置，这与地球物理资料相吻合。可以设想，在山链形成历史过程中，最高山峰也自北经南迁移，至今在尼泊尔韧性剪切带前缘形成世界最高的山峰。因此喜马拉雅山链主要是推覆成山的。

5.2 山链的类型及板块构造演化

长时间以来，经典板块理论认为俯冲（即洋壳插入陆壳之下）是洋壳板块消减的唯一形式。玛托耶等人根据阿尔卑斯、喜马拉雅等山链的研究提出：仰冲是板块运动的又一重要形式，它所形成的山链不同于俯冲型山链（如安第斯山链）（Mattauer, M., 1981）。喜马拉雅山链的雅鲁藏布江带蛇绿岩构造研究表明，这种仰冲作用在板块碰撞前的大洋消减阶段就开始了，可以设想这种仰冲剪切作用很容易发生在仅几公里厚的洋壳内，特别是应力薄弱地带（如洋脊）。剪切作用深度可以达到洋壳下的上地幔内，并致使上地幔岩石发生强烈的塑性流变，因此，洋内仰冲是板块相对运动的第一阶段，洋壳内的相对运动必然加速了板块靠拢及碰撞时间，这一点可以较理想地解释宽达 3000km 的东特提斯洋（J_3—K_1）为什么能在 20Ma 期间很快闭合（据古地磁资料）。洋内剪切作用时期大致在 100Ma 左右。

随洋内剪切作用连续，在 80Ma 期间，洋壳仰冲于印度板块北缘，形成壳幔型韧性推覆剪切带，并造就了印度板块北缘最早的山链——仰冲型山链。与此同时，在拉萨板块南侧形成火山岛弧及弧前复理石楔（日喀则盆地），在印度板块北侧由于推覆形成含外来岩块复理石混杂堆积。壳幔型韧性推覆剪切带伴随着高压变质作用。

40Ma 期间，东特提斯闭合，两板块发生碰撞事件，收缩应变发生在日喀则群及混杂堆积内，并叠加于上述已形成韧性推覆剪切带之上。与此同时产生陆内俯冲作用，形成康马-定日韧性推覆剪切带。

20Ma 期间，陆内俯冲作用继续，形成尼泊尔韧性推覆剪切带。

壳内型韧性推覆剪切带存在表明板块碰撞后，俯冲没有停止，而在陆壳内部进行。

图 13 扼要表示了山链形成的板块动力学模式，我们可以看到通过微构造方法来研究板块聚合带变形，在板块动力学解释方面所起到的重要作用。

野外工作期间与布尔格，陈国铭先生合作，透射电镜及方解石工作得到布尔格、洛朗及艾切戈巴先生帮助，陈晶同志协助测试部分橄榄石组构，在此一并致谢。

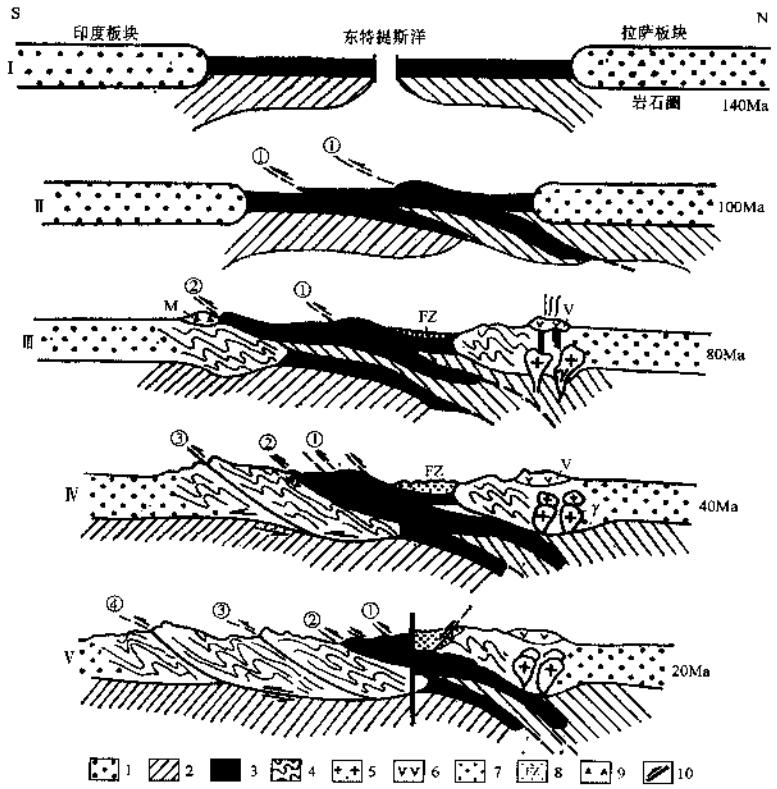

图 13 喜马拉雅山链形成的板块动力学模式

Ⅰ—东特提斯洋的扩张(J_3—K_1)；Ⅱ—洋内剪切，幔内型韧性推覆剪切带形成(100Ma)，Ⅲ—蛇绿岩仰冲，壳幔型韧性推覆剪切带、仰冲型山链形成(80Ma)；Ⅳ—碰撞，缝合带。收缩应变及陆内俯冲、康马-定日韧性推覆剪切带形成(20~40Ma)；Ⅴ—陆内继续俯冲，"尼泊尔"韧性推覆剪切带形成(20Ma)

1—陆壳；2—上地幔；3—洋壳；4—造山带；5—花岗岩；6—火山岩；7—K_2 日喀则群复理石；8—第三纪红色磨拉石；9—混杂堆积；10—逆冲断层

参 考 文 献

许志琴，1984，阿尔卑斯旋回中喜马拉雅山链和阿尔卑斯山链的主要变形特征。中国地质科学院院报，第 9 号。

许志琴，1984，地壳变形及显微构造。地质出版社。

肖序常等，1980，中国特提斯喜马拉雅蛇绿岩及其地质意义。国际交流地质学术论文集(一)，构造地质、地质力学。地质出版社。

肖序常，高延林，1982，西藏雅鲁藏布江缝合带高压低温绿片岩相的新资料。中国地质科学院地质研究所所刊，第 5 号。

Bard, J.P., Maluski, H., Matte, Ph., and Proust, F., 1980, The Kohistan Sequence: Crust and Mantle of an Obducted island Arc. Proc. Intern. Commit. Geodynamics, Grp. 6, Mtg. Peshawar, Nov. 23-29, 1079; Spec. Issue, Geol. Bull. Univ. Peshawar Vol. 13, 1980.

Boucher, J.L., 1977, Plastic deformation of quartzites in an area of natural strain gradient and low temperature. Tectonophysics, 39, 25~50.

Boucher, J.L., & Pecher, A., 1981, The Himalayan Main Thrust pile and its quartz rich tectonites in Central Nepal. Tectoni-

physics, 78, 23～50.

Boudier, F., Nicolas, A., Boucher, J. L., Crambert, S., Dahl, R., et Juteau, T., 1980, Les ophiolites des Nappes de Semail (Oman): Structures internes des massif de Nakhl et de Rustaq. Sci. Géol., Bull., 36, 1, P. 17～33, Strasbourg, 1983.

Boullier, A.M., et Boucher, J. L., 1978, Le *quartz en rubans* dans les *mylonites*. Bull. Soc.Geol.Fr., 1978, n 3.

Brunel, M., & Andrieux, J., 1980, Sur un modele tectonique explicatif du métamorphisme "inverse"himalayen. C. R. Acad. Sc. Paris, t. 291, Ser. D, 509～612.

Brunel, M., Etude Pétro-structurale des chevauchements ductiles en Himalaya (Nepal oriental et Himalaya du Nordouest). 1983, Thèse, presentéeà l'université de paris VII pour l' obtention du titre de Docteurdes Sciences.

Carter, N. L., Christie, J. M, & Griggs, D. T., 1961, Experimentally produced déformation lamellae and others structures in quartz sand'Abst.) Am. Géophys. Union. Trans. 66. P. 2518.

Carter, N. L., Christie, J. M., & Griggs, D. T., 1964, Experimental déformation and recrystallization of quartz, J. Geol., 72, 687～733.

Mattauer, M., 1975, Sur le mécanisme de formation de la schisite dans l'Himalaya. Earth and planetary Science Letters, 28, pp. 144～154.

Mattauer. M., e' Mercier, J. L., 1980, Microtectonique et grande tectonique Mem. h. ser. Soc. géol. de France N. 10.

Mattauer, M., 1980, Les déformations des matériaux de l' écorce terrestre. Ed. Herman. Paris.

Mattauer, M., 1981, La formation des chaines de montagnes. Science édition francaise de scientific américan, N. 46, pp. 40～56.

Nicolas, A., Boucher, J. L., & Boudier, F., 1972, Interprération cinématique des déformations plastiques dans le Massif de Iherzolites de Lanzo (Alpes piémontaires). Tectonophysics 14, 143～171.

Nicolas, A., Boudier, F., and Boullier, A. M., 1973, Mechanisms of flow in naturally and experimentally deformed peridotites. Am. Jour. Sci, 273, 853～876.

Large shear zones in the main orogenic belts of China[●]

During the last ten and more years, detailed research has been undertaken on the geometry, kinematics and dynamics of more than 50 large shear zones in the main orogenic belts of China, including the Himalayas, the East Kunlun Mountains, the Bayan Har-Songpan-Ganzê, the Qilian Mountains, the Qinling-Dabie, the Tianshan Mountains and the intracontinental mountain chains of eastern China. New classifications of the shear zones are proposed. The dynamic process of formation of the initial mountain chains by plate convergence has been reconstructed using the concepts of 'palaeo-intraoceanic' and 'palaeo-subduction' types of ductile shear zones. In addition, the mechanisms of orogenesis during the formation of the main continental mountain chains in China have been re-established. It is suggested that different types of large shear zone resulted from main orogeny-, post-orogeny-or re-orogeny-phases respectively, in both the 'collision' and 'intracontinental' types of mountain chain.

The classification of large shear zones and some examples

The large shear zones of China have been defined on the basis of three criteria:

- The nature of the boundary between interacting plates.
- The regional tectonic regime.
- The P-T conditions during shear zone formation.

Details of the classification and some examples of the various types of shear zone are given in Table 1.

The intraoceanic type

The Yarlung Zangbo River suture zone is an example of a palaeo-intraoceanic ductile shear zone. There, an ophiolite zone, developed a ductile thrust-nappe system with a transverse (N-S) stretching lineation), and with garnet amphibole schist characterising the base of an obducted part. Fabric and dislocation structures in minerals in mantle-derived peridotite, indicate the existence of a (010)[100] slip system representing high temperature and flow of the upper mantle and a N-S slip vector. This demonstrates that, before the formation of the initial mountain chain of the Himalayas, the closure of the Tethys oceanic basin (J-K_1) had involved intraoceanic shearing, with the oceanic crust being thrust southward onto the continental margin of the Indian plate.

● Episodes, Vol. 18, nos. 1 & 2.

Table 1 Types of large shear zones in different orogenic belts

Classification criterion	Shear type	Typical example
Nature of the boundary between interacting plates	1. Intraoceanic	Zoulang Nanshan, northern Qilian Mountains, Yarlung Zangbo River
	2. Subduction (Obduction)	Northern Qilian Mountains, central Kunlun (A'nyêmaqên), Yushu-Jinsha River
	3. Collision and plate convergence	Himalayas, south Kunlun, north Qiling
	4. Non-collision	Shandong-Liaoning, south China
Regional tectonic regime	1. Contraction: a Decollement b Thrust nappe	South Qinling, Shandong-Liaoning, western Sichuan (Danba), Tanggula Mountains, Eastern Sichuan, Himalayas, south Kunlun, Dabie, north Qinling, south China
	2. Extension	Western Shandong, southern Liaoning, central Qilian, western Sichuan, north Himalayas
	3. Strike slip	Xianshui River, central Qinling, southern Kunlun, south edge of north Qilian, south edge of north Tianshan, Lancang River, Jinsha River, Honghe River
P-T conditions during shear zone formation	High T-ultra High P (25~30) 105KPa, >840℃	Southern Shandong, Dabie
	High T-Medium P (6) 105KPa, > 500℃	Western Sichuan (Danba)
	High T-Low P (3~4) 105KPa, >650℃	Western Sichuan (Yajiang, Xianshui River)
	High P-Low T (7.5) 105KPa, 300~400℃	North Qilian, Yarlung Zangbo River, southern Kunlun
	Low T-Low P (2~3) 105KPa, 250~300℃	Tanggula Mountains

The subduction type

The Zoulang Nanshan Caledonian subduction complex zone, located between the Alxa block and the Qilian block in the Sino-Korean plate, is composed of multiple accretionary volcanic island arcs, high-pressure metamorphic belts (glaucophane, eclogite), flysch accretionary wedges, décollement mylonite zones and remnants of ophiolites. It belongs to a subductive, complex ductile shear zone system along a palaeo-plate boundary. Finite strain analysis shows that the northward subduction of the Qilian block beneath the Alxa block involved simple shearing dynamics. The metamorphism during subduction progressed through three stages: low-P metamorphism (greenschist facies), high-P metamorphism (blueschist facies), and low-T metamorphism (low greenschist facies). Evidently the Qilian block underwent subduction and then returned to the surface. In addition, the stage of high-P metamorphism can be subdivided into three stages: the initial stage accompanied with S1 cleavage, the main stage accompanied by S2 cleavage and the lag stage with isobar-temperature increase (zonal glaucophane). A Caledonian retrotrench subduction model with northward subduction of the Qilian block resulting in the development of the initial Qilian Mountains has been suggested. The elapsed time

from subduction to return was 450～408Ma and the subduction rate was 14cm/a.

The contraction-type

Data on shear vectors and transverse stretching lineations of large thrust-nappes and décollements have shown that there was lithospheric contraction during the main orogenic stage in the Upper Proterozoic, Palaeozoic, Mesozoic and Cenozoic orogenic belts of China.

Shear zones in the Upper Proterozoic orogenic belts

The recognition of Upper Proterozoic orogenic belts of China is based on the discovery of an Upper Proterozoic high P-ultrahigh P (coesite) metamorphic zone, an ophiolite zone and a metamorphosed volcanic rock zone (700～800Ma) in the southern Shandong-Dabie-Qinling-north-western Sichuan in central China. A glaucophane metamorphic zone accompanied by relics of oceanic crust (700Ma) has also been found in Aksu, west Tianshan Mountains (Xiao Xuchang and Maruyama *et al*., 1990). Evidence that the Sino-Korean plate subducted southward below the palaeo-Yangtze plate, causing the formation of the Upper Proterozoic collision orogenic belt is provided by the presence of:

- Transverse stretching lineations, SSE 140°～160°.
- Shear strain (slipping from south to north) in the high P (ultrahigh P) -high T ductile shear zones in the root of the subduction belt
- A synchronous thrust-nappe ductile shear system with a slip direction of south-north.

In the south Qinling and western Sichuan, the early S-N ductile decollement shear zone (Anz) has also been found between the Pt_{2-3} metamorphosed volcanic rock and the Pz cover below the Indian decollement belt (200Ma).

Shear zones in the Palaeozoic orogenic belts

In the 'Qinling-Qilian-Kunlun' Palaeozoic central orogenic belt, there is a large Caledonian-Variscan thrust-nappe ductile shear system with shear vector-stretching lineation perpendicular to the strike of the mountain chains (north Qinling: S-N; north Qilian: NE-SW; east Kunlun: S-N). Shear strains show that the shear directions of the north Qinling, north Qilian and east Kunlun are from north to south, from north-east to south-west and from south to north respectively, which suggests that the Yangtze plate subducted northward beneath the Sino-Korean plate, the Qilian block subducted northward beneath the Alxa block and the Qaidam-north Kunlun block subducted southward beneath the Yangtze plate (southern Kunlun). The genesis of these shear zones may have included subduction, collision or intracontinental scenarios.

Shear zones in the Mesozoic and Cenozoic orogenic belts

In the south Qinling Mountains, a deep decollement shear zone lying between the basement (Pt_3 metamorphosed volcanic rocks) and the cover (Z-T) was formed in the Indosinian stage (190～200Ma) with a slip direction from north to south. It is accompanied by a high-pressure metamorphic belt, which the product of intracontinental subduction brought about by

the northward subduction of the Yangtze plate beneath the Sino-Korean plate.

The concentric fold belt composed of J-K strata in the Tanggula Mountains and the fold belt composed of T-J_3 strata in the eastern Sichuan Province, are related to the shallow ductile décollement zones formed in the Cretaceous, the slip directions of which are from north to south and from west to east respectively.

From north to south, the ductile thrust system of the Himalayan chain consists of:

- the Yarlung Zangbo 'crust-mantle type' ductile thrust shear zone (YCMT), 80Ma;
- the Lhagoi Kangri-Kangma ductile thrust shear zone (KMT), 40Ma;
- the north Himalayas ductile thrust shear zone (NHT), 40～20Ma;
- the main central ductile thrust fault (MCT), 20Ma and;
- the main boundary ductile-brittle thrust fault (MBT), 10Ma.

All of these zones dip gently northward, have a shear direction from north to south and their ages show a southward migration with time. The thrust of the YCMT has caused deep mantle rock to move 130km southward, and the MCT has made the Himalayan crystalline rock sheet thrust southward onto the microlithon composed of Palaeozoic slightly metamorphosed sedimentary rocks. The distance of this thrust is about 70～115km. All the ductile shear zones mentioned above formed by the continous northward subduction of the Indian wedge. From north to south, they show the following changes:

- the formation age becomes younger;
- the depth becomes shallower;
- the temperature becomes lower;
- the palaeostress and strain rate becomes lower, and;
- the deformation changes from ductile to brittle.

The partial melting of the crust accompanying the late-stage shearing led to the development of syntectonic granites.

Intracontinental shear zones in the Mesozoic

Since the Mesozoic, the continental regions of eastern China have undergone intensive structural alteration and orogeny, resulting in large-scale intracontinental deep thrust-décollement structures overlapping the palaeo-Asian tectonic system (Palaeozoic). The most typical example is the Jiao (eastern Shandong)-Liao (eastern Liaoning) orogenic belt. A sub-horizontal amphibole mylonite zone, 2km wide characterising the deep décollement, lies between the Archaeozoic Anshan group metamorphic basement (Ar), the Proterozoic Liaohe group low metamorphic basement and the sedimentary cover (Z-P).

The nearly east-west (90°～110°) transverse stretching lineation; sheath folding; the east-west strain direction and partial melting caused by shear heating can be clearly observed in the shear zone. The décollement age falls in the Indosinian period (198Ma). A décollement granite mylonite zone striking east-west, possibly of the same age, has been founded in the eastern Shandong, superimposed on the earlier strained rock beds and was modified by the Yun-shanian granite.

Postorogenic extensional shear zones

Extension-type ductile shear zones which may be normal or strike slip, can be divided into three types: 'lag extension', 'gravity extension' and 'thermal uplifting-extension'.

Typical examples of the lag extension type of shear zone include a series of low-angle ductile normal shear zones in the backland of the north Himalaya and in the Xainza-Ñam Co ductile décollement between the Gangdise composite basement and the Mesozoic-Cenozoic sedimentary cover at the north slope of Gangdise-Nyainqêntanglha Mountain. This resulted from stress relaxation on the backland of the thrust.

In the Shandong-Liaoning and Songpan-Ganze orogenic belts, there are ductile shear zones, with syntectonic migmatisation and dynamic partial melting accompanying postorogenic uplift of the metamorphic basement and the thermal dome as a result of granite intrusion.

In southern Liaoning, dynamic myrmekites, which developed perpendicular to the foliation, have also been discovered in the deep décollement mylonite zone and in felsic veins. The dynamic myrmekites with the features of the syn-rotation or reverse-rotation, have developed along the direction from high-strain energy (plagio-clase) to low-strain energy (K-feldspar), and some of them developed parallel to the foliation, deformational lamina and twin crystals. Our studies suggest that the myrmekite does not come from deep high-temperature fluids (the formation temperature is about 570℃), but is the product of the dynamic partial melting and alteration. The structural features of the myrmekite reflect the stress status as vertical, which indicates that the orogeny had changed from contraction to extension.

The formation of the Laiyang Basin (J_3-K_2) to the north of southern Shandong is related with the ENE ductile normal-strikeslip shear zone on the south margin of the basin (Yang Tiannan, 1994). From the en échelon arrangement of Mesozoic-Cenozoic continental facies basins on an Archaeozoic metamorphic basement, it can be inferred that the basin and range system in West Shandong was controlled by a ductile shear zone with north-south slip.

Strike-slip shear zones in the Variscan

The Qinling orogenic belt:

The Shangdan mylonite zone, 2km wide and located between the south Qinling and the north Qinling belt, exhibits sinistral strike-slip movement. This demonstrates the westward movement of the north Qinling with respect to the south Qinling since 315Ma and that the zone is related to the subduction of the Yangtze plate beneath the Sino-and Korean plate.

The Qilian orogenic belt:

The ductile strike-slip shear zones on the north and south edges of the Qilian Mountains which are parallel to the trend of the mountain chain and intersect the Caledonian fold belt, developed 300～299Ma ago and reflect rotation between the Alxa and the Qilian blocks.

The Tianshan orogenic belt:

The existence of the huge strike-slip ductile shear zone with a width over 10km at the south edge of north Tianshan Mountain indicates large-scale dextral strike slip movement between the north Tianshan and the central Tianshan since the Variscan stage.

The Kunlun orogenic belt:

Large-scale sinistral strike-slip movement occurred at the end of the Indosinian stage along the southern Kunlun suture zone ($P\text{-}T_1$), when the syntectonic granite zone was formed (198Ma, 150Ma).

Tertiary shear zones

Most Tertiary shear zones lie on the east edge of the Qinghai-Xizang Plateau. The Xianshuihe sinistral strike-slip shear zone, aligned NW-SE, was formed at 15Ma and divides the Songpan-Ganzê orogenic belt into two parts. Sinistral displacement reaches 80km. The Jinshajiang, Lancangjiang and Honghe sinistral strike-slip zones were formed at 15～20Ma. The strike-slip of the eastern edge of Qinghai-Xizang Plateau is related to the eastward extrusion of the China continent due to the plunge of the Indian wedge beneath Eurasia.

Reference

Cui, Junwen, Zhu, Hong, Wu, Changde, 1992, Deformation and dynamics of the lithosphere in Qinghai-Xizang (Tibet) Plateau: Geological Memoirs, ser. 5, no. 17, 165 pp. (in Chinese).

Tapponnier, P, and Molnar, P, 1976, Slip-linefield theory and large scale continental tectonics: Nature, no. 264, pp. 319～324.

Xiao, Xuchang, Li, Tingdong, Li, Guangcen, Chang, Chengfa and Yuan, Xuecheng, 1988, Tectonic evolution of the lithosphere of the Himalayas (General Principles): Geological Memoirs, ser. 5, no. 5, 236pp. (in Chinese).

Xu, Zhiqin, Hou, Liwei and Wang, Zonxiu, 1992, Orogenic processes of the Songpan-Ganze Orogenic Belt of China: Geological Publishing House, Beijing, 190 pp. (in Chinese).

Xu, Zhiqin, Xu, Huifeng, Zhang, Jianxin, Li, Haibing, Zhu, Zhizhi, Qu, Jingchuan, Chen, Daizhang and Chen, Jinlu, 1994, The Zhoulangnanshan Caledonian subductive complex in the Northern Qilian Mountains and its dynamics: Acta Geologica Sinica, vol.68, no. 1, pp. 1～15 (in Chinese).

Zhiqin Xu is a senior research fellow at the Institute of Geology, Chinese Academy of Geological Sciences and a member of the IUGS Commission on Tectonics. She has been engaged in research on tectonics and structural geology, mainly focused on the deformational dynamics of the main orogenic belts of China. She is vice-president of the Chinese Academy of Geological Sciences and Director of the Institute of Geology.

松潘-甘孜造山带的变形构造体制●

许志琴[1]　侯立玮[2]　王大可[2]　王宗秀[1]
（1. 地质科学院地质所　100037；2. 四川地质矿产局地质研究所　610082）

摘　要　通过变形构造动力学的研究，将松潘-甘孜早-中中生代造山带重新划分为四个基本构造单元：西部义敦岛弧碰撞平移-逆冲岩片，巴颜喀拉-西康三叠系复合型复理石推覆体，扬子陆块西缘逆冲叠置岩片及前陆逆冲系。提出松潘-甘孜造山带的特殊倒三角形几何形态，两个板块聚合矢量（近南北及近东西）、弧形构造及两个前陆体系（龙门山及盐源），是与特提斯洋（P_2—T_2）闭合后的扬子俯冲板块、劳亚仰冲板块及羌塘-昌都仰冲板块的相互作用及会聚有关。强调扬子板块俯冲过程中在主动大陆边缘（劳亚以南及羌塘-昌都以东）形成三叠系复理石增生楔与扬子陆块被动边缘沉积一起组成复合型复理石楔，大规模平卧褶皱及底部滑脱层的存在表明复理石楔往东叠置于扬子陆块之上而形成大型推覆体。

1　前言

位于扬子板块西北部以川西高原及巴颜喀拉山为主体的松潘-甘孜造山带是一个几何形态特殊，构造变动剧烈及演化历史极为复杂的造山带，加之恶劣的自然地理环境，获有“中国地质百慕大”之称[1]。

松潘-甘孜造山带是一个典型的早-中中生代碰撞型造山带，其北侧以阿尼玛卿印支缝合带与劳亚板块相隔[2]~[5]，西侧以义敦岛弧碰撞带（包含甘孜-理塘印支蛇绿混杂岩带、金沙江东蛇绿混杂岩带及义敦岛弧岩浆带）[6][7]与羌塘-昌都微板块毗邻，东缘以龙门山-锦屏山与扬子克拉通相连。造山带西部（巴颜喀拉）呈东西向条带状展布，而东部（川西高原）却犹如一个倒三角形的大口袋往南急剧收敛，在云南省中甸以北尖灭[8]，使在西部羌塘-昌都微板块基础上发育起来的“金沙江-澜沧江-怒江”中生代造山带直接与扬子克拉通相接触。

松潘-甘孜造山系的滋生是发生在古特提斯洋（P_2—T_2）的消亡之后，如今标志古特提斯洋存在的蛇绿混杂岩残片及复理石增生楔仍保留在山体中。

造山过程包含了诺利-瑞替期以来劳亚陆块、羌塘-昌都陆块及扬子陆块拼贴、碰撞及陆内会聚作用。在陆块相互作用过程中，羌塘-昌都陆块在北部向北俯冲于劳亚板块之下；在东部，拼贴并焊接于上述两陆块之间的扬子陆块，作为仰冲板块向北及向西分别同时俯冲于作为仰冲板块的劳亚板块及羌塘-昌都板块之下，因此在整个造山过程中存在着不同的板块

● 中国大陆构造论文集，1992 年 4 月。

聚合矢量:西部(巴颜喀拉)为近南北向,较简单;而往东,川西高原则处于由近南北向及近东西向2个互相垂直的聚合矢量同时作用的复杂应力状况之下。

大量晚三叠世末期磨拉石的出现表明此时松潘-甘孜造山带强烈褶皱作用结束,继而山体隆升扩展及燕山期花岗岩大量侵入;与此同时新特提斯洋在冈底斯-念青唐古拉地块之南部打开,然后新特提斯洋底的向北俯冲及印度板块和欧亚板块于80Ma期间碰撞及大规模陆内俯冲的继续,致使作为喜马拉雅碰撞带后陆一侧的松潘-甘孜造山带发生了强烈的扭转,并深深地打上喜马拉雅的烙印,因此松潘-甘孜造山带保存了连续造山事件的极为复杂的构造体制。

2 基本构造单元

在前人工作基础上,笔者对研究区构造单元重新划分的尝试是基于考虑以下主要因素:稳定陆块、造山带及碰撞接合带的不同构造部位,造山带基本地壳结构及板块作用的运动学和动力学方式。

2.1 板块单元

(1)劳亚仰冲板块:位于造山带北侧的古生代末北方联合大陆板块,在印支阶段作为仰冲一侧叠置于扬子及羌塘-昌都陆块之上。

(2)羌塘-昌都仰冲微板块:位于造山带西侧,晚古生代期间与冈底斯陆块一起作为基墨里大陆的一部分(Sengör,1979)从冈瓦那古陆分裂及离散出来,而在晚三叠世—中侏罗世期间同劳亚、扬子板块拼合,并向东推覆在扬子之上,而往北俯冲于劳亚板块之下。由于板块叠置及相互作用在羌塘-昌都微板块上形成与东部的松潘-甘孜造山带相邻的怒江-澜沧江-金沙江造山带。

(3)扬子俯冲板块:东部为稳定克拉通,西北部边缘在基墨里期因俯冲于劳亚及羌塘-昌都板块之下而卷入松潘-甘孜造山事件中。其北界阿尼玛卿印支缝合带往东至西秦岭逐渐尖灭,经研究中朝板块(北中国板块)与扬子板块(南中国板块)在秦岭—大别地区于泥盆纪已开始碰撞[9]。西部以两条蛇绿混杂岩带(理塘-甘孜蛇绿混杂岩带及金沙江东蛇绿混杂岩带)及所夹持的义敦印支岩浆岛弧带一起组成的岛弧碰撞带于晚三叠世晚期与羌塘-昌都陆块相聚。

2.2 松潘-甘孜造山带的构造单元

松潘-甘孜造山带是由巨大三叠系复理石增生楔、扬子板块西缘活动带、羌塘-昌都陆块以东的义敦岛弧带及前陆体系组成。以构造岩片为基本单位可划分如下造山带构造单元(表1,图1)。

3 西部义敦岛弧碰撞带的平移—逆冲复合体系

造山带西部以近南北向东凸出的义敦岛弧碰撞带与昌都-羌塘微板块相接。由三叠纪义敦群浅变质火山岩系及印支—燕山期中酸性侵入岩组成的岛弧岩浆带被夹持于扬子与羌塘-昌都微板块之间,东以理塘-甘孜蛇绿混杂岩带(P_2-T_3^1)[7]为界,西以金沙江东蛇绿混杂岩带(P_2-T_2)为界,在此,笔者认为金沙江缝合带[6]的确切位置应移至中咱地块东侧的盖

表 1 松潘-甘孜造山带(V)构造单元划分

Table 1 Tectonic units of the Sonpan-Ganzi orogenic belt(V)

V_1	义敦岛弧碰撞逆冲-平移复合系	①金沙江逆冲平移带 ②金沙江东蛇绿混杂岩带 ③中咱逆冲岩片 ④义敦岛弧逆冲岩片 ⑤甘孜-理塘蛇绿混杂岩带
V_2	巴颜喀拉-西康三叠系 复合型复理石推覆体	①西部三叠系主动大陆边缘复理石增生楔推覆体 ②东部三叠系被动大陆边缘复理石推覆体
V_3	扬子陆块西缘叠置构造岩片	①丹巴弧形逆冲-滑脱叠置岩片 ②木里弧形逆冲-滑脱叠置岩片 ③松潘隐伏陆块
V_4	造山带前陆逆冲系	①东缘龙门山前陆逆冲系 ②南缘盐源前陆逆冲系

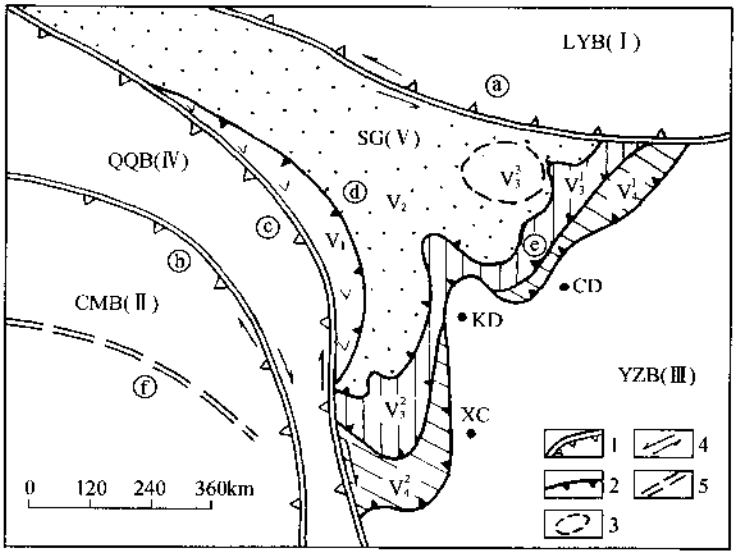

图 1 松潘-甘孜造山带的大地构造背景及单元划分示意图

Fig.1 Tectonic setting and tectonic units of the Songpan Ganzi orogenic belt

LYB(Ⅰ):劳亚俯冲陆块;CMB(Ⅱ):基墨里俯冲陆块;YZB(Ⅲ):扬子俯冲陆块;QQB(Ⅳ):羌塘-昌都俯冲微陆块;SG(Ⅴ):松潘-甘孜造山带;V_1—义敦岛弧碰撞平移—逆冲复合系,V_2 巴颜喀拉-西康三叠系复合型复理石推覆体,V_3—扬子陆块西缘叠置构造岩片(V_3^1—丹巴弧形逆冲滑脱叠置岩片,V_3^2—木里弧形逆冲-滑脱叠置岩片,V_3^3—松潘隐伏陆块),V_4—造山带前陆逆冲系(V_4^1—龙门山前陆逆冲系,V_4^2—盐源前陆逆冲系)。CD:成都;KD:康定;XC:西昌。古特提斯体系:a:昆仑南缘印支缝合带;b:丁青-怒江缝合带,c:金沙江东蛇绿混杂岩带(P_2—T_2);d:理塘-甘孜蛇绿混杂岩带(T_{1-2});e:复理石楔底部滑脱带;f:雅鲁藏布江新特提斯缝合带(T_3—J_2)。1—古特提斯陆块边界;2—松潘-甘孜造山带内部构造单元界线;3—隐伏陆块边界;4—平移;5—新特提斯缝合带

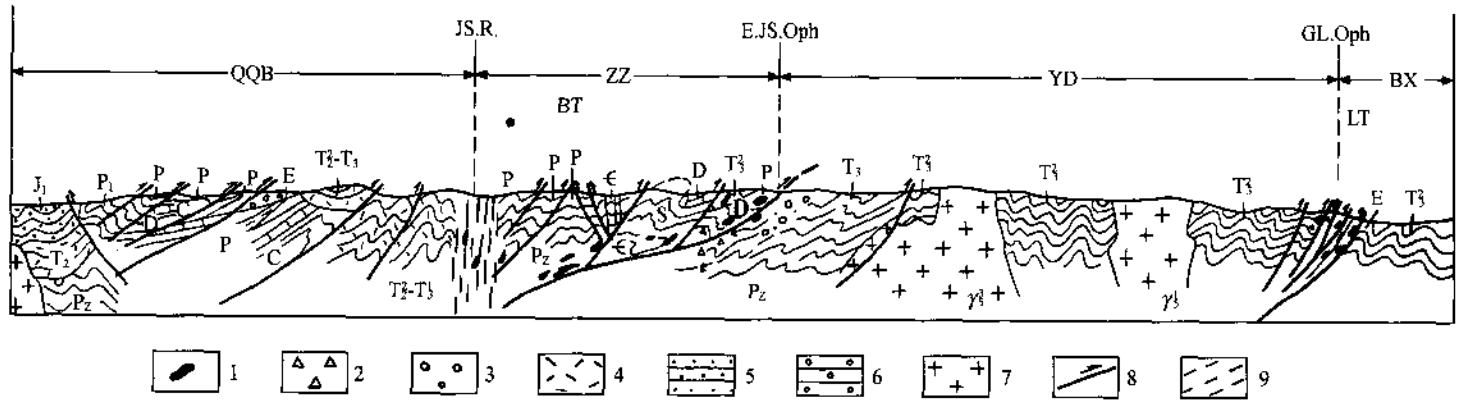

图 2　横穿造山带西部(理塘—海通)构造示意剖面

Fig.2　Schematic cross section showing structures for the Western Part of the Songpan-Garze orogenic belt (Litang-Haitong)

QQB:羌塘-昌都陆块;ZZ:中咱逆冲岩片;YD:义敦岛弧带;BX:巴颜喀拉-西康复理石增生楔推覆体;E.JS.Oph:金沙江东蛇绿混杂岩带;GL.Oph,甘孜-理塘蛇绿混杂岩带;J.S.R:金沙江平移带;BT:巴塘; LT:理塘。1—超基性岩;2—混杂岩;3—泥砾混杂岩;4—火山岩;5—陆相碎屑岩;6—陆相磨拉石;7—花岗岩;8—逆冲断层;9—劈理化带

玉-定曲带,其主要原因是:①金沙江带为后期形成的直立平移带;②金沙江以东"中咱地块"的古生界地层中与昌都板块古生界地层岩性相似;③"中咱地块"古生界地层中相继发现大量平卧(A型及B型)褶皱,表明并非为稳定的原地地块而应为羌塘-昌都仰冲板块自西往东推覆在义敦岛弧上的前缘逆冲岩片;④作为中咱岩片底部的盖玉-定曲韧性逆冲断层带(向西缓倾)由超基性岩、辉长岩、放射虫硅质岩、基性火山熔岩及混杂堆积组成的蛇绿混杂带,后经逆冲—平移剪切而沿金沙江及岩片内出露;⑤中咱逆冲岩片以东的 T_3^{1-2} 陆相碎屑岩中含大量来自西部的石炭纪—二叠纪灰岩岩块组成了泥砾混杂岩[6],可视为逆冲前缘的滑塌堆积(图2)。

义敦岛弧带主要构造线方向从北往南由NWW-SEE→NW-SE→SN,在西北部德格柯鹿洞一带发现早期的350°～10°方向拉伸线理、"A"型平卧褶皱、剑鞘褶皱,显示存在有自南往北逆冲推覆;往南义敦、巴塘一带,中咱岩片以及义敦岛弧带内微构造特征表现为105°～120°方向的拉伸线理、"A"型褶皱,以及一系列平行展布的西倾的糜棱岩带。

垂直于弧形构造带的逆冲矢量(35°→120°的变化)及旋转应变确定了羌塘-昌都陆块整个向东推覆于义敦岛弧带之上,在此剪切应变基础上,又叠加了垂直于缝合带方向挤压而形成的同劈理直立褶皱、扇形断裂体系及新生代以来强大的平移走滑体系。

由于盖玉-定曲带及理塘-甘孜带从晚华力西—印支阶段开始的先后往西俯冲,在昌都及义敦带内分别形成了 P_2—T_3^1 陆缘火山岩和 T_3 岛弧火山岩,以及晚华力西、印支—燕山期花岗岩(246～169Ma)[1]。

4 巴颜喀拉-西康三叠系复合型复理石推覆体

三叠系巴颜喀拉群(西部)及西康群(东部)巨厚复理岩系构成了松潘-甘孜造山带的主体。关于此套复理石岩系生成的构造背景曾有如下观点:①张勤文(1981)[10]认为三叠纪沉积作用主要是在新生洋壳(晚二叠世海相玄武岩)上进行的,并提出新生洋壳系三叠纪弧后扩张形成的边缘海盆;②Sengör 提出(1981)[11]并强调(1987)了三叠纪时增生的混杂岩及复理石复合体充填于松潘-甘孜古特提斯残海中的论点;③俞如龙等(1989)则认为三叠纪西康群复理石岩系为扬子陆块被动大陆的前缘复理石推覆体。

近年来,对西康群及巴颜喀拉群三叠纪复理石岩系沉积特征及物源的研究表明,南巴颜喀拉三叠纪复理石为次深海-深海环流的古浊流沉积作用产物,发育大规模海底浊积扇,其物源区为北面的东昆仑造山带[12];而在西部义敦三叠系中-下统复理石及深海浊积扇的研究[13]表明其物源来自西部羌塘-昌都陆块。

上述情况结合扬子板块向北及向西俯冲及甘孜-理塘蛇绿混杂岩带出露,提供了复理石体之西部及西北部作为在洋壳俯冲过程中形成的主动大陆边缘增生楔的依据。复理石体东部马尔康、雅江一带早三叠世为斜坡相复理石,松潘地区由于隐伏陆块存在发育稳定碳酸岩台地,中三叠世东部海槽沉降加大,以半深海复理石为主,晚三叠世以边缘海复理石沉积为代表。上述表明东部西康群属于扬子被动大陆边缘的复理石为主沉积,由于板块相互会聚、被动及主动大陆边缘水域相通及洋壳消减,在三个板块之间形成庞大的复合型复理石楔。

三叠系复理石楔向东仰冲于扬子陆块上是沿其底部由 T_1 薄层凝灰岩及薄板状灰岩组成柔性层(上滑脱层)在上三叠统刚性海相枕状玄武岩层上的滑动而进行的,玄武岩与下面

$P_2^1 + P_1^1$ 薄层质及钙质岩柔性层(下滑脱层)也产生相对滑动。上、下滑脱层均发生动力变质,达绿片岩—低角闪岩相,并含应力矿物黑硬绿泥石及硬绿泥石。

在板块作用过程中(俯冲→碰撞→陆内聚合),三叠系复理石楔沿底部蛇绿混杂岩带及滑脱层继续进行大规模滑移,形成了庞大的复理石楔纳布。叠加应变及应变机制的研究重塑了早期纳布阶段所具有的剪切应变特征:大型平卧褶皱的发育,特别是靠近底部滑脱层的 T_{1-2} 中强烈流面劈理、拉伸线理及大量不同规模紧密的"A"型平卧褶皱及剑鞘褶皱的存在。

上述事实表明,三叠纪复理石岩系主要是活动大陆及被动大陆边缘联合形成的复合型复理石楔,板块继续作用,致使增生体遭受强烈剪切应变,叠置于扬子陆块上形成巨大的复理石推覆体,并使扬子陆块边缘古生界变形变质。

5 扬子陆块西缘叠置构造岩片

扬子陆块西缘活动带(位于龙门山锦屏山西侧)由浅变质的古生代(Z-P)浅海碳酸盐岩、碎屑岩及前震旦系(AnZ)变质基底组成,在北部松潘一带,航磁资料表明存在一个隐伏刚性磁性地块,推测为 AnZ 的扬子变质基底。边缘活动带的构造线呈现近东西向并向南凸出的弧形特征,其地表结构由 2 个超叠构造岩片组成:北部的丹巴弧形滑脱-逆冲岩片及南部的木里弧形滑脱-逆冲岩片。

图 3 为横穿丹巴弧形岩片东侧的构造变形剖面,主滑脱面发育在前震旦系变质火山岩与盖层之间,前震旦系的上部岩系均已糜棱岩化,厚达 0.5～1km,盖层岩片之下部(Z—S)以发育强烈剪切应变的"A"型平卧褶皱、流劈理及自北西往南东向的滑移为特征,并伴随局部熔融生成的混合质脉,在志留系中还出现中压变质的蓝晶石-硅线石-十字石矿物组合。盖层岩片自下而上(D—P)逐渐变成向北西倾斜的同斜褶皱,并伴随一系列脆性逆冲断层(平面上呈弧形)及滞后正断层。由于后期叠加挤压应变及逆冲作用,使深层滑脱界面重褶、上隆且冲断,在丹巴岩片之前沿出露了多个前震旦系变质岩构造窗。丹巴岩片向东及向南整体地叠置于龙门山前陆体系之上。

木里岩片(图 3)的主滑脱层位于下奥陶统之间,底盘为玄武岩(O_1^2)及混合岩化变质岩(AnO_1^2),上盘为浅变质碎屑岩及碳酸盐岩(O_1^3—T_3)组成的强烈褶皱(平卧及同斜褶皱)岩片,并伴随自北向南的逆冲体系及前沿推覆体,木里岩片向南整体地叠置在盐源前陆体系之上。

6 前陆逆冲系

松潘-甘孜造山带东侧及南侧与扬子陆块相接的前陆部位出露以宝兴杂岩(816Ma)和彭灌杂岩(1017～1043Ma)为代表的前震旦系变质基底及震旦系至中、下三叠统的浅海沉积盖层,它们之大部均卷入造山带的前陆逆冲体系中。造山带的前陆逆冲体系由东侧的北东向龙门山前陆逆冲岩片及南侧的东西向盐源弧形逆冲岩片组成(图 4)。

绵延 600km 的 NNE 向龙门山前陆逆冲系包括了被一系列收缩性的西倾缓式、铲式断层分割的 6 个叠置岩片,自东往西、自上而下依次为:

(1)后龙门山岩片(Sa):继续分布在后龙门山,由微变质的古生代褶皱地层组成,褶皱轴面向北西缓倾。

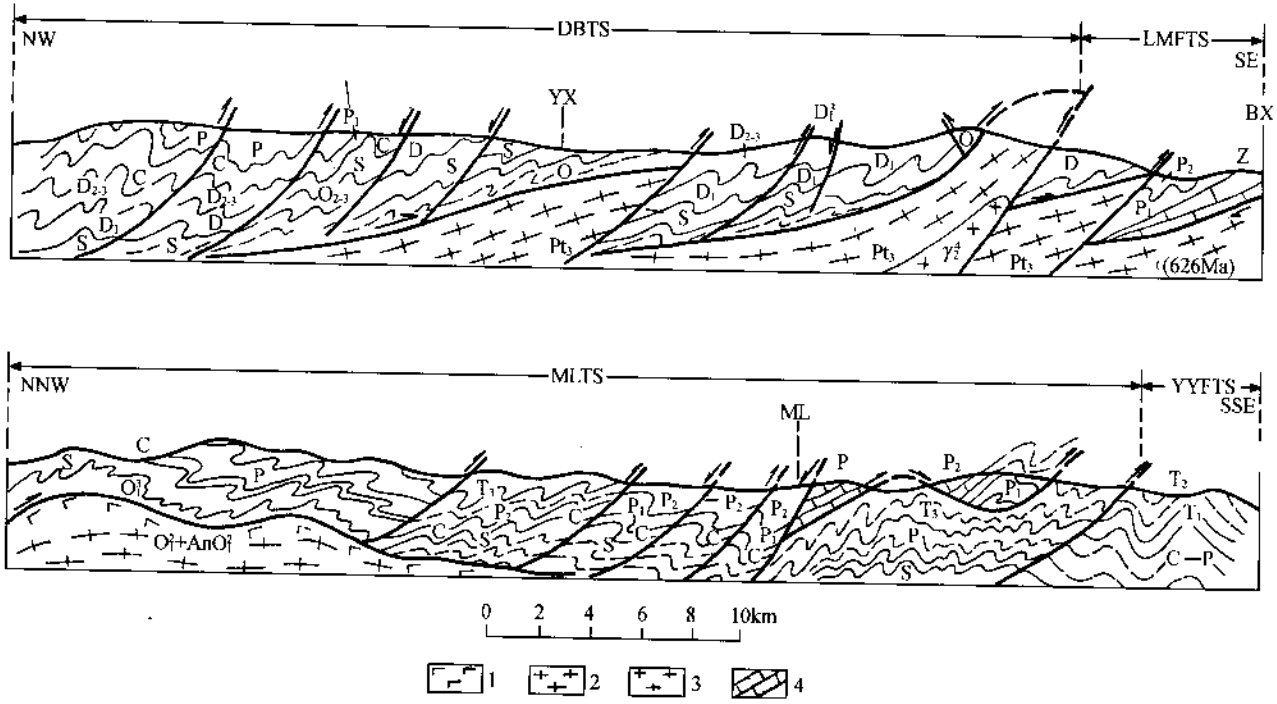

图 3 横穿丹巴及木里构造岩片的剖面

Fig. 3 Cross sections of Danba and Moli tectonic Slabs

DBTS:丹巴逆冲岩片;MLTS:木里逆冲岩片;LMFTS:龙门山前陆逆冲岩片;YYFTS:盐源前陆逆冲岩片。1—玄武岩;2—叶理化变质岩;3—花岗岩;4—碳酸盐岩。YX:永兴;BX:宝兴;ML:木里

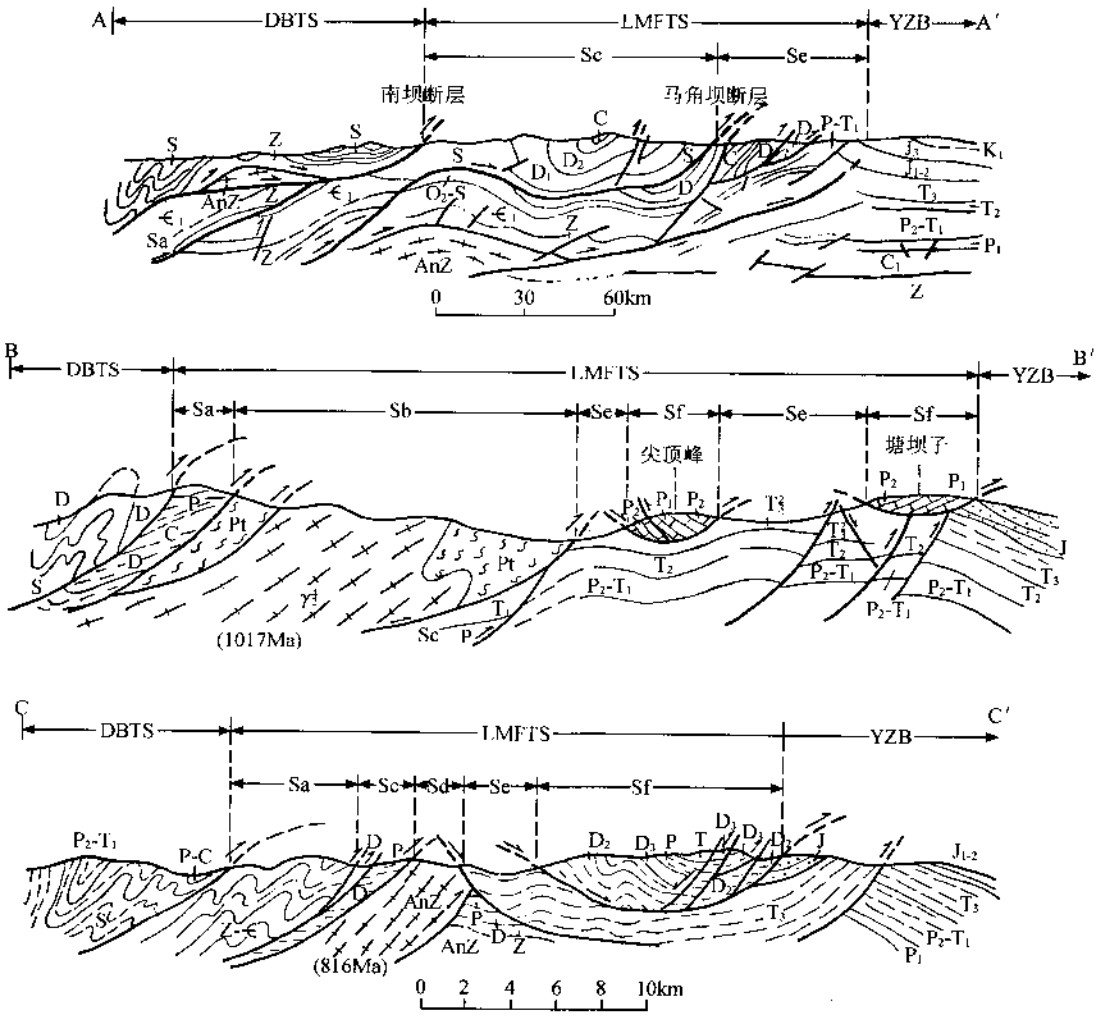

图 4　龙门山前陆逆冲体系剖面图

Fig. 4　Cross sections for the foreland thrust system of the Longmen Mountain

DBTS：丹巴逆冲岩片；LMFTS：龙门山前陆逆冲岩片；YZB：扬子陆块；Sa：后龙门山逆冲岩片；Sb：彭灌杂岩逆冲楔；Sc：唐王寨逆冲岩片；Sd：宝兴杂岩逆冲楔；Se：前龙门山逆冲片；Sf：龙门山前缘推覆体。剖面 AA′根据宋文海(1989)的龙门山区 L55 测线地震，地质综合解释剖面图

(2)彭灌杂岩逆冲楔(Sb)：由前震旦系彭灌变质杂岩及厚度不大的震旦系和泥盆至下三叠统碳酸岩组成的刚性岩楔。

(3)唐王寨逆冲岩片(Sc)：主要位于江油之北西，岩片内的志留系至石炭系碳酸盐及碎屑岩组成了同心褶皱，并发育反冲断层及切割侏罗系陆相红色砂砾岩的前缘逆冲断层系。

(4)宝兴杂岩逆冲楔(Sd)：位于龙门山西南部，由前震旦系宝兴变质杂岩及上覆古生代盖层组成的刚性岩楔。

(5)前龙门山逆冲岩片(Se)：由上三叠统煤系地层及以下的浅海相沉积层组成的岩片，岩片内的逆冲断层被侏罗系红色岩系不整合覆盖。

(6)龙门山前缘推覆体(Sf)(黄汲清,1929):近 20 个大小飞来峰展布在灌县至宝兴一带[14],作为外来岩块的志留-泥盆系至中三叠统碳酸盐岩刚性体自北西往南东推覆在 Se 岩片及扬子陆块的中生代(T_3—K)陆相地层(原地岩块)上。龙门山推覆体可分为三类:伴随平卧褶皱及劈理的褶皱推覆体、变形微弱的冲断推覆体及由后期重力形成的变质杂岩滑覆体。褶皱推覆体靠近龙门山,其根部可能位于彭灌及宝兴杂岩的东南缘,远离龙门山的冲断推覆体可能来自彭灌杂岩及宝兴杂岩逆冲楔(Sb 及 Sd)中的上部盖层。

龙门山前陆叠置逆冲岩片中各岩片的生成顺序为 Se(早于 J_1)→Sb(晚于 J_1)→Sc→Sb→Sa,为自东往西一倒退式(上叠式)逆冲序列,形成于印支—燕山末或喜马拉雅初期。

龙门山前陆逆冲岩片的西缘北东向边界逆冲断层(茂汶一带)由于后期喜马拉雅运动影响又发生右行平移作用。

在造山带南部的盐源前陆弧形逆冲岩片中以下三叠统石膏层为滑脱层将岩片划分为上岩片(T_2)及下岩片(Z—T_1),下岩片的南部发育前缘逆冲断层系,盐源岩片自北往南推覆在扬子陆块之上。

7 变形构造体制及动力学初探

(1)与阿尔卑斯及喜马拉雅等碰撞型造山带一样,由扬子陆块西缘活动带、三叠系复合型复理石楔、岛弧带及前陆体系组成的松潘-甘孜造山带实体,具典型的薄壳结构。

(2)造山带所处的特殊大地构造部位(位于三板块之间)使其本身在印支造山阶段同时遭受了近南北向及近东西向的两个剪切矢量及聚合矢量的影响。总体近南北和近东西向拉伸线理以及近东西和近南北两套弧形构造体制(包括滑脱-逆冲系及韧性剪切带)的存在提供直接依据。自北往南及自西往东的剪切指向表明了劳亚及羌塘-昌都为仰冲板块,而扬子为俯冲板块。

(3)燕山末至新生代开始,印度板块向欧亚大陆俯冲的板块驱动力使喜马拉雅碰撞带后陆发生强大的右行扭转:造山带西部(理塘带、金沙江带)及东侧(后龙门山带)叠加了右行平移作用,造山带内部及前陆叠置了浅层推覆构造和共轭剪切断裂系统。

参 考 文 献

[1] 俞如龙、郝子文、侯立玮,1989,川西高原中生代碰撞造山带的大地构造演化,四川地质学报,第 9 卷,第 1 期,第 27～38 页。

[2] 李春昱,1975,用板块构造学说对中国部分地区构造发展的初步分析,地球物理学报,第 18 卷,第 1 期,第 52～76 页。

[3] 朱志直、赵民、施立新,1984,东昆仑南缘西大滩混杂堆积,中国地质科学院院报,第 10 号,第 129～136 页。

[4] 曲景川,1984,藏东、川西及青海南部二叠-三叠纪时期地质构造特征的讨论——地块自身的解体和敛合,中国地质科学院院报,第 10 号,第 117～128 页。

[5] 姜春发、冯秉贵等,1986,昆仑地质构造轮廓,中国地质科学院地质研究所所刊,第 15 号,第 70～80 页。

[6] 张之孟、金蒙,1979,川西南乡城—得荣地区的两种混杂岩及其构造意义,地质科学,第 3 期。

[7] 刘宝田、曲景川,1983,四川理塘—甘孜一带古洋壳的发现及对板块构造的意义,青藏高原地质文集(12),地质出版社。

[8] 陈炳尉等,1987,怒江—澜沧江—金沙江地区大地构造,地质出版社。

[9] Mattauer Xu Zhiqin, 1985, Tectonics of the Qinling Belt: build-up and evolution of eastern Asia, Nature, Vol.317, No.6037, p.496~500。

[10] 张勤文,1981,松潘-甘孜印支地槽西康群复理石建造沉积特征及其大地构造背景,地质论评,第27卷,第5期,第405~412页。

[11] Sengr, A.M.C., 1987, 特提斯的故事:大洋神有多少后妃? 张渝昌译,石油地质与实验,1988,增刊1,第128~142页。

[12] 邹定邦,饶荣标、陈水明、陈冉琨,1984,南巴颜喀拉山三叠系浊积岩,青藏高原地质文集,第15期,第27~42页。

[13] 唐茂蛟,1989,川西义敦地区三叠系下、中统复理石与浊积扇,四川地质学报,第9卷,第4期,第12~16页。

[14] 赵友年,1985,龙门山推覆构造之初步研究,四川地质学报,第5卷,第2期。

The Deformation Structure System of the Songpan-Garzê Orogenic Belt

Xu Zhiqin* Hou Liwei** Wang Dake* Wang Zongxiu*

Abstract The Songpan-Garzê orogenic system lying in southwestern China originated after the closure of Palaeo-Tethys. The orogenic process involved collage, collision and intracontinental convergence of the Laurasia, Qangtang-Qamdo and Yangtze plates since the Norian-Rhaetian. The orogenic belt embraces a structural system combining the Palaeo-Tethyan and Neo-Tethyan orogenic events. On the basis of the study of the deformation structural dynamics, the orogenic belt may be divided into four basic tectonic units: (1) the strike slip-thrust sheet of the Yidun island-arc collision zone in the western part, (2) the Triassic Bayan Har-Xikang composite flysch wedge nappe, (3) the thrust sheets superposed on the western margin of the Yangtze plate (including the Danba arcuate detachment-thrust sheet and Muli arcuate detachment thrust sheet, and (4) the foreland thrust system (including the Longmen Mt. and Yanyuan foreland thrust slabs). It is emphasized that the Triassic accretionary flysch on the margins of the active continent (Laurasia and Qangtang-Qamdo) in the process of subduction of the Yangtze plate and the flysch and flyschoid sediments on the margins of the passive continent (Yangtze) formed a composite flysch wedge. Large-scale recumbents in the flysch wedge and the existence of detachments indicate that the flysch wedge was eastwards superposed on the Yangtze plate to form a largescale nappe. The establishment of the deformation structure system has confirmed that the orogenic belt has a thin-skinned structure.

* Chinese Academy of Geological Sciences.

** Geological Bureau of Sichuan Province.

“西康式”褶皱及其变形机制❶

——一种新的造山带褶皱类型

许志琴[1]　侯立玮[2]　王大可[2]　王宗秀[1]
（1. 地科院地质所；2. 四川地矿局地质所）

摘　要　在松潘-甘孜造山带的三叠系西康群复理石岩系中，普遍发育着一种特殊的同劈理直立褶皱，作者称为“西康式”褶皱。这类褶皱的特点是：其褶皱枢纽倾伏角是变化的；具有圆滑—同心褶皱、尖棱褶皱及过渡型褶皱等多种复合褶皱形式；由不同类型劈理构成复杂的折射劈理图形；在流劈理面上发育有垂直的拉伸线理。根据微构造分析和有限应变测量表明，这类褶皱是由压扁，纯剪切、纯剪切＋简单剪切等三种变形机制的产物。其动力学基础是在三个板块和近于垂直的南北及东西方向挤压应力作用下，形成的叠加褶皱，推测形成深度为10～15km“西康式”褶皱的构造特征、形成机制及壮观程度上，完全可与世界著名的“侏罗山”型，“彭尼内”型造山带褶皱相媲美，它是造山带中一种新的褶皱类型。

1　引言

西欧地质学家在研究阿尔卑斯造山带时，曾提出过两种世界著名的褶皱类型；①“侏罗山”(Jura)型褶皱，即发育在阿尔卑斯山前的无劈理同心—等厚—箱形褶皱；②“彭尼内(Pennine)型褶皱。即发育在阿尔卑斯造山带内部的同劈理平卧褶皱[1]。研究表明，前者为地壳浅层次褶皱(约5～8km深)，与阿尔卑斯山前的深层大滑脱(在三叠系石膏层内)有关；后者为地壳深层次褶皱(大于15km)，是板块俯冲而导致的大规模推覆作用的产物。这两种类型的褶皱，在中国及世界上许多造山带中均存在。

位于中国西南部的松潘-甘孜造山带是一个具特殊几何形态(倒三角形)的早-中中生代造山带。组成造山带主体的川西高原，其大部分(约15万km^2)为三叠系西康群巨厚复理石岩系所覆盖。西康群为扬子被动大陆西缘的斜坡相复理石及半深海复理石类型的沉积(包含局部碳酸岩台地相)[1]，它与西部及西北部(巴颜喀拉群)的主动大陆(劳亚大陆及羌塘-昌都微陆块)边缘的洋壳增生复理石楔一起，构成了迄今保存在大陆内部的世界上最大的复理石复合体[1](图1)。由于古特提斯洋(P_2—T_2)闭合后三个板块(劳亚仰冲板块、羌塘-昌都仰冲微板块及扬子俯冲板块)的相互作用，继后的陆内会聚以及第三纪以来印度板块的影响，致使西康群复理石岩系遭受多期构造应变及多种变形机制的影响。形成十分复杂的构

❶ 中国区域地质，1991年第1期。

造样式[2]。本文所提出的"西康式"褶皱类型,是界于"侏罗山型"及"彭尼内型"之间的一种特殊的同劈理直立褶皱,它的突出特点除了劈理及拉伸线理直立以外,还具有褶皱枢纽变化,褶皱样式交替、复合以及劈理类型复杂的特征。通过微构造分析在确定此一新褶皱类型的基础上,研究了"西康式"褶皱的变形机制,应变参数及生成条件,并进行了板块动力学的解释。

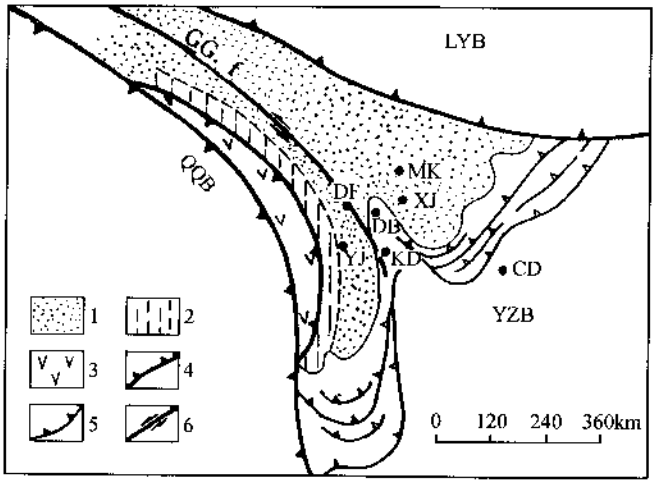

图1 西康群分布区的大地构造背景图

Fig.1 Map showing the tectonic settings in the region of distribution of the Xikang Group

1—西康群(T)复理石岩系;2—洋壳复理石增生楔;3—三叠系火山岛弧;4—古特提斯蛇绿混杂岩带;5—逆冲断层;6—平移断层。LYB—劳亚大陆,YZB—扬子陆块,QQB—羌塘、昌都陆块,GG.f—贡嘎半移断层,CD—成都,KD—康定,DB—丹巴,MK—马尔康,DF—道孚,YJ—雅江

2 "西康式"褶皱特征及变形机制

2.1 "西康式"褶皱的主要特征

"西康式"褶皱是一种同劈理直立褶皱,广泛发育在由巨厚砂板岩组成的三叠系西康群复理石岩系中,微构造的详细研究表明,此类褶皱不同于一般简单的同劈理直立褶皱(图2),它的突出特点如下:

(1)褶皱枢纽的倾伏角是变化的(+90°→-90°);

(2)由于岩层能干性差异而形成复合褶皱样式,包括无劈理(或少劈理)的圆滑—同心褶皱、同劈理的尖棱褶皱及过渡型褶皱;

(3)伴随多种类型的劈理(破劈理、板劈理及流劈理),并构成复杂的折射劈理图案;

(4)在直立的流劈面上发育垂直的拉伸线理。

小金东麻子桥中三叠统杂谷脑砂岩的变形构造剖面(图3),表明了劈理面走向稳定(NWW290°~304°),但褶皱枢纽倾伏角有很大变化。马尔康一带"西康式"褶皱枢纽测量反映了枢纽走向及倾伏角均具变化。

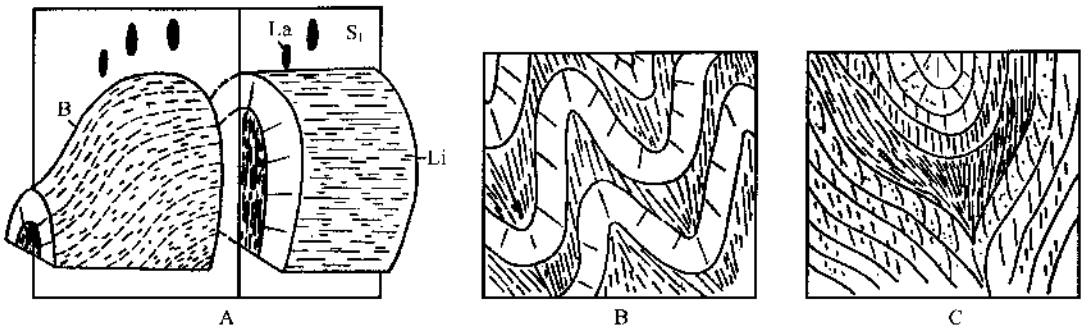

图 2　"西康式"褶皱的微构造特征及立体模式

Fig.2　Microstructural characteristics and stereoscopic model of "Xikang-type"folds

A—西康式褶皱的立体模式:褶皱枢纽(B)倾伏角的变化,具直立的劈理面(S_1),垂直的拉伸线理(La),交面线理(Li)平行于褶皱枢纽;B—圆滑褶皱与尖棱褶皱组成的复合褶皱样式;C—折射劈理

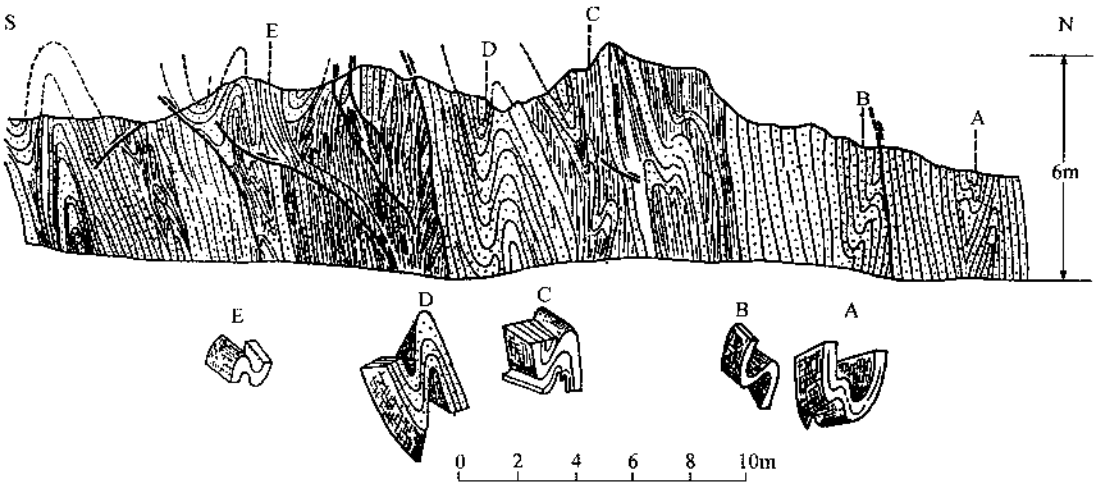

图 3　小金东麻子桥中三叠统砂岩的构造变形剖面

Fig.3　Section of structural deformation of Middle Triassic sandstones at Dongmaziqiao, Xiaojin County

"西康式"褶皱的轴面轨迹在区域范围内显示了 NWW—EW—NEE 总体向南凸出的弧形。以北西向贡嘎断裂带(原名鲜水河断裂)为界可划分成两个弧形构造体制:东北部的马尔康弧形构造及西南部的雅江弧形构造,这两个弧形构造错位达几十公里很可能与第三纪以来(?)贡嘎韧性剪切带(糜棱岩带)的强大左行平移有关。

2.2　"西康式"褶皱的变形机制

变形机制的研究是通过微构造分析(特别是拉伸线理的剖析)[3]及有限应变测量[4]而得的。"西康式"褶皱的垂直拉伸线理通常表现为以下几种形式:黄铁矿及石榴石的压力影,拉伸的氧化膜,水平裂隙中垂直生长的结晶矿物(方解石及石英)纤维以及布丁构造(包括双凸形布丁及双凹形(骨形)布丁)等。根据研究将"西康式"褶皱的变形机制划分为以下三种类型:

2.2.1 纯剪切机制

在劈理面上黄铁矿压力影呈对称型，影子部的方解石或石英纤维生长垂直于黄铁矿边壁，并与其它形式的拉伸线理方向(X)一致，沿 Y 轴却无结晶纤维生长，表明具有沿 X 轴拉伸、Y 轴不变的纯剪切应变特征(图 4A)。

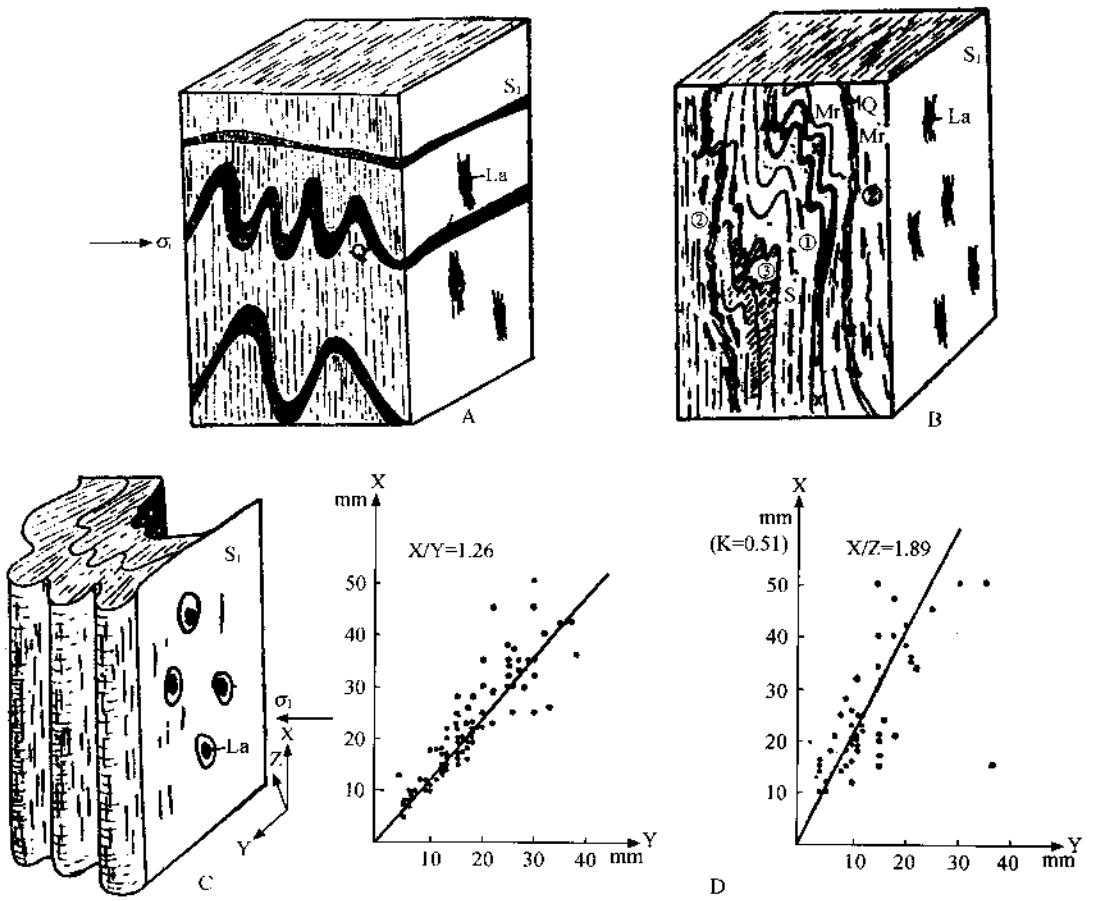

图 4 "西康式"褶皱的变形机制

Fig.4 Deformation mechanism of"Xikang-type"folds

A—纯剪切机制，B—纯剪切＋简单剪切机制，C—压扁机制，D—雅江北两河口氡化膜(T_2 砂岩中)的有限应变测量(主轴比法)。La—拉伸线理，S_1—劈理面，Q—石英，Mr—长英质

2.2.2 纯剪切＋简单剪切机制

在丹巴以东半扇门一带的下三叠纪含黑云母变质砂板岩中，"西康式"褶皱的变形机制显示了复杂情况。广泛发育的长英质脉由于高应变而形成骨形布丁(即双凹形布丁)[5,6]，骨形布丁之间的裂隙被石英充填形成凸起部，并在垂直褶皱轴面的露头上显示了斜方对称与单斜对称两种组构特征。骨形布丁的斜方对称(图 4B①)与黄铁矿压力影特征(y 轴不拉伸)相结合可解释为纯剪切机制的结果。骨形布丁的单斜对称是由于布丁之间结晶充填物的重新定向所造成，可作为剪切指向的标志(即简单剪切机制的产物)本处骨形布丁所显示

的不同剪切指向的单斜对称组构(图 4-$B_②$,有左行剪切及右行剪切)表明,在纯剪切的总背景下,由于塑性基质能干性、刚性拉伸层及骨形布丁之间结晶充填物的流变性质差异而形成的不同指向的简单剪切机制分量。布丁脉及早期剪理面(S_1)的重褶(图 4-$B_③$)也可能是这种分量的产物。

2.2.3　压扁机制

在雅江—道孚一带及雅江以东的上三叠统"西康式"褶皱中,劈理面上的拉伸线理表现为黄铁矿周围的石英结晶纤维沿两个方向(X 轴及 Y 轴)生长,并且 X＞Y;雅江北两河口变形氧化膜的有限应变测量获得富林(Flinn)指数 K＝0.51[7],说明褶皱形成为压扁机制所致(图 4-C、D)。

3　"西康式"褶皱的形成及动力学解释

在讨论"西康式"褶皱的生因问题时,应考虑以下三方面的因素:①NWW—EW—NEE向的"西康式"褶皱具倾伏角变化的枢纽,表明它是一种叠置褶皱,其形成需要一个近南北向延伸及倾角变化的面理(层理或劈理)作为基础。因此重塑"西康式"褶皱形成前的早期应变十分必要;②包含有复杂微构造内容的"西康式"褶皱的应变参数:形成深度、应力大小及岩层的流变学性质;③力的来源及动力学解释与三个板块相互作用的关系。

3.1　"西康式"褶皱形成前的早期应变

西康群不同应变阶段的变形特征及变形机制的重塑,揭示了"西康式"褶皱形成之前所经历的早期应变有两种不同的情况。

(1)以近南北向"A"型平卧褶皱为基础,叠加了近南北向挤压应力。在雅江、马尔康一带所发现的"西康式"褶皱叠置在早已形成的三叠系韧性推覆(或滑脱)剪切带中,剪切应变表现为近水平流劈理、南北向拉伸线理、南北向褶皱枢纽及自北往南的旋转应变。"西康式"褶皱为 S_1(或 S_{0-1})重褶而形成,并伴随直立的 S_2 劈理,西康式褶皱枢纽陡倾部分即为原"A"型褶皱的转折部位(图 5 左图)。

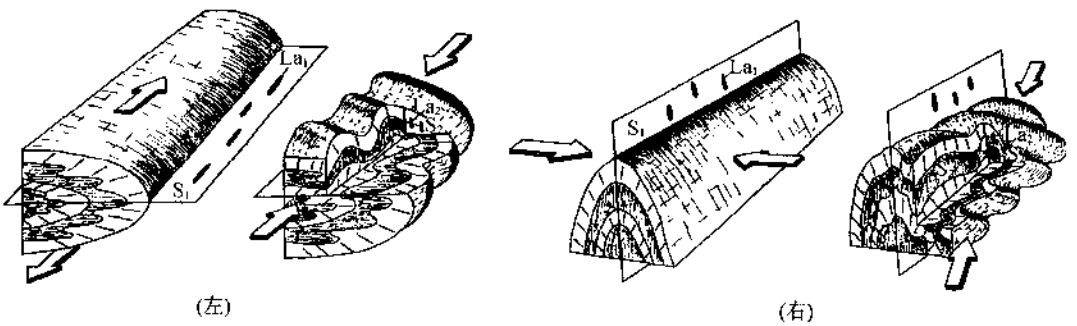

图 5　"西康式"褶皱形成模式

Fig.5　Model for the formation of "Xikang-type" folds

左图:由"A"型平卧褶皱→"西康式"褶皱;右图:由"B"型直立褶皱→"西康式"褶皱。S_1—第一期劈理面,La_1—第一期拉伸线理;S_2—第二期劈理面,La_2—第二期拉伸线理

(2)以近东西向"B"型同劈理直立(或同斜)褶皱为基础,叠加了与南北方向呈一角度的挤压应力,形成 290°～300°轴向、枢纽变化的"西康式"褶皱(图 5 右图)。在丹巴—道孚一带的"西康式"褶皱属此类型。

3.2 应变参数的估计

(1)根据"西康式"褶皱形成的同变质条件(绿片岩相)及劈理类型(破劈理+流劈理),推测其形成深度约 10～15km,介于"侏罗山"式褶皱及"彭尼内"式褶皱之间。

(2)不同褶皱类型(圆滑+尖棱)交替及折射劈理的发育,表明西康群砂板岩中不同岩性能干性差异是重要应变参数。柔性层(泥岩、泥灰岩)组成相似褶皱,并发育流劈理;而强性层(灰岩、石英岩)则生成圆滑同心褶皱,发育破劈理。

(3)根据小金东部多处"西康式"褶皱幅度的定量计算(仅对枢纽水平的直立褶皱),获得地壳平均缩短量为 65%～85%。贡嘎断裂以东西康群地层出露宽度(南北向)以 300km 计,估算地壳缩短 900km,原宽度约为 1200km,这说明它是在一个近南北向强挤压应力下形成的。

3.3 动力学初步解释

具特殊几何形态(例三角形)的松潘-甘孜中生代造山带,由三个板块相互聚敛而成。变形构造动力学的研究表明两个近于垂直的聚合矢量(近南北向及近东西向)作用于造山带,并形成两个相互垂直的收缩体系,即自北往南的收缩体系及自西往东的收缩体系[2]。前者主要呈现在扬子被动大陆边缘,后者主要显示在羌塘—昌都板块之东侧。发育在扬子被动大陆边缘三叠系复理石岩系,在中生代阶段主要经历了三期构造应变:1. 扬子板块向北俯冲于劳亚板块之下,形成自北往南的大规模剪切应变,表现为沿推覆(或滑脱)韧性剪切带的南北向"A"型平卧褶皱及远离韧性剪切带的近东西向"B"型直立褶皱的形成;2. 扬子与劳亚板块碰撞以后,陆内会聚所形成的南北向挤压作用塑造了西康式褶皱;3. 来自扬子板块西缘的东西向收缩体制,不断在板内向东扩展,使早期生成(南北向收制缩体制)的近东西向(或略带弧形)构造线进一步弯曲,呈向南明显突出的弧形构造。由于构造应变影响到较深的范围,故"西康式"褶皱样式在三叠系以下岩层中也存在。

4 结语

(1)"西康式"褶皱是一种叠置褶皱,为发育在造山带内部复杂应力作用的产物;

(2)"西康式"褶皱具直立劈理、垂直拉伸线理、变化的褶皱枢纽,复合的褶皱样式及折射劈理等特征;

(3)"西康式"褶皱生成深度 10～15km,岩层能干性差异使其形成复合的褶皱及劈理样式;

(4)"西康式"褶皱的变形机制为纯剪切、纯剪切+简单剪切及压扁;

在广阔的川西高原上,"西康式"褶皱重重叠叠、此起彼伏,犹如蛟龙腾飞,在百丈陡壁上构成一幅令人惊叹的宏伟画卷。这种类型的褶皱目前在中国的祁连山、南秦岭造山带及辽南地区均有发现。"西康式"褶皱无论从其特征、机制及壮观程度而言,完全可与世界著名"侏罗山"型及"彭尼内"型褶皱相媲美。

参 考 文 献

[1] Debelmas. J., 1970, AIpes-Savoie et Dauphine. Masson Paris.

[2] 许志琴、侯立玮、王大可、王宗秀，松潘—甘孜造山带的变形构造体制。"大陆构造及成矿作用"论文集，中国地质大学。

[3] 许志琴，1989，拉伸线理及其构造意义，四川地质学报，第9卷第2期，P.9～15。

[4] Ramsay. J. G., 1967. Folding and Fracturing of Rocks. McGraw Hill, New-York. P. 568.

[5] Goldstein A. G., 1988, Factors affecting the Kinematic interpretation of asymmetric boudinage in Shear zones. Journal of Structural Geology, Vol. 10, NO. 7, P. 707～715.

[6] Malavielle. J., and Lacassin. R., 1988, "Bone-shaped" boudins in progressive shearing. Journal of Structural Geology, Vol. 10, No. 4, P. 335～345.

[7] Flinn. D., 1965, On the Symmetry principle and the Deformation Ellipsoide. Geo. May, 102, n°1.

"XIKANG-TYPE" FOLDS AND THEIR DEFORMATION MECHANIISM ——A NEW FOLD TYPE IN OROGENIC BELTS

Xu Zhiqin Hou Liwei Wang Dake and Wang Zongxiu

Abstract (Omit)

阿尔卑斯旋回中喜马拉雅山链和阿尔卑斯山链的主要变形特征[●]

MAJOR DEFORMATION FEATURES OF THE ALPINE CHAIN AND THE HIMALAYAN CHAIN IN THE ALPINE CYCLE

许志琴
（中国地质科学院地质研究所）

特提斯—阿尔卑斯山系是当今世界两大造山带之一，它自加勒比海开始，横贯欧亚大陆南部，直达印度尼西亚。这一山系的形成经历新特提斯洋打开至闭合的整个过程。特提斯洋是在华力西造山运动之后（T—J）联合大陆由西太平洋开始剪切张开而形成的；晚侏罗世至老第三纪时期，由于大西洋由南往北张开造成特提斯洋闭合[3]。与此同时大洋内及洋壳和陆壳间发生俯冲或仰冲，以致大洋消亡，南北大陆板块碰撞（有些地段无碰撞）。

阿尔卑斯山链及喜马拉雅山链是特提斯—阿尔卑斯山链中的二个著名山链（图1），笔

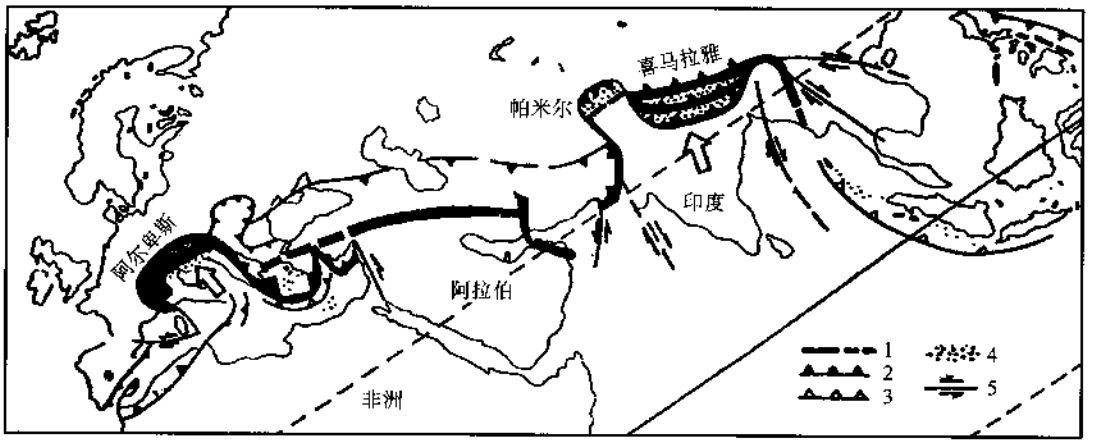

图1　欧亚南部的特提斯—阿尔卑斯山系
（据 Aubouin, 1980, 简化）
Fig. 1　A simplified map of the Tethys-Alpine system
1—蛇绿岩残片；2—逆掩前缘；3—俯冲带；4—超碰撞带；5—走滑断层

● 中国地质科学院院报，1984年第9号。

者在本文中将通过对阿尔卑斯山链(法国 Gronoble-Briançon 剖面,Grave 地区及瑞士 Rose 地区)(1981,1982)及喜马拉雅山链(西藏萨嘎—聂拉木剖面及雅鲁藏布江缝合带南北地带)(1982)所进行的地壳变形的显微构造初步研究❶ 及对比来讨论这两个山链在阿尔卑斯旋回中主要变形特征及山链构造演化过程。

1 推覆构造是山链的主要构造类型

本文讨论的两个山链都是弧形山链,具复杂的多期变形特征。而最主要最明显变形则表现为在阿尔卑斯旋回大规模推覆构造的存在。

阿尔卑斯山链位于法国、瑞士及意大利境内,是欧亚板块和非洲—意大利板块在聚合及碰撞过程中形成的向北西突出的弧形高应变带。从西往东可分为三个以华力西结晶地块为基底的构造单元[6]:

1.1 外带(Helve 带)

厚 2～5km 的中新生代浅海碎屑岩碳酸岩相、复理石及磨拉石沉积层组成简单的构造。Gronoble 及 Grave 以西的剖面观察表明了本带由一系列简单背向斜组成,并被叠瓦式冲断层所切割。背斜核部往往有石膏粘上层(T_{2-3},有时形成底辟)(图 2),向斜核部为中新世地层。褶皱内发育直立轴面劈理,以破劈理及折射劈理为主。华力西结晶地块由于断裂作用而呈带状断裂,地块间的盖层遭受强烈挤压。

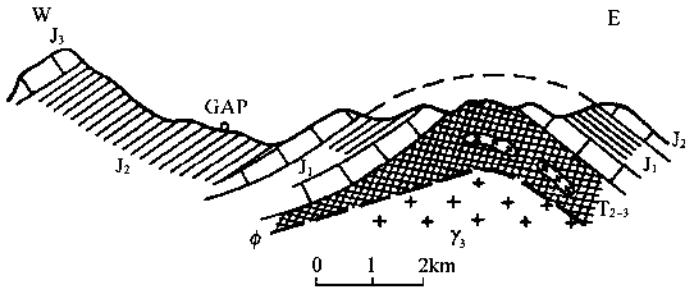

图 2 阿尔卑斯外带 REMOLLON 穹隆示意剖面

Fig.2 A sectional view of REMOLLON dome on the outer zone of the Alps

T_{2-3}—石膏层;J_1、J_2—碎屑岩及灰岩;J_3—灰岩;γ_3—华力西花岗岩;φ—冲断层

1.2 中带(Pennine 带)

自西往东变形逐渐强烈,西部三叠系至始新统浅海沉积层组成向东倾斜的倒转褶皱及平卧褶皱,发育向东倾斜和近水平的流劈理及一系列韧性冲断层(图 3)。东部洋壳蛇绿岩套呈叠瓦岩片覆于侏罗系至下白垩统光泽片岩系(绿片岩)之上(图 4)。本带变形构造以发育著名的"奔尼"式(Pennine)纳布(推覆 nappe)构造为特征,即一系列以平卧褶皱、近水平劈理及垂直山链的拉伸线理为特征的韧性推覆剪切带。

❶ 据"地壳变形及显微构造"(许志琴,1983,未刊);"雅鲁藏布江壳幔型及壳内型韧性推覆剪切带""西藏定日—康马壳内型韧性推覆剪切带"(许志琴,未刊)。

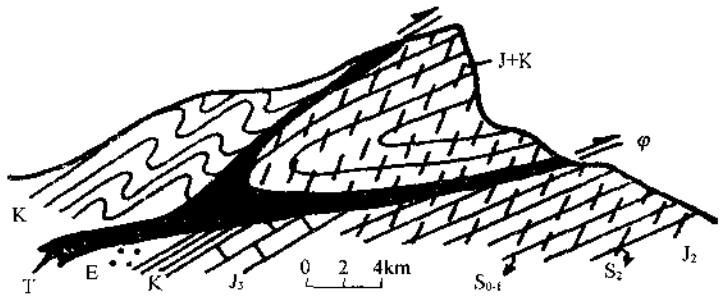

图 3 阿尔卑斯中带西部 MORGON 推覆构造示意剖面

Fig. 3 A sectional view of MORGON nappe structure in the western part of the middle zone of the Alps

S_{0-1}—层理及第一期劈理；S_2—第二期劈理；J_2—碎屑岩；J_3—灰岩；J+K—碎屑岩及灰岩；K—碎屑岩；E—复理石岩系

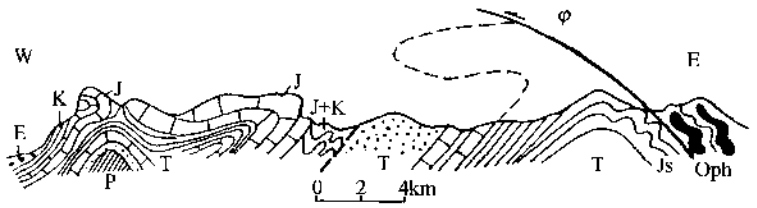

图 4 阿尔卑斯中带东部 BRIANCON 推覆构造剖面

Fig. 4 A sectional view of BRIANCON nappe structure in the eastern part of the middle zone of the Alps

P—浅海碎屑岩；T. J. K 及 J+K—浅海碎屑岩及碳酸盐；E—复理石岩系；Js—光泽片岩；Oph—蛇绿岩套；φ—冲断层

1.3 内带(Autra alpin 带)

为意大利—非洲板块的边缘地带。以中生代碳酸岩(T?)为主的盖层与欧亚板块有明显差异。近西部发育"奔尼"式推覆构造，往东为阶梯状断裂所代替(逆断层或平移断层组合)。

以上三个构造单元之间都呈自东向西推覆构造接触关系，蛇绿岩套呈夹在两陆块间的东倾窄带。推覆构造还明显表现在原地岩块之上叠置了许多外来岩块(飞来峰)，如外带上的 Ultrahelv。异地岩(来自中带)，中带上的 D. Blanche, M^t. Mary, Emilun, M^t. Rafray, Bec de Nana 和 Pillonet 飞来峰(来自内带)(图 5)，推覆距离可达上百公里。

雄伟壮观的喜马拉雅山链总体呈向南凸出的弧形。根据变形构造特征，由北往南可分五个构造单元[2](图 6)：

Ⅰ. 藏北构造带：古生代变质基底及早白垩世以前的中生代海相地层遭受大规模向南推覆作用，晚白垩世日喀则群弧后盆地沉积，混杂岩及老第三纪红色磨拉石建造均遭受板块碰撞产生的收缩作用影响，这种作用并叠加在早期推覆作用影响的地层上。

Ⅱ. 雅鲁藏布江蛇绿岩带：一系列向南的韧性冲断层使蛇绿岩套残缺不全，并呈叠瓦片状夹于两个陆块之间。本带与Ⅰ带之间的雅鲁藏布江缝合线为板块碰撞产物。

Ⅲ. 藏南构造带：以巨厚的晚三叠统浅变质绿片岩相为主体，发育"奔尼"式推覆构造。

Ⅳ. 高喜马拉雅构造带：巨厚的前寒武纪晚期至始新世浅海沉积中发育一系列向南的韧性冲断层。

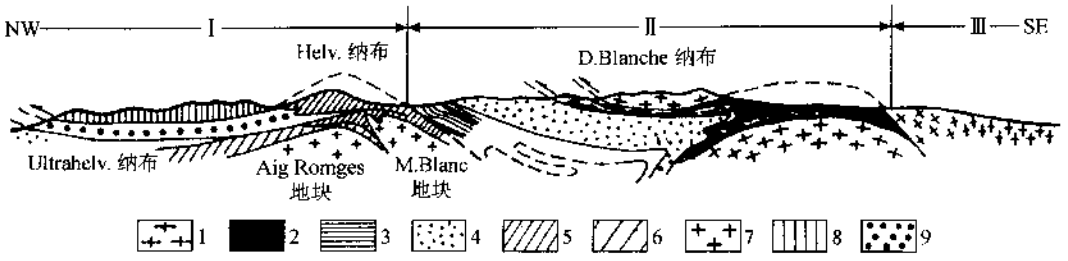

图 5　横穿阿尔卑斯山链(法国、瑞士境内)的构造剖面

Fig.5　Atransverse section of the Alpine Chain (within France and Switzerland)

I 阿尔卑斯外带, II 阿尔卑斯中带, III 阿尔卑斯内带

1—内带华力西基底;2—洋壳蛇绿岩(J_3—K_1);3—光泽片岩(J_3—K_4);4—复理石岩系(K—E);5—外带中生代外来岩块(Helve. 纳布);6—外带原地岩块的中生代盖层;7—外带华力西基底;8—来自中带及内带的中生代外来岩块;9—Ultrahelv. 纳布

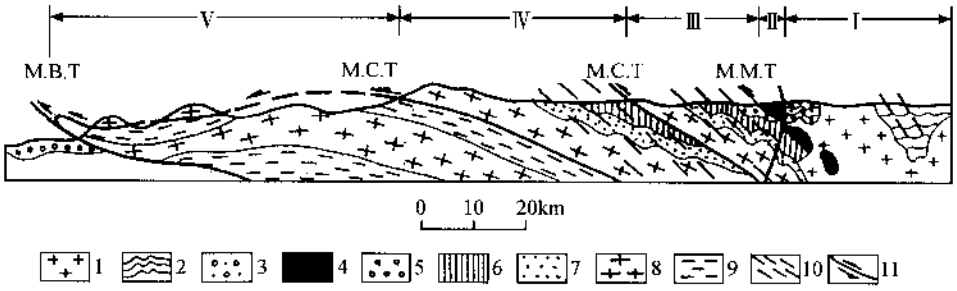

图 6　横穿喜马拉雅山链的构造示意剖面

(据常承法 1979, 修改)

Fig.6　A transverse section of the Himalayan Chain

I 藏北构造带; 1—冈底斯花岗岩; 2—中生代地层(T—K_4);3—日喀则群(K_2);II 雅鲁藏布江蛇绿岩带;4—蛇绿岩; III 藏南构造带, IV 高喜马拉雅带; 5—始新世—中新世磨拉石建造; 6—中生代地层;7—古生代地层; 8—前寒武系变质岩; V 低喜马拉雅构造带;9—前奥陶系变质岩;10—劈理化带;11—冲断层;M.M.T—主幔冲断层;M.C.T 主中冲断层;M.B.T—主边冲断层

V. 低喜马拉雅构造带:由前寒武系至古生代变质岩系组成,高喜马拉雅结晶变质岩系推覆其上,岩系内包含一系列叠瓦构造。

以上单元与阿尔卑斯一样,都是呈构造接触,并且自北往南推覆叠置,其中规模最大者可向南推移百多公里(如低喜马拉雅带上的高喜马拉雅结晶变质岩系外来岩块),(图 6)。

2　深部推覆具韧性剪切的特点

在阿尔卑斯山链及喜马拉雅山链内各构造单元之间的界限曾用主幔冲断层(M.M.T),主中冲断层(M.C.T)及主边冲断层(M.B.T)命名之。但是研究表明这些界面并不具明显的破裂特征,而是表现为以主界面为中心的数公里厚地壳范围内的强烈塑性流动及剪切应变,也就是以一系列韧性推覆剪切带形式表现出来:发育在洋壳蛇绿岩内为"幔内型",洋壳

蛇绿岩与陆壳间为"壳幔型",在陆壳内为"壳内型",如喜马拉雅山链自北往南发育雅鲁藏布江"幔内型"及"壳幔型"韧性推覆剪切带,定日-康马"壳内型"韧性推覆剪切带及尼泊尔"壳内型"韧性推覆剪切带[4];再往南在低喜马拉雅构造带边缘发育冲断层,使下古生代变质岩系逆掩于锡伐里克磨拉石砾岩之上。同样在阿尔卑斯山链中自蛇绿岩纳布往西,也显示了从"幔内型"→"壳幔型"→"壳内型"韧性推覆剪切带→冲断层的变化。

韧性推覆剪切带是逆掩断层在地壳深部的再现,在韧性推覆剪切带内发育一系列无明显破裂面的逆掩断层带、平卧褶皱、近平行的流劈理以及垂直山链的拉伸线理。

2.1 无明显破裂面的逆掩断层带

韧性推覆剪切带实际由一系列无明显破裂面的韧性逆掩断层组成。如喜马拉雅山链中雅鲁藏布江剪切带的构造主界面(M.M.T)位于蛇绿岩与硅铝质陆壳之间,在蛇绿岩内部存在一系列叠瓦式的韧性逆掩断层(图 7),变形是连续过度的,厚达数公里。阿尔卑斯山链中带的奔尼式纳布构造就是具有这种性质的推覆剪切带。

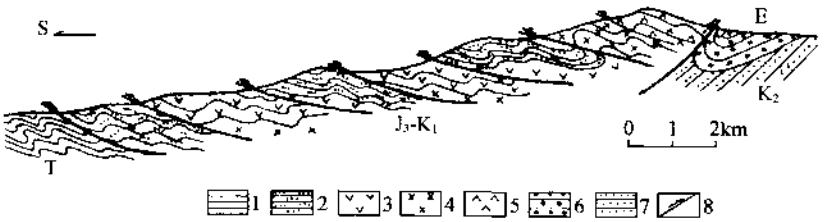

图 7 雅江西部萨嘎构造剖面图

Fig.7 A sectional view of the structure of Saga in the west of the Yarlong Zangbo River

1—复理石沉积;2—放射虫硅质岩;3—基性火山岩;4—辉长岩;5—辉橄岩;6—红色砾岩;7—砂岩;8—冲断层

2.2 拉伸线理

拉伸线理代表了剪切运动矢量,是深部剪切应变在岩石叶理或劈理面上留下的痕迹。无论在陆壳内,还是在洋壳中;在盖层内,还是在基底中,在两个山链中到处发育了横穿山链的拉伸线理。这种线理具有穿透性的特点,其发育在每一个劈理或叶理面上,而在区域上方向一致。如在阿尔卑斯山链到处发育 110°－120°方向的拉伸线理,喜马拉雅山链中普遍存在近南北向拉伸线理。

拉伸线理的表现形式是多种多样的,普遍存在的有矿物及矿物集合体(石英集合体为多)的拉伸,正片麻岩中包体拉伸,大理岩及石英岩中杆状构造,布丁及香肠构造;此外还有变形砾岩中的拉伸砾石(如阿尔卑斯中带上侏罗统砾岩中的拉伸砾石)及拉伸或截断的化石(如阿尔卑斯外带里阿斯统的拉伸箭石及菊石,雅鲁藏布江韧性推覆剪切带内中生代类蓝闪石片岩中变形圆球虫等)。

阿尔卑斯及喜马拉雅蛇绿岩中(特别在上地幔岩—橄榄岩及二辉橄榄岩中)拉伸线理的存在具特殊的意义,它是洋内剪切标志,代表了洋间剪切运动的矢量。上地幔岩中拉伸线理是通过斜方辉石及橄榄石的拉伸表现出来的。

2.3 褶皱与叶理

在大规模推覆作用阶段,伴随着剪切带内有不同规模的平卧褶皱,发育一系列近水平的

叶理,这是由于在劈理面上矿物优选方位所造成的。在剪切带内,岩石变形强度是不均一的,因为变形是岩性及构造部位的函数。靠近推覆的主界面,岩石叶理化强,而且糜棱岩化(糜棱岩叶理平行区域叶理);而在远离主界面处,流劈理(叶理)变成破劈理甚至无劈理。如阿尔卑斯山链中远离蛇绿岩和陆壳之间的 M.M.T 主界面的华力西地块(玫瑰山和阿班地块)内部,或在洋壳辉橄岩内部,几乎没有劈理,石英组构分析[5]表现了无优选方位的图像;同样,喜马拉雅山链的雅鲁藏布江韧性推覆剪切带中,在具较完整的蛇绿岩吉丁剖面的辉橄岩内部,变形极微。

剪切带中所有岩系都遭受了褶皱,呈现了平卧或同斜褶皱形式。它们的轴近平行于拉伸线理方向,这些规模不等的平卧及近平卧的褶皱发育在逆冲主界面附近几公里范围内。在大部分情况下,层理(S_0)被流劈理(S_1)所置换,只有近平卧褶皱转折部位,S_1 与 S_0 斜交乃至直交。而远离主界面平卧褶皱的轴面逐渐倾斜,变为同斜褶皱。同斜褶皱轴面倾向剪切运动力源方向(在无后期叠加作用情况下)。微构造研究(拉伸线理、旋转变形、有限应变分析及岩组分析等)表明这些平卧及同斜褶皱并非压扁作用产物,而是剪切应变的结果。

在逆冲主界面下部局部会出现一种特殊类型的"a"型箭鞘褶皱,其剖面上呈眼状,平面上呈舌状,褶皱轴方向垂直山链且平行于拉线理。箭鞘褶皱作为简单剪切机制的产物已被模拟实验所证实(Cobbold, 1979)。因此它可以作为剪切应变的一个典型标志。

在阿尔卑斯及喜马拉雅山链的 M.M.T 界面下部,可以看到这种类型的褶皱,但一般是小规模的,唯在瑞士阿尔卑斯中带蛇绿岩纳布之下,陆壳中生代地层中发现两个目前可能规模最大的箭鞘褶皱[8],褶皱轴向 120°,和拉伸线理方向一致,褶皱核部由三叠系大理岩及石英岩组成,四周为二叠系的云母片岩,组成一对闭合的眼睛(图 8),这是由于蛇绿岩纳布推覆在陆壳上而形成的。

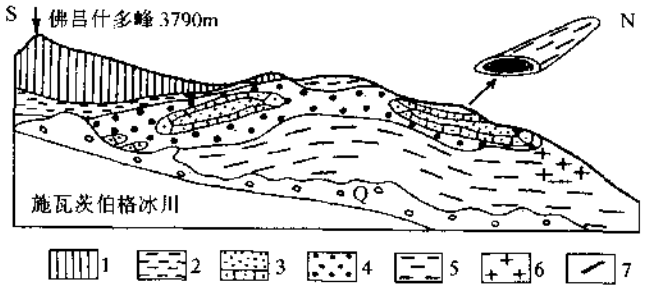

图 8　瑞士阿尔卑斯马特马克箭鞘褶皱示意剖面
(剖面据 Bearth, 1967)

Fig.8　A sectional view of Mattauer Mark sheath fold in the Alps of Switzerland
1—蛇绿岩;2—侏罗系;3—三叠系;4—二叠系;5—华力西期副变质岩;6—华力西期正变质岩;7—拉伸线理

2.4　旋转变形及有限应变分析、确定变形机制

对上述两山链中的旋转变形及有限应变分析表明具有强大的简单剪切作用存在,韧性推覆剪切是简单剪切机制的产物,并且确定了剪切运动的方向(图 9)。

(1) 阿尔卑斯山链中带玫瑰山(Rose,瑞士)地区的观察表明通过次级褶皱指向、压力影

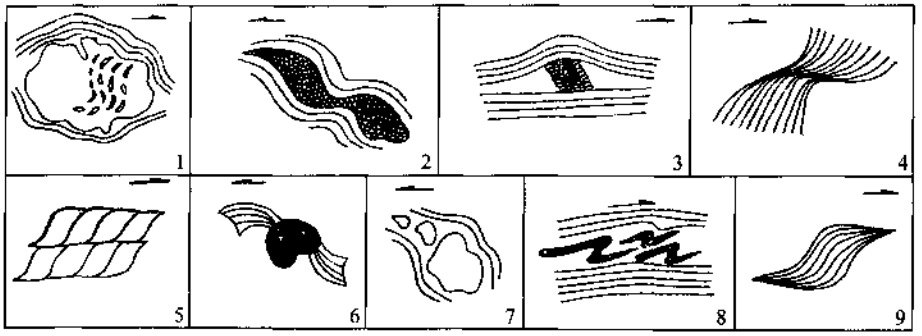

图 9　阿尔卑斯及喜马拉雅山链韧性推覆剪切带中旋转变形例示

Fig. 9　Examples showing rotational deformation in the ductile shear zone of the Alpine Chain and the Himalayan Chain

1—5：雅鲁藏布江韧性推覆剪切带中旋转变形；1—变形石英中包体排列的旋转；2—石英集合体扭动；3—变形石英中张裂隙（充填石英）与剪切方向斜交；4—云母组成显微韧性断层；5—杏仁构造；6—9：阿尔卑斯韧性推覆剪切带中旋转变形：6—压力影（刚体为菊石）；7—曲颈状长石；8—次级揉皱脉；9—S形云母

矿物（长石、石榴石、菊石、黄铁矿等）的旋转、劈理与剪切面之间关系等判断剪切运动方向为自东往西，组构分析也证实这点。笔者（1982）曾利用该区蛇绿岩纳布构造之下的侏罗系变质砾岩进行了有限应变分析，野外测得砾石的构造椭球体主轴比如下：

$$\frac{X_T}{Z_T}=5.9,\quad \frac{X_T}{Z_T}=2.97,\quad \frac{X_T}{Y_T}=5$$

根据 R_0/R_T 图表（Ramsay, 1969）求得原始椭球体的主轴比：

$$\frac{Y_0}{Z_0}=2.25,\quad \frac{X_0}{Z_0}=4.5,\quad \frac{X_0}{Y_0}=2$$

则 $x/y/z=4/1/0.25$（据 R_T/φ 的 Dunnet 图解），获得富林指数● $K\approx1$，这个数据与 Mallavielel(1982)[5]计算中带阿班（Ambin）地块侏罗系变质砾岩中石英砾石 $x/y/z=2.64/1/0.44$，及 $x/y/z=4/1/0.2$，获得 $K=1.23-1.3$ 相似。外带变形量分析也有类似结果：Haute-Provence 地区里阿斯统千枚岩中变形箭石测量[9]获 $x/y/z=2.3/1/0.42$ $K=0.96$；B.K. Tank(1973)[10]对瑞士 Windgällen 区里阿斯统中变形箭石研究获得 $K>0.95$，表明机制的存在。

（2）喜马拉雅山链的“幔内”、“壳幔”、“壳内”型韧性推覆剪切带内岩石显示了丰富多彩的旋转变形。指示了剪切方向自北往南。从石英及方解石组构分析也得到佐证。

雅鲁藏布江壳幔型韧性推覆剪切带内中生代类蓝闪石片岩中变形圆球虫的有限应变分析获得 $x/y/z=2.03/1.43/1$，$K=0.87$；定日-康马壳内韧性推复剪切带中马拉山花岗岩变

● 富林指数 K 是用以确定变形机制的指数，$K=\dfrac{\frac{X}{Y}-1}{\frac{Y}{Z}-1}$，当 $0<K<1$，为压扁型；$K=1$ 为剪切型；$1<K<\infty$，为收缩型。

形石英的变形分析获 $x/y/z=1.88/1/10.6$；$K=1.3$。表明是剪切作用结果。

旋转变形及有限应变分析是确定变形机制及运动矢量的重要方法，也为板块动力学模式提供了依据。

3 糜棱岩带及高压变质带

在"壳幔型"推覆剪切带中心部位，往往发育一定规模的糜棱岩带及高压变质带，这是高应变集中的产物。

喜马拉雅山链最大的糜棱岩带是雅鲁藏布江糜棱岩带。以仲巴、加加、宁嘎、日喀则一直到罗布莎以东，宽数公里，延展 400 多公里。糜棱岩带以 M.M·T 为中心，北带位于洋壳蛇绿岩中，称"蛇绿糜棱岩"(包括辉橄糜棱岩、辉长糜棱岩及硅质千糜岩等)；南带主要位于三叠系复理石岩系北缘，称"陆壳糜棱岩"，主要由千糜岩组成。辉橄糜棱岩结构可分为残碎斑状结构，条带结构及镶嵌结构。具变形纹、扭折、吕德尔线，多边形亚结构及不均匀消光等变形特征，三峰分布明显，其特征与阿尔卑斯型"橄榄糜棱岩"十分相似。辉橄糜棱岩基质中晶粒极细小(直径可达 6μm)。在南带千糜岩中含有蓝闪石类矿物，表明糜棱岩带是高应变作用产物。

作为高压变质带，阿尔卑斯西部具有目前世界上最大的蓝片岩带，此带位于中带西侧，包含在盖层及基底中。其主要矿物组合为蓝闪石-硬柱石-多硅白云母-硬玉，估计形成在6~8kb，200~400℃温压条件下。此外，在近内带中还发育另一高压相——榴辉岩相，高压相是在阿尔卑斯初期(晚白垩世)发育的，蓝闪石及硬柱石在某些地带中结晶时间可持续到很晚。

雅鲁藏布江高压带与糜棱岩带的分布位置大体一致(或更宽些)，以蓝闪石类、文石、硬玉、硬柱石、绿纤石组合为特征，蓝闪石不典型，主要为冻蓝闪石及碱性蓝闪石。蓝闪石带以南分布有硬绿泥石带[1]。糜棱岩带及高压变质带是洋壳仰冲在陆壳上大规模推覆作用中产生(Mattauer，1980)。

4 变形及变质作用的穿时性

变形及变质作用是同时发生的，而且具有穿时特点，主要表现为：

(1)无论是纳布或是原地地块，无论是基底或是盖层，都卷入了大规模推覆构造之中，都具有相同的矿物组合类型。

(2)以韧性推覆剪切带主界面为中心向两侧，变形作用及变质作用逐渐减弱，如阿尔卑斯山链中，从 M.M.T 往西，褶皱作用由平卧→等斜→直立，面状构造表现为由流劈理→折射劈理→破劈理。阿尔卑斯变质作用自东到西可分以下三个相带：高压相带、绿片岩相带及沸石相带，由高压→中压变化。雅鲁藏布江的壳幔型韧性剪切带内也有类似的变化规律，至定日—康马一带变形又加强，出现流劈理及平卧褶皱。喜马拉雅期变质相带从北往南为蓝片岩相带至黑硬绿泥石带。

另外在两山链中，变形作用前峰远远超过变质作用的前峰。

5 叠加变形

在两山链中变形构造表现了复杂的多期性叠加的特点。

玫瑰山地区(瑞士)及阿班地区[5]变形的显微构造研究表明主要存在二期变形构造。

推覆(纳布)阶段的剪切应变是最强大的一次变形,使原来古老地块的早期变形痕迹大大削弱,基底连同盖层全部卷入这次重大构造事件中。在玫瑰山地块的变质岩中发育 N60°的线理构造,被东西向区域性拉伸线理所切,很可能是前纳布阶段的产物,后纳布阶段变形主要表现为纳布阶段生成的线理,劈理(叶理),褶皱及纳布主界面又重新褶皱,褶皱轴垂直于拉伸线理。如玫瑰山北面的 Mischabel 背斜为纳布后构造,其轴向为 NE—SW,轴面倾向西,劈理发育程度与岩性有关,一般在片岩中明显,在石英岩及大理岩中不明显,在转折端发育交叉或细褶纹线理。这是叠加在第一世代上的变形往往显示了局部具细褶纹线理的垂直轴面的小型褶皱特点。在喜马拉雅山链中,以与山链方向一致的直立褶皱为特征的收缩作用叠加在早期大规模推覆构造之上。如在雅鲁藏布江缝合带南北侧遭受剪切作用的下白垩统及其前下白垩统地层中普遍发育了切割早期南北向拉伸线理的东西向细褶纹线理,或者拉伸线理及早期劈理又重新褶皱,褶皱轴平行于细褶纹线理方向。在上白垩统日喀则群中收缩作用显示了扇形褶皱的发育(中部褶皱轴面直立,北侧轴面南倾,南侧轴面北倾),由于日喀则群为在剪切作用后形成的复理石盆地楔,故没有第一世代剪切应变的痕迹,收缩作用同时伴随逆断层及走滑断层产生。上述两山链中的后期收缩作用是在板块碰撞阶段及以后产生的。

6 变形迁移及构造演化

根据山链的变形构造研究,阿尔卑斯与喜马拉雅山链的主要变形特征十分相似,因此山链应具有类似的成因机理及演化阶段。推测山链形成的演化阶段如下:

6.1 洋内仰冲阶段

主要依据是完整蛇绿岩剖面存在、蛇绿岩中推覆构造存在及蛇绿岩拉伸线理所提供的洋内剪切运动的矢量[7]。喜马拉雅山链形成前的洋内仰冲在早、晚白垩世之间,阿尔卑斯山链形成前的洋内仰冲大约在晚白垩世(100 百万年)。

6.2 仰冲阶段

洋壳仰冲于陆壳之上,一系列推覆构造形成,同时在 M.M.T 上界面附近形成糜棱岩带及高压变质带。喜马拉雅仰冲阶段大致发生在晚白垩世至老第三纪,阿尔卑斯在晚白垩世末至老第三系(80 百万~60 百万年)。

6.3 碰撞阶段

特提斯洋最终闭合、收缩作用叠加在推覆构造之上。此阶段大致发生 60 百万年左右,(可能比喜马拉雅早一些)。与此同时,阿尔卑斯山链中带形成绿片岩相。喜马拉雅山链的雅鲁藏布江蓝片岩相带以南形成硬绿泥石带。

6.4 陆内超碰撞阶段

碰撞后,俯冲作用并未停止,它以较缓慢速度在大陆岩石圈中进行,造成岩石圈加厚。

变形作用由于壳幔滑脱不断从中心向两侧扩展,形成地壳加积构造,伴随有大型逆冲断层及走滑断层(Mattauer,1983)两个山链的这种大陆岩石套下冲构造都为最新地球物理资料所证实,它们的演化模式是可以对比的(图 10)。

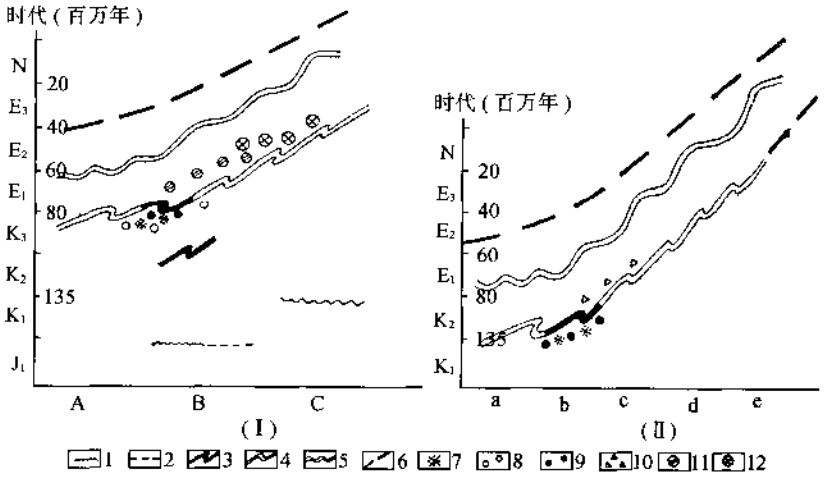

图 10　阿尔卑斯山链及喜马拉雅山链变形迁移及构造演化示意图

Fig. 10　A map showing the deformational migration and structural evolution of the Alpine Chain and the Himalayan Chain

Ⅰ阿尔卑斯山链;A. 内带,B. 中带,C. 外带;Ⅱ喜马拉雅山链:a)藏北构造带,b)雅鲁藏布江蛇绿岩带,c)藏南构造带,d)高喜马拉雅构造带,e)低喜马拉雅构造带;

1—角度不整合,2—假整合,3—洋内剪切,4—推覆作用,5—收缩作用,6—脆性断裂作用,7—糜棱岩,8—榴辉岩相,9—蓝片岩相,10—硬绿泥石带,11—绿片岩相,12—沸石相

在上述构造演化过程中,变形作用随时间自内向外显示了明显的迁移性:

(1)推覆剪切带类型,从"幔内型"→"壳幔型"→"壳内型"→逆断层;

(2)深度上,从深到浅;

(3)变形性质上,从韧性到脆性,阿尔卑斯晚期脆性变形还向西扩展到法国中央地块,东西向挤压作用叠加在比利牛斯南北挤压的应力场之上;喜马拉雅山链中晚期脆性形变表现为第四纪的东西向拉张作用在西藏高原的普遍存在(Tapponnier 和韩同林,1981)。图 10 表示了变形迁移及构造演化的关系。

7　结论

(1)在新特提斯洋闭合过程中形成的阿尔卑斯及喜马拉雅山链具有十分相似的变形特征,以大规模剪切作用为主,叠加了收缩作用。这两个山链的主要变形机制是简单剪切。

(2)具有类似的变形迁移特点及变形和变质作用的穿时性。

(3)具相类似的板块构造演化规律及动力学模式,经历了从洋内仰冲→洋陆仰冲→大陆碰撞→陆内超碰撞(陆内俯冲)阶段。

参 考 文 献

[1] 肖序常、高延林，1982，西藏雅鲁藏布江缝合带高压低温绿片岩相的新资料。中国地质科学院地质研究所所刊，第5号。

[2] 常承法、郑锡澜、潘裕生，1978，喜马拉雅的地质发展历史、构造带的划分和隆起原因探讨。国际交流地质学术论文集(1)，地质出版社。

[3] Aubouin, J., Debelmas, J., Latreille, M., 1980, Les chaines alpines issues de la Téthys: Introduction générale. Publications du 26e Congrès géologique international Paris 7～17. Juillet 1980.

[4] Brunal, M. et Andrieux, J., 1977, Déformations superposées et mécanismes associes an Chevauchement Central Himalayan "M.C.T"; Nepal Oriental. "Himalaya" sciences de la terre. Colloques.

[5] Malaviellc, J., 1982, Etude tectonique et microtectonique de la déformation ductile dans de grands chevauchements crustaux: Exemple des Aples Franco-Italiennes et de la Corse. Thèse, Acad. de Montpellier. U.S.T.L.

[6] Mattauer, M., 1980, Les déformation des Materiaux de l'écorce Terrestre. Ed. Herman Paris.

[7] Mattauer, M. et Mercier, J.L., 1980, Microtectonique et grande tectonique. Mem. H. ser. Soc. geol. de France N.10.

[8] Mattauer, M., 1982, Plis en Fourreau d'échelle plurikilometrique dans la zone interne des Aples Suisses(Couverture nord de la Nappe du Mont Rose). C.R.A.S., a paraitre.

[9] Subieta, T.A., 1977, Analyse quantitative de la déformation dans un secteur de la zone externe des Alpes. Thèse. Acad. de Montpellier. U.S.T.L.

[10] Tank, B.K., 1973, Determinations of strain ellipses from deformed ammonoids. Tectonophysics No.16, pp.89～101.